UNIVERSITEIT GENT

Academic year 2013-2014

Thesis submitted in partial fulfilment of the requirements for the degree of Doctor in Science: Biology

Palaeolimnological reconstruction of Holocene climate and relative sea-level change in Lützow Holm Bay (East Antarctica)

Paleolimnologische reconstructie van Holocene klimaat- en relatieve zeespiegelveranderingen in Lützow Holm Bay (Oost-Antarctica)

Ines Tavernier

Promoter: Prof. Dr. Wim Vyverman
Co-promoter: Dr. Elie Verleyen

Faculty of Sciences, Biology Department

Research group Protistology & Aquatic Ecology

belspo

iwt

PROTISTOLOGY AQUATIC ECOLOGY

Members of the examination committee:

Members of the reading committee:

Dr. Dominic A. Hodgson (British Antarctic Survey, Cambridge, UK)

Dr. Sébastien Bertrand (Ghent University)

Prof. Dr. Dirk Verschuren (Ghent University)

Other members of the examination committee:

Prof. Dr. Wim Vyverman (Ghent University)

Prof. Dr. Koen Sabbe (Ghent University)

Dr. Elie Verleyen (Ghent University)

Prof. Dr. Luc Lens (Ghent University) (Chairman)

Public thesis defence: May 20, 2014

Content

Dankwoord

Een doctoraat schrijf je niet alleen, velen hebben hieraan op een of andere manier bijgedragen. In deze post-doctoraat fase wil ik iedereen graag persoonlijk komen bedanken want op papier is maar op papier. Dankjewel allemaal!

The past is the key to the future

Chapter 1. General introduction

Ice-sheet dynamics and climate regime of Antarctica

The Antarctic ice-sheets and the Southern Ocean play a crucial role in the global climate system (Turner et al. 2009). Moreover, the Antarctic ice-sheets contain approximately 90% of the continental ice on Earth (Vaughan & Spouge 2002). Several coastal glaciers, in particular those of the marine-based West Antarctic Ice-Sheet (WAIS) and in the Antarctic Peninsula (AP), are currently experiencing a negative mass balance as a result of accelerated flow. This process, known as dynamic thinning, results from the melting of floating ice shelves, which induce progressive drawdown and thinning of glaciers (Pritchard et al. 2009; 2012). Both observational and modelling data support the hypothesis that ice shelves and ice tongues buttress fast-flowing ice streams and outlet glaciers, preventing faster flow and ice-sheet shrinkage or collapse (Alley et al. 2005; Pritchard et al. 2012). In total, 87% of AP glaciers retreated during the past 61 years (Cook et al. 2005), and 14,000 km² of ice shelves have recently collapsed (Roberts et al. 2008). Melting of (parts of) the ice-sheets can significantly contribute to global sea-level rise (Pfeffer et al. 2008). In addition, freshwater fluxes from the ice-sheets may also affect the Meridional Overturning Circulation (MOC) as deepwater formation occurs immediately adjacent to the ice-sheets under the ice shelves (Alley et al. 2005). These freshwater fluxes can thus influence the formation of Antarctic Bottom Water (ABW), the densest and coldest bottom water in the oceans and a major driver of the MOC (Foldvik et al. 2004). As such, melting of the ice-sheets can affect the global climate system (Hu et al. 2011).

The current climate regime of the Antarctic is mainly controlled by its geographic position, as well as by its strong degree of atmospheric and hydrographic isolation from other land masses. As the Antarctic continent is one of the few major orographic features present in the Southern Ocean, the main atmospheric and oceanic currents flow virtually uninterrupted in an eastward direction around the continent (Fig. 1) (Summerhayes et al. 2009). The Antarctic Circumpolar Current (ACC) isolates the Southern Ocean from the other oceans, with the boundary formed by the Polar Frontal Zone (PFZ; Fig. 1). Climate variability in the Southern Hemisphere (SH) high-latitudes is mainly dominated by the SH annular mode, which is a large-scale pattern of variability characterised by fluctuations in the strength of the circumpolar vortex. There is a trend towards a stronger circumpolar flow which has contributed to the observed warming over the AP and a non-significant cooling over East Antarctica (EA) and the Antarctic Plateau (Fig. 2; Thompson & Solomon 2002; Steig et al. 2009). This increase in tropospheric circumpolar westerly flows is linked to the depletion of ozone in the stratosphere (Perlwitz et al. 2008). Furthermore, West Antarctica (WA) has been warming during the past decades because of a warming atmosphere, making the AP one of the fastest warming regions on Earth, with temperatures rising at a rate of six times the global mean (Vaughan et al. 2003). On the contrary, the temperature change in the interior of the East Antarctic Ice-Sheet (EAIS) continent was not significant (Thompson & Solomon 2002; Steig et al. 2009).

Figure 1. Overview map of Antarctica indicating the regions mentioned in the text. EA=East Antarctica, WA=West Antarctica. The eastward flow of the oceanic and atmospheric current is indicated (blue arrow), as well as the Polar Frontal Zone (red line).

The mechanisms underlying the current changes in the Earth's climate are not yet fully understood. Investigation of palaeo-archives can provide valuable insights into the magnitude and nature of past climate changes and their effects on Antarctic ice-sheets and the pristine Antarctic environments. This will allow us to determine whether the ongoing current climate changes, amplified at the higher latitudes (e.g. Vaughan et al. 2001) are within the range of natural Holocene climate variability. Although the dramatic climate disruption at the Pleistocene-Holocene transition, Termination I, has received

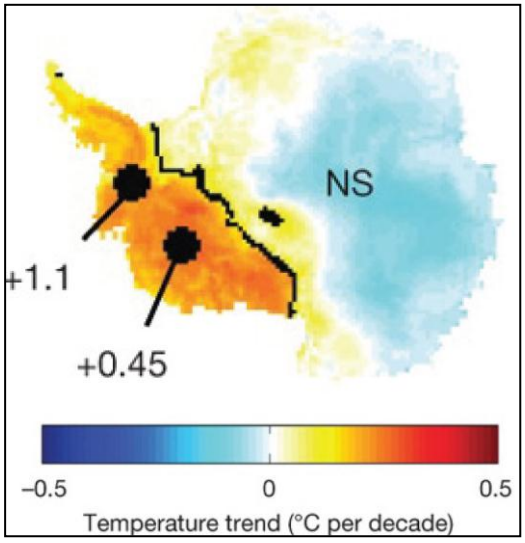

Figure 2. Spatial pattern of temperature trends (degree Celsius per decade) from reconstructions using infrared satellite data. Mean annual trends for 1969-2000. Black lines enclose areas with statistically significant trends (95% confidence). NS = not significant. Black circles: location of Siple and Byrd Stations with their respective trends for 1979-1997. Figure from Steig et al. 2009.

considerable attention (e.g. Denton et al. 2010; Shakun & Carlson 2010; Fiedel 2011), less is known about Holocene climate variability (Mayewski et al. 2004; Divine et al. 2010). Furthermore, the majority of high-resolution Holocene climate records originate from the Northern Hemisphere (NH), while such records are still relatively rare from the SH high-latitudes (see the supplementary material of Mann et al. 2009 for an overview). A better understanding of the effects of current and future climate changes on polar ecosystems and on the cryosphere therefore requires additional well-dated palaeoclimate records and geological constraints on ice-sheet dynamics from the SH high-latitudes (Mann et al. 2008). Insights into the Holocene glacial history are particularly important to understand and predict present and future ice-sheet behaviour and global sea-level rise in a warming world (Hall 2009). As discussed below, significant progress has recently been made in documenting Holocene climate and ice-sheet dynamics in Antarctica. However, several areas remain understudied, such as the sector between 0° and 60°E, including Lützow Holm Bay (Fig. 1; Mackintosh et al. 2013; Verleyen et al. 2011 in Appendix 2), where the current ice-sheet models fail to correctly reconstruct the extent of the Last Glacial Maximum (LGM) ice-sheet (Bassett et al. 2007).

Past ice-sheet dynamics and climate changes in Antarctica

After the LGM, the deglaciation of the Antarctic Peninsula Ice-Sheet (APIS), the WAIS and the EAIS, appears to be asynchronous (Anderson et al. 2002). While the APIS retreated from the continental shelf from 18 ka onwards (Heroy & Anderson 2007), the WAIS started to retreat between 15 and 12 ka (Anderson et al. 2002) and continued to retreat during the Holocene (Stone et al. 2003). The EAIS started to melt shortly before the Early-Holocene Climate Optimum (EHCO; 11.5 - 9 ka BP; Verleyen et al. 2011 in Appendix 2) in most regions, and ice recession was well underway by the Early-Holocene. Apart from the general differences between these ice-sheets, regional scale variability in ice-sheet behaviour is also becoming evident. For instance, a major retreat of the Ross Ice-Sheet (Fig. 1) only occurred around c. 7.5 ka BP (Hall & Denton 1999; 2000; Hall et al. 2004); and on Stornes in the Larsemann Hills (Fig. 1), the ice-sheet only receded by c. 4 ka BP (Hodgson et al. 2001). In most regions, ice extent was at or close to its present-day positions by the Mid-Holocene (Hall 2009), but ice advances during that period have also been suggested for certain regions, for instance in the Vestfold Hills (Fig. 1; Verleyen et al.

2005a).

The disintegration of parts of the EAIS has often been linked to the EHCO, as well as to a warming ocean and/or to eustatic sea-level rise caused by the melting of large parts of the NH ice-sheets (Mackintosh et al. 2011; Verleyen et al. 2011 in Appendix 2). The EHCO has been detected in the majority of lake (e.g. Cromer et al. 2005; Hodgson et al. 2005) and coastal marine records (e.g. Finocchiaro et al. 2005; Crosta et al. 2007) across the entire Antarctic continent, as well as in ice cores (e.g. Masson-Delmotte et al. 2010; Stenni et al. 2010). During the EHCO, lakes became seasonally ice-free and biogenic sediments accumulated in several ice-free regions, such as the Larsemann Hills (Hodgson et al. 2005), Vestfold Hills (Cromer et al. 2005), Rauer Islands (Berg et al. 2010), Amery Oasis (Wagner et al. 2004; Fink et al. 2006), and Bunger Hills (Verkulich et al. 2002) (Fig. 1). Increased primary production was likely related to increased nutrient inputs from the catchment area and a reduction in snow and ice cover (Wagner et al. 2004). Also in marine bays, biogenic sedimentation started in the Windmill Islands (Cremer et al. 2003), and sea-ice was less present compared to present-day situations, accompanied by a prolonged spring-summer growing season off Terre Adélie (Crosta et al. 2007) (Fig. 1). However, little information is available for certain regions such as Dronning Maud Land, Enderby Land, and Mac Robertson Land (Verleyen et al. 2011 in Appendix 2; Fig. 1).

The period following the EHCO in EA shows complex and less consistent patterns than those observed at Termination I. Moreover, little information is available for vast sectors along the continent, such as Dronning Maud Land, Enderby Land and Terre Adélie (Verleyen et al. 2011 in Appendix 2; Fig. 1). The available records of shallow marine and coastal terrestrial climate anomalies show large regional differences in amplitude, timing and duration. For example, a marine optimum inferred near the Larsemann Hills (Hodgson et al. 2005) and the Rauer Islands (Berg et al. 2010) appears to be out of phase with temperature trends on land, or even coincident with a cooling trend in ice cores and other terrestrial records (Stenni et al. 2010; Verleyen et al. 2011 in Appendix 2), from for example the Vestfold Hills (Gibson unpubl. res.) and Bunger Hills (Verkulich et al. 2002) (Fig. 1). This suggests that regional, rather than global forcing mechanisms, such as local deglaciation, dominated the climate in East Antarctic ice-free regions during that period (Verleyen et al. 2011 in Appendix 2). It has been suggested that these disparities might be related to differences in heat capacity between the ocean and land (Renssen et al. 2005) and the fact that marine biotic assemblages largely reflect spring-summer-autumn conditions, whereas lacustrine assemblages reflect mainly summer conditions (Hodgson & Smol 2008). This is important because orbitally-forced insolation maxima and minima differ between seasons (Bentley et al. 2009). It has however been shown that lake planktonic primary production may also occur during spring and autumn, under dim and cold conditions when lakes are ice-covered (Tanabe et al. 2008).

A Mid- to Late-Holocene warm period is inferred from a range of coastal records across the entire continent but was most pronounced in the AP (Hodgson et al. 2004b; Sterken et al. 2012). Although there are some regional differences in the timing of this warm period, it typically occurs between 4.7 and 1 ka BP (Verleyen et al. 2011 in Appendix 1). The differences in the timing of these warm events indicates a number of mechanisms and processes that have to be identified, such as regional changes in albedo

and problems associated with dating uncertainties. This warm period was evidenced by relatively wet conditions leading to increased water levels in the Larsemann Hills (Verleyen et al. 2004b) and decreased lake salinities in the Vestfold Hills (Roberts & McMinn 1996; 1999) (Fig. 1). It also coincided with local deglaciation and/or snow melt and the formation of glacial lakes on Stornes in the Larsemann Hills (Hodgson et al. 2001), and increased organic matter deposition in lakes in the Amery Oasis and the AP (Wagner et al. 2004; Sterken et al. 2012) (Fig. 1). This climate optimum has been linked to ice-sheet growth in EA as a result of increased snowfall (Goodwin 1998), but geological constraints of the dynamics of the EAIS during the Holocene are still too rare to fully test this hypothesis. Interestingly, this climate optimum is not well-resolved in ice cores (Divine et al. 2010) and marine sediment cores (Crosta et al. 2007), which generally display a Neoglacial cooling from c. 4 ka BP onwards (Divine et al. 2010). This Antarctic Mid- to Late-Holocene optimum is furthermore out of phase with climate anomalies recorded in the NH (Mayewski et al. 2004; Wanner et al. 2008).

From c. 2 ka BP onwards, most Antarctic regions experienced a Neoglacial cooling, evidenced as drier conditions in for instance the Larsemann Hills (Hodgson et al. 2005), and the Vestfold Hills (Fulford-Smith & Sikes 1996) (Fig. 1). Little or only circumstantial evidence is available for an event similar to the NH Medieval Climate Anomaly (MCA; 1050 - 650 cal. yr BP), or Little Ice Age (LIA; 500 - 100 cal. yr BP) (Goosse et al. 2012). These climate anomalies appear to be either absent from palaeoclimate records or their relative intensities and timings are inconsistent between regions (Masson-Delmotte et al. 2010).

Aims

The overall goal of this thesis is to contribute to the knowledge of regional Holocene deglaciation, relative sea-level (RSL) changes, and climate history of EA by studying lake sediment records from the ice-free regions in Lützow Holm Bay (Figs. 3 & 4). With respect to the palaeoclimate reconstruction, the underlying strategy was that by combining a number of well-dated lake sediment records, we could address the near total lack of palaeolimnological studies from the region. As such, it should be possible to identify common patterns of local or external forcing and palaeoenvironmental changes throughout the Holocene in this region and compare these with other regions in EA. A second objective was addressing the lack of independent records of regional deglaciation. Thirdly, we aimed to provide an isolation basin perspective on RSL change to supplement the existing raised beach data from the region (Miura et al. 1998). An isolation lake approach allows a more detailed reconstruction of RSL changes for several reasons. First, raised beaches only provide a minimum limit of sea-level high stands. Second, problems associated with the marine reservoir effect can be circumvented by dating lacustrine sediments that are in equilibrium with the atmosphere (e.g. Verleyen et al. 2005a). Third, problems associated with the observation that *Laternula elliptica* occurs at a range of water depths are not present when using isolation lakes. And fourth, material in beaches can be translocated, at least by the magnitude of the tidal range. By applying this approach, we would be able to identify the altitude and age of the RSL high stand; define the duration of that high stand; provide constrained age and altitude data to reconstruct Holocene RSL fall; and compare these new RSL constraints with the existing raised beach

data.

To achieve our aims, radiocarbon-dated sediment cores from a total of three glacial and four isolation lakes from Lützow Holm Bay (Figs. 4a & b) were analysed for geochemical [total carbon (TC), organic carbon (TOC), nitrogen (TN), sulphur (TS) and fossil pigments], sedimentological [(mass-specific) magnetic susceptibility (MS) and gamma ray density (GRD)] and biological proxies (diatoms). As there is increasing evidence that significant regional differences in diatom species composition and ecology exist within Antarctica, a surface diatom training dataset and transfer function were constructed to aid in palaeoecological reconstructions. To this end, 27 lakes were sampled (littoral and deep samples) and cored if possible (Figs. 4a, b & c). Lakes were chosen based on (i) their accessibility, (ii) depth (sediment cores should be undisturbed by wind and ice action) and (iii) sill height (to cover both isolation and glacial basins). Glacial lakes include Ura Ike (WO5), Higashi Ike (WO6), and Nishi Ike (WO8); isolation lakes include Yumi Ike (WO1), Ô-Ike (WO4), Mago Ike (SK1) and Kobachi Ike (SK4). For an illustration on the formation of isolation lakes the reader is referred to Fig. 6. Certain sediment cores were studied at a higher resolution based on their higher temporal resolution (i.e. high sedimentation rates) (Mago Ike in Chapter 3 and Ô-Ike in Chapter 4) or because of their potential to gain more insight into the regional RSL history (Kobachi Ike in Chapters 5 and 6). Despite the fact that Kobachi Ike is located above the currently accepted regional Holocene marine limit [20 m above sea-level (a.s.l.); Igarashi et al. 1995; Miura et al. 1998], the presence of *in situ* fossilized polychaete tubes at an altitude of 32.7 m a.s.l. prompted a detailed study of its sediments. Sediment cores from Yumi Ike, Ura Ike, Higashi Ike and Nishi Ike were principally used to support the reconstructions of changes in primary production in the Ô-Ike sediment cores (Chapter 4). Ura Ike and Higashi Ike were additionally included in the study to gain more insight into the deglaciation history of the region (Chapter 6). This thesis contributes to the BelSPO funded project “Holocene climate variability and ecosystem change in coastal East and Maritime Antarctica” (HOLANT) which aims to determine how the climate of coastal (Sub-)Antarctic regions has varied during the Holocene.

Study area

Lützow Holm Bay is located within the quadrangle 69 - 70°S and 35 - 40°E in Dronning Maud Land, EA (Fig. 1). Eight main ice-free areas and islands are present along the coast and include the Ongul Islands, Skarvsnes, Langhovde and Skallen (Fig. 3; Miura et al. 1998). The ice-sheet margin is located on the eastern side of the region. The research station, Syowa Station, is situated on the northern coast of East Ongul Island (69°00’22’’S - 39°35’24’’E), from where seismic observations (Kaminuma et al. 1998) and hourly meteorological data have been collected since 1957 (Sato & Hirasawa 2007). Although Antarctica is generally considered to be an aseismic region, some relatively large earthquakes have occurred near Syowa Station (Kaminuma et al. 1998). Meteorological data of the region indicate that the mean temperature over the past 50 years is -10.5°C, and the mean wind speed is 6.6 m/s with a predominant northeasterly direction (Sato & Hirasawa 2007). Trends in cloud cover and radiative fluxes point to a gradual increase of annual mean cloud cover at a rate of 0.01⁄year over the past 50 years (Yamanouchi & Shudou 2007).

In Lützow Holm Bay, as in many other coastal Antarctic ice-free regions, raised beaches and marine deposits are present (Hayashi & Yoshida 1994), containing mollusc fossils (mainly *L. elliptica;* Miura et al. 1998) and polychaete worm tubes. These raised beaches were formed in response to isostatic uplift after retreat of the regional ice-sheet. In Lützow Holm Bay, the raised beach deposits place the Holocene marine limit at approximately 20 m (Miura et al. 1998; Nakada et al. 2000) and they are composed of coarse sand with gravel and occasional bedrock (Hayashi & Yoshida 1994). Radiocarbon ages of *in situ* mollusc fossils (*L. elliptica*) from the region can be divided into two groups, namely Holocene fossils (< 8 ka BP) and fossils with a radiocarbon age between 48 and 33 ka BP (Fig. 5; Miura et al. 1998). However, there is some dating uncertainty about the latter, as electron spin resonance (ESR) dating indicate that they might be as old as Marine Isotope Stage (MIS) 6 - 7 (Takada et al. 2003). These radiocarbon ages indicate that prior to the LGM, the EAIS had probably retreated from the northern Sôya Coast, and more specifically from the Ongul Islands and Langhovde, and did not readvance over the region during the LGM (Fig. 5; Miura et al. 1998). By contrast, exposure ages from Skarvsnes (Fig. 5) indicate that this region only became ice-free between 10 and 6 ka BP; the last deglaciation occurred there in the Holocene (Yamane et al. 2011).

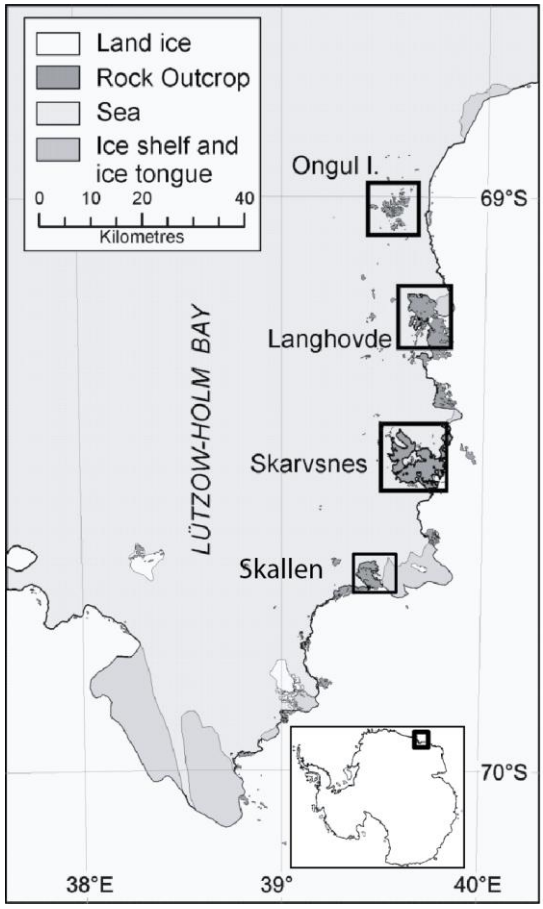

Figure 3. Map of the study sites: the Ongul Islands, Langhovde, Skarvsnes, and Skallen in Lützow Holm Bay. Inset shows the position of Lützow Holm Bay.

Near the Ongul Islands, a drowned glacial trough, the Fuji Submarine Valley, occurs under Ongul Strait, extending northwards from Langhovde Glacier (Fig. 5). The highest point is 47.6 m a.s.l. on West Ongul Island (7.8 km²) and 44 m on East Ongul Island (2.6 km²; Miura et al. 1998). Langhovde (52 km²), located 20 - 30 km south of the Ongul Islands, has the highest point of 496.5 m a.s.l. of the region and is bounded on the east by the Langhovde Glacier (Fig. 5; Miura et al. 1998). Skarvsnes (61 km²) is the largest ice-free area of Lützow Holm Bay with a peak called Skjegget, 400 m a.s.l. The Hönnor Glacier occurs to the north of Skarvsnes, and the Telen and Skallen Glaciers to the south (Fig. 5; Yamane et al. 2011). Glacial striae indicate that ice in this region flowed NW-SE (Yoshida 1983). Skallen is located 20 km southwest of the extremity

of Skarvsnes; it is a small peninsula (14.4 km²) protruding northwestward from the ice-sheet. The floating ice tongue of Skallen Glacier flows northwards, close to the eastern coast of Skallen (Miura et al. 1998). The Shirase Glacier, located to the south of Skallen (Fig. 5) is characterised by a surface velocity of up to 2700 m/year at the calving front, making it one of the fastest outlet glaciers draining the EAIS (Pattyn & Derauw 2002; Nakamura et al. 2007; Rignot et al. 2011). It does not calve directly into the sea, but ends in a 40 km long floating ice tongue (Pattyn & Derauw 2002) and its mass output at the calving front is estimated to be 12.5 Gt/year (Fujii 1981). Satellite data indicate that its flow direction is turning eastward (Nakamura et al. 2007).

Numerous lakes and ponds occur in these ice-free regions, ranging from freshwater to hypersaline (Kimura et al. 2010). The lakes originated as a result of past ice-sheet melting. Based on their origin, two main lake types can be distinguished: isolation basins and glacial lakes. Isolation lakes were once situated below sea-level and originated after isostatic uplift of the continent in response to regional ice-sheet retreat or because of tectonic processes (Bentley et al. 2005; Fig. 6). They became either hypersaline due to evaporation, or diluted because of meltwater input, varying then from freshwater to brackish-water lakes. The ionic composition is variable and depends on the amount of meltwater entering the lake from the catchment area, the amount of marine-derived ions and nutrients, and the amount of precipitation (Roberts & McMinn 1996; Verleyen et al. 2012 in Appendix 1). Glacial lakes are located above the maximum marine limit and were filled with meltwater derived from retreating glaciers or the ice-sheet. They thus contain generally freshwater and are (ultra-)oligotrophic, unless they experienced a long-term negative moisture balance and/or a relatively high marine-derived nutrient or ion input due to regular visits by sea birds or mammals (Hodgson et al. 2010; Verleyen et al. 2012 in Appendix 1). During the austral winter, the surfaces of freshwater and saline lakes in the region are covered by up to 1.7 m and less than 1 m of ice respectively, which yearly melts during the 2 - 3 months ice-free period (Kimura et al. 2010). Some of the lakes that were formerly connected to the sea are meromictic, such as Suribati Ike in Skarvsnes (Kimura et al. 2010), but the majority are holomictic, being mixed throughout the summer ice-free period (Verleyen et al. 2012 in Appendix 1). However, a meltwater surface layer may occur during and just after melting of the lake-ice and temporarily prevent full mixing as has likely been observed in Kobachi Ike (Chapter 5; Kimura et al. 2010).

All cored lakes were at the time of sampling fed by snow banks from the catchment area. However, no active outflow streams were noted during field work except in the case of WO2 which received an outflow stream draining from Yumi Ike. Kobachi Ike was partly ice-covered with redistributed ice because of wind action. All study lakes are oligotrophic (Verleyen et al. 2012 in Appendix 1).

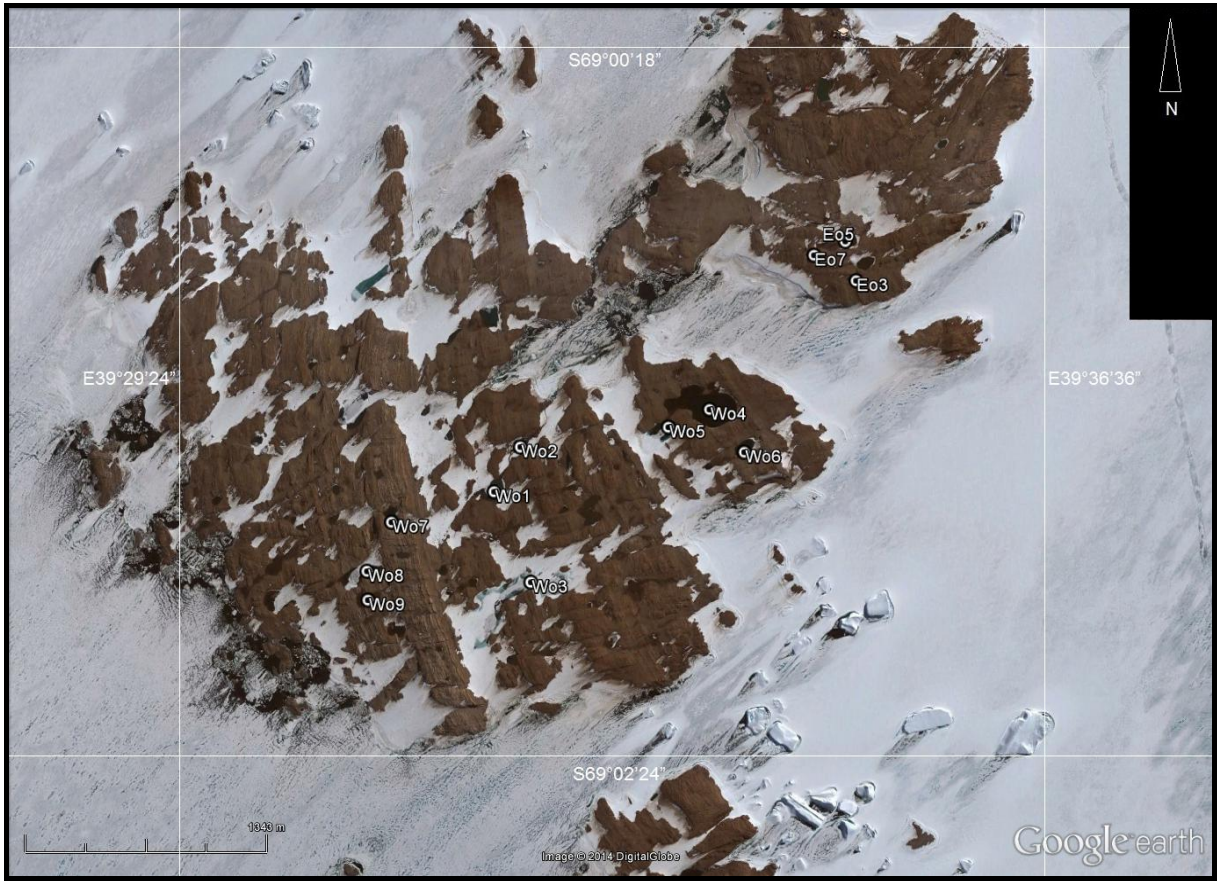

Figure 4a. Aerial photo of the Ongul Islands indicating the study lakes: Yumi Ike (WO1), Ô-Ike (WO4), Ura Ike (WO5), Higashi Ike (WO6), and Nishi Ike (WO8) on West Ongul Island. Lakes used for the transfer function are indicated: Wo codes (West Ongul Island), and Eo codes (East Ongul Island).

Figure 4b. Map of Skarvsnes indicating the study lakes: Mago Ike (SK1) and Kobachi Ike (SK4). Lakes used for the transfer function are indicated with Sk codes.

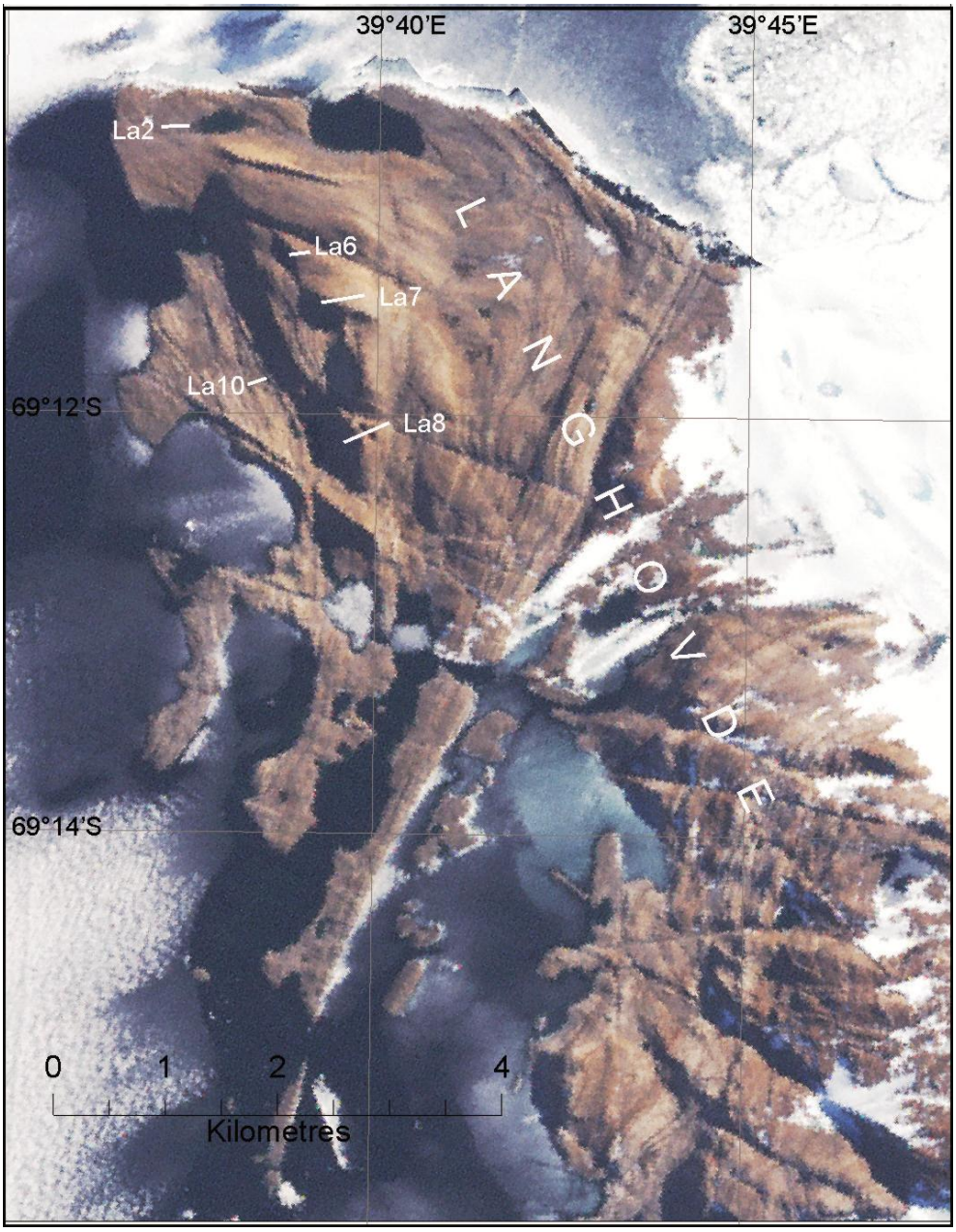

Figure 4c. Map of the Langhovde. Lakes used for the transfer function are indicated with La codes.

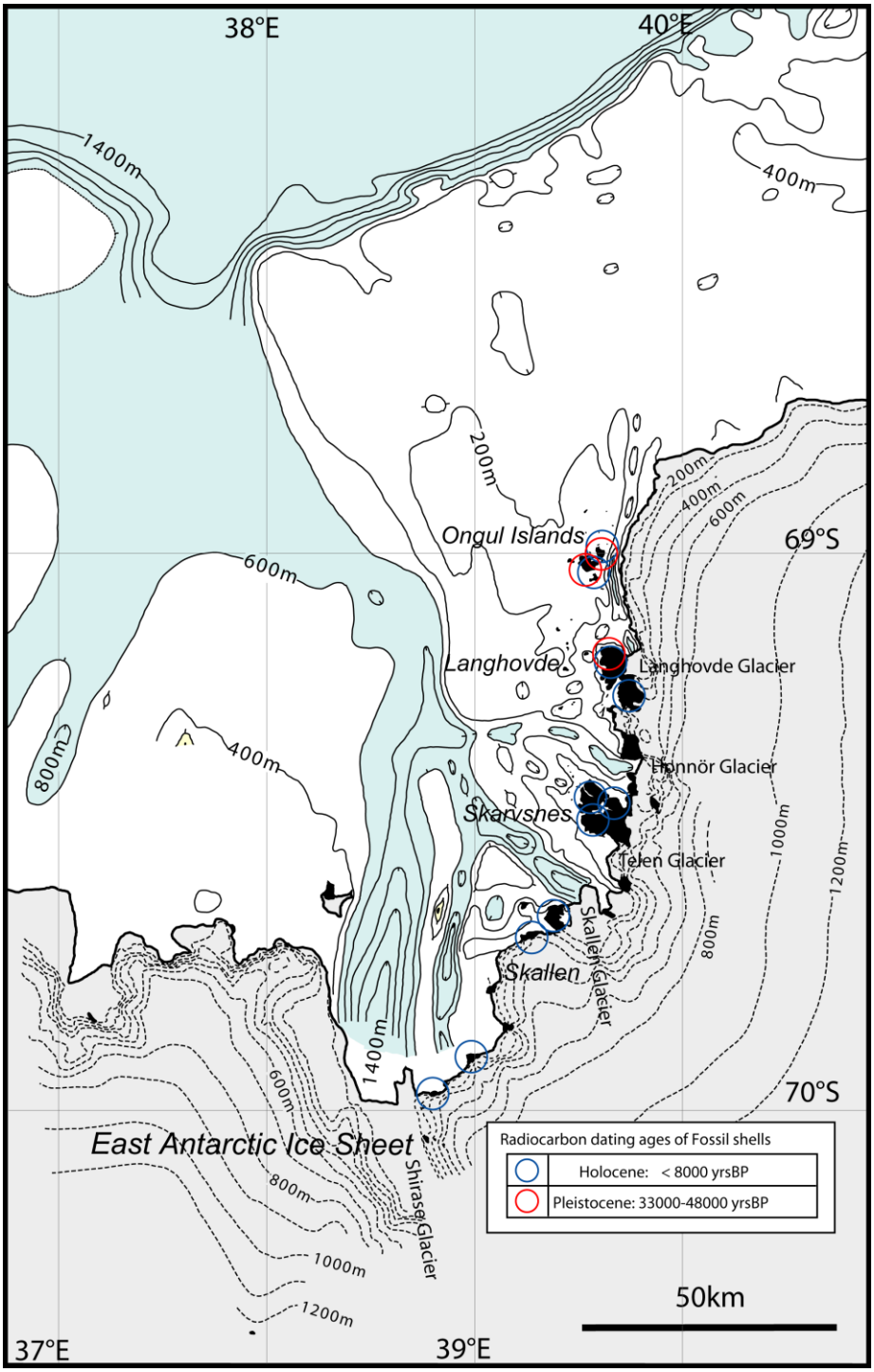

Figure 5. Map adapted from Miura et al. (in prep.), indicating the location of fossil shells from Holocene (blue) and Pleistocene (red) age. Regional glaciers are also indicated.

Research methodologies

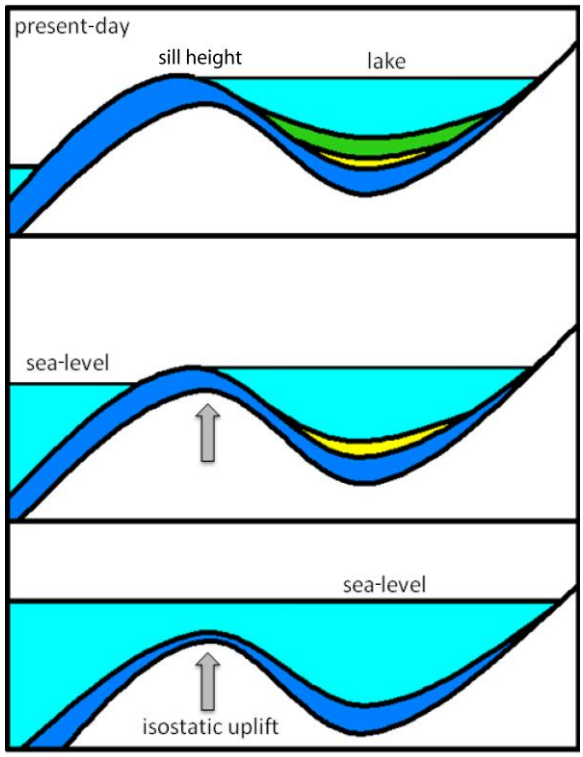

Figure 6. Schematic presentation illustrating the formation of an isolation basin due to isostatic uplift after retreat of the regional ice-sheet. Note that these basins can also be formed due to tectonic processes (Bentley et al. 2005). Sediment colours: blue = marine diatoms, yellow = brackish water diatoms, green = lacustrine diatoms.

Ice cores from the continental Antarctic plateau often do not allow to fully resolve the more subtle Holocene climate anomalies (e.g. Mayewski et al. 2004) due to small differences in isotopic ratios in the interior of Antarctica in response to temperature variability. Coastal ice cores, which are often more sensitive to small-scale climate variability, are relatively rare because the ice-sheet in coastal regions is typically too dynamic, which prevents the establishment of reliable reconstructions and chronologies (Hodgson & Smol 2008). Valuable alternatives are deposits of marine birds and mammals as bio-indicators of ecosystem and environmental changes (e.g. Sun et al. 2004) and shallow marine and lake sediments (e.g. Sterken et al. 2012). Records of penguin populations and abandoned colonies (Emslie et al. 1998; Sun et al. 2000) can provide information about the impact of climate changes on penguin distributions, whereas seal populations can be used as an indicator of changes in the Antarctic marine environment (Sun et al. 2004). Shallow marine and lake sediments can contain high temporal resolution records providing information regarding climatic effects on lake ecosystems such as the duration of ice cover (e.g. Verleyen et al. 2004a), primary production (e.g. Sterken et al. 2012), moisture balance (e.g. Hodgson et al. 2005) and community structure (e.g. Verleyen et al. 2004b; Bissett et al. 2005; Hodgson et al. 2006; 2009a). In Antarctica, lake primary production is influenced by the surface air temperature (Doran et al. 2002; Quayle et al. 2002). Increased surface air temperatures lead to increased water temperatures and a subsequent increase in the number of ice-free days. In turn this stimulates primary production (Quayle et al 2002). The draining of exposed catchment areas as well as the development of soils and in-lake biotic communities might also increase nutrient availability in these lakes (Quayle et al. 2002). The development of soils is a phenomenon of Maritime Antarctica and the AP, whereas this is rather limited in the Antarctic continent. Lakes and particularly closed basins furthermore record quantitative changes in

the moisture balance, which can be reconstructed using diatom-based transfer functions (e.g. Verleyen et al. 2003). In East Antarctic lakes, lake water specific conductance results from the balance between direct precipitation in the form of snow and inputs of meltwater from multi-year snow banks and glaciers, and outputs from outflow, evaporation and ablation. The latter are affected by temperature, atmospheric humidity and wind strength (Verleyen et al. 2012 in Appendix 1). The moisture balance in lakes is furthermore influenced by the amount of snow, which is blown from the interior of the continent to the coastal regions by katabatic winds.

Proxy data for lake primary production, such as organic matter accumulation and fossil pigment concentrations have been shown to be sensitive tools for reconstructing past temperature variability and have provided detailed records of the MCA and LIA in the NH in for instance the Canadian Arctic (MacDonald et al. 2009) and Iceland (Geirsdóttir et al. 2009). In Antarctica, these proxies enabled the detection of millennial-scale Holocene warm periods (Verleyen et al. 2011 in Appendix 2; Sterken et al. 2012) and short-term temperature excursions (Cremer et al. 2007). They are furthermore useful for delineating marine-lacustrine transitions, as the carbon content is generally higher in lake sediments because of carbon fixation by benthic microbial-mats.

Potential limitations of these proxies are differential preservation of fossil pigments and diatoms, and the lack of modern analogues in the diatom-based inference models. With respect to pigment preservation, a comparison between diatom biovolume and diatom marker pigments in sediment cores from Antarctic isolation basins has revealed that both proxies are readily preserved in marine sediments, while some degradation might occur in lacustrine environments (Verleyen et al. 2004c). This should be taken into account when interpreting diatom and pigment stratigraphies from these records. In general however, pigment degradation is expected to be of relatively minor importance due to the relatively rapid burial of autotrophic organisms in benthic microbial mats (Verleyen et al. 2005b). In addition, pigments produced by benthic autotrophs are not exposed to factors occurring in the water column that affect pigment degradation. This is important, as the most rapid degradation occurs in the water column due to grazing and during sinking, when exposed to high irradiance, oxygen concentrations and temperatures (Louda et al. 2002). Hence, a lower pigment concentration might not necessarily imply a lower primary production. Alternatively, it might point to a shift from benthic primary production to one dominated by planktonic autotrophs. The latter might be important, for example during the dim conditions in spring and autumn when lake ice starts to form (Tanabe et al. 2008), or during prolonged ice-free conditions leading to the establishment of a planktonic autotrophic community (Quayle et al. 2002). The robustness of environmental reconstructions using transfer functions based on diatom community structure depends on preservation and the presence of modern analogue communities. Dissolution of diatom frustules is generally of minor importance in freshwater lakes with a circum-neutral pH (Ryves et al. 2006). By contrast, valve dissolution is sometimes high in saline and alkaline lakes (Ryves et al. 2009). For example, a multivariate analysis of factors influencing diatom dissolution revealed that salinity is a significant predictor in Greenland lakes (Ryves et al. 2006). Weakly silicified frustules are less degradation-resistant compared to heavily silicified diatom valves and resting spores (Crosta et al. 1997; Ryves et al. 2001; 2009). Losses of

valves due to dissolution can thus lead to a bias in the composition towards the more robust taxa, and lead also to a reduction in the number of valves accumulating in the sediments (Battarbee et al. 2001). Species-specific preservation is seen as the most serious concern; however, differences between living and fossil assemblages can also include resuspension and reworking of older sediments by wind-action (Batterbee et al. 2001). These possible limitations for the use of diatoms as a proxy evidently also apply to diatom-based transfer functions (Ryves et al. 2009). Limitations for the use of transfer functions can furthermore be the lack of modern analogues, both modern analogues of diatom species and of lake types (freshwater - brackish - saline; Birks 1998). Generally, a consistent and detailed taxonomy is also a prerequisite for using these proxies (Birks 1998).

Past primary production in lake sediments can be quantified using several proxies, which enable the reconstruction of palaeoenvironmental and palaeoclimatic changes. These proxies include the total organic matter content (Birks et al. 2004), the total carotenoid and chlorophyll content (Hodgson et al. 2005) and total diatom concentration when one is interested to quantify the importance of this part of the autotrophic community. While the total organic matter content is a widely used proxy in palaeolimnological studies, some problems may remain with interpretation of these data. First, during sample preparation freeze-drying is preferred over air-drying or oven-drying as the latter techniques may result in the loss of volatile, organic compounds (Meyers & Teranes 2001). Second, the use of sediment standards with known composition is important to test the accuracy of the method. For example, larger errors were found for TOC analysis compared to TC and TN analysis (King et al. 1998), indicating differences in analytical techniques and thus requiring care in interpreting these results. Also the errors on both the analysis by the Organic Elemental Analyzer and on the weighing steps need to be considered, especially if samples only contain very small (organic) carbon and nitrogen concentrations. When TC is used to infer lake productivity, there may be problems in those cases where carbonate accumulation occurs. In two of the studied lakes, TC contents were very low and were not considered as a proxy for changes in lake productivity. In those lakes with higher TC, analyses of TC and TOC (based on acidification of filtered and homogenised samples with 5% HCl,), indicated that only Kobachi Ike sediments contained significant amounts of total inorganic carbon (TIC). Therefore, throughout this thesis and where possible, TC was used as a secondary indicator of changes in primary production, which was primarily assessed using pigment-based indicators (i.e., fluxes of total chlorophylls, and carotenoids). In Kobachi Ike, TOC content was additionally measured, because the TIC content appeared to be high.

The concentration of magnetisable minerals can be studied by measuring the MS of sediments, which is a non-destructive analysis. MS can be measured continuously on whole or split core sections, and discretely on individual subsamples. Continuous measurements are performed using core loggers. MS varies with the content of iron-bearing minerals. As these are common in nearly all rocks and their weathering products, MS can be regarded as a proxy for the minerogenic contribution to the sediment (Zolitska et al. 2001). Moreover, environmental changes might result in different erosional, weathering, transport and deposition conditions, resulting in differences in the sediment composition and hence MS (Nowaczyk 2001). In Antarctica for example, changes in the

amount of meltwater input can lead to differences in the minerogenic input, which in turn is expected to affect the MS of the sediments. Moreover, in combination with other proxies, differences in MS between marine and lacustrine sediments in Antarctic isolation lakes, allows to identify when the lakes became isolated from the ocean (e.g. Watcham et al. 2011; Roberts et al. 2011). MS can also be used to correlate different sediment cores from the same location/composites from different sites. Volume-specific MS can be converted to mass-specific MS, which reflects the sediment magnetic composition more accurately. This is because environmental studies often measure materials with widely different bulk densities, which may account for differences in volume-specific MS (Dearing 1994). The conversion can be done by dividing the MS measured with the core logger by the dry bulk density (DBD). GRD can be measured at the same time as volume-specific MS and is converted to DBD using a dry weight percentage of each sample at a certain depth. GRD measurements are also non-destructive. The principle of the method relies on attenuation of gamma rays as they pass through the sediments. GRD is used as a parameter for physical characterisation of sediment cores, which gives information on lithological changes and enables to correlate different cores from the same site. Another important application of the converted DBD from the wet bulk density is as a parameter to calculate accumulation rates (Zolitschka et al. 2001). The mass accumulation rate (MAR) can be calculated as the multiplication of the DBD (g/cm^3) and the sedimentation rate (SR; cm/yr) based on the constructed age-depth model. Multiplying the MAR with the concentration by weight at a certain depth, gives the flux of a proxy. This approach prevents the influence of variable SRs and large changes in the proportion of organic, siliciclastic and biogenic components (Street-Perrot et al. 2007).

As the backbone of palaeoenvironmental studies is formed by age-depth models, modelling software should enable exploration of different assumptions, such as model type, hiatuses, age offsets, outliers and extrapolation (Blaauw 2010). Calibration of ^{14}C dates often results in widened, asymmetrical and multi-peaked calendar age uncertainties (Telford et al. 2004), preventing the use of classical interpolation techniques which assume normally distributed errors (Blaauw 2010). The entire calibrated distribution of the dates is taken into account using bootstrap or Monte Carlo sampling when modelling the accumulation of a sequence through time. As the accuracy of ^{14}C dates should not be overestimated (i.e., every time an analytical ^{14}C measurement is repeated under identical conditions and on an identical sample, a slightly different result is obtained) (Scott et al. 2007), the 'best' age-depth estimate derived from the model is based on all dating information and contains an interpretation of the likely accumulation history of the site (Blaauw 2010). CLAM uses classical age-depth modelling and allows using common types of age-depth models (e.g. linear interpolation, linear or higher order polynomial regression, and cubic, smoothed or locally weighted splines); outliers and hiatuses can be identified before modelling. The goodness-of-fit ('the lower the value, the better'), based on the product of the probabilities of the modelled ages of the dated depths, is used as an indicator for the quality of the model. Confidence intervals for the undated levels are calculated using the Monte Carlo approach. To low-resolution dated sites, Bayesian age-depth modelling may not add much additional value (Blaauw 2010), however, it should be considered as a next step in the age-depth modelling process (Blockley et al. 2007) and should be preferred in the case of more complicated sedimentation conditions. The

Bayesian BACON software aims to produce more environmentally realistic age-depth models by reconstructing the underlying processes (i.e., the accumulation/sedimentation process), instead of by fitting a curve through the dated points as classical modelling (CLAM) does (Blaauw & Christen 2011).

Outline

In **Chapter 2**, type material of *Luticola* species (and other diatom species originally described by West & West) has been revised, which led to the description of a new species, *Luticola pseudomurrayi* Van de Vijver et Tavernier sp. nov., which was previously usually misidentified as *Navicula murrayi*. A diatom taxonomy revision was necessary to improve the quality of the transfer function (Chapter 3) and will aid in future biogeographical studies (Verleyen et al. in prep.).

In **Chapter 3**, a regional diatom-based transfer function for inferring specific conductance has been constructed using samples from 27 lakes from East and West Ongul Island, Langhovde and Skarvsnes (Figs. 4a, b & c). Late-Holocene environmental changes were reconstructed by applying this transfer function to the lacustrine sediments from Mago Ike (Fig. 4b; Skarvsnes), while interpretation of changes in marine sediments from this isolation basin were based on published information on diatom ecology. Interpretation of these diatom-based data was combined with analyses of fossil pigments, TC, TN, MS, and GRD.

Chapter 4 discusses the Holocene climate and environmental changes on West Ongul Island and the time of deglaciation of the region, based on a multi-proxy analysis (diatoms, fossil pigments, TC, TN, mass-specific MS, and GRD) of sediments from the isolation lakes Ô-Ike (at a higher resolution), and Yumi Ike and the glacial basins Nishi Ike, Ura Ike and Higashi Ike (Fig. 3).

In **Chapter 5**, the Holocene evolution of the brackish-water isolation basin Kobachi Ike (Fig. 4b; Skarvsnes) is discussed. Information about the deglaciation history of Skarvsnes is obtained, as well as information about environmental and RSL changes. Besides diatoms, fossil pigments, TC, TN, mass-specific MS, and GRD, TOC, TIC, and TS are also used as proxies.

Chapter 6 deals with RSL changes in Lützow Holm Bay during the Holocene. For this purpose, an existing RSL curve based on marine terraces from the region (Nakada et al. 2000) has been extended and improved by adding data from both isolation (Mago Ike, Kobachi Ike, Yumi Ike and Ô-Ike) and glacial lakes (Ura Ike, Higashi Ike, and Nishi Ike) (Figs. 4a & b) as well as by adding published data from isolation lakes from Skallen (Fig. 3; Takano et al. 2012).

Appendix 1 contains the limnological data of 27 lakes in Lützow Holm Bay on which the transfer function (Chapter 3) is based.

Appendix 2 is a review paper regarding post-glacial regional climate variability along the East Antarctic coast.

References

Alley RB, Clark PU, Huybrechts P, Joughin I (2005) Ice-sheet and sea-level changes. *Science,* **310**: 456-460.

Anderson JB, Shipp SS, Lowe AL, Wellner JS, Mosola AB (2002) The Antarctic Ice Sheet during the Last Glacial Maximum and its subsequent retreat history: a review. *Quaternary Science Reviews*, **21**: 49-70.

Bassett SE, Milne GA, Bentley MJ, Huybrechts P (2007) Modelling Antarctic sea-level data to explore the possibility of a dominant Antarctic contribution to meltwater pulse IA. *Quaternary Science Revieuws,* **26**: 2113-2127.

Battarbee RW, Jones VJ, Flower RJ, Cameron NG, Bennion H, Carvalho L, Juggins S (2001) Diatoms. *In:* Smol JP, Birks HJ, Last WM (Eds.) Tracking environmental change using lake sediments. Volume 3: Terrestrial, algal, and siliceous indicators. Kluwer Academic publishers, Dordrecht, The Netherlands. pp 155-202.

Bentley MJ, Hodgson DA, Smith JA, Cox NJ (2005) Relative sea level curves for the South Shetland Islands and Marguerite Bay, Antarctic Peninsula. *Quaternary Science Reviews,* **24**: 1203 – 1216.

Bentley MJ, Hodgson DA, Smith JA, Cofaigh CÓ, Domack EW, Larter RD, Roberts SJ, Brachfeld S, Leventer A, Hjort C, Hillenbrand C-D, Evans J (2009) Mechanisms of Holocene palaeoenvironmental change in the Antarctic Peninsula region. *The Holocene,* **19(1)**: 51-69.

Berg S, Wagner B, Cremer H, Leng MJ, Melles M (2010) Late Quaternary environmental and climate history of Rauer Group, East Antarctica. *Palaeogeography, Palaeoclimatology, Palaeoecology,* **297**: 201-213.

Berkman PA, Andrews JT, Bjorck S, Colhoun EA, Emslie SD, Goodwin ID, Hall BL, Hart CP, Hirakawa K, Igarashi A, Ingolfsson O, Lopez-Martinez J, Lyons WB, Mabin MCG, Quilty PG, Taviani M, Yoshida Y (1998) Circum-Antarctic coastal environmental shifts during the Late Quaternary reflected by emerged marine deposits. *Antarctic Science,* **10(3)**: 345-362.

Birks HJB (1998) Numerical tools in palaeolimnology - progress, potentialities, and problems. *Journal of Paleolimnology,* **20**: 307-332.

Birks HJB, Monteith DT, Rose NL, Jones VJ, Peglar SM (2004) Recent environmental change and atmospheric contamination on Svalbard as recorded in lake sediments - modern limnology, vegetation, and pollen deposition. *Journal of Paleolimnology*, **31**: 411-431.

Bissett A, Gibson JAE, Jarman SN, Swadling KM, Cromer L (2005) Isolation, amplification, and identification of ancient copepod DNA from lake sediments. *Limnology and Oceanography: Methods,* **3**: 533-542.

Blaauw M (2010) Methods and code for 'classical' age-modelling of radiocarbon sequences. *Quat Geochr,* **5**: 512-518.

Blaauw M, and Christen JA (2011) Flexible paleoclimate age-depth models using an autoregressive gamma process. *Bayesian Analysis,* **6(3):** 457-474.

Blockley SPE, Blaauw M, Bronk Ramsey C, van der Plicht J (2007) Assessing uncertainties in age modelling sedimentary records in the Lateglacial and Early Holocene. *Quaternary Science Reviews,* **26:** 1915-1926.

Cook AJ, Fox AJ, Vaughan DG, Ferrigno JG (2005) Retreating glacier fronts on the Antarctic Peninsula over the past half-century. *Science,* **308**: 541-544.

Corner GD, Yevzerov VY, Kolka VV, Moller JJ (1999) Isolation basin stratigraphy and Holocene relative sea-level change at the Norwegian-Russian border north of Nikel, northwest Russia. *Boreas,* **28**: 146-166.

Corner GD, Kolka VV, Yevzerov VY, Moller JJ (2001) Postglacial relative sea-level change and stratigraphy of raised coastal basins on Kola Peninsula, northwest Russia. *Global and Planetary Change,* **31**: 155-177.

Cremer H, Gore D, Melles M, Roberts D (2003) Palaeoclimatic significance of late Quaternary diatom assemblages from southern Windmill Islands, East Antarctica. *Palaeogeography, Palaeoclimatology, Palaeoecology,* **195**: 261-280.

Cremer H, Heire O, Wagner B, Wagner-Cremer F (2007) Abrupt climate warming in East Antarctica during the early Holocene. *Quat Sci Rev*, **26**: 2012-2018.

Cromer L, Gibson JAE, Swadling KM, Ritz DA (2005) Faunal microfossils: indicators of Holocene ecological change in a saline Antarctica lake. *Palaeogeography, Palaeoclimatology, Palaeoecology,* **221**: 83-97.

Crosta X, Pichon J-J, Labracherie M (1997) Distribution of Chaetoceros resting spores in modern peri-Antarctic sediments. *Marine Micropaleontology,* **29**: 283 – 299.

Crosta X, Debret M, Denis D, Courty MA, Ther O (2007) Holocene long- and short-term climate changes off Adelie Land, East Antarctica. *Geochemistry Geophysics Geosystems,* **8(11)**: Q11009, doi:10.1029/2007GC001718.

Dearing J (1994) Environmental magnetic susceptibility. Using the Bartington MS2 system. Kenilworth, Chi Publ.

Denton GH, Anderson RF, Toggweiler JR, Edwards RL, Schaefer JM, Putnam AE (2010) The last glacial termination. *Science,* **328**: 1652-1656.

Divine DV, Koç N, Isaksson E, Nielsen S, Crosta X, Godtliebsen (2010) Holocene Antarctic climate variability from ice and marine sediment cores: Insights on ocean-atmosphere interaction. *Quaternary Science Reviews,* **29**: 303-312.

Doran PT, Priscu JC, Lyons WB, Walsh JE, Fountain AG, McKnight DM, Moorhead DL, Virginia RA, Wall DH, Clow GD, Fritsen CH, McKay CP, Parsons AN (2002) Antarctic climate cooling and terrestrial ecosystem response. *Nature,* **415:** 517-520.

Douglas MSV, Ludlam S, Feeney S (1996) Changes in diatom assemblages in Lake C2 (Ellesmere Island, Arctic Canada): response to basin isolation from the sea and to other environmental changes. *Journal of Paleolimnology,* **16**: 217-226.

Emslie SD, Fraser WR, Smith RC, Walker W (1998) Abandoned penguin colonies and environmental change in the Palmer Station areas, Anvers Island, Antarctic Peninsula. *Antarctic Science,* **3**: 257-268.

Fiedel SJ (2011) The mysterious onset of the Younger Dryas. *Quaternary International,* **242**: 262-266.

Fink D, McKelvey B, Hambrey MJ, Fabel D, Brown R (2006) Pleistocene deglaciation chronology of the Amery Oasis and Radok Lake, northern Prince Charles Mountains, Antarctica. *Earth and Planetary Science Letters,* **243**: 229-243.

Finocchiaro F, Langone L, Colizza E, Fontolan G, Giglio F, Tuzzi E (2005) Records of early Holocene warming in a laminated sediment core from Cape Hallett Bay (Northern Victoria Land, Antarctica). *Glob. Planet. Ch.,* **45**: 193-206.

Foldvik A, Gammelsrod T, Osterhus S, Fahrbach E, Rohardt G, Schröder M, Nicholls KW, Padman L, Woodgate RA (2004) Ice shelf water overflow and bottom water formation in the southern Weddell Sea. *Journal of Geophysical Research*, **109**: doi:10.1029/2003JC002008.

Fujii Y (1981) Aerophotographic interpretation of surface features and estimation of ice discharges at the outlet of the Shirase drainage basin, Antarctica. *Antarct. Rec.,* **72**: 1-15.

Fulford-Smith SP, and Sikes EL (1996) The evolution of Ace Lake, Antarctica, determined from sedimentary diatom assemblages. *Palaeogeography, Palaeoclimatology, Palaeoecology,* **124**: 73-86.

Geirsdóttir Á, Miller GH, Thordarson T, Ólafsdóttir KB (2009) A 2000 year record of climate variations reconstructed from Haukadalsvatn, West Iceland. *J Paleolimnol*, **41**: 95-115.

Goodwin ID (1998) Did changes in Antarctic ice volume influence Late Holocene sea-level lowering? *Quaternary Science Reviews,* **17**: 319-332.

Goosse H, Braida M, Crosta X, Mairesse A, Masson-Delmotte V, Mathiot P, Neukom R, Oerter H, Philippon G, Renssen H, Stenni B, van Ommen T, Verleyen E (2012) Antarctic temperature changes during the last millennium: evaluation of simulations and reconstructions. *Quaternary Science Reviews,* **55**: 75-90.

Hall BL (2009) Holocene glacial history of Antarctica and the sub-Antarctic islands. *Quaternary Science Reviews,* **28**: 2213-2230.

Hall B, and Denton G (1999) New relative sea-level curves for the southern Scott Coast, Antarctica: evidence for Holocene deglaciation of the western Ross Sea. *J. Quat. Sci.,* **14**: 641-650.

Hall B, and Denton G (2000) Extent and chronology of the Ross Sea Ice Sheet and the Wilson Piedmont Glacier along the Scott Coast at and since the Last Glacial Maximum. *Geogr. Ser. Phys. Geogr.,* **82A**: 337-363.

Hall B, Baroni C, Denton G (2004) Holocene relative sea-level history of the southern Victoria Land Coast, Antarctica. *Global Planet. Change,* **42**: 241-263.

Hayashi M, and Yoshida Y (1994) Holocene raised beaches in the Lützow-Holm Bay region, East Antarctica. *Mem. Natl Inst. Polar res., Spec. Issue,* **50**: 49-84.

Heroy DC, and Anderson JB (2007) Radiocarbon constraints on Antarctic Peninsula Ice Sheet retreat following the Last Glacial Maximum (LGM) *Quaternary Science Reviews,* **26**: 3286-3297.

Hodgson DA, Noon PE, Vyverman W, Bryant CL, Gore DB, Appleby P, Gilmour M, Verleyen E, Sabbe K, Jones VJ, Ellis-Evans JC, Wood PB (2001) Were the Larsemann Hills ice-free through the Last Glacial Maxium? *Antarctic Science,* **13(4)**: 440-454.

Hodgson DA, Doran PT, Roberts D, McMinn A (2004) Paleolimnological studies from the Antarctic and Subantarctic islands. *In*: Pienitz R, Douglas MSV, Smol JP (Eds.) Long-term environmental changes in Arctic and Antarctic lakes. Dordrecht, The Netherlands. pp. 419-474.

Hodgson DA, Verleyen E, Sabbe K, Squier AH, Keely BJ, Leng MJ, Saunders KM, Vyverman W (2005) Late Quaternary climate-driven environmental change in the Larsemann Hills, East Antarctica, multi-proxy evidence from a lake sediment core. *Quaternary Research,* **64**: 83-99.

Hodgson DA, Roberts D, McMinn A, Verleyen E, Terry B, Corbett C, Vyverman W (2006) Recent rapid salinity rise in three East Antarctic lakes. *Journal of Paleolimnology,* **36**: 385-406.

Hodgson DA, and Smol JP (2008) High latitude palaeolimnology. *In*: Vincent WF, Laybourn-Parry J (Eds.) Polar Lakes and Rivers - Arctic and Antarctic Aquatic Ecosystems. Oxford University Press, Oxford, UK. pp 43-64.

Hodgson DA, Roberts SJ, Bentley MJ, Carmichael EL, Smith JA, Verleyen E, Vyverman W, Geissler P, Leng MJ, Sanderson DCW (2009a) Exploring former subglacial Hodgson Lake, Antarctica. Paper II: palaeolimnology. *Quaternary Science Reviews,* **28(23-24)**: 2310-2325.

Hodgson DA, Verleyen E, Vyverman W, Sabbe K, Leng MJ, Pickering MD, Keely BJ (2009b) A geological constraint on relative sea level in Marine Isotope Stage 3 in the Larsemann Hills, Lambert Glacier region, East Antarctica (31366 – 33228 cal yr BP). *Quaternary Science Reviews,* **28(25-26)**: 2689-2696.

Hodgson DA, Convey P, Verleyen E, Vyverman W, McInnes SJ, Sands CJ, Fernández-Carazo R, Wilmotte A, De Wever A, Peeters K, Tavernier I, Willems A (2010) The limnology and biology of the Dufek Massif, Transantarctic Mountains 82° South. *Polar Science,* **4(2)**: 197-214.

Hu A, Meehl GA, Han W, Yin J (2011) Effect of the potential melting of the Greenland Ice Sheet on the Meridional Overturning Circulation and global climate in the future. *Deep-Sea Research II,* **58**: 1914-1926.

Kaminuma K, Kanao M, Kubo A (1998) Local earthquake activity around Syowa Station, Antarctica. *Polar Geosci.,* **11**: 23-31.

Kimura S, Ban S, Imura S, Kudoh S, Matsuzaki M (2010) Limnological characteristics of vertical structure in the lakes of Syowa Oasis, East Antarctica. *Polar Science,* **3**: 262-271.

King P, Kennedy H, Newton PP, Jickells TD, Brand T, Calvert S, Cauwet G, Etcheber H, Head B, Khripounoff A, Manighetti B, Miquel JC (1998) Analysis of total and organic carbon and total nitrogen in settling oceanic particles and a marine sediment: an interlaboratory comparison. *Marine Chemistry,* **60**: 203-216.

Louda JW, Liu L, Baker EW (2002) Senescence- and death-related alteration of chlorophylls and carotenoids in marine phytoplankton. *Organic Geochemistry,* **33(12)**: 1635-1653.

MacDonald GM, Porinchu DF, Rolland N, Kremenetsky KV, Kaufman DS (2009) Paleolimnological evidence of the response of the central Canadian treeline zone to radiative forcing and hemispheric patterns of temperature change over the past 2000 years. *J Paleolimnol*, **41**: 129-141.

Mackintosh A, Golledge N, Domack E, Dunbar R, Leventer A, White D, Pollard D, DeConto R, Fink D, Zwartz D, Gore D, Lavoie C (2011) Retreat of the East Antarctic ice sheet during the last glacial termination. *Nature Geoscience,* **4**: 195-202.

Mackintosh AN, Verleyen E, O'Brien PE, White DA, Selwyn Jones R, McKay R, Bunbar R, Gore DB, Fink D, Post AL, Miura H, Leventer A, Goodwin I, Hodgson DA, Lilly K, Crosta X, Golledge NR, Wagner B, Berg S, van Ommen T, Zwartz D, Roberts SJ, Vyverman W, Masse G (2013) Retreat history of the East Antarctic Ice Sheet since the Last Glacial Maximum. *Quaternary Science Reviews*, 1-21.

Mann ME, Zhang Z, Hughes MK, Bradley RS, Miller SK, Rutherford S, Ni F (2008) Proxy-based reconstructions of hemispheric and global surface temperature variations over the past two millennia. *PNAS,* **105(36)**: 13252-13257.

Mann ME, Zhang ZH, Rutherford S, Bradley RS, Hughes MK, Shindell D, Ammann C, Faluvegi G, Ni FB (2009) Global signatures and dynamical origins of the Little Ice Age and Medieval Climate Anomaly. *Science*, **326**: 1256-1260.

Masson-Delmotte V, Stenni B, Pol K, Braconnot P, Cattani O, Falourd S, Kageyama M, Jouzel J, Landais A, Minster B, Barnola JM, Chappellaz J, Krinner G, Johnsen S, Rothlisberger R, Hansen J, Mikolajewicz U, Otto-Bliesner B (2010) EPICA Dome C record of glacial and interglacial intensities. *Quat Sci Rev*, **29**: 113-128.

Mayewski PA, Rohling EE, Stager JC, Karlén W, Maasch KA, Meeker LD, Meyerson EA, Gasse F, van Kreveld S, K, Lee-Thorp J, Rosqvist G, Rack F, Staubwasser M, Schneider RR, Steig EJ (2004) Holocene climate variability. *Quaternary Research,* **62**: 243-255.

Meyers PA, and Teranes JL (2001) Sediment organic matter. *In:* Last WM, and Smol JP (Eds.) Tracking environmental change using lake sediment. Volume 2: Physical and geochemical methods. Kluwer Academic Publishers, Dordrecht, The Netherlands. pp 239-270.

Miura H, Maemoku H, Igarashi A, Moriwaki K (1998) Late Quaternary raised beach deposits and radiocarbon dates of marine fossils around Lützow Holm Bay. *Special map series of National Institute of Polar Research,* **6:** pp. 46.

Nakada M, Kimura R, Okuno J, Moriwaki W, Miura H, Maemoku H (2000) Late Pleistocene and Holocene melting history of the Antarctic ice sheet derived from sea-level variations. *Marine Geology,* **167**: 85-103.

Nakamura K, Doi K, Shibuya K (2007) Why is Shirase Glacier turning its flow direction eastward? *Polar Science,* **1**: 63-71.

Nowaczyk NR (2001) Logging of magnetic susceptibility. *In:* Last WM, and Smol JP. Tracking environmental change using lake sediments. Volume 1: Basin analysis, coring, and chronological techniques. Kluwer Academic Publishers, Dordrecht, The Netherlands. pp 155-170.

Pattyn F, and Derauw D (2002) Ice-dynamic conditions of Shirase Glacier, Antarctica, inferred from ERS SAR interferometry. *Journal of Glaciology,* **48(163)**: 559-565.

Perlwitz J, Pawson S, Fogt R, Nielsen JE, Neff W (2008) The impact of stratospheric ozone hole recovery on Antarctic climate. *Geophysical Research Letters,* **35**: L08714, doi:10.1029/2008GL033317.

Pfeffer WT, Harper JT, O'Neill S (2008) Kinematic constrains on glacier contributions during the 21st-century sea-level rise. *Science,* **321**: 1340-1343.

Pritchard HD, Arthern RJ, Vaughan DG, Edwards LA (2009) Extensive dynamic thinning on the margins of the Greenland and Antarctic ice sheets. *Nature,* **461**: 971-975.

Pritchard HD, Ligtenberg SRM, Fricker HA, Vaughan DG, van den Broeke MR, Padman L (2012) Antarctic ice-sheet loss driven by basal melting of ice shelves. *Nature,* **484**: 502-505.

Quayle WC, Peck LS, Peat H, Ellis-Evans JC, Harrigan PR (2002) Extreme responses to climate change in Antarctic lakes. *Science,* **295**: 645.

Renssen H, Goosse H, Fichefet T, Masson-Delmotte V, Koc N (2005) Holocene climate evolution in the high-latitude Southern Hemisphere simulated by a coupled atmosphere-sea ice-ocean-vegetation model. *Holocene*, **15(7)**: 951-964.

Rignot E, Mouginot J, Scheuchl B (2011) Ice flow of the Antarctic Ice Sheet. *Science,* **333**: 1427-1430.

Roberts D, and McMinn A (1996) Relationships between surface sediment diatom assemblages and water chemistry gradients in saline lakes in the Vestfold Hills, Antarctica. *Antarctic Science,* **8**: 331-341.

Roberts D, and McMinn A (1999) A diatom-based palaeosalinity history of Ace Lake, Vestfold Hills, Antarctica. *Holocene,* **9**: 401-408.

Roberts SJ, Hodgson DA, Bentley MJ, Smith JA, Millar IL, Olive V, Sugden DE (2008) The Holocene history of George VI ice shelf, Antarctic Peninsula from clast-provenance analysis of epishelf lake sediments. *Palaeogeography, Palaeoclimatology, Palaeoecology,* **259**: 258-283.

Roberts SJ, Hodgson DA, Bentley MJ, Sanderson DCW, Milne G, Smith JA, Verleyen E, Balbo A (2009) Holocene relative sea-level change and deglaciation on Alexander Island, Antarctic Peninsula, from elevated lake deltas. *Geomorphology,* **112(1-2)**: 122-134.

Roberts SJ, Hodgson DA, Sterken M, Whitehouse PL, Verleyen E, Vyverman W, Sabbe K, Balbo A, Bentley MJ, Morteton S (2011) Geological constraints on glacio-isostatic adjustment models of relative sea-level change during deglaciation of Prince Gustav Channel, Antarctic Peninsula. *Quaternary Science Reviews,* **30(25-26)**: 3603-3617.

Ryves DB, Juggins S, Fritz SC, Battarbee RW (2001) Experimental diatom dissolution and the quantification of microfossil preservation in sediments. *Palaeogeography, Palaeoclimatology, Palaeoecology,* **172**: 99-113.

Ryves DB, Battarbee RW, Juggins S, Fritz SC, Anderson NJ (2006) Physical and chemical predictors of diatom dissolution in freshwater and saline lake sediments in North America and West Greenland. *Limnol. Oceanogr.,* **51(3)**: 1355-1368.

Ryves DB, Battarbee RW, Fritz SC (2009) The dilemma of disappearing diatoms: incorporating diatom dissolution data into palaeoenvironmental modelling and reconstruction. *Quaternary Science Reviews,* **28**: 120-136.

Sato K, and Hirasawa N (2007) Statistics of Antarctic surface meteorology based on hourly data in 1957-2007 at Syowa Station. *Polar Science,* **1**: 1-15.

Scott EM, Cook GT, Naysmith P (2007) Error and uncertainty in radiocarbon measurements. *Radiocarbon,* **49(2)**: 427-440.

Shakun JD, and Carlson AE (2010) A global perspective on Last Glacial Maximum to Holocene climate change. *Quaternary Science Reviews,* **29**: 1801-1816.

Steig EJ, Schneider DP, Rutherford SD, Mann ME, Comiso JC, Shindell DT (2009) Warming of the Antarctic ice-sheet surface since the 1957 International Geophysical Year. *Nature,* **457**: 459-463.

Stenni B, Masson-Delmotte V, Selmo E, Oerter H, Meyer H, Rothlisberger R, Jouzel J, Cattani O, Falourd S, Fischer H, Hoffmann G, Lacumin P, Johnsen SJ, Minster B, Udisti R (2010) The deuterium excess records of EPICA Dome C and Dronning Maud Land ice cores (East Antarctica). *Quatern. Sci. Rev*., **29**: 146–159.

Sterken M, Roberts SJ, Hodgson DA, Vyverman W, Balbo AL, Sabbe K, Moreton SG, Verleyen E (2012) Holocene glacial and climate history of Prince Gustav Channel, northeastern Antarctic Peninsula. *Quaternary Science Reviews,* **31**: 93-111.

Stone JO, Balco GA, Sugden DE, Caffee MW, Sass III LC, Cowdery SG, Siddoway C (2003) Holocene deglaciation of Marie Byrd Land, West Antarctica. *Science,* **299**: 99-102.

Street-Perrot FA, Barker PA, Swain DL, Ficken KJ, Wooller MJ, Olago DO, Huang Y (2007) Late Quaternary changes in ecosystems and carbon cycling on Mt. Kenya, East Africa: a landscape-ecological perspective based on multi-proxy lake-sediment fluxes. *Quaternary Science Reviews,* **26**: 1838-1860.

Summerhayes C, Ainley D, Barrett P, Bindschadler R, Clarke A, Convey P, Fahrbach E, Gutt J, Hodgson D, Meredith M, Murray A, Pörtner H-O, di Prisco G, Schiel S, Speer K, Turner J, Verde C, Willems A (2009) The Antarctic environment in the global system. *In*: Turner J, Bindschadler R, Convey P, di Prisco G, Fahrbach E, Gutt J, Hodgson D, Mayewski P, Summerhayes C. Antarctic Climate Change and the Environment (ACCE). pp. 1-32.

Sun L, Xie Z, Zhao J (2000) Palaeoecology: a 3,000-year record of penguin populations. *Nature,* **407**: 858.

Sun L, Liu X, Yin X, Zhu R, Xie Z, Wang Y (2004) A 1500-year record of Antarctic seal populations in response to climate change. *Polar Biol,* **27**: 495-501.

Takada M, Tani A, Miura H, Moriwaki K, Nagatomo T (2003) ESR dating of fossil shells in the Lützow-Holm Bay region, East Antarctica. *Quaternary Science Reviews,* **22**: 1323-1328.

Takano Y, Tyler JJ, Kojima H, Yokoyama Y, Tanabe Y, Sato T, Ogawa NO, Ohkouchi N, Fukui M (2012) Holocene lake development and glacial-isostatic uplift at Lake Skallen and Lake Oyako, Lützow Holm Bay, East Antarctica, based on biogeochemical facies and molecular signatures. *Applied Geochemistry,* doi: http://dx.doi.org/10.1016/j.apgeochem.2012.08.009.

Tanabe Y, Kudoh S, Imura S, Fukuchi M (2008) Phytoplankton blooms under dim and cold conditions in freshwater lakes of East Antarctica. *Polar Biol,* **31**: 199-208.

Telford RJ, Heegaard E, Birks HJB (2004) The intercept is a poor estimate of a calibrated radiocarbon age. *The Holocene*, **14**: 296-298.

Thompson DWJ, and Solomon S (2002) Interpretation of recent Southern Hemisphere climate change. *Science,* **296**: 895-899.

Turner J, Bindschadler R, Convey P, di Prisco G, Fahrbach E, Gutt J, Hodgson D, Mayewski P, Summerhayes C (2009) Antarctic climate change and the Environment. pp. 526.

Vaughan DG, and Spouge JR (2002) Risk estimation of collapse of the West Antarctic Ice Sheet. *Climatic Change,* **52**: 65-91.

Vaughan DG, Marshall GJ, Connolley WM, King JC, Mulvaney R (2001) Devil in detail. *Science,* **293**: 1777-1779.

Vaughan DG, Marshall GJ, Connolley WM et al. (2003) Recent rapid regional climate warming on the Antarctic Peninsula. *Climatic Change,* **60**: 243-274.

Verkulich SR, Melles M, Hubberten HW, Pushina ZV (2002) Holocene environmental changes and development of Figurnoye Lake in the Southern Bunger Hills, East Antarctica. *J. Paleolim.,* **28**: 253-267.

Verleyen E, Hodgson DA, Vyverman W, Roberts D, McMinn A, Vanhoutte K, Sabbe K (2003) Modelling diatom responses to climate induced fluctuations in the moisture balance in continental Antarctic lakes. *J Paleolimnol*, **30**: 195-215.

Verleyen E, Hodgson DA, Sabbe K, Vanhoutte K, Vyverman W (2004a) Coastal oceanographic conditions in the Prydz Bay region (East Antarctica) during the Holocene recorded in an isolation basin. *The Holocene,* **14(2)**: 246-257.

Verleyen E, Hodgson DA, Sabbe K, Vyverman W (2004b) Late Quaternary deglaciation and climate history of the Larsemann Hills (East Antarctica). *Journal of Quaternary Science,* **19(0)**: 1-15.

Verleyen E, Hodgson DA, Leavitt PR, Sabbe K, Vyverman W (2004c) Quantifying habitat-specific diatom production: a critical assessment using morphological and biogeochemical markers in Antarctic marine and lake sediments. *Limnol. Oceanogr.,* **49(5)**: 1528-1539.

Verleyen E, Hodgson DA, Milne GA, Sabbe K, Vyverman W (2005a) Relative sea-level history from the Lambert glacier region, East Antarctica, and its relation to deglaciation and Holocene glacier readvance. *Quaternary Research,* **63**: 45-52.

Verleyen E, Hodgson DA, Sabbe K, Vyverman W (2005b) Late Holocene changes in ultraviolet radiation penetration recorded in an East Antarctic lake. *Journal of Paleolimnology,* **34**: 191-202.

Verleyen E, Hodgson DA, Sabbe K, Cremer H, Emslie SD, Gibson J, Hall B, Imura S, Kudoh S, Marshall GJ, McMinn A, Melles M, Newman L, Roberts D, Roberts SJ, Singh SM, Sterken M, Tavernier I, Verkulich S, Van de Vyver E, Van Nieuwenhuyze W, Wagner B, Vyverman W (2011) Post-glacial regional climate variability along the East Antarctic coastal margin - evidence from shallow marine and coastal terrestrial records. *Earth Sci Rev,* **104**: 199-212.

Verleyen E, Hodgson DA, Gibson J, Imura S, Kaup E, Kudoh S, De Wever A, Hoshino T, McMinn A, Obbels D, Roberts D, Roberts SJ, Sabbe K, Souffreau C, Tavernier I, Van Nieuwenhuyze W, Van Ranst E, Vindevogel N, Vyverman W (2012) Chemical limnology in coastal East Antarctic lakes: monitoring future climate change in centres of endemism and biodiversity. *Antarctic Science,* **24(1)**: 23-33.

Wagner B, Cremer H, Hultzsch N, Gore DB, Melles M (2004) Late Pleistocene and Holocene history of Lake Terrasovoje, Amery Oasis, East Antarctica, and its climatic and environmental implications. *Journal of Paleolimnology,* **32**: 321-339.

Wanner H, Beer J, Bütikofer J, Crowley TJ, Cubasch U, Flückiger J, Goosse H, Grosjean M, Joos F, Kaplan JO, Küttel M, Müller SA, Prentice IC, Solomina O, Stocker TF, Tarasov P, Wagner M, Widmann M (2008) Mid- to Late Holocene climate change: an overview. *Quaternary Science Reviews,* **27**: 1791-1828.

Watcham EP, Bentley MJ, Hodgson DA, Roberts SJ, Fretwell PT, Lloyd JM, Larter RD, Whitehouse PL, Leng MJ, Monien P, Moreton SG (2011) A new Holocene relative sea level curve for the South Shetland Islands, Antarctica. *Quaternary Science Reviews,* **30**: 3152-3170.

Yamane M, Yokoyama Y, Miura H, Maemoku H, Iwasaki S, Matsuzaki H (2011) The last deglacial history of Lützow-Holm Bay, East Antarctica. *Journal of Quaternary Science,* **26(1)**: 3-6.

Yamanouchi T, and Shudou Y (2007) Trends in cloud amount and radiative fluxes at Syowa Station, Antarctica. *Polar Science,* **1**: 17-23.

Yoshida Y (1983) Physiography of the Prince Olav and Prince Harald Coasts, East Antarctica. *Memoirs of National Institute of Polar Research, Ser. C (Earth Science),* **13**: pp. 83.

Zolitschka B, Mingram J, van der Gaast S, Fred Jansen JH, Naumann R (2001) Sediment logging techniques. *In:* Last WM, and Smol JP. Tracking environmental change using lake sediments. Volume 1: Basin analysis, coring, and chronological techniques. Kluwer Academic Publishers, Dordrecht, The Netherlands. pp 155-170.

Chapter 2. Revision of type materials of Antarctic diatom species (Bacillariophyta) described by West & West (1911), with the description of two new species

PUBLISHED PAPER. Van de Vijver B, Tavernier I, Kellogg TB, Gibson J, Verleyen E, Vyverman W, Sabbe K (2012) Revision of type materials of Antarctic diatom species (Bacillariophyta) described by West & West (1911), with the description of two new species. Fottea, ***12(2)****: 149-169.*

Author's contribution: description of the ecology of Luticola pseudomurrayi and the associated diatom flora, diatom size measurements of Luticola pseudomurrayi.

Key-words: Antarctica, Bacillariophyta, diatoms, morphology, new species, type material, West & West

Abstract

In 1911, W & GS West published a detailed account of freshwater algae collected by James Murray in the vicinity of Cape Royds on Ross Island (Antarctic Continent). Out of 84 algal taxa reported, 30 were diatoms. Although the majority of the diatoms were considered (at that time) to be cosmopolitan, eight diatom species and two varieties were described as new. While most of these new taxa are still commonly reported from Antarctic and Subantarctic localities, the exact identity of some remains uncertain. Here we document the morphology of these species from the original type material using light and scanning electron microscopy; the taxonomic identities are discussed and, where necessary, the taxonomy is updated. For several species, lectotypes are designated. In addition, two Antarctic species are described as new: *Luticola pseudomurrayi* VAN DE VIJVER ET TAVERNIER sp. nov. and *Chamaepinnularia gibsonii* VAN DE VIJVER sp. nov.

Introduction

The oldest diatom records from the Antarctic Continent date back to the beginning of the 20th century (Holmboe 1902; Van Heurck 1909; West & West 1911; Fritsch 1912; 1917; Carlson 1913; Brown 1920) when diatoms, including new species, were described from collections made during Belgian, British, German and Danish Polar Expeditions. One of the most important contributions of this pioneer era was made by William West (Roebuck 1914) and his son George Stephen West (Grove 1919) with their publication in 1911 of a detailed account of freshwater algae collected in 1908 and 1909 by James Murray in the vicinity of the winter quarters of the British Expedition near Cape Royds on Ross Island (77°30' S – 168°00' E). Among the 84 algal species reported in their paper, they list and describe 30 diatom taxa. Although the majority of these diatoms were at the time considered to be cosmopolitan, West & West also described eight new diatom species. Several of these, such as *Chamaepinnularia cymatopleura* (W West et GS West) CAVACINI, *Muelleria peraustralis* (W WEST ET GS WEST) SPAULDING ET STOERMER, and *Luticola murrayi* (W West et GS West) DG MANN (all originally described as *Navicula* species), *Navicula shackletoni* W & GS WEST and *Craspedostauros laevissimus* (W West et GS West) SABBE (originally *Tropidoneis laevissima*) are commonly reported in publications on

contemporary diatoms from the Antarctic Continent (Spaulding et al. 1997; Sabbe et al. 2003; Gibson et al. 2006).

The present paper discusses the morphology and phenotypic variability of the new species described in West & West (1911) using modern SEM and LM techniques. The original description and drawings are verified and discussed on the basis of the original West & West slides. For each species, light micrographs of the original type slides and scanning electron micrographs (using other materials from recent collections) are provided and comparisons with other taxa are made in order to clarify the taxonomical position of the West & West species. West & West (1911) did not designate holotype slides. Since apart from *Chamaepinnularia cymatopleura* (Cavacini et al. 2006), this was never done for the other species described in West & West (1911), we formally lectotypify all new species described in their paper, except for *Navicula muticopsiforme*, as we did not find the species in the slides.

Additionally, *Luticola pseudomurrayi* VAN DE VIJVER ET TAVERNIER sp. nov. and *Chamaepinnularia gibsonii* VAN DE VIJVER sp. nov., both observed on the Antarctic Continent, are described as new species.

Material & Methods

Table 1 lists all original slides made by West & West (1911), stored in the British Museum, together with the available sample information. Light micrographs from the original slides have been made for species described as new by West & West (1911) in order to document the morphological variability of the populations. Since no raw materials of the original slides were kept, samples from recent collections from similar environments in other regions on the Antarctic Continent (viz. the Bunger Hills, East Antarctica and Taylor Valley, McMurdo Dry Valleys) have been investigated in order to provide SEM observations of specimens fully matching the original West & West species. Table 2 lists all samples used. Diatom samples of this material were prepared following the method of Van der Werff (1955). Small parts of the samples were cleaned by adding 37% H_2O_2 and heating to 80 °C for about 1h where after the reaction was completed by addition of $KMnO_4$. Following digestion and centrifugation (3 times 10 minutes at 3500 rpm), the material was diluted with distilled water to avoid excessive concentrations of diatom valves that may hinder reliable observations. Cleaned diatom valves were mounted in Naphrax®. LM observations were conducted using an Olympus BX51 microscope equipped with Differential Interference Contrast (Nomarski) optics. For SEM, part of the suspension was filtered through polycarbonate membrane filters with a pore diameter of 3 µm, pieces of which were fixed on aluminium stubs after air-drying. The stubs were sputter-coated with 50 nm of Au and studied in a JEOL-5800LV at 20 kV.

Terminology of frustule morphology is based on Hendey (1964), Barber & Haworth (1981) and Round et al. (1990). Samples and slides from the Bunger Hills and Taylor Valley are stored at the National Botanic Garden of Belgium (BR), Department of Bryophytes and Thallophytes.

Observations and Discussion

In their original publication, West & West (1911) reported 30 diatom taxa belonging to (following the taxonomical concepts of that time) 16 genera. Eight species and two varieties were described as new for science. For a list of these 30 species with their current taxonomic identity and/or status, we refer to this published manuscript (Van de Vijver et al. 2012).

Several taxa such as *Navicula* (*Pinnularia*) *globiceps* Gregory, *Stauroneis anceps* EHRENBERG and *Achnanthes brevipes* var. *intermedia* (KÜTZING) CLEVE were illustrated but wrongly identified in West & West and later described as new species by other authors, viz. *Luticola gaussii* (HEIDEN) DG MANN (Heiden & Kolbe 1928), *Stauroneis latistauros* VAN DE VIJVER ET LANGE-BERTALOT (Van de Vijver et al. 2004), and *Achnanthes taylorensis* KELLOGG ET KELLOGG (Kellogg et al. 1980) respectively. For all other taxa listed in West & West (1911), no illustrations or descriptions were provided, making it sometimes impossible to verify their identity, as they were apparently quite rare in the samples and could not be found during a re-examination of the slides. Finally, a considerable portion of the reported species has a marine origin, e.g. *Trachyneis aspera* (EHRENBERG) CLEVE, *Triceratium arcticum* BRIGHTWELL or *Hemiaulus ambiguus* JANISCH.

Based on our re-analysis of the original West & West material, it is clear that two Antarctic taxa, which to date have been wrongly identified and/or force-fitted to species described by West & West, actually constitute species in their own right. One of these is usually identified as *Navicula murrayi* W & GS WEST and is here described as *Luticola pseudomurrayi* VAN DE VIJVER ET TAVERNIER sp. nov. A second taxon resembles *Chamaepinnularia cymatopleura* and is described here as *Chamaepinnularia gibsonii* VAN DE VIJVER sp. nov.

Species newly described by W & GS WEST (1911)

***Chamaepinnularia cymatopleura* (W ET GS WEST) CAVACINI** (Figs 1-23)

Basionym: *Navicula (Pinnularia) cymatopleura* W & GS WEST

Original description (West & West 1911): *Navicula minutissima, valves sublinearis, diametro 4 ¼ -5 2/5-plo longioribus, lateribus triundulatis, undulo mediana levissime majori, polis subcapitatis, platea centrali magna et longitudinaliter elliptica, platea axiali lata, striis brevibus et laevibus, 20-21 in 10 µm, leviter radiates in parte mediana (adversus plateam centralem). Longitudo 17-27 µm, latitudo 4-5 µm.*

Translation of the original description: Very small *Navicula*, sublinear valves, 4 ¼- 5 2/5-fold longer than wide. Margins triundulate, the middle undulation slightly larger. Apices subcapitate. Central area large and apically elliptical. Axial area broad. Striae short and smooth, 20-21 in 10 µm, slightly radiate in the middle part of the valve (near the central area). Length 17-27 µm, width 4-5 µm.

Lectotype: slide BM34146 (Natural History Museum, London, UK)

Synonyms: *Navicula deltaica* KELLOGG ET KELLOGG in Kellogg et al., *Navicula quaternaria* KELLOGG ET KELLOGG in Kellogg et al.

LM observations: Frustules in girdle view rectangular (Fig. 12). Larger valves linear to linear-elliptical with (tri-)undulate margins and subcapitate apices; smaller specimens more broadly elliptical with a (slightly) convex central part and broadly rounded to slightly rostrate-capitate ends (Fig. 1-11). Valve length 15-36 µm, width 3.6-5.1 µm (n=30). Axial area wide, lanceolate, with slightly triundulate margins in the larger specimens. Towards the apices, the axial area widens to form a wedge-shaped hyaline area around the terminal raphe fissures. Central area lanceolate to elliptical. Raphe straight, filiform with expanded, pore-like central endings and hooked terminal fissures. Transapical striae slightly radiate in the middle, parallel to convergent towards the poles, 20-24 in 10 µm.

SEM observations (Bunger Hills 11): Alveoli covered by hymenes (Fig. 19). When eroded, alveoli are slit-like, not interrupted near the valve face/mantle junction (Fig. 20). Central raphe endings small, expanded, pore-like, almost straight to weakly deflected (Fig. 20). Terminal fissures hooked, continuing on the valve mantle (Fig. 19). Internally, proximal raphe endings short, bent in the same direction (Figs 21, 23). Terminal raphe with small helictoglossae (Fig. 22). Internally, small, blunt, spine-like structures are present on the virgae close to the valve face/mantle junction (Fig. 23).

Distribution: *Chamaepinnularia cymatopleura* is widespread on the Antarctic Continent (see Kellogg & Kellogg 2002 – as *Pinnularia cymatopleura* - and references therein, Sabbe et al. 2003, Cavacini et al. 2006). To date there are no confirmed records from the Maritime and Subantarctic Regions.

Taxonomical remarks: Cavacini et al. (2006) analysed the type material of *Navicula (Pinnularia) cymatopleura* and concluded that the species should be transferred to *Chamaepinnularia,* although the alveoli are not interrupted on the valve face/mantle junction contrary to what is claimed (Cavacini et al. 2006, p. 60 & 64). While *C. cymatopleura* is larger than most *Chamaepinnularia* species, all other features typical for the genus are present, such as the uniseriate striae (contrary to *Pinnularia* which has multiseriate striae), and therefore the transfer to *Chamaepinnularia* proposed by Cavacini et al. (2006) appears to be justified.

Spaulding et al. (1997) and Sabbe et al. (2003) synonymised *Navicula deltaica* and *N. quaternaria* on the basis of their close resemblance to smaller specimens of *C. cymatopleura*. Both species were never validly described because the types of both species were never deposited in the Academy of Natural Sciences of Philadelphia (Cavacini et al. 2006). We analysed the original materials used by Kellogg et al. (1980) and confirm that both taxa belong to the smaller end of the size range of *C. cymatopleura* (Figs 13-16). During our analyses, an unknown taxon, similar to *C. cymatopleura*, was found in the Bunger Hills samples. This taxon is described as a new species, *Chamaepinnularia gibsonii*, below.

***Craspedostauros laevissimus* (W et GS West) Sabbe** (Figs 24-39)

BASIONYM: *Tropidoneis laevissima* W ET GS WEST

Original description (West & West 1911): *T. parva, delicatissima et laevissima; valves oblongo-linearis, diametro 8-11-plo longioribus, in parte mediana marginibus parallelibus,*

apices versus leviter et gradatim angustiaribus, polis obtuse rotundatis, raphe recta sed juxta polos levissime curvata nodulo centrali in staurum transversum producto, stauro angustissimo plerumque valvae margines versus paullulo dilatato, alis (vel carinis) carentibus, striis non visis. Cellulae in aspectu cingulato anguste oblongo-rectangulari, medio constricta, lateribus convexis et angulis rotundatis.

Translation of the original description: Small *Tropidoneis* species, very delicate and smooth. Valves oblong-linear, 8-11 times longer than wide. Margins parallel in the middle part. Valves gradually narrower towards the apices. Apices obtusely rounded. Raphe straight but near the apices very slightly curved, forming a central nodule in the stauros. Stauros very narrow in most of the valves with very slightly widened valve margins, lacking wings or keels. Striae not visible. Cells in girdle view narrow, oblong-rectangular, constricted in the middle part with convex margins and rounded edges.

Lectotype (here designated): slide BM34122 (Natural History Museum, London, UK)

LM observations: Frustules in girdle view more or less biarcuate (Figs 29-30). Valves linear to linear-lanceolate, sometimes slightly constricted in the centre, with broadly rounded to cuneate apices (Figs 24-28). Margins sometimes irregular, probably due to flattening and rupture of the thin valves. Valve length 35-88 µm, width 4.8-7.8 µm (n=20). Axial area narrow, linear. Central area narrow, rectangular to bow tie-shaped. Raphe filiform, straight to slightly undulate, with slightly expanded central raphe endings. Terminal raphe endings bent to the same side, clearly visible in LM. Striae parallel to slightly radiate near the central area, 26-28 in 10 µm. Areolae not discernible in LM.

SEM morphology (Bunger Hills 14): Areolae rounded, closed externally by cribra with four (or more alongside the raphe sternum) small peripheral pores and occasionally one small central pore (Figs 36, 37). Central raphe endings expanded, straight to weakly deflected (Fig. 36). Terminal fissures clearly bent, terminating on the valve face margin (Fig. 38). Pores continue around the apices. Internally, raphe sternum well-developed, raised (Fig. 39). Central area internally with a narrow stauros lying in a wider hyaline fascia (Fig. 39). Internal central raphe endings terminate in a small double helictoglossa (Fig. 39). Internal areola openings more or less square to rounded.

Distribution: *Craspedostauros laevissimus* is a widespread endemic species restricted to the Antarctic Continent [Eastern Antarctica and Victoria land (see Kellogg & Kellogg 2002 – as *Tropidoneis laevissima* – and references therein, Sabbe et al. 2003)]. The species has never been observed outside continental Antarctica.

Taxonomical remarks: *Craspedostauros laevissimus* can be found under different names in the Antarctic literature. The species was originally placed in the genus *Tropidoneis*. Patrick & Reimer (1975) rejected the genus *Tropidoneis* and included all its species in the genus *Plagiotropis* which has priority. It is clear that *C. laevissimus* does not belong to the latter genus, which has a different areolar structure without cribra and a different internal raphe structure, without central helictoglossae. While Paddock (1988), without studying material of *C. laevissimus*, suggested that the species might belong to *Stauroneis*, it was finally transferred to the new genus *Craspedostauros* (Cox 1999) in Sabbe et al. (2003) on the basis of areolar, raphe and cingulum structure.

Navicula glaberrima W ET GS WEST (Figs 40-43)

Original description (West & West 1911): *Navicula minutissima et laevissima ; valvis rhomboideis vel rhomboideo-ellipticis cum lateribus paene rectis, polis levissime rotundatis, raphe rectissima, nodulis terminalibus conspicuis, striis non visis. Longitudo valvae 19 µm, latitudo 5,1 µm.*

Translation of the original description: Very small and smooth *Navicula*. Valves rhomboid to rhomboid-elliptic with almost straight margins and very slightly rounded apices. Raphe very straight with distinct terminal nodules. Striae not visible. Valve length 19 µm, with 5.1 µm.

Lectotype (here designated): slide BM34117 (Natural History Museum, London, UK)

LM morphology: Valves lanceolate to rhombic-lanceolate, apices sub-rostrate to rostrate (Figs 40-42). Valve length 19-20 µm, width 4.9-5.1 µm (n=2). Axial area very narrow, linear, central area absent. Raphe filiform with straight, expanded central pores. Terminal fissures not visible in LM. Transapical striae parallel to weakly radiate throughout the entire valve, ca. 22 in 10 µm. Areolae not visible in LM.

SEM morphology: So far, the only record of this species has been in the West & West (1911) publication. It has been impossible to find other samples containing *N. glaberrima*. Therefore, no SEM observations could yet be made.

Distribution: The species has so far only been found in a large lake on the west side of McMurdo Sound, at 25 miles from the Cape Royds Camp (77°45'S) (West & West 1911).

Taxonomical remarks: *N. glaberrima* most probably does not belong to the genus *Navicula* s.s. but resembles several members of the genus *Craticula* (Lange-Bertalot 2001). Since only two valves could have been investigated in LM, it is probably too early to draw conclusions about its taxonomic status. It is possible that *N. glaberrima* is conspecific to *C. submolesta* (HUSTEDT) LANGE-BERTALOT based on valve outline, dimensions and stria density and hence represents a younger synonym of the latter. *Craticula submolesta* has never been observed on the Antarctic Continent (Kellogg & Kellogg 2002) although it was reported from the South Shetland Islands (Håkansson & Jones 1994) and Horseshoe Island (Wasell & Håkansson 1992; Wasell 1993). On the Antarctic Continent, a second *Craticula* species has been regularly found in larger populations than *N. glaberrima*. The species has been for a long time identified as *Craticula* (*Navicula*) *molesta* (KRASSKE) LANGE-BERTALOT ET WILLMANN, a species described in 1938 from Spitsbergen by G Krasske (or as *Navicula zizix* VAN LANDINGHAM as it was called later). Recently, the morphology of the species was thoroughly investigated and based on the results, it was described as a separate species, *Craticula antarctica* VAN DE VIJVER ET SABBE (Van de Vijver et al. 2010). Possible conspecificity between *N. glaberrima* and *C. antarctica* has to be excluded based on differences in valve outline and dimensions.

***Luticola murrayi* (W ET GS WEST) DG MANN** (Figs 44-50)

Basionym: *Navicula (Pinnularia) murrayi* W ET GS WEST

Original description (West & West 1911): *Navicula parva, lineari-ellipticis, diametro circiter 4-plo longioribus, polis obtusis laevissime dilatatis, platea centrali transverse expansa, marginem utrinque paene attingente cum puncta solitaria asymmetrica, platea axiali angusta, striis 14 in 10 µm, punctulatis, in toto radiates, in parte mediana 4 (circ.) utrobique multe brevioribus.*

Translation of the original description: Small *Navicula*. Valves linear-elliptical, four times longer than wide. Apices obtuse, very slightly widened. Central area transversely expanded, almost reaching the margins on both sides with an asymmetrical solitary puncta. Axial area narrow. Striae 14 in 10 µm, punctate, radiate throughout the entire valve. In the middle part of the valve, 4 shorter striae present on both sides.

Lectotype (here designated): slide BM34129 (Natural History Museum, London, UK)

Synonyms: *Navicula muticopsis* f. *murrayi* (W ET GS WEST) KO-BAYASHI, *Luticola laeta* SPAULDING ET ESPOSITO, *L. murrayi* var *elegans* W ET GS WEST

LM observations: Valves elongated, linear-lanceolate to narrowly elliptical with broadly rounded to rostrate-capitate apices (Figs 44-48). Valve length 20-45 µm, width 8-11 µm (n=5). Axial area rather broad, linear. Central area forming a rectangular fascia. Isolated stigma present, positioned about halfway between the valve margin and the axial area. Raphe straight, filiform; central raphe endings simple, deflected in the same direction, away from the stigma. Terminal raphe fissures short, bent in the same direction as the central raphe endings, lying in a hyaline area near the apices. Transapical striae radiate throughout the entire valve, 14-18 in 10 µm. Striae clearly punctate, composed of 4-7 small areolae.

SEM observations: Due to the extreme rarity of the species in the investigated samples, we were as yet unable to observe it in SEM.

Distribution: Because of the confused identity of this species (see below), most published reports are unreliable and its exact geographic distribution remains unclear. To date, *L. murrayi* has only been reported with certainty from the type locality ('in pond, and moraines near camp, Cape Royds' on Ross Island) and various localities in the McMurdo Dry Valleys (based on the illustrations shown on the Antarctic Freshwater Diatoms website Spaulding et al. 2011).

Taxonomical remarks: No specimens matching the original type description and drawing (West & West 1911, PlXXVI, Fig. 129, reproduced here as Fig. 49) could be found in the West & West materials. In other samples from the McMurdo Dry Valleys, we did find some specimens (Figs 44-48, see also Spaulding et al. 2011) matching the valve shape and the lower range of the stria density (as shown in the type illustration and description) and possessing a stigma (as described in the protologue, but not shown in the type illustration!). Despite the fact that in our specimens the stria density range was considerably larger (14-18 striae in 10 µm), we believe that these specimens should be considered true *L. murrayi*, as the differences in stria density range may be due to the

fact that West & West (1911) probably only saw a single specimen. The fact that the stigma is mentioned in the type description but not shown in the accompanying illustration also leads us to believe that the drawing is inaccurate (note also that the central raphe endings are shown as being straight). The identity of *L. murrayi* has been confused in several taxonomic treatments. This confusion is likely traced to the studies of Kobayashi (1963) and Hustedt (1961-1966). Both authors discuss the morphology and variability of *L. murrayi* but show specimens with distinctly capitate, wide apices, while according to the original protologue the apices are obtuse ('*obtusis*') and only very slightly expanded ('*laevissime dilatatis'*). The taxon illustrated by Kobayashi (1963) and Hustedt (1961-1966) is therefore described as a new species below, viz. *Luticola pseudomurrayi* VAN DE VIJVER ET TAVERNIER sp. nov. The case of *Luticola murrayi* thus presents a classic example of taxonomic drift. Due to this confusion, published reports of this species are not trustworthy.

Our 'new' concept of *L. murrayi* largely overlaps with the description of *L. laeta*, which was described by Esposito et al. (2008). The latter taxon is most probably a later synonym of *L. murrayi*, but due to the rarity of *L. murrayi* we still refrain from formally synonymising *L. laeta* with *L. murrayi* until further populations can be analyzed. Note that West & West also described a new variety belonging to this species, viz. *N. murrayi* var. *elegans*, which is smaller, narrower, and has produced subcapitate apices (West & West 1911, PlXXVI, Fig. 130, reproduced here as Fig. 50). This specimen (apparently here as well has only one specimen been observed) matches the description of *L. laeta* even better, but may also fall within the range of *L. murrayi*.

***Muelleria peraustralis* (W ET GS WEST) SPAULDING & STOERMER** (Figs 52-62)

Basionym: *Navicula peraustralis* W ET GS WEST

Original description (West & West 1911): *Navicula parva, valves anguste lineari-lanceolatis, diametro circiter 4 1/3-plo longioribus, lateribus triundulatis inflatione mediana majori, polis inflato-capitatis et levissima angularibus, platea centrali parva et elliptica, platea axiali angusta, striis validis 18 in 10 µm, leviter radiates, a plateis lateralibus duobus interruptis. Longitudo 47,7 µm, latitudo 11,1 µm.*

Translation of the original description: Small *Navicula*. Valves narrowly linear-lanceolate, 4 1/3 times longer than wide. Margins triundulate with the largest thickening in the middle. Apices inflated, capitate and very slightly angled. Central area small, elliptical. Axial area narrow. Striae robust, 18 in 10 µm, slightly radiate, interrupted by two hyaline zones. Length 47.7 µm, width 11.1 µm.

Lectotype (here designated): slide BM34127 (Natural History Museum, London, UK)

LM observations: Valves elliptical with a gibbous central part and produced broadly rounded to slightly rostrate-capitate ends (Figs 52-54). Valve face/mantle margin gently sloping into a rather deep mantle. Valve length 30-65 µm, width 7.5-12.5 µm (n=15). Axial area narrow, linear, only slightly widening towards an elliptical central area. Raphe filiform with distant central raphe endings, deflected in the same direction, sometimes reaching the areolae. Terminal raphe endings deflected in the same direction as the

central raphe endings. Transapical striae radiate near the valve centre, becoming parallel and convergent towards the apices, 20-21 in 10 µm at the valve centre, 22-24 in 10 µm towards the apices. Areolae clearly discernible in LM.

SEM observations (Taylor Valley, C14-77-1B): Striae composed of small, transapically elongated areolae (Figs 56, 58, 59). The row of areolae adjacent to the raphe sternum is often separated from the next longitudinal row by slightly wider vimines (Figs 56, 58). Internally, this longitudinal hyaline band corresponds to longitudinal canals on both sides of the raphe sternum (Fig. 60). Near the terminal raphe endings, the canals end externally in two puncta on the mantle (Fig. 57). Internally, a well-developed rectelevatum (Van de Vijver et al. 2010) is present in the central area (Fig. 61). Areolae occluded by vela (Fig. 62).

Distribution: *Muelleria peraustralis* has only been observed on the Antarctic Continent where it is found commonly in East Antarctica and Victorialand (Spaulding & Steromer 1997; Spaulding et al. 1999). No record exists in the Maritime Antarctic Region or the Subantarctic islands where in similar habitats other *Muelleria* species are found (Van de Vijver et al. 2010).

Taxonomical remarks: *Muelleria peraustralis* was transferred to the genus *Muelleria* (Spaulding & Stoermer 1997) on the basis of typical *Muelleria* features such as the canal puncta, rectelevatum, strongly bent central raphe endings and a stria structure with more widely spaced striae around the central area (Van de Vijver et al. 2010).

***Navicula muticopsiforme* W ET GS WEST** (Fig. 51)

ORIGINAL DESCRIPTION (WEST & WEST 1911): *Navicula minutissima, valves subellipticis, diametro circiter duplo longioribus, parte mediana parva cum marginibus parallelis, polis longe cuneiformis et obtuse rotundatis, platea centrali magna et transverse dilatata, platea axiali lata, striis 17 utrobique (16 in 10 µm), punctatis, in parte mediana (adversus plateam centralem) striis tribus brevibus e puncto singulo elliptico formatis, ceteris radiates e punctis duobus formatis. Longitudo 11.3 µm, latitudo 5.3 µm.*

Translation of the original description: Very small *Navicula*, valves subelliptical, length almost twice the width, middle part of the valve small with parallel margins, apices elongated, cuneate and obtusely rounded, central area large and transversely widened, axial area broad, 17 striae on both sides (16 in 10 µm), punctate, in the middle part (opposite the central area) three short striae formed of only one single rounded pore, the other striae radiate, composed of two pores. Length 11.3 µm, width 5.3 µm.

Taxonomical remarks: We were not able to find any specimens matching the protologue in the material from Clear Lake, the type locality mentioned by West & West (1911). Several valves with a similar outline were observed but these had a different central area and striae composed of at least 2-3 areolae. It is possible, considering the fact that only one measurement was given for both length and width, that the description was based on only a single specimen.

In material studied by Fritsch (1917) collected during the British Antarctic Expedition of 1910 from Cape Adare, the species was also reported. Careful examination however of that slide also did not reveal any specimens (although the name was written on the label). On the contrary, many valves could be identified as *Luticola muticopsis* f. *reducta* and f. *evoluta* .

In more recent years, the species was only mentioned once in fossil material from McMurdo Sound (Kellogg & Kellogg 1987).

Hustedt (1966) considered *N. muticopsiforme* as part of the size reduction cycle of *Luticola* (*Navicula*) *muticopsis*, reducing the taxon to a synonym of the latter. Based on our analysis of both the original West & West (1911) slide and the Fritsch (1917) slide, this is probably a correct interpretation and until populations matching the description of *N. muticopsiforme* are observed on the Antarctic Continent, we suggest accepting this hypothesis.

***Navicula shackletoni* W ET GS WEST** (Figs 63-81)

Original description (West & West 1911): *Navicula minuta, valvis anguste elliptico-lanceolatis cum polis valde productis levissime subcapitatis et obtusis, platea centrali minuta, platea axiali angustissima, striis 10-12 in 10 µm, leviter radiatis, validis et non punctulatis, in medio striis duobus utrobique adversus plateam centralem delicatissimis et valde indistinctis. Cellula in aspectu cingulato anguste lineari-oblonga. Longitudo 25-29 µm, latitudo 4-5 µm.*

Translation of the original description: Small *Navicula*. Valves narrowly elliptic-lanceolate with strongly produced, obtusely rounded, slightly subcapitate apices. Central area small. Axial area very narrow. Striae 10-12 in 10 µm, slightly radiate, robust but not punctate. In the middle, two very small, almost indistinct striae present on both sides of the central area. Cells in girdle view narrowly linear-oblong. Length 25-29 µm, width 4-5 µm.

Lectotype (here designated): slide BM34128 (Natural History Museum, London, UK)

LM morphology: Frustules rectangular in girdle view (Fig. 72). Valves lanceolate with rostrate to capitate apices (Figs 63-70). Valve length 20-38 µm, width 3.8-5.8 µm (n=24). Axial area narrow, linear, gradually widening towards the central area. Central area forming a rectangular fascia bordered by 2-3 shortened striae. Raphe filiform, weakly curved with straight, only very slightly expanded central pores. Terminal fissures hooked, clearly visible in LM. Transapical striae parallel to weakly radiate, to convergent near the apices, 12-14 in 10 µm.

SEM morphology (Bunger Hills 14): Striae composed of apically elongated lineolae, 50-60 in 10 µm (Figs 76, 77). Virgae wider than the striae (Fig. 77). Proximal raphe endings almost straight and not or only very weakly expanded (Fig. 79). Distal raphe endings with thin, strongly hooked fissures (Fig. 77). A short slit is present at both poles near the end of the terminal raphe fissures (Fig. 76). Internally, areolae covered by hymenes (Figs 78, 80). Striae lying in grooves, sunk beneath the internal valve face, bordered by well developed virgae (Figs 80, 81). Raphe sternum asymmetrically thickened due to the presence of a

pronounced accessory rib (Fig. 80). Distal raphe endings terminating in small helictoglossae (Fig. 81).

Distribution: *Navicula shackletoni* has so far only been reported from the Antarctic Continent (East Antarctica, Victorialand) and seems to be absent from the Subantarctic and Maritime Antarctic (see Kellogg & Kellogg 2002 and references therein).

Taxonomical remarks: *N. shackletoni* clearly belongs to *Navicula* s.s. (sect. *Naviculae lineolatae* sensu CLEVE 1895) (Lange-Bertalot 2001) although Mills (1933-1935) transferred the species to the genus *Pinnularia*, most probably because West & West (1911) indicated that the species might belong to this genus. West & West (1911) also described a variety '*pellucida*' that, according to the authors, should be separated from the nominate variety type on one hand by having two shorter striae on either side of the central area and on the other hand by having a much great width in girdle view. Since mixed populations containing both morphotypes can be found in the same sample, it is rather unclear whether they should be separated or not based on this one feature. We suggest therefore considering this variety as a synonym of *Navicula shackletoni*.

In 2000, Alfinito & Cavacini described a new species, *Navicula skuae*, which appears to be closely related to *N. shackletoni*. The features used to distinguish both species were based on the original drawings from West & West of *N. shackletoni*. These drawings and the original description however do not show or mention the presence of hooked terminal raphe fissures we observed in the type material of this species, the lack of which was consequently used by Alfinito & Cavacini 2000 to separate *N. skuae* from *N. shackletoni*. A second discriminating feature used, was the number of transapical striae in 10 µm being 16-20 in *N. skuae* but only 10-12 in *N. shackletoni*. Both our own observations and Sabbe et al. (2003) contradict these findings in counting 12-14 for *N. shackletoni* and 14-15 for *N. skuae* (illustrations in Alfinito & Cavacini 2000). We therefore have to conclude that both species are conspecific and that *N. skuae* should be considered as a synonym of *N. shackletoni*.

***Nitzschia westiorum* KELLOGG ET KELLOGG in Kellogg et al.** (Figs 82-92)

Basionym: *Nitzschia westii* KELLOGG ET KELLOGG in Kellogg et al. (1980), Palaeogeography, Palaeoclimatology, Palaeoecology 30: p. 185, Plate 2 Fig. 7.

Original name in West & West (1911): *Fragilaria tenuicollis* Heib. var. *antarctica* W ET GS WEST

Original description (West & West 1911): *Var. polis valvae valde productis et leviter subcapitatis ; striis non radiatis, 16 in 10 µm. Longitudo valvae 37 µm, latitudo 3 µm.*

Translation of the original description: Variety with valve poles strongly produced and slightly subcapitate. Striae not radiate, 16 in 10 µm. Valve length 37 µm, width 3 µm.

Lectotype (here designated): slide BM34122 (Natural History Museum, London, UK)

LM morphology: Valves linear with parallel margins (Figs 82-87). Apices rostrate to capitate-produced. Valve length 16-45 µm, width 3-4 µm (n=25). Transapical striae

parallel and equidistant throughout the entire valve, 14-16 in 10 µm. Valves crossed by transapical, raised ribs. Near the valve margin, some striae are bifurcating. Areolae not discernible in LM.

SEM morphology (Taylor Valley, C14-77-1B): Raphe keel rather narrow, slightly elevated, situated at the valve margin (Fig. 89). Striae biseriate composed of two rows of small, rounded areolae, occasionally a third row of areolae is visible near the raphe keel (Fig. 90). Striae separated by thickened costae, almost as broad as the striae, connected to the raphe keel. Raphe continuous from pole to pole (Fig. 89). Internally, double or triple rows of areolae visible in the striae (Fig. 92). Fibulae very small. Distal raphe endings terminating in small helictoglossae, visible in the last foramen before the apices (Fig. 91, see arrow).

Distribution: *Nitzschia westiorum* is a typical Antarctic endemic and has so far been observed in the Ross Sea Embayment (Taylor Valley, McMurdo, Victoria Land) (Kellogg & Kellogg 2002 and references therein) and East Antarctica (a.o. Spaulding et al. 1997). The species is absent from the Maritime Antarctic Region.

Taxonomical remarks: This taxon was described by West & West (1911) as a variety of *Fragilaria tenuicollis*. West & West (1911) however could not observe in LM the particular ultrastructure outlined above. Baker (1967) found the species in Lake Miers (South Victoria Land) and reported it as *Nitzschia antarctica* (W ET GS WEST) BAKER, a name that was however already in use for a marine species (Okuno 1954). Kellogg et al. (1980) renamed it *Nitzschia westii* in honour of West & West who originally described it. Since Kellogg et al. (1980) stated that the specific epithet was given in honour of both W West & GS West, the name should be '*westiorum*' and not '*westii*' (ICBN, Article 61, McNeill et al. 2006).

Species described as new in this paper

***Luticola pseudomurrayi* VAN DE VIJVER ET TAVERNIER sp. nov.** (Figs 93-110)

Diagnosis: Valvae lanceolatae ad late ellipticae parte centrali paene elliptica apicibusque clare constrictis, late rotundatis, capitatis ad subcapitatis. Longitudo 15.5-50.0 µm, latitudo 7.5-12.0 µm. Area axialis angusta, linearis, leviter dilatata ad aream centralem. Zona hyaline adest in apicibus. Area centralis formans fasciam rectangularem ad transverse-ellipticam, emarginatam striis irregulariter abbreviates. Stigma solitaria adest. Raphe recta, filiformis terminationibus centralibus indistinctis, leviter deflexis. Fissurae terminales curtae, leviter deflexae. Striae radiatae apud aream centralem, magis radiatae ad apices, 17-20 in 10 µm, 21-22 in 10 µm ad apices. Areolae 4-5 per striam, discernendae in microscopio photonico.

Holotypus (here designated): BR-4245 (National Botanic Garden, Meise, Belgium)

Isotypi: PLP-193 (University of Antwerp, Belgium), BRM-ZUHXXX (Hustedt Collection, Bremerhaven, Germany)

Type locality: Lake LA9 (69°12.111'S-39°38.966'E), Langhovde, Lützow Holm Bay, East Antarctica

Etymology: The specific epithet '*pseudomurrayi*' refers to the confusion that has existed for a long time with *Luticola murrayi*.

LM observations: Valves broadly lanceolate to broadly elliptical with an almost elliptical central part and clearly constricted, broadly rounded rostrate to capitate (Figs 93-104). Valve length 15.5-50.0 µm, width 7.5-12.0 µm, apex width 4.5-9.0 µm (n=35). Axial area narrow, linear, slightly widening towards the central area and the apices, where a wedge-shaped hyaline area is present. Central area elliptical to rectangular, bordered by several irregularly shortened striae. One isolated stigma present. Raphe filiform, straight. Central raphe endings simple, weakly deflected away from the stigma. Terminal raphe endings short, weakly deflected. Transapical striae radiate near the valve centre to more or less radiate near the apices, 17-20 in 10 µm to 21-22 near the apices. Each stria composed of 4-5 areolae.

SEM observations: Striae composed of 4-5 transapically elongated areolae of variable size, which sometimes appear to be merged in more eroded valves (Figs 105-107). Striae bordering the central area on the stigma-bearing side composed of 2-3 areolae, on the other side only one areola is present in the striae (Fig. 106). Stigma slit-like externally (Fig. 106). Central raphe endings simple, deflected (Fig. 106). Terminal raphe endings very short, deflected, ending near the last striae (Fig. 107). Internal structure difficult to resolve due to erosion of the valves (Fig.108). Occlusion type unknown due to erosion. Internal stigma opening consisting of an almost rounded, irregularly lipped slit (Fig. 109). Central raphe endings internally slightly deflected towards the stigma, terminating in a weakly raised central nodule. Terminal raphe endings with small helictoglossae (Fig. 110).

Ecology and associated diatom flora: Out of 27 studied lakes (Tavernier et al., unpublished data, Chapter 3) from four regions in Lützow Holm Bay (East and West Ongul Island, Langhovde and Skarvsnes), *L. pseudomurrayi* has been observed in 22 lakes. The largest population was found in lake LA9, where the species occurred co-dominantly with *Chamaepinnularia cymatopleura* in a littoral epipsammic mat sample. The diatom community was furthermore composed of *Amphora veneta* KÜTZING and *Navicula gregaria* DONKIN in relatively small abundances. The lake has an alkaline pH (8.17) with a very high specific conductance (4.03 mS/cm) compared to lakes in the region, and very low nutrient levels. Another important population was found in lake LA8 (Akebi Lake, 69°12.089'S-39°39.047'E), where the community was composed of the same diatom species, along with *Achnanthes brevipes* C.AGARDH and *Navicula phyllepta* KÜTZING in small abundances.

Taxonomical remarks: To date, *Luticola pseudomurrayi* has usually been identified as *Luticola murrayi* on the basis of the original description and illustration of *L. murrayi* by West & West (1911). *L. pseudomurrayi* however does not fit into this description (cf. discussion under *Luticola murrayi*). Even the largest specimens of *L. pseudomurrayi* never have the typical *L. murrayi* valve outline.

L. pseudomurrayi resembles *Luticola gaussii*, a taxon found in similar environments on the Antarctic Continent that was reported and illustrated by West & West (1911) as *Navicula* (*Pinnularia*) *globiceps*. Both species however can be separated by differences in valve outline, shape of the apices and stria structure. *L. gaussii* has a rounded central area

whereas in *L. pseudomurrayi* it is more elliptic-lanceolate. Moreover, *L. gaussii* has distinctly capitate apices with a narrow constriction between the valve center and the apices. This constriction is less pronounced in *L. pseudomurrayi*. The striae in *L. gaussii* are composed of maximum 3, sometimes 4 small areolae (in contrast with *L. pseudomurrayi* which has 4-5 areolae). Other capitate *Luticola* species such as *L. gigamuticopsis* VAN DE VIJVER or *L. caubergsii* VAN DE VIJVER have so far never been observed on the Antarctic Continent and seem to be restricted to the Maritime Antarctic Region (Van de Vijver & Mataloni 2008). *Luticola gigamuticopsis* has a more elliptic valve outline with larger valve dimensions whereas *L. caubergsii* has typically rostrate apices (Van de Vijver & Mataloni 2008). The most widespread *Luticola* species in the Antarctic Region is *L. muticopsis* (VAN HEURCK) DM MANN. However, the valve outline with one straight and one convex margin, the typical raphe system with the short, bent proximal raphe endings and the lower areola number per stria make confusion with *L. pseudomurrayi* entirely impossible (Van de Vijver & Mataloni 2008).

***Chamaepinnularia gibsonii* VAN DE VIJVER sp. nov.** (Figs 111-127)

Diagnosis: Frustulae in aspectu cingulari rectangulares. Cellulae solitariae, numquam formantes colonias. Valvae lineares marginibus parallellis clare triundulatis, apicibusque subcapitatis, late rotundatis, etiam in speciminibus minutissimis. Valvae lanceolatae vel lineari-ellipticae numquam observatae. Longitudo 29-39 µm, latitudo 6.1-7.2 µm. Area axialis lata, linearis, dilatata ad aream centralem. Ad apices, area axialis abrupte dilatata formans zonam hyalinam ellipticam. Area centralis lata, elliptico-lanceolata ad ovalis, formata striis centralibus graduatim abbreviates. Raphe filiformis, recta terminationibus centralibus non deflexis, leviter expansis. Fissurae terminals uncinatae. Striae leviter radiatae in medio parte valvae, convergentes ad apices, 22-24 in 10µm. In apices, striae irregulariter interruptae.

Holotypus (here designated): BR-4246 (National Botanic Garden, Meise, Belgium)

Isotypi: PLP-194 (University of Antwerp, Belgium), BRM-ZUHXXX (Hustedt Collection, Bremerhaven, Germany)

Type locality: Lake 14, Bunger Hills, Antarctic Continent (coll. date January 2000)

Etymology: The species is named after our colleague Dr. John Gibson (University of Tasmania, Australia) in recognition of his Antarctic research.

LM observations: Frustules in girdle view rectangular (Fig. 121). Valves always linear-rectangular with slightly tri-undulated margins and rostrate-capitate, broadly rounded apices. Valve length 29-39 µm, width 6.1-7.2 µm (n=17). Axial area broad, linear, widening to the central area. Near the apices, axial area wider, forming an elliptical to circular hyaline area. Central area wide, elliptic-lanceolate to oval. Raphe filiform, straight to slightly expanded, in LM almost straight central raphe endings. Terminal fissures hooked, distinct in LM. Transapical striae slightly radiate near the valve center, becoming convergent towards the apices, 22-24 in 10 µm. Near the apices, striae appear irregularly interrupted around the raphe sternum.

SEM observations: Externally, alveoli covered by hymen (Fig. 124). Striae continue across the valve face/mantle margin (Fig. 125). Central raphe endings expanded and slightly deflected to the opposite side of the terminal fissures (Figs 122, 124). Terminal fissures long, hooked, continuing onto the mantle (Fig. 122). Internally, alveoli not occluded (Fig. 123). Close to the apices, striae may partly be covered (Fig. 127). Near the valve face/mantle margin, short, blunt spine-like projections are internally present on the virgae (Figs 126, 127; cf. *C. cymatopleura*). Internal central raphe endings bent in the same direction (Fig. 126). Central nodule only weakly developed (Fig. 126). Terminal raphe endings lying in small helictoglossae (Fig. 127).

Ecology and associated diatom flora: So far *C. gibsonii* has only been observed in one lake of the Bunger Hills but due to confusion with the widespread *Chamaepinnularia cymatopleura*, it is possible that the exact distribution is not precisely known. Lake 14 in the Bunger Hills where the species was found, is a relatively large saline lake covered with an orange/brown microbial mat (Gibson et al. 2006). Dominant species in the lake include *Craspedostauros laevissimus*, *Navicula directa* (W SMITH) RALFS, *N. shackletoni* and several so far unidentified *Amphora*, *Navicula* and *Nitzschia* species.

Taxonomical remarks: *Chamaepinnularia gibsonii* closely resembles *C. cymatopleura* (Figs 1-23) but can be separated in valve width shape (6.1-7.2 µm vs. 4.5-5.1 µm in *C. cymatopleura*) and shape (always linear-rectangular). In the typical *C. cymatopleura* populations of the Bunger Hills, valves with a *C. gibsonii* morphology are completely absent despite the fact that specimens of similar length (30-35 µm) were present. Moreover, the apices of *C. gibsonii* are always wider than the valve center, a feature never observed in *C. cymatopleura*. *Chamaepinnularia gibsonii* cannot be confused with other *Chamaepinnularia* species present in the Antarctic Region (such as *C. krookii*, *C. krookiiformis* or *C. australomediocris*, Sterken et al. unpubl. data.).

Acknowledgments

The authors wish to thank Mr. Marcel Verhaegen and Mrs. Myriam de Haan for their technical support with the SEM. Mr. Pierre Compère is thanked for stimulating discussions on the International Code of Botanic Nomenclature. Prof. Dr. David G. Mann is thanked for his valuable taxonomic comments. Dr. Sarah Spaulding is acknowledged for giving us the permission to reproduce the *Luticola murrayi* pictures from the Freshwater Antarctic Diatoms website. Dr. Paolo Cavacini is thanked for the pictures of *Navicula glaberrima*. Dr. David Williams (Natural History Museum) is thanked for sending the West & West slides. Elie Verleyen is a post-doctoral fellow at the FWO.

References

Alfinito S & Cavacini (2000) *Navicula skuae* sp. nov., a freshwater dieton from Continental Antarctica. *Diatom Research,* **15**: 1–9.

Baker AN (1967) Algae from Lake Miers, a solar-heated Antarctic lake. *New Zealand Journal of Botany*, **5**: 453-468.

Barber HG & Haworth EY (1981) A guide to the morphology of the diatom frustule. *Freshwater Biological Association Scientific Publication*, **44**: 1-111.

Brown NE (1920) Some new and old diatoms from the Antarctic Region. *English Mechanic and World of Science*, **111**: 210-211.

Carlson GWF (1913) Süsswasseralgae aus der Antarktis, Südgeorgien und den Falkland Inseln. *Wissenschaftliche Ergebnisse der Schwedischen Südpolar-Expedition 1901-1903, unter leitung von dr. Otto Nordenskjøld*, **4** (Botanique): 1-94 + 3 plates.

Cavacini P, Tagliaventi N, Fumanti B (2006) Morphology, Ecology and distribution of an endemic Antarctic lacustrine diatom: *Chamaepinnularia cymatopleura* comb. nov. *Diatom Research*, **21**: 57-70.

Cox EJ (1999) *Craspedostauros* gen. nov., a new diatom genus for some unusual marine raphid species previously placed in *Stauroneis* Ehrenberg and *Stauronella* Mereschkowsky. *European Journal of Phycology*, **34**: 131-148.

Cremer H, Roberts D, McMinn A, Gore D, Melles M (2003) The Holocene Diatom Flora of Marine Bays in the Windmill Islands, East Antarctica. *Botanica Marina*, **46**: 82-106.

Esposito RMM, Spaulding SA, McKnight DM, Van de Vijver B, Kopalová K, Lubinski D, Hall B, Whittaker T (2008) Inland diatoms from the McMurdo Dry Valleys and James Ross Island, Antarctica. *Botany*, **86**: 1378-1392.

Fritsch FE (1912) Freshwater algae. In: Natural History. London. British Museum. *National Antarctic Expedition 1901-1904. v.6 (Zoology & Botany):* 1-60.

Fritsch FE (1917) Freshwater algae. British Antarctic ("Terra Nova") Expedition, 1910. *Natural History Report*: 1-17.

Gibson JAE, Roberts D, Van de Vijver B (2006) Salinity control of the distribution of diatoms in lakes of the Bunger Hills, East Antarctica. *Polar Biology*, **29**: 694-704.

Grove WB (1919) George Stephen West, MA, DSc, FLS (1876-1919.) *Journal of Botany*, **57**: 283-284.

Håkansson H, and Jones VJ (1994) The compiled freshwater diatom taxa list for the maritime region of the South Shetland and South Orkney Islands. *In*: Hamilton PB (Eds.), Proceedings of the Fourth Arctic-Antarctic Diatom Symposium Workshop, Canadian Technical report of Fisheries and Aquatic Sciences No. **157**: 77-83.

Heiden H, and Kolbe RW (1928) Die marinen Diatomeen der Deutschen Südpolar-Expedition 1901-1903. *In*: Deutsche Südpolar-Expedition 1901-1903 im Auftrage des Reichsministeriums des Innern. (Ed. By E. von Drygalsky), Vol. **8/5** (Botanik): 447-715. Walter de gruyter & co, Berlin und Leipzig.

Hendey NI (1964) An introductory account of the smaller algae of British coastal waters. Part V. Bacillariophyceae (Diatoms). London: her Majesty's Stationery Office. 317pp + 44 plates.

Holmboe JD (1902) IV. *Navicula mutica* Kütz. Aus dem antarktischen Festlande. *Nyt Magazin for Naturvidenskaberne, Christiana*, **40**: 221-222.

Hustedt F (1961-1966) Die Kieselalgen Dutschlands, Österreichs unde der Schweiz mit Berücksicht der übrigen Länder Europas sowie der Angrenzenden Meeresgebiete. *In*: Dr. Rabenhirst Kryptogamen Flora von Deutschland, Österreich und der Schweiz **7**: 1-815.

Kellogg DE, Stuiver M, Kellogg TB, Denton GHD (1980) Non-marine diatoms from Late Wisconsin perched deltas in Taylor Valley, Antarctica. *Palaeogeography, Palaeoclimatology, Palaeoecology*, **30**: 157–189.

Kellogg DE, and Kellogg TB (1987) Diatoms of the McMurdo Ice Shelf, Antarctica. *Palaeogeograpgy, Palaeoclimatology, Palaeoecology*, **60**: 77-96.

Kellogg TB, and Kellogg DE (2002) Non-marine and littoral diatoms from Antarctic and subantarctic regions. Distribution and updated taxonomy. *Diatom monographs*, **1**: 1-795.

Ko-Bayashi T (1963) Variations on some pennate diatoms from Antarctica (Part 1): III. Variations of *Navicula muticopsis* Van Heurck var. *muticopsis* f. *murrayi* (W & GS West) Ko-Bayashi. Japanese Antarctic Research Expedition 1956-1962, Scientific Reports Series E 18: 1-20 + 16 plates.

Krasske G (1938) Beiträge zur Kenntnis der Diatomeenflora von Island und Spitzbergen. *Archiv für Hydrobiologie und Planktonkunde*, **33**: 503-533.

Lange-Bertalot H (2001) *Navicula* sensu stricto, 10 genera separated from *Navicula* sensu lato, *Frustulia*. *Diatoms of Europe*, **2**: 1-526.

McNeill J, Barrie FR, Burdet HM, Demoulin V, Hawksworth DL, Marhold K, Nicolson DH, Prado J, Silva PC, Skog JE, Wiersema JH, Turland NJ (2006) International Code of Botanical Nomenclature, Vienna Code. ARG Gantner Verlag KG, Ruggell, Liechtenstein.

Mills FW (1933-1935) An index to the genera and species of the Diatomaceae and their synonyms 1816-1932. London, Wheldon & Wesley.

Okuno H (1954) Electron microscopical study on Antarctic diatoms. *Journal of Japanese Botany*, **29**: 18-25.

Paddock TBB (1988) *Plagiotropis* PFITZER and *Tropidoneis* CLEVE, a summary account. *Bibliotheca Diatomologica*, **16**: 1-152.

Patrick R, and Reimer CW (1975) The diatoms of the United States exclusive of Alaska and Hawaii. Entomoneidaceae, Cymbellaceae, Gomphonemaceae, Epithemiaceae. *Monographs of the Academy of Natural Sciences of Philadelphia,* **2**: 213pp.

Roebuck WD (1914) In memory of William West (1848-1914.) (with portrait). *Journal of Botany*, **52**: 161-164.

Round FE, Crawford RM, Mann DG (1990) The diatoms. Biology & Morphology of the genera. Cambridge University Press, Cambridge, UK. 747pp.

Sabbe K, Verleyen E, Hodgson DA, Vanhoutte K, Vyverman W (2003) Benthic diatom flora of freshwater and saline lakes in the Larsemann Hills and Rauer Islands, East-Antarctica. *Antarctic Science*, **15**: 227-248.

Spaulding SA, and Stoermer EF (1997) Taxonomy and distribution of the genus *Muelleria* Frenguelli. *Diatom Research*, **12**: 95-115.

Spaulding SA, McKnight DM, Stoermer EF, Doran PT (1997) Diatoms in sediments of perennially ice-covered Lake Hoare, and implications for interpreting lake history in the dry valleys region of Antarctica. *Journal of Paleolimnology*, **17**: 403-420.

Spaulding SA, Kociolek JP, Wong D (1999) A taxonomic and systematic revision of the genus *Muelleria* (Bacillariophyta). *Phycologia*, **38**: 314-341.

Spaulding S, Esposito R, Lubinski D, Horn S, Cox M, McKnight D, Alger A, Hall B, Mayernick M, Whittaker T, Yang C (2011) Antarctic Freshwater Diatoms web site, McMurdo Dry Valleys LTER, visited 18 Mar 2011 at http://huey.colorado.edu/diatoms/

Van de Vijver B, Beyens L, Lange-Bertalot H (2004) The genus *Stauroneis* in Arctic and Antarctic locations. *Bibliotheca Diatomologica*, **51**: 1-311.

Van de Vijver B, and Mataloni G (2008) New and interesting species in the genus *Luticola* D.G. MANN (Bacillariophyta) from Deception Island (South Shetland Islands). *Phycologia*, **47**: 451-467.

Van de Vijver B, Mataloni G, Stanish L, Spaulding SA (2010) New and interesting species of the genus *Muelleria* (Bacillariophyta) from the Antarctic Region and South Africa. *Phycologia*, **49**: 22-41.

Van de Vijver B, Sterken M, Vyverman W, Mataloni G, Nedbalová L, Kopalová K, Elster J, Verleyen E, Sabbe K (2010) Four new non-marine diatom taxa from the Subantarctic and Antarctic Regions. *Diatom Research*, **25**: 431-443.

Van der Werff A (1955) A new method for cleaning and concentrating diatoms and other organisms. *Verhandlungen der Internationalen Vereinigung für theoretische und angewandte Limnologie*, **12**: 276-277.

Van Heurck H (1909) Diatomées. *In*: Résultats du Voyage du SY Belgica en 1897-1898-1899. Rapports Scientifiques. Botanique 6: 1-129. Antwerpen: Imprimerie J-E Buschmann.

Wasell A, and Håkansson H (1992) Diatom stratigraphy in a lake on Horseshoe Island, Antarctica: a marine-brackish-freshwater transition with comments on the systematics and ecology of the most common diatoms. *Diatom Research*, **7**: 157–194.

Wasell A (1993) Diatom Stratigraphy and evidence of Holocene environmental changes in selected lake basins in the Antarctic and South Georgia. Stockholm University, Department of Quaternary Research, PhD Thesis.

West W, and West GS (1911) Freshwater algae. British Antarctic Expedition (1907-1909) Science Report, Biology **1**: 263-298.

Figure captions

Figures 1-23. *Chamaepinnularia cymatopleura*. Figs 1-11. Light microscopical images of a population present on the original W. & G.S. West slides. Fig. 12. Girdle view from the original population. Figs 13-16. LM images of *Navicula deltaica* and *Navicula quaternaria* from the type slide C14-77-1. Figs 17-18. Original drawings from West & West (1911). Fig. 19. Scanning Electron Microscope (SEM) external view of an entire valve. Fig. 20. SEM external view of the central area of an eroded valve. Note the striae running over the valve face/mantle margin. Fig. 21. SEM internal view of an entire valve. Fig. 22. SEM internal detail of the apex with a small helictoglossa. Fig. 23. SEM internal view of the central area. Note the presence of blunt spines on the virgae. Scale bar represents 10 µm except for figs. 19-23 where scale bar = 2 µm.

Figures 24-39. *Craspedostauros laevissimus*. Figs 24-30. Light microscopical images of a population present on the original W. & G.S. West slides. Figs 31-35. Original drawings from West & West (1911). Fig. 36. Scanning Electron Microscope (SEM) external view of the central area. Fig. 37. SEM external detail of the areola structure. Fig. 38. SEM external view of the apex. Fig. 39. SEM internal view of the central area. Scale bar represents 10 µm except for figs. 36-39 where scale bar = 1 µm.

Figures 40-43. *Craticula glaberrima*. Figs 40-42. Light microscopical images of a population present on the original W. & G.S. West slides. Fig. 43. Original drawing from West & West (1911).

Figures 44-50. *Luticola murrayi*. Figs 44-48. Light microscopical images of a population on the Antarctic Continent (photos: courtesy of Dr. Sarah Spaulding). Fig. 49. Original drawing of *Navicula murrayi* by West & West (1911). Fig. 50. Original drawing of *Navicula murrayi* var. *elegans* by West & West (1911).

Figure 51. *Navicula muticopsiforme*. Fig. 51. Original drawing by West & West (1911).

Figures 52-62. *Muelleria peraustralis*. Figs 52-54. Light microscopical images of a population present on the original W. & G.S. West slides. Fig. 55. Original drawings by West & West (1911). Fig. 56. Scanning Electron Microscope (SEM) external view of an entire valve. Fig. 57. SEM external view of the apex with the bifurcating terminal raphe fissure and the presence of canal puncta. Fig. 58. SEM external view of the central area. Fig. 59. SEM external view of the areolae. Fig. 60. SEM internal view of an entire valve. Fig. 61. SEM internal view of the central area with the rectelevatum. Fig. 62. SEM internal view of the apex showing the longitudinal canals and the helictoglossa. Scale bar represents 10 µm except for fig. 57 where scale bar = 1 µm.

Figures 63-81. *Navicula shackletoni*. Figs 63-70. Light microscopical images of a population present on the original W. & G.S. West slides. Figs 71-73. Original drawings of *Navicula shackletoni* by West & West (1911). Figs. 74-75. Original drawings of *Navicula shackletoni* var. *pellucida* by West & West (1911). Fig. 76. Scanning Electron Microscope (SEM) external view of an entire frustule in girdle view. Fig. 77. SEM external view of two entire valves. Fig. 78. SEM internal view of an entire valve. Fig. 79. SEM external view of the central area. Fig. 80. SEM internal view of the central area. Fig. 81. SEM internal view of the apex with the helictoglossa. Scale bar represents 10 µm except for figs. 79-81 where scale bar = 1 µm.

Figures 82-92. *Nitzschia westiorum*. Figs 82-87. Light microscopical images of a population present on the original W. & G.S. West slides. Fig. 88. Original drawings of *Fragilaria tenuicollis* var. *antarctica* by West & West (1911). Fig. 89. Scanning Electron Microscope (SEM) external view of an entire valve. Fig. 90. SEM external detail of the striae with 2-3 rows of areolae. Fig. 91. SEM internal view of the valve apex with the helictoglossa. Fig. 92. SEM internal view of the striae showing the absence of fibulae. Scale bar represents 10 µm except for figs. 90-92 where scale bar = 1 µm.

Figures 93-110. *Luticola pseudomurrayi*. Figs 93-104. Light microscopical images of the type population of Langhovde, Antarctica. Fig. 105. Scanning Electron Microscope (SEM) external view of

an entire valve. Fig. 106. SEM external detail of the central area showing the position of the stigma. Fig. 107. SEM external detail of the apex with the very short terminal fissures. Fig. 108. SEM internal view of an entire valve. Fig. 109. SEM internal view of the central area. Fig. 110. SEM internal view of the valve apex with the helictoglossa. Scale bar represents 10 µm except for figs. 106-107 and 109-110 where scale bar = 1 µm.

Figures 111-127. *Chamaepinnularia gibsonii*. Figs 111-120. Light Microscopical (LM) images of the type population of Bunger Hills, Antarctica. Fig. 121. LM girdle view. Fig. 122. Scanning Electron Microscope (SEM) external view of an entire valve. Fig. 123. SEM internal view of an entire valve. Fig. 124. SEM external detail of the central area of an non-eroded valve. Fig. 125. SEM external detail of the valve face/mantle margin of an eroded valve. Note the uninterrupted striae continuing over the margin. Fig. 126. SEM internal view of the central area. Fig. 127. SEM internal view of the valve apex with the helictoglossa. Scale bar represents 10 µm except for figs. 124-127 where scale bar = 1 µm.

Table 1. List of West & West samples present in the Natural History Museum, London.

Slide number	Sample description	Collector	Additional information on slide label
BM 34116	Green Lake, Cape Royds	Coll. J. Murray	G.S. West, Rec'd 8.12.1911
BM 34117	Lake W. side of McMurdo Sound, Jan 1909.	Coll. R.E. Priestley	G.S. West, Rec'd 8.12.1911
BM 34118	Lake W. side of McMurdo Sound, Jan 1909.	Coll. R.E. Priestley	G.S. West, Rec'd 8.12.1911
BM 34119	Lake W. side of McMurdo Sound, Jan 1909.	Coll. R.E. Priestley	G.S. West, Rec'd 8.12.1911
BM 34120	Moraine, Mt. Erebus.	?	G.S. West, Rec'd 8.12.1911
BM 34121	Clear Lake, Cape Royds	Coll. J. Murray	G.S. West, Rec'd 8.12.1911
BM 34122	Clear Lake, Cape Royds	Coll. J. Murray	G.S. West, Rec'd 8.12.1911
BM 34123	Dried up Lake, Cape Royds.	?	G.S. West, Rec'd 8.12.1911
BM 34124	Moraine, Mt. Erebus.	?	G.S. West, Rec'd 8.12.1911
BM 34125	Pony Lake, Cape Royds	Coll. J. Murray	G.S. West, Rec'd 8.12.1911
BM 34126	Moraine, Mt. Erebus.	?	G.S. West, Rec'd 8.12.1911
BM 34127	Cape Royds, Ross Island.	?	G.S. West ?
BM 34128	Clear Lake, Cape Royds	Coll. J. Murray	G.S. West, Rec'd 8.12.1911
BM 34129	Pond, Cape Royds.	Coll. J. Murray	G.S. West, Rec'd 8.12.1911
BM 34130	Pond, Cape Royds.	Coll. J. Murray	G.S. West, Rec'd 8.12.1911
BM 34131	Green Lake, Cape Royds	Coll. J. Murray	G.S. West, Rec'd 8.12.1911
BM 34132	Green Lake, Cape Royds	Coll. J. Murray	G.S. West, Rec'd 8.12.1911

BM 34202	Pony Lake, Cape Royds	Coll. J. Murray	G.S. West, Rec'd 21.5.1920
BM 34228	Brit. Antarctica Expediton (Terra Nova), 1910, Cape Adare.	Fritsch slide	
BM 34229	Brit. Antarctica Expediton (Terra Nova), 1910, Cape Adare.	Fritsch slide	

Table 2. List of recent samples used for the Scanning Electron Microscopy analysis.

Sample ID	**Sampling date**	**Sample location**	**Habitat**	**Published in**
BH11	January 2000	Bunger Hills, East Antarctica	microbial mat	Gibson et al. (2006)
BH14	January 2000	Bunger Hills, East Antarctica	microbial mat	Gibson et al. (2006)
C14-77-1B	1977	Taylor Valley, Victorialand, Antarctica	sediment core	Kellogg et al. (1980)
Lake LA9	2009	Langhovde	microbial mat	unpublished

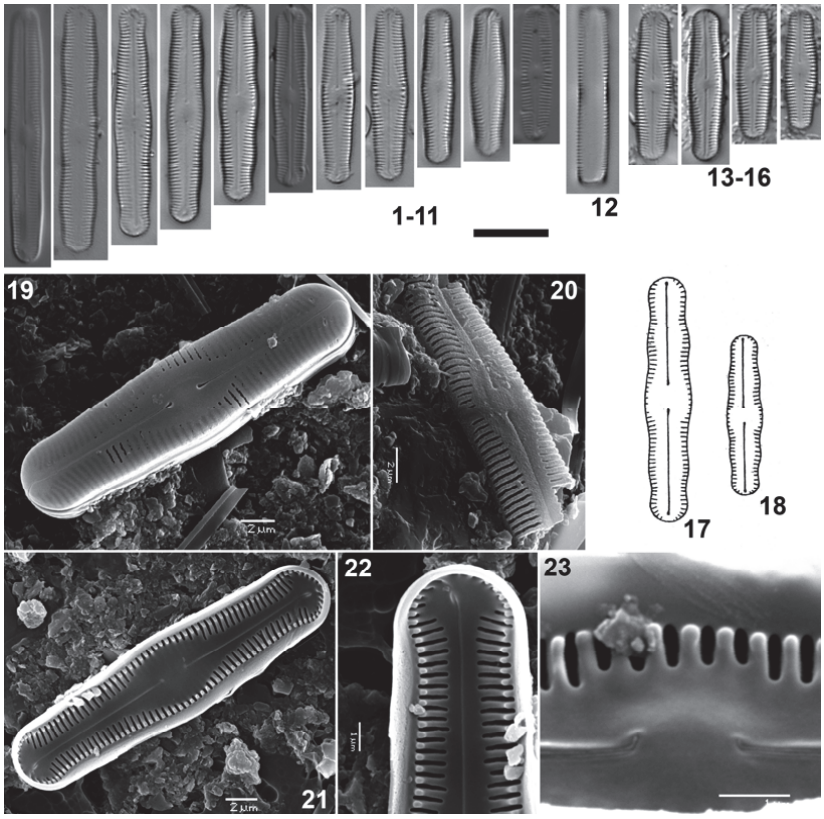
1-11
12
13-16
19
20
17
18
21
22
23

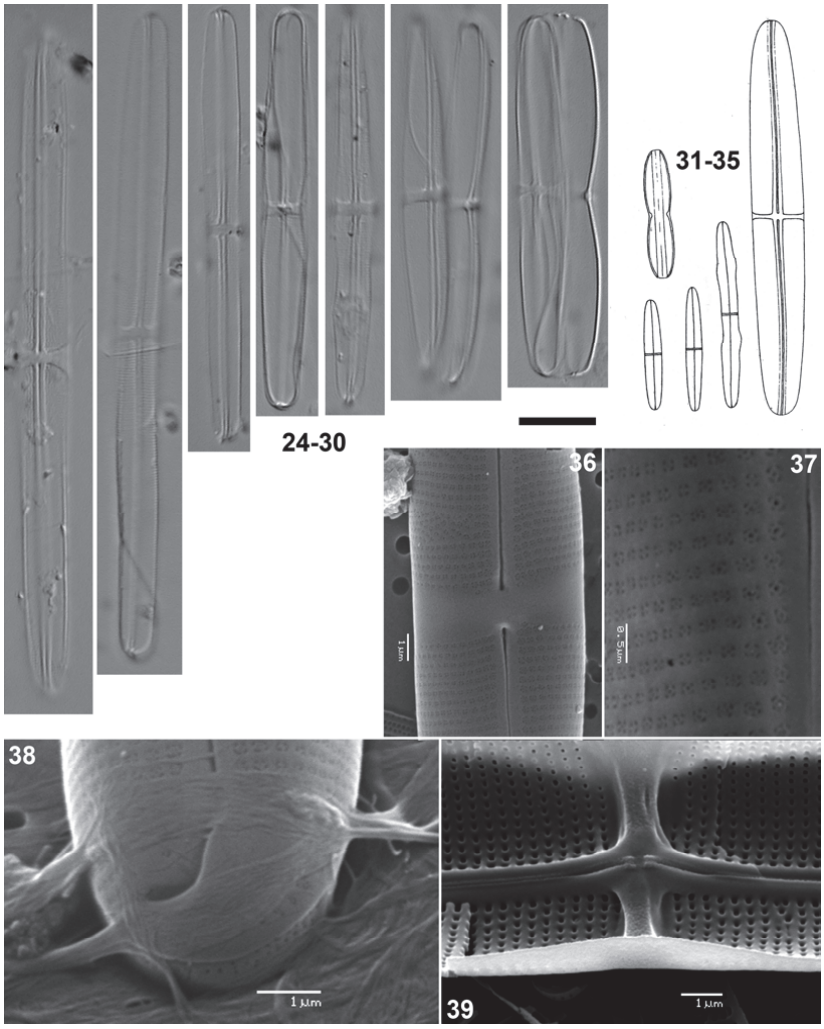
24-30
31-35
36
37
38
39
1 µm
1 µm
1 µm
1 µm

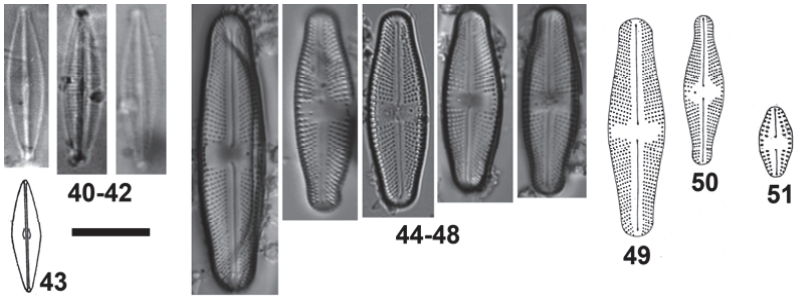
40-42
43
44-48
49
50
51

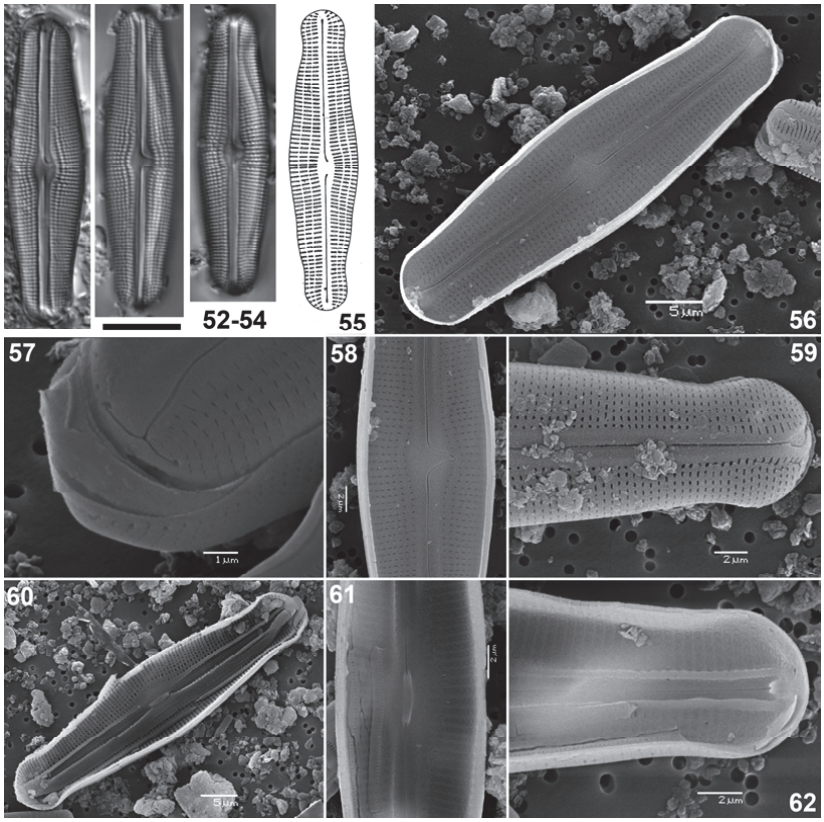
52-54
55
5 µm
56
57
1 µm
58
2 µm
59
2 µm
60
5 µm
61
2 µm
62
2 µm

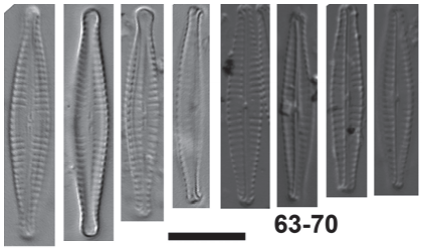
63-70

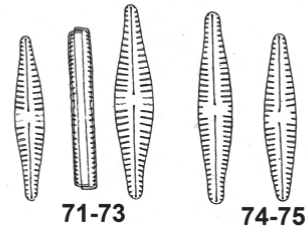
71-73
74-75

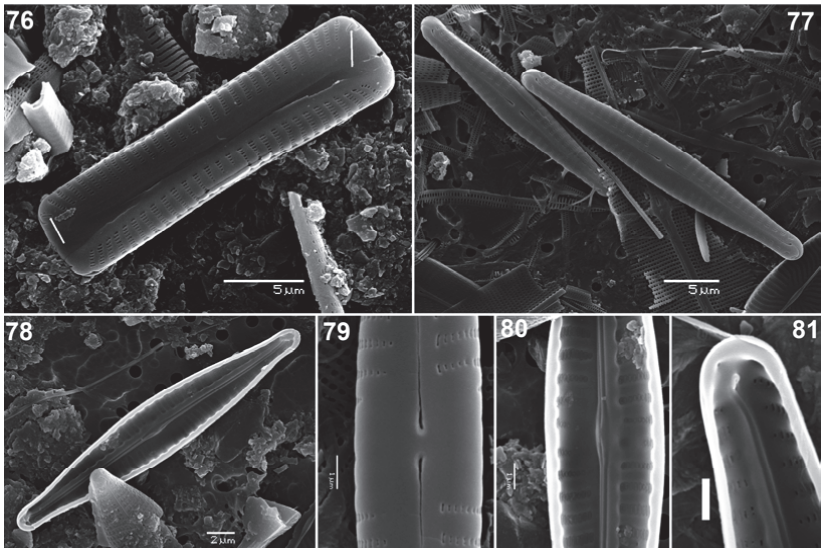
76
5 µm
77
5 µm
78
2 µm
79
80
81

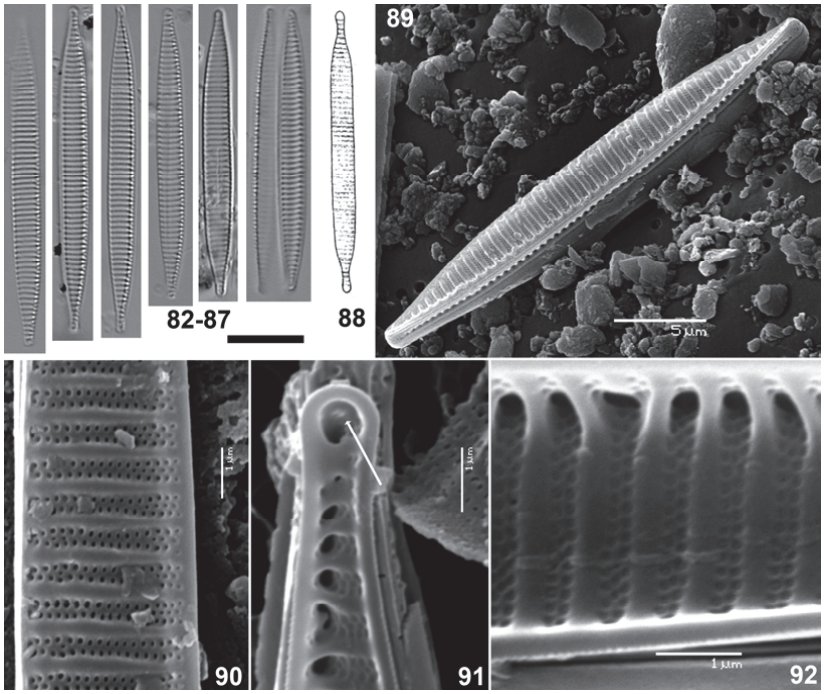
82-87
88
89
5 µm
90
1 µm
91
1 µm
92
1 µm

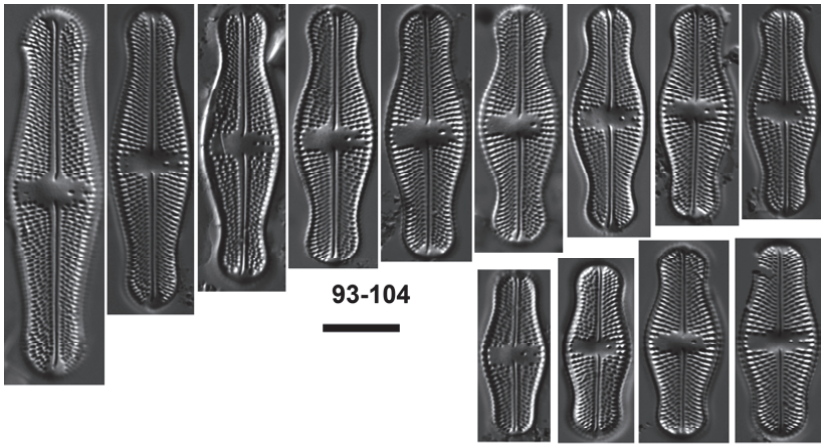
93-104

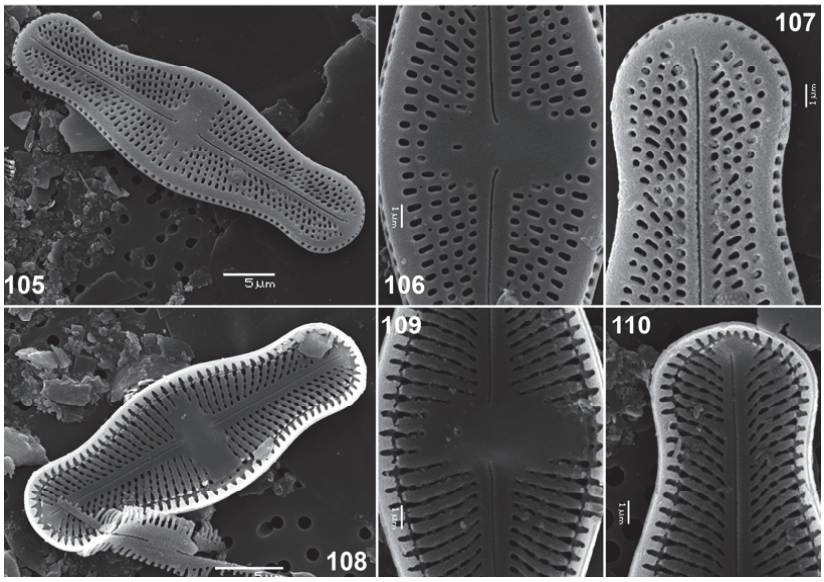
105
5 µm
106
1µm
107
1µm
108
109
1µm
110
1µm

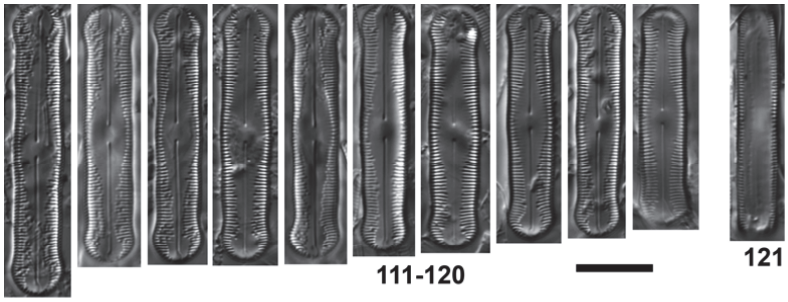
111-120
121

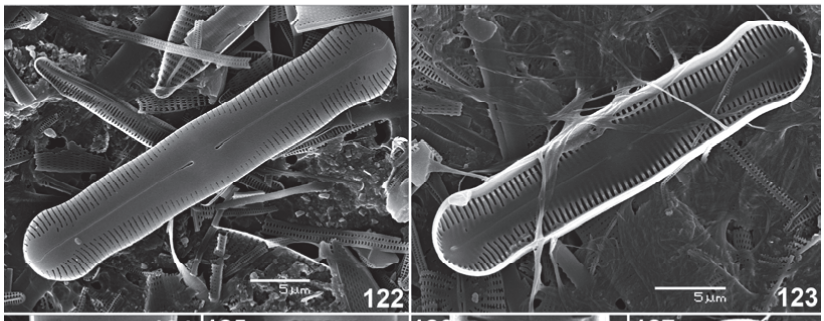
5 µm
122
5 µm
123

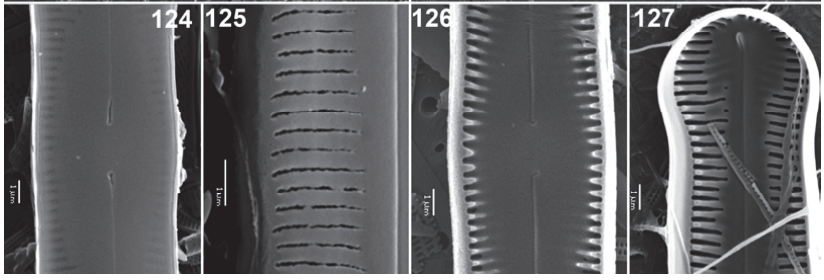
124
125
126
127

Chapter 3. Absence of a Medieval Climate Anomaly, Little Ice Age and Twentieth Century Warming in Skarvsnes, Lützow Holm Bay, East Antarctica

Running title: Palaeoclimate changes in Skarvsnes

PUBLISHED PAPER. Ines Tavernier, Elie Verleyen*, Dominic A. Hodgson, Katrien Heirman, Stephen J. Roberts, Satoshi Imura, Sakae Kudoh, Koen Sabbe, Marc De Batist, Wim Vyverman (* shared first authorship). Antarctic Science (in press).*

Key-words: Syowa Oasis, diatom-based transfer function, isolation basin, palaeoclimatology, Holocene climate changes

Abstract

Palaeoclimate changes such as the Medieval Climate Anomaly and the Little Ice Age, are well-defined in the Northern Hemisphere during the past 2000 years. In contrast, these anomalies appear to be either absent, or less well-defined, in high-latitude regions of the Southern Hemisphere. Here, we inferred environmental changes during the past two millennia from proxies in a sediment core from Mago Ike, an East Antarctic lake in Skarvsnes (Lützow Holm Bay). Variations in lake primary production were inferred from fossil pigments, sedimentological and geochemical proxies and combined with absolute diatom counts to infer past diatom productivity and community changes. Three distinct stratigraphic zones were recognized, resulting from a shift from marine to lacustrine conditions with a clear transition zone in between. The presence of open-water marine diatoms indicates a coastal zone seasonally free of sea-ice between c. 2120 and 1500 cal. yr BP. Subsequently the lake became isolated from the ocean due to isostatic uplift. Freshwater conditions were established from c. 1120 cal. yr BP onwards after which the proxies are considered highly sensitive to temperature changes. There is no evidence for a Medieval Climate Anomaly, Little Ice Age or Twentieth Century Warming in our lake sediment record suggesting that studies that have force-fitted Northern Hemisphere climate anomalies onto Southern Hemisphere palaeoclimate records should be treated with caution.

Introduction

The past two millennia are of particular interest to the understanding of the Earth's climate system because, apart from the human-induced rise in greenhouse gas concentrations, the boundary conditions of the climate system have not changed dramatically. During this period, the Northern Hemisphere (NH) experienced three main climate anomalies, namely the Medieval Climate Anomaly (MCA; 1050 - 650 yr BP), the Little Ice Age (LIA; 500 - 100 yr BP) and the recent temperature increase (Twentieth-Century Warming, TCW) (Mann *et al.* 2009). In the Southern Hemisphere (SH) high-latitudes, these climate anomalies appear to be either absent from palaeoclimate records or their relative intensities and timings are regionally inconsistent (Verleyen *et al.* 2011 in Appendix 2).

In the NH, the MCA started with a rate of temperature increase which exceeded that of the modern late-20th century (1961 - 1990 AD) in some regions, but remained below the most recent global temperature rise (from 1990 AD onwards; Mann *et al.* 2009). It has been observed in palaeoclimate reconstructions from the North Atlantic region, Southern Greenland, the Eurasian Arctic and parts of North America (Mann *et al.* 2009). Evidence for an event coeval with the MCA in Antarctica, or even in the SH, seems to be rather limited and far from unequivocal (Bentley *et al.* 2009, Verleyen *et al.* 2011 in Appendix 2). In the Antarctic Peninsula (AP), there is some evidence of a warm event coeval with the MCA, but these reconstructions are mostly limited to marine records (Bentley *et al.* 2009 and references therein). In most continental ice cores, there is no evidence for a well-defined temperature rise during or following the NH MCA (Masson *et al.* 2000). In addition, there is no or only limited palaeoenvironmental evidence along the Antarctic coastline for an event equivalent to the NH MCA (Bentley *et al.* 2009, Verleyen *et al.* 2011 in Appendix 2).

The LIA is observed in almost all NH records and culminated between 500 and 100 yr BP when NH summer temperatures dropped significantly below the mean of the second half of the 20th century (Matthews & Briffa 2005). As with the MCA, the LIA is regarded as a NH phenomenon with only limited evidence in certain places in Antarctica for a climate anomaly with similar features and timing (Bertler *et al.* 2011, Verleyen *et al.* 2011 in Appendix 2). A mild 'LIA'-event has been reported from the Vestfold Hills, as a period of lower evaporation between c. 200 and 150 yr BP (Roberts *et al.* 2001). In the McMurdo Dry Valleys, the Wilson Piedmont Glacier was more extensive in some areas between 400 and 100 yr BP than today (Hall & Denton 2002). However, the magnitude of this change was less than the glacier advances recorded in the NH during the LIA (Hall & Denton 2002), and no other glacier advances have been reported simultaneously across the Antarctic continent at the same time. Lake sediment (e.g. Roberts *et al.* 2001), ice core and marine sediment core evidence (e.g. Bertler *et al.* 2011) are thus equivocal, as recorded cold palaeoclimate anomalies of the last 2000 years appear to be rather mild, short in duration, and occurred only at a local scale.

Globally, the TCW is most pronounced in the Arctic and the AP. In the AP, temperatures have increased at > 0.1°C per decade during the past 50 years and in the Arctic, a modest temperature increase near the start of the 20th century has been followed by a sharp increase over the past 30 years (Turner *et al.* 2007). In East Antarctica (EA), the climate shows complex temperature patterns, with non-significant cooling in some regions, but the continent-wide average is slightly positive (Steig *et al.* 2009). Trends associated with continental Antarctica are less clear although a precipitation anomaly is present in the Law Dome ice core near the coast of Wilkes Land, with snow accumulation during the past few decades exceeding natural variability of the past 750 years (van Ommen & Morgan 2010). On the AP, recent studies revealed that a gradual warming interrupted Neoglacial cooling already c. 600 years ago (Sterken *et al.* 2012) followed by accelerated warming in the last 100 years (Mulvaney et al. 2012).

It is still not certain whether the observed differences in the timing and amplitude of climate anomalies between both hemispheres during the past two millennia are real or rather related to the overall lack of comparable well-dated palaeoclimate

reconstructions from the SH (Mann *et al.* 2009, Verleyen *et al.* 2011 in Appendix 2). Antarctic ice cores from the continental plateau are often unable to fully resolve climates of the past two millennia, being better suited to track past atmospheric composition and temperature variability over glacial-interglacial cycles. Coastal ice cores are often more sensitive to small-scale climate anomalies, but are relatively rare because coastal ice-sheets are dynamic. A valuable alternative is lake sediment records.

In EA, lake sediments record quantitative changes in the moisture balance which can be reconstructed using diatom-based inference models. The moisture balance, and therefore salinity and specific conductance in East Antarctic lakes is a complex balance between inputs of meltwater from multi-year snow banks and glaciers in the catchment area and precipitation, and outputs including evaporation and sublimation. The latter are affected by both increasing temperature and wind strength. Conversely, decreased wind speeds and lower temperatures lead to lower evaporation and sublimation rates, positively affecting the moisture balance (Verleyen *et al.* 2012 in Appendix 1). However, this relationship is complicated in regions where (katabatic) winds transport snow from the interior to the coastal regions. Primary production in polar lakes is, in turn, a function of surface air temperatures. Increased air temperatures generally result in higher water temperatures and an increase in the number of ice-free days (Quayle *et al.* 2002). Furthermore, in Maritime Antarctica and the AP, soil development on newly exposed ice-free ground in lake catchments can result in increased nutrient export leading to a further increase in lake primary production. These multiple changes have been shown to be amplified in maritime Antarctic lakes, and have resulted in an extreme ecological response to the recent temperature changes (Quayle *et al.* 2002). Proxy data for lake primary production such as organic matter accumulation and fossil pigment concentrations have been shown to be sensitive tools for reconstructing past temperature variability and have provided detailed records of the MCA and the LIA in for instance the Canadian Arctic (MacDonald *et al.* 2009). In Antarctica, proxies for lake primary production have enabled the detection of millennial-scale Holocene warm periods (Verleyen *et al.* 2011 in Appendix 2, Sterken *et al.* 2012) and short-term temperature excursions during the Early-Holocene, but so far, there is limited evidence for the MCA and LIA in lake sediment cores from the Antarctic margin (Verleyen *et al.* 2011 in Appendix 2).

Here we aim to study palaeoenvironmental changes occurring during the past two millennia in Skarvsnes, Lützow Holm Bay (69°00'S - 39°35'E; Fig. 1) (EA) using a high-resolution, well-dated palaeolimnological approach. Fluxes of fossil pigments were used to reconstruct temperature-related changes in lake primary production. This was combined with fluxes of total carbon (TC) as well as absolute diatom counts to infer past diatom production. Past changes in the moisture balance were quantitatively reconstructed using a newly developed diatom-based transfer function.

Site description

Several ice-free areas and islands are present along Syowa Coast in Lützow Holm Bay. These include East and West Ongul Island (Fig. S1 in the Supplementary Material), and the two main peninsulas Langhovde (Fig. S2 in the Supplementary Material) and Skarvsnes (Fig. 1). Lakes range from hypersaline and dry lake beds in low-altitude areas in Skarvsnes

and on the eastern part of Langhovde to freshwater lakes in the other areas. Low-altitude lakes have been isolated from the sea following postglacial isostatic uplift (Bentley *et al.* 2005) and subsequently became hypersaline due to evaporation or diluted as a result of meltwater inputs from snow banks in their catchment areas (Roberts & McMinn 1996; Verleyen *et al.* 2012 in Appendix 1). These lakes, called isolation basins, contain both marine and lacustrine sediments.

Mago Ike (SK1; 69°28.450'S - 39°36.674'E) is an isolation basin situated at 1.5 m above sea-level (a.s.l.) on Kizahasi Beach in Skarvsnes (Fig. 1) and is seasonally ice-free. The lake is characterized by a maximum depth of 5.8 m, a pH of 8.95 and a specific conductance of 0.48 mS/cm. During the time of sampling, the water-column was completely mixed and the lake was fed by a small meltwater stream. Mago Ike was specifically chosen for this study on account of its high sediment accumulation rate during the past two millennia, which enabled the transition from marine-lacustrine sediments and post-isolation palaeoenvironmental changes to be studied at a higher temporal resolution than is available in other small Antarctic lakes our research group have generally studied (e.g. Sterken *et al.* 2012).

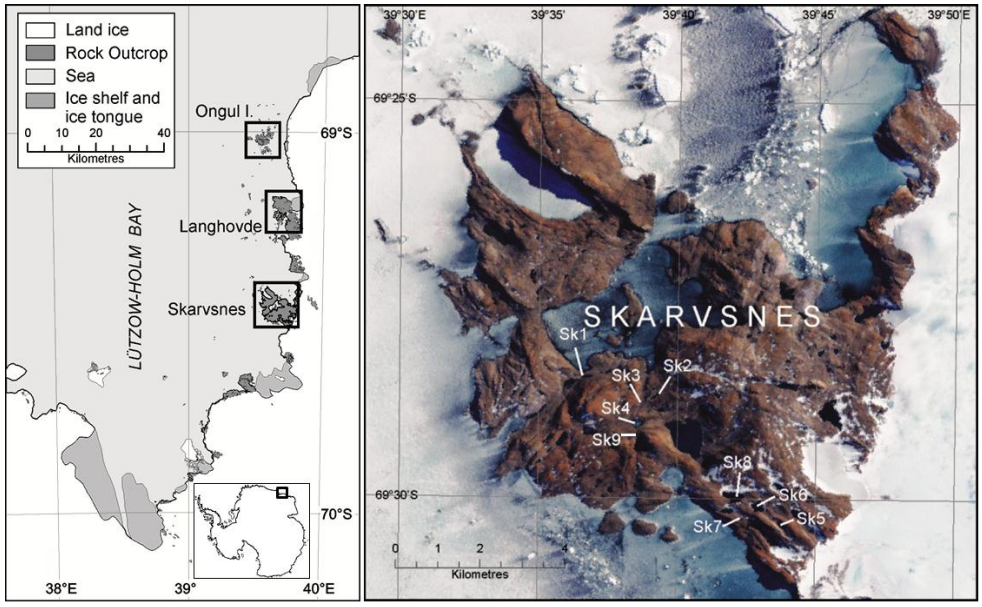

Figure 1. Map of Lützow Holm Bay, East Antarctica with boxes showing the four study areas (the Ongul Islands, Langhovde and Skarvsnes) along with a detailed satellite image of the main study region Skarvsnes. Study lakes on Skarvsnes on which the transfer function is based are indicated with codes Sk1-9. Mago Ike is indicated as Sk1. For a detailed map of the Ongul Islands and Langhovde (with indication of the study lakes included in the transfer function), the reader is referred to respectively Fig. S1 and S2 in the Supplementary Material. Inset shows the position of the Lützow Holm Bay region relative to the Antarctic continent.

Methods

Transfer function and calibration data set

Surface sediments and water-chemistry data were collected from 27 lakes in Lützow Holm Bay. Surface sediments generally consisted of benthic microbial mats and were collected from the deepest part of the lakes and from the littoral zones with a UWITEC gravity corer, and manual sampling, respectively. Samples were stored at -20°C. Limnological data included measurements of water-column specific conductance, pH, oxidation-reduction potential (ORP), and lake water depth. These parameters were measured using a YSI 600 water-quality meter. Water samples for analyses of major ions (Mg, K, Ca, Fe, Na, SO_4, Al), nutrients (silicate, NH_4-N, total nitrogen, NO_3-N, PO_4-P), total organic carbon (TOC) and dissolved organic carbon (DOC) were collected in acid-washed Nalgene bottles and frozen prior to analysis. Methods are described in more detail in Verleyen *et al.* (2012 in Appendix 1).

Sediment coring, lithostratigraphical, geophysical and geochemical analysis

Fieldwork took place in January 2007. Sediments were collected at the deepest part of the lake using a UWITEC gravity corer for the upper 57 cm of the sediments and a square-rod piston sampler for the deeper sediments, with an overlap of at least 20 cm between four successive drives to a total of 254 cm.

Before splitting, the sediment cores were scanned with a GEOTEK multi-sensor core logger measuring gamma ray density (GRD) and volume-specific magnetic susceptibility (MS) in 0.2-cm steps. GRD was converted to dry bulk density (DBD) by using a dry weight conversion factor. To obtain this, a weighted sample was dried for 48h at a temperature of 60°C in an oven and subsequently re-weighted. The percentage dry weight was calculated as the ratio between the weight of the dried sample to that of the wet sample. Volume-specific MS was used to correlate different overlapping sections of the sediment cores and has been converted to mass-specific MS by dividing it by the DBD. This was subsequently used to calculate the mass accumulation rate (MAR) (as in Street-Perrot *et al.* 2007). Macroscopic descriptions included sediment texture (qualitative grain size, sorting, etc.) and structure (laminations, grading, etc.).

Concentrations of TC and total nitrogen (TN) were carried out using a Flash 2000 Organic Elemental Analyzer (subsamples taken at maximum 8-cm interval). These measurements were carried out by dry combustion at high temperature (left furnace: 950°C and right furnace: 840°C) followed by separation and detection of the gaseous products. The data were processed using the Eager Xperience software. Reproducibility and reliability of the analyses were tested using standards of sulphanilamide. Caution is required when interpreting TC as a palaeoproductivity indicator because besides organic carbon, this can also include inorganic carbonates. Therefore, TC is only used to support palaeoproductivity indications of fluxes of chlorophylls, carotenoids and diatoms.

Chronology

Nineteen samples from the Mago Ike sediment cores were dated using AMS ^{14}C by the UK Natural Environment Research Council (NERC) Radiocarbon Laboratory and/or the Beta Analytic Radiocarbon Dating Laboratory. The results are reported as conventional radiocarbon years BP with two-sigma (2σ) standard deviation errors. Absolute percentage of modern carbon (pMC) data were corrected according to ^{13}C/^{12}C isotopic ratios from measured pMC, where a 'modern' pMC value is defined as 100% (AD 1950), and the 'present-day' pMC value is defined as 107.5% (AD 2010). Calibration of ^{14}C ages was carried out in OXCAL v. 4.1 (Bronk Ramsey 2009). The pMC values from samples at 0.5, 3.5, 5.5, 9.5 and 13.5 cm depth, which returned a 'modern' radiocarbon age, were calibrated in CALIBomb using the SH1 compilation of SH datasets (Hua & Barbetti 2004; Calibration curve A; Table 1 & S1 in the Supplementary Material). Freshwater samples were calibrated using the SHCal04.14C SH atmosphere dataset (McCormac *et al.* 2004; Calibration curve B; Table 1 & S1). In the marine-influenced sections of the core, the Marine09 calibration curve (100% marine) was used (Reimer *et al.* 2009). The Antarctic marine reservoir effect for this locality was constrained by using a ΔR value of 720 ± 100 years based on 1120 ± 100 years minus the global marine reservoir of 400 years (Calibration curve C; Table 1 & S1). This value is recommended as a regional correction for the Lützow Holm Bay region; the error of ± 100 years was calculated from original radiocarbon data in Yoshida & Moriwaki (1979).

Radiocarbon age data are reported as conventional radiocarbon years BP (^{14}C yr BP) ± 1σ, and as 2σ (95.4%) calibrated age ranges, mean ± 1σ, and median calibrated ages (cal. yr BP relative to AD 1950) (Table 1 & S1 in the Supplementary Material). Calibrated ages are rounded to the nearest 5 years where measured radiocarbon age errors were less than ± 50 ^{14}C years and to the nearest 10 years where measured radiocarbon age errors were greater than ± 50 ^{14}C years.

The most likely age-depth sequence of calibrated ages was determined in OXCAL v. 4.1 using 95.4%, 2σ error calibration data, and a standard Poisson distribution Bayesian age-depth deposition model, which was applied separately to lacustrine and marine sediments (flexibility, k, was set to 100, and MCMC set to 1000k). Interpolated ages in the text were rounded to the nearest 10 years and derived from the 'best-fit' age of the CLAM v. 2.1 (Blaauw 2010) age-depth models.

Diatom analysis

Quantitative diatom analysis followed standard methods (Sabbe *et al.* 2003). Diatoms were counted using a Zeiss axiophot light microscope under oil immersion with at least 400 valves (> 2/3 intact or unmistakably the middle part of the raphe system) counted in each sample, except for 13 samples in the surface dataset in which diatom concentrations were too low. 97 samples were analyzed from the core (subsamples taken at a maximum 4-cm interval) and 68 surface samples were analyzed from regional lakes and ponds to develop the calibration dataset. Where possible, more than one sample was taken to ensure that the different habitats (e.g. littoral vs. deep water) were included in the dataset. *Chaetoceros* resting spores were counted in addition to the diatom valves.

Taxonomic identification was mainly based on Sabbe *et al.* (2003) for the lacustrine diatoms and Cremer *et al.* (2003) for the marine diatoms.

Fossil pigment analysis

Fossil pigments were extracted and analyzed following standard methods (Van Heukelem & Thomas). The High Performance Liquid Chromatography (HPLC) components included an Agilent 1100 HPLC, pump, auto-sampler, DAD-diode-array detector and Agilent Eclipse XDB-C8 column. The method uses three solvents, methanol (80%) - ammonium acetate (20%), acetonitrile (90%) and ethyl acetate. The system was calibrated using authentic pigment standards and compounds isolated from reference cultures (Jeffrey *et al.* 1997). The identification of the pigments was based on Jeffrey *et al.* (1997) and pigments of unknown affinity were assigned as derivatives of the pigment with which they showed the closest match based on the retention time and the absorption spectrum, or as 'unknown'. Concentrations of individual pigments in the samples were calculated using the response factors of standard pigments. The response factors of unknown carotenoids, dinoxanthin and neoxanthin were calculated as the mean of the response factors of the other carotenoids, and for unknown mixtures of carotenoids and chlorophylls a mean response factor for all carotenoids and chlorophylls was used. The abundance of individual pigments is reported as percentages of total chlorophylls or carotenoids (%).

Statistical techniques and the construction of the diatom-based transfer function

Species and environmental variables (except pH) were log- (x+1) transformed, to reduce the influence of dominant taxa and to reduce or remove skewness in the data. Ordinations were performed using Canoco 4.5 for Windows (ter Braak & Šmilauer 2002). Before statistical analysis, detection of outliers/unusual samples was accomplished by running a correspondence analysis (CA) of the species data. A detrended correspondence analysis (DCA) was used to determine the length of gradient, and identify whether unimodal or linear models were suitable for further analyses (ter Braak & Šmilauer 2002). The length of gradient equaled 5.0 so the unimodal method canonical correspondence analysis (CCA) was used to select those variables explaining the largest amount of variation in the species data (ter Braak & Šmilauer 2002). The significance ($P \leq 0.05$) of each variable was assessed with forward selection using an unrestricted Monte Carlo permutation test involving 999 permutations. Subsequently, a CCA was performed with the environmental variable of interest as the only explanatory variable in order to calculate the ratio of the eigenvalue for the first (constrained) axis to the eigenvalue for the second (unconstrained) axis, which is an indication of the importance of that variable in explaining the variance in the species data (ter Braak & Šmilauer 2002).

Weighted averaging-partial least squares (WA-PLS) was applied using the C2 software package (Juggins 2003). WA-PLS was chosen over simple weighted averaging (WA) as it generally outperforms WA over long compositional gradients (3-22 standard deviation units) and when there is a secondary gradient, the root-mean-square error of prediction (RMSEP) may be reduced by 50% (Birks 1998). The final model was selected based on the lowest prediction error (RMSEP), and highest jack-knifed r^2. To be considered as 'useful', a component should give a reduction in RMSEP of more than 5%

compared to WA (Birks 1998). Sample-specific errors of reconstructed specific conductance were calculated using C2 (Juggins 2003) with 999 bootstrapped cycles.

Proxy data which are potentially influenced by variable sedimentation rates (SRs) and large changes in the proportion of organic, siliciclastic and biogenic components are represented as fluxes (Street-Perrot *et al.* 2007). The MAR (g/cm^2 yr) was calculated as the multiplication of the DBD (g/cm^3) and the SR (cm/yr). Gamma ray density (GRD) was converted to DBD using a dry weight percentage of the samples. The flux of each proxy was calculated as the multiplication of the MAR and the concentration by weight at that depth. The diatom and pigment stratigraphy was divided into zones using a constrained cluster analysis (CONISS) and plotted using Tilia and Tilia Graph View (Grimm 2004). The significance of the zones was assessed using a broken-stick model in the Rioja package for R (Juggins 2009).

Results

Transfer function development

Initially, a total of 41 diatom species, including marine diatoms, were identified in the calibration dataset. Occasional marine diatoms and taxa occurring with a maximum relative abundance of 0.5% in at least one sample or occurring in less than five samples were removed.

All samples were retained in the analysis, because no outliers were detected in a DCA of the species data (Fig. 2). CCA with forward selection and Monte Carlo permutation tests involving 999 permutations revealed that the variance in diatom composition was significantly ($P \leq 0.05$) explained by sulfate, sampling depth, pH, aluminum, TN, DOC, ORP and specific conductance. The most significant variable was specific conductance (Fig. 2). The ratio of the eigenvalue of the first axis (0.475) to the eigenvalue of the second axis (0.388) indicated that this was a suitable variable for creating a transfer function.

The specific conductance transfer function was constructed without two littoral samples from lake LA7 (Langhovde) whose WA residuals exceeded the standard deviation of specific conductance. WA-PLS with two components showed an increase in apparent r^2 of 6.77%, an increase in jack-knifed r^2 of 6.76% and a decrease in RMSEP of 13.5% compared with the WA-PLS model with one component, hence this model was selected. Jack-knifed r^2 and apparent r^2 were both high in the transfer function, respectively 0.85 and 0.90 and RMSEP was relatively low (0.26 mS/cm) (see Table S2 in the Supplementary Material for comparison with data obtained from the literature). WA optima and tolerances of the lacustrine species for specific conductance are summarized in Table S3 in the Supplementary Material.

A plot of the observed versus predicted specific conductance for all samples indicated a close agreement between inferred and measured specific conductance with no apparent outliers (Fig. S3 in the Supplementary Material). However, the residual trend of the retained samples used for the WA-PLS2 transfer function, indicates that the low and high end of the specific conductance gradient is slightly overestimated, while values in the middle of the gradient are somewhat underestimated (Fig. S4 in the Supplementary Material).

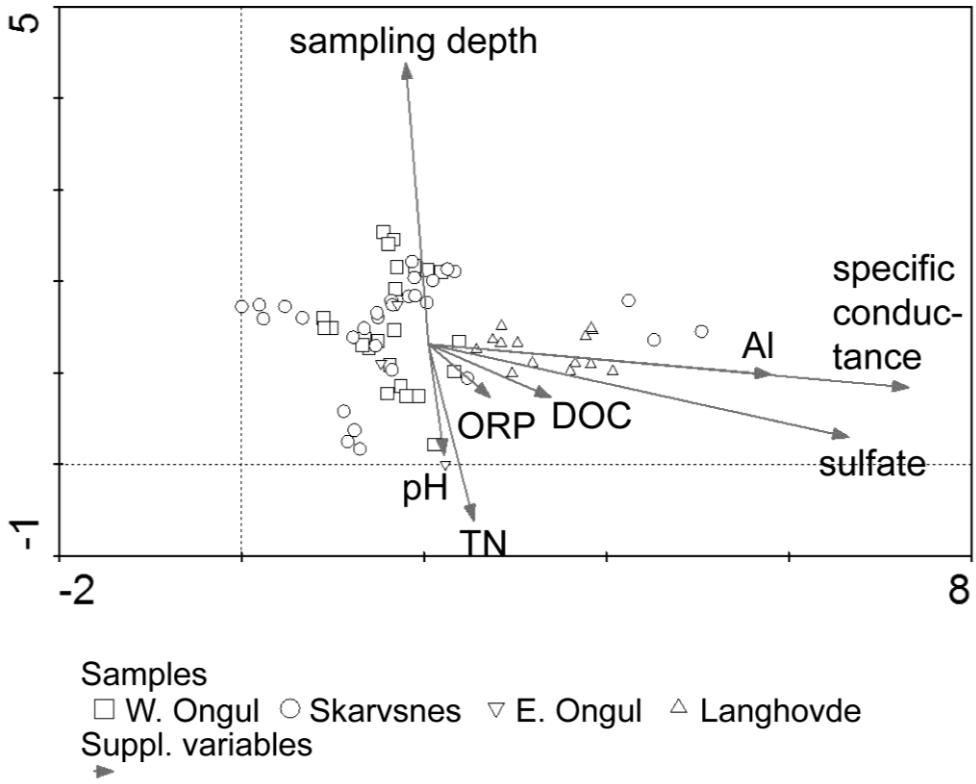

Figure 2. DCA scatter plot of the Lützow Holm Bay samples, with the significant variables plotted as supplementary variables.

Lithostratigraphical, geophysical and geochemical analysis

The sediment cores indicated three main stratigraphic units based on their geophysical and sedimentological characteristics (Figs. 3a & b). For the upper 6 cm of the sediments, only retrieved with the UWITEC gravity corer, no geophysical or geochemical data are available. For consistency with the other Chapters, a simplified lithology of the sediments is presented in Fig. S5 in the Supplementary Material. As volume-specific MS and mass-specific MS follow the same pattern throughout the sediments, only the first is described. The water content of the sediments is plotted in Fig. S6 in the Supplementary Material.

Unit 1 (254 - 136 cm, c. 2120 - 1420 cal. yr BP) consisted of mud (silty clay) laminations with some sand and marine shell fragments, and sponge spicules. Between 237 and 208 cm, there were no laminations and the sediment comprised a heterogeneous and possibly disturbed mixture of sand, clay and silt with only broken sponge spicules and very rare shell fragments. Between 202 and 136 cm, there were a number of discrete levels of coarse sand or small pebbles. This unit had the highest GRD and volume-specific MS compared to the rest of the core with notable peaks linked to the presence of coarse sand laminations or small pebbles. The TN flux remained relatively low in this unit, except for two higher values in the bottom of the core (at 253 and 245 cm).

The TC flux fluctuated and was relatively high likely related to the presence of shell fragments (Fig. 4).

Unit 2 (136 - 111 cm, c. 1420 - 710 cal. yr BP) was characterized by a strong decrease in volume-specific MS and a steady decrease in GRD. Lacustrine microbial-mat remains occurred for the first time in this unit. TC and TN fluxes were both very low throughout this unit.

Unit 3 (111 - 6 cm, c. 710 cal. yr BP - recent) consisted of laminated lacustrine microbial mats with varying degrees of lamina thickness. GRD and volume-specific MS were at their lowest in the core with the exception of c. 66 cm depth, where a pebble was present. TC and TN fluxes were relatively high and variable with peaks between 90 and 75 cm and at 6 cm.

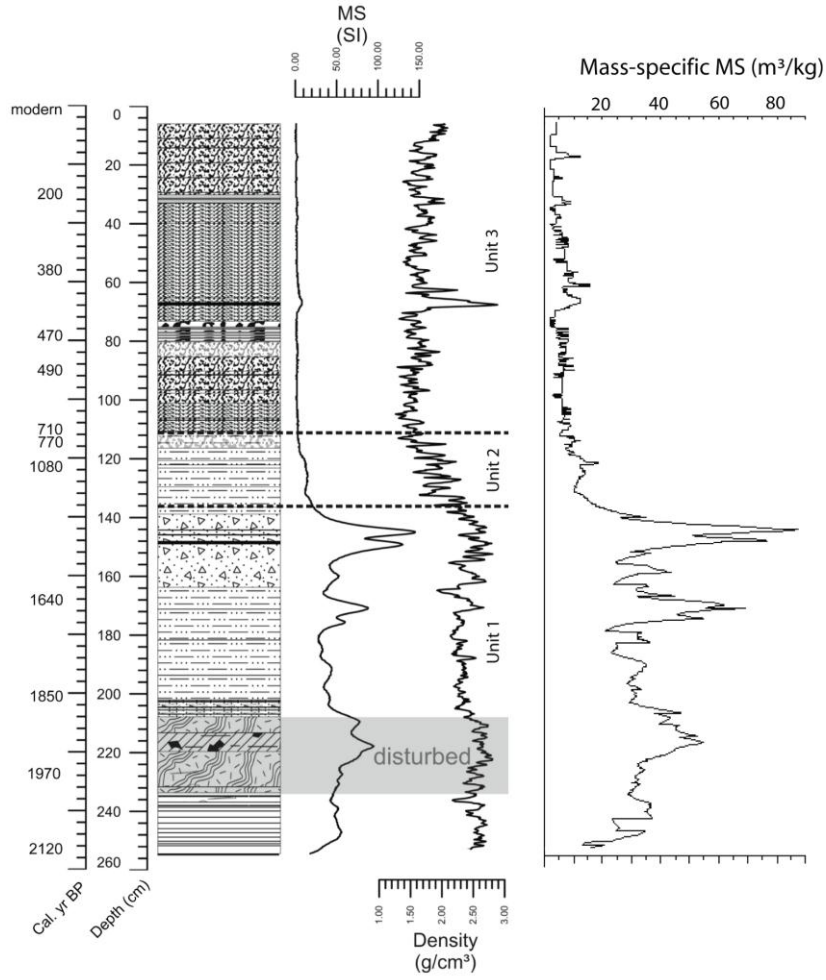

Figure 3a. Diagram of the lithology (the legend is shown in Figure 3b for visibility), volume-specific magnetic susceptibility (MS) (SI), gamma ray density (GRD; g/cm³), and mass-specific MS (m³/kg) of the Mago Ike sediment cores. Calibrated radiocarbon dates are indicated.

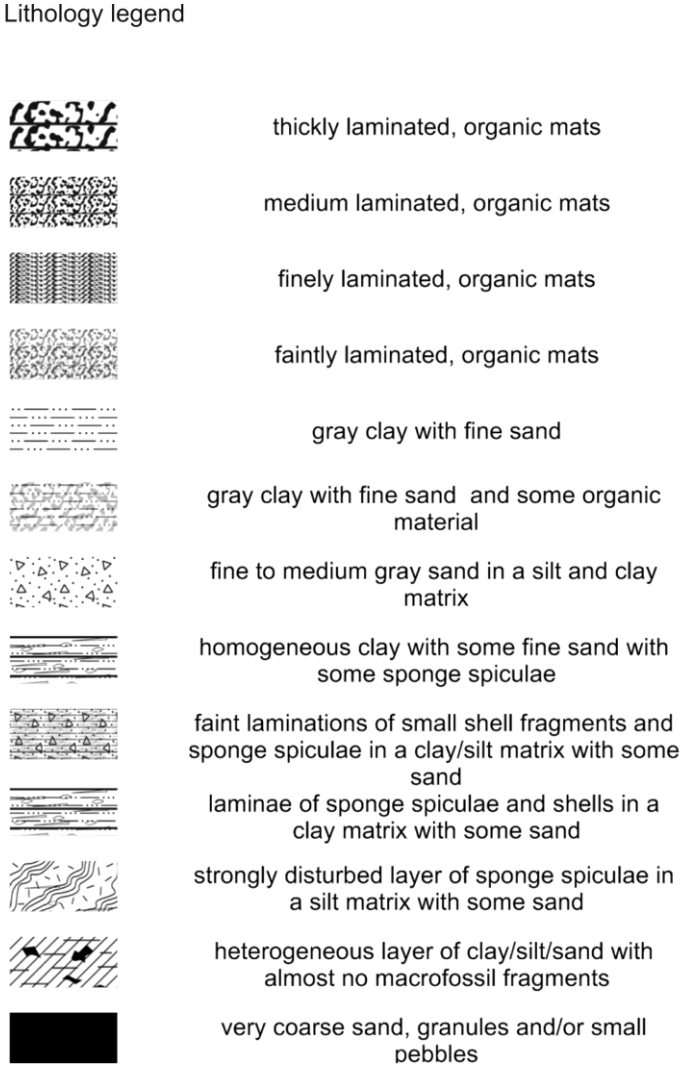

Figure 3b. Legend of the lithology of the Mago Ike sediment cores.

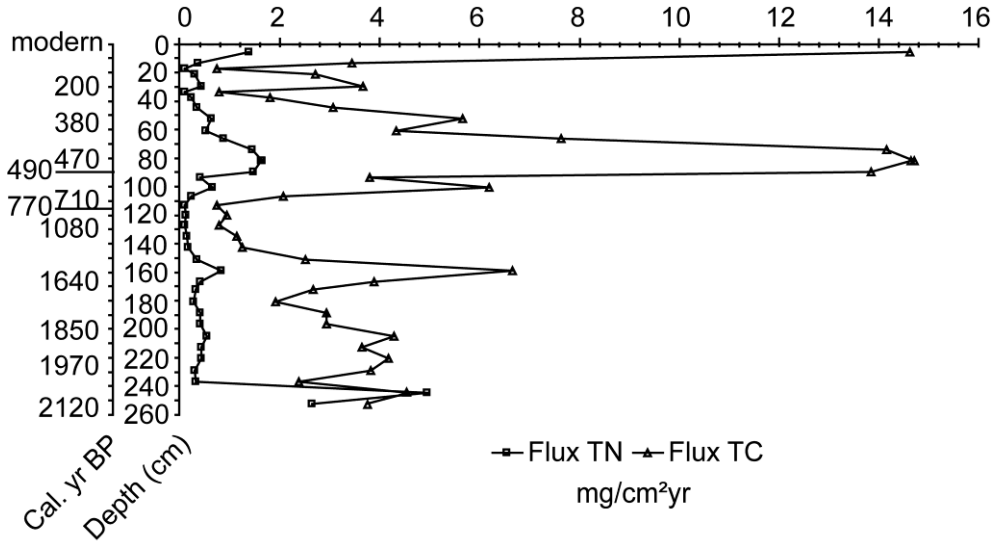

Figure 4. Total Carbon (TC) and Total Nitrogen (TN) fluxes (mg/cm²yr) throughout the Mago Ike sediment cores.

Radiometric dating

Radiocarbon dating of the cores showed that the ages, with the exception of BETA-261160 at 7 cm depth, were in stratigraphic order (Table 1 & S1 in the Supplementary Material; Fig. 5). Since classical and Bayesian age-depth modelling approaches produced broadly similar results, for simplicity, we present the classical age-depth modelling results undertaken in CLAM v. 2.1 (Fig. 5; Table 1 & S1 in the Supplementary Material). Furthermore, CLAM also enabled us to produce continuous whole core marine-lacustrine age-depth sequence models.

Calibration of 'post-bomb' samples, traditionally defined as 'modern', suggests that the top 13 cm of sediments were either deposited very rapidly between 1957 and 1959 AD, or deposition occurred more gradually between 1957 and 2005 AD (Table 1 & S1 in the Supplementary Material). We considered the second scenario to be more likely, firstly because the sediment sequence is repeatedly laminated, possibly representing several years of ice-covered/ice-free conditions, and, secondly, because both the sequence of calibrated and modelled modern-surface ages from 1957 to 2004 AD are broadly in line with modern-day sedimentation rates and adequately reproduce the date the cores were extracted. Sample BETA-261160 at 7 cm was excluded from the age-depth model as this was the uppermost sample taken from the square-rod piston sampler core, which meant that it was potentially water-washed during extraction, and could have been contaminated by older carbon. Moreover, this sample had a radiocarbon age that was non-sequential, and bracketed by 'modern' radiocarbon ages which were obtained from a UWITEC surface core that had been sectioned at 0.5-cm intervals, bagged and frozen in the field. The UWITEC samples are, therefore better suited for radiocarbon dating of this section of the core compared with the surface of the square-rod piston sampler core (sample BETA-261160).

The other terrestrial dates were all retained, producing a straightforward age profile that increases with depth without age-reversals. Radiocarbon ages from the marine-influenced section of the core showed a potential offset between bulk and macrofossil ages. Measured radiocarbon ages of the two macrofossil samples were both c. 300 ^{14}C years younger than radiocarbon ages of the bulk sediment matrix from which they were extracted. To test the effect of this offset on the timing of isolation, we undertook three calibration model runs in OXCAL and in CLAM (Table 1 & S1 in the Supplementary Material; Fig. 5): Model 1 (based on 'as-measured' radiocarbon data), 2 (bulk and macrofossil 'as-measured' radiocarbon ages combined into a single calibrated age range), and 3 (an additional 300 ± 100 ^{14}C years offset applied to all bulk sediment 'as-measured' radiocarbon age data before calibration). Details about this analysis can be found in the Supplementary Material (Protocol S1).

A bulk-macrofossil age offset could not be entirely ruled out; therefore, we retained both Model 2 as a maximum possible age-depth sequence, and Model 3 as a minimum possible age-depth sequence (Fig. 5). Model 3 could be considered more reliable, but it would require significantly more data from the region to unequivocally determine the existence and scale of the bulk sediment age offset. Therefore, in this paper, Model 2 median calibrated ages were used.

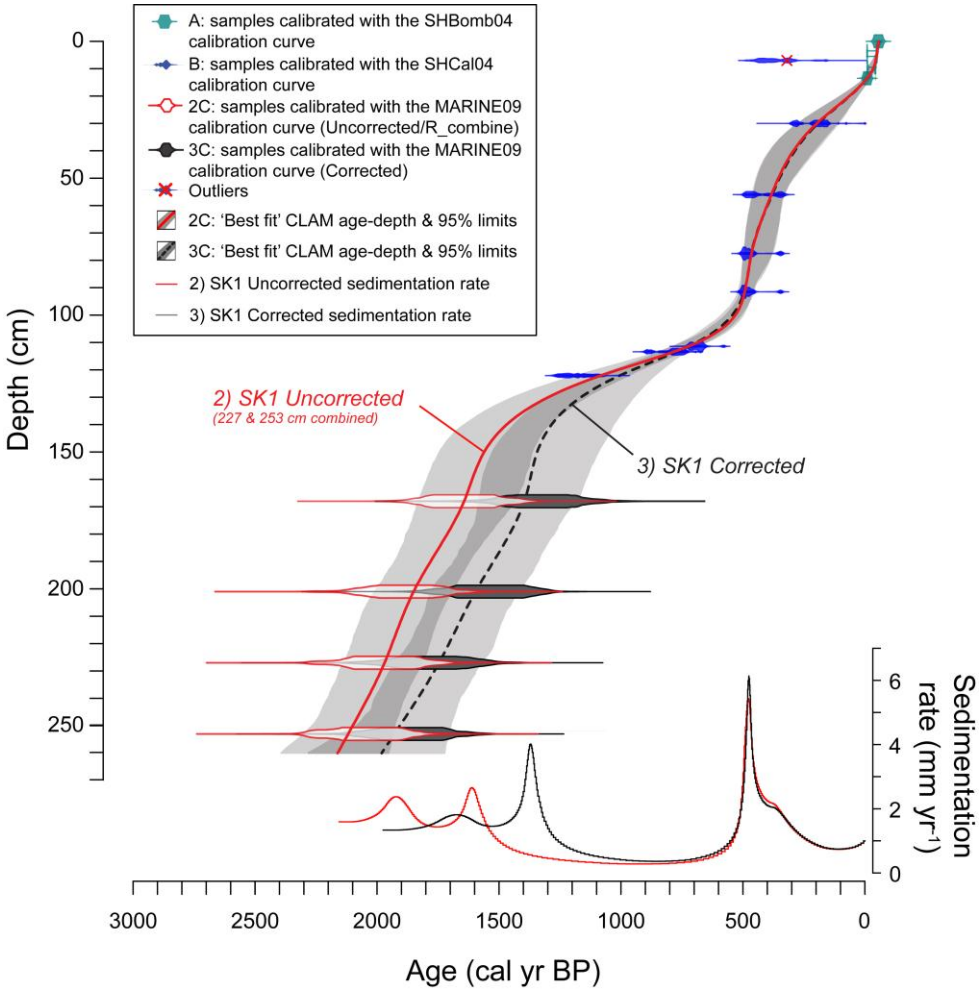

Figure 5. Stratigraphic age-depth plot undertaken in CLAM v. 2.1 (Blaauw 2010). Calibrated radiocarbon ages and Models 2 and 3 are as defined in Table 1 & S1 and Protocol S1 in the Supplementary Material. Data not included in the age-depth model are indicated by a red cross (see text for explanation).

Lab. ID	Depth (cm)	Unit	T/M	Material dated	Carbon content (wt %)	$d^{13}C_{VPDB}$ (‰)	pMC (%±1s)	CRA (^{14}C yr BP ± 1s)	Oxcal 95.4% calibration data (cal. yr BP; yr AD where stated) Models 1 (normal font) & 2 (italics)	Model 3
SUERC-18335	0.5	3	T	a	17.5	-17.3	106.4 ± 0.5	-	>2004 or	>-54 or
				a				-	1957 - 1958 AD	-7 - -8
BETA-306507	3.5	3	T	a	-	-16.2	110.2 ± 0.4	-	1958 - 2000 AD	-8 - -50
BETA-322263	5.5	3	T	a	-	-15.9	110.7 ± 0.3	-	1958 - 1999 AD	-8 - -49
BETA-261160	7	3	T	a	-	-17.9	96.1 ± 0.6	320 ± 50	490 - 150	490 - 150
BETA-322264	9.5	3	T	a	-	-15.1	114.2 ± 0.3	-	1959 - 1994 AD	-9 - -44
BETA-322265	13.5	3	T	a	-	-15.5	107.4 ± 0.3	-	1957 - 1958 AD	-7 - -8
BETA-306508	30	3	T	b	0.0	-14.6	97.2 ± 0.4	230 ± 30	310 - -5	310 - -5
SUERC-19466	56	3	T	c	4.1	-16.7	94.7 ± 0.4	413 ± 37	505 - 320	505 - 320
BETA-306509	77.5	3	T	c	-	-14.0	94.6 ± 0.4	450 ± 30	520 - 330	520 - 330
BETA-306510	91.5	3	T	a	-	-15.8	94.4 ± 0.4	460 ± 30	525 - 335	525 - 335
SUERC-19467	111.4	2	T	c	10.0	-14.5	90.7 ± 0.4	788 ± 37	740 - 570	740 - 570
SUERC-19468	113.4	2	T	d	3.0	-14.5*	89.2 ± 0.4	919 ± 37	910 - 690	910 - 690
BETA-261161	122.1	2	T	e	-	-*	85.0 ± 0.4	1300 ± 40	1275 - 1065	1275 - 1065
SUERC-18048	168	1	M	f	0.7	-17.5	70.7 ± 0.3	2785 ± 35	1880 - 1380	1570 - 1050
SUERC-18049	201	1	M	f	0.5	-16.2	68.9 ± 0.3	2993 ± 37	2145 - 1605	1810 - 1290
SUERC-18050	227_{bulk}	1	M	g	0.5	-17.3	67.1 ± 0.3	3208 ± 35	2380 - 1865	2070 - 1490
SUERC-18348	227_{macro}	1	M	h	12.1	-0.3	69.7 ± 0.3	2902 ± 35	2035 - 1515	
	$227_{bulk}/227_{macro}$			**					*2250 - 1710*	
SUERC-18062	253_{bulk}	1	M	i	0.5	-17.2	66.5 ± 0.3	3274 ± 37	2510 - 1925	2130 - 1590
SUERC-18349	253_{macro}	1	M	j	11.5	-0.1	69.1 ± 0.3	2974 ± 35	2125 - 1590	
	$253_{bulk}/253_{macro}$			**					*2310 - 1800*	

Table 1. Radiocarbon table of the Mago Ike sediments. Radiocarbon dates, calibrated age ranges, publication codes, and the nature of material dated are given. Greyed out data are considered least likely or as outliers. Carbon content is not routinely measured by BETA analytical; T=terrestrial (lacustrine); M=marine; CRA=Conventional Radiocarbon Age; *=estimated value due to small sample. Material dated: a = medium laminated microbial-mat; b = fine-medium laminated mat transition; c = finely laminated microbial-mat; d = grey clay with fine sand, some organics; e = grey clay with fine sand; f = bulk grey clay with fine sand; g = sandy-silt bulk matrix - no macros; h = sponge spicules; i = sandy-clay bulk matrix - no macros; j = carbonate shells. ** = R_combine (Model run 2 - see Protocol S1) (Fig. 5). Unit 1-2-3 refers to the lithological units in Fig. 3a. For more details about the Model Runs 1-3: the reader is referred to Protocol S1.

Microfossil analysis and reconstructed lake-water specific conductance

A total of 112 diatom taxa were identified of which 25 taxa are plotted (Fig. 6). These taxa occurred with a minimum abundance of 2% in at least three samples. All lacustrine species are currently present in the extant diatom flora of the Lützow Holm Bay region. Based on a broken-stick and CONISS cluster analysis, four distinct diatom zones were identified, namely MIDA1 (Mago Ike Diatom Analysis) to MIDA4.

Zone MIDA1 (254 - 175 cm, c. 2120 - 1680 cal. yr BP) is dominated by marine taxa, including unknown *Fragilaria* species (for pictures, see Fig. S7 in the Supplementary Material), *Chaetoceros* resting spores, *Pseudostaurosira perminuta*, and *Navicula directa*. The most abundant species is an unknown *Fragilaria* species. *Fragilariopsis curta, N. directa* and *Chaetoceros* resting spores all occur at relatively low densities. The diatom concentration (number of diatoms g^{-1} dry weight) is relatively low throughout this zone, with a peak at 180.6 cm. The diatom flux is similarly relatively low and variable.

Zone MIDA2 (175 - 143 cm, c. 1680 - 1500 cal. yr BP) is composed of the same marine community as the previous zone, but *N. directa, Chaetoceros* resting spores and *Tryblionella marginulata* increase in abundance while the concentration of the unknown *Fragilaria* species decreases. *Chaetoceros* resting spores become the most dominant species of the diatom community. The diatom concentration remains relatively low. The diatom flux is comparable to the previous zone.

Zone MIDA3 (143 - 123 cm, c. 1500 - 1120 cal. yr BP) is characterized by a decrease in the relative abundance and the subsequent disappearance of marine taxa, and an increase in the brackish-water species *Navicula phyllepta,* which becomes the most abundant species. The diatom concentration slightly increases near the end of this zone, while the diatom flux is very low throughout this zone.

Zone MIDA4 (123 - 0 cm, c. 1120 cal. yr BP - recent) is dominated by fluctuating abundances of freshwater taxa including *Halamphora veneta* and *Craticula antarctica* and occasional spikes of *Navicula gregaria*. Diatom concentration and flux rapidly increase at the beginning of this zone (from c. 92 cm), and remain relatively high and very variable. Three zones with a higher diatom concentration occur between 92.5 and 82.5 cm (with peaks at 92.5, 88.5 and 82.5 cm), between 46.3 and 43.6 cm, and to a lesser extent in the recent sediments from 4 cm onwards. The diatom flux is high between 92 and 84 cm and then shows an overall decrease towards the upper part of the core. Diatom-inferred specific conductance in the lacustrine section of the core reaches a maximum value of 1.13 mS/cm at 120 cm after which it rapidly decreases to 0.45 mS/cm at 119 cm (Fig. 7). Above 119 cm, specific conductance ranges between 0.52 and 0.72 mS/cm. The fluctuations of inferred specific conductance are small and fall within the error of the model.

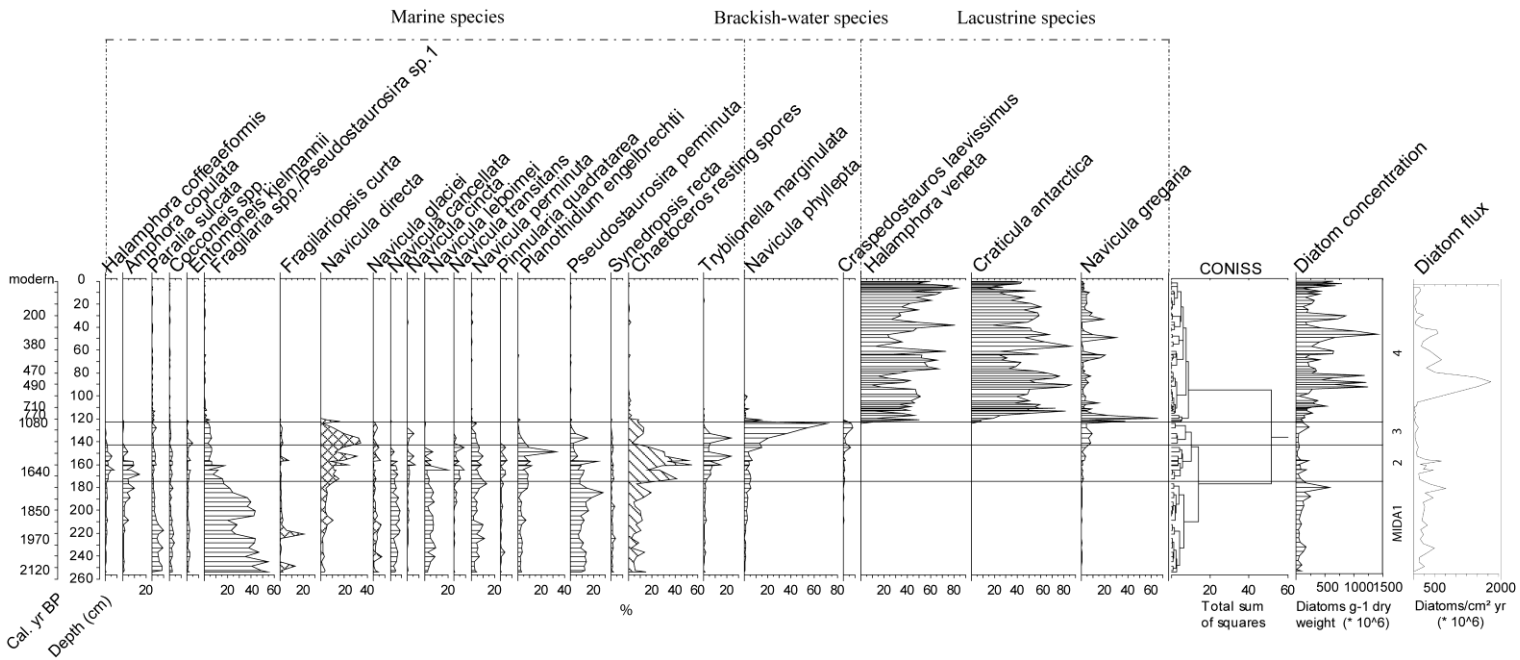

Figure 6. Diatom stratigraphy of the Mago Ike sediments. Zoning (MIDA1-4; Mago Ike Diatom Analysis) is based on a broken-stick and CONISS cluster analysis. Species data are expressed as relative abundances. Sea-ice indicator species are indicated with cross-hatching lines and open-water indicator species with left-diagonal lines. Marine, brackish-water and lacustrine diatom species are indicated with brackets. The species listed as lacustrine are also present in the diatom flora of the Lützow Holm Bay region. Diatom concentration is expressed as the number of diatoms g^{-1} dry weight. Diatom flux is expressed in the number of valves/cm²yr. Calibrated radiocarbon dates are indicated.

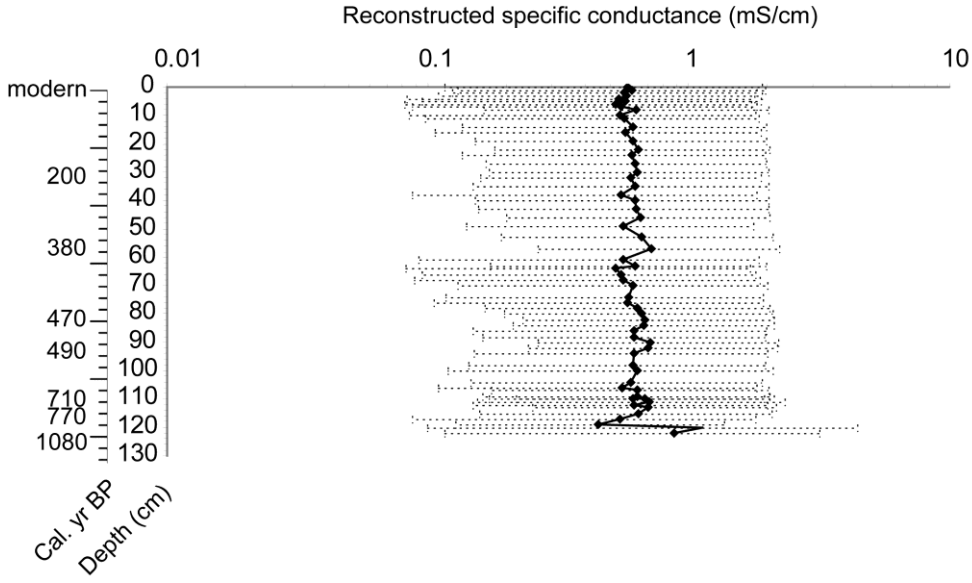

Figure 7. Diatom-based inferred specific conductance throughout the lacustrine sediments of Mago Ike (mS/cm). Uncertainty ranges are the sample-specific errors.

Fossil pigment analysis

Based on the broken-stick model and CONISS cluster analysis, four distinct pigment zones were identified, namely MIPA1 (Mago Ike Pigment Analysis) to MIPA4 (Fig. 8). Only pigments occurring in a minimum of three samples were plotted on the figure, meaning that chlorophyll c2 and neoxanthin were not included.

Zone MIPA1 (254 - 210 cm, c. 2120 - 1890 cal. yr BP) is characterized by very low concentrations and fluxes of total carotenoids and total chlorophylls. Chlorophyll *a* and phaeophytin *a* (a chlorophyll *a* derivative) dominate the chlorophylls, whereas the most abundant carotenoids are diatoxanthin (present in diatoms, dinophytes and chrysophytes), lutein (green algae, red seaweeds), and unknown carotenoids.

ZONE MIPA2 (210 - 149 cm, c. 1890 - 1550 cal. yr BP) is characterized by a decrease in chlorophyll *a* and an increase in phaeophytin *a.* The most abundant carotenoids are β-carotene (green algae, chromophyte algae, some phototrophic bacteria) which appears at 221 cm, and unknown carotenoids. Diatoxanthin and lutein decrease in abundance. Total chlorophylls and total carotenoids and their fluxes remain low.

ZONE MIPA3 (149 - 74 cm, c. 1550 - 450 cal. yr BP) is characterized by relatively high total chlorophyll and total carotenoid concentrations. Chlorophyll and carotenoid fluxes are relatively low in the beginning of this zone to become relatively high from 105 cm onwards. Peaks in fluxes are observed between 90 and 71 cm. Phaeophytin *a* decreases in abundance whereas the concentration of chlorophyll *a* increases. Unknown chlorophylls also increase in abundance. The most abundant carotenoids are lutein, violaxanthin (green algae, euglenophytes, brown seaweeds), zeaxanthin (cyanobacteria,

green algae, and possibly mosses), β-carotene, hexanoyloxyfucoxanthin (haptophytes, dinophytes) and unknown carotenoids. Zeaxanthin reaches high abundances between 122 and 90 cm.

ZONE MIPA4 (74 - 6 cm, c. 450 cal. yr BP - recent) is characterized by relatively lower concentrations of total chlorophylls and total carotenoids. Chlorophyll and carotenoid fluxes are relatively low to show slightly increasing values from 14 cm onwards. Chlorophyll *a* and phaeophytin *a* remain the most abundant chlorophylls. Unknown carotenoids are the most abundant carotenoids, followed by lutein, zeaxanthin and diatoxanthin.

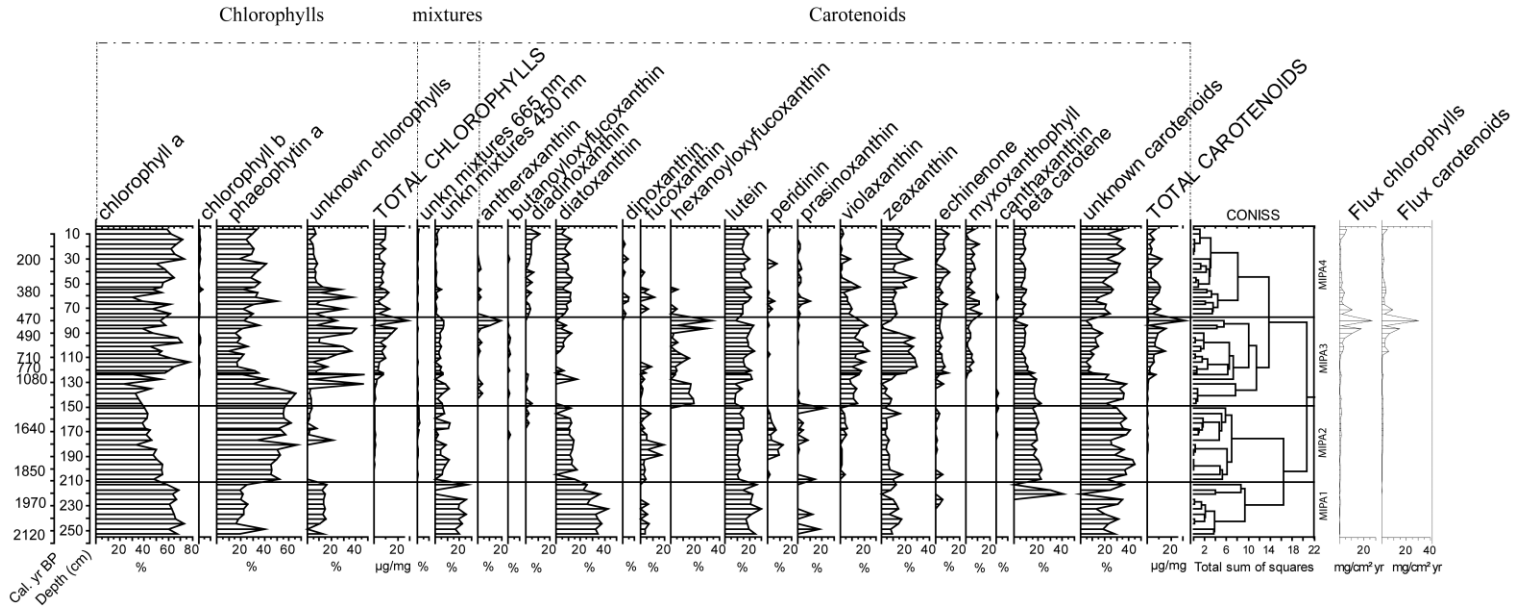

Figure 8. Stratigraphy of fossil pigments in the Mago Ike sediments. Zoning (MIPA1-4; Mago Ike Pigment Analysis) is based on a broken-stick and CONISS cluster analysis. The abundance of individual pigments is reported as percentages to total chlorophylls or carotenoids (%). Total chlorophylls and total carotenoids are reported in µg/mg and plotted with an exaggeration factor of 20 to increase the visibility of the graph. The fluxes of carotenoids and chlorophylls are expressed in mg/cm²yr. Calibrated radiocarbon dates are indicated.

Discussion

Ecological changes and lake evolution

The distinct stratigraphic zones in the cores based on diatom (Fig. 6), pigment (Fig. 8), and lithostratigraphic (Fig. 3a) analyses correspond to a shift from marine to lacustrine conditions with a clear transition zone in between. These changes are related to lake formation as a result of isostatic uplift of the basin and coincident relative sea-level fall. These zones provide information on coastal oceanographic conditions in Skarvsnes between c. 2120 and 1500 cal. yr BP (253 - 143 cm), and on limnological conditions from c. 1500 cal. yr BP onwards (143 - 0 cm).

Changes in the proxies of the marine zone most likely reflect ecological changes associated with isostatic uplift such as a decreasing sea water depth and related differences in sea-ice dynamics and light regimes, rather than climate variability. Conditions were characterized by seasonal open-water and sea-ice coverage during the majority of the year, which is similar to those observed today and in coastal marine sediment cores elsewhere in EA during this time interval (Verleyen *et al.* 2011 in Appendix 2). The most striking changes in the marine diatom record are the increase in *Chaetoceros* resting spores and *Navicula directa*, and the decrease in an unknown *Fragilaria* species (Figs. 6 & S7). The increase in *Chaetoceros* resting spores points to seasonal stratification of the water-column (Crosta *et al.* 2004) due to the melting of sea-ice and/or the inflow of meltwater from the nearby terrestrial environment. The ecological significance of the decrease in *Fragilaria* sp. during the marine stage is not entirely clear as no detailed auto-ecological data are available for this taxon. However, it is possible that it is an open-water marine species, declining when the site became isolated from the ocean. This is further supported by a decrease in the abundance of *Paralia sulcata*, a tychoplanktonic species. Furthermore, along with the benthic taxon *N. directa*, other benthic species start to increase, such as *Halamphora coffeaeformis* and *Amphora copulata*. This might indicate a higher availability of light due to the uplift of the basin from the ocean and hence decreasing water depth, which is an important structuring factor in Antarctic benthic diatom communities (Cunningham & McMinn 2004).

All proxies analyzed point to the isolation of Mago Ike from the ocean between c. 1500 and 1120 cal. yr BP (143 - 123 cm). The rapid increase in total chlorophylls and total carotenoids indicates a quick colonization of the lake by cyanobacteria, diatoms and green algae after isolation (Fig. 8). The microbial turnover after lake isolation is similar to patterns observed from other Antarctic regions, such as the Larsemann Hills (Verleyen *et al.* 2004) and characterized by an increase in brackish-water diatom species (*Navicula phyllepta, Craspedostauros laevissumus* and *Tryblionella marginulata;* Fig. 6), a rapid increase in cyanobacteria-derived pigments, the appearance of diatom- and green algae-related pigments (Fig. 8) and the subsequent establishment of a freshwater diatom community (Fig. 6). A sudden decrease in MS and GRD (Fig. 3a) coincided with these changes and points to changes in sediment composition, provenance and delivery. While the sediments in the marine part of the cores likely contained ice-rafted debris (IRD) from icebergs, which might have originated elsewhere, the lacustrine sediments are composed

of wind-blown material and local debris from the catchment area which was transported by the inflow stream.

After the early succession phase (c. 1120 cal. yr BP; 123 cm), well-developed microbial-mats colonized the lake and dominated primary production as indicated by the pigment composition, which is composed of marker pigments of cyanobacteria (zeaxanthin, echinenone and myxoxanthophyll; Fig. 8). Green algae (lutein, violaxanthin, ß-carotene and antheraxanthin) and diatoms (fucoxanthin, diatoxanthin) likely occurred as co-dominants. The higher nitrogen values (Fig. 4) are also consistent with the relatively high abundance of nitrogen-fixing cyanobacteria, which commonly occur in East Antarctic lakes (Verleyen *et al.* 2010) and which are largely absent in the Southern Ocean. Specific conductance only slightly fluctuated during the lacustrine phase, and was highest just after lake isolation when lake water remained temporarily enriched with marine salts derived from the Southern Ocean (Fig. 7). This points to a relatively rapid transition from brackish water to freshwater conditions as a result of the positive moisture balance. After this transition phase, changes in the moisture balance are relatively small. This is likely related to the relatively dilute nature of Mago Ike, and the observation that shallow and brackish to saline lakes respond quickly to changes in the precipitation-evaporation/sublimation balance (Verleyen *et al.* 2012 in Appendix 1), while freshwater lakes are less sensitive.

Palaeoclimate reconstruction

Changes in proxies for primary production in the lacustrine sediments such as an increased flux of total chlorophylls, total carotenoids (90 - 71 cm) (Fig. 8), diatoms (92 - 84 cm) (Fig. 6), and TC and TN (90 - 75 cm) (Fig. 4) can be attributed to a slightly warmer period in Skarvsnes between c. 490 and 440 cal. yr BP (92 - 71 cm). This warmer period has only a very short duration and does not coincide with the NH MCA time interval (1050 - 650 yr BP). Therefore, a MCA event in Skarvsnes appears to be absent, which is similar to a range of other proxy records in the SH (Bentley *et al.* 2009). On the AP, records of an event only broadly similar in timing to the MCA, and of a shorter duration, are mainly restricted to marine records (Bentley *et al.* 2009). These include for instance a higher MS between 700 and 500 cal. yr BP interpreted as a signal of warmer surface water temperatures in eastern Bransfield Bay. This was however only one of several events, all of comparable amplitude and duration, suggesting intrinsically unstable climatic conditions during the Late-Holocene in Bransfield Bay (Khim *et al.* 2002). Exposed terrestrial material indicated that the ice edge was at or even behind its present position at Anvers Island between 970 and 700 yr BP. This appears to have had a regional expression in the western and northern AP (Hall *et al.* 2010 and references therein). However, in most continental ice cores, there is no clear evidence for a well-defined temperature rise corresponding to the NH MCA (Masson *et al.* 2000), although some records show a warm period which immediately post-dates the NH MCA. For example the deuterium excess record from the Law Dome ice core exhibits higher values corresponding to warmer conditions, between 650 and 450 yr BP, followed by a decreasing trend until 100 yr BP (Masson *et al.* 2000). This was confirmed by model simulations where the surface temperature in the Southern Ocean appears to be higher between 650 and 500 yr BP by at least 0.17°C compared to the mean over the period

1000 - 200 yr BP in all simulations (see Goosse *et al.* 2012). The proposed lag mechanism between the NH and SH records involves the formation of slightly warmer North Atlantic deep water when slightly milder conditions prevailed at the NH high-latitudes, followed by a centennial transport and upwelling in the Southern Ocean. However, a newer version of the LOVECLIM model weakens this result, and this lagged warmer period is less clear in the new simulations. This is attributed to the smaller solar forcing applied, which led to weaker temperature changes in the North Atlantic (Goosse *et al.* 2012). Moreover, this warm event appeared to be model-dependent as it was not found using the model MPI-RSM-E2 (Goosse *et al.* 2012), so its occurrence must be questioned. A lagged warm period between 810 and 663 yr BP (i.e. only corresponding to the last 150 years of the MCA) has been interpreted from a McMurdo Dry Valleys ice core and has been linked to warmer summers accompanied by increased snow accumulation and higher sea surface temperatures in the Ross Sea Region (Bertler *et al.* 2011). A synthesis of 11 ice cores revealed relatively warmer conditions before 1000 yr BP, but not during the past 1000 years when colder conditions prevailed (PAGES 2k 2013). Lake sediment evidence for a MCA event in Antarctica is similarly either absent or unconvincing. Studies from both EA [e.g. Pup Lagoon in the Larsemann Hills (see Verleyen *et al.* 2011 in Appendix 2)] and the AP [e.g. Lake Beak 1 on Beak Island (Sterken *et al.* 2012)] do not show any evidence for a MCA event. Only a small number of studies include evidence of warmer and wetter conditions during the past 1000 years. For example, wetter conditions were inferred in Lake Fryxell (Taylor Valley) after 1000 BP, indicating an increased meltwater supply to the lake, attributed to an increase in the number of snowless days and/or higher summer temperatures (Wagner *et al.* 2006). Collectively, the absence of a warm period coinciding with the NH MCA signal is thus in agreement with other East Antarctic studies (Verleyen *et al.* 2011 in Appendix 2, Goosse *et al.* 2012).

Fluxes of fossil pigments (Fig. 8), TC, TN (Fig. 4), and diatoms (Fig. 6) show an overall decrease between c. 440 cal. yr BP and the recent sediments (71 - 14 cm) and a slight increase again between 14 cm and the surface. These relatively low concentrations are comparable to those recorded in the period before 490 - 440 cal. yr BP and the therefore clear and well-defined LIA cooling observed between 500 and 100 cal. yr BP in the NH appears to be absent in this part of Antarctica. This is consistent with the absence of an LIA analogue in Antarctica (Verleyen *et al.* 2011 in Appendix 2). Overall, there is no consistent palaeoclimate signal between records, even when these are from nearby localities. An ice core record from the Victoria Lower Glacier (McMurdo Dry Valleys) indicates colder summers and decreased snow accumulation between 662 and 143 yr BP (Bertler *et al.* 2011). However, in a summary of 11 ice cores overall colder conditions were inferred from 1000 yr BP onwards compared with the preceding 1000 years, but a LIA could not be observed (PAGES 2k 2013). Furthermore, in agreement with our record, most lake sediment evidence from both EA (Verleyen *et al.* 2011 in Appendix 2) and the AP (e.g. Sterken *et al.* 2012) indicate the absence of a LIA in Antarctica. One exception is a mild and short cold event recorded in the Vestfold Hills, as evidenced by a period of lower evaporation between c. 200 and 150 yr BP (Roberts *et al.* 2001). However, because of the very short duration of this event and its relatively recent occurrence, this cannot be regarded as a LIA analogue. The same applies for the marine environment, as in the vast majority of the records there is no analogue for the LIA or the chronologies are too poorly

resolved for a direct comparison. Only in the MS record from Bransfield Basin was an excursion suggested to co-occur with the LIA (Khim *et al.* 2002). However, this was just one of a series of climatic events, all comparable in duration and amplitude. It is thus becoming evident that a number of studies have probably force-fitted NH climate anomalies onto Antarctic palaeoclimate records or that regional differences dominate over Antarctic-wide trends in temperature variability.

In the recent sediments, increased chlorophyll, carotenoid (Fig. 8), TC and TN fluxes (Fig. 4) were observed, although smaller than the peaks evidenced between c. 490 and 440 cal. yr BP. This might be related to taphonomical issues rather than an increase in lake primary production. In summary there is no direct evidence for a response of the lake to recent TCW. This is consistent with weather station data from the region and generally elsewhere in EA, which revealed no significant trend in temperature during the past decennia (Sato & Hirasawa 2007, Steig *et al.* 2009). This observation clearly contrasts with records from the AP, where there is clear evidence for an effect of the recent TCW trend on lacustrine ecosystems (Quayle *et al.* 2002, Sterken *et al.* 2012).

Conclusions

A shift from marine to lacustrine conditions with a clear transition zone in between is inferred from all the proxies analyzed in Mago Ike, Skarvsnes, Lützow Holm Bay, EA. Between c. 2120 and 1500 cal. yr BP, seasonally open-water conditions occurred in this region of the Southern Ocean, comparable to other East Antarctic coastal regions during that time window and the present-day situation. The lake became isolated from the ocean around c. 1500 cal. yr BP due to isostatic uplift and freshwater conditions occurred from c. 1120 cal. yr BP onwards. From c. 1120 cal. yr BP proxies in the lake sediment record are considered highly sensitive to regional temperature changes.

Our multi-proxy evidence suggests that both the MCA and LIA are absent in Skarvsnes and only a brief period of slightly increased primary production occurred between c. 490 and 440 cal. yr BP, clearly post-dating the NH MCA and shorter in duration. It is therefore becoming clear that a number of studies have force-fitted NH climate anomalies onto Antarctic palaeoclimate events, as few of the latter are consistent in timing, duration and magnitude with their NH counterparts. There is no evidence of a recent climate anomaly in our record consistent with the TCW, which is in agreement with instrumental observations which have revealed only a relatively modest warming in EA.

Acknowledgements

This research was funded by the Belspo project ‘Holocene climate variability and ecosystem change in coastal East and Maritime Antarctica’ (HOLANT) and the British Antarctic Survey ‘Chemistry and Past Climate programme’. IT was funded by the Institute for the Promotion of Innovation by Science and Technology in Flanders. EV and KH were funded by the Fund for Scientific Research Flanders. Dirk Vangansbeke is thanked for the help with the CN analyses, Ilse Daveloose for the pigment analyses, Renaat Dasseville for the SEM-photos, Peter Fretwell for making the maps, Bart Van De Vijver for his help with the diatom identification, Ann-Eline Debeer for making the slides, and Bart Aelterman for his help with the CLAM software. Two anonymous reviewers are thanked for their

valuable comments on an earlier version of the paper. This work contributed to the PAGES Antarctica2k programme.

References

BENTLEY, M.J. HODGSON, D.A., SMITH, J.A. & COX, N.J. 2005. Relative sea – curves for the South Shetland Islands and Marguerite Bay, Antarctic Peninsula. *Quaternary Science Reviews,* **24,** 1203 – 1216.

BENTLEY, M.J., HODGSON, D.A., SMITH, J.A., COFAIGH, C.O., DOMACK, E.W., LARTER, R.D., ROBERTS, S.J., BRACHFELD, S., LEVENTER, A., HJORT, C., HILLENBRAND, C.D. & EVANS, J. 2009. Mechanisms of Holocene palaeoenvironmental change in the Antarctic Peninsula region. *Holocene*, **19**, 51-69.

BERTLER, N.A.N., MAYEWSKI, P.A. & CARTER, L. 2011. Cold conditions in Antarctica during the Little Ice Age - Implications for abrupt climate change mechanisms. *Earth Planetary Science Letters*, **308**, 41-51.

BIRKS, H.J.B. 1998. Numerical tools in palaeolimnology - progress, potentialities, and problems. *Journal of Paleolimnology,* **20**, 307-332.

BLAAUW, M. 2010. Methods and code for 'classical' age-modelling of radiocarbon sequences. *Quaternary Geochronology*, **5**, 512-518.

BRONK RAMSEY, C. 2009. Bayesian analysis of radiocarbon dates. *Radiocarbon,* **51(1)**, 337-360.

CREMER, H., ROBERTS, D., MCMINN, A., GORE, D. & MELLES, M. 2003. The Holocene diatom flora of marine bays in the Windmill Islands, East Antarctica. *Botanica Marina*, **46**, 82-106.

CROSTA, X., STURM, A., ARMAND, L. & PICHON, J.J. 2004. Late Quaternary sea ice history in the Indian sector of the Southern Ocean as recorded by diatom assemblages. *Marine Micropaleontology*, **50**, 209-223.

CUNNINGHAM, L. & MCMINN, A. 2004. The influence of natural environmental factors on benthic diatom communities from the Windmill Islands, Antarctica. *Phycologia*, **43**, 744 -755.

GOOSSE, H., BRAIDA, M., CROSTA, X., MAIRESSE, A., MASSON-DELMOTTE, V., MATHIOT, P., NEUKOM, R., OERTER, H., PHILIPPON, G., RENSSEN, H., STENNI, B., VAN OMMEN, T. & VERLEYEN E. 2012. Antarctic temperature changes during the last millennium: evaluation of simulations and reconstructions. *Quaternary Science Reviews,* **55**, 75-90.

GRIMM, E.C. 2004. TGView Version 202. Illinois State Museum, Springfield.

HALL, B.L., KOFFMAN, T. & DENTON, G.H. 2010. Reduced ice extent on the western Antarctic Peninsula at 700-970 cal yr BP. *Geology*, **38**, 635-638.

HALL, B.L. & DENTON, G.H. 2002. Holocene history of the Wilson Piedmont Glacier along the southern Scott Coast, Antarctica. *Holocene,* **12**: 619-627.

HUA, Q. & BARBETTI, M. 2004. Review of tropospheric bomb C-14 data for carbon cycle modeling and age calibration purposes. *Radiocarbon*, **46**, 1273-1298.

JEFFREY, S.W., MANTOURA, R.F.C. & BJORNLAND, T. 1997. Data for the identification of 47 key phytoplankton pigments. *In* JEFFREY, S.W., MANTOURA, R.F.C. & WRIGHT, S.W., *eds. Phytoplankton pigments in oceanography, guidelines to modern methods.* UNESCO Publishing, 447-554.

JUGGINS, S. 2003. *C2 User Guide - Software for Ecological and Palaeoecological Data Analysis and Visualisation*. University of Newcastle, Newcastle.

JUGGINS, S. 2009. *Rioja, analysis of Quaternary science data*. http://www.staff.ncl.ac.uk/staff/stephen.juggins/

KHIM, B.K., YOON, H.I., KANG, C.Y. & BAHK, J.J. 2002. Unstable climate oscillations during the late Holocene in the eastern Bransfield Basin, Antarctic Peninsula. *Quaternary Research*, **58**, 234-245.

MACDONALD, G.M., PORINCHU, D.F., ROLLAND, N., KREMENETSKY, K.V. & KAUFMAN D.S. 2009. Paleolimnological evidence of the response of the central Canadian treeline zone to radiative forcing and hemispheric patterns of temperature change over the past 2000 years. *Journal of Paleolimnology*, **41**, 129-141.

MANN, M.E., ZHANG, Z.H., RUTHERFORD, S., BRADLEY, R.S., HUGHES, M.K., SHINDELL, D., AMMANN, C., FALUVEGI, G. & NI, F.B. 2009. Global signatures and dynamical origins of the Little Ice Age and Medieval Climate Anomaly. *Science,* **326**, 1256-1260.

MASSON, V., VIMEUX, F., JOUZEL, J., MORGAN, V., DELMOTTE, M., CIAIS, P., HAMMER, C., JOHNSEN, S., LIPENKOV, V.Y., MOSLEY-THOMPSON, E., PETIT, J.R., STEIG, E.J., STIEVENARD, M. & VAIKMAE, R. 2000. Holocene climate variability in Antarctica based on 11 ice-core isotopic records. *Quaternary Research,* **54**, 348-358.

MATTHEWS, J.A. & BRIFFA, K.R. 2005. The 'Little Ice Age': Re-evaluation of an evolving concept. *Geografiska Annaler*, **87A**, 17-36.

MCCORMAC, F., HOGG, A., BLACKWELL, P., BUCK, C., HIGHAM, T. & REIMER, P. 2004. Shcal04 Southern Hemisphere calibration 0-11.0 cal kyr BP. *Radiocarbon,* **46**, 1087-1092.

MULVANEY, R., ABRAM, N.J., HINDMARSH, R.C.A., ARROWSMITH, C., FLEET, L., TRIEST, J., SIME, L.C., ALEMANY, O., FOORD, S. 2012. Recent Antarctic Peninsula warming relative to Holocene climate and ice-shelf history. Nature, 489, 141-144.

PAGES 2k CONSORTIUM. 2013. Continental-scale temperature variability during the past two millennia. *Nature Geoscience,* **6**, 339-346.

QUAYLE, W.C., PECK, L.S., PEAT, H., ELLIS-EVANS, J.C. & HARRIGAN, P.R. 2002. Extreme responses to climate change in Antarctic lakes. *Science*, **295**, 645-645.

REIMER, P.J., BAILLIE, M.G.L., BARD, E., BAYLISS, A., BECK, J.W., BERTRAND, C.J.H., BLACKWELL, P.G., BUCK, C.E., BURR, G.S., CUTLER, K.B., DAMON, P.E., EDWARDS, R.L., FAIRBANKS, R.G., FRIEDRICH, M., GUILDERSON, T.P., HOGG, A.G., HUGHEN, K.A., KROMER, B., MCCORMAC, G., MANNING, S., RAMSEY, C.B., REIMER, R.W., REMMELE, S., SOUTHON, J.R., STUIVER, M., TALAMO, S., TAYLOR, F.W., VAN DER PLICHT, J. & WEYHENMEYER, C.E. 2009. Intcal04 Terrestrial radiocarbon age calibration, 0-26 cal kyr BP. *Radiocarbon*, **46**, 1029-1058.

ROBERTS, D. & MCMINN, A. 1996. Relationships between surface sediment diatom assemblages and water chemistry gradients in saline lakes in the Vestfold Hills, Antarctica. *Antarctic Science,* **8**, 331-341.

ROBERTS, D. & MCMINN A. 1998. A weighted-averaging regression and calibration model for inferring lakewater salinity from fossil diatom assemblages in saline lakes of the Vestfold Hills: a new tool for interpreting Holocene lake histories in Antarctica. Journal of Paleolimnology, 19, 99-113.

ROBERTS, D., MCMINN, A., CREMER, H., GORE, D.B. & MELLES, M. 2004. The Holocene evolution and palaeosalinity history of Beall Lake, Windmill Islands (East Antarctica) using an expanded diatom-based weighted averaging model. Palaeogeography, Palaeoclimatology, Palaeoecology, 208, 121-140.

ROBERTS, D., VAN OMMEN, T.D., MCMINN, A., MORGAN, V. & ROBERTS, J.L. 2001. Late-Holocene East Antarctic climate trends from ice-core and lake-sediment proxies. *Holocene*, **11**, 117-120.

SABBE, K., VERLEYEN, E., HODGSON, D.A., VANHOUTTE, K. & VYVERMAN, W. 2003. Benthic diatom flora of freshwater and saline lakes in the Larsemann Hills and Rauer Islands, East Antarctica. *Antarctic Science*, **15**, 227-248.

SATO, K., & HIRASAWA, N. 2007. Statistics of Antarctic surface meteorology based on hourly data in 1957-2007 at Syowa Station. *Polar Science,* **1**, 1-15.

STEIG, E.J., SCHNEIDER, D.P., RUTHERFORD, S.D., MANN, M.E., COMISO, J.C. & SHINDELL, D.T. 2009. Warming of the Antarctic ice-sheet surface since the 1957 International Geophysical Year. *Nature*, **460**, 766-766.

STERKEN, M., ROBERTS, S.J., HODGSON, D.A., VYVERMAN, W., BALBO, A.L., SABBE, K., MORETON, S.G., & VERLEYEN, E. 2012. Holocene glacial and climate history of Prince Gustav Channel, northeastern Antarctic Peninsula. *Quaternary Science Reviews*, **31**, 93-111.

STREET-PERROT, F.A., BARKER, P.A., SWAIN, D.L., FICKEN, K.J., WOOLLER, M.J., OLAGO, D.O. & HUANG, Y. 2007. Late Quaternary changes in ecosystems and carbon cycling on Mt. Kenya, East Africa: a landscape-ecological perspective based on multi-proxy lake-sediment fluxes. *Quaternary Science Reviews,* **26**, 1838-1860.

TER BRAAK, C.J.F. & ŠMILAUER, P. 2002. *CANOCO reference Manual and Canodraw for Windows User's Guide: Software for Canonical Community Ordination (version 45)*. Microcomputer Power, Ithaca NY.

TURNER, J., OVERLAND, J.E. & WALSH, J.E. 2007. An Arctic and Antarctic perspective on recent climate change. *International Journal of Climatology*, **27**, 277-293.

VAN HEUKELEM, L. & THOMAS, C.S. 2001. Computer-assisted high-performance liquid chromatography method development with applications to the isolation and analysis of phytoplankton pigments. *J. Chromatogr.,* **910**, 31-49.

VAN OMMEN, T.D., & MORGAN, V. 2010. Snowfall increase in coastal East Antarctica linked with southwestWestern Australian drought. *Nature Geoscience*, 1-6.

VERLEYEN, E., HODGSON, D.A., GIBSON, J., IMURA, S., KAUP, E., KUDOH, S., DE WEVER, A., HOSHINO, T., MCMINN, A., OBBELS, D., ROBERTS, D., ROBERTS, S.J., SABBE, K., SOUFFREAU, C., TAVERNIER, I., VAN NIEUWENHUYZE, W., VAN RANST, E., VINDEVOGEL, N. & VYVERMAN, W. 2012. Chemical limnology in coastal East Antarctic lakes: monitoring future climate change in centres of endemism and biodiversity. *Antarctic Science*, **24(1)**, 23-33.

VERLEYEN, E., HODGSON, D.A., SABBE, K., CREMER, H., EMSLIE, S.D., GIBSON, J., HALL, B., IMURA, S., KUDOH, S., MARSHALL, G.J., MCMINN, A., MELLES, M., NEWMAN, L., ROBERTS, D., ROBERTS, S.J., SINGH, S.M., STERKEN, M., TAVERNIER, I., VERKULICH, S., VAN DE VYVER, E., VAN NIEUWENHUYZE, W., WAGNER, B. & VYVERMAN, W. 2011. Post-glacial regional climate variability along the East Antarctic coastal margin - evidence from shallow marine and coastal terrestrial records. *Earth-Science Reviews*, **104**, 199-212.

VERLEYEN, E., HODGSON, D.A., SABBE, K., VANHOUTTE, K. & VYVERMAN, W. 2004. Coastal oceanographic conditions in the Prydz Bay region (East Antarctica) during the Holocene recorded in an isolation basin. *Holocene*, **14**, 246-257.

VERLEYEN, E., HODGSON, D.A., VYVERMAN, W., ROBERTS, D., MCMINN, A., VANHOUTTE, K. & SABBE, K. 2003. Modelling diatom responses to climate induced fluctuations in the moisture balance in continental Antarctic lakes. Journal of Paleolimnology, 30, 195-215.

VERLEYEN, E., SABBE, K., HODGSON, D.A., GRUBISIC, S., TATON, A., COUSIN, S., WILMOTTE, A., DE WEVER, A., VAN DER GUCHT, K. & VYVERMAN, W. 2010. Structuring effects of climate-related environmental factors on Antarctic microbial mat communities. *Aquatic Microbial Ecology*, **59**, 11-24.

WAGNER, B., MELLES, M., DORAN, P.T., KENIG, F., FORMAN, S.L., PIERAU, R. & ALLEN, P. 2006. Glacial and postglacial sedimentation in the Fryxell Basin, Taylor Valley, southern Victoria Land, Antarctica. *Palaeogeography Palaeoclimatology Palaeoecology*, **241**, 320-337.

YOSHIDA, Y. & MORIWAKI, K. 1979. Some consideration on elevated coastal features and their dates around Syowa Station, Antarctica. *Memoirs of National Institute of Polar Research. Special Issue*, **13**, 220-226.

Supplementary material

Protocol S1. Detailed description of the analysis of three calibration model runs in OXCAL v. 4.1 and CLAM v. 2.1 (100,000 iterations, smoothing = 0.3; Table 1 & S1; Fig. 5). The radiocarbon ages from the marine-influenced section of the core were challenging, indicating a potential offset between bulk and macrofossil ages. To test the effect of the age-depth model on the timing of isolation, we undertook three calibration model runs in OXCAL and in CLAM: Model 1 (no bulk-macro offsets applied to bulk marine sediment; best-fit age-depth curve based solely on as measured radiocarbon data), Model 2 (no bulk-macro offsets applied to bulk marine sediment; bulk and macrofossil 'as-measured' radiocarbon ages at 227 and 253 cm combined into a single calibrated age range), and Model 3 (an additional 300 ± 100 ^{14}C years offset applied to all bulk sediment 'as-measured' radiocarbon age data before calibration). Model 1 produced too many age-reversals in the marine-influenced section to be usable. Therefore, only Model 2 and Model 3 were considered 'reasonable'.

The calibrated median ages of bulk marine sediments were 370 ± 180 and 360 ± 190 cal. yr BP older than those of the sponge spicules and carbonate shells (Table 1). The bulk-macrofossil offset is, therefore, consistent at two independent depths, and could indicate that bulk sediment ages are 300-400 years too old, but it is a small dataset. However, as there is a significant overlap between the bulk marine sediment and the equivalent sponge spicule calibrated age ranges, bulk and macrofossil ages could be considered to be statistically indistinguishable. Because a bulk-macrofossil age offset cannot be entirely ruled out, we have retained both Model 2 as a maximum possible age-depth sequence, and Model 3 as a minimum possible age-depth sequence (Fig. 5). Model 3 could be considered more reliable, but it would require significantly more data from the region to unequivocally determine the existence and scale of a bulk sediment age offset. Therefore, in this paper, we use Model 2 median calibrated ages.

Lacustrine data (Calibration curve B) was used as baseline input data for CLAM age-depth model runs, with full post-bomb (Calibration curve A) and full marine probability distributions (Calibration curve C) for individual calibrated ages generated in OXCAL and imported into CLAM as text files at specified depths (recommended method; Blaauw, pers. comm.). All marine ages in model runs 1-3 were calibrated using a ΔR value of 720 ± 100 (reflecting the regional marine reservoir correction of 1120 ± 100 for the Lützow Holm Bay region; Yoshida & Moriwaki 1979) in OXCAL and imported into CLAM. For model runs 1-3, a smooth-spline curve produced the best-fit to data (as shown by comparatively lower -log values) (Fig. 5).

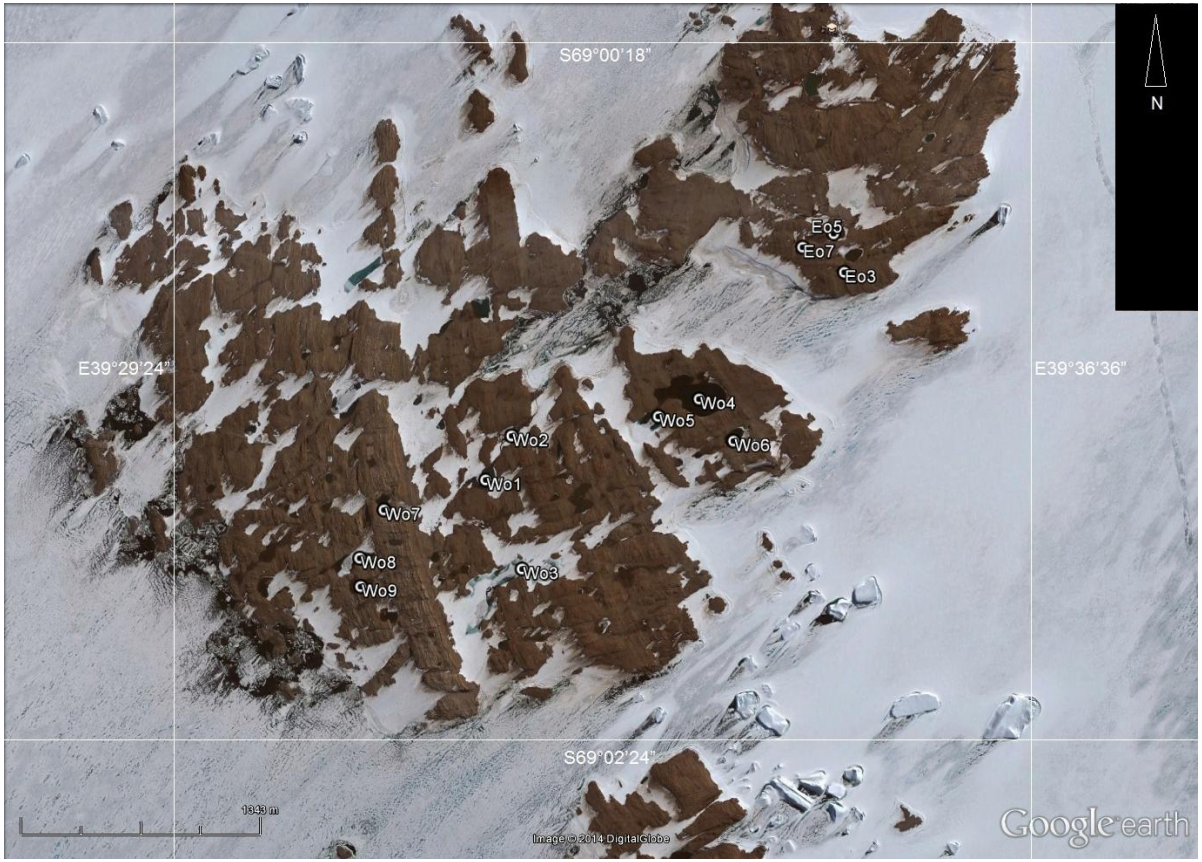

Figure S1. Aerial photo of East and West Ongul Island (Lützow Holm Bay, East Antarctica). Study lakes on which the transfer function is based are indicated with codes Eo3, Eo5, Eo7, and Wo1-9.

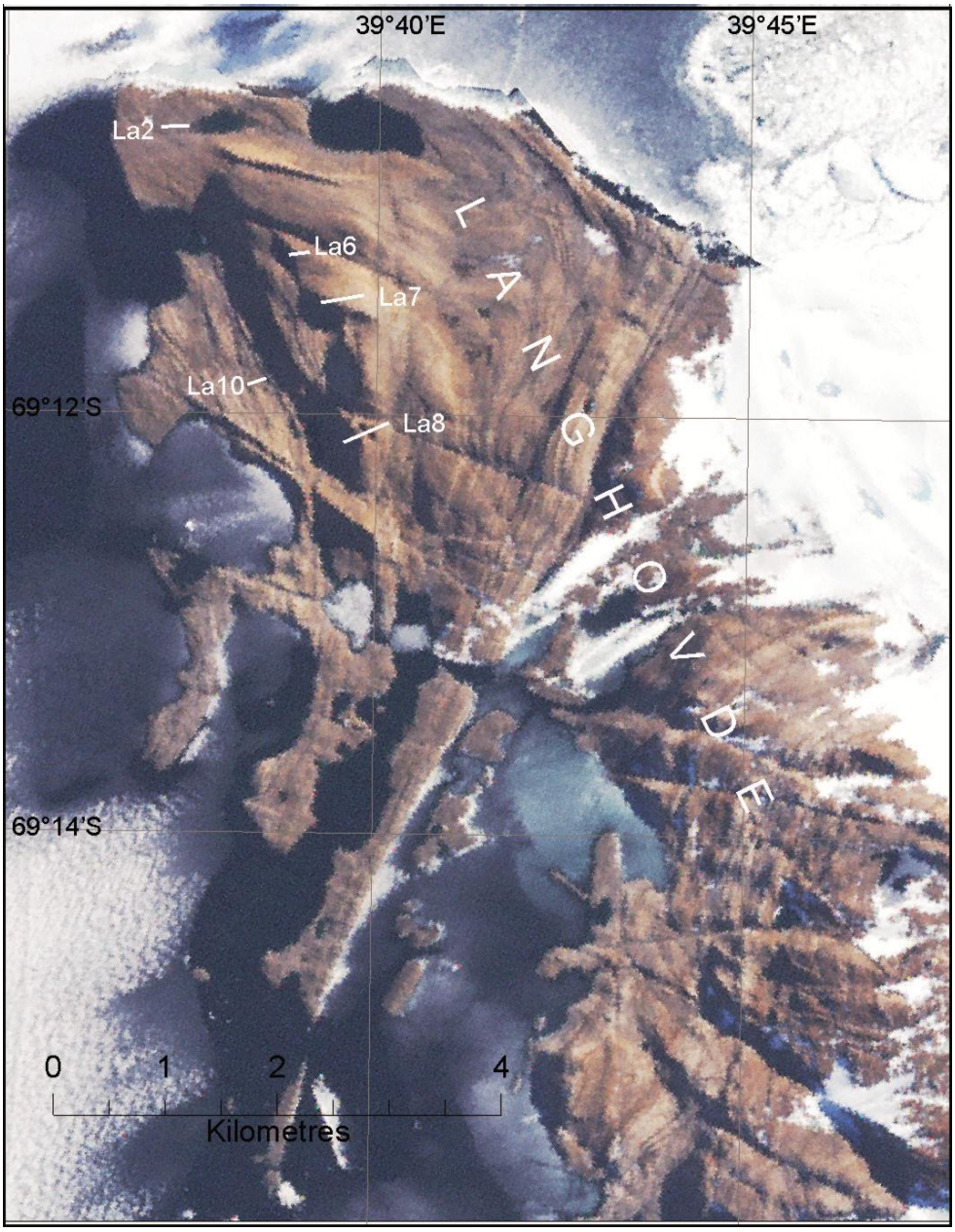

Figure S2. Detailed map of Langhovde (Lützow Holm Bay, East Antarctica). Study lakes on which the transfer function is based are indicated with codes La2, La6, La8, and La10.

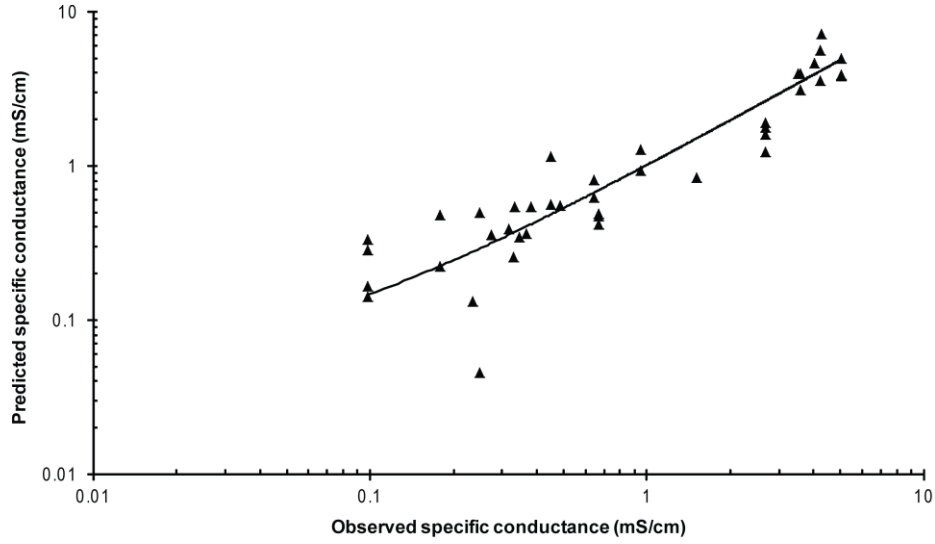

Figure S3. Plot showing inferred and observed specific conductance for the samples of the surface dataset from Lützow Holm Bay, used to construct the transfer function.

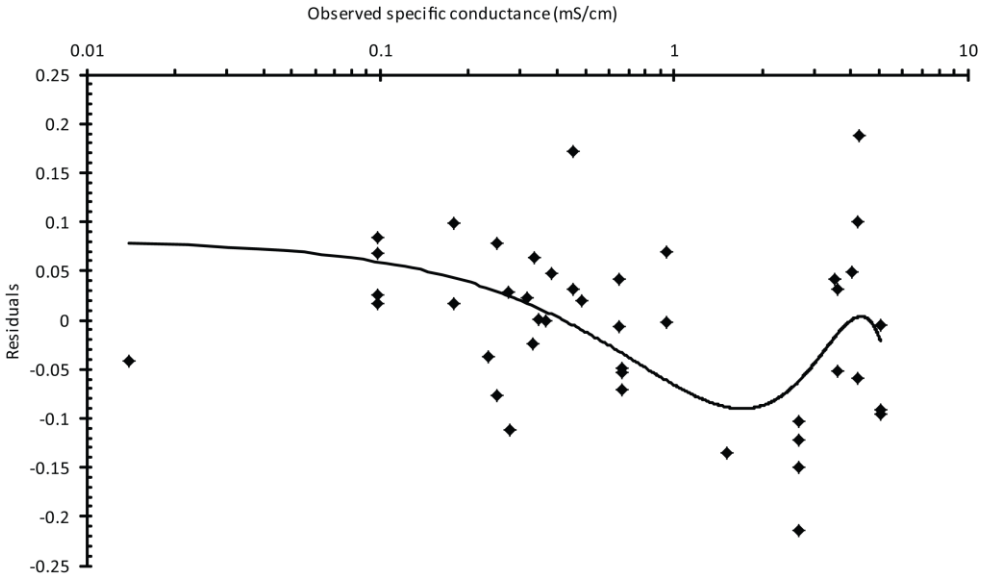

Figure S4. Residuals (predicted minus observed values) versus observed specific conductance. Trends in the residuals are highlighted with a polynomial trendline.

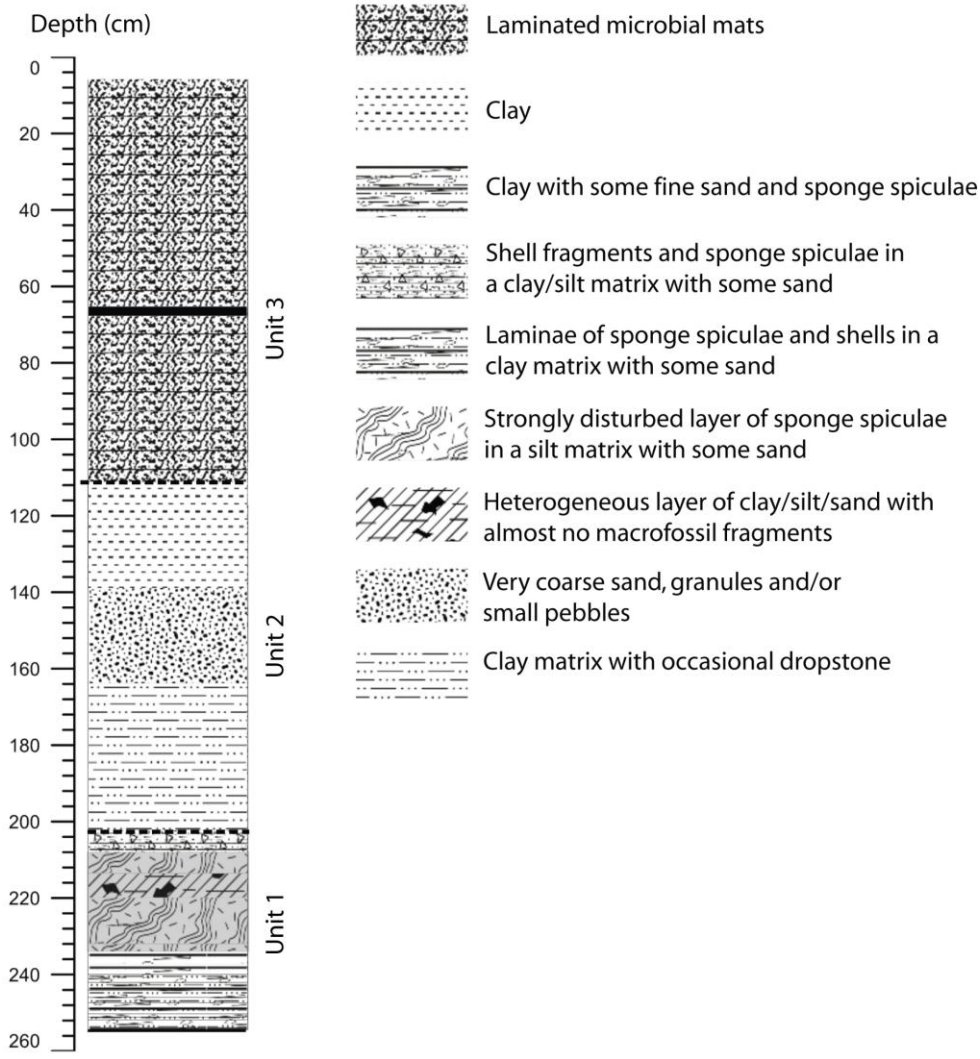

Figure S5. Simplified lithology with accompanying legend of the Mago Ike sediment core.

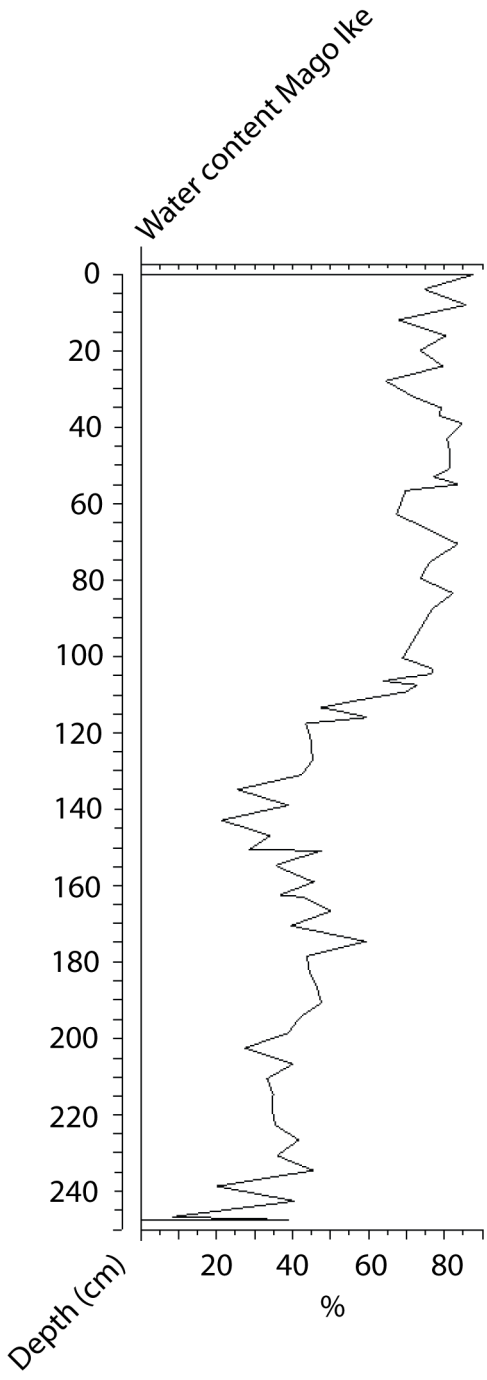

Figure S6. Water content of the Mago Ike sediments.

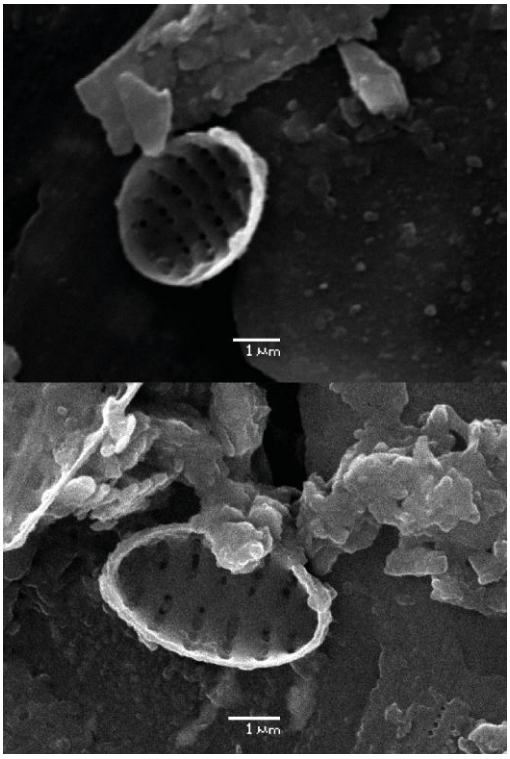

Figure S7. Scanning Electron Microscope (SEM) pictures of the unidentified *Fragilaria* sp. from the sediments of Mago Ike, Skarvsnes, taken with a JEOL JSM5600LV (JEOL, Tokyo, Japan).

Depth (cm)	Models 2 (normal font) and 3 (italics)		Model 3		Calibration curve
	Mean±1s	Median	Mean±1s	Median	
0.5	>2004 or	>2004 or	>-54 or	>-54 or	A
	1958 ± 1	1958	-8 ± 1	-7)	(x - SEQ)
3.5	1996 ± 9	1998 AD	-46 ± 9	-48	A
5.5	1994 ± 10	1997 AD	-44 ± 10	-47	A
7	360 ± 75	375	360 ± 75	375)	(x - RW)
9.5	1987 ± 12	1992 AD	-37 ± 12	-42	A
13.5	1959 ± 8	1958 AD	-9 ± 8	-8	A
30	205 ± 60	195	205 ± 60	195	B
56	420 ± 55	440	420 ± 55	440	B
77,5	460 ± 50	480	460 ± 50	480	B
91.5	475 ± 45	490	475 ± 45	490	B
111.4	685 ± 30	685	685 ± 30	685	B
113.4	795 ± 55	780	795 ± 55	780	B
122.1	1175 ± 60	1180	1175 ± 60	1180	B
168	1640 ± 125	1640	1320 ± 130	1320	C
201	1885 ± 135	1885	1540 ± 130	1540	C
227_{bulk}	2140 ± 130	2145	1770 ± 140	1770	C
227_{macro}	1770 ± 130	1775			C
$227_{bulk}/227_{macro}$	*1965 ± 130*	*1965*			C
253_{bulk}	2220 ± 140	2220	1860 ± 130	1860	C
253_{macro}	1860 ± 135	1860			C
$253_{bulk}/253_{macro}$	*2040 ± 130*	*2040*			C

Table S1. Radiocarbon table for the Mago Ike sediment cores (part 2). Mean ± 1σ, and median calibrated ages (cal. yr BP relative to AD 1950). Greyed out data are considered least likely or as outliers. Out-of-sequence data, marked as x-SEQ, or ages where reworking of sediment appears likely, marked as x-RW, were both excluded from the age-depth model. Model Runs 1-3: for detailed information, see the Supplementary Material (Protocol S1). All marine ages were calibrated using a ΔR value of 720 ± 100 (Yoshida & Moriwaki 1979) (Fig. 5).

Region(s)	Model	Apparent r^2	Jack-knifed r^2	RMSEP	Reference
Syowa Oasis	WA-PLS1	0.84	0.79	0.32	This study
Syowa Oasis	WA-PLS2	0.90	0.85	0.26	This study
saline lakes VH		0.80	0.73	0.37	Roberts and McMinn 1998
BI, LH, RI, VH, WI		0.86	0.83	0.31	Verleyen et al. 2003
VH, WI		0.85	0.79	0.36	Roberts et al. 2004

Table S2. Overview of the apparent r^2, jack-knifed r^2 and RMSEP of different East Antarctic transfer functions. VH = Vestfold Hills, BI = Bølingen Islands, LH = Larsemann Hills, RI = Rauer Islands, WI = Windmill Islands.

Lacustrine diatom species in the surf. dataset	Occurrence in 27 lakes (%)	Mean rel. abundance (%)	WA optima spec. cond.	WA tolerances spec. cond.
Achnanthes taylorensis	22.22	0.36	2.48	0.76
Chamaepinnularia cymatopleura	66.67	7.36	3.33	0.50
Craspedostauros laevissimus	22.22	1.31	4.24	0.04
Craticula antarctica	70.37	6.45	0.73	0.33
Diadesmis australis	59.26	18.10	0.23	0.18
Halamphora veneta	81.48	19.40	0.61	0.37
Hantzschia cf. *amphioxys*	25.93	0.20	0.20	0.05
Luticola australomutica	11.11	0.12	1.31	0.93
Luticola austroatlantica	70.37	2.87	0.99	0.63
Luticola gaussii	18.52	0.08	0.37	0.11
Luticola murrayi	25.93	0.06	0.77	0.55
Luticola muticopsis	22.22	0.08	2.14	0.99
Luticola pseudomurrayi	81.48	6.02	1.70	0.81
Navicula gregaria	81.48	15.30	0.74	0.88
Navicula phyllepta	25.93	5.47	4.42	0.15
Navicula shackletoni	33.33	0.69	0.95	0.66
Nitzschia commutata	33.33	0.60	0.23	0.22
Psammothidium papilio	66.67	10.05	0.27	0.15
Psammothidium stauroneioides	25.93	0.80	0.06	0.61
Pseudostaurosira sp. 1	18.52	1.08	0.28	0.08
Stauroneis latistauros	55.56	1.21	0.15	0.13

Table S3. WA optima and tolerances for specific conductance of the lacustrine species.

Chapter 4. Holocene climate and environmental changes on West Ongul Island (East Antarctica)

Author's contribution: diatom analysis of Yumi Ike, Nishi Ike, and part of Ô-Ike, supervision of the diatom analysis of part of Ô-Ike, supervision of the pigment analysis of Ô-Ike, geochemical analyses (TC, TN) of all the cores, construction of the age-depth models, writing parts of the manuscript.

Other contributors are listed alphabetically: Ilse Daveloose, Dominic A. Hodgson, Satoshi Imura, Annelies Jacques, Sakae Kudoh, Koen Sabbe, Elie Verleyen, Wim Vyverman

Note: not all contributors commented on this manuscript

Key-words: East Antarctica - Holocene - lakes - Mid- to Late-Holocene warm period - deglaciation

Abstract

In order to better understand the effects of current and future climate changes on polar ecosystems and the cryosphere, there is a need for well-dated Holocene palaeoclimate records, particularly from the Southern Hemisphere. Here we conducted a multi-proxy analysis of five lake sediment records from West Ongul Island (Lützow Holm Bay, East Antarctica) in order to examine the onset of deglaciation of the island and to identify the presence and timing of Holocene climate anomalies against a background of local environmental changes. The oldest radiocarbon date recovered from a glacial lake is c. 11.2 cal. ka BP, suggesting an Early-Holocene deglaciation of West Ongul Island. This is however in contrast with marine fossils from raised beaches on the island and the nearby East Ongul Island, which predate the Last Glacial Maximum (LGM). Our results suggest that the island was covered by permanent snowbanks during the LGM. Primary production remained low in the glacial lakes, possibly until c. 6290 cal. yr BP, which might have been related to partial ice and/or snow cover in the lake catchments. At that time (c. 6530 - 5000 cal. yr BP), marine sediments in the isolation lakes suggest the presence of sea-ice and seasonally stratified open-water conditions, which is comparable to the present-day situation in Lützow Holm Bay. A Mid- to Late-Holocene warm period could be inferred between c. 4170 and 940 cal. yr BP based on primary production data and changes in the moisture balance of the closed basins. A period of Neoglacial cooling could be inferred from c. 940 cal. yr BP onwards. There is no evidence for a Medieval Climate Anomaly, or a Little Ice Age event in any of the studied sediment records.

Introduction

In order to have a better understanding of the effects of current and future climate changes on both ecosystems and the cryosphere, there is a need for adequate regional coverage of well-dated palaeoclimate records spanning the Holocene. This is because current rates of air temperature warming and changes in ice-sheet mass balance show large geographical differences between and within each of the polar regions (ACIA 2004;

Steig et al. 2009; King et al. 2012). In the Northern Hemisphere (NH) these palaeoclimate data are becoming increasingly available (e.g. Axford et al. 2009; Kaufman et al. 2009). By contrast, they are still largely lacking from the Southern Hemisphere (SH) high-latitudes (Mann et al. 2008). In particular, coastal areas in vast sectors of Continental Antarctica remain understudied, such as Dronning Maud Land, Enderby Land and Terre Adélie (Fig. 1; Verleyen et al. 2011 in Appendix 2).

Ice cores from the continental plateau are often unable to fully resolve the more subtle Holocene climate anomalies (e.g. Mayewski et al. 2004) due to the small variations in isotopic composition compared to coastal ice cores (e.g. Mayewski et al. 2009; Steig et al. 2013). The latter are thus often more sensitive to small-scale climate variability. However, they are relatively rare because the ice-sheet is more dynamic in coastal regions, often preventing the establishment of a reliable chronology and reconstruction (Hodgson & Smol 2008). In coastal regions, long-term monitoring studies in both Continental and Maritime Antarctica have demonstrated that lake ecosystems are very sensitivity to recent climate changes (Doran et al. 2002; Quayle et al. 2002). Their sediments potentially hold high-resolution records of climate change and have been shown to be very useful in linking climate records derived from ice cores from the continental plateau with marine sediment cores from the Southern Ocean (e.g. Verleyen et al. 2004a; Hodgson et al. 2005). Together with the dominance of physical forcing on lake ecosystems and the virtual absence of bioturbation, this makes them suitable to gain more insight into the apparent phase differences between terrestrial and marine Holocene climate optima (Verleyen et al. 2004a; 2011 in Appendix 2).

Current evidence indicates that the Pleistocene-Holocene transition in Antarctica is characterised by a circum-Antarctic Early-Holocene Climate Optimum (EHCO) between 11.5 and 9 ka BP (Mayewski et al. 2009; Masson-Delmotte et al. 2010). This thermal optimum is well-resolved in coastal and continental ice cores (e.g. Masson et al. 2000; Mayewski et al. 2009; Masson-Delmotte et al. 2010), as well as in the majority of terrestrial (e.g. Cromer et al. 2005; Hodgson et al. 2005) and coastal marine records (e.g. Finocchiaro et al. 2005; Crosta et al. 2007). Together with eustatic sea-level rise resulting from the disintegration of parts of the continental ice masses (Mackintosh et al. 2011), this climate optimum appears to be coincident with the deglaciation of several coastal regions in East Antarctica (EA) (Verleyen et al. 2011 in Appendix 2), such as the Windmill Islands, the continental shelf in Mac Robertson Land and parts of Lützow Holm Bay (Mackintosh et al. 2013). However, deglaciation is asynchronous in the different ice-free regions along the East Antarctic coastline. For example in Wilkes Land (Fig. 1), substantial ice-sheet thinning and lateral retreat of the East Antarctic Ice-Sheet (EAIS) had started prior to this optimum and continued during and after the EHCO (Mackintosh et al. 2013). Some coastal oases such as the Larsemann Hills and Bunger Hills (Fig. 1) were ice-free since before the Last Glacial Maximum (LGM) (Hodgson et al. 2001; Gore et al. 2001), while others became only partially ice-free during the Mid-Holocene (Hodgson et al. 2001). This is probably also the case in Lützow Holm Bay (Fig. 1); based on *in situ* fossils in raised beaches, it has been suggested that the Ongul Islands (Fig. 1) were ice-free during the LGM (Miura et al. 1998) and even since Marine Isotope Stage (MIS) 6 or 7 (Takada et

al. 2003). By contrast, Skarvsnes, only c. 60 km from East Ongul Island, became ice-free during the Early-Holocene (Yamane et al. 2011; Chapter 5). These regional differences in deglaciation history of the EAIS are likely related to differences in bedrock geomorphology and related ice-sheet flow and direction, grounding line position, ocean currents transporting warm/cold waters to the continental shelf, and/or regional climate variability (Mackintosh et al. 2013). However, terrestrial records enabling the reconstruction of the deglaciation history in the Ongul Islands are still lacking.

After the EHCO, climate anomalies detected in shallow marine and coastal terrestrial records appear to be out of phase and show large regional differences in amplitude, timing and duration, suggesting that regional climate dynamics following the EHCO were more complex (Verleyen et al. 2011 in Appendix 2). The disparity between marine and terrestrial records might be related to differences in heat capacity between the ocean and the continent (Renssen et al. 2005), in combination with the observation that biotic indicators in marine records reflect spring, summer and autumn conditions (Bentley et al. 2009), while in lacustrine sediment cores they largely reflect summer conditions when the lakes are free of snow and ice and primary production is highest. However, primary production in the water column might also occur during spring and autumn, under dim conditions and lake ice cover (Tanabe et al. 2008), which calls the last argument into question. Also dating uncertainties may account for part of this disparity. In general, an overall cooling trend between c. 9 and 4 ka BP has been observed in terrestrial records of EA and the Antarctic Peninsula (AP) (e.g. Verleyen et al. 2004a; Hodgson et al. 2005; Bentley et al. 2009), whereas certain marine records contain evidence for a marine climate optimum until c. 4 ka BP (e.g. Verleyen et al. 2004a; Berg et al. 2010).

A Mid- to Late-Holocene warm period is inferred from a range of terrestrial records in Maritime and East Antarctic coastal regions (see Bentley et al. 2009 and Sterken et al. 2012 for a review). The onset of this optimum appears to have varied regionally, for example at the northeastern tip of the AP (c. 3170 cal. yr BP; Sterken et al. 2012), the South Orkney Islands to the north (c. 3800 cal. yr BP; Hodgson & Convey 2005), and the Amery Oasis (c. 3.5 ka BP; Wagner et al. 2004; Newman et al. unpubl. res.), Larsemann Hills (c. 4 ka BP; Verleyen et al. 2004a; b), and Vestfold Hills (c. 4.7 ka BP; Björck et al. 1996) in EA. In some cases, these differences in timing may be related to the buffering effect of ocean currents as was suggested for the Prince Gustav Channel (eastern AP) where the Weddell Gyre may have promoted a regional cooling around 4000 cal. yr BP (Sterken et al. 2012), while a warming was observed over the western part of the AP, likely attributed to a poleward displacement of the Southern Westerlies bringing warm, moist air to this region (Bentley et al. 2009). This climate optimum in terrestrial environments might be the result of low-altitude coastal sites being closer to the 0°C threshold, making them very responsive to climate change. Therefore, relatively small changes in temperature, lake ice-extent, snow cover, light availability, and albedo can have a significant impact on the ecology (Quayle et al. 2002). In EA, regional differences in the timing of the onset of this climate optimum might be related to local processes. For example in the Larsemann Hills (Fig. 1), some catchments deglaciated during this period

(Hodgson et al. 2001), which resulted in albedo changes. In turn, this possibly caused local warming, which affected lake dynamics. However, it remains unclear whether this local deglaciation was the result of the climate optimum or rather the trigger for it (Verleyen et al. 2011 in Appendix 2).

In general, the Mid-Holocene climate optimum was followed by a Neoglacial cooling from c. 2 ka BP onwards, which is evidenced as colder and/or dryer conditions on land (Verleyen et al. 2011 in Appendix 2). In EA, Neoglacial cooling has been inferred from lake records in the Larsemann Hills around c. 2 ka BP (Hodgson et al. 2005), in the Amery Oasis from c. 2.3 ka BP onwards (Wagner et al. 2004), in the Vestfold Hills from c. 3 ka BP onwards (Fulford-Smith & Sikes 1996) and in the Windmill Islands from c. 1 ka BP onwards (Cremer et al. 2003) (Fig. 1). Much attention has been paid to detect climate anomalies in SH records similar in timing, duration and amplitude to the NH Medieval Climate Anomaly (MCA; c. 1050 - 650 yr BP) and Little Ice Age (LIA; c. 500 - 100 yr BP) (Mann et al. 2009). Although some regions such as Dronning Maud Land (Fig. 1) remain understudied, the available lake records along the East Antarctic coastline (Verleyen et al. 2011 in Appendix 2) and the vast majority of the Antarctic ice core records (e.g. Steig et al. 1998; 2013; Mulvaney et al. 2002; Masson-Delmotte et al. 2004) do not show any evidence for these climate anomalies (Goosse et al. 2012; Verleyen et al. 2011 in Appendix 2; Tavernier et al. in press. - Chapter 3).

Using sediment records from five lakes on West Ongul Island (Lützow Holm Bay), we aimed to (1) examine the onset of deglaciation of the region; (2) assess the consistency of environmental signals between records, and more specifically, determine to which extend these signals are consistent among sites and thus reflect regional drivers of environmental changes; and (3) compare the timing of Holocene climate anomalies with other East Antarctic regions. To achieve our aims, we performed a multi-proxy analysis on radiocarbon-dated sediment cores from two isolation lakes and three glacial lakes. Initial radiocarbon dates of the Ô-Ike (WO4) sediments revealed that a higher temporal resolution could be obtained in this core compared with the others. It was therefore studied in most detail. To date, sediment cores from Yumi Ike (WO1), Nishi Ike (WO8), Ura Ike (WO5), and Higashi Ike (WO6) were analysed at a lower resolution, but additional analyses are underway to increase the temporal resolution.

Site description

Lützow Holm Bay (within the quadrangle 69 - 70°S and 35 - 40°E) is a 220 km-wide bay on the eastern coast of Dronning Maud Land (EA) (Miura et al. 1998) (Fig. 1). The Ongul Islands are situated in the northeast of Lützow Holm Bay along Sôya Coast and are separated from the Prince Olav Coast by the Ongul Strait, holding a drowned glacial trough, the Fuji Submarine Valley (Miura et al. 1998). The islands are comprised of more than ten small islands, of which West Ongul Island (7.8 km²) is the largest (Yanai et al. 1974) (Fig. 1). A narrow sea way, Naka-no-seto Strait, which was ice-free during the sampling period in 2007, separates it from East Ongul Island (Fig. 1). It is furthermore separated from Teöya by the Minami-no-seto Strait and from Ongul Kalven Island by the Nishi-no-seto Strait (Yanai et al. 1974) (Fig. 1). Meteorological measurements over the

past 50 years at Syowa Station on East Ongul Island (Fig. 1) indicate a mean annual temperature of -10.5°C and a mean wind speed of 6.6 m/s, predominantly blowing northeasterly (Sato & Hirasawa 2007).

The geomorphology on West Ongul Island consists of low-altitude hills with a rounded glacial topography and shallow valleys. Raised beach deposits are found in the lower areas along the coast (Yanai et al. 1974). Numerous ponds occur on the island, as a result of water occupying depressions in the terrain exposed during the last deglaciation.

Ô-Ike (Fig. 1) (69°1.329'S - 39°33.715'E) is situated on the northeastern side of the island at 13 m above sea-level (a.s.l.). The lake is characterised by a maximum depth of 12 m, a pH of 7.6 and a specific conductance of 0.33 mS/cm. The lake has no outflow stream and is fed with meltwater derived from multiyear snowbanks in the catchment. Yumi Ike (Fig. 1) (69°1.581'S - 39°32.094'E) is situated 10 m a.s.l. The lake is characterised by a maximum depth of 5 m, a pH of 8.1 and a specific conductance of 0.25 mS/cm. During the sampling period, it had an active inflow stream originating from snow banks in the catchment. An active outflow stream drained into a small pond and subsequently into the sea. Nishi Ike (Fig. 1) (69° 1.859'S - 39° 31.032'E) is situated 23 m a.s.l. and characterised by a maximum depth of 6 m, a pH of 7.7, and a specific conductance of 0.27 mS/cm. The southern side of the lake was at the time of sampling characterised by sandy shorelines, and the eastern side by the presence of a large snow bank which provided meltwater to the lake. Ura Ike (Fig. 1) (69° 1.417'S - 39° 33.479'E) is situated 17 m a.s.l. and characterised by a maximum depth of 12 m, a pH of 7.6 and a specific conductance of 0.28 mS/cm. The lake was closed and fed by meltwater from multiyear snowbanks in the catchment. It is situated above Ô-Ike and close to Higashi Ike (Fig. 1). The latter (69° 1.473'S - 39° 34.170'E) is situated 18 m a.s.l. and characterised by a maximum depth of 5 m, a pH of 7.6 and a specific conductance of 0.67 mS/cm. During the time of sampling, the lake was fed by a large snow bank but had no active outflow stream.

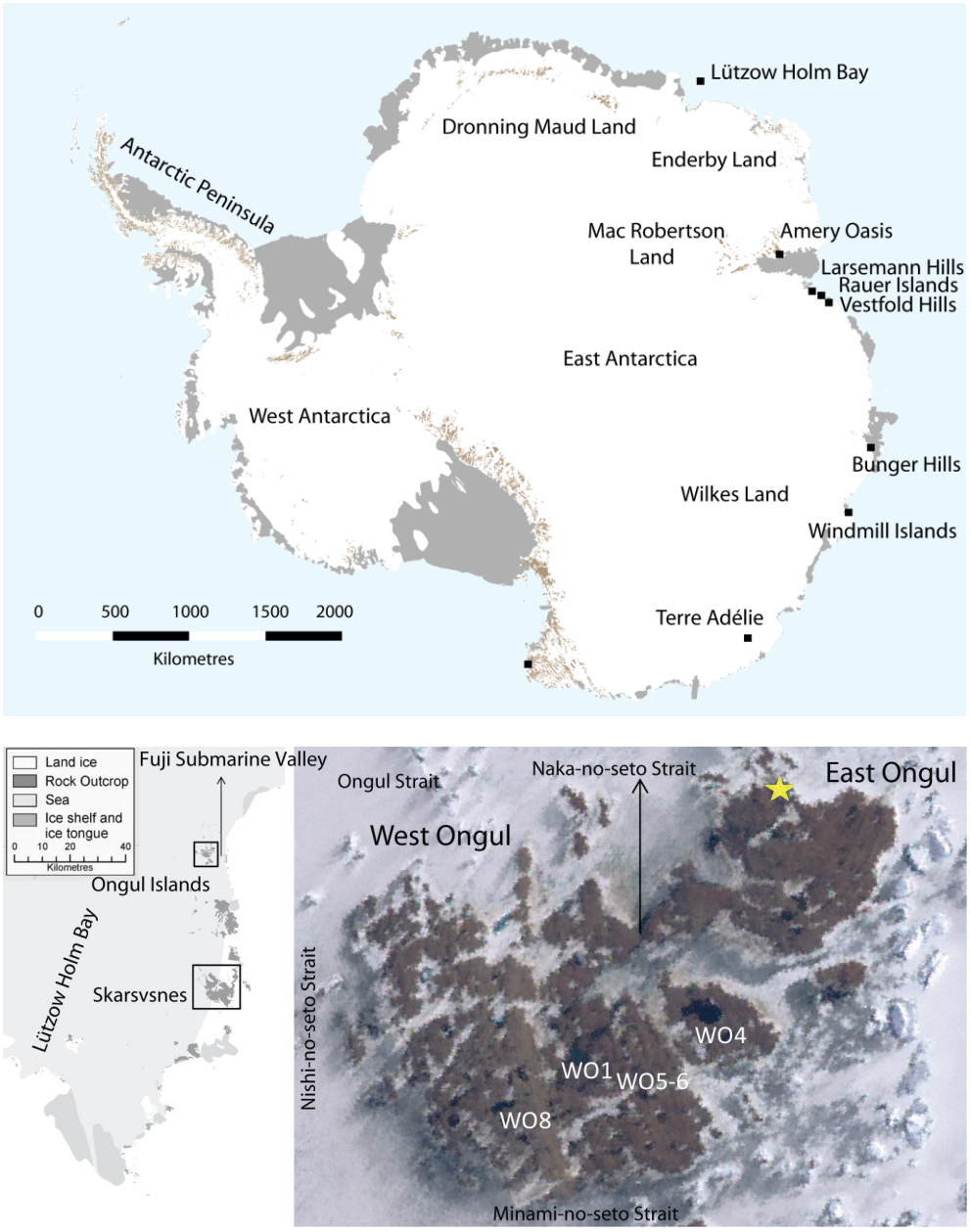

Figure 1. Top: overview map of Antarctica showing the location of the regions mentioned in the text. Bottom: map of Lützow Holm Bay, and the Ongul Islands (East and West Ongul Island), along with the Straits mentioned in the text, and the study lakes (Ô-Ike=WO4, Yumi Ike=WO1, Nishi Ike=WO8, Ura Ike=WO5, and Higashi Ike=WO6). The main location of Syowa Station on East Ongul Island is indicated with a yellow star.

Materials and methods

Lake sediment coring

Sediments were collected in January 2007 at the deepest part of the lakes using a UWITEC gravity corer for the upper centimeters of the sediment and a square-rod piston sampler (Wright 1967) for the deeper sediments. During coring, the bedrock was most likely reached in all lakes.

Radiocarbon dating

Twelve samples from Ô-Ike, six from Yumi Ike, eight from Nishi Ike, five from Ura Ike, and three from Higashi Ike were dated using AMS ^{14}C by the UK Natural Environment Research Council (NERC) Radiocarbon Laboratory or the Beta Analytic Radiocarbon Dating Laboratory. Dated samples from the lacustrine parts of the sediments were composed of microbial-mats, whereas those from the marine parts (indicated with an asterisk in the radiocarbon table; Table 1), were composed of bulk matrix. The results are reported as conventional radiocarbon years BP with two-sigma (2σ) standard deviation errors. Dates were calibrated using the SHCal04.14C calibration curve for freshwater sediments (McCormac et al. 2004; Reimer et al. 2004), or the Marine09.14C calibration curve for marine sediments (Reimer et al. 2009). As the SHCal04.14C curve only extends to 11 cal. ka BP, the age-depth model of Nishi Ike was run with the NH curve, IntCal09.14C (Reimer et al. 2009) glued at the bottom of SHCal04.14C, applying an appropriate SH offset, as recommended by Blaauw (2010). The AMS ^{14}C dates of the marine sediments were corrected for the marine carbon reservoir effect by subtracting a regional reservoir correction of 1120 years, following Yoshida & Moriwaki (1979). An error of ±100 years for the reservoir effect has been applied based on the Yoshida & Moriwaki (1979) dates. Age-depth modelling was undertaken using OXCAL v. 4.1 (Bronk Ramsey 2009) and the CLAM v. 2.1 software in R (Blaauw 2010). For all models, 10,000 iterations weighted by calibrated probabilities at 95% confidence ranges were performed. All reported ages in the text are rounded to the nearest 10 years.

Lithostratigraphical, geophysical and geochemical analyses

Before splitting, the intact sediment cores were scanned with a GEOTEK multi-sensor core logger measuring gamma ray density (GRD) and volume-specific magnetic susceptibility (MS) in 0.2-cm steps. These data are only available for the Ô-Ike sediments between 176.8 and 86.6 cm, for the Yumi Ike sediments between 69 and 0 cm, and for the Higashi Ike sediments between 64.6 and 27.6 cm. GRD was converted to dry bulk density (DBD) by using a dry weight conversion factor. To obtain this, a weighted sample was dried for 48h at a temperature of 60°C in an oven and subsequently re-weighted. The percentage dry weight was calculated as the ratio between the weight of the dried sample to that of the wet sample. When GRD data were not available, a mean GRD value of the sediments of that specific lake was used to calculate DBD. Volume-specific MS was used to correlate different overlapping sections of the sediment cores and has been converted to mass-specific MS by dividing it by the DBD. This was subsequently used to calculate the mass

accumulation rate (MAR) (as in Street-Perrot et al. 2007). Macroscopic descriptions included sediment texture (qualitative grain size, sorting, etc.) and structure (laminations, grading, etc.).

Concentrations of total carbon (TC) and total nitrogen (TN) were analysed using a Flash 2000 Organic Elemental Analyzer. Measurements were carried out by dry combustion at high temperature (left furnace: 950°C and right furnace: 840°C; King et al. 1998). The data were processed using the Eager Xperience software. Samples were all ran at least twice to detect and exclude possible erroneous values. Outliers were excluded and the mean value of replicates was plotted. Reproducibility within and between different runs was tested using standards of sulphanilamide, with a known carbon and nitrogen content of respectively 41.84 and 16.27%. This analysis revealed that our method is reproducible as these samples yielded an average carbon concentration of 41.8%, ranging between 41.2 and 42.5%, and an average nitrogen concentration of 16.3%, ranging between 15.3 and 17.0%. The analytical error of the TC and TN analysis was calculated based on the measured sulphanilamide standards, as well as on a sample from each lake which had been run multiple times. The highest and hence most conservative error obtained was applied. In Ô-Ike, 189 samples were analysed from the cores, in Yumi Ike 84 samples, in Nishi Ike 88 samples, in Ura Ike 48 samples, and in Higashi Ike 56 samples. A number of samples were treated with 5% HCl to remove carbonates. This revealed that samples contained little inorganic carbon and that TC can be cautiously used as an approximation of total organic carbon (TOC) (See also Chapter 1, p. 15). However, the presented TC data here were only used to support hypotheses made based on other proxies, which directly reflect primary production (i.e., fluxes of total chlorophylls, carotenoids, and diatoms). While samples were analysed for TC and TN throughout the entire sediment cores from Ô-Ike, Yumi Ike, and Nishi Ike, data are currently only available for the intact stored parts of the sediment cores from Ura Ike and Higashi Ike (i.e., between 74 - 37 cm and 67 - 23 cm coring depth respectively).

Diatom analysis

Diatom analysis was performed on the Ô-Ike, Yumi Ike and Nishi Ike sediment cores only. Quantitative analysis followed standard methods (Battarbee & Kneen 1982; Renberg 1990). Diatoms were counted using a Zeiss axiophot light microscope under oil immersion at a magnification of 10x100. At least 400 valves (>2/3 intact or unmistakably the middle part of the raphe system) were counted in each sample, except when concentrations were too low to reach this number. In Ô-Ike, 99 samples were analysed from the cores, in Yumi Ike 20 samples, and in Nishi Ike 21 samples (all subsamples taken at a maximum interval of 4 cm). Taxonomic identification was mainly based on Sabbe et al. (2003), Ohtsuka et al. (2006) and Esposito et al. (2008) for the freshwater diatoms and Cremer et al. (2003) and Scott & Thomas (2005) for the marine and brackish-water diatoms. A constrained cluster analysis (CONISS) was performed and the significance of the zones was assessed using a broken-stick model (Bennett 1996) in the Rioja package in R (Juggins 2009). Stratigraphic data were plotted using Tilia and Tilia Graph (Grimm 2004). Specific conductance in the lacustrine zones of the cores was reconstructed using a weighted

averaging-partial least squares (WA-PLS2) transfer function which was developed using the C2 package (Juggins 2003) (see Tavernier et al. in press. - Chapter 3). Sample-specific errors of reconstructed specific conductance were calculated using C2 (Juggins 2003) with 999 bootstrapped cycles.

Fossil pigment analysis

Fossil pigment analysis was performed on the sediment cores from Ô-Ike only. Fossil pigments were extracted and analysed following Van Heukelem & Thomas (2001). The system was calibrated using authentic pigment standards and compounds isolated from reference cultures [Scientific Committee on Oceanic Research (SCOR) protocols; DHI, Denmark]. The identification of the pigments was based on Jeffrey et al. (1997) and pigments of unknown affinity were assigned as derivatives of the pigment with which they showed the closest match based on retention times and absorption spectra, or as 'unknown'. Concentrations of individual pigments in the samples were calculated using the response factors of standard pigments. The response factors of unknown carotenoids, eta eta-carotene and vaucheriaxanthin were calculated as the mean of the response factors of the other carotenoids, because no standards were analysed for these pigments. Similarly, the response factors of unknown chlorophylls and phaeophorbide *a* were calculated as the mean of the response factors of the other chlorophylls, and for unknown mixtures of carotenoids and chlorophylls, a mean response factor for all carotenoids and chlorophylls was used. The abundance of individual pigments is reported as percentage of total chlorophylls or carotenoids.

Fluxes of proxy data

Proxy data are represented as fluxes to take into account the influence of variable sedimentation rates (SRs) and large changes in the proportion of organic, siliciclastic and biogenic components on changes in primary production indicators (Street-Perrot et al. 2007). The MAR (g/cm^2yr) was calculated as the multiplication of the DBD (g/cm^3) and the SR (cm/yr). The flux of each proxy was calculated as the multiplication of the MAR and the concentration (by weight) or the absolute counts at that depth. Due to the presence of air in the sediment cores of Nishi Ike and Ura Ike, no reliable GRD values were obtained, hence no flux data are available for these two lakes.

Results

Radiocarbon dating and age-depth modelling

For Ô-Ike, a smooth-spline model was chosen with a smoothing factor of 0.4, as indicated by the lowest goodness-of-fit (Fig. 2). The bottom layers of the sediment are c. 7010 cal. yr BP old (168 cm). Dates were in stratigraphic order except for those at 104 and 92 cm. These were excluded from the age-depth model (Table 1). The sample at 171 cm failed to generate sufficient CO_2 for reliable AMS-analysis because the carbon content was less than 0.1% dry weight. The sediment accumulation rate was lowest in the bottom sediments (0.005 cm/yr) and increased to 0.073 cm/yr between 132 cm and the top sediment core (Fig. 2).

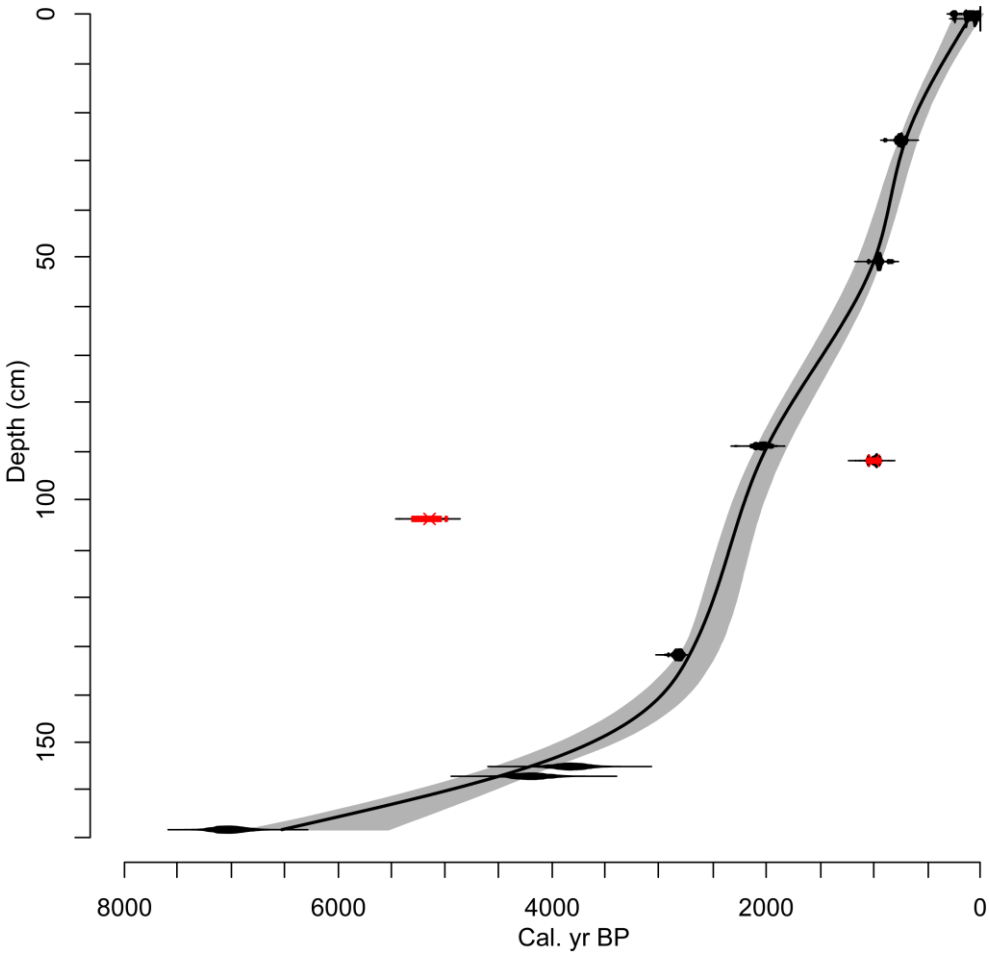

Figure 2. Stratigraphic age-depth plot undertaken in OXCAL v. 4.1 (Bronk Ramsey 2009) and CLAM v. 2.1 (Blaauw 2010) for Ô-Ike. Outliers are indicated in red. Calibrated radiocarbon ages are shown in Table 1. A smooth-spline model was chosen with a smoothing factor of 0.4.

For Yumi Ike, a smooth-spline model with a smoothing factor of 0.1 was chosen, as indicated by the lowest goodness-of-fit (Fig. 3). The bottom layers of the sediment core are c. 5560 cal. yr BP old (73 cm; Table 1). Dates were in stratigraphic order. The sediment accumulation rate was highest in the bottom sediments until 39 cm (on average 0.033 cm/yr) and was lower between 39 cm and the top sediments (on average 0.009 cm/yr) (Fig. 3).

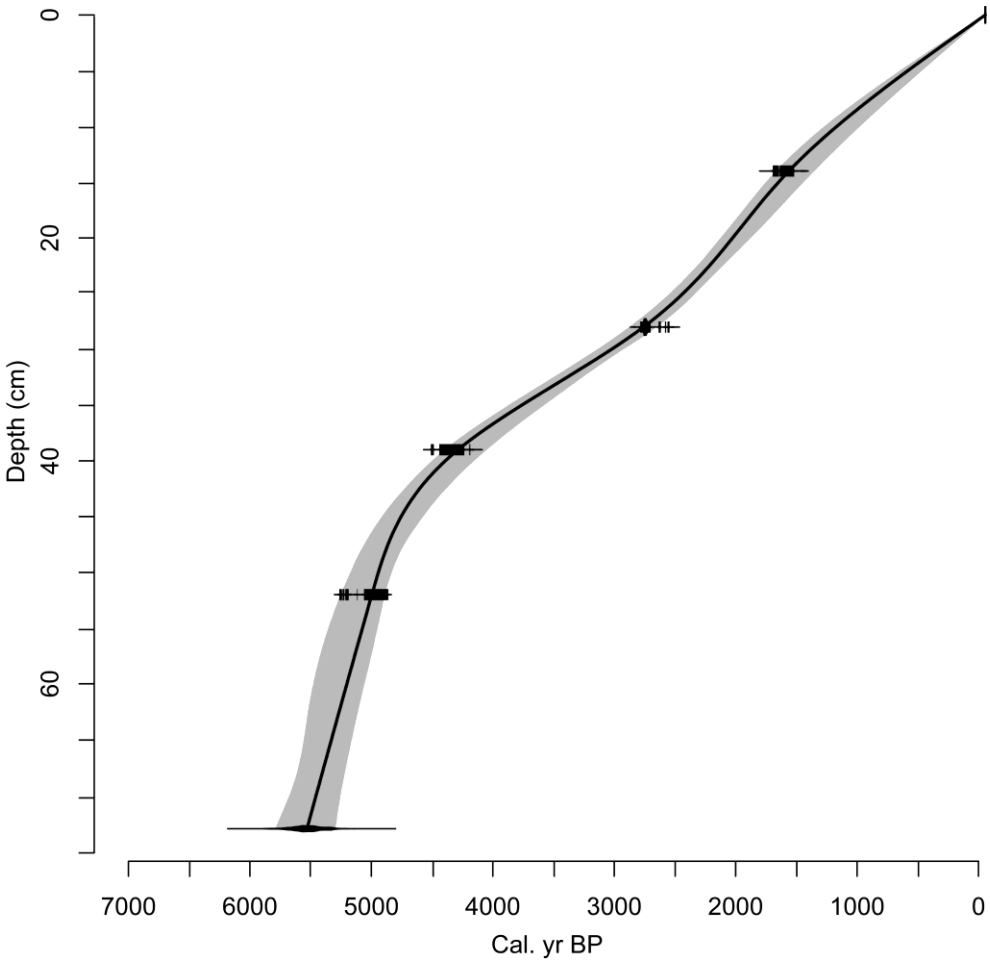

Figure 3. Stratigraphic age-depth plot undertaken in OXCAL v. 4.1 (Bronk Ramsey 2009) and CLAM v. 2.1 (Blaauw 2010) for Yumi Ike. Calibrated radiocarbon ages are shown in Table 1. A smooth-spline model was chosen with a smoothing factor of 0.1.

For Nishi Ike, a cubic-spline model was chosen, based on the lowest goodness-of-fit (Fig. 4). The bottom layers of the sediment core (71 cm) failed to generate sufficient CO_2 for reliable AMS-analysis, as the carbon content was less than 0.1% dry weight; so the bottom age remains unknown (Table 1). The sample at 60 cm was c. 11,240 cal. yr BP old. Dates were in stratigraphic order. The sediment accumulation rate was lowest between the bottom of the core and 40 cm (on average 0.003 cm/yr), after which it was higher (on average 0.010 cm/yr) (Fig. 4).

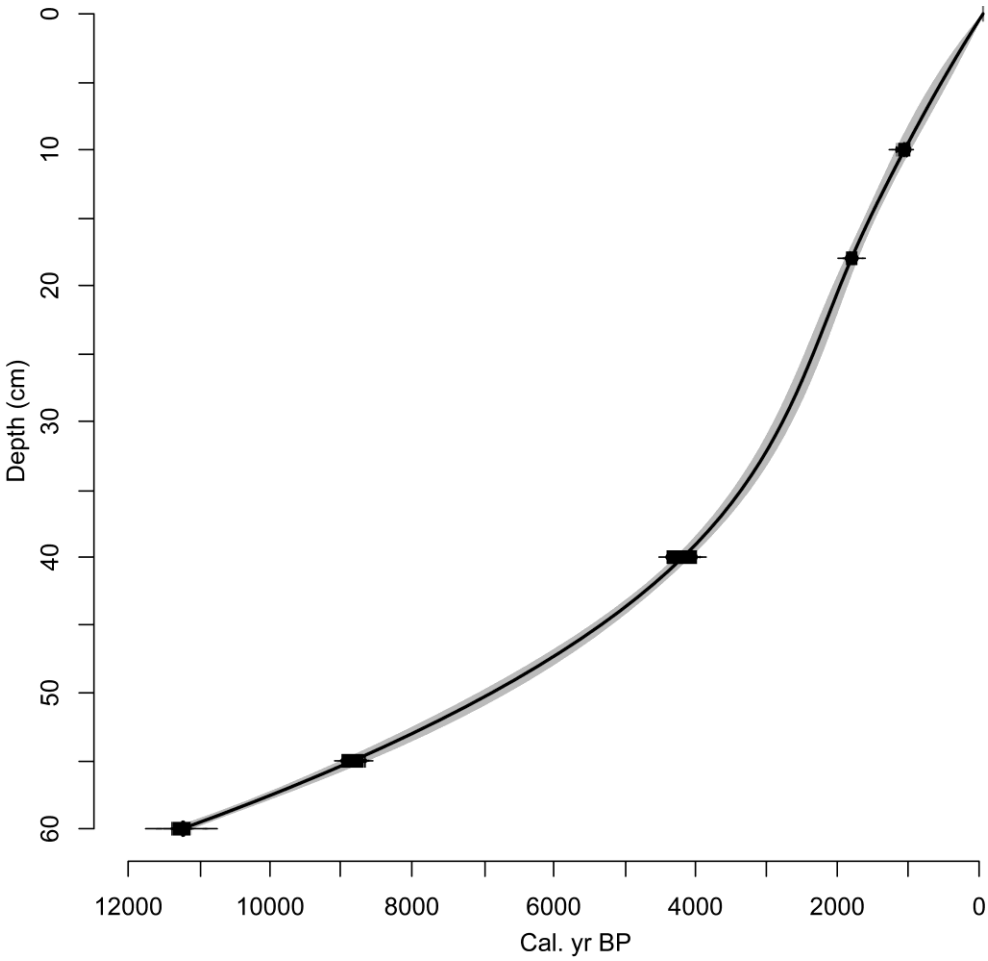

Figure 4. Stratigraphic age-depth plot undertaken in OXCAL v. 4.1 (Bronk Ramsey 2009) and CLAM v. 2.1 (Blaauw 2010) for Nishi Ike. Calibrated radiocarbon ages are shown in Table 1. A cubic-spline model was chosen.

In Ura Ike, the oldest radiocarbon date taken, is c. 6290 cal. yr BP (51 cm; Table 1). Additional radiocarbon dates from the bottom sediments of the core (73 cm) are required to determine the age of the oldest sediments in this lake.

The bottom layers of the Higashi Ike sediment core (65 cm) failed to generate sufficient CO_2 for a reliable AMS-analysis, because the carbon content was less than 0.1% dry weight; so the bottom age remains unknown (Table 1). The sample at 51 cm was dated at c. 4560 or 4520 cal. yr BP.

Table 1. Conventional and calibrated radiocarbon dates, dated material, publication code and the inferred dates using the age-depth models constructed with OXCAL v. 4.1 (Bronk Ramsey 2009) and CLAM v. 2.1 (Blaauw 2010). Dates indicated with an asterisk were corrected for the marine reservoir effect (1120 years; Yoshida & Moriwaki 1979). CRA = Conventional Radiocarbon Age. The most likely calibrated age of the oldest radiocarbon date used as bottom age of the sediments is mentioned below each table for each lake.

Ô-Ike depth (cm)	Dated material	Publication code	^{14}C enrichment (% modern ± 1σ)	Carbon content (% by wt.)	$\delta^{13}C_{VPDB}$ ‰ ± 0.1	CRA (yr BP ± 1σ)	Cal. using CALIB (yr BP)	Rel. area under probability distribution	Best fit according to the model (cal. yr BP)	2σ age range (cal. yr BP)
0	microbial-mat	SUERC - 18342	98.16 ± 0.43	8.9	-14.2	149 ± 35	0-32	0.228	80	230 - -30
							57-122	0.477		
							133-144	0.071		
							224-255	0.224		
1	microbial-mat	Beta - 279333	102.0 ± 0.5	-	-12.5	40 ± 40	0-0	0.324	100	250 - 0
							29-58	0.443		
							121-135	0.225		
							234-236	0.008		
26	microbial-mat	Beta - 279334	-	-	-12.8	880 ± 40	688-702	0.141	700	750 - 590
							719-774	0.812		
							782-787	0.047		
51	microbial-mat	Beta - 279335	-	-	-21.2	1080 ± 40	911-973	1	990	1150 - 940
89	microbial-mat	Beta - 261170	-	-		2130 ± 40	1992-2072	0.705	1990	2080 - 1810
							2076-2114	0.295		
92	microbial-mat	Beta - 261171	-	-		1130 ± 40	935-945	0.105	outlier	outlier
							953-1002	0.633		
							1031-1051	0.263		
104	microbial-mat	Beta - 261172	-	-	-15.1	4570 ± 40	5056-5187	0.728	outlier	outlier
							5214-5223	0.048		
							5236-5243	0.036		
							5261-5296	0.188		
132	microbial-mat	Beta - 322269	-	-	-13.1	2790 ± 30	2783-2856	1	2720	2820 - 2470
155*	bulk matrix	SUERC - 18067	56.52 ± 0.25	1.5	-23.2	4583 ± 36	3680-3966	1	4210	4530 - 4000
157*	bulk matrix	SUERC - 18068	54.63 ± 0.26	0.9	-23.6	4856 ± 38	4066-4367	1	4500	4810 - 4240
168*	bulk matrix	Beta - 261174				7240 ± 50	6893-7158	1	6530	6850 - 5530
171	bulk matrix					insufficient CO_2				

The most likely calibrated age of the oldest radiocarbon date (7240 ± 50), used as bottom age of the sediments: 7010 cal. yr BP

Yumi Ike depth (cm)	Dated material	Publication code	^{14}C enrichment (% modern ± 1σ)	Carbon content (% by wt.)	$\delta^{13}C_{VPDB}$ ‰ ± 0.1	CRA (yr BP ± 1σ)	Cal. using CALIB (yr BP)	Rel. area under probability distribution	Best fit according to the model (cal. yr BP)	2σ age range (cal. yr BP)
0	microbial-mat	SUERC - 18338	102.85 ± 0.47	8.4	-14.6	modern			-60	-50 - -60
14	microbial-mat	Beta - 322266	-	-	-16.2	1730 ± 30	1533-1612	1	1560	1660 - 1360
28	microbial-mat	Beta - 322267	-	-	-8.3	2660 ± 30	2723-2758	1	2760	2870 - 2660
39	microbial-mat	SUERC - 18056	61.00 ± 0.27	0.7	-21.6	3970 ± 35	4294-4334	0.336	4290	4390 - 4060
							4337-4419	0.664		
52	microbial-mat	Beta - 322268	-	-	-21.7	4460 ± 30	4879-4939	0.428	5000	5240 - 4890
							4955-4985	0.223		
							4993-5039	0.349		
73*	bulk matrix	SUERC - 18066	48.02 ± 0.23	0.1	-18.5	5893 ± 38	5416-5654	1	5530	5780 - 5300

The most likely calibrated age of the oldest radiocarbon date (5893 ± 38), used as bottom age of the sediments: 5560 cal. yr BP

Nishi Ike depth (cm)	Dated material	Publication code	^{14}C enrichment (% modern ± 1σ)	Carbon content (% by wt.)	$\delta^{13}C_{VPDB}$ ‰ ± 0.1	CRA (yr BP ± 1σ)	Cal. using CALIB (yr BP)	Rel. area under probability distribution	Best fit according to the model (cal. yr BP)	2σ age range (cal. yr BP)
0	microbial-mat	SUERC - 18345	106.16 ± 0.49	12.4	-13.7	modern			-60	- 50 - -60
10	microbial-mat	Beta - 322270	-	-	-11	1200 ± 30	978-1039	0.661	1050	1170 - 970
							1043-1077	0.339		
18	microbial-mat	Beta - 322271	-	-	-12.8	1920 ± 30	1737-1762	0.23	1800	1880 - 1720
							1772-1830	0.574		
							1844-1864	0.195		
40	microbial-mat	Beta - 322272	-	-	-16.2	3900 ± 30	4156-4207	0.328	4170	4270 - 4080
							4221-4297	0.533		
							4330-4351	0.109		
							4373-4380	0.029		
40	microbial-mat	Beta - 327120	-	-		3790 ± 30	3994-4039	0.384	4170	4270 - 4080
							4076-4103	0.243		
							4107-4149	0.373		
55	microbial-mat	SUERC - 18071	36.85 ± 0.18	0.2	-21.2	8019 ± 40	8728-8736	0.029	8830	8990 - 8650
							8755-8813	0.261		
							8824-8873	0.233		
							8876-8979	0.478		
60	microbial-mat	Beta - 322273	-	-	-23.4	9870 ± 60	11213-11324	1	11240	11390 - 11120
71	microbial-mat					insufficient CO_2				

The most likely calibrated age of the oldest radiocarbon date (9870 ± 60), used as bottom age of the sediments: 11240 cal. yr BP

Ura Ike depth (cm)	Dated material	Publication code	^{14}C enrichment (% modern ± 1σ)	Carbon content (% by wt.)	$\delta^{13}C_{VPDB}$ ‰ ± 0.1	CRA (yr BP ± 1σ)	Cal. using CALIB (yr BP)	Rel. area under probability distribution	Best fit according to the model (cal. yr BP)	2σ age range (cal. yr BP)
0	microbial-mat	SUERC - 18343	96.56 ± 0.45	9,5	-28,4	281 ± 37	154-171	0,159		
							179-189	0,062		
							192-206	0,093		
							278-324	0,646		
							416-424	0,039		
37	microbial-mat	Beta - 327121	-	-	-29,9	4340 ± 30	4831-4867	1		
37	microbial-mat	Beta - 326318	-	-	-30,6	4500 ± 30	4970-5065	0,571		
							5111-5121	0,039		
							5184-5217	0,182		
							5221-5271	0,209		
40	microbial-mat	SUERC - 18070	53.07 ± 0.25	1,6	-31,1	5090 ± 38	5721-5769	0,337		
							5786-5792	0,026		
							5805-5891	0,637		
50	microbial-mat	SUERC - 18069	50.42 ± 0.24	1,2	-30	5500 ± 38	6209-6251	0,596		
							6262-6292	0,404		
51	microbial-mat	SUERC - 18058	50.25 ± 0.23	0,8	-30,7	5528 ± 37	6213-6243	0,403		
							6269-6306	0,597		

The most likely calibrated age of the oldest radiocarbon date taken (5528 ± 37): 6290 cal. yr BP

Higashi Ike depth (cm)	Dated material	Publication code	^{14}C enrichment (% modern ± 1σ)	Carbon content (% by wt.)	$\delta^{13}C_{VPDB}$ ‰ ± 0.1	CRA (yr BP ± 1σ)	Cal. using CALIB (yr BP)	Rel. area under probability distribution	Best fit according to the model (cal. yr BP)	2σ age range (cal. yr BP)
0	microbial-mat	SUERC - 18344	105.88 ± 0.49	5.3	-13.9	modern				
51	microbial-mat	Beta - 326319	-		-15.3	4130 ± 30	4448-4467	0.123		
							4517-4616	0.746		
							4765-4784	0.13		
64	microbial-mat					insufficient CO_2				

The most likely calibrated age of the oldest radiocarbon date (4130 ± 30), used as bottom age of the sediments: 4520 or 4560 cal. yr BP

Lithostratigraphical and geophysical analysis

The Ô-Ike sediments between 176 and 155.8 cm are composed of dark, grey clay with some sand (Fig. 5a). The upper 155.8 cm of the sediments are composed of finely laminated microbial-mats. Mass-specific MS increases from the bottom sediments to a maximum value at 163 cm to decrease to very low values (close to zero) between c. 151 and 86.6 cm (Fig. 5a). GRD is slightly higher and variable between the bottom sediments and c. 154.8 cm, to become relatively lower and more stable between c. 151 and 86.6 cm (Fig. 5a).

The Yumi Ike sediments are composed of grey clay between 83.4 and c. 44 cm, and turn into clay-sand between c. 44 and 6 cm (Fig. 5b). In the upper c. 6 cm of the sediments, less consolidated microbial-mats occur. Colors range from orange-rust, to grey, brown and black. Mass-specific MS is highly variable throughout the sediments (Fig. 5b). Values decrease from the bottom sediments until c. 56 cm, to increase and reach a maximum at 37.2 cm. Values decrease again until c. 20 cm to become relatively higher in the upper sediments. GRD is relatively high between 69 and c. 55.6 cm and then lower until c. 38 cm (Fig. 5b). Between 38 and c. 21.6 cm, values are relatively high after which GRD shows a decreasing trend until c. 11 cm. From then onwards GRD increases again to become highest in the upper c. 5 cm.

The Nishi Ike sediments are fairly homogeneous between 72 and c. 43 cm, and are mainly composed of black clay (Fig. 5c). Between c. 43 and 20 cm, sediments are composed of clay with some sand. The upper 20 cm of the sediments are more laminated and consist of black, grey and rust-coloured microbial-mats.

The Ura Ike sediments are between 74 and 43 cm composed of a fairly homogeneous mixture of grey clay, which turns into slightly more laminated, black clay with some sand in the upper 43 cm (Fig. 5d).

The Higashi Ike sediments are composed of a homogeneous mixture of clay between 67 and c. 21 cm (Fig. 5e). The upper 21 cm of the sediments is composed of less consolidated darker grey clay-sand. Both Mass-specific MS and GRD values show an overall decreasing trend from the bottom sediments until 27.6 cm (Fig. 5e).

Water content data of the Ô-Ike, Yumi Ike and Higashi Ike sediment cores are plotted in Fig. S1 of the Supplementary Material.

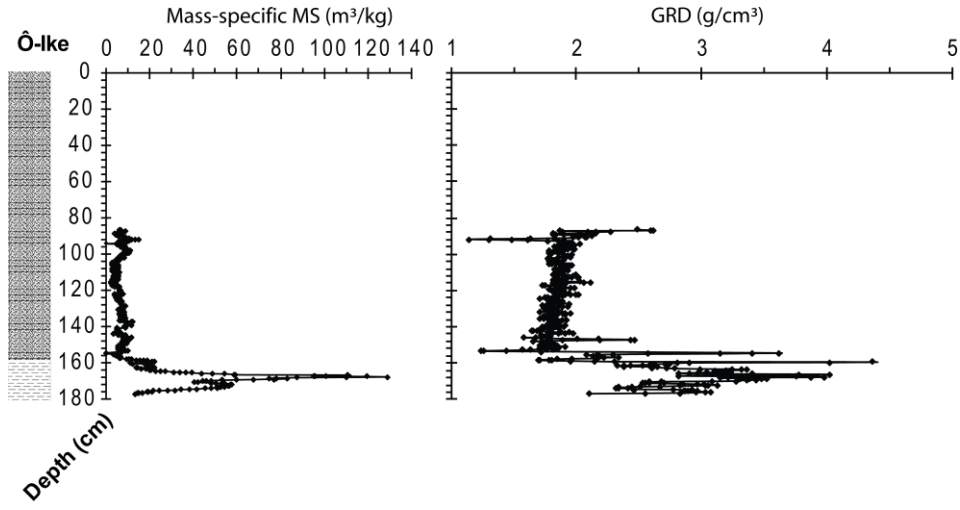

Figure 5a. Lithology (legend in Fig. 5f), mass-specific magnetic susceptibility (MS) and gamma ray density (GRD) of the Ô-Ike sediments.

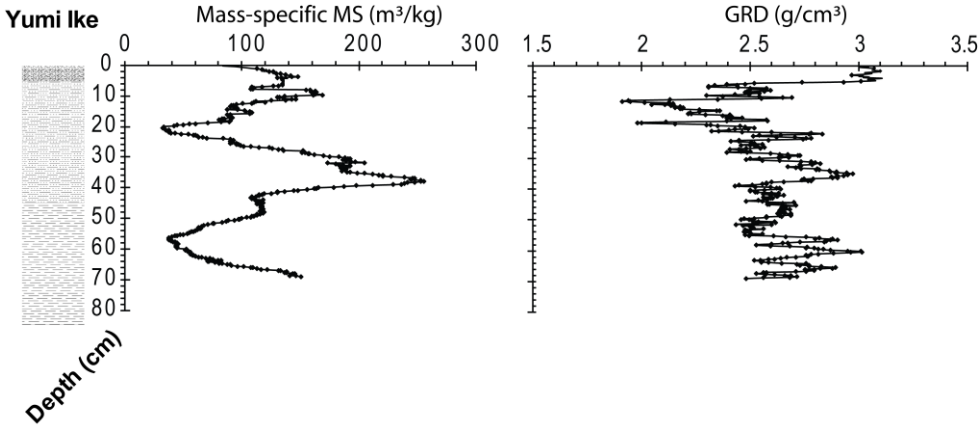

Figure 5b. Lithology (legend in Fig. 5f), mass-specific magnetic susceptibility (MS) and gamma ray density (GRD) of the Yumi Ike sediments.

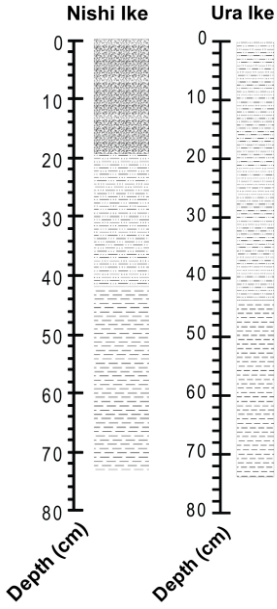

Figure 5c and 5d. Lithology (legend in Fig. 5f) of the Nishi Ike (left) and Ura Ike (right) sediments.

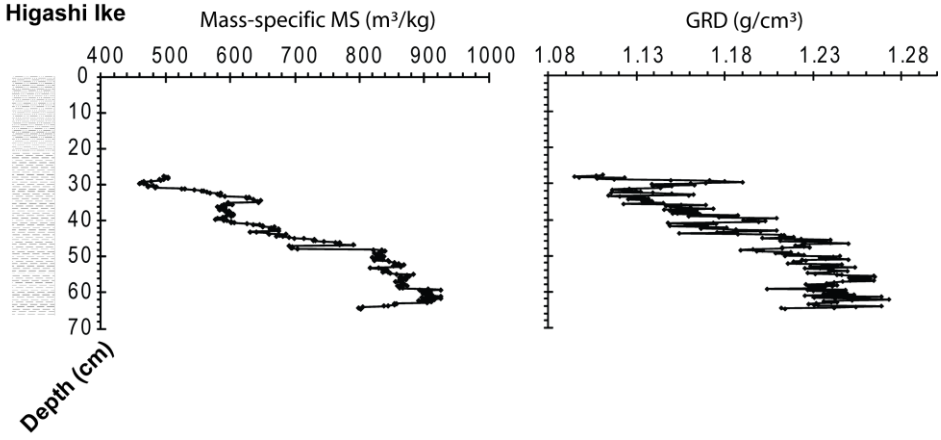

Figure 5e. Lithology (legend in Fig. 5f), mass-specific magnetic susceptibility (MS) and gamma ray density (GRD) of the Higashi Ike sediments.

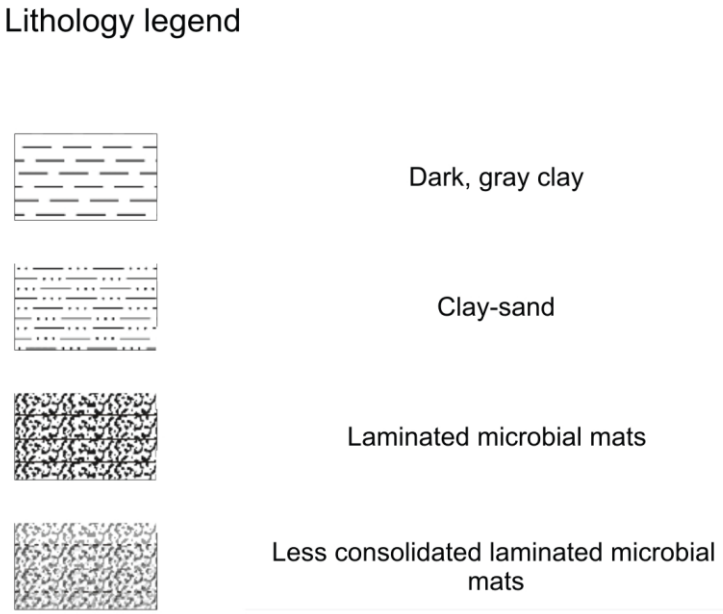

Figure 5f. Lithology legend of the Ô-Ike, Yumi Ike, Nishi Ike, Ura Ike, and Higashi Ike sediments.

Geochemical analysis

The analytical error of the TC and TN analysis calculated using the sulphanilamide standards yielded an error of respectively 0.66% and 0.97%. The multiple run of samples resulted in an error of 2.5, 0.22, 0.35, 0.05, and 0.14% for the TC analysis, and an error of 0.17, 0.01, 0.03, 0.02, and 0.01% for the TN analysis in respectively Ô-Ike, Yumi Ike, Nishi Ike, Ura Ike and Higashi Ike. The most conservative error was used namely the error of 0.66% and 0.97% based on the sulphanilamide standards, except for the TC analysis of Ô-Ike (2.5%). In the Higashi Ike sediments, TC content was within the analytical error and is therefore not considered in the discussion. For TN concentrations, this was the case for all lakes (Figs. 7a and b).

The lakes differ strongly in their sediment TC content (Fig. 6a). TC concentrations are highest in Ô-Ike. They are very low between 172 and 158 cm and show a generally increasing trend until 64 cm where a minimum occurs. TC is relatively high between 58 and 9 cm and decreases towards the top of the sediments. In Yumi Ike, TC concentrations are a lot lower than in Ô-Ike and showed no clear long-term trend with maxima being present at 28, 16 and 12 cm. In Nishi Ike, TC concentrations are very low between 72 and 60 cm and gradually increase between 56 and 44 cm. They reach relatively high values between 40 and 20 cm and at 4 cm depth. In Ura Ike, TC concentrations are very low between 74 and 54 cm, and show an increasing trend until 38 cm.

In Ô-Ike, the TC flux (Fig. 6b) is very low between 172 and 158 cm. It increases until 114 cm, and exhibits a general decreasing trend afterwards with the exception of one peak at 44 cm. In Yumi Ike, the TC flux is a lot lower than in Ô-Ike and shows an increasing trend until 60 cm. It decreases towards the upper sediments where TC values are close to zero.

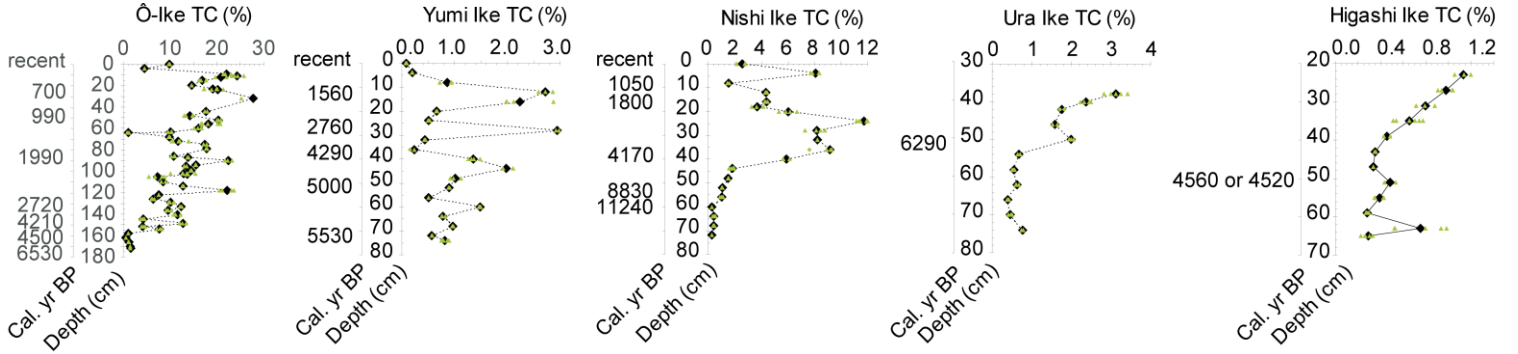

Figure 6a. Total carbon (TC) concentrations of the sediment cores from Ô-Ike, Yumi Ike, Nishi Ike, Ura Ike and Higashi Ike. Symbols: black=average of the samples, green=samples used to calculate the average. Calibrated radiocarbon dates are indicated.

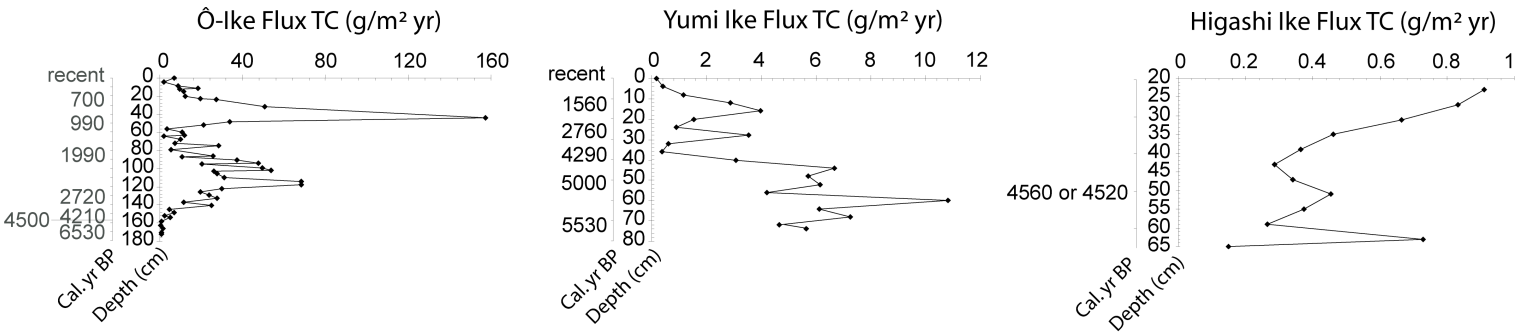

Figure 6b. Total carbon (TC) fluxes of the sediment cores from Ô-Ike, Yumi Ike, and Higashi Ike. Calibrated radiocarbon dates are indicated. Only the averaged values from figure 6a were used.

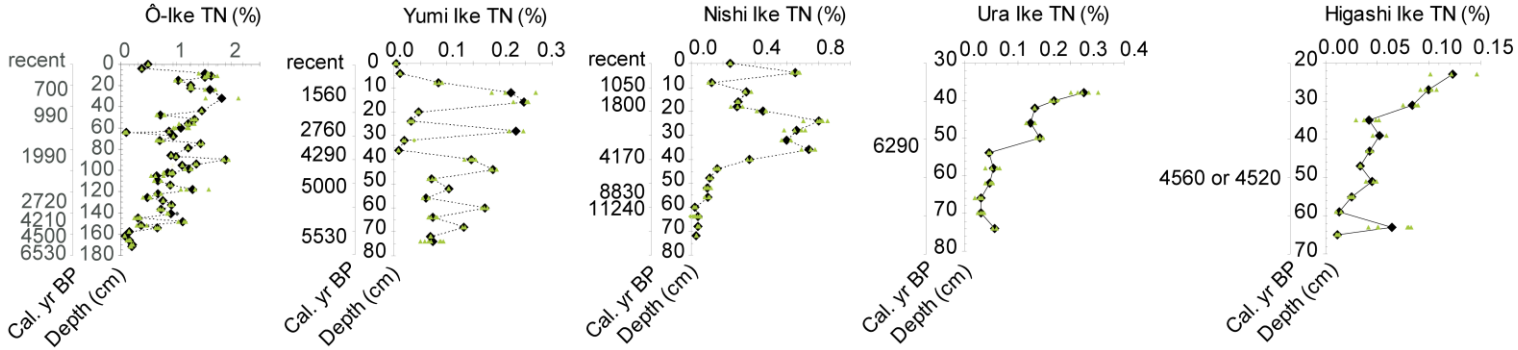

Figure 7a. Total nitrogen (TN) analyses of the sediment cores from Ô-Ike, Yumi Ike, Nishi Ike, Ura Ike and Higashi Ike. Symbols: black=average of the samples, green=samples used to calculate the average. Calibrated radiocarbon dates are indicated.

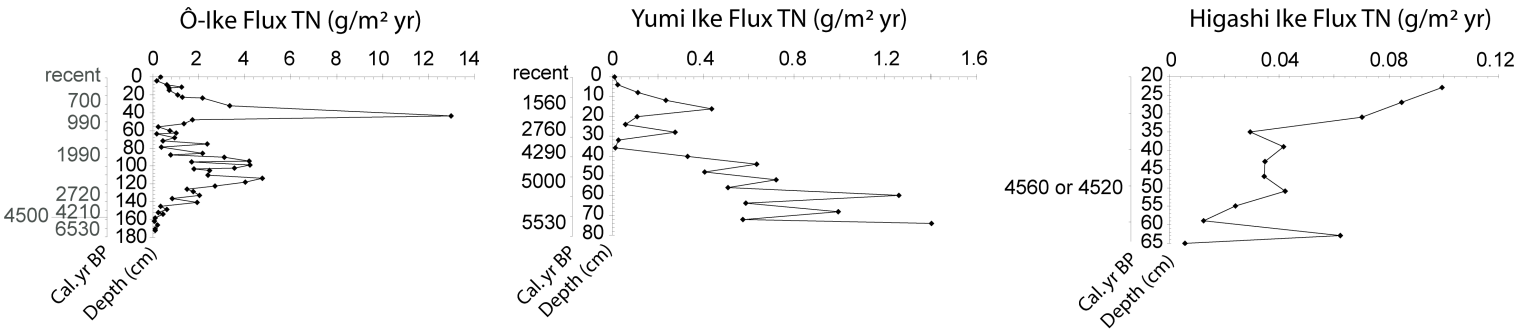

Figure 7b. Total nitrogen (TN) fluxes of the sediment cores from Ô-Ike, Yumi Ike, and Higashi Ike. Calibrated radiocarbon dates are indicated. Only the averaged values from figure 7a were used.

Diatom analysis and inferred specific conductance

In the Ô-Ike sediment cores, a total of 80 diatom taxa were identified of which 16 taxa with a minimum abundance of 2% in at least 3 samples were plotted (Fig. 8). In Yumi Ike, 76 diatom taxa were identified of which 20 taxa with a minimum abundance of 1% in at least 3 samples or a minimum abundance of 10% in at least 1 sample were plotted (Fig. 9). In the Nishi Ike sediment core, a total of 14 diatom taxa were identified and plotted in Fig. 10. Four distinct and significant diatom zones were identified in Ô-Ike (OIDA1-4; Ô-Ike Diatom Analysis), three zones in Yumi Ike (YIDA1-3; Yumi Ike Diatom Analysis), and three zones in Nishi Ike (NIDA1-3; Nishi Ike Diatom Analysis) based on the broken-stick analysis.

Ô-Ike and Yumi Ike are characterised by the presence of both marine and freshwater sediments (Figs. 8 & 9). *Chaetoceros* resting spores, indicators for stratified, open-water conditions, is the most abundant diatom taxon in the marine sediments of Ô-Ike (zone OIDA1; 176 - 160 cm, c. 6530 - 5000 cal. yr BP; Fig. 8) and Yumi Ike (zone YIDA1; 74 - 54 cm, c. 5530 - 5050 cal. yr BP; Fig. 9). Marine sea-ice indicator species, such as *Navicula glaciei, Navicula directa, Fragilariopsis cylindrus* and *Fragilariopsis curta* also occur (Krebs et al. 1987; Crosta et al. 2004; 2008). Brackish-water species, such as *Navicula phyllepta* and *Chamaepinnularia cymatopleura* occur in low abundances; *N. phyllepta* is nearly absent from the Ô-Ike core. In both basins, *Chaetoceros* resting spores decrease, while *N. glaciei* increases in abundance towards the transition zone to lacustrine conditions. The diatom flux in Ô-Ike is relatively low during the marine phase (Fig. 8), whereas in Yumi Ike, the diatom flux is relatively high in the marine sediments, decreases throughout this zone, and increases again at the end of this phase (Fig. 9).

In Ô-Ike, the transition zone between marine and lacustrine sediments is relatively short as evidenced by the lack of a distinct brackish-water period (Fig. 8). By contrast, zone YIDA2 in Yumi Ike (54 - 46 cm, c. 5050 - 4800 cal. yr BP) is characterised by a high abundance of the brackish-water species *N. phyllepta* (Fig. 9). This transition zone in Yumi Ike has a high inferred specific conductance caused by high abundances of the brackish-water species *N. phyllepta* (Fig. 9). However, the reconstruction is somewhat less reliable due to the lower number of counts and a high sample-specific error; Fig. 12). Caution is furthermore required because the inferred specific conductance in the transition zone of Yumi Ike exceeds the range used in the dataset to construct the transfer function (0.01 - 5.05 mS/cm; Tavernier et al. in press - Chapter 3). The diatom flux is relatively low in both lakes (Figs. 8 & 9).

The lacustrine zone OIDA2 in Ô-Ike (160 - 132 cm, c. 5000 - 2720 cal. yr BP) is dominated by freshwater diatoms (Fig. 8). *Craticula antarctica* was relatively abundant between 160 and 144 cm (c. 5000 - 3170 cal. yr BP), after which it decreased in abundance. The inferred specific conductance is somewhat higher than in the more recent samples, which probably reflects the presence of small amounts of relict marine salts inherited during the isolation of the lake. Again, caution is required when interpreting these results because of high sample-specific errors (Fig. 11). Zones OIDA3 (132 - 47 cm, c. 2720 - 930 cal. yr BP) and OIDA4 (47 - 0 cm, c. 930 cal. yr BP - recent) are dominated by fluctuating abundances of *Halamphora veneta*, and *Diadesmis australis.*

Stauroneis latistauros occurs from 130 cm (c. 2670 cal. yr BP) onwards. *Navicula gregaria* occurs in lower abundances compared to zone OIDA2. The diatom flux is relatively higher in zone OIDA4 with peaks between 47 and 31.5 cm (930 - 770 cal. yr BP) (Fig. 8). The inferred specific conductance is highly variable, with several minima between 92 and 31.5 cm and more stable from 30.5 cm onwards (c. 760 cal. yr BP - present) (Fig. 11). These minima can be linked to a decrease in *H. veneta* accompanied by an increase in *D. australis* and/or *Psammothidium papilio* (Fig. 8).

In Yumi Ike, the lacustrine zone YIDA3 (46 - 0 cm, c. 4800 cal. yr BP - recent) is characterised by the appearance and dominance of freshwater species (Fig. 9). *H. veneta* is the most abundant species between 46 and 8 cm (c. 4800 - 940 cal. yr BP). *N. gregaria* is abundant between 20 and 8 cm (c. 2030 - 940 cal. yr BP). *P. papilio* and *D. australis* increase in abundance towards the end of the zone. The diatom flux is highest between 28 and 8 cm (c. 2760 - 940 cal. yr BP; Fig. 9). The inferred specific conductance is rather constant throughout the lacustrine part of the sediments (Fig. 12); the apparent maximum at 16 cm (c. 1730 cal. yr BP) can be explained by a higher abundance of the brackish-water species *C. cymatopleura* (Fig. 9). The maximum at 36 cm (c. 3900 cal. yr BP) is less reliable because this sample contains a high relative abundance of *Diadesmis gallica,* a species which was absent in the surface dataset used to create the transfer function, whereas the maximum at 44 cm (c. 4700 cal. yr BP) can be considered less reliable due to a lower number of counted valves (Figs. 9 & 12). *N. directa* occurred abundantly in that sample. A diatom analysis at a higher temporal resolution needs to confirm the duration of these apparent maxima and minima.

The diatom community in Nishi Ike is dominated by freshwater species throughout the entire sediments (Fig. 10). Marine and brackish-water species only sporadically occur. Zone NIDA1 (72 - 34.5 cm, c. > 11,240 - 3280 cal. yr BP) is characterised by the almost complete absence of diatoms. Due to the low number of retrieved valves in these sediments, specific conductance has not been reconstructed in this zone. Zone NIDA2 (34.5 - 22 cm, c. 3280 - 2110 cal. yr BP) is dominated by *D. australis* (Fig. 10) and thus by very low reconstructed specific conductance values (Fig. 13). The value at 32 cm (c. 2980 cal. yr BP) is less reliable because of the high relative abundance of *Diadesmis gallica*. In zone NIDA1 (22 - 0 cm, c. 2110 cal. yr BP - recent), *H. veneta* is dominant and *D. australis* less abundant; *N. gregaria* dominates in the top of the core (Fig. 10). The diatom concentration is highest between 33 and 16 cm (c. 3090 - 1630 cal. yr BP) and (close to) zero in the layers above and below (Fig. 10). The inferred specific conductance is higher in zone NIDA1 compared with zone NIDA2, with maxima at 20 and 0 cm (c. 1960 cal. yr BP and recent), caused by higher abundances of *H. veneta* and/or *N. gregaria* (Fig. 13). However, these maxima have high sample-specific errors. Similar to Ô-Ike, the changes in salinity are relatively modest. A diatom analysis at a higher temporal resolution needs to confirm the duration of these apparent maxima and minima.

The residual trend of the samples used for the transfer function (see Fig. S3 in Chapter 3) indicates that all reconstructed specific conductance values for Ô-Ike, Yumi Ike and Nishi Ike are slightly overestimated, whereas the peaks at 36 and 16 cm in Yumi Ike are somewhat underestimated.

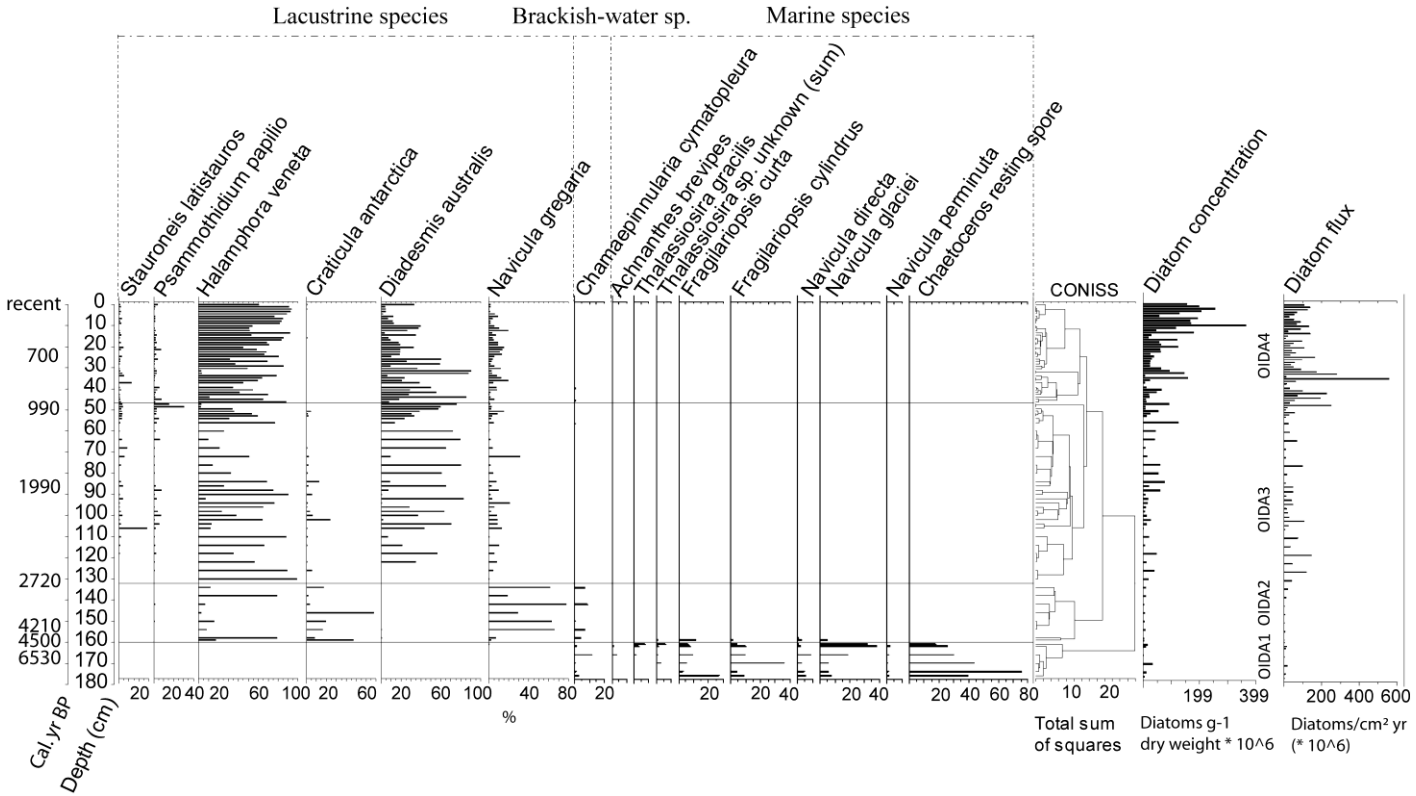

Figure 8. Diatom stratigraphy of the Ô-Ike sediment cores. Zoning (OIDA1-4; Ô-Ike Diatom Analysis) is based on a CONISS constrained cluster analysis. Marine, brackish-water and lacustrine diatom species are indicated with brackets.

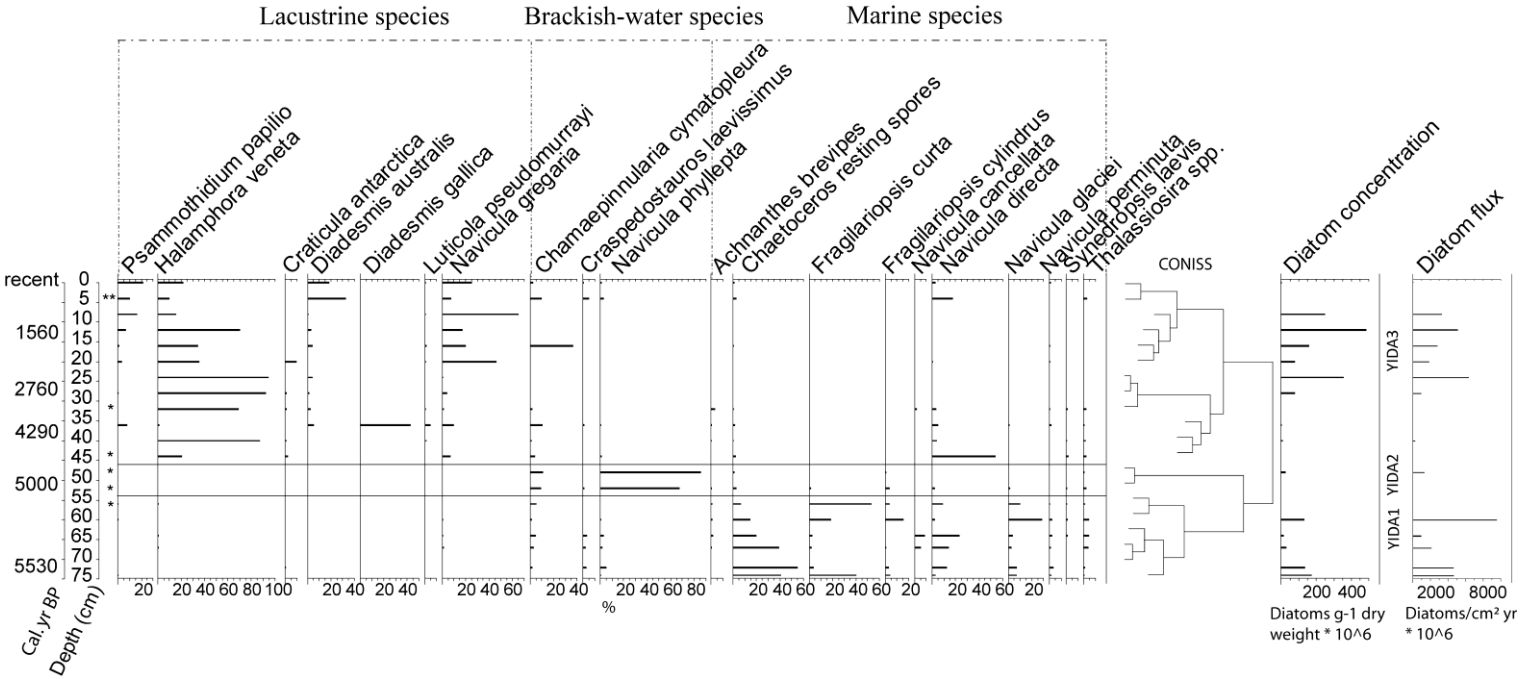

Figure 9. Diatom stratigraphy of the Yumi Ike sediment cores. Zoning (YIDA1-3; Yumi Ike Diatom Analysis) is based on a CONISS constrained cluster analysis. Marine, brackish-water and lacustrine diatom species are indicated with brackets. Samples with less than 400 valves counted are indicated with an asterisk (*: 50-400 valves, **: <50 valves).

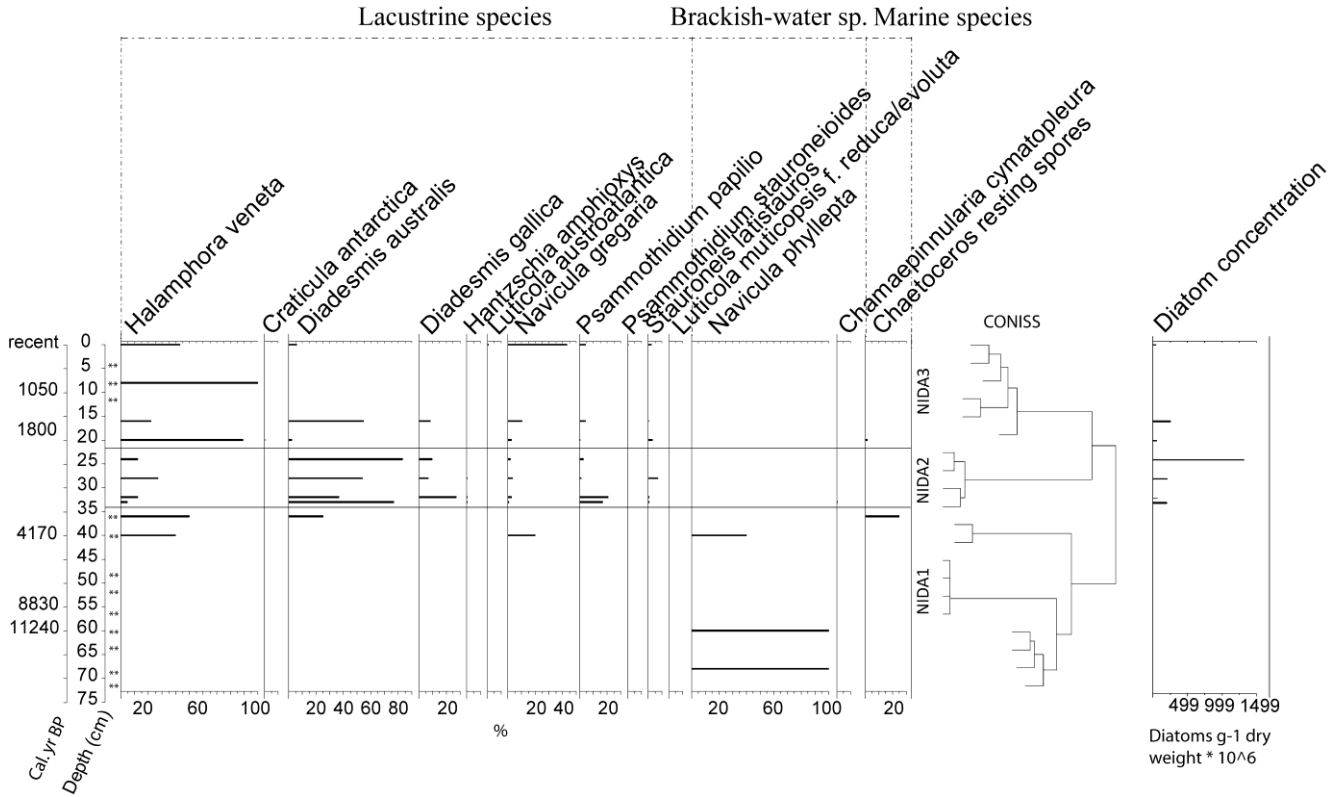

Figure 10. Diatom stratigraphy of the Nishi Ike sediment cores. Zoning (NIDA1-3; Nishi Ike Diatom Analysis) is based on a CONISS constrained cluster analysis. Marine, brackish-water and lacustrine diatom species are indicated with brackets. Samples with less than 400 valves counted are indicated with an asterisk (**: <50 valves).

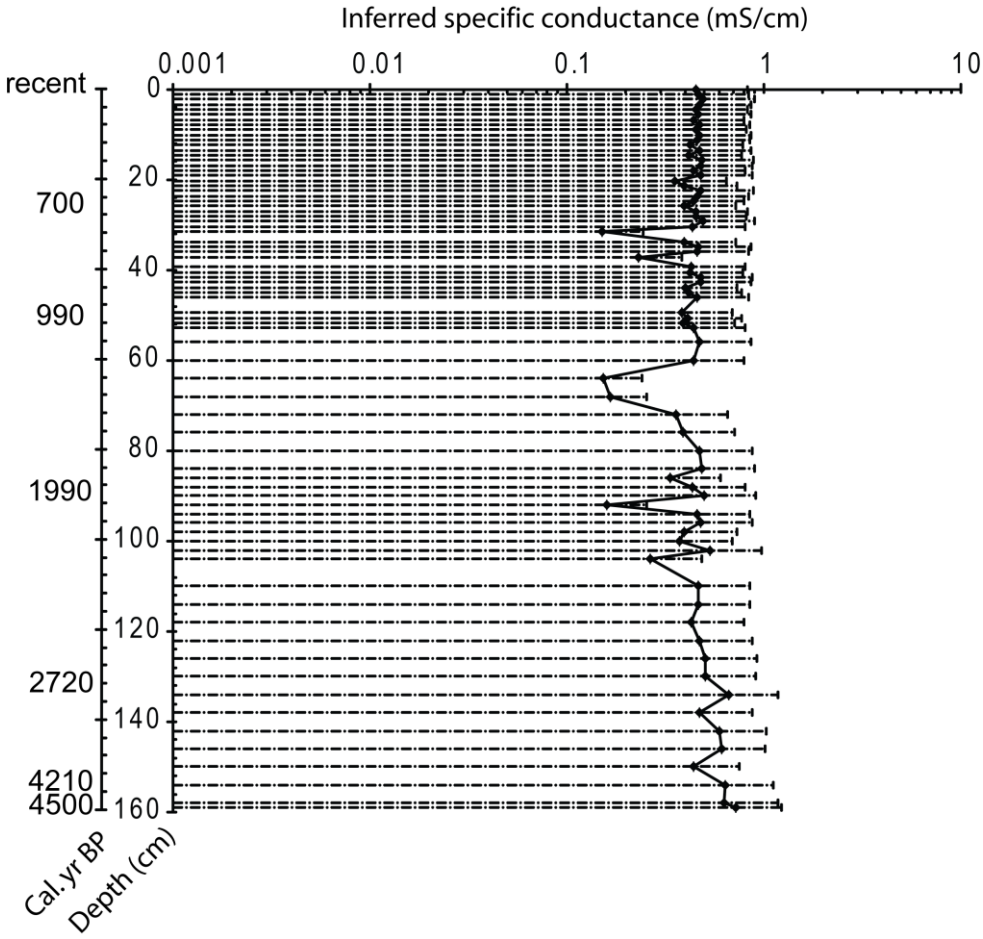

Figure 11. Inferred specific conductance for the lacustrine Ô-Ike sediments with indication of the sample-specific errors.

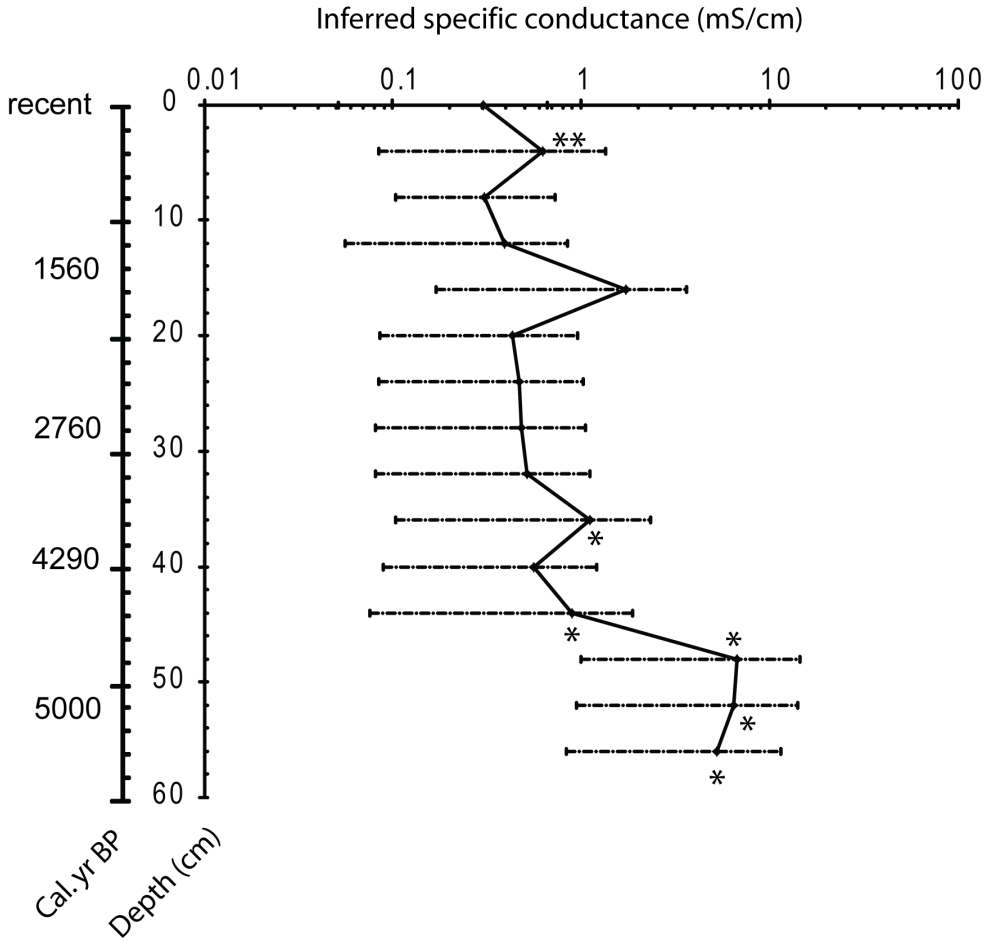

Figure 12. Inferred specific conductance for the transitional (54 - 46 cm) and lacustrine (46 - 0 cm) Yumi Ike sediments, with indication of the sample-specific errors. Reconstructions based on a smaller amount of valves: *: 50-400 valves, **: <50 valves; the sample at 36 cm (*) contained *Diadesmis gallica,* a species which was absent from the surface dataset on which the transfer function was based.

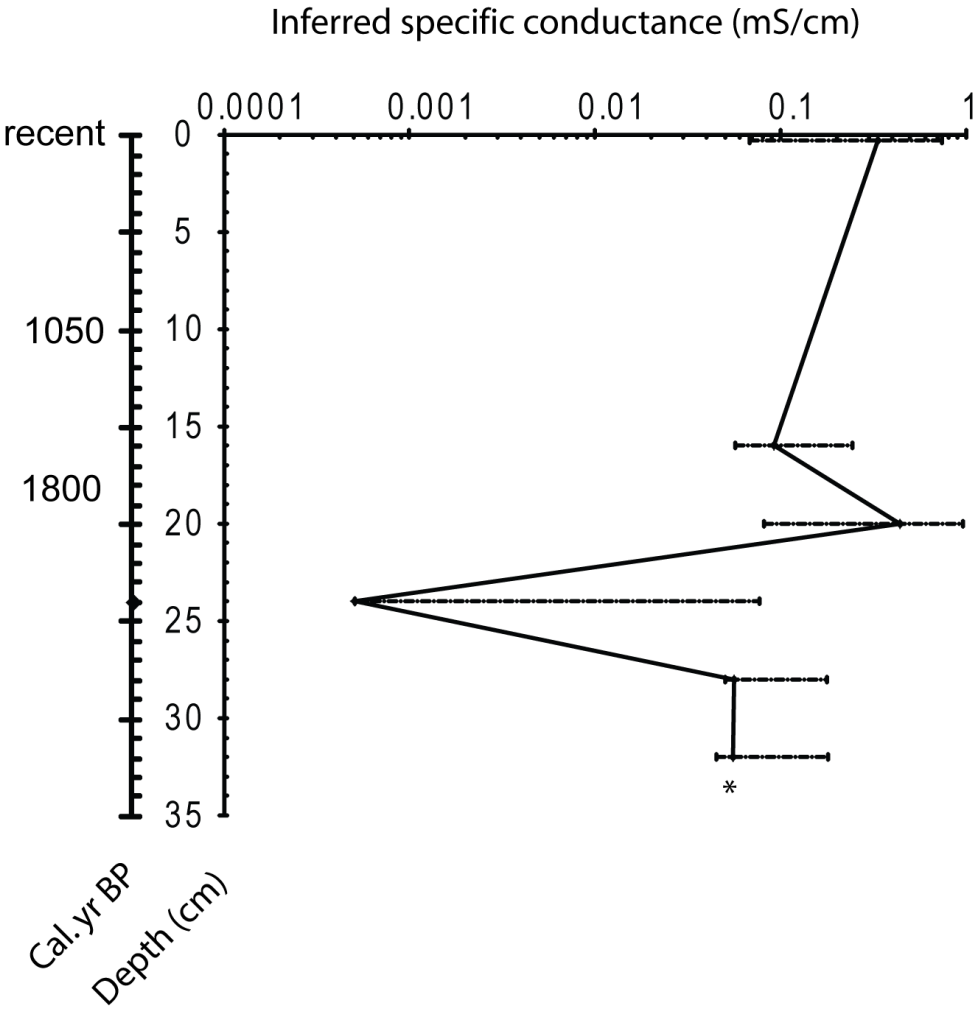

Figure 13. Inferred specific conductance for part of the lacustrine (32 - 0 cm) Nishi Ike sediments with indication of the sample-specific errors. Samples containing (almost) no diatoms (4, 8, 12, 36, 40, 44, 48, 52, 56, 60, 64, 68, and 72 cm) have been left out of this reconstruction. *: this sample contained *Diadesmis gallica*, a species which was absent from the surface dataset on which the transfer function was based.

Fossil pigment analysis

The broken-stick analysis did not reveal any significant zones for the pigment data in the Ô-Ike sediment record. Therefore, the marine and lacustrine zone based on the diatom zonation are indicated on Fig. 14. The pigment composition in the bottom part of the sediments (170 - 160 cm, c. 6530 - 5000 cal. yr BP) is characterised by very low fluxes of total carotenoids and total chlorophylls. Immediately preceding lake isolation, pigment fluxes increase. Phaeophytin *a*, which is a chlorophyll *a* derivative, is the most abundant chlorophyll throughout the entire core. Alloxanthin (cryptophytes, dinophytes), zeaxanthin (cyanobacteria, green algae, and possibly mosses), lutein (green algae, red seaweeds and possibly mosses) and diatoxanthin (diatoms, xanthophytes, haptophytes, dinophytes) dominate the carotenoid fraction. At the start of the lacustrine phase, pigment fluxes increase further with lutein and to a lesser extent zeaxanthin, being the dominant carotenoids. Canthaxanthin (cyanobacteria) and vaucheriaxanthin (xanthophytes, eustigmatophytes) appear for the first time. From 138 cm (c. 2890 cal. yr BP), myxoxanthophyll, a cyanobacteria marker pigment, becomes subdominant; zeaxanthin and lutein remain the most abundant carotenoids. Apart from a gradual increase in the lutein and beta carotene fraction and some minor fluctuations in less abundant pigments, the pigment composition remains more or less constant between 138 and 12 cm (c. 2890 - 400 cal. yr BP). The total carotenoid and chlorophyll fluxes are however more variable and reach maxima between 102 and 94cm (c. 2230 - 2090 cal. yr BP). From 12 cm until the top of the core, the pigment composition is characterised by the absence of myxoxanthophyll and the dominance of lutein, with the exception of one sample at 1 cm depth in which beta carotene is more abundant. Chlorophyll *a* becomes the most abundant chlorophyll in some samples between 12 and 0 cm.

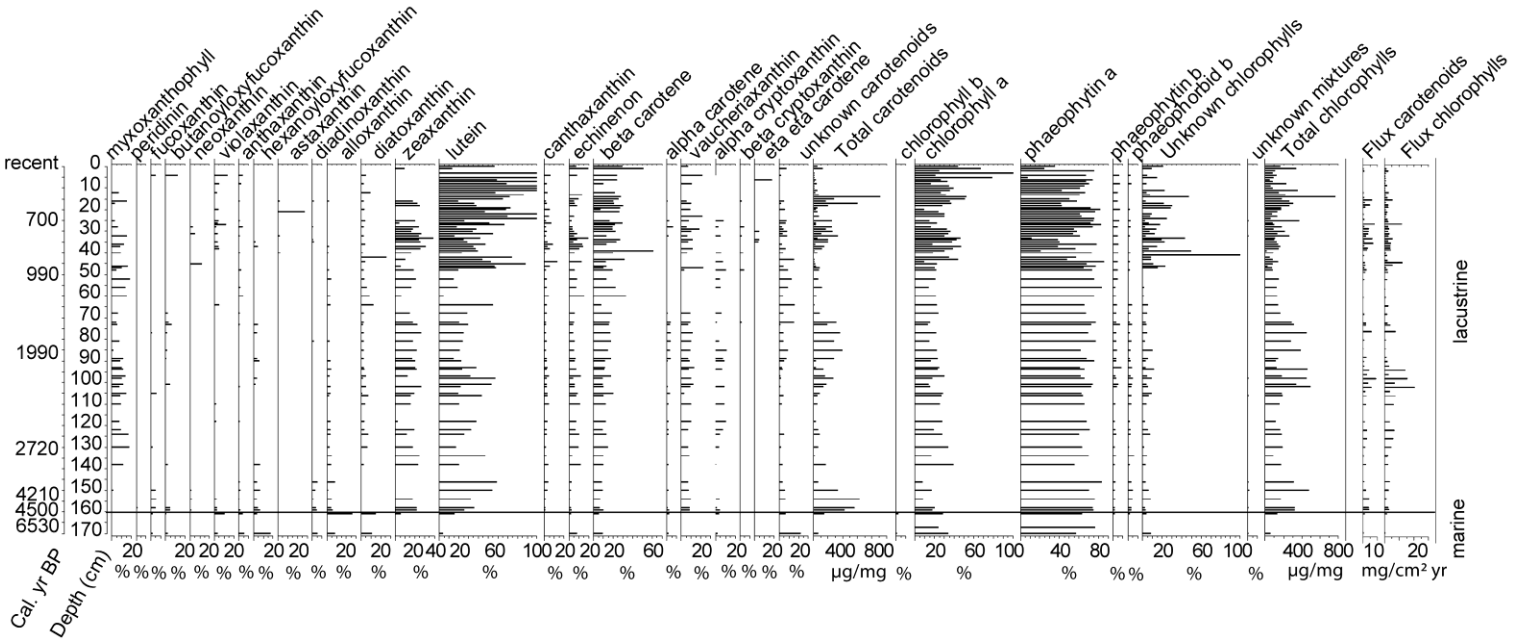

Figure 14. Stratigraphy of fossil pigments in the Ô-Ike sediment cores. Calibrated radiocarbon dates, and the marine and lacustrine zone are indicated.

Discussion

Deglaciation

The presence of glacial sediments in Nishi Ike and the subsequent increase in TC which likely reflects the onset of organic carbon accumulation at c. 11,240 cal. yr BP (Table 1; Fig. 6a), indicates that this part of West Ongul Island (Fig. 1) was probably covered by the EAIS during the LGM and deglaciated in the Early-Holocene (see overview Fig. 15). This scenario is consistent with geomorphological evidence of glacial over-riding, including the presence of erratics and glacial striae in the region (Hirakawa et al. 1999). It also corresponds to most other East Antarctic regions, such as for instance Mac. Robertson Land (Mackintosh et al. 2007), the Windmill Islands (Roberts et al. 2004) and some areas in Prydz Bay (Rauer Islands, parts of the Vestfold Hills and Larsemann Hills) (Fig. 1), which were ice-covered during the LGM and became ice-free immediately before the Holocene or during the EHCO (Hall 2009; Verleyen et al. 2011 in Appendix 2; Mackintosh et al. 2013). This scenario is however in disagreement with evidence from raised beaches from the Ongul Islands. The majority of the Holocene raised beaches from the region (Fig. 1) agree with this proposed minimum age of deglaciation, as the oldest Holocene ^{14}C date recovered is 10,800 cal. yr BP. However, intact shells of *Laternula elliptica*, found in a trench in a raised beach deposit on West Ongul Island predate the LGM (Takada et al. 2003). This would suggest that some parts of the Ongul Islands were ice-free during MIS3 and possibly even during MIS6-7 (Miura et al. 1998; Takada et al. 2003) and were not overridden by an erosive glacier during the LGM. This is in clear contrast with the peninsulas further south (excluding parts of Langhovde), which became ice-free during the Early-Holocene (Chapter 5). Regional differences in the deglaciation history were also detected in ice-free regions in Prydz Bay (Larsemann Hills) (Fig. 1). For example, some peninsulas became only ice-free during the Late-Holocene, while Broknes remained ice-free during the LGM (Hodgson et al. 2001). This was probably due to the presence of a subglacial bedrock ridge leading to the diversion of the ice-sheet and an increased flow of the Dålk Glacier (Hodgson et al. 2001). A similar process might have occurred in Lützow Holm Bay. If the glacier flowed through the Fuji Submarine Valley (Fig. 1), a deep valley located between the Ongul Islands and the Prince Olav Coast, it would have been diverted around the Ongul Islands. Another possible scenario is that the Ongul Islands were ice-free during the LGM, but permanently snow-covered preventing lake primary production. As a consequence, a large gap would exist between the timing of deglaciation and the actual onset of biogenic sedimentation (Gore 1997). A third possibility might be that both islands were ice-covered during the LGM but that the fragile *L. elliptica* shells in the raised beaches were preserved under a more or less inactive, non-erosive glacier. Given the fragile nature of these shells and the fact that they are preserved in the original feeding position, the latter hypothesis is however less likely (Mackintosh et al. 2013).

Early-Holocene climate history

The relatively recent age of the radiocarbon date in the sediments of Higashi Ike (c. 4560 or 4520 cal. yr BP; Table 1) suggests that the site was ice- or snow-covered during the Early-Holocene. In Nishi Ike, diatom concentration (Fig. 10), and the TC content (Fig. 6a)

remained relatively low until c. 4170 cal. yr BP (40 cm). This might suggest that this lake also remained partially ice-covered or at least permanently snow-covered until the Mid-Holocene, preventing the break-up of lake ice and limiting primary production (cf. Gore 1997; Fig. 15). Combined, these data indicate that the region possibly remained partially snow/ice-covered during the Early-Holocene and that terrestrial habitats only fully deglaciated or became free of permanent snow during the Mid-Holocene.

Mid- to Late-Holocene

After c. 4170 cal. yr BP, primary production likely started/increased in Nishi Ike as indicated by an increased concentration of diatoms (Fig. 10) and TC (Fig. 6b), although caution is required because no flux data are available for this record, implying that increases/decreases in proxies can also result from variable SRs and changes in sediment composition (Street-Perrot et al. 2007). In the isolation lakes, lacustrine conditions became established during the Mid- to Late-Holocene. In Yumi Ike, a brief brackish transition period was present between c. 5050 and 4800 cal. yr BP (Figs. 9 & 12), whereas in Ô-Ike, we did not detect brackish-water conditions (Figs. 8 & 11). These differences in lake evolution are likely related to the interplay between basin morphometry and volume, the surface area and geomorphology of the catchment area, the amount and exposure (south versus north facing) of snowbanks in the catchment area, and the uplift rate. The latter generally follows an exponential decrease with the highest rate immediately after ice-sheet disintegration (e.g. Roberts et al. 2011). A relative sea-level (RSL) curve developed for the region indeed confirmed that the uplift rate was higher when Ô-Ike became isolated from the sea compared with Yumi Ike (Chapter 6). These differences might have led to a more prolonged connection to the ocean and a subsequent sea water input in Yumi Ike resulting in a brackish water phase. Similar observations were made in isolation lakes from both Maritime (Watcham et al. 2011; Sterken et al. 2012) and Continental Antarctica (Verleyen et al. 2004a).

After lake isolation, fluxes in diatoms (Fig. 8), total chlorophylls and carotenoids (Fig. 14), but particularly TC (Fig. 6b), started to increase in Ô-Ike. This is possibly related to relatively high nutrient concentrations inherited from the sea water. Between c. 2230 and 2090 cal. yr BP (102 - 94 cm), the total carotenoid and chlorophyll fluxes are highest compared to the entire Ô-Ike sediment record (Fig. 14). This coincides with a period of relatively higher TC fluxes, between c. 2970 and 2010 cal. yr BP (140 - 90 cm; Fig. 6b). Together, this suggest relatively warm conditions leading to an increase in the number of ice-free days and hence in primary production (Quayle et al. 2002). In Yumi Ike, a period of relatively high diatom flux is similarly detected between c. 2760 and 940 cal. yr BP (28 - 8 cm; Fig. 9). In Nishi Ike, reconstructed specific conductance is relatively low between c. 2980 and 2260 cal. yr BP (32 - 24 cm; Fig. 13), whereas in Ô-Ike an overall yet small decreasing trend can be detected between c. 2720 and 1290 cal. yr BP (132 - 64 cm; Fig. 11). However, sample-specific errors are high for the latter reconstruction. Possibly, these observations are related to increased snow melt centred around the climate optimum, resulting in more dilute lake water. Yumi Ike on the other hand has an outflow stream, making it less sensitive to changes in the moisture balance (Verleyen et al. 2012 in

Appendix 1), although specific conductance maxima have been inferred but require a higher-temporal analysis for further interpretation (Fig. 12). Interestingly, in the Kobachi Ike sediment record on Skarvsnes (Chapter 5), a change in lithology from sediments dominated by coarse sand to sand-clay-silt-rich sediments, along with a decrease in mass-specific MS was observed from c. 2010 cal. yr BP onwards. This might point to the (partial) disappearance of multi-year snow banks in the catchment, which might similarly be related to warmer conditions. Taken together, available evidence suggests that both West Ongul Island and Skarvsnes experienced a thermal optimum between c. 4170 and 940 cal. yr BP, which can be linked to the Mid- to Late Holocene climate optimum.

The presence of this Mid- to Late-Holocene warm period is in accordance with other East Antarctic records and has been inferred from various lake sediment records. Although dating uncertainty is quite high in some records, this climate optimum occurs between c. 4.7 and 1 ka BP (Verleyen et al. 2011 in Appendix 2). Its presence in EA has been attributed to a poleward displacement of the Southern Westerlies, possibly in combination with local processes such as albedo effects following partial deglaciation and/or a high sensitivity of low-altitude coastal lakes because these ecosystems are situated close to the 0°C threshold. Hence, relatively small changes in temperature, lake ice-extent, snow cover, light availability and albedo can have a significant impact on their ecology (Verleyen et al. 2011 in Appendix 2).

Neoglacial cooling is inferred from c. 940 cal. yr BP onwards (Fig. 15), as evidenced by relatively lower total carotenoid and chlorophyll fluxes (Fig. 14), and TC flux (after one high peak at c. 900 cal. yr BP; 44 cm; Fig. 6b) in Ô-Ike. The Yumi Ike sediments are characterized by low diatom (Fig. 9) and TC fluxes (Fig. 6b) from then onwards. At approximately the same time, specific conductance slightly increased in Nishi Ike [Fig. 13; i.e., from c. 1960 cal. yr BP (20 cm) until present], which is possibly related to a lower amount of water entering the lake. Similar dry conditions linked to Neoglacial cooling were observed in sediment cores from lakes in the Larsemann Hills (Verleyen et al. 2004a) and Vestfold Hills (Fuldford-Smith & Sikes 1996) (Fig. 1). In the marine environment, a more persistent sea-ice cover was evidenced in the Windmill Islands, as well as a decrease in primary production (Kirkup et al. 2002; Cremer et al. 2003) (Fig. 1).

There is no substantial evidence for a MCA, or a LIA event in any of the cores. This is consistent with other lake records (Verleyen et al. 2011 in Appendix 2; Tavernier et al. in press - Chapter 3) as well as with ice cores (Goosse et al. 2012) and suggests that previous NH palaeoclimate reconstructions may have been force-fitted to these Antarctic climate anomalies. A recent synthesis of records in the SH however, suggests that warmer conditions generally prevailed after the peak warming of the NH MCA and cold conditions were more or less coincident with the LIA (Neukom et al. 2014). High-resolution studies (e.g. Chapter 3) are evidently needed to fully understand past climate changes along the Antarctic coastline during the past millennium.

There is no circumstantial evidence for a recent warming or a warming initiated c. 500-600 years ago on West Ongul Island as was observed on the AP (Mulvaney et al. 2012; Sterken et al. 2012). In the upper 10 cm of the Ô-Ike sediments, corresponding to

the past c. 350 years, the relative abundance of the cyanobacteria marker pigment myxoxanthophyll decreased (Fig. 14), whereas lutein (linked to green algae) increased. It is unclear why these shifts in autotrophic community structure occur in the upper part of the sediment core, but one possibility is an increase in planktonic primary production which could be related to climate warming. This hypothesis is however far from certain as fluxes in TC (Fig. 6b) but also chlorophylls (Fig. 14) are actually relatively low during the past c. 500-600 years in the sediment cores studied.

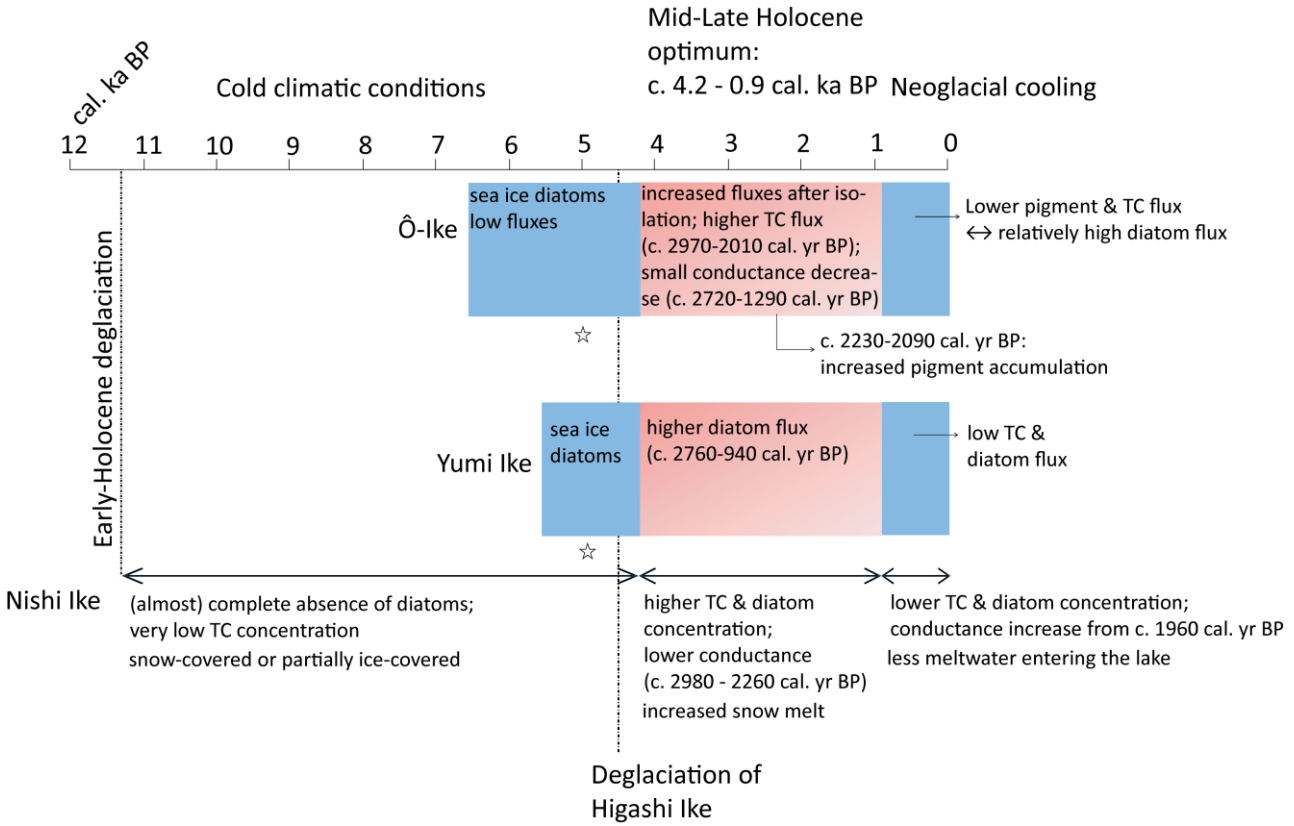

Figure 15. Overview figure of the inferred Holocene climate anomalies in the Ô-Ike, and Yumi Ike sediments, supported by proxies from the Nishi Ike sediments. Red = inferred warm climatic conditions, blue = inferred cold climatic conditions. A star indicates the isolation of the lake.

Acknowledgements

This research was funded by the Belspo project SD/CA/01 'Holocene climate variability and ecosystem change in coastal East and Maritime Antarctica' (HOLANT) and the British Antarctic Survey Chemistry and Past Climate programme. The members of JARE 48 are thanked for logistic support and Tamotsu Hoshino is thanked for his help in the field. IT was funded by the Institute for the Promotion of Innovation by Science and Technology in Flanders (IWT). EV is funded by FWO Vlaanderen and Ghent University.

References

ACIA (2004) Arctic Climate Impact Assessment. Cambridge University Press. 140 pp.

Ampel L, Bigler C, Wohlfarth B, Risberg J, Lotter AF, Veres D (2010) Modest summer temperature variability during DO cycles in western Europe. *Quaternary Science Reviews,* **29**: 1322-1327.

Axford Y, Briner JP, Cooke CA, Francis DR, Michelutto N, Miller GH, Smol JP, Thomas EK, Wilson CR, Wolfe AP (2009) Recent changes in a remote lake are unique within the past 200,000 years. *PNAS,* **106(44)**: 18443-18446.

Battarbee RW, and Kneen M (1982) The use of electronically counted microspheres in absolute diatom analysis. *Limnology and Oceanography,* **27**: 184-188.

Bennett KD (1996) Determination of the number of zones in a biostratigraphical sequence. *New Phytologist,* **132:** 155-170.

Bentley MJ, Hodgson DA, Smith JA, Cofaigh CO, Domack EW, Larter RD, Roberts SJ, Brachfeld S, Leventer A, Hjort C, Hillenbrand CD, Evans J (2009) Mechanisms of Holocene palaeoenvironmental change in the Antarctic Peninsula region. *Holocene,* **19**: 51-69.

Berg S, Wagner B, Cremer H, Leng MJ, Melles M (2010) Late Quaternary environmental and climate history of Rauer Group, East Antarctica. *Palaeogeography, Palaeoclimatology, Palaeoecology,* **297**: 201-213.

Björck S, Olsson S, Ellis-Evans C, Håkansson H, Humlum O, Delirio JM (1996) Late Holocene palaeoclimatic records from lake sediments on James Ross Island, Antarctica. *Palaeogeography, Palaeoclimatology, Palaeoecology,* **121**: 195-220.

Blaauw M (2010) Methods and code for 'classical' age-modelling of radiocarbon sequences. *Quat Geochr,* **5**: 512-518.

Bronk Ramsey C (2009) Bayesian analysis of radiocarbon dates. *Radiocarbon,* **51(1)**: 337-360.

Cremer H, Gore D, Melles M, Roberts D (2003) Palaeoclimatic significance of Late Quaternary diatom assemblages from Southern Windmill Islands, East Antarctica. *Palaeogeogr. Palaeoclimatol. Palaeoecol.,* **195**: 261–280.

Cromer L, Gibson JAE, Swadling KM, Ritz DA (2005) Faunal microfossils: indicators of Holocene ecological change in a saline Antarctica lake. *Palaeogeography, Palaeoclimatology, Palaeoecology,* **221**: 83-97.

Crosta X, Sturm A, Armand L, Pichon J-J (2004) Late Quaternary sea ice history in the Indian sector of the Southern Ocean as recorded by diatom assemblages. *Marine Micropaleontology,* **50**: 209-223.

Crosta X, Debret M, Denis D, Courty MA, Ther O (2007) Holocene long- and short-term climate changes off Adelie Land, East Antarctica. *Geochemistry Geophysics Geosystems,* **8(11)**: Q11009, doi:10.1029/2007GC001718.

Crosta X, Denis D, Ther O (2008) Sea ice during the Holocene, Adélie Land, East Antarctica. *Marine Micropaleontology,* **66(3-4):** 222-232.

Doran PT, Priscu JC, Lyons WB, Walsh JE, Fountain AG, McKnight DM, Moorhead DL, Virginia RA, Wall DH, Clow GD, Fritsen CH, McKay CP, Parsons AN (2002) Antarctic climate cooling and terrestrial ecosystem response. *Nature,* **415:** 517-520.

Esposito RMM, Spaulding SA, McKnight DM, Van de Vijver B, Kopalová K, Lubinski D, Hall B, and Whittaker T (2008) Inland diatoms from the McMurdo Dry Valleys and James Ross Island, Antarctica. *Botany,* **86**: 1378-1392.

Finocchiaro F, Langone L, Colizza E, Fontolan G, Giglio F, Tuzzi E (2005) Records of early Holocene warming in a laminated sediment core from Cape Hallett Bay (Northern Victoria Land, Antarctica). *Glob. Planet. Ch.,* **45**: 193-206.

Fulford-Smith SP, and Sikes EL (1996) The evolution of Ace Lake, Antarctica, determined from sedimentary diatom assemblages. *Palaeogeography, Palaeoclimatology, Palaeoecology,* **124**: 73-86.

Gore DB (1997) Blanketing snow and ice; constraints on radiocarbon dating deglaciation in East Antarctic oases. *Antarctic Science,* **9(3)**: 336-346.

Goosse H, Braida M, Crosta X, Mairesse A, Masson-Delmotte V, Mathiot P, Neukom R, Oerter H, Philippon G, Renssen H, Stenni B, van Ommen T, Verleyen E (2012) Antarctic temperature changes during the last millennium: evaluation of simulations and reconstructions. *Quaternary Science Reviews,* **55**: 75-90.

Grimm EC (2004) TGView Version 2.0.2. Illinois State Museum, Springfield, Illinois.

Hall BL (2009) Holocene glacial history of Antarctica and the sub-Antarctic islands. *Quaternary Science Reviews,* **28**: 2213-2230.

Hodgson DA, Noon PE, Vyverman W, Bryant CL, Gore DB, Appleby P, Gilmour M, Verleyen E, Sabbe K, Jones VJ, Ellis-Evans JC, Wood PB (2001) Were the Larsemann Hills ice-free through the Last Glacial Maximum? *Antarctic Science,* **13(4)**: 440-454.

Hodgson DA, and Convey P (2005) A 7000-year record of oribatid mite communities on a Maritime-Antarctic Island: Responses to climate change. *Arctic, Antarctic, and Alpine Research,* **37(2)**: 239-245.

Hodgson DA, Verleyen E, Sabbe K, Squier AH, Keely BJ, Leng MJ, Saunders KM, Vyverman W (2005) Late Quaternary climate-driven environmental change in the Larsemann Hills, East Antarctica, multi-proxy evidence from a lake sediment core. *Quat. Res.,* **64**: 83–99.

Hodgson DA, and Smol JP (2008) High latitude palaeolimnology. *In*: Vincent WF, Laybourn-Parry J (Eds.) Polar Lakes and Rivers - Arctic and Antarctic Aquatic Ecosystems. Oxford University Press, Oxford, UK, pp 43-64.

Jeffrey SW, Mantoura RFC, Bjornland T (1997) Data for the identification of 47 key phytoplankton pigments. *In*: Jeffrey SW, Mantoura RFC, Wright SW. Phytoplankton pigments in oceanography, guidelines to modern methods. UNESCO Publishing, Paris, p. 447-554.

Juggins S (2003) C2 User Guide - Software for Ecological and Palaeoecological Data Analysis and Visualisation. University of Newcastle, Newcastle.

Juggins S (2009) Rioja, analysis of Quaternary science data.
http://www.staff.ncl.ac.uk/staff/stephen.juggins/.

Kaufman DS, Schneider DP, McKay NP, Ammann CM, Bradley RS, Briffa KR, Miller GH, Otto-Bliesner BL, Overpeck JT, Vinther BM, Arctic Lakes 2k Project Members (2009) Recent warming reverses long-term Arctic cooling. *Science,* **325**: 1236-1239.

King P, Kennedy H, Newton PP, Jickells TD, Brand T, Calvert S, Cauwet G, Etcheber H, Head B, Kheipounoff A, Manighetti B, Miquel JC (1998) Analysis of total and organic carbon and total nitrogen in settling oceanic particles and a marine sediment: an interlaboratory comparison. *Marine Chemistry,* **60**: 203-216.

King MA, Bingham RJ, Moore P, Whitehouse PL, Bentley MJ, Milne GA (2012) Lower satellite-gravimetry estimates of Antarctic sea-level contribution. *Nature,* **491**: 586-590.

Kirkup H, Melles M, Gore DB (2002) Late Quaternary environment of Southern Windmill Islands, East Antarctica. *Antarct. Sci.,* **14**: 385-394.

Krebs WN, Lipps JH, Burckle LH (1987) Ice diatom floras, Arthur Harbor, Antarctica. *Polar Biol,* **7**: 163-171.

MacKintosh A, White D, Fink D, Gore DB, Pickard J, Fanning PC (2007) Exposure ages from mountain dipsticks in Mac. Robertson Land, East Antarctica, indicate little change in ice-sheet thickness since the Last Glacial Maximum. *Geology*, **35**: 551-554.

Mackintosh A, Golledge N, Domack E, Dunbar R, Leventer A, White D, Pollard D, DeConto R, Fink D, Zwartz D, Gore D, Lavoie C (2011) Retreat of the East Antarctic ice sheet during the last glacial termination. *Nature Geoscience,* **4**: 195-202.

Mackintosh AN, Verleyen E, O'Brien PE, White DA, Selwyn Jones R, McKay R, Dunbar R, Gore DB, Fink D, Post AL, Miura H, Leventer A, Goodwin I, Hodgson DA, Lilly K, Crosta X, Golledge NR, Wagner B, Berg S, van Ommen T, Zwartz D, Roberts SJ, Vyverman W, Masse G (2013) Retreat history of the East Antarctic Ice Sheet since the Last Glacial Maximum. *Quaternary Science Reviews,* http://dx.doi.org/10.1016/j.quascirev.2013.07.024.

Mann ME, Zhang Z, Hughes MK, Bradley RS, Miller SK, Rutherford S, Ni F (2008) Proxy-based reconstructions of hemispheric and global surface temperature variations over the past two millennia. *PNAS,* **105(36)**: 13252-13257.

Mann ME, Zhang ZH, Rutherford S, Bradley RS, Hughes MK, Shindell D, Ammann C, Faluvegi G, Ni FB (2009) Global signatures and dynamical origins of the Little Ice Age and Medieval Climate Anomaly. *Science*, **326**: 1256-1260.

Masson V, Vimeux F, Jouzel J, Morgan V, Delmotte M, Ciais P, Hammer C, Johnsen S, Lipenkov VY, Mosley-Thompson E, Petit JR, Steig EJ, Stievenard M, Vaikmae R (2000) Holocene climate variability in Antarctica based on 11 ice-core isotopic records. *Quat. Res.,* **54**: 348-358.

Masson-Delmotte V, Stenni B, Jouzel J (2004) Common millennial-scale variability of Antarctic and Southern Ocean temperatures during the past 5000 years reconstructed from the EPICA Dome C ice core. *The Holocene,* **14**:145-151.

Masson-Delmotte V, Stenni B, Pol K, Braconnot P, Cattani O, Falourd S, Kageyama M, Jouzel J, Landais A, Minster B, Barnola JM, Chappellaz J, Krinner G, Johnsen S, Rothlisberger R, Hansen J, Mikolajewicz U, Otto-Bliesner B (2010) EPICA Dome C record of glacial and interglacial intensities. *Quat Sci Rev*, **29**: 113-128.

Mayewski PA, Rohling EE, Stager JC, Karlen W, Maasch KA, Meeker LD, Meyerson EA, Gasse F, Van Kreveld S, Holmgren K, Lee-Thorp J, Rosqvist G, Rack F, Staubwasser M, Schneider RR, Steig EJ (2004) Holocene climate variability. *Quat. Res.,* **62**: 243-255.

Mayewski PA, Meredith MP, Summerhayes CP, Turner J, Worby A, Barrett PJ, Casassa G, Bertler NAN, Bracegirdle T, Garabato ACN, Bromwich D, Campbell H, Hamilton GS, Lyons WB, Maasch KA, Aoki S, Xiao C, Van Ommen T (2009) State of the Antarctic and Southern Ocean Climate System. *Rev. Geophys.,* **47**: 1–38.

McCormac F, Hogg A, Blackwell P, Buck C, Higham T, Reimer P (2004) Shcal04 Southern Hemisphere calibration 0-11.0 cal kyr BP. *Radiocarbon,* **46**: 1087-1092.

Miura H, Maemoku H, Igarashi A, Moriwaki K (1998) Late Quaternary raised beach deposits and radiocarbon dates of marine fossils around Lützow-Holm Bay. *Special map series of National Institute of Polar Research,* **6:** pp. 46.

Mulvaney R, Oerter H, Peel DA, Graf W, Arrowsmith C, Pasteur EC, Knight B, Littot GC, Miners WD (2002) 1000 year ice-core records from Berkner Island, Antarctica. *Annals of Glaciology,* **35**: 45-51.

Mulvaney R, Abram NJ, Hindmarsh RCA, Arrowsmith C, Fleet L, Triest J, Sime LC, Alemany O, Foord S (2012) Recent Antarctic Peninsula warming relative to Holocene climate and ice-shelf history. *Nature,* doi: 10.1038/nature11391.

Ohtsuka T, Kudoh S, Imura S, Ohtani S (2006) Diatoms composing benthic microbial mats in freshwater lakes of Skarvsnes ice-free area, East Antarctica. *Polar Biosci.,* **20**: 113-130.

Quayle WC, Peck LS, Peat H, Ellis-Evans JC, Harrigan PR (2002) Extreme responses to climate change in Antarctic lakes. *Science,* **295**: 645.

Reimer PJ, Baillie MGL, Bard E, Bayliss A, Beck JW, Bertrand CJH, Blackwell PG, Buck CE, Burr GS, Cutler KB, Damon PE, Edwards RL, Fairbanks RG, Friedrich M, Guilderson TP, Hogg AG, Hughen KA, Kromer B, McCormac G, Manning S, Ramsey CB, Reimer RW, Remmele S, Southon JR, Stuiver M, Talamo S, Taylor FW, Van Der Plicht J, Weyhenmeyer CE (2004) Intcal04 Terrestrial radiocarbon age calibration, 0-26 cal kyr BP. *Radiocarbon*, **46**: 1029-1058.

Reimer PJ, Baillie MGL, Bard E, Bayliss A, Beck JW, Blackwell PG, Bronk Ramsey C, Buck CE, Burr GS, Edwards RL, Friedrich M, Grootes PM, Guilderson TP, Hajdas I, Heaton TJ, Hogg AG, Hughen KA, Kaiser KF, Kromer B, McCormac FG, Manning SW, Reimer RW, Richards DA, Southon JR, Talamo S, Turney CSM, van der Plicht J, Weyhenmeyer CE (2009) IntCal09 and Marine09 radiocarbon age calibration curves, 0-50,000 years cal BP. *Radiocarbon*, **51**: 1111-1150.

Renberg I (1990) A procedure for preparing large sets of diatom slides from sediment cores. *Journal of Paleolimnology,* **4**: 87-90.

Renssen H, Goosse H, Fichefet T, Masson-Delmotte V, Koc N (2005) Holocene climate evolution in the high-latitude Southern Hemisphere simulated by a coupled atmosphere-vegetation model. *Holocene,* **15(7)**: 951-964.

Roberts D, McMinn A, Cremer H, Gore DB, Melles M (2004) The Holocene evolution and palaeosalinity history of Beall Lake, Windmill Islands (East Antarctica) using an expanded diatom-based weighted averaging model. *Palaeogeogr. Palaeoclimat. Palaeoecol.,* **208**: 121-140.

Roberts SJ, Hodgson DA, Sterken M, Whitehouse PL, Verleyen E, Vyverman W, Sabbe K, Balbo A, Bentley MJ, Morteton S (2011) Geological constraints on glacio-isostatic adjustment models of relative sea-level change during deglaciation of Prince Gustav Channel, Antarctic Peninsula. *Quaternary Science Reviews,* **30(25-26)**: 3603-3617.

Sabbe K, Verleyen E, Hodgson DA, Vanhoutte K, Vyverman W (2003) Benthic diatom flora of freshwater and saline lakes in the Larsemann Hills and Rauer Islands, East Antarctica. *Antarct Sci,* **15**: 227-248.

Sato K, and Hirasawa N (2007) Statistics of Antarctic surface meteorology based on hourly data in 1957-2007 at Syowa Station. *Polar Science,* **1**: 1-15.

Scott FJ, and Thomas DP (2005) Diatoms. *In:* Scott FJ, and Marchant HJ (Eds.) Antarctica marine protists. Hobart, Australia. p. 13 – 201.

Steig EJ, Brook EJ, White JWC, Sucher CM, Bender ML, Lehman SJ, Morse DL, Waddington ED, Clow GD (1998) Synchronous climate changes in Antarctica and the North Atlantic. *Science,* **282**: 92-95.

Steig EJ, Schneider DP, Rutherford SD, Mann ME, Comiso JC, Shindell DT (2009) Warming of the Antarctic ice-sheet surface since the 1957 International Geophysical Year. *Nature*, **460**: 766-766.

Steig EJ, Ding Q, White JWC, Küttel M, Rupper SB, Neumann TA, Neff PD, Gallant AJE, Mayewski PA, Taylor KC, Hoffmann G, Dixon DA, Schoenemann SW, Markle BR, Fudge TJ, Schneider DP, Schauer AJ, Teel RP, Vaughn BH, Burgener L, Williams J, Korotkikh E (2013) Recent climate and ice-sheet changes in West Antarctica compared with the past 2,000 years. *Nature Geoscience,* **6**: 372-375.

Sterken M, Roberts SJ, Hodgson DA, Vyverman W, Balbo AL, Sabbe K, Moreton SG, Verleyen E (2012) Holocene glacial and climate history of Prince Gustav Channel, northeastern Antarctic Peninsula. *Quaternary Science Reviews,* **31**: 93-111.

Street-Perrot FA, Barker PA, Swain DL, Ficken KJ, Wooler MJ, Olago DO, Huang Y (2007) Late Quaternary changes in ecosystems and carbon cycling on Mt. Kenya, East Africa: a landscape-ecological perspective based on multi-proxy lake-sediment fluxes. *Quaternary Science Reviews,* **26**: 1838-1860.

Takada M, Tani A, Miura H, Moriwaki K, Nagatomo T (2003) ESR dating of fossil shells in the Lützow-Holm Bay region, East Antarctica. *Quaternary Science Reviews,* **22**: 1323-1328.

Tanabe Y, Kudoh S, Imura S, Fukuchi M (2008) Phytoplankton blooms under dim and cold conditions in freshwater lakes of East Antarctica. *Polar Biol,* **31**: 199-208.

Van Heukelem L, and Thomas CS (2001) Computer-assisted high-performance liquid chromatography method development with applications to the isolation and analysis of phytoplankton pigments. *Journal of Chromatography A*, **910**: 31-49.

Verleyen E, Hodgson DA, Sabbe K, Vyverman W (2004a) Late Quaternary deglaciation and climate history of the Larsemann Hills (East Antarctica). *J. Quat. Sci.,* **19**: 361-375.

Verleyen E, Hodgson DA, Leavitt PR, Sabbe K, Vyverman W (2004b) Quantifying habitat-specific diatom production: A critical assessment using morphological and biogeochemical markers in Antarctic marine and lake sediments. *Limnol. Oceanogr.,* **49(5)**: 1528-1539.

Verleyen E, Hodgson DA, Sabbe K, Cremer H, Emslie SD, Gibson J, Hall B, Imura S, Kudoh S, Marshall GJ, McMinn A, Melles M, Newman L, Roberts D, Roberts SJ, Singh SM, Sterken M, Tavernier I, Verkulich S, Van de Vyver E, Van Nieuwenhuyze W, Wagner B, Vyverman W (2011) Post-glacial regional climate variability along the East

Antarctic coastal margin - evidence from shallow marine and coastal terrestrial records. *Earth Sci Rev*, **104**: 199-212.

Verleyen E, Hodgson DA, Gibson J, Imura S, Kaup E, Kudoh S, De Wever A, Hoshino T, McMinn A, Obbels D, Roberts D, Roberts SJ, Sabbe K, Souffreau C, Tavernier I, Van Nieuwenhuyze W, Van Ranst E, Vindevogel N, Vyverman W (2012) Chemical limnology in coastal East Antarctic lakes: monitoring future climate change in centres of endemism and biodiversity. *Antarctic Science,***24(1)**: 23-33.

Wagner B, Cremer H, Hultsch N, Gore DB, Melles M (2004) Late Pleistocene and Holocene history of Lake Terrasovoje, Amery Oasis, East Antarctica, and its climatic and environmental implications. *J. Paleolimnol.,* **32**: 321-339.

Watcham EP, Bentley MJ, Hodgson DA, Roberts SJ, Fretwell PT, Lloyd JM, Larter RD, Whitehouse PL, Leng MJ, Monien P, Moreton SG (2011) A new Holocene relative sea-level curve for the South Shetland Islands, Antarctica. *Quaternary Science Reviews,* **30**: 3152-3170.

Wright HE (1967) A square-rod piston sampler for lake sediments. *J Sed Pet,* **37**: 975-976.

Yamane M, Yokoyama Y, Miura H, Maemoku H, Iwasaki S, Matsuzaki H (2011) The last deglacial history of Lützow-Holm Bay, East Antarctica. *Journal of Quaternary Science,* **26(1)**: 3-6.

Yanai K, Kizaki K, Tatsumi T, Kikuchi T (1974) Explanatory text of geological map of East Ongul Island, Antarctica. *Antarctic Geological map series, Sheet 1 East Ongul Island,* pp. 13.

Yoshida Y, and Moriwaki K (1979) Some consideration on elevated coastal features and their dates around Syowa Station, Antarctica. *Memoirs of National Institute of Polar Research. Special Issue*, **13**: 220-226.

Supplementary material

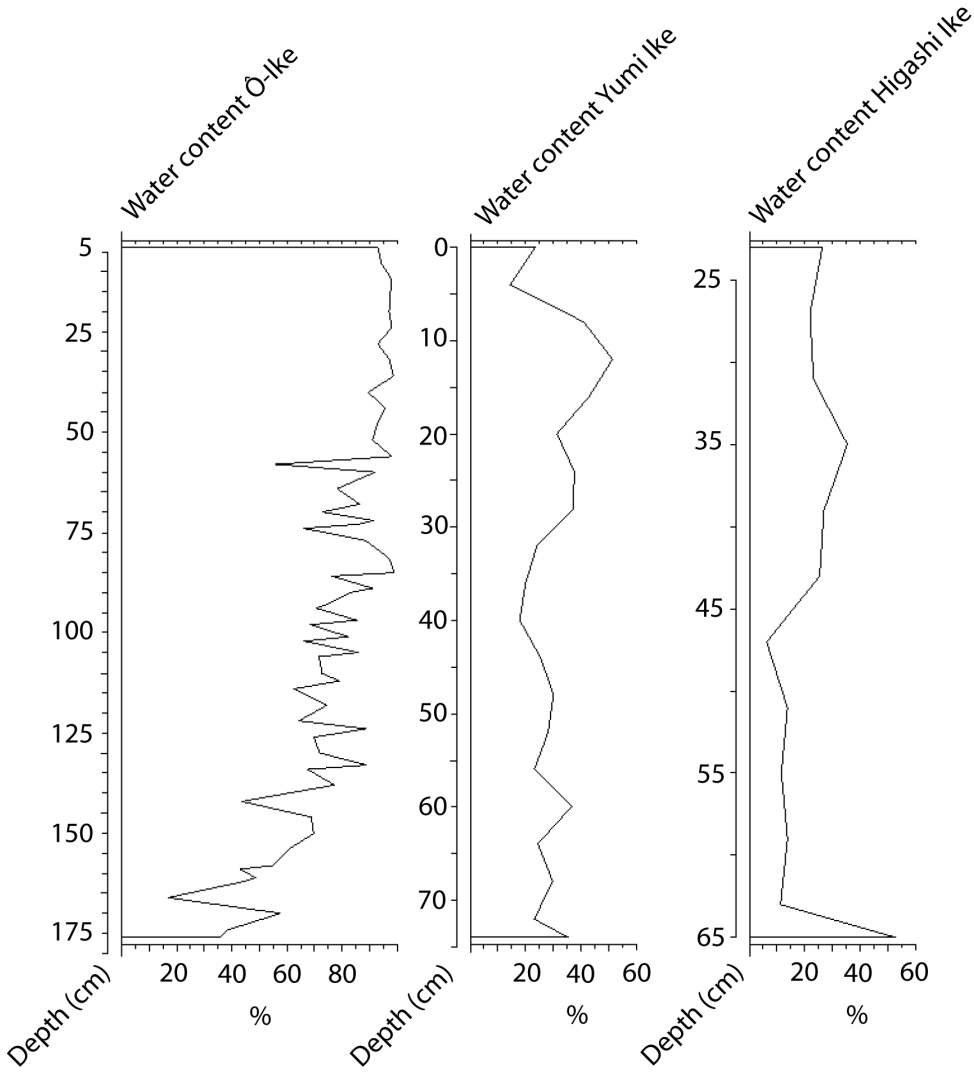

Figure S1. Water content (%) of the Yumi Ike, Ô-Ike and Higashi Ike sediments.

Chapter 5. Holocene palaeoenvironmental and relative sea-level changes on Skarvsnes, Lützow Holm Bay, East Antarctica

Author's contribution: diatom analysis of the Kobachi Ike sediment cores, fossil pigment analysis, geochemical analyses (TN, TOC, TS), writing parts of the manuscript.

Ines Tavernier, Elie Verleyen, Dominic A. Hodgson, Stephen J. Roberts, Katrien Heirman, Ilse Daveloose, Koen Sabbe, Marc De Batist, Satoshi Imura, Sakae Kudoh, Wim Vyverman

Note: not all contributors commented on this manuscript

Key-words: Mid- to Late-Holocene warm period, isolation basin, deglaciation, relative sea-level, East Antarctica

Abstract

The combined analysis of fossil pigments, siliceous microfossils, sedimentology and geochemical variables in radiocarbon-dated sediment cores from Kobachi Ike (Skarvsnes, Lützow Holm Bay, East Antarctica) provides insights into the onset of regional deglaciation, relative sea-level (RSL) changes and the emergence and palaeoecological evolution of this coastal Antarctic lake. The site deglaciated not earlier than c. 7240 cal. yr BP, narrowing down available cosmogenic isotope dates, which placed deglaciation of the peninsula roughly between 10 and 6 ka BP. The period following deglaciation was characterised by relatively cold coastal climatic conditions, as evidenced by low fluxes of palaeoproductivity indicators. The regional RSL maximum could be placed at 28.7 m, which is 8.7 m higher than previous estimates based on raised beach data alone. From c. 4580 cal. yr BP onwards, primary production increased in the marine environment. The site was then possibly a shallow marine lagoon, only suitable for a limited number of diatom taxa as evidenced by monospecific assemblages of a currently unknown *Navicula* species. Between c. 4450 and 3670 cal. yr BP, a more diverse diatom community dominated by *Chaetoceros* resting spores with sea-ice diatoms being co-dominant, indicates the presence of marine, seasonally open-water conditions. Around c. 3670 cal. yr BP, the lake basin became isolated from the ocean due to isostatic uplift as indicated by the presence of myxoxanthophyll, which is produced by lacustrine cyanobacteria. Alternatively, lake isolation may have started earlier, around c. 4030, when the relative abundance of the brackish water diatom *Navicula phyllepta* started to increase. The lacustrine phase is dominated by cyanobacteria, green algae and brackish-water diatoms, including the abundant *Chaetoceros* resting spores. Around c. 2010 cal. yr BP, a shift in the lithology towards finer sediments, a decrease in magnetic susceptibility, and an increase in brackish-water diatoms is observed. This possibly indicates the (partial) disappearance of multi-year snow banks in the catchment area, which might be linked to the Mid- to Late-Holocene warm period recorded in several palaeorecords from Antarctica. From c. 1200 cal. yr BP onwards, Neoglacial cooling could be inferred based on decreased fluxes in palaeoproductivity proxies.

Introduction

Only 0.35% of the Antarctic continent is ice-free (Fox & Cooper 1994) of which 1 to 2% consists of coastal oases (Hodgson et al. 2004). In these regions many lakes occur, with a wide range in physical and chemical properties (Laybourn-Parry & Pearce 2007; Vincent et al. 2008; Verleyen et al. 2012 in Appendix 1). The limnological diversity is related to the combined effect of several factors, including lake ontogeny, catchment size and geomorphology, basin morphometry, the time of deglaciation, the amount of nutrients and ions entering the lake via sea spray, visits by marine animals and meltwater streams, and past and present climate dynamics. The latter include in particular the ablation rate, the precipitation-evaporation balance and the melting rate of snow banks and ice caps in the catchment area (Verleyen et al. 2012 in Appendix 1). The vast majority of coastal Antarctic lakes was formed in response to ice-sheet or glacier dynamics during the Holocene (Laybourn-Parry & Pearce 2007; Pienitz et al. 2008) and are therefore of relatively recent origin. However, there is increasing evidence for significant regional differences in lake age and the related deglaciation history of coastal regions in East Antarctica (EA). Some lakes escaped full glaciation during the Last Glacial Maximum (LGM), such as Lake Reid in the Larsemann Hills (Hodgson et al. 2005) and Lake Abraxas in the Vestfold Hills (Gibson et al. 2009) (Fig. 1a), while others were ice-covered and gradually deglaciated between c. 13.5 and 4 ka BP (Verleyen et al. 2011 in Appendix 2 and references therein). Accumulated sediments in Antarctic lakes can therefore provide insights into the deglaciation of a region, but they also contain valuable records of environmental and climatological change, as well as information on regional colonization-extinction dynamics of biota. Moreover, sediments in isolation basins can be used to develop relative sea-level (RSL) curves. These lakes were once inundated by the sea as a result of ice-sheet loading and originated due to isostatic uplift (e.g. Verleyen et al. 2005). By dating the transition from marine to lacustrine sediments and measuring the sill height of the lake, changes in the RSL can be reconstructed. In turn, RSL curves can be used to estimate the volume and dynamics of the ice-sheets during and after the LGM (Bassett et al. 2007).

The ice-free area on Skarvsnes (69°19’ - 69°32’S and 39°27’ - 39°53’E) (Fig. 1b) in eastern Dronning Maud Land (EA) is the largest in Lützow Holm Bay (Fig. 1a). Terrestrial cosmogenic nuclide dating of glacial erratic boulders exposed following retreat of the LGM ice-sheet suggests that the ice-sheet on Skarvsnes was at least 350 m thick during the LGM and that the peninsula became ice-free between 10 and 6 kyr ago (Yamane et al. 2011). Skarvsnes contains numerous lakes, but relatively few have been studied for their long-term sedimentary records (Matsumoto et al. 2006; 2010). The latter studies showed a good preservation of organic components, sedimentary facies, and isotope ratios of organic carbon and nitrogen in radiocarbon-dated sediment cores of Namazu Ike, Ô-Ike, and Lake Skallen Oike and thus their potential for palaeolimnological studies.

Kobachi Ike [28 m above sea-level (a.s.l.); Fig. 1b], was identified as an interesting coring site because of its location in the central part of the peninsula and the presence of *in situ* fossilized polychaete tubes in deposits on its highest sill at an altitude

of 32 m a.s.l. Therefore, the lake provides an opportunity to determine the maximum RSL high stand in the region, which was previously reconstructed to be only 20 m based on ^{14}C dates of marine fossil remains in raised beaches (Igarashi et al. 1995; Miura et al. 1998). Furthermore, the lake is brackish, with a specific conductance of 5.0 - 11.4 mS/cm (surface - bottom). This is a rather uncommon situation for a lake at such altitude according to available data from many Antarctic lakes (Verleyen et al. 2012 in Appendix 1), and might be due to either a negative precipitation-evaporation balance, input of salt via aerosols derived from the hypersaline Suribati Ike (Fig. 1b) that is located in the same area but at an altitude of -33 m a.s.l., and/or the presence of relict marine waters. This chapter describes sediment cores from the lake with the aim to (1) determine the onset of deglaciation of Skarvsnes, (2) constrain the local RSL maximum, and (3) document the changes in the lake since its isolation in response to Holocene environmental changes. To achieve this, we analysed fossil pigments, siliceous microfossils (diatoms), sedimentology, total organic (TOC) and inorganic carbon (TIC), nitrogen (TN), and sulfur (TS) in radiocarbon-dated sediment cores.

Site description

Skarvsnes is part of Syowa Oasis (unofficial name), a 200 km² ice-free region in Lützow Holm Bay composed of a series of islands and peninsulas (Miura et al. 1998). The highest altitude is Mount Suribati which rises to 400 m a.s.l. (Miura et al. 1998). The ice-sheet margin is located on the eastern side of the peninsula and the coast is seasonally free of sea-ice (Sawagaki & Hirakawa 1997). North and south of the peninsula, three glaciers occur, namely the Honnör glacier to the north, and the Telen and Skallen glaciers to the south (Yamane et al. 2011). The ice-free areas are covered by scoured bedrock, resulting from glacial erosion (Sawagaki & Hirakawa 1997) by a formerly more extensive ice-sheet (Yoshida 1983). Striations with a NW-SE flow (Yoshida 1983) and scattered erratic boulders are common (Miura et al. 1998). Raised beaches and emerged marine deposits occur on ice-free rocks around the coves and lakes, and include bivalve mollusks and worm tubes (Miura et al. 1998). The mean temperature and wind speed over the past 50 years are -10.5°C and 6.6 m/s respectively, and the predominant wind direction is northeasterly (Sato & Hirasawa 2007).

Skarvsnes contains numerous fresh to brackish water lakes (Kimura et al. 2010). The study lake, Kobachi Ike (SK4; 69°29.025'S - 39°38.575'E; Fig. 1b) is an oligotrophic, brackish water lake located 28.7 m a.s.l. in the vicinity of Mount Suribati. It is several weeks ice-free during the austral summer and has a length of 0.24 km, a width of 0.18 km, and a surface area of 0.041 km² (Kimura et al. 2010). At the time of sampling, the lake was fed by a small stream draining the southern part of the catchment, including the nearby Magobati Ike (SK9; Fig. 1b) (which has a specific conductance of 0.33 mS/cm; Table S1 in Appendix 1), but there was no active outflow stream from Kobachi Ike. To the east of Mount Suribati, the largest water body in the region, Suribati Ike (SK10), is situated. This hypersaline and meromictic lake has a specific conductance of 32.9 mS/cm (Table S1 in Appendix 1).

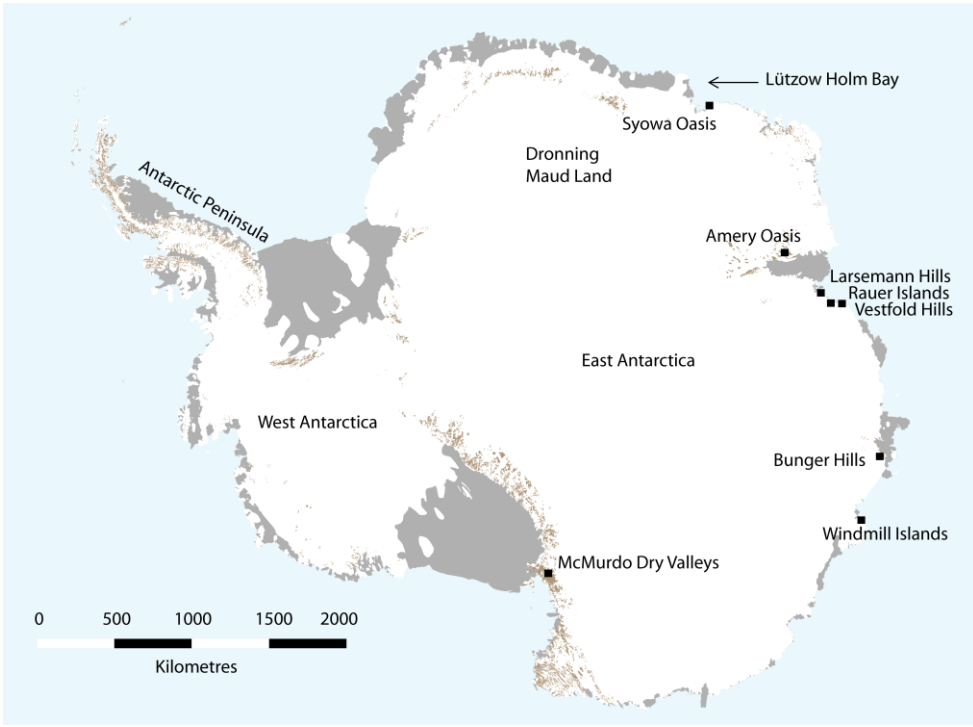

Figure 1a. Overview map of Antarctica indicating the study region Lützow Holm Bay and other main ice-free areas referred to in the text.

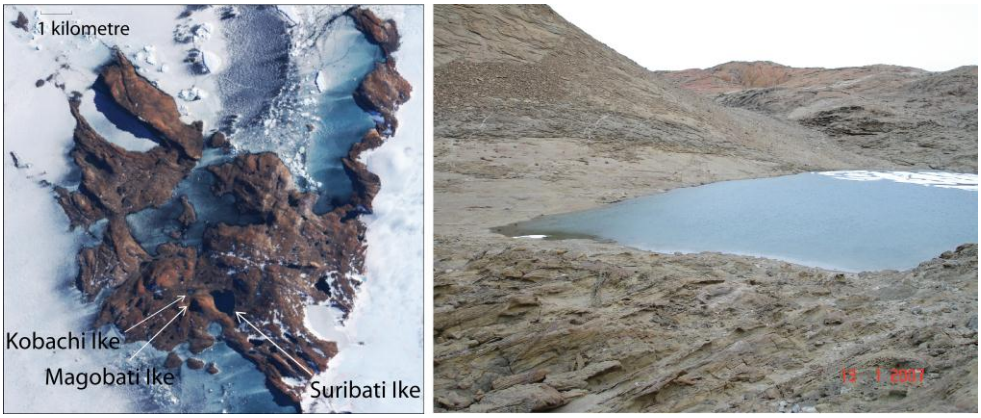

Figure 1b. Left: Map of Skarvsnes with indication of the study lake Kobachi Ike and the nearby lakes Suribati Ike and Magobati Ike. Right: Picture of Kobachi Ike at the time of sampling.

Materials and methods

Fieldwork took place on 14-15 January 2007. Water samples for the analysis of the major ions, nutrients, TOC, and dissolved organic carbon (DOC) were collected in acid-washed Nalgene bottles and kept frozen prior to analysis. Vertical profiles of specific conductance, pH and temperature were measured using an YSI 600 water-quality meter. Sediments were collected at the deepest part of the lake using a square-rod piston sampler (Wright 1967) with an overlap of at least 15 cm between different successive drives. Four cores were retrieved with a total sediment depth of 280.8 cm and stored at -20°C prior to analysis.

The sill height of Kobachi Ike was surveyed using a Trimble 5700 base station GPS cross-referenced to the IGS station at Syowa (code SYOG). As a test of the vertical accuracy, Geodetic Station No 39-02 was resurveyed giving an ellipsoidal error of ± 0.97 cm. Altitudes were referenced to vertical datum WGS84 with the EGM96 geoid separation ranging from 21.14 to 22.02 m.

Before splitting, the cores were scanned with a GEOTEK multi-sensor core logger measuring gamma ray density (GRD) and volume-specific magnetic susceptibility (MS) in 0.2-cm steps. GRD was converted to dry bulk density (DBD) by using a dry weight conversion factor. To obtain this, a weighted sample was dried for 48h at a temperature of 60°C in an oven and subsequently re-weighted. The percentage dry weight was calculated as the ratio between the weight of the dried sample to that of the wet sample. Volume-specific MS was used to correlate different overlapping sections of the sediment cores and was converted to mass-specific MS by dividing it by the DBD. Macroscopic descriptions included sediment texture and structure.

Nineteen samples were dated using AMS ^{14}C by the UK Natural Environment Research Council (NERC) Radiocarbon Laboratory and/or the Beta Analytic Radiocarbon Dating Laboratory. Results are reported as conventional radiocarbon years BP with two-sigma (2σ) standard deviation errors. Dates were calibrated using the SHCal04.14C atmosphere calibration curve for lacustrine sediments (McCormac et al. 2004; Reimer et al. 2004), and the Marine09 calibration curve for marine sediments (Reimer et al. 2009). The AMS ^{14}C dates of the marine sediments were corrected for the marine carbon reservoir effect by adding a ΔR value of 720±100 years based on 1120±100 years minus the global marine reservoir of 400 years, as recommended by Yoshida & Moriwaki (1979). We preferred Bayesian (BACON) instead of classical (CLAM) age-depth modeling in the case of the Kobachi Ike sediments as these appeared to be challenging and rather complicated. Bayesian age-depth modeling uses more advanced, robust and flexible numerical methods (Blockley et al. 2007) and the BACON software (Blaauw & Christen 2011) aims to produce more environmentally realistic age-depth models by reconstructing the underlying processes (i.e., the accumulation/sedimentation process), instead of simply fitting a curve through the dated points as classical (CLAM) modeling does (Blaauw & Christen 2011). The model included 7,080,000 iterations, 0.5-cm resolution steps and all ages used in the text are rounded off to the nearest 10 years.

Concentrations of total carbon (TC), TOC, TN, and TS were measured using a Flash 2000 Organic Elemental Analyzer (subsamples taken at a maximum interval of 8 cm). Filtered and homogenised samples for TOC analysis were pretreated overnight with 5% HCl to remove carbonates. Samples for sulfur analysis were treated with vanadium pentoxide to ensure complete combustion of the sulfur. Measurements were carried out by dry combustion at high temperature (left furnace: 950°C and right furnace: 840°C; King et al. 1998). This was followed by separation and detection of the gaseous products. The data were processed using the Eager Xperience software. Samples for TC, TOC and TN were ran all at least twice to detect and exclude possible erroneous values. Where appropriate, outliers were excluded and the mean value of replicates was used. TIC is derived from the difference between TC and TOC. For TS analysis, eight samples were run at least twice to ensure reproducibility. Of those, the mean value was used. Reproducibility within and between runs was furthermore ensured by running standards of sulphanilamide. This analysis revealed that our method is reproducible as these samples yielded an average carbon concentration of 41.8%, ranging between 41.4 and 42.0%, and an average nitrogen concentration of 16.3%, ranging between 16.0 and 16.6%. The analytical error for TOC appeared to be ± 0.45% and for TN ± 0.31%, based on measured sulphanilamide standards. Based on a sample which had been run multiple times, this error was respectively ± 0.05% and ± 0.01%. The highest and most conservative error was applied. For the TS analysis, no analytical error was calculated.

Diatom analysis followed standard protocols (Battarbee & Kneen 1982; Renberg 1990). Taxonomic identification was mainly based on Cremer et al. (2003) and Scott & Thomas (2005). In all samples, at least 400 valves were counted, except when diatom concentrations were too low. The diatom stratigraphy was divided into zones using stratigraphically constrained cluster analysis (CONISS) in R and plotted using Tilia and Tilia Graph (Grimm 2004). The significance of the zones was assessed using a broken-stick model (Bennett 1996) in the Rioja package in R (Juggins 2009).

Fossil pigments were extracted from bulk sediments and analysed with a High Performance Liquid Chromatography (HPLC) system comprising an Agilent 1100 HPLC, DAD-diode-array detector and Agilent Eclipse XDB-C8 column. Pigment analysis followed Van Heukelem & Thomas (2001), using three solvents, namely 80:20 methanol - ammonium acetate, 90:10 acetonitril - water and ethyl acetate. The system was calibrated using authentic pigment standards and compounds isolated from reference cultures following Scientific Committee on Oceanic Research (SCOR) protocols (DHI, Denmark). Pigment identification was based on Jeffrey et al. (1997). Pigments of unknown affinity were assigned as derivatives of the pigment with which they shared the closest retention times and absorption spectra, or as 'unknown'. Concentrations of individual pigments in the samples were calculated using the response factors of pigment standards. The pigment stratigraphy was analyzed as described above for the diatom stratigraphy.

As proxy data can be influenced by variable sedimentation rates (SRs) (Street-Perrot et al. 2007), they were calculated as fluxes. The mass accumulation rate (MAR; g/cm^2 yr) was calculated as the multiplication of the DBD (g/cm^3) and the SR (cm/yr). The

flux of proxies was then calculated as the multiplication of the MAR and their concentration by dry weight or the absolute counts at a certain depth.

Results

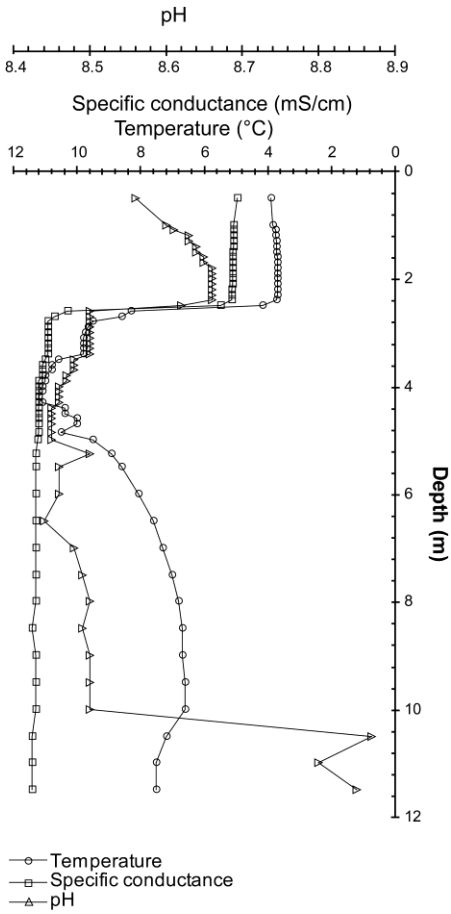

Figure 2. Vertical profiles of pH, specific conductance (mS/cm), and temperature (°C) of Kobachi Ike.

Limnological characteristics

Limnological measurements revealed that Kobachi Ike has a maximum depth of 11.5 m, a pH of 8.6 - 8.9 (surface - bottom) and a specific conductance of 5.0 - 11.4 mS/cm (surface - bottom). Vertical profiles indicate a primary thermocline at c. 2.4 m and a pronounced warmer water lens between c. 6 and 10 m (Fig. 2), which was most probably resulting from the accumulation of cold meltwater with a low salinity in the surface waters and trapping of heat in the more saline deeper part of the water column. At the time of sampling, ice covered about one third of the lake surface. This remarkable vertical stratification is likely a temporary feature as high dissolved oxygen (DO) values were measured throughout the water column by Kimura et al. (2010) [see Fig. S1 in the Supplementary Material for the profiles presented in Kimura et al. (2010) for comparison]. In general, our observed physical profiles closely match those from Kimura et al. (2010; Fig. S1), similarly indicating a thermocline around 2.4 m water depth. The warmer water lens was located between c. 4 and 6 m. The salinity profile in Kimura et al. (2010) resembles our specific conductance profile, and the pH profiles also closely match, although pH measured in the Kimura et al. (2010) study was overall slightly lower. Although no oxygen measurements were taken at the time of sampling, we did not observe any indication for reducing conditions in the bottom waters either. It thus appears that later during the summer period, the lake is completely mixed.

Radiometric dating

All samples except the sample at 240 cm provided reliable AMS dating results (Table 1) and all dates were retained in the age-depth model (Fig. 3). As the $C_{organic}/N_{total}$ ratio is clearly different in the zone between 260 and 231 cm (Fig. 4) (see further), this might

indicate that the dominant carbon source is most likely of terrestrial origin, so a marine reservoir correction was not applied on these dates. An increased SR of up to 14.3 mm/yr is suggested between c. 4570 and 3670 cal. yr BP (244 - 110 cm). Between c. 6740 and 4580 cal. yr BP (280 - 245 cm), the SR was between 0.05 and 2.56 mm/yr, while during the period between c. 3650 cal. yr BP and present (109 - 0 cm), the SR was between 0.13 and 1.70 mm/yr.

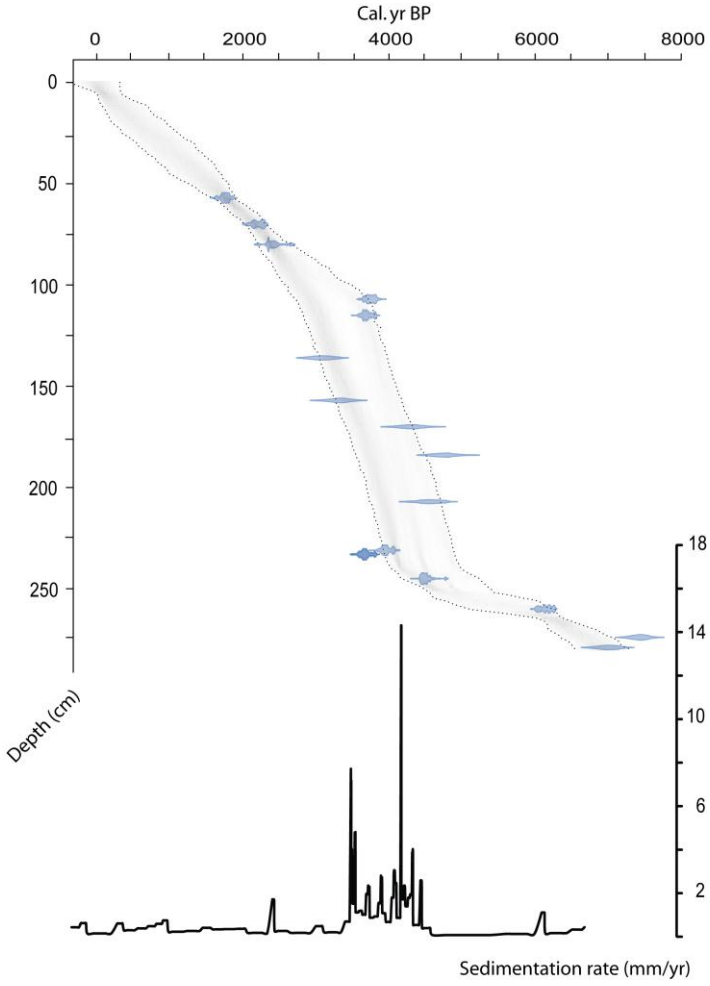

Figure 3. Stratigraphic age-depth model of the Kobachi Ike sediment cores undertaken in BACON (Blaauw & Christen 2011), along with the sedimentation rate. Calibrated radiocarbon ages are shown in Table 1.

Lithostratigraphical, geophysical, and geochemical analysis

Between 280.8 and 271.3 cm, the sediments were composed of grey clay and white-yellow platy fragments (Fig. 4). The zone between 271.3 and 217.7 cm was composed of

fine to medium laminae, alternated with laminae of silty clay. This sequence was covered by a 2-cm layer of grey clay and medium sand. Thick to medium laminae alternated with yellow laminae between 214.4 and 155.3 cm. From 155.3 cm upwards the laminae were richer in sand and alternated with yellow colored laminae or coarse sand laminae. The sediments changed at 68.8 cm into finely laminated layers of fine-medium sand with some clay-silt, alternated with white-yellow clay-silt and fine white-yellow sand, until 58.2 cm. Between 54.7 and 26.5 cm, the fine laminations were only faintly visible. A fine white-yellowish sand layer was present between 37.6 and 31.8 cm. The upper 26.5 cm of the sediments were composed of fine or medium sand, alternated with laminated clay silt. For readability, the lithology figure has also been added to the Supplementary Material (Fig. S2).

TN values ranged between 0.02 and 0.18% (Fig. 4). Values were low in the bottom sediments (280 - 240 cm; 0.02 - 0.09%), increased slightly between 236 and 235.2 cm (0.10 - 1.18%), to become overall low again between 231.2 and 89 cm (0.03 - 0.09%). From then onwards, TN increased, and ranged between 0.03 and 0.18%. However, TN concentrations fall within the range of analytical error based on the measured sulphanilamide standards (± 0.31%) and were therefore not further interpreted. TS values ranged between 0.11 and 1.37% (Fig. 4). Values were relatively high between 280 and 268 cm (0.97 - 1.37%) to become relatively low between 268 and 113 cm (0.11 - 0.77%). The upper 113 cm of the sediments again contained on average higher TS amounts (between 0.32 and 0.86%). TOC values ranged between 0.22 and 1.35% (Fig. 4). Values were relatively low between 280 and 268 cm (0.30 - 0.48%), to become higher between 260 and 235.2 cm (0.22 - 1.28%). Between 235.2 and 64 cm, TOC values were again relatively low (0.23 - 0.78%), whilst the upper 64 cm of the sediments contained relatively high TOC values (0.58 - 1.35%). TIC values ranged between 0.01 and 2.74% (Fig. 4) and were highest between 280 and 235.2 cm (0.26 - 2.74%). From then onwards, values were relatively low (0.01 - 1.00%). The $C_{organic}/N_{total}$ ratio is relatively low in the bottom sediments (280 - 260 cm), increases between 260 and 235 cm, and becomes relatively low afterwards (Fig. 4). Mass-specific MS was relatively low until c. 235 cm, and then relatively high between c. 235 and 65 cm, returning to relatively lower values in the upper 65 cm (Fig. 4). GRD values were relatively stable throughout the sediments to fluctuate slightly more in the upper 60 cm (Fig. 4). Overall patterns throughout the sediments can be summarized as follows: between 280 and 236 cm, sediments were characterized by a low MS, stable GRD and the highest TIC values compared to the entire sediments. TOC was relatively high between 260 and 236 cm. The significantly higher $C_{organic}/N_{total}$ ratio might indicate a terrestrial influence in this part of the sediments. Between 236 and 115 cm, sediments were characterized by relatively lower TIC, TOC and TN values, and a higher MS and stable GRD. The upper 115 cm of the sediments was then characterized by a low MS, slightly more variable GRD and higher TOC and TN values.

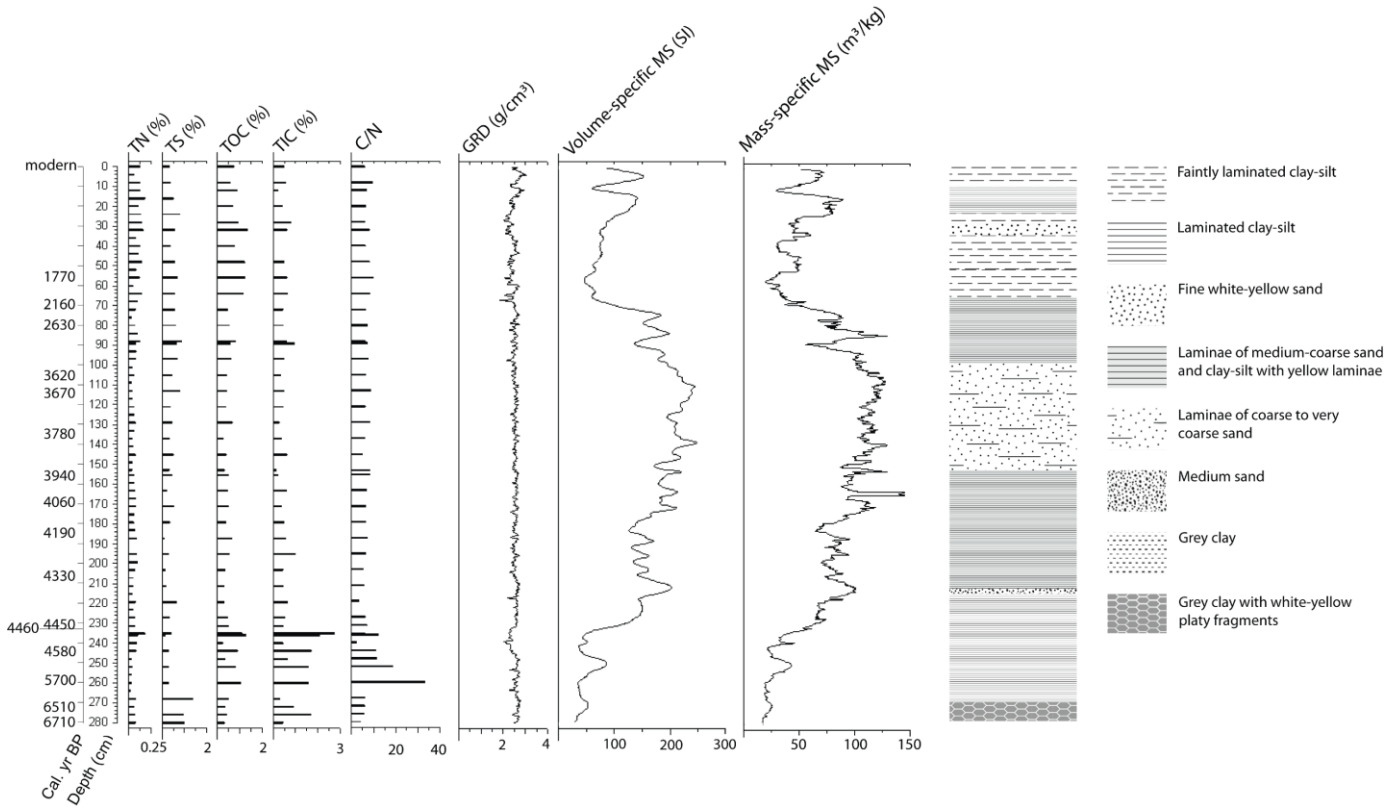

Figure 4. Diagram with total nitrogen (TN), total sulfur (TS), total organic carbon (TOC), total inorganic carbon (TIC), the $C_{organic}/N_{total}$ ratio along with the volume-specific magnetic susceptibility (MS) and mass-specific MS, gamma ray density (GRD), and lithology (with accompanying legend) of the Kobachi Ike sediment cores.

Microfossil analysis

A total of 92 diatom taxa were identified, with 24 taxa having a minimum abundance of 1% in at least 2 samples (Fig. 5). Samples in which less than 100 valves were found are indicated with an asterisk. Based on a constrained cluster (see Fig. S3 in the Supplementary Material) and broken-stick analysis, five significant diatom zones were identified.

Sediments from zone 1 (280 - 245 cm, c. 6740 - 4580 cal. yr BP) contained very low concentrations of diatom frustules. In the bottom sample, the marine and brackish-water diatom species *Navicula phyllepta, Navicula directa* and *Trachyneis aspera* were encountered, while towards the top of this zone, some *Chaetoceros* resting spores were observed.

Zone 2 (245 - 230 cm, c. 4580 - 4450 cal. yr BP) was characterised by an almost monospecific assemblage of an unknown *Navicula* species (*N.* sp. 1; see Fig. S4 in the Supplementary Material), together with some specimens of *Halamphora veneta, Chaetoceros* resting spores, and *Thalassiosira oliverana.* To our knowledge, this *Navicula* species has not been reported before from (Sub-)Antarctica and is not listed in a recent compilation of diatoms from over 400 freshwater and brackish lakes from Maritime Antarctica, Sub-Antarctica and EA (Verleyen et al. unpubl. results). Moreover, it was absent in both older and younger sediments in the Kobachi Ike sediment cores. Further taxonomic research is currently being performed (Sabbe et al. in prep). The diatom concentration was slightly higher compared with the previous zone.

In zone 3 (230 - 99 cm, c. 4450 - 3290 cal. yr BP) sediments were characterised by a relatively high diatom concentration, which was dominated by *Chaetoceros* resting spores, an indicator of marine open-water and stratified conditions (Crosta et al. 2004). Vegetative forms of *Chaetoceros,* however, were not present, which might indicate that dissolution occurred. As Ryves et al. (2009) point out, diatom dissolution is a widespread phenomenon, particularly in marine and saline settings, and here it might have been the case that the heavily silicified and more dissolution-resistant *Chaetoceros* resting spores (Crosta et al. 1997) were preserved while vegetative cells did not. This might also lead to an underestimation of the abundance of other little silicified species such as *Craspedostauros laevissimus*. Alternatively, valve dissolution might not have been a problem and these resting spores indeed made up the majority of the diatom assemblages in the sediments. In other Antarctic regions (e.g. the Gerlache Strait, Ross Sea), *Chaetoceros* resting spores have also been commonly found in the neritic zone (the coastal waters) (Ferrario et al. 1998; Armand et al. 2005). Resting spore formation is seen as a common phenomenon and is often triggered by low light conditions in polar waters and as such, these spores are regarded as the 'waiting' or 'seeding' population (Ferrario et al. 1998 and references therein). In the beginning of this zone, a peak in *Tryblionella marginulata* occurred. Around 200 cm (c. 4270 cal. yr BP), the relative abundance of the brackish-water, littoral species *N. phyllepta* started to increase. The assemblage further included *Fragilaria* sp./*Pseudostaurosira* sp., and the sea-ice taxa *Navicula glaciei, N. directa, Fragilariopsis curta* and *Fragilariopsis cylindrus* (Crosta et al. 2004).

ZONE 4 (99 - 17 cm, c. 3290 - 630 cal. yr BP) was characterised by samples with a very high relative abundance of the brackish-water diatom *N. phyllepta,* whereas a smaller amount of samples contained very high abundances of *Chaetoceros* resting spores. The latter can be *in situ* produced, or were transported to the lake via sea spray or washed-in from raised beach deposits within the catchment area. *C. laevissimus* and *Chamaepinnularia cymatopleura,* two brackish-water species occurring in Antarctic coastal lakes (e.g. Sabbe et al. 2003), were sub-dominant. Diatom concentration was relatively low compared to the previous zone.

ZONE 5 (17 - 0 cm, c. 630 cal. yr BP - recent) was characterised by a very low diatom concentration. Apart from the upper samples, which were dominated by benthic species, and in particular *N. phyllepta,* the assemblage was generally composed of *Chaetoceros* resting spores.

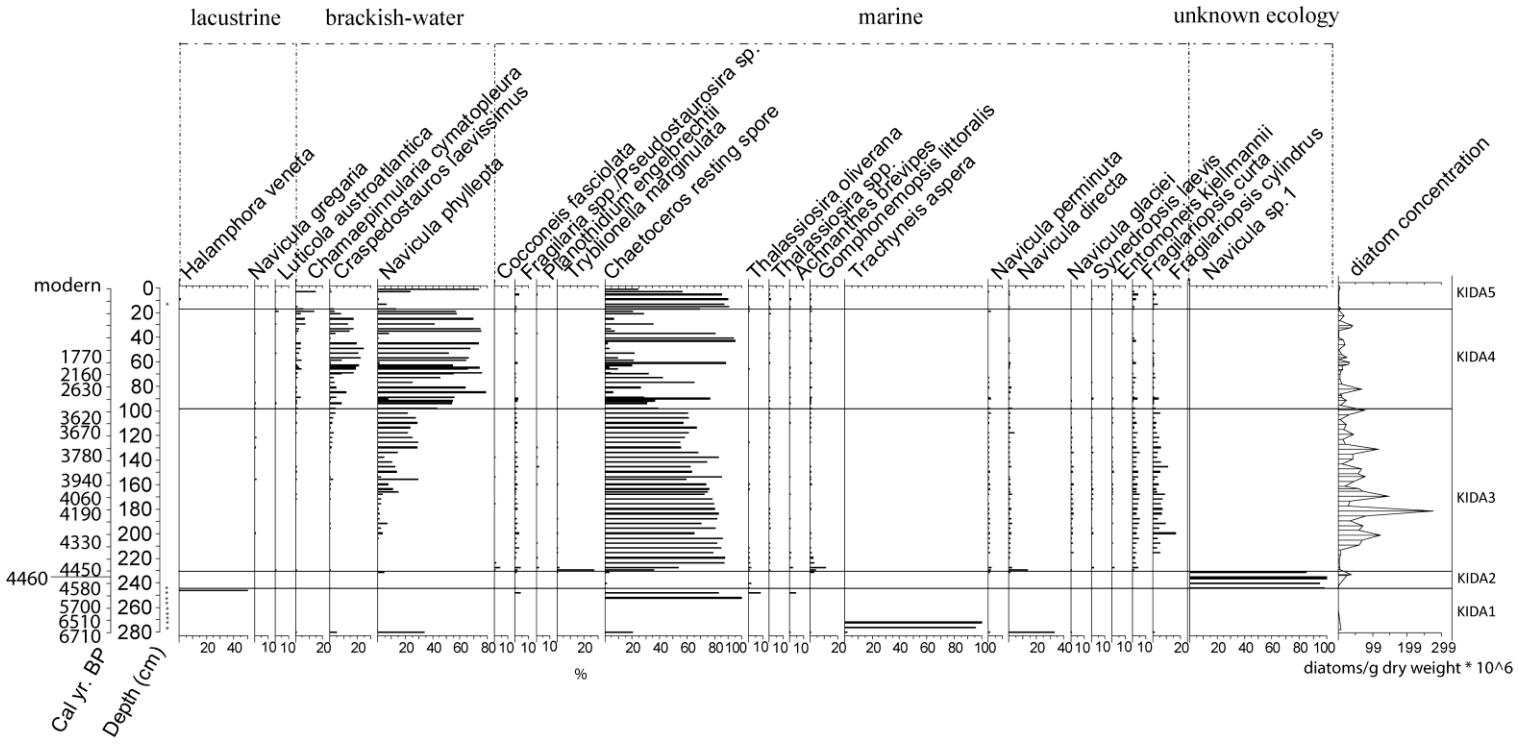

Figure 5. Diatom stratigraphy of the Kobachi Ike sediment cores. Zoning (KIDA1-5; Kobachi Ike Diatom Analysis) is based on a CONISS constrained cluster analysis (see Fig. S3 in the Supplementary Material). Apart from the diatom concentration, all data are expressed as relative abundances. Marine, brackish-water and lacustrine diatom species are indicated with brackets, as well as species with an unknown ecology. Diatom concentration is expressed as the number of diatoms per gram dry weight. The samples indicated with an asterisk along the right side of the depth axis contained a very small amount of diatoms preventing the analysis of 400 valves. Calibrated radiocarbon dates are indicated.

Fossil pigment analysis

Four significant pigment zones were identified based on a constrained cluster (see Fig. S5 in the Supplementary Material) and broken-stick analysis. Overall, total chlorophyll and carotenoid concentrations were very low in zone 1 and 2, slightly higher in zone 3, to become highest in zone 4. Zone 1 and 2 overall match the distinct zones based on the diatom communities.

Zone 1 (280 - 237.5 cm, c. 6740 - 4480 cal. yr BP) was characterised by very low concentrations of total chlorophylls and carotenoids, except for one peak in total chlorophylls at the top of the zone. The chlorophyll *a* derivative phaeophytin *a* dominated the chlorophyll fractions, whereas the most abundant carotenoids throughout the zone were lutein (present in green algae, and red seaweeds) and unknown carotenoids; vaucheriaxanthin (xanthophytes, eustigmatophytes) in the bottom part of this zone, and diatoxanthin (diatoms, dinophytes, chrysophytes) near the top of this zone.

Zone 2 (237.5 - 213 cm, c. 4480 - 4350 cal. yr BP) was characterised by large peaks in prasinoxanthin (prasinophytes) and diatoxanthin. Zeaxanthin (cyanobacteria, green algae, and possibly mosses) occurred in the bottom of zone 1, was then no longer detected and re-appeared at 227 cm in this zone. Phaeophytin *a* remained the most abundant chlorophyll. Total chlorophyll and total carotenoid concentrations remained low.

Zone 3 (213 - 131 cm, c. 4350 - 3740 cal. yr BP) was characterised by slightly higher amounts of total chlorophylls and carotenoids compared to the two previous zones. Chlorophyll *a* was the dominant chlorophyll, whereas lutein and vaucheriaxanthin were the most abundant carotenoids. The latter was found in the bottom sediments in zone 1, but was no longer detected and only re-appeared at the beginning of this zone. Diatoxanthin, fucoxanthin (diatoms, brown seaweeds), and prasinoxanthin were almost absent in this zone.

Zone 4 (131 - 0 cm, c. 3740 cal. yr BP - recent) was characterised by higher amounts of total chlorophylls and carotenoids compared to the previous zones. Chlorophyll *a* remained the most abundant chlorophyll, while lutein and vaucheriaxanthin were the most abundant carotenoids. This zone was furthermore characterised by the appearance of myxoxanthophyll (cyanobacteria) at 115 cm (c. 3670 cal. yr BP) which was only detected once in the previous zone at 207.2 cm (c. 4330 cal. yr BP). Phaeophytin *a* increased in abundance compared to the previous zone, as well as the group of unknown carotenoids and diatoxanthin. Violaxanthin (green algae, euglenophytes) decreased in abundance.

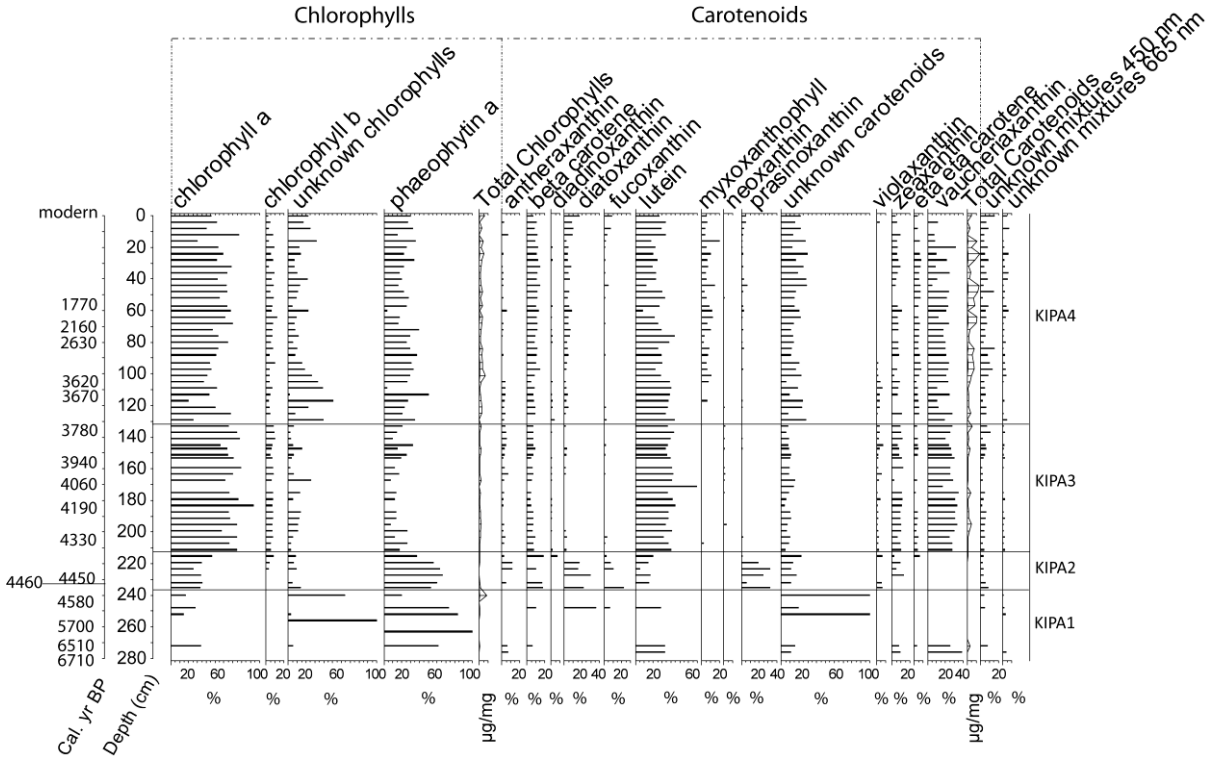

Figure 6. Stratigraphy of fossil pigments in the Kobachi Ike sediments. The abundance of individual pigments is reported as percentages to total chlorophylls or carotenoids. Total chlorophylls and total carotenoids are reported in µg/mg and plotted with an exaggeration factor of 20 to increase visibility of the figure.

Palaeoproductivity indicators

To account for variable SRs, palaeoproductivity indicators (diatom concentration, TN, TS, TOC, total chlorophylls and carotenoids) were calculated as fluxes (Street-Perrot et al. 2007). The water content of the Kobachi Ike sediments is plotted in Fig. S6 in the Supplementary material.

Between 280 and 245 cm (c. 6740 - 4580 cal. yr BP), all palaeoproductivity indicators were relatively low (Fig. 7), as well as in the upper 113 cm (c. 3670 cal. yr BP - recent). Between 245 and 113 cm, values were higher and showed more variation. The pattern of the diatom flux (Fig. 7) is comparable to the diatom concentration (Fig. 5), with higher values between c. 215 and 113 cm (c. 4360 - 3670 cal. yr BP). One peak occurred at 207 cm (c. 4330 cal. yr BP). The TN, TS and TOC fluxes exhibited higher values between c. 245 and 113 cm (c. 4580 - 3670 cal. yr BP) (Fig. 7) and lower values in the upper and lower sediments. The TOC flux slightly decreases in the upper 40 cm (c. 1200 cal. yr BP). This is a different pattern compared to the raw data which were relatively higher in the bottom and upper sediments (Fig. 4). The total carotenoid and chlorophyll fluxes exhibited the same pattern as the TN, TS and TOC fluxes (Fig. 7). This pattern is again different compared to the raw carotenoid and chlorophyll concentration data as these were relatively high in the upper 113 cm as well (Fig. 6).

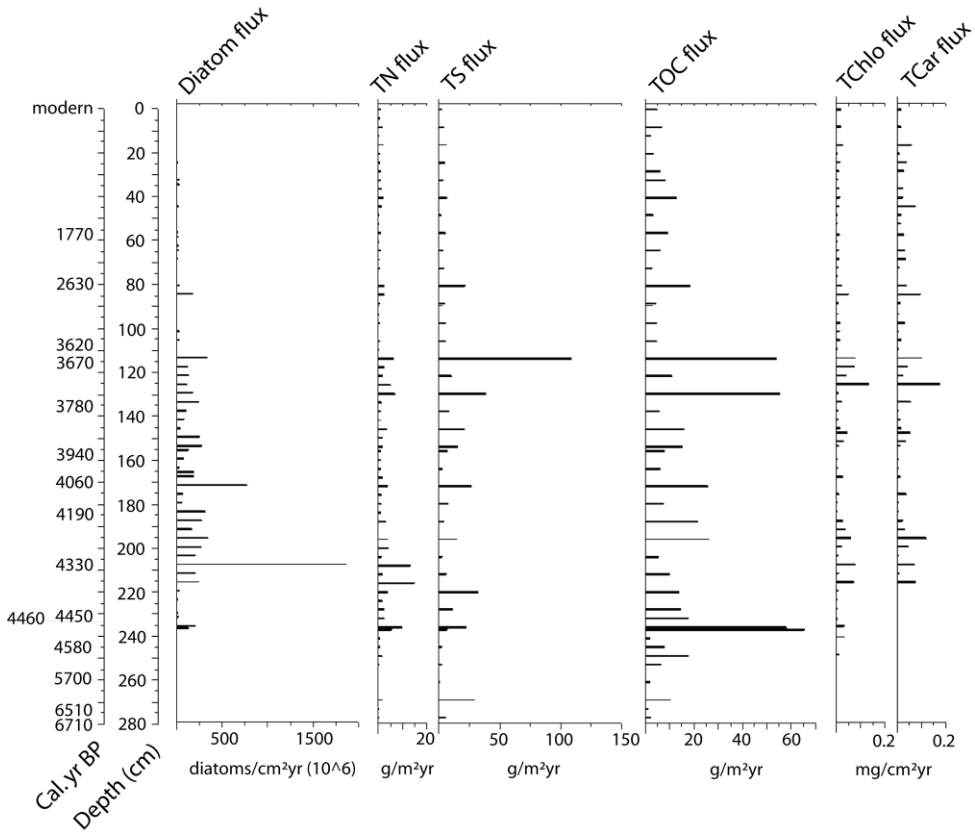

Figure 7. Fluxes of the palaeoproductivity indicators throughout the Kobachi Ike sediments: diatoms, total nitrogen (TN), total sulfur (TS), total organic carbon carbon (TOC), total chlorophylls (TChlo), and total carotenoids (TCar).

Discussion

Deglaciation history of Skarvsnes

Radiometric and cosmogenic isotope dating campaigns revealed that the majority of the currently ice-free coastal oases in EA deglaciated slightly prior to or at the start of the Holocene (Mackintosh et al. 2013). However, some regions became ice-free during the Late-Holocene (Verleyen et al. 2011 in Appendix 2), while others were ice-free for at least the past 120,000 years (Hodgson et al. 2001). The radiocarbon dating of the bottom sediments of Kobachi Ike provides a minimum age of deglaciation of this part of the peninsula of c. 7240 cal. yr BP (Table 1; Fig. 8), which is later than in most other coastal Antarctic oases. Our date falls within the time window (10 to 6 ka BP) of deglaciation obtained using terrestrial cosmogenic nuclide (TCN) exposure ages from glacial erratics in Skarvsnes (Yamane et al. 2011). Mount Suribati, in the immediate vicinity of Kobachi Ike, was exposed at its base (56 m a.s.l.) around c. 8.66 ± 0.90 ka BP and at its top (259 m a.s.l.) around c. 6.42 ± 1.08 ka BP (mean of three ^{10}Be ages; Yamane et al. 2011), which agrees well with our radiocarbon date of the onset of sedimentation in Kobachi Ike. The relatively wide range of glacial erratic ages might be related to long-term burial, persistent snow cover, long-term erosion, and problems with quantification of nuclides (Yamane et al. 2011) and should thus be interpreted with caution. Overall, however, they indicate an Early-Holocene melting of the ice-sheet of at least 350 m in this region (Yamane et al. 2011). In agreement with this, ^{14}C dates from marine sediment cores from the region, located less than 50 km offshore, are all younger than c. 16 ka BP (Igarashi et al. 2001) and therefore suggest that the ice-sheet covered the region during the LGM and contracted during the Early-Holocene.

A deglaciation during the Late- to Mid-Holocene is in clear contrast with the nearby Ongul Islands and Langhovde where ^{14}C ages of fossils preserved *in situ* in raised beaches suggest that these regions were ice-free during the LGM (Miura et al. 1998; Takada et al. 2003). These differences are also supported by the relatively unweathered and intensely striated rocks on Skarvsnes, compared to deeply weathered rocks on the Ongul Islands and Langhovde (Miura et al. 1998). These regional differences in deglaciation history might be related to geomorphological differences, but to determine this, marine geological surveys, including multi-beam swath bathymetry and deep-tow side-scan sonar, together with ^{14}C dates of marine sediment cores would be useful. Although offshore troughs have been identified in front of the largest glaciers along the coast of Lützow Holm Bay, no detailed offshore geological or geophysical studies have been conducted in the region so far (Anderson et al. 2002). Such studies could provide strong evidence for ice-sheet grounding as for example in the Ross Sea region, where glacial lineations provide indisputable evidence that the ice-sheet grounded on the continental shelf (Shipp et al. 1999; Mosola & Anderson 2006). It is thus possible that the ice-sheet grounded on the continental shelf leading to a relatively late deglaciation of the near-shore environment of Skarvsnes during the Holocene.

The RSL maximum and onset of RSL fall

Understanding and documenting the behaviour of (parts of) the East Antarctic Ice-Sheet (EAIS) is key for understanding its present and future dynamics (Mackintosh et al. 2013), especially under climate warming. Numerical predictions of glaciation-induced sea-level change underestimated the isostatic component of the sea-level response in the Syowa Oasis region of the EAIS, indicating that the maximum ice thickness has been underestimated in the majority of the ice-sheet models available (Bassett et al. 2007). According to data derived from marine fossils (*Laternula elliptica*) from raised beach deposits, sea-level fell at this site from around 20 m a.s.l. (Miura et al. 1998; Hirakawa & Sawagaki 1998). The presence of marine diatom species in the sediments dated between c. 6740 and 3670 cal. yr BP in Kobachi Ike (Fig. 5) indicates that this was an isolation basin, which became isolated from the ocean after c. 3670 cal. yr BP (115 cm). This could be inferred from the presence of the cyanobacterial pigment myxoxanthophyll (Fig. 6), the increase of brackish water diatoms such as *N. phyllepta, C. laevissimus,* and *C. cymatopleura,* and the decrease of sea-ice indicator species such as *F. cylindrus* and *F. curta* (Fig. 5). Alternatively, lake isolation started around c. 4030 cal. yr BP when the abundance of *Navicula phyllepta* started to increase (Fig. 5). In any case, this isostatic uplift occurred in response to regional ice-sheet retreat possibly in combination with neotectonic processes (Watcham et al. 2011). It can be assumed however that the contribution of the latter is smaller than ice-sheet disintegration, but neotectonics cannot be excluded given the fact that Skarvsnes is situated over a fault (Ishikawa et al. 1976). Our data thus revealed that the local RSL high stand is 28.7 m a.s.l., which is 8.7 m higher than previous estimates (Miura et al. 1998; Hirakawa & Sawagaki 1998). Compared with other East Antarctic regions, a RSL of this magnitude is relatively high (e.g. Zwartz et al. 1998; Verleyen et al. 2005). This might be related to (i) a larger difference in ice-sheet volume since deglaciation and/or (ii) the relatively recent deglaciation. This is not captured by any of the ice models used in Bassett et al. (2007), where there is relatively little ice volume change in EA and Holocene variability is neglected. Our data thus call for a re-evaluation of the existing ice-sheet models in the Lützow Holm Bay region. More information can be found in Chapter 6.

Holocene environmental changes

After regional deglaciation, low fluxes of TOC, total carotenoids, chlorophylls and diatoms (Figs. 7 & 8) indicate a low level of primary production in and around the lake during the period between c. 6740 and 4580 cal. yr BP (280 - 245 cm). Also the sediment accumulation rate was relatively low compared to the rest of the core (Figs. 3 & 7). These low fluxes of primary productivity indicators are consistent with lake sedimentary records from nearby West Ongul Island (Chapter 4), suggesting cold climatic conditions and the prevalence of undeveloped, slowly weathering catchments. Cold conditions were similarly being experienced during this period in other locations in EA. For example the marine environment in the Windmill Islands was relatively cold between c. 10.5 and 4 cal. ka BP (Cremer et al. 2003) and in the Rauer Islands between c. 8.2 and 5.7 ka BP, as evidenced by high abundances of diatom sea-ice indicator species (Berg et al. 2010). In

the Bunger Hills, a marine optimum between c. 9.4 and 7.6 ka BP was followed by cold marine conditions between c. 7.6 and 4.5 ka BP (Kulbe et al. 2001) (Fig. 1a).

Between c. 4580 and 4450 cal. yr BP (245 - 230 cm), primary production increased, as evidenced by higher fluxes of TOC, diatoms, and chlorophylls (Fig. 7). As strongly indicated by RSL data from the Lützow Holm Bay region, it is highly unlikely that the lake was isolated from the ocean during this period. However, it is difficult to explain the unusual combination of proxy data as well as the exact timing of this period. First, in contrast to the above-mentioned indications for increased primary productivity, the diatom assemblage in this zone was dominated by an almost monospecific assemblage of an as yet unknown *Navicula* species (Fig. S4 in the Supplementary Material), which was furthermore absent from both older and younger sediments (Fig. 5). Other primary producers, such as prasinophytes, may have been important as well as revealed by the pigment composition (Fig. 6). Interestingly, the main carbon source might be of terrestrial origin, as indicated by a significantly higher $C_{organic}/N_{total}$ ratio (Fig. 4). This ratio is often used to identify proportions of lake/marine algal and terrestrial organic matter. Organic matter from lake and marine algae has typically lower C/N values compared to terrestrial plants so elevated values can indicate a terrigenous input (Meyers 2003; Perdue & Koprivnjak; Hodgson et al. 2009a; b). Therefore, we did not apply a marine reservoir correction on these dates (Fig. 3; Table 1). If correct, this terrestrial input of organic material into the marine environment might have been derived from an increased melt of the regional ice-sheet and possibly originated from the in-wash of terrestrial mosses. TIC values were however high (Fig. 4), which suggests that the sediments are rather of a marine origin. Based on the available evidence, we therefore cautiously conclude that during this period Kobachi Ike was a shallow, sheltered marine lagoon harbouring a specific near-shore environment and receiving significant input of organic material from the surrounding terrestrial environment.

Between c. 4450 and 3670 cal. yr BP (230 - 115 cm), seasonally open-water marine conditions in the area can be inferred from the presence of a more diverse and productive community of marine and sea-ice associated diatoms (Figs. 5 & 8). This is also consistent with the higher levels of diatoxanthin (Fig. 6). Between c. 4480 and 4380 cal. yr BP (235 - 219 cm; Fig. 6), the high concentration of prasinoxanthin suggests higher abundances of prasinophytes, a group known to occasionally form blooms in Antarctic waters (Bird & Karl 1992). From c. 4380 cal. yr BP onwards (219 cm and above), green algae and/or red seaweeds became more dominant as indicated by the increasing relative concentration of lutein (Fig. 6). This might indicate that the marine basin became slightly shallower, favoring the development of attached, benthic macroalgae. The diatom community composition throughout this zone is similar to the marine composition of for instance the Prydz Bay region (Larsemann Hills; Verleyen et al. 2005) (Fig. 1a). Mass-specific MS values were high throughout this zone (Fig. 4), possibly because sediments contained ice-rafted debris (IRD) which originated elsewhere and had another ferromagnetic mineral content than those in the catchment of the basin.

Kobachi Ike became likely isolated after c. 3670 cal. yr BP (115 cm) (Fig. 8), as indicated by the appearance of myxoxanthophyll (Fig. 6) pointing to the colonization of

the basin by mat-forming cyanobacteria. However, it may also be possible that lake isolation started around c. 4030 cal. yr BP (165 cm) when an increase in *Navicula phyllepta* is observed (Fig. 5). The subsequent lacustrine phase is characterized by the dominance of green algae (lutein) and cyanobacteria (myxoxanthophyll; Fig. 6) and the presence of brackish water diatoms (*N. phyllepta, C. laevissimus,* and *C. cymatopleura*; Fig. 5). However, a freshwater diatom community (as for instance present in nearby Mago Ike; Tavernier et al. in press - Chapter 3), never became established, which is likely related to the interplay between the moisture balance and the lake morphometry. Kobachi Ike is deeper than Mago Ike, implying that the latter was more easily flushed due to meltwater input. By contrast, the relatively deep nature of Kobachi Ike likely led to stratification of the water column. In turn, this prevented the rapid dilution of the bottom water and led to the formation of a freshwater lens on top of the saline/brackish hypolimnion. This process is similarly observed today (Fig. 2). It is furthermore notable that the diatom flux was low during the entire lacustrine phase while fluxes of TOC, and pigments were more variable and exhibited peaks at certain depths (Fig. 7). The reason for that may be that cyanobacteria, and possibly also chlorophytes, dominate over diatoms in this brackish lake.

Around c. 2010 cal. yr BP (65 cm), a decrease in mass-specific MS and a change in lithology towards finer sediments (Fig. 4) might be linked to either a further retreat of local glaciers or - more likely - to the (partial) disappearance of multi-year catchment snow banks during the Mid- to Late-Holocene warm period (Fig. 8), which is detected in EA roughly between c. 4.7 and 1 ka BP (Verleyen et al. 2011 in Appendix 2), and in the nearby Ongul Islands between c. 4.2 and 0.9 cal. ka BP (Chapter 4). There are no clear indications for a primary productivity increase at the resolution studied, although the TOC flux was then slightly higher (Fig. 7). The (partial) disappearance of multi-year snow banks in the catchment area would have led to a decreased inflow of meltwater and terrigenous material into Kobachi Ike, explaining the presence of finer sand, clay and silt in the sediment record, which would also be reflected in the mass-specific MS trend (Fig. 4). Another consequence was the slightly increased salinity resulting from a relative increase in evaporative water loss relative to inflow of water. This is evidenced by an increase in *C. cymatopleura* and *C. laevissimus,* two brackish-water diatom species (Fig. 5). However, specific conductance could not be quantified using the constructed transfer function for this region (Tavernier et al. in press - Chapter 3) because of a lack of modern analogues in the surface dataset. The latter contained a low number of brackish and saline lakes, thus preventing us from performing a reliable reconstruction. Also combining our dataset with those from other East Antarctic regions (e.g. from the saline lakes in the Vestfold Hills; Roberts & McMinn 1998) was not possible because of large differences in regional diatom composition (Verleyen et al. unpubl. res.). Combined with data on nearby West Ongul Island where increased accumulation of total chlorophylls and total carotenoids occurred between c. 2230 and 2090 cal. yr BP (Chapter 4), the data from Kobachi Ike suggest the presence of a Mid- to Late-Holocene warm period.

From c. 1200 cal. yr BP (40 cm), the TOC flux decreases slightly more (Fig. 7), possibly indicating colder climatic conditions which could be linked to a Neoglacial cooling

(Fig. 8). However, a higher resolution of the samples is required here to verify this. This is similar to other East Antarctic regions, as in general colder and/or dryer conditions have been inferred from c. 2 ka BP onwards (Verleyen et al. 2011 in Appendix 2), for example in the Larsemann Hills (Hodgson et al. 2005), Amery Oasis (Wagner et al. 2004), Vestfold Hills (Fulford-Smith & Sikes 1996) and Windmill Islands (Cremer et al. 2003) (Fig. 1a).

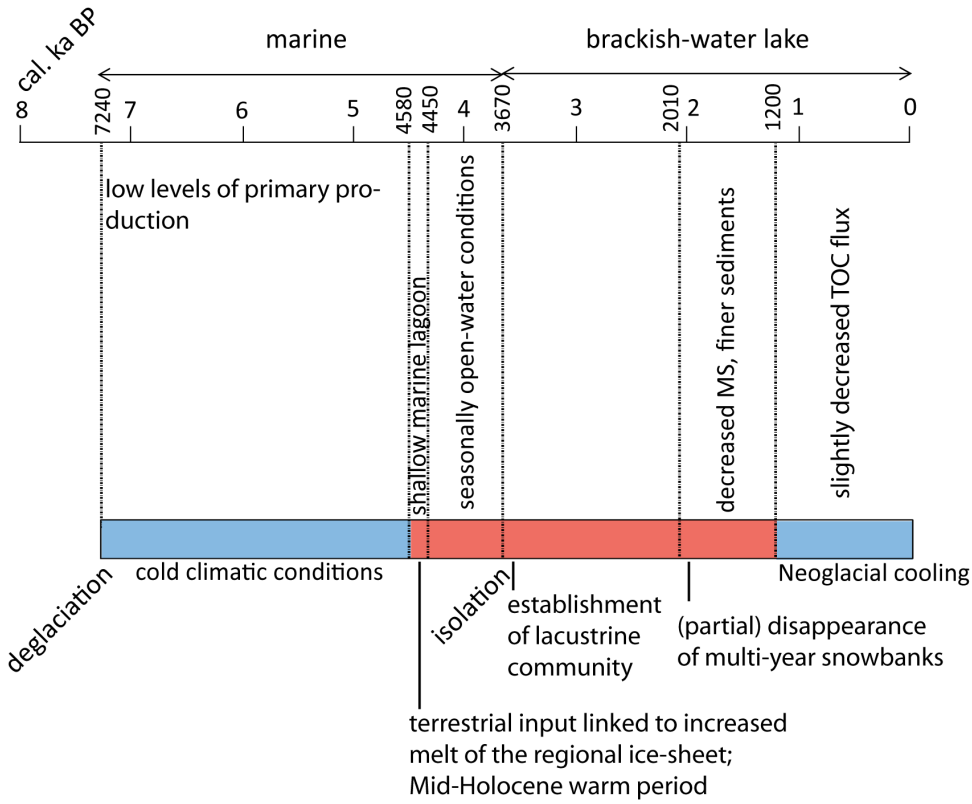

Figure 8. Overview figure of the inferred climatological and environmental changes in Skarvsnes and the Kobachi Ike site.

Conclusions

Multi-proxy analysis of the Kobachi Ike sediment cores revealed:

1. A local minimum age for deglaciation of 7240 cal. yr BP which confirms the exposure ages of nearby Mount Suribati (c. 8.66 - 6.42 ka BP) as assessed using cosmogenic isotope dating of erratics (Yamane et al. 2011).

2. A RSL maximum above 28.7 m a.s.l., which is 8.7 m higher than previous estimates based on raised beach deposits (Miura et al. 1998; Hirakawa & Sawagaki 1998).

3. The basin became isolated from the sea after between c. 4030 and 3670 cal. yr BP as revealed by the presence of cyanobacterial pigments, a decline in sea-ice diatoms and an increase in brackish water species. Brackish water conditions remained until the present-day.

4. Around c. 2010 cal. yr BP, a reduced meltwater influx could be inferred, which was possibly linked to the (partial) disappearance of multi-year snow banks in the catchment area, coincident with the Mid- to Late-Holocene warm period.

Acknowledgements

This research was funded by the Belspo project SD/CA/01 'Holocene climate variability and ecosystem change in coastal East and Maritime Antarctica' (HOLANT) and the British Antarctic Survey Chemistry and Past Climate programme. IT was funded by the Institute for the Promotion of Innovation by Science and Technology in Flanders (IWT).

References

Anderson JB, Shipp SS, Lowe AL, Wellner JS, Mosola AB (2002) The Antarctic Ice Sheet during the Last Glacial Maximum and its subsequent retreat history: a review. *Quaternary Science Reviews*, **21**: 49-70.

Armand LK, Crosta X, Romero O, Pichon J-J (2005) The biogeography of major diatom taxa in Southern Ocean sediments: 1. Sea ice related species. *Palaeogeography, Palaeoclimatology, Palaeoecology,* **223**: 93-126.

Bassett SE, Milne GA, Bentley MJ, Huybrechts P (2007) Modelling Antarctic sea-level data to explore the possibility of a dominant Antarctic contribution to meltwater pulse IA. *Quaternary Science Reviews,* **26**: 2113-2127.

Battarbee RW, and Kneen M (1982) The use of electronically counted microspheres in absolute diatom analysis. *Limnology and Oceanography,* **27**: 184-188.

Bennett KD (1996) Determination of the number of zones in a biostratigraphical sequence. *New Phytologist,* **132:** 155-170.

Berg S, Wagner B, Cremer H, Leng MJ, Melles M (2010) Late Quaternary environmental and climate history of Rauer Group, East Antarctica. *Palaeogeography, Palaeoclimatology, Palaeoecology,* **297**: 201-213.

Bird DF, and Karl (1992) Prasinophyte bloom in the northern Gerlach Strait. *Journal of Phycology,* **28(No. 3 suppl.)**: 16.

Blaauw M, and Christen JA (2011) Flexible paleoclimate age-depth models using an autoregressive gamma process. *Bayesian Analysis,* **6(3):** 457-474.

Blockley SPE, Blaauw M, Bronk Ramsey C, van der Plicht J (2007) Assessing uncertainties in age modelling sedimentary records in the Lateglacial and Early Holocene. *Quaternary Science Reviews,* **26:** 1915-1926.

Cremer H, Gore D, Melles M, Roberts D (2003) Palaeoclimatic significance of Late Quaternary diatom assemblages from Southern Windmill Islands, East Antarctica. *Palaeogeogr. Palaeoclimatol. Palaeoecol.,* **195**: 261–280.

Crosta X, Pichon J-J, Labracherie M (1997) Distribution of Chaetoceros resting spores in modern peri-Antarctic sediments. *Marine Micropaleontology*, **29**: 283 – 299.

Crosta X, Sturm A, Armand L, Pichon J-J (2004) Late Quaternary sea ice history in the Indian sector of the Southern Ocean as recorded by diatom assemblages. *Marine Micropaleontology,* **50**: 209-223.

Crosta X, Romero O, Armand LK, Pichon J-J (2005) The biogeography of major diatom taxa in Southern Ocean sediments: 2. Open ocean related species. *Palaeogeography, Palaeoclimatology, Palaeoecology,* **223**: 66-92.

Ferrario ME, Sar EA, Vernet M (1998) Chaetoceros resting spores in the Gerlache Strait, Antarctic Peninsula. *Polar Biology,* **19**: 286-288.

Fox AJ, and Cooper APR (1994) Measured properties of the Antarctic ice sheet derived from the SCAR Antarctic digital database. *Polar Rec.* **30**: 204.

Fukuda R, Ogawa H, Nagata T, Koike I (1998) Direct determination of carbon and nitrogen contents of natural bacterial assemblages in marine environments. *Applied and Environmental Microbiology*, **64(9)**: 3352-3358.

Fulford-Smith SP, and Sikes EL (1996) The evolution of Ace Lake, Antarctica, determined from sedimentary diatom assemblages. *Palaeogeography, Palaeoclimatology, Palaeoecology,* **124**: 73-86.

Gibson JAE, Paterson KS, White CA, Swadling KM (2009). Evidence for the continued existence of Abraxas Lake, Vestfold Hills, East Antarctica during the Last Glacial Maximum. *Antarctic Science*, **21**: 269-278.

Grimm EC (2004) TGView Version 2.0.2. Illinois State Museum, Springfield, Ilinois.

Hall BL (2009) Holocene glacial history of Antarctica and the sub-Antarctic islands. *Quaternary Science Reviews*, **28**: 2213-2230.

Hirakawa K, and Sawagaki T (1998) Radiocarbon dates of fossil shells from raised beach sediments along the Sôya Coast, East Antarctica - A report on a geomophological survey during JARE-35 (1993-94). *Antarctic Record,* **42**: 151-167.

Hodgson DA, Noon PE, Vyverman W, Bryant CL, Gore DB, Appleby P, Gilmour M, Verleyen E, Sabbe K, Jones VJ, Ellis-Evans JC, Wood PB (2001) Were the Larsemann Hills ice-free through the Last Glacial Maximum? *Antarctic Science*, **13(4):** 440-454.

Hodgson DA, Doran PT, Roberts D, McMinn A (2004) Paleolimnological studies from the Antarctic and Subantarctic islands. *In:* Pienitz R, Douglas MSV, Smol JP (Eds.) Long-term environmental change in Arctic and Antarctic lakes, pp. 419-474.

Hodgson DA, Verleyen E, Sabbe K, Squier AH, Keely BJ, Leng MJ, Saunders KM, Vyverman W (2005) Late Quaternary climate-driven environmental change in the Larsemann Hills, East Antarctica, multi-proxy evidence from a lake sediment core. *Quaternary Research*, **64**: 83-99.

Hodgson DA, Roberts SJ, Bentley MJ, Smith JA, Johnson JS, Verleyen E, Vyverman W, Hodson AJ, Leng MJ, Cziferszky A, Fox AJ, Sanderson DCW (2009a) Exploring former subglacial Hodgson Lake, Antarctica Paper I: site description, geomorphology and limnology. *Quaternary Science Reviews,* **28(23-24):** 2295-2309.

Hodgson DA, Roberts SJ, Bentley MJ, Carmichael EL, Smith JA, Verleyen E, Vyverman W, Geissler P, Leng MJ, Sanderson DCW (2009b) Exploring former subglacial Hodgson Lake, Antarctica Paper II: palaeolimnology. *Quaternary Science Reviews,* **28(23-24):** 2310-2325.

Igarashi A, Harada N, Moriwaki K (1995) Marine fossils of 30-40 ka in raised beach deposits, and late Pleistocene glacial history around Lutzow-Holm Bay, East Antarctica. *In:* Proceedings of the NIPR Symposium on Antarctic Geosciences, vol. 8, pp. 219–229.

Igarashi A, Numanami H, Tsuchiya Y, Fukuchi M (2001) Bathymetric distribution of fossil foraminifera within marine sediment cores from the eastern part of Lützow-Holm Bay, East Antarctica, and its paleoceanographic implications. *Marine Micropaleontology,* **42**: 125-162.

Ishikawa T, Tatsumi K, Kizaki K, Yanai H, Ando T, Kikuchi Y, Yoshida Y (1976) Explanatory text of geological map of Langhovde, Antarctica. *Ant. Geol. Map Ser. Sheet 5, Langhovde, Natl. Inst. Polar Res.* 12.

Jeffrey SW, Mantoura RFC, Bjornland T (1997) Data for the identification of 47 key phytoplankton pigments. *In*: Jeffrey SW, Mantoura RFC, Wright SW (Eds.) Phytoplankton pigments in oceanography, guidelines to modern methods. UNESCO Publishing, Paris, pp. 447-554.

Juggins S (2009) Rioja, analysis of Quaternary science data.
http://www.staff.ncl.ac.uk/staff/stephen.juggins/.

King P, Kennedy H, Newton PP, Jickells TD, Brand T, Calvert S, Cauwet G, Etcheber H, Head B, Khripounoff A, Manighetti B, Miquel JC (1998) Analysis of total and organic carbon and total nitrogen in settling oceanic particles and a marine sediment: an interlaboratory comparison. *Marine Chemistry,* **60**: 203-216.

Kimura S, Ban S, Imura S, Kudoh S, Matsuzaki M (2010) Limnological characteristics of vertical structures in the lakes of Syowa Oasis, East Antarctica. *Polar Science,* **3**: 262-271.

Krebs WN, Lipps JH, Burckle LH (1987) Ice diatom floras, Arthur Harbor, Antarctica. *Polar Biology,* **7**: 163-171.

Kulbe T, Melles M, Verkulich SR, Pushina ZV (2001) East Antarctic climate and environmental variability over the last 9400 years inferred from marine sediments of the Bunger Oasis. *Arct. Ant. Alp. Res.,* **33**: 223-230.

Laybourn-Parry J, and Pearce DA (2007) The biodiversity and ecology of Antarctic lakes: models for evolution. *Phil. Trans. R. Soc. B,* **362(1488)**: 2273-2289.

Lazerte BD (1983) Stable carbon isotope ratios: implications for the source of sediment carbon and for phytoplankton carbon assimilation in Lake Memphremagog, Quebec. *Canadian Journal of Fisheries and Aquatic Sciences*, **40**: 1658–1666.

Mackintosh AN, Verleyen E, O'Brien PE, White DA, Selwyn Jones R, McKay R, Bunbar R, Gore DB, Fink D, Post AL, Miura H, Leventer A, Goodwin I, Hodgson DA, Lilly K, Crosta X, Golledge NR, Wagner B, Berg S, van Ommen T, Zwartz D, Roberts SJ, Vyverman W, Masse G (2013) Retreat history of the East Antarctic Ice Sheet since the Last Glacial Maximum. *Quaternary Science Reviews*, 1-21.

Matsumoto GI, Komori K, Enomoto A, Imura S, Takemura T, Ohyama Y, Kanda H (2006) Environmental changes in Syowa Station area of Antarctica during the last 2300 years inferred from organic components in lake sediment cores. *Polar Biosci.,* **19:** 51-62.

Matsumoto GI, Tani Y, Seto K, Tazawa T, Yamamuro M, Watanabe T, Nakamura T, Takemura T, Imura S, Kanda H (2010) Holocene paleolimnological changes in Lake Skallen Oike in the Syowa Station area of Antarctica inferred from organic components in a sediment core (Sk4C-02). *J. Paleolimnol.,* **44:** 677-693.

Meyers PA (2003) Applications of organic geochemistry to paleolimnological reconstructions: a summary of examples from the Laurentian Great Lakes. *Organic Geochemistry,* **34:** 261-289.

McCormac F, Hogg A, Blackwell P, Buck C, Higham T, Reimer P (2004) Shcal04 Southern Hemisphere calibration 0-11.0 cal kyr BP. *Radiocarbon,* **46**: 1087-1092.

Miura H, Maemoku H, Igarashi A, Moriwaki K (1998) Late Quaternary raised beach deposits and radiocarbon dates of marine fossils around Lützow-Holm Bay. Explanatory text. *Special map series of National Institute of Polar Research,* **6**. pp. 46.

Mosola AB, and Anderson JB (2006) Expansion and rapid retreat of the West Antarctic Ice Sheet in eastern Ross Sea: possible consequence of over-extended ice streams? *Quaternary Science Reviews,* **25**: 2177-2196.

Ohtsuka T, Kudoh S, Imura S, Ohtani S (2006) Diatoms composing benthic microbial mats in freshwater lakes of Skarvsnes ice-free area, East Antarctica. *Polar Biosci.,* **20**: 113-130.

Perdue EM, Koprivnjak J-F (2007) Using the C/N ratio to estimate terrigenous inputs of organic matter to aquatic environments. *Estuarine, Coastal and Shelf Science,* **73:** 65-72.

Pienitz R, Doran PT, Lamoureux SF (2008) Origin and geomorphology of lakes in the polar regions. In: Vincent WF, and Laybourn-Parry J (Eds.) Polar lakes and rivers. Limnology of Arctic and Antarctic aquatic ecosystems, pp. 25-42.

Rankin LM, Gibson JAE, Franzmann PD, Burton HR (1999) The chemical stratification and microbial communities of Ace lake, Antarctica: a review of the characteristics of a marine-derived meromictic lake. *Polarforschung*, **66(1/2)**: 33-52.

Reimer PJ, Brown TA, Reimer RW (2004) Discussion: reporting and calibration of post-bomb 14C data. *Radiocarbon*, **46**: 1299-1304.

Reimer PJ, Baillie MGL, Bard E, Bayliss A, Beck JW, Bertrand CJH, Blackwell PG, Buck CE, Burr GS, Cutler KB, Damon PE, Edwards RL, Fairbanks RG, Friedrich M, Guilderson TP, Hogg AG, Hughen KA, Kromer B, McCormac G, Manning S, Ramsey CB, Reimer RW, Remmele S, Southon JR, Stuiver M, Talamo S, Taylor FW, Van Der Plicht J, Weyhenmeyer CE (2009) Intcal04 Terrestrial radiocarbon age calibration, 0-26 cal kyr BP. *Radiocarbon*, **46**: 1029-1058.

Renberg I (1990) A procedure for preparing large sets of diatom slides from sediment cores. *Journal of Paleolimnology,* **4**: 87-90.

Roberts D, and McMinn A (1998) A weighted-averaging regression and calibration model for inferring lakewater salinity from fossil diatom assemblages in saline lakes of the Vestfold Hills: a new tool for interpreting Holocene lake histories in Antarctica. *Journal of Paleolimnology,* **19**: 99-113.

Roberts EC, Laybourn-Parry J, McKnight DM, Novarino G (2000) Stratification and dynamics of microbial loop communities in Lake Fryxell, Antarctica. *Freshwater Biol.*, **44**: 649-661.

Roberts D, McMinn A, Cremer H, Gore DB, Melles M (2004) The Holocene evolution and palaeosalinity history of Beall Lake, Windmill Islands (East Antarctica) using an expanded diatom-based weighted averaging model. *Palaeogeography, Palaeoclimatology, Palaeoecology,* **208**: 121-140.

Ryves DB, Battarbee RW, Fritz SC (2009) The dilemma of disappearing diatoms: incorporating diatom dissolution data into palaeoenvironmental modelling and reconstruction. *Quaternary Science Reviews*, **28**: 120-136.

Sato K, and Hirasawa N (2007) Statistics of Antarctic surface meteorology based on hourly data in 1957-2007 at Syowa Station. *Polar Science,* **1**: 1-15.

Sawagaki T, and Hirakawa K (1997) Erosion of bedrock by subglacial meltwater, Soya Coast, East Antarctica. *Geografiska Annaler. Series A, Physical Geography,* **79(4)**: 223-238.

Scott FJ, and Thomas DP (2005) Diatoms. *In:* Antarctic marine protists. Scott FJ, and Marchant HJ (Eds.), ABRS, Canberra and AAD, Hobart, pp. 13-201.

Shipp S, Anderson JB, Domack EW (1999) Seismic signature of the Late Pleistocene fluctuation of the West Antarctic Ice Sheet system in Ross Sea: a new perspective, Part I. *Geological Society of America Bulletin*, **111**: 1486-1516.

Street-Perrot FA, Barker PA, Swain DL, Ficken KJ, Wooller MJ, Olago DO, Huang Y (2007) Late Quaternary changes in ecosystems and carbon cycling on Mt. Kenya, East Africa: a landscape-ecological perspective based on multi-proxy lake-sediment fluxes. *Quaternary Science Reviews*, **26**: 1838-1860.

Takada M, Tani A, Miura H, Moriwaki K, Nagatomo T (2003) ESR dating of fossil shells in the Lützow-Holm Bay region, East Antarctica. *Quaternary Science Reviews,* **22:** 1323-1328.

Tominaga H, and Fukui F (1981) Saline lakes at Syowa Oasis, Antarctica. *Hydrobiologia*, **82**: 375-389.

Van Heukelem L, and Thomas CS (2001) Computer-assisted high-performance liquid chromatography method development with applications to the isolation and analysis of phytoplankton pigments. *Journal of Chromatography A*, **910**: 31-49.

Verleyen E, Hodgson DA, Sabbe K, Vanhoutte K, Vyverman W (2004a) Coastal oceanographic conditions in the Prydz Bay region (East Antarctica) during the Holocene recorded in an isolation basin. *The Holocene,* **14(2):** 246-257.

Verleyen E, Hodgson DA, Sabbe K, Vyverman W (2004b) Late quaternary deglaciation and climate history of the Larsemann Hills (East Antarctica). *Journal of Quaternary Science,* **19(0):** 1-15.

Verleyen E, Hodgson DA, Milne GA, Sabbe K, Vyverman W (2005) Relative sea-level history from the Lambert Glacier region, East Antarctica, and its relation to deglaciation and Holocene glacier readvance. *Quaternary Research,* **63**: 45-52.

Verleyen E, Sabbe K, Hodgson DA, Grubisic S, Taton A, Cousin S, Wilmotte A, De Wever A, Van der Gucht K, Vyverman W (2010) Structuring effects of climate-related environmental factors on Antarctic microbial mat communities. *Aquatic Microbial Ecology*, **59**: 11-24.

Verleyen E, Hodgson DA, Gibson J, Imura S, Kaup E, Kudoh S, De Wever A, Hoshino T, McMinn A, Obbels D, Roberts D, Roberts SJ, Sabbe K, Souffreau C, Tavernier I, Van Nieuwenhuyze W, Van Ranst E, Vindevogel N, Vyverman W (2012) Chemical limnology in coastal East Antarctic lakes: monitoring future climate change in centres of endemism and biodiversity. *Antarctic Science,* **24(1)**: 23-33.

Verleyen E, Hodgson DA, Sabbe K, Cremer H, Emslie SD, Gibson J, Hall B, Imura S, Kudoh S, Marshall GJ, McMinn A, Melles M, Newman L, Roberts D, Roberts SJ, Singh SM, Sterken M, Tavernier I, Verkulich S, Van de Vyver E, Van Nieuwenhuyze W, Wagner B, Vyverman W (2011) Post-glacial regional climate variability along the East Antarctic coastal margin - evidence from shallow marine and coastal terrestrial records. *Earth Sci Rev,* **104**: 199-212.

Vincent ZF, MacIntyre S, Spigel RH, and Laurion I (2008) The physical limnology of high-latitude lakes. *In:* Vincent WF, Laybourn-Parry J (Eds.) Polar lakes and rivers. Limnology of Arctic and Antarctic aquatic ecosystems, pp. 65-81.

Wagner B, Cremer H, Hultsch N, Gore DB, Melles M (2004) Late Pleistocene and Holocene history of Lake Terrasovoje, Amery Oasis, East Antarctica, and its climatic and environmental implications. *J. Paleolimnol.,* **32**: 321-339.

Watcham EP, Bentley MJ, Hodgson DA, Roberts SJ, Fretwell PT, Lloyd JM, Larter RD, Whitehouse PL, Leng MJ, Monien P, Moreton SG (2011) A new Holocene relative sea-level curve for the South Shetland Islands, Antarctica. *Quaternary Science Reviews,* **30**: 3152-3170.

Wright HE (1967) A square-rod piston sampler for lake sediments. *J Sed Pet,* **37**: 975-976.

Yamane M, Yokoyama Y, Miura H, Maemoku H, Iwasaki S, Matsuzaki H (2011) The last deglacial history of Lützow-Holm Bay, East Antarctica. *Journal of Quaternary Science,* **26(1)**: 3-6.

Yoshida Y (1983) Physiography of the Prince Olav and the Prince Harald Coasts, East Antarctica. *Memoirs of the National Institute of Polar Research*, **13**: 1-76.

Yoshida Y, and Moriwaki K (1979) Some consideration on elevated coastal features and their dates around Syowa Station, Antarctica. *Memoirs of National Institute of Polar Research. Special Issue*, **13**: 220-226.

Zwartz D, Bird, M, Stone J, Lambeck K (1998) Holocene sea-level change and ice-sheet history in the Vestfold Hills, East Antarctica. *Earth and Planetary Science Letters,* **155**: 131-145.

Tables

Table 1. Conventional and calibrated radiocarbon dates, dated material, and the inferred dates using the age-depth model constructed with BACON (Blaauw & Christen 2011). Dates indicated with an asterisk were corrected for the marine reservoir effect.

Kobachi Ike Depth (cm)	Dated material	CRA (yr BP ± 1σ)	Publication code	pMC (%±1σ)	Carbon content (wt %)	$d^{13}C_{VPDB}$ (‰)	Cal. age using CALIB (yr BP)	Rel area under prob distr	Best fit according to the model (cal. yr BP)	2σ age range (cal. yr BP)
0	Laminated microbial-mat	modern	SUERC – 18336	109.62 ± 0.51	2	-25.8	-8 - -9 or -46	1		
57	Laminated microbial-mat	1875 ± 35	SUERC – 18051	79.18 ± 0.35	0.9	-25.4	1714-1813	1	1770	1890 - 1610
70	Laminated microbial-mat	2234 ± 35	SUERC – 18063	75.72 ± 0.33	0.6	-25.5	2123-2183	0.425	2160	2330 - 2010
							2199-2202	0.01		
							2235-2305	0.564		
80	Laminated microbial-mat	2410 ± 40	Beta – 261164	-	-	-24.4	2335-2370	0.461	2630	2710 - 2210
							2386-2458	0.539		
107	Laminated microbial-mat	3527 ± 38	SUERC – 18352	64.47 ± 0.3	0.2	-24.5	3691-3736	0.378	3620	3720 - 2700
							3740-3778	0.287		
							3788-3827	0.335		
115	Laminated microbial-mat	3490 ± 30	Beta – 326312	-	-	-23.4	3636-3723	0.867	3670	3810 - 2820
							3797-3816	0.133		
136*	Bulk matrix	3980 ± 30	Beta – 326313	-	-	-23.7	2824-3346	1	3780	4010 - 3050
157*	Bulk matrix	4176 ± 35	SUERC – 18353	59.46 ± 0.26	0.3	-23.6	3050-3597	1	3940	4210 - 3260
170*	Bulk matrix	4940 ± 30	Beta – 326314	-	-	-22.6	3995-4598	1	4060	4350 - 3440
184*	Bulk matrix	5282 ± 37	SUERC – 18354	51.81 ± 0.24	0.5	-22.2	4445-5037	1	4190	4530 - 3580
207*	Bulk matrix	5120 ± 40	Beta – 326315	-	-	-22.4	4274-4827	1	4330	4730 - 3760
231	Bulk matrix	3700 ± 30	Beta – 311995	-	-	-19.6	2450-3024	1	4450	4890 - 3930
233	Bulk matrix	3466 ± 36	SUERC – 18355	64.96 ± 0.29	0.9	-17.9	2209-2220	0.005	4460	4900 - 3940
							2225-2235	0.004		
							2240-2730	0.991		
233	Bulk matrix	3480 ± 30	Beta – 326316	-	-	-18.9	2246-2742	1		
240	Bulk matrix	insufficient CO_2							4490	4990 - 4010
245	Bulk matrix	4080 ± 30	Beta – 311996	-	-	-17.3	2924-3455	1	4580	5280 - 4160
260	Bulk matrix	5420 ± 40	Beta – 326317	-	-	-18.3	4682-5275	1	5700	6320 - 5110
274*	Bulk matrix	7650 ± 60	Beta – 261166	-	-	-	7335-7545	1	6510	7030 - 6310
279*	Bulk matrix	7219 ± 41	SUERC – 18356	40.71 ± 0.21	0.1	-21.5	6814-7314	1	6710	7210 - 6510

The most likely calibrated age of the bottom sediments: 7240 cal. yr BP

Supplementary material

Figure S1. Vertical profiles of Kobachi Ike of dissolved oxygen (DO; mg/l), temperature (°C), salinity (%) and pH as in Kimura et al. (2010), indicating a thermocline between 2 and 3 m depth.

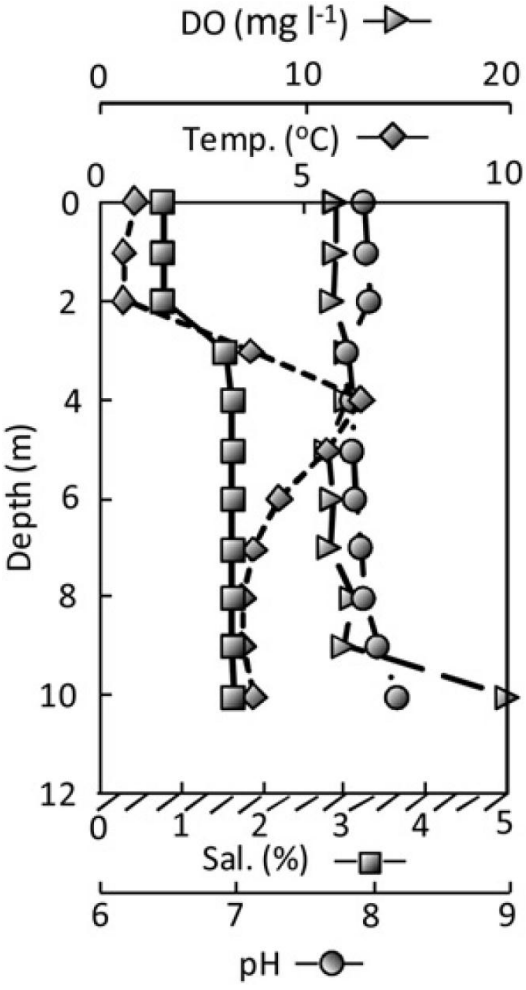

Figure S2. Enlarged lithology of the Kobachi Ike sediments, along with the accompanying legend.

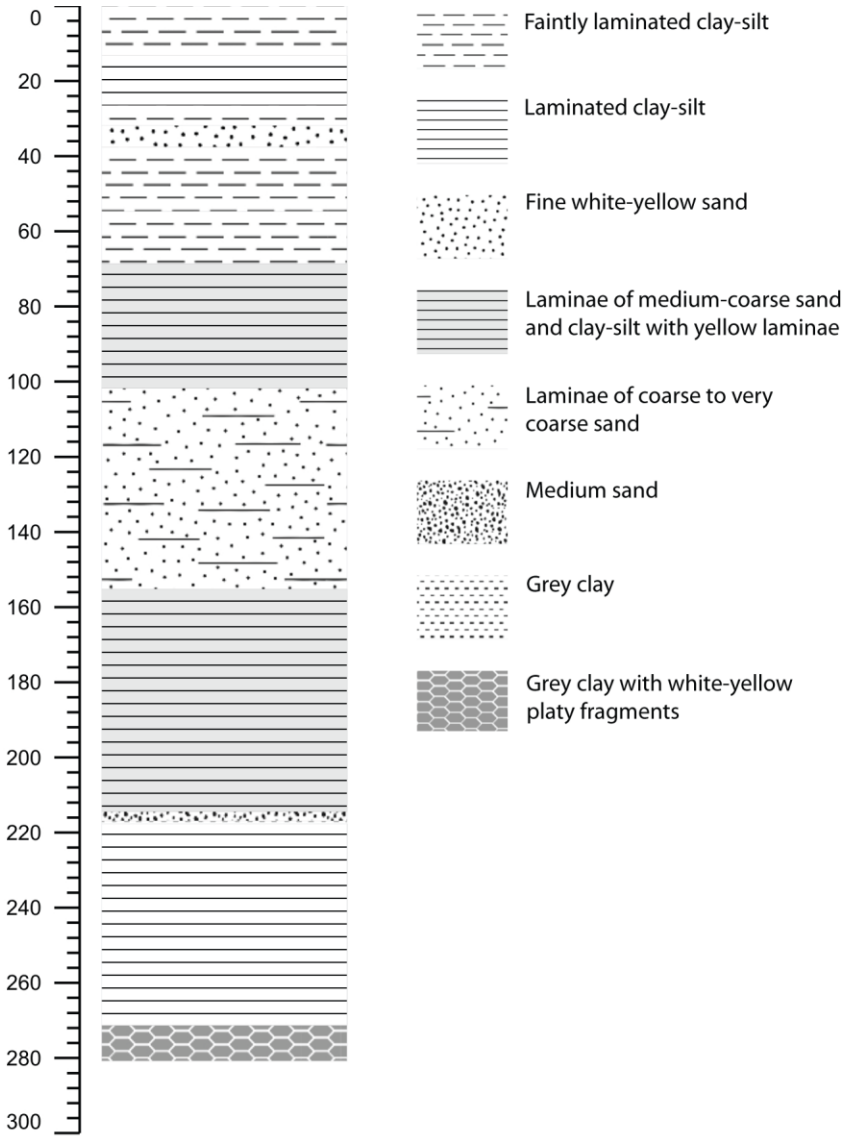

Figure S3. Diatom cluster analysis (CONISS) indicating the significant zones based on the broken-stick analysis.

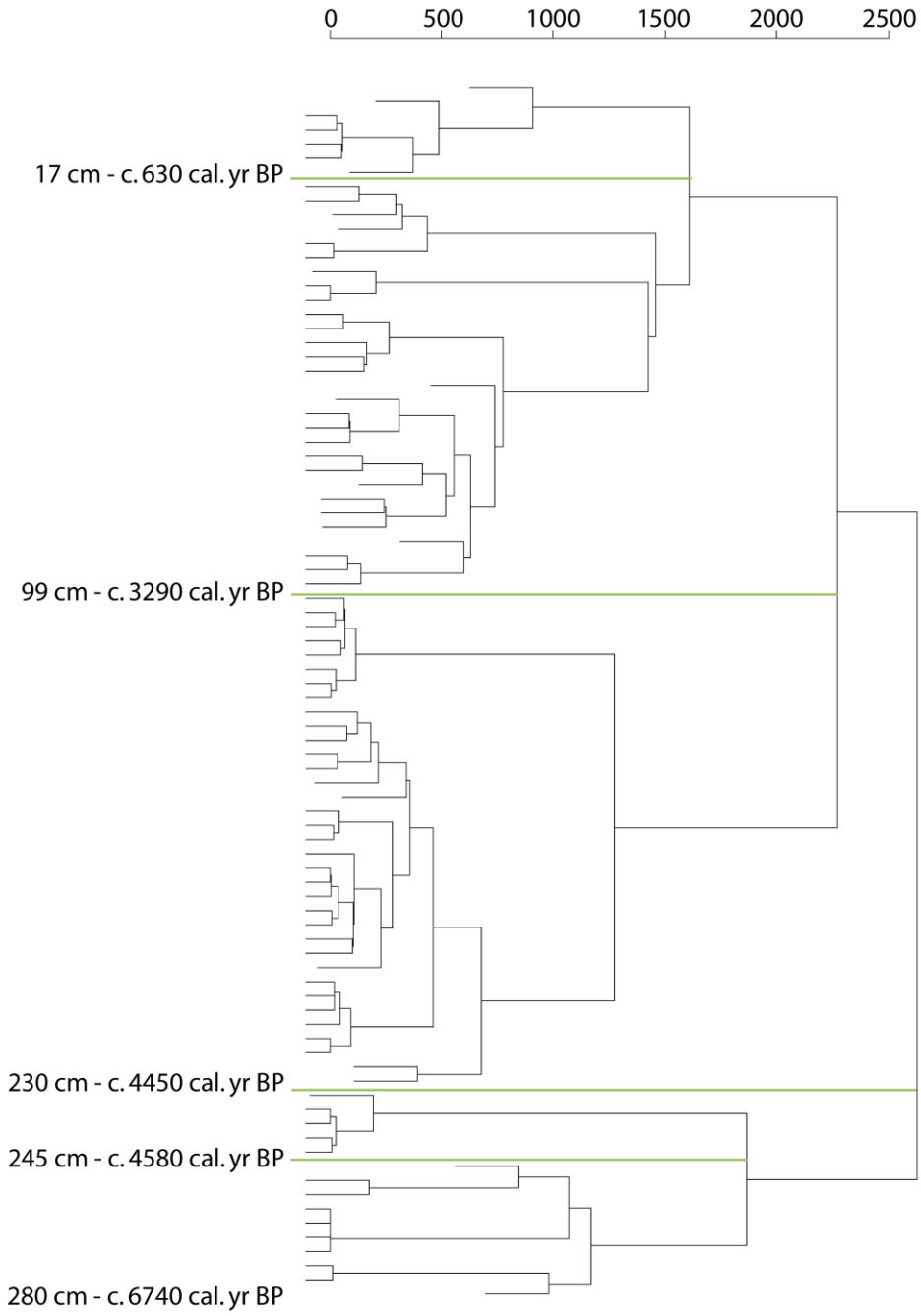

Figure S4. SEM (left) and LM (right) photograph of the unknown *Navicula* species retrieved from the Kobachi Ike sediments. Valves narrowly elliptical to lanceolate, with cuneate apices. Valve length 13.9-25.0 µm (n=6), width 4.4-6.0 µm (n=16). Raphe filiform and straight. Central raphe endings deflected in the same direction, central fissures hooked in the same direction. Terminal raphe endings deflected in the same direction, terminal fissures strongly hooked in the same direction. Axial area lanceolate, raphe sternum distinct in LM. Central area more or less round with a distinct central nodule, bordered by shortened striae. Striae 13-16 in 10 µm (n=6), radial to slightly parallel-convergent near the apices.

N. sp. 1 can mainly be distinguished from the sea-ice diatom *N. glaciei* in the shape of the central area, which is distinctly round in *N. sp.* 1, while it is rectangular in *N. glaciei*.

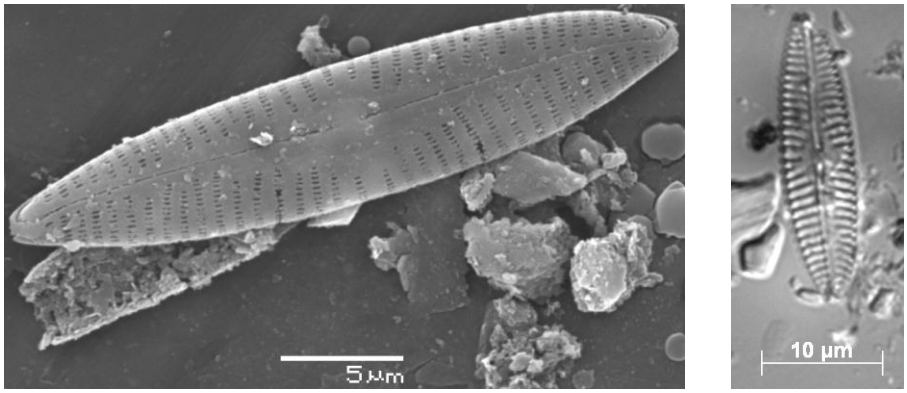

Figure S5. Pigment cluster analysis (CONISS) indicating the significant zones based on the broken-stick analysis.

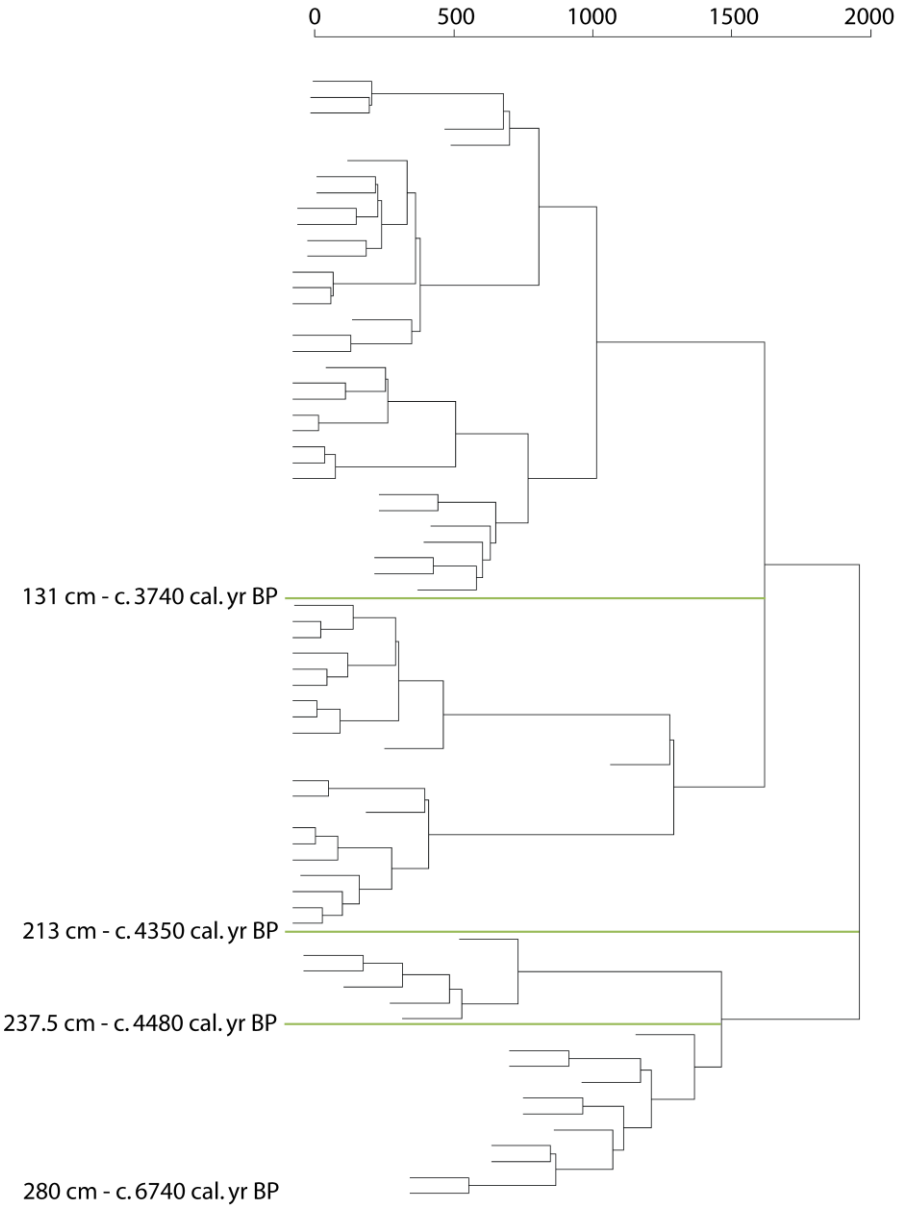

Figure S6. Water content (%) of the Kobachi Ike sediments.

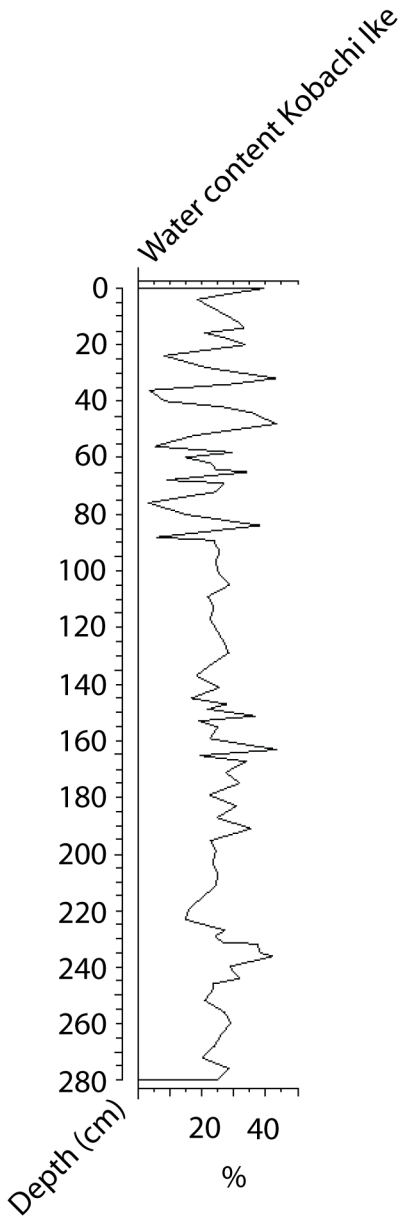

Chapter 6. Regional differences in Late-Holocene relative sea-level changes in the Lützow Holm Bay region, East Antarctica

Author's contributions: diatom analysis of the different lake sediment cores, geochemical analyses (TC, TN), construction of some of the age-depth models, writing parts of the manuscript.

Other contributors are listed alphabetically: Marc De Batist, Katrien Heirman, Dominic A. Hodgson, Hideki Imura, Satoshi Imura, Sakae Kudoh, Koen Sabbe, Elie Verleyen, Wim Vyverman

Note: not all contributors commented on this manuscript.

Key-words: Dronning Maud Land, Syowa Oasis, isostatic uplift, relative sea-level, isolation lake, Holocene, neotectonics

Abstract

Compared to the other continental ice masses, the East Antarctic Ice-Sheet (EAIS) has few field data to constrain its past volume and contribution to global sea-level changes since the Last Glacial Maximum. We developed a new relative sea-level (RSL) curve for Lützow Holm Bay by using marine to freshwater transitions in sediment cores from four isolation lakes and radiocarbondating of macrofossils in raised beaches. These data were combined with radiocarbon dating of the transitions from glaciogenic to organic-richer sediments in three glacial lakes to obtain the minimum age of deglaciation and the maximum sea-level high stand. Our results were integrated with published raised beach data and records from two isolation lakes. In West Ongul Island, the maximum marine limit was 17 m at 10,500 ^{14}C yr BP. RSL fall was relatively rapid (15 mm/yr) between c. 5000 cal. yr BP and 4800 cal. yr BP. The uplift rate equaled 2.1 mm/yr during the past c. 4800 cal. yr BP, which was similar to that in Skallen (2 mm/yr during the past 4690 ± 100 cal. yr BP). In Skarvsnes, the maximum marine limit was 32.7 m at 5410 ± 40 ^{14}C (5265 - 4653 cal. yr BP). RSL fall was very rapid (14.5 mm/yr) between c. 3670 and 1905 cal. yr BP. Between c. 1905 and 1500 cal. yr BP, RSL fall dropped to 2.1 mm/yr and from c. 1500 cal. yr BP onwards, it was c. 1 mm/yr. The RSL changes on West Ongul Island and Skallen are in agreement with previous findings from the region. By contrast, the RSL curve for Skarvsnes differs in shape and maximum marine limit from previous reconstructions and those from nearby regions and elsewhere in East Antarctica. These regional differences are likely related to neotectonic faulting, and complicate estimations of the contribution of this part of the EAIS to past sea-level changes.

Introduction

Estimates of the contribution of continental ice-sheets to recent and future global sea-level rise are still relatively imprecise (Bromwich & Nicolas 2010), partly as a result of very sparse near-field relative sea-level (RSL) records from Greenland and Antarctica (Whitehouse et al. 2012). Accurate RSL data are however needed to validate the numerical models, which are used for predicting changes in ice-sheet dynamics and their potential contribution to future global sea-level rise (Watcham et al. 2011). Moreover RSL

reconstructions, together with GPS-derived data, are needed to calculate regional differences in the rate of glacial isostatic adjustment (GIA) following deglaciation of the Last Glacial Maximum (LGM) ice-sheets (Chen et al. 2009). These GIA estimates are critical for correcting the satellite-derived measurements of changes (GRACE) in the height of the ice-sheets, which are used to monitor current regional variability in their mass balance (Wu et al. 2010). Potential biases related to extrapolation between sparse GIA measurements are subsequently aliased into mass balance calculations. This might for example be the case in East Antarctica (EA), where satellite-derived measurements suggest that some coastal parts of the East Antarctic Ice-Sheet (EAIS) started to melt very recently, whereas there was no detectable trend for the interior part (Rignot et al. 2011). This observation might point to (i) regional differences in mass balance and sensitivity to Holocene climate changes and/or (ii) inaccurate data on the regional differences in the rate of GIA. Therefore, increasing the spatial resolution of RSL reconstructions is a recognized research priority (Watcham et al. 2011).

RSL reconstructions are also a powerful tool to better constrain the past contribution of ice-sheets to the c. 125 ± 5 m global sea-level rise (Yokoyama et al. 2001) since the LGM (e.g. Bassett et al. 2007). Post-LGM changes in RSL of previously glaciated regions reflect principally three processes, namely eustatic sea-level rise, regional GIA, and neotectonic events (Stewart et al. 2000). The latter are generally assumed to be of minor importance, but in tectonically active regions appropriate corrections need to be applied because post-glacial faulting can significantly affect RSL changes (Watcham et al. 2011). For example, neotectonic processes along existing faults have been suggested to underlie regional variability in RSL in regions c. 90 km apart in Sweden (e.g. Risberg et al. 2005) and have had a pervasive influence on regional sea-level changes in the southern part of the Strait of Magellan and southernmost Tierra del Fuego (Bentley & McCulloch 2005). Therefore, if RSL changes are significantly influenced by neotectonic faulting, such records should be cautiously used to validate the numerical models aimed at predicting past and future ice-sheet dynamics (Watcham et al. 2011).

Of the global ice-sheets, the Antarctic ice-sheets have probably least RSL field data (Hall 2009), which resulted in a wide range of model-based estimates, varying between 35 m (Nakada & Lambeck 1988) and as low as 9 ± 1.5 m (Whitehouse et al. 2012). Given (i) the capacity of the EAIS to raise global sea-level by up to 50 m (Huybrechts et al. 2002) and (ii) indications that the melting of the EAIS likely contributed to the Eemian sea-level high stand, which was 6 to 10 m higher than today (Pingree et al. 2011), identifying those areas of the EAIS that respond to Holocene and recent climate changes is critical.

Traditionally, RSL reconstructions in Antarctica relied on radiocarbon dating of marine fossils in raised beaches as direct evidence of former sea-level changes (e.g. Berkman et al. 1998; Miura et al. 1998). This approach typically provides only minimum and maximum ^{14}C ages for sea-level high and low stands. Another approach is based on isolation lakes, which provide more precise constraints on RSL changes because of their distinct sills of which the height can be determined with more precision compared to fossils in raised beaches that might have been translocated at least by the magnitude of the tidal range, and because they circumvent problems associated with the marine

reservoir effect as lacustrine sediments can be dated which are in equilibrium with atmospheric CO_2 (Bentley et al. 2005; Verleyen et al. 2005). At the time of isolation, lake water salinity is relatively high. Brackish and saline lakes are known to have a less extensive ice cover during winter compared with freshwater lakes (Kimura et al. 2010) and seasonally ice-free conditions allow sufficient CO_2-exchange between the lake-water and the atmosphere. There is thus no reason to assume a lake reservoir effect. Isolation basins are natural depressions in the bedrock, which have been inundated by and subsequently isolated from the sea as a result of RSL fall (Verleyen et al. 2004). RSL curves are developed by studying markers of marine and lacustrine phases (e.g. diatoms and fossil pigments) in the sediments of these basins situated at different altitudes, and by subsequently dating the marine-lacustrine transitions (Zwartz et al. 1998). RSL curves based on isolation lakes have previously been developed for some islands near the Antarctic Peninsula (AP; Bentley et al. 2005; Hall 2010; Roberts et al. 2011; Watcham et al. 2011) and a few ice-free regions along the East Antarctic coastline, such as the Vestfold Hills (Zwartz et al. 1998), Windmill Islands (Goodwin & Zweck 2000), Rauer Islands (Berg et al. 2010; Hodgson et al. in prep.) and Larsemann Hills (Verleyen et al. 2005) (Fig. 1a). A recent comparison between existing ice-sheet models and geological data revealed that in the latter two regions the amount of ice present during the LGM was less than predicted by the models (Whitehouse et al. unpubl. res.). For other East Antarctic oases, such as the ice-free islands and peninsulas in Lützow Holm Bay (Fig. 1b), a similar approach revealed that ice-sheet volume was higher than predicted by the models (Bassett et al. 2007). However, the RSL curve used in the latter comparison was based on raised beach data alone and can be considered as less accurate.

Here, we present new RSL constraints for islands and peninsulas in the Lützow Holm Bay region based on two coastal lakes from Skarvsnes and five lakes from West Ongul Island situated at different elevations. We combined our data with recently published records from isolation basins from Skallen and Skarvsnes (Takano et al. 2012), as well as with raised beach data from Skallen, Skarvsnes, and West Ongul Island (Miura et al. 1998; Fig. 1b).

Site description

Lützow Holm Bay comprises several ice-free peninsulas and islands in the eastern part of Dronning Maud Land (Fig. 1a; Miura et al. 1998). Some of the larger East Antarctic glaciers, such as the Shirase Glacier, drain into the bay (Rignot et al. 2011). West Ongul Island is the largest ice-free island in Lützow Holm Bay (Fig. 1b) and separated from the Antarctic continent by a c. 600 m deep glacial trough, which is likely the result of ice scouring from the Langhovde and Hazuki Glaciers (Miura et al. 1998). West Ongul Island is furthermore separated from East Ongul Island by the Naka-no-seto Strait. Based on ^{14}C dates of *in situ* fossils of the marine bivalve *Laternula elliptica* and other marine macrofossils in raised beaches on the Ongul Islands, it was suggested that this part of the region was ice-free during the LGM and Marine Isotope Stage (MIS) 3 (Nakada et al. 2000), or even MIS 6-7 (Takada et al. 2003). The maximum Holocene marine limit for the region was estimated to be 17 m (10,500 ^{14}C yr BP). Several fault systems are present on the islands; one runs through Naka-no-Seta Strait.

Skarvsnes is one of the two largest peninsulas in Lützow Holm Bay (Fig. 1b) and situated in between glacial troughs in front of the Honnör and Telen Glaciers (Miura et al. 1998). All but one of the ^{14}C-dated fossils derived from raised marine deposits are of Holocene age (Miura et al. 1998), suggesting that the region was ice-covered during the LGM. This is confirmed by a recent cosmogenic isotope dating campaign which revealed that Skarvsnes emerged from an at least 350 m thick ice mass between 10 and 6 ka BP (Yamane et al. 2011). The maximum marine limit at 8440 ^{14}C yr BP was set at c. 20 m based on raised beach data. A fault system separates the eastern from the western part of the peninsula (Ishikawa et al. 1976), with our study lakes being situated on the eastern side of the fault.

Skallen is a smaller peninsula to the south-west of Skarvsnes nearby the Skallen and Telen Glaciers (Takano et al. 2012) (Fig. 1b). All the fossils sampled in raised beach deposits are of Holocene age. The minimum marine limit is 12 m and dated to be 4720 ^{14}C yr BP old. No geomorphological maps were available to assess the presence of faults.

For the location of the glaciers mentioned in the text, we refer to Fig. 5 in Chapter 1 (General Introduction).

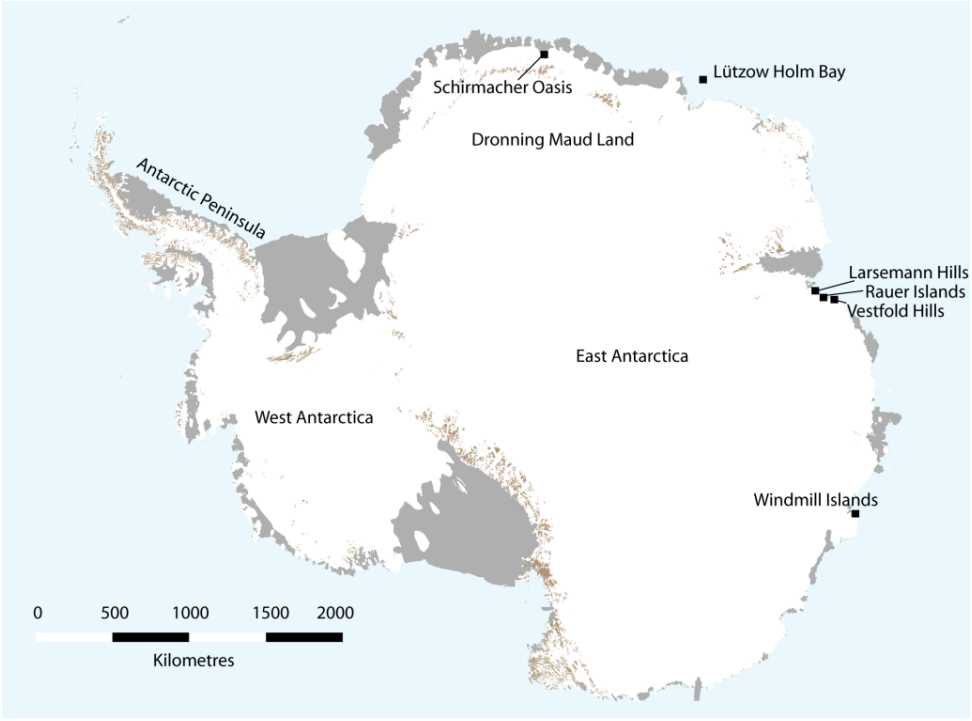

Fig. 1a. Overview map of Antarctica with indication of the regions mentioned in the text.

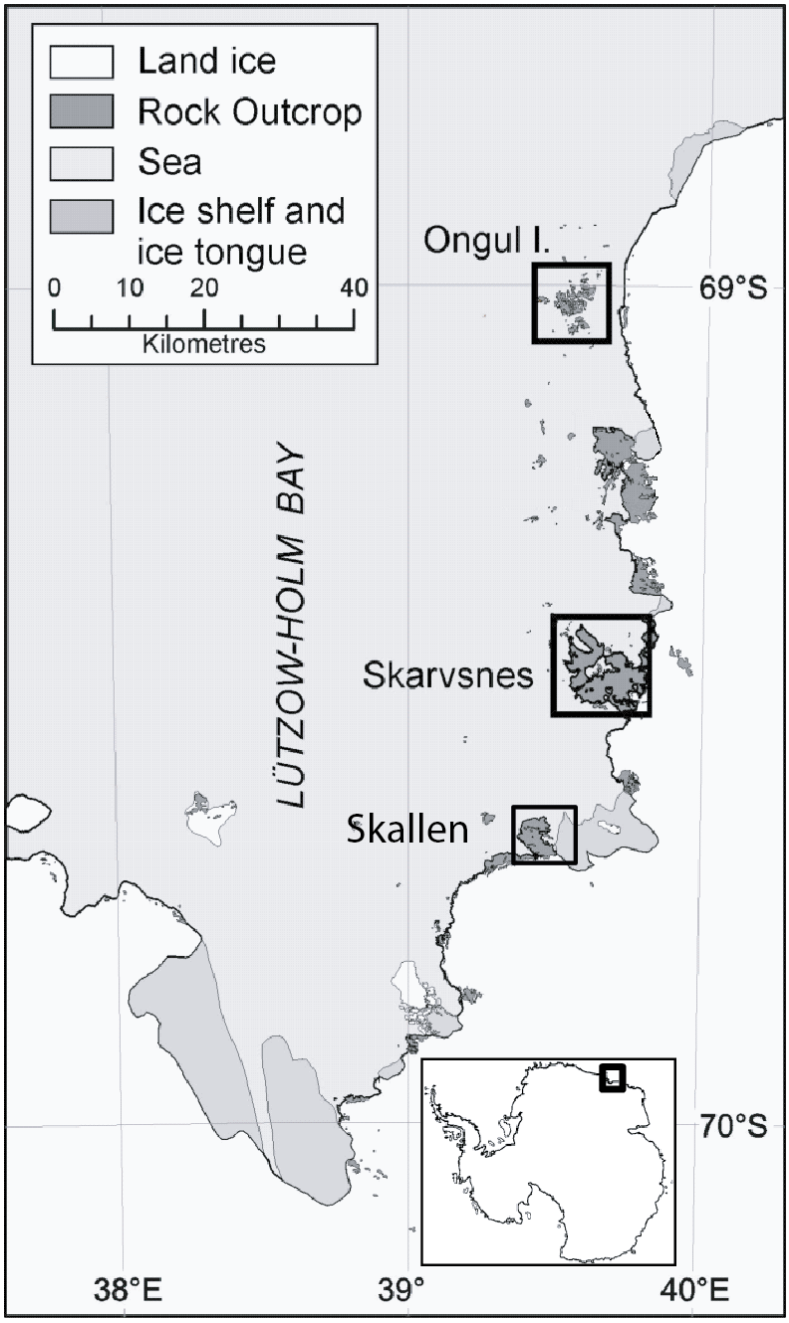

Fig. 1b. Map of the study sites in Lützow Holm Bay: the Ongul Islands, Skarvsnes and Skallen. Inset shows the location of Lützow Holm Bay.

Material and methods

Sill heights of the lakes, raised beach deposits and marine limits were surveyed using a Trimble 5700 base station GPS cross-referenced to the IGS station at Syowa (code SYOG). As a test of the vertical accuracy, Geodetic Station No 39-02 was resurveyed giving an ellipsoidal height error of ± 0.97 cm. Altitudes were referenced to vertical datum WGS84 with the EGM96 geoid separation ranging from 21.14 to 22.02 m (mean 21.62 m between the ellipsoidal height and the orthometric height). Where data could not be referenced to the IGS station, spot heights of the sills of the lakes were used from previous mapping surveys (http://polaris.nipr.ac.jp/~penguin/Terrestrial/regal/DataBase/index.htm).

Sediment cores were extracted from five lakes on West Ongul Island [Yumi Ike (WO1), Ô-Ike (WO4), Ura Ike (WO5), Higashi Ike (WO6), and Nishi Ike (WO8)] and two lakes on Skarvsnes [(Mago Ike (SK1) and Kobachi Ike (SK4)] using a UWITEC gravity corer for surface sediments and a square-rod piston sampler (Wright 1967) for intermediate to basal sediments. The bedrock of the lakes has most likely been reached during coring in all cases. Three marine macrofossils were sampled in raised beaches at different altitudes in Skarvsnes. Lake sediment samples and marine macrofossils were dated using AMS ^{14}C by the UK Natural Environment Research Council Radiocarbon Laboratory (NERC) and/or by the Beta Analytic Radiocarbon Dating Laboratory (Table 1). Where possible, discrete macrofossils were dated (cyanobacterial mats, worm tubes, sponge spicules or shells). The results are reported as conventional radiocarbon years BP with one-sigma (1σ) standard deviation error. The raised beach data were calibrated using the Marine09.14C calibration curve in CALIB (Reimer et al. 2009; Table S1 in the Supplementary Material). Dates from the sediment cores were calibrated using the SHCal04.14C calibration curve for freshwater deposits (McCormac et al. 2004; Reimer et al. 2004), and the Marine09.14C calibration curve for marine sediments. As the SHCal04.14C curve only extends to 11 cal. ka BP, the age-depth model of Nishi Ike was run with the Northern Hemisphere (NH) curve, IntCal09.14C (Reimer et al. 2009) glued at the bottom of SHCal04.14C, applying an appropriate Southern Hemisphere (SH) offset (Blaauw 2010). The AMS ^{14}C dates of the marine sediments and marine fossils in the raised beaches were corrected for the marine reservoir effect following Yoshida & Moriwaki (1979). An error of ± 100 years for the reservoir effect has been calculated based on the Yoshida & Moriwaki (1979) dates. No reservoir correction was applied to dates from lacustrine sediments, because surface-sediment dates indicate that ^{14}C in the modern lakes is in near-equilibrium with modern atmospheric CO_2 (Table 1). Age-depth modelling was undertaken using OXCAL v. 4.1 (Bronk Ramsey 2009) and the CLAM v. 2.1 software in R (Blaauw 2010). For Kobachi Ike, an age-depth model was constructed using the Bayesian software BACON (Blaauw & Christen 2011). For all models, 10,000 iterations weighted by calibrated probabilities at 95% confidence ranges were performed. All ages are rounded to the nearest 10 years. We combined our raised beach data with the data obtained from the isolation lakes and raised beach data from Miura et al. (1998).

Table 1. Conventional and calibrated radiocarbon dates of lakes Yumi Ike, Ô-Ike, Mago Ike, Kobachi Ike, Ura Ike, Higashi Ike, and Nishi Ike, along with the publication codes, dated material, and the inferred dates using the age-depth models constructed with Oxcal v. 4.1 (Bronk Ramsey 2009) and CLAM v. 2.1 (Blaauw 2010). The age-depth model for Kobachi Ike has been constructed using BACON (Blaauw & Christen 2011). Dates indicated with an asterisk were corrected for the marine reservoir effect (1120 years; Yoshida & Moriwaki 1979). CRA=Conventional Radiocarbon Age. The bottom table from Kobachi Ike reports conventional and calibrated dates from macrofossils from the vicinity of Kobachi Ike, not used in the age-depth model. For more information regarding the Mago Ike radiocarbon table, we refer to Chapter 3 (Tavernier et al. in press).

Yumi Ike depth (cm)	Dated material	Publication code	^{14}C enrichment (% modern ± 1σ)	Carbon content (% by wt.)	$\delta^{13}C_{VPDB}$ ‰ ± 0.1	CRA (yr BP ± 1σ)	Cal. using CALIB (yr BP)	Rel. area under probability distribution	Best fit according to the model (cal. yr BP)	2σ age range (cal. yr BP)
0	microbial mat	SUERC - 18338	102.85 ± 0.47	8.4	-14.6	modern			-60	-50 - -60
14	microbial mat	Beta - 322266	-	-	-16.2	1730 ± 30	1533-1612	1	1560	1660 - 1380
28	microbial mat	Beta - 322267	-	-	-8.3	2660 ± 30	2723-2758	1	2760	2860 - 2660
39	microbial mat	SUERC - 18056	61.00 ± 0.27	0.7	-21.6	3970 ± 35	4294-4334	0.336	4300	4390 - 4130
							4337-4419	0.664		
52	microbial mat	Beta - 322268	-	-	-21.7	4460 ± 30	4879-4939	0.428	4970	5070 - 4890
							4955-4985	0.223		
							4993-5039	0.349		
73*	bulk matrix	SUERC - 18066	48.02 ± 0.23	0.1	-18.5	5893 ± 38	5416-5654	1	5270	5550 - 5040

The most likely calibrated age of the oldest radiocarbon date (5893 ± 38), used as bottom age of the sediments: 5560 cal. yr BP

Ô-lke depth (cm)	Dated material	Publication code	^{14}C enrichment (% modern ± 1σ)	Carbon content (% by wt.)	$\delta^{13}C_{VPDB}$ ‰ ± 0.1	CRA (yr BP ± 1σ)	Cal. using CALIB (yr BP)	Rel. area under probability distribution	Best fit according to the model (cal. yr BP)	2σ age range (cal. yr BP)
0	microbial mat	SUERC - 18342	98.16 ± 0.43	8.9	-14.2	149 ± 35	0-32	0.228	70	230 - -30
							57-122	0.477		
							133-144	0.071		
							224-255	0.224		
1	microbial mat	Beta - 279333	102.0 ± 0.5	-	-12.5	40 ± 40	0-0	0.324	100	250 - 0
							29-58	0.443		
							121-135	0.225		
							234-236	0.008		
26	microbial mat	Beta - 279334	-	-	-12.8	880 ± 40	688-702	0.141	700	750 - 590
							719-774	0.812		
							782-787	0.047		
51	microbial mat	Beta - 279335	-	-	-21.2	1080 ± 40	911-973	1	990	1150 - 930
89	microbial mat	Beta - 261170	-	-		2130 ± 40	1992-2072	0.705	2000	2090 - 1830
							2076-2114	0.295		
92	microbial mat	Beta - 261171	-	-		1130 ± 40	935-945	0.105	outlier	outlier
							953-1002	0.633		
							1031-1051	0.263		
104	microbial mat	Beta - 261172	-	-	-15.1	4570 ± 40	5056-5187	0.728	outlier	outlier
							5214-5223	0.048		
							5236-5243	0.036		
							5261-5296	0.188		
132	microbial mat	Beta - 322269	-	-	-13.1	2790 ± 30	2783-2856	1	2730	2830 - 2490
155*	bulk matrix	SUERC - 18067	56.52 ± 0.25	1.5	-23.2	4583 ± 36	3680-3966	1	3980	4390 - 3670
157*	bulk matrix	SUERC - 18068	54.63 ± 0.26	0.9	-23.6	4856 ± 38	4066-4367	1	4220	4640 - 3810
168*	bulk matrix	Beta - 261174				7240 ± 50	6893-7158	1	5910	6360 - 4630
171	bulk matrix					insufficient CO_2				

The most likely calibrated age of the oldest radiocarbon date (7240 ± 50), used as bottom age of the sediments: 7010 cal. yr BP

Mago Ike Lab. ID	Strat. Depth (cm)	Unit	T/M	Material dated	Carbon content (wt %)	$d^{13}C_{VPDB}$ (‰)	pMC (%±1s)	CRA (^{14}C yr BP ± 1s)	Models 1 (normal font) & 2 (italics) OXCAL 95.4% calibration data (cal yr BP; yr AD where stated)			Model 3 OXCAL 95.4% calibration data (cal yr BP)			
									from - to	Mean±1s	Median	Max-Min	Mean±1s	Median	Calibration curve
SUERC-18335	0.5	3	T	Medium laminated microbial mat	17.5	-17.3	106.4 ± 0.5	-	>2004 or	>2004 or	>2004 or	>-54 or	>-54 or	>-54 or	A
				Medium laminated microbial mat				-	1957 - 1958	1958 ± 1	1958	-7 - -8	-8 ± 1	-7	x - SEQ
BETA-306507	3.5	3	T	Medium laminated microbial mat	-	-16.2	110.2 ± 0.4	-	1958 - 2000	1996 ± 9	1998 AD	-8 - -50	-46 ± 9	-48	A
BETA-322263	5.5	3	T	Medium laminated microbial mat	-	-15.9	110.7 ± 0.3	-	1958 - 1999	1994 ± 10	1997 AD	-8 - -49	-44 ± 10	-47	A
BETA-261160	7	3	T	Medium laminated microbial mat	-	-17.9	96.1 ± 0.6	320 ± 50	490 - 150	360 ± 75	375	490 - 150	360 ± 75	375	x - RW
BETA-322264	9.5	3	T	Medium laminated microbial mat	-	-15.1	114.2 ± 0.3	-	1959 - 1994	1987 ± 12	1992 AD	-9 - -44	-37 ± 12	-42	A
BETA-322265	13.5	3	T	Medium laminated microbial mat	-	-15.5	107.4 ± 0.3	-	1957 - 1958	1959 ± 8	1958 AD	-7 - -8	-9 ± 8	-8	A
BETA-306508	30	3	T	Fine-medium laminated mat transition	-	-14.6	97.2 ± 0.4	230 ± 30	310 - -5	205 ± 60	195	310 - -5	205 ± 60	195	B
SUERC-19466	56	3	T	Finely laminated microbial mat	4.1	-16.7	94.7 ± 0.4	413 ± 37	505 - 320	420 ± 55	440	505 - 320	420 ± 55	440	B
BETA-306509	77.5	3	T	Thickly laminated microbial mat	-	-14.0	94.6 ± 0.4	450 ± 30	520 - 330	460 ± 50	480	520 - 330	460 ± 50	480	B
BETA-306510	91.5	3	T	Medium laminated microbial mat	-	-15.8	94.4 ± 0.4	460 ± 30	525 - 335	475 ± 45	490	525 - 335	475 ± 45	490	B
SUERC-19467	111.4	2	T	Finely laminated microbial mat	10.0	-14.5	90.7 ± 0.4	788 ± 37	740 - 570	685 ± 30	685	740 - 570	685 ± 30	685	B
SUERC-19468	113.4	2	T	Grey clay with fine sand, some organic	3.0	-14.5*	89.2 ± 0.4	919 ± 37	910 - 690	795 ± 55	780	910 - 690	795 ± 55	780	B
BETA-261161	122.1	2	T	Grey clay with fine sand	-	-*	85.0 ± 0.4	1300 ± 40	1275 - 1065	1175 ± 60	1180	1275 - 1065	1175 ± 60	1180	B
SUERC-18048	168	1	M	Bulk grey clay with fine sand	0.7	-17.5	70.7 ± 0.3	2785 ± 35	1880 - 1380	1640 ± 125	1640	1570 - 1050	1320 ± 130	1320	C
SUERC-18049	201	1	M	Bulk grey clay with fine sand	0.5	-16.2	68.9 ± 0.3	2993 ± 37	2145 - 1605	1885 ± 135	1885	1810 - 1290	1540 ± 130	1540	C
SUERC-18050	227_{bulk}	1	M	Sandy-silt bulk matrix - no macros	0.5	-17.3	67.1 ± 0.3	3208 ± 35	2380 - 1865	2140 ± 130	2145	2070 - 1490	1770 ± 140	1770	C
SUERC-18348	227_{macro}	1	M	Sponge spicules	12.1	-0.3	69.7 ± 0.3	2902 ± 35	2035 - 1515	1770 ± 130	1775				C
	227_{bulk}/227_{macro}			*R_combine (Model run 2)*					*2250 - 1710*	*1965 ± 130*	*1965*				C
SUERC-18062	253_{bulk}	1	M	Sandy-clay bulk matrix - no macros	0.5	-17.2	66.5 ± 0.3	3274 ± 37	2510 - 1925	2220 ± 140	2220	2130 - 1590	1860 ± 130	1860	C
SUERC-18349	253_{macro}	1	M	Carbonate shells	11.5	-0.1	69.1 ± 0.3	2974 ± 35	2125 - 1590	1860 ± 135	1860				C
	253_{bulk}/253_{macro}			*R_combine (Model run 2)*					*2310 - 1800*	*2040 ± 130*	*2040*				C

The most likely calibrated age of the oldest radiocarbon date, used as bottom age of the sediments: 2120 cal. yr BP

Kobachi Ike Depth (cm)	Dated material	CRA (yr BP ± 1σ)	Publication code	pMC (%±1σ)	Carbon content (wt %)	$d^{13}C_{VPDB}$ (‰)	Cal. age using CALIB (yr BP)	Rel area under prob distr	Best fit according to the model (cal. yr BP)	2σ age range (cal. yr BP)
0	Laminated microbial mat	modern	SUERC – 18336	109.62 ± 0.51	2	-25.8	-8 - -9 or -46	1		
57	Laminated microbial mat	1875 ± 35	SUERC – 18051	79.18 ± 0.35	0.9	-25.4	1714-1813	1	1770	1890 - 1610
70	Laminated microbial mat	2234 ± 35	SUERC – 18063	75.72 ± 0.33	0.6	-25.5	2123-2183	0.425	2160	2330 - 2010
							2199-2202	0.01		
							2235-2305	0.564		
80	Laminated microbial mat	2410 ± 40	Beta – 261164	-	-	-24.4	2335-2370	0.461	2630	2710 - 2210
							2386-2458	0.539		
107	Laminated microbial mat	3527 ± 38	SUERC – 18352	64.47 ± 0.3	0.2	-24.5	3691-3736	0.378	3620	3720 - 2700
							3740-3778	0.287		
							3788-3827	0.335		
115	Laminated microbial mat	3490 ± 30	Beta – 326312	-	-	-23.4	3636-3723	0.867	3670	3810 - 2820
							3797-3816	0.133		
136*	Bulk matrix	3980 ± 30	Beta – 326313	-	-	-23.7	2824-3346	1	3780	4010 - 3050
157*	Bulk matrix	4176 ± 35	SUERC – 18353	59.46 ± 0.26	0.3	-23.6	3050-3597	1	3940	4210 - 3260
170*	Bulk matrix	4940 ± 30	Beta – 326314	-	-	-22.6	3995-4598	1	4060	4350 - 3440
184*	Bulk matrix	5282 ± 37	SUERC – 18354	51.81 ± 0.24	0.5	-22.2	4445-5037	1	4190	4530 - 3580
207*	Bulk matrix	5120 ± 40	Beta – 326315	-	-	-22.4	4274-4827	1	4330	4730 - 3760
231	Bulk matrix	3700 ± 30	Beta – 311995	-	-	-19.6	2450-3024	1	4450	4890 - 3930
233	Bulk matrix	3466 ± 36	SUERC – 18355	64.96 ± 0.29	0.9	-17.9	2209-2220	0.005	4460	4900 - 3940
							2225-2235	0.004		
							2240-2730	0.991		
233	Bulk matrix	3480 ± 30	Beta – 326316	-	-	-18.9	2246-2742	1		
240	Bulk matrix	insufficient CO_2							4490	4990 - 4010
245	Bulk matrix	4080 ± 30	Beta – 311996	-	-	-17.3	2924-3455	1	4580	5280 - 4160
260	Bulk matrix	5420 ± 40	Beta – 326317	-	-	-18.3	4682-5275	1	5700	6320 - 5110
274*	Bulk matrix	7650 ± 60	Beta – 261166	-	-	-	7335-7545	1	6510	7030 - 6310
279*	Bulk matrix	7219 ± 41	SUERC – 18356	40.71 ± 0.21	0.1	-21.5	6814-7314	1	6710	7210 - 6510

Sample name	Dated material	CRA (yr BP ± 1σ)	Publication code	pMC (%±1σ)	Carbon content (wt %)	$d^{13}C_{VPDB}$ (‰)	Cal. age using CALIB (yr BP)	Rel area under prob distr	Height (m)	Location
SK4MLLAT	carbonate shell	4730 ± 40	Beta-261167	-	-	0.2	4340 - 3726	1	8.6	69°28′54.9″S - 39°38′58.6″E
SK4ML POLY	polychaete worm tube	6800 ± 40	Beta-261167	-	-	0.2	6743 - 6278	1	8.6	69°28′54.9″S - 39°38′58.6″E
SK3ML	carbonate shell	5410 ± 40	Beta-261169	-	-	-0.8	5265 - 4653	1	32.7	69°28′57.4″S - 39°38′29.8″E

The most likely calibrated age of the bottom sediments: 7240 cal. yr BP

Ura Ike depth (cm)	Dated material	Publication code	^{14}C enrichment (% modern ± 1σ)	Carbon content (% by wt.)	$\delta^{13}C_{VPDB}$ ‰ ± 0.1	CRA (yr BP ± 1σ)	Cal. using CALIB (yr BP)	Rel. area under probability distribution	Best fit according to the model (cal. yr BP)	2σ age range (cal. yr BP)
0	microbial-mat	SUERC - 18343	96.56 ± 0.45	9,5	-28,4	281 ± 37	154-171	0,159		
							179-189	0,062		
							192-206	0,093		
							278-324	0,646		
							416-424	0,039		
37	microbial-mat	Beta - 327121	-	-	-29,9	4340 ± 30	4831-4867	1		
37	microbial-mat	Beta - 326318	-	-	-30,6	4500 ± 30	4970-5065	0,571		
							5111-5121	0,039		
							5184-5217	0,182		
							5221-5271	0,209		
40	microbial-mat	SUERC - 18070	53.07 ± 0.25	1,6	-31,1	5090 ± 38	5721-5769	0,337		
							5786-5792	0,026		
							5805-5891	0,637		
50	microbial-mat	SUERC - 18069	50.42 ± 0.24	1,2	-30	5500 ± 38	6209-6251	0,596		
							6262-6292	0,404		
51	microbial-mat	SUERC - 18058	50.25 ± 0.23	0,8	-30,7	5528 ± 37	6213-6243	0,403		
							6269-6306	0,597		

The most likely calibrated age of the oldest radiocarbon date taken (5528 ± 37): 6290 cal. yr BP

Higashi Ike depth (cm)	Dated material	Publication code	^{14}C enrichment (% modern ± 1σ)	Carbon content (% by wt.)	$\delta^{13}C_{VPDB}$ ‰ ± 0.1	CRA (yr BP ± 1σ)	Cal. using CALIB (yr BP)	Rel. area under probability distribution	Best fit according to the model (cal. yr BP)	2σ age range (cal. yr BP)
0	microbial mat	SUERC - 18344	105.88 ± 0.49	5.3	-13.9	modern				
51	microbial mat	Beta - 326319	-		-15.3	4130 ± 30	4448-4467	0.123		
							4517-4616	0.746		
							4765-4784	0.13		
64	microbial mat					insufficient CO_2				

The most likely calibrated age of the oldest radiocarbon date (4130 ± 30), used as bottom age of the sediments: 4520 or 4560 cal. yr BP

Nishi Ike depth (cm)	Dated material	Publication code	^{14}C enrichment (% modern ± 1σ)	Carbon content (% by wt.)	$\delta^{13}C_{VPDB}$ ‰ ± 0.1	CRA (yr BP ± 1σ)	Cal. using CALIB (yr BP)	Rel. area under probability distribution	Best fit according to the model (cal. yr BP)	2σ age range (cal. yr BP)
0	microbial mat	SUERC - 18345	106.16 ± 0.49	12.4	-13.7	modern			-60	- 50 - -60
10	microbial mat	Beta - 322270	-	-	-11	1200 ± 30	978-1039	0.661	1050	1170 - 970
							1043-1077	0.339		
18	microbial mat	Beta - 322271	-	-	-12.8	1920 ± 30	1737-1762	0.23	1800	1880 - 1720
							1772-1830	0.574		
							1844-1864	0.195		
40	microbial mat	Beta - 322272	-	-	-16.2	3900 ± 30	4156-4207	0.328	4170	4270 - 4080
							4221-4297	0.533		
							4330-4351	0.109		
							4373-4380	0.029		
40	microbial mat	Beta - 327120	-	-		3790 ± 30	3994-4039	0.384	4170	4270 - 4080
							4076-4103	0.243		
							4107-4149	0.373		
55	microbial mat	SUERC - 18071	36.85 ± 0.18	0.2	-21.2	8019 ± 40	8728-8736	0.029	8830	8990 - 8650
							8755-8813	0.261		
							8824-8873	0.233		
							8876-8979	0.478		
60	microbial mat	Beta - 322273	-	-	-23.4	9870 ± 60	11213-11324	1	11330	11390 - 11120
71	microbial mat					insufficient CO_2				

The most likely calibrated age of the oldest radiocarbon date (9870 ± 60), used as bottom age of the sediments: 11240 cal. yr BP

To identify marine to freshwater transitions, multiple biological and sedimentological proxies were analysed. Gamma ray density (GRD) and volume-specific magnetic susceptibility (MS) were analysed using a Bartington 1 ml MS2G sensor for those cores which were transported unsliced. GRD was converted to dry bulk density (DBD) using a dry weight percentage of the samples. To obtain this, a weighted sample was dried for 48h at a temperature of 60°C in an oven and subsequently re-weighted. The percentage dry weight was calculated as the ratio between the weight of the dried sample to that of the wet sample. Volume-specific MS was converted to mass-specific MS by dividing it by the DBD. The total carbon (TC), and total organic carbon (TOC) concentrations were analysed using a Flash 2000 Organic Elemental Analyzer. Measurements were carried out by dry combustion at high temperature (left furnace: 950°C and right furnace: 840°C; King et al. 1998). This was then followed by separation and detection of the gaseous products. The data were processed using the Eager Xperience software. Samples were all run at least twice to detect and exclude possible erroneous values. Outliers were excluded and the mean value of replicates was used. Reproducibility within and between different runs was tested using standards. Diatoms were prepared following standardized protocols (Renberg 1990), with absolute abundances calculated following Battarbee & Kneen (1982). Diatoms were counted under oil immersion using a Zeiss axiophot light microscope. At least 400 valves (>2/3 intact or unmistakably the middle part of the raphe system) were counted in each sample, except when concentrations were too low to reach this number. In the latter case samples were first concentrated and then slides were screened entirely. Taxonomic identification was mainly based on Sabbe et al. (2003), Ohtsuka et al. (2006) and Esposito et al. (2008) for the freshwater diatoms, and Cremer et al. (2003) and Scott & Thomas (2005) for the marine and brackish-water diatoms. Diatoms were grouped into freshwater, brackish and marine species. Species were considered as freshwater taxa when their WA-optimum is below 1.5 mS/cm (Tavernier et al. in press - Chapter 3). Species were considered to be brackish-water taxa when (i) their WA-optimum exceeds 1.5 mS/cm, (ii) and was lower than 4.42 mS/cm (Tavernier et al. in press - Chapter 3). Fossil pigments were extracted and analysed following Van Heukelem & Thomas (2001). The system was calibrated using authentic pigment standards and compounds isolated from reference cultures following Scientific Committee on Oceanic Research (SCOR) protocols (DHI, Denmark). The identification of the pigments was based on Jeffrey et al. (1997) and pigments of unknown affinity were assigned as derivatives of the pigment with which they showed the closest match based on retention times and absorption spectra, or as 'unknown'. Concentrations of individual pigments in the samples were calculated using the response factors of standard pigments. The abundance of the cyanobacteria marker pigments myxoxanthophyll, echinenone, and zeaxanthin, is reported as percentage of the total carotenoids (%). Note that zeaxanthin is also produced by green algae and mosses and hence its presence does not necessary imply the occurrence of cyanobacteria. Stratigraphic data were plotted using Tilia and Tilia Graph (Grimm 2004).

Results

Isolation lakes

Yumi Ike - 10 m above sea-level (a.s.l.)

Three main zones were identified in the Yumi Ike cores (Fig. 2), namely a marine zone (WO1 I), a lacustrine freshwater zone (WO1 III) and a transition zone (WO1 II) in between. Between 74 and 54 cm (c. 5530 - 5050 cal. yr BP), marine diatoms dominate and the TC concentration is relatively low. Mass-specific MS values decrease towards the end of this zone whereas GRD is relatively stable. The zone between 54 and 46 cm (c. 5050 - 4800 cal. yr. BP) is a transition zone containing a mixture of brackish-water and marine diatom species. The TC concentration remains low. Mass-specific MS values slightly increase, whereas GRD remains stable. From 46 cm until the surface sediments (c. 4800 cal. yr. BP until recent), freshwater diatoms are dominant and brackish and marine diatoms occasionally occur, likely as a result of sea spray and/or the visit of the lake by marine birds or mammals. The TC concentration is more variable than in the other two zones. Mass-specific MS values further increase to reach a maximum at 37.2 cm, decrease until c. 21 cm, to increase again. GRD remains relatively stable to become slightly higher in the upper 5 cm of the sediments.

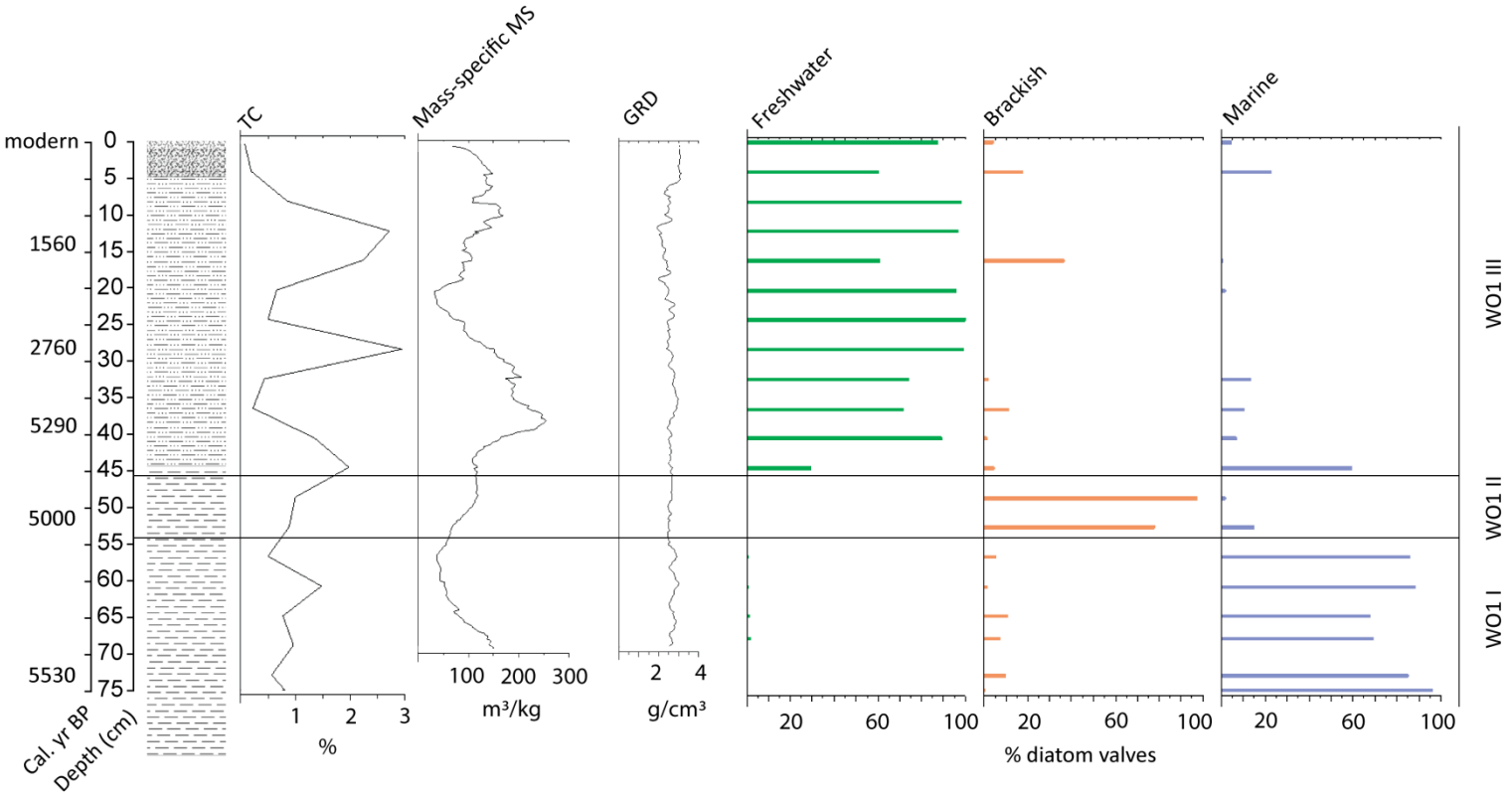

Figure 2. Summary diagram of the Yumi Ike sediment core showing the lithology, total carbon content (TC; %), mass-specific magnetic susceptibility (MS; m^3/kg), gamma ray density (GRD; g/cm^3), and the percentage of lacustrine freshwater, brackish and marine diatoms. Lithology legend as in fig. 9.

Ô–Ike - 13 m a.s.l.

Similar to Yumi Ike, three main zones were identified in the Ô-Ike sediment cores (Fig. 3), namely a marine zone (WO4 I), a lacustrine freshwater zone (WO4 III) and a very short transition zone in between (WO4 II). In zone WO4 I, between 176 and 160 cm (c. 6530 - 5000 cal. yr BP), the cyanobacteria-specific pigments, total carotenoid and chlorophyll concentrations, as well as TC concentrations are low, while GRD and mass-specific MS are relatively high. The latter decreases towards the end of this zone. This zone is dominated by marine diatoms, while freshwater species are absent. In WO4 II, between 160 and 158 cm (c. 5000 - 4660 cal. yr BP), TC concentrations are still low, while all the cyanobacterial pigments, and the total chlorophyll and carotenoid concentrations increase. This zone is dominated by marine and brackish diatom species. GRD and mass-specific MS decrease throughout this zone. In WO4 III, between 158 and 0 cm (c. 4660 cal. yr BP - recent), the TC concentration is relatively high. The total chlorophyll and carotenoid concentrations and the abundance of cyanobacteria marker pigments are generally high in this zone but also variable. WO4 III is dominated by freshwater diatoms. GRD is initially high to decrease and remain relatively stable until 86.6 cm. Mass-specific MS is low and stable throughout this zone.

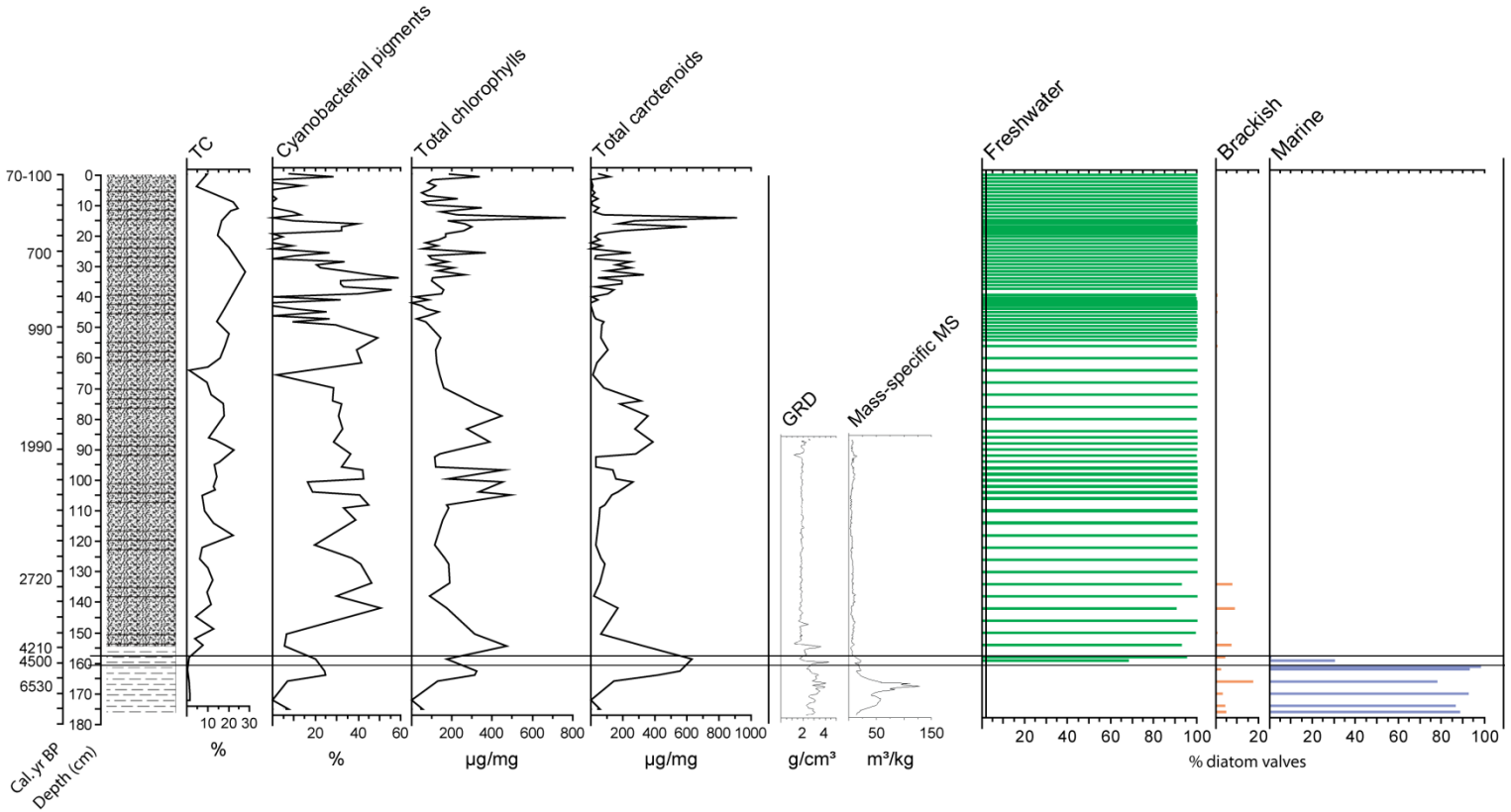

Figure 3. Summary diagram of the Ô-Ike sediment core showing the lithology (lithology legend as in fig. 9), total carbon content (TC; %), the relative abundance of cyanobacteria marker pigments (%), the total chlorophyll and carotenoid concentration (µg/mg), gamma ray density (GRD; g/cm³), mass-specific magnetic susceptibility (MS; m³/kg), and the percentage of lacustrine freshwater, brackish and marine diatoms (%).

Mago Ike - 1.5 m a.s.l.

Again, three main zones were identified (Fig. 4), namely a marine zone (SK1 I), a lacustrine freshwater zone (SK1 III) and a transition zone in between (SK1 II). Between 254 and 143 cm (c. 2120 - 1500 cal. yr BP), the TC concentration is very low, as well as the total carotenoid and chlorophyll concentrations and the relative abundance of cyanobacteria-specific marker pigments. GRD and mass-specific MS are relatively high and the latter increases towards the end of the zone. Marine diatoms dominate, while brackish-water and particularly freshwater species are only present in low abundances. Between 143 cm and 123 cm (c. 1500 - 1120 cal. yr BP), TC, the total chlorophyll and carotenoid concentrations and the relative abundance of cyanobacteria marker pigments start to increase. GRD decreases in SK1 II while mass-specific MS reaches a maximum and subsequently drops sharply. The relative abundance of brackish-water diatoms increases towards the upper part of this zone, while the percentage of marine diatoms decreases. Between 123 cm and the top of the core (c. 1120 cal. yr BP until present), TC concentration is high, as are the total chlorophyll and carotenoid concentrations and the relative abundance of cyanobacteria marker pigments. GRD and mass-specific MS are relatively low in SK1 III. This zone is dominated by freshwater diatoms; some brackish-water and marine diatoms occasionally occur at the beginning of this zone.

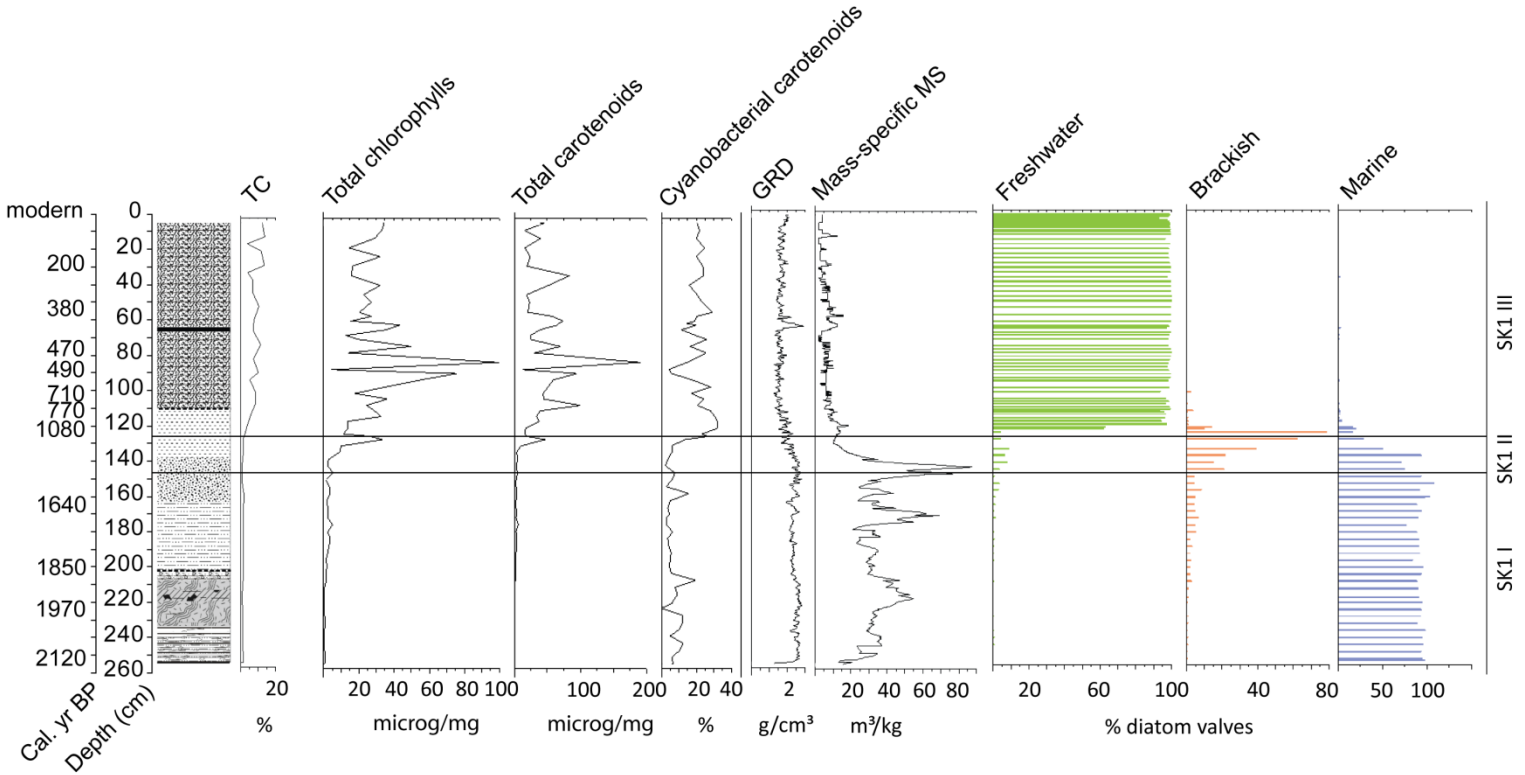

Figure 4. Summary diagram of the Mago Ike sediment core showing the lithology (lithology legend as in fig. 9), total carbon content (TC; %), total chlorophyll and carotenoid concentrations (microg/mg), relative abundance of cyanobacteria marker pigments (%), gamma ray density (GRD; g/cm³), mass-specific magnetic susceptibility (MS; m³/kg), and the percentage of lacustrine freshwater, brackish and marine diatoms (%).

Kobachi Ike - 28 m a.s.l.

The evolution of Kobachi Ike is more complex. The sediment cores can again be subdivided in three main zones (Fig. 5), namely a zone consisting of glacial sediments (SK4 I), and a marine zone (SK4 II) which gradually evolves towards a lacustrine zone (SK4 III). Between 280 and 245 cm (c. 7240 - 4580 cal. yr BP), the total chlorophyll and carotenoid concentrations as well as the relative abundance of cyanobacterial carotenoids, mass-specific MS and total diatom concentration (Chapter 5) are low. From 260 cm onwards, zone SK4 I is further characterised by relatively high TOC concentrations. Myxoxanthophyll is absent throughout this zone. Between 245 and 115 cm (c. 4580 - 3670 cal. yr BP), the TOC concentrations, and the total chlorophyll and carotenoid concentrations are low. Myxoxanthophyll is almost completely absent in zone SK4 II, which is furthermore characterised by relatively high mass-specific MS values. Marine diatoms are dominant, but brackish-water species become more abundant towards the end of this zone. In zone SK4 III, between 115 cm (c. 3670 cal. yr BP) and the top of the core, the TOC, chlorophyll and carotenoid concentrations are relatively high. Myxoxanthophyll becomes a subdominant pigment. Mass-specific MS gradually decreases until 65 cm (c. 2010 cal. yr BP). GRD values were relatively stable throughout the sediments to fluctuate slightly more in the upper 60 cm. The majority of the samples are dominated by brackish-water diatoms, but spores from marine *Chaetoceros* species are an important member of the assemblages in some samples. These can be *in situ* produced, although it is also possible that they were transported to the lake through sea spray, or alternatively that they were washed-in from raised beach deposits within the catchment area (see Chapter 5 for a more detailed description).

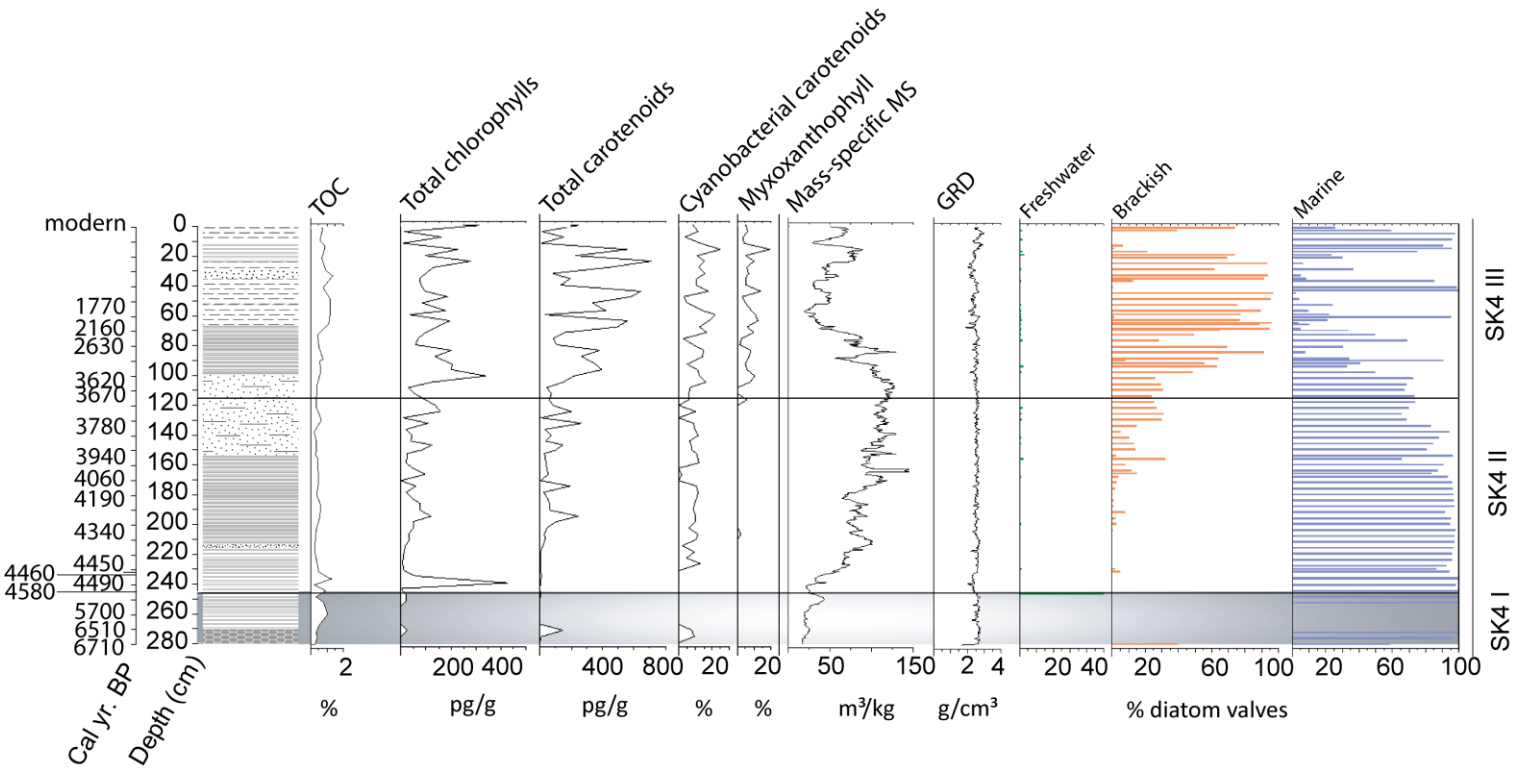

Figure 5. Summary diagram of the Kobachi Ike sediment core showing the lithology (lithology legend as in fig. 9), total organic carbon content (TOC; %), total chlorophyll and carotenoid concentration (pg/g), relative abundance of cyanobacteria marker pigments (%), and the percentage of myxoxanthophyll (%); a pigment exclusively produced by cyanobacteria. Also shown are the gamma ray density (GRD; g/cm³) and mass-specific magnetic susceptibility (MS; m³/kg), and the percentage of lacustrine freshwater, brackish and marine diatoms (%). The grey horizontal bar represents a zone of low diatom productivity (see Chapter 5 for more details).

Glacial lakes

All the samples analysed in Ura Ike (17 m a.s.l.), Higashi Ike (18 m a.s.l.) and Nishi Ike (23 m a.s.l.) were dominated by freshwater lacustrine diatoms. The TC concentrations in Nishi Ike are very low in the bottom sediments and start to increase from 40 cm onwards (Fig. 8). The bottom age of the Higashi Ike and Nishi Ike sediment cores equals c. 4520 or 4560 and c. 11,240 cal. yr BP, respectively. The latter dating was obtained from a sample immediately preceding the increase of the TC concentration (Fig. 8). In Ura Ike, the oldest radiocarbon date taken, is c. 6290 cal. yr BP. However, the age of the bottom sediments remains unknown. Combined, these data suggest that these basins were situated above the marine limit throughout the entire Holocene and probably originated from beneath the ice-sheet or permanent snow fields during the Early- to Mid-Holocene.

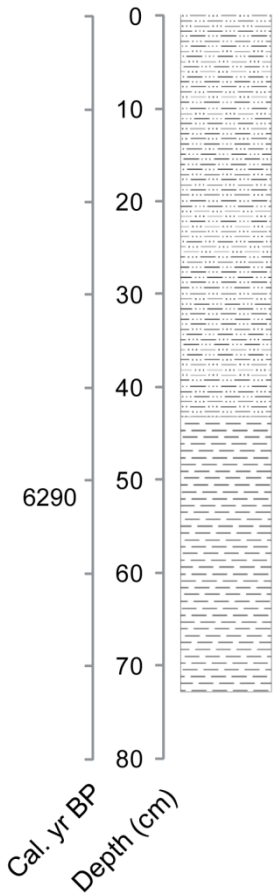

Figure 6. Lithology (lithology legend as in fig. 9) of the sediment core of Ura Ike.

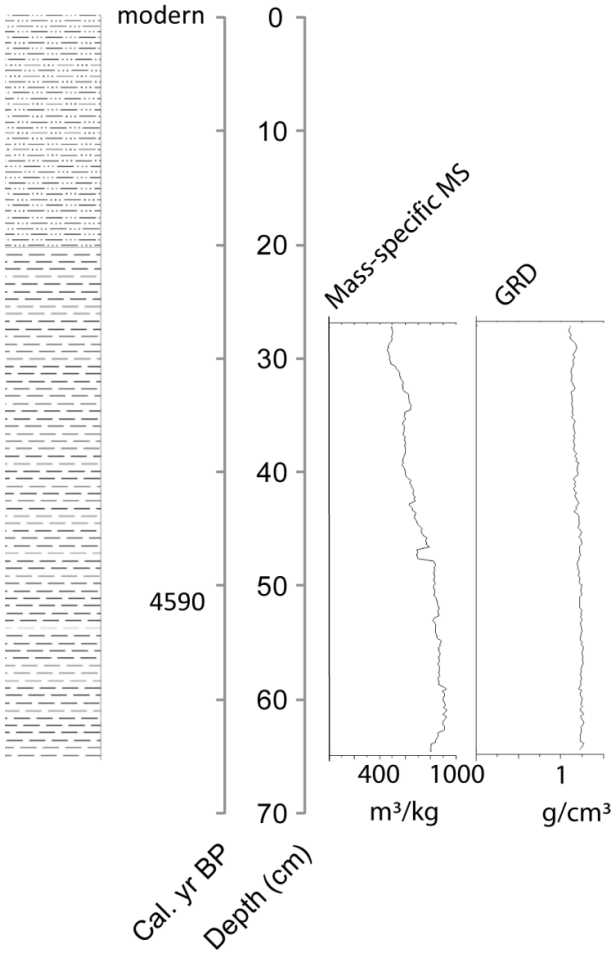

Figure 7. Summary diagram showing the lithology (lithology legend as in fig. 9), mass-specific magnetic susceptibility (MS; m^3/kg), and gamma ray density (GRD; g/cm^3) of (part of) the sediment cores of Higashi Ike.

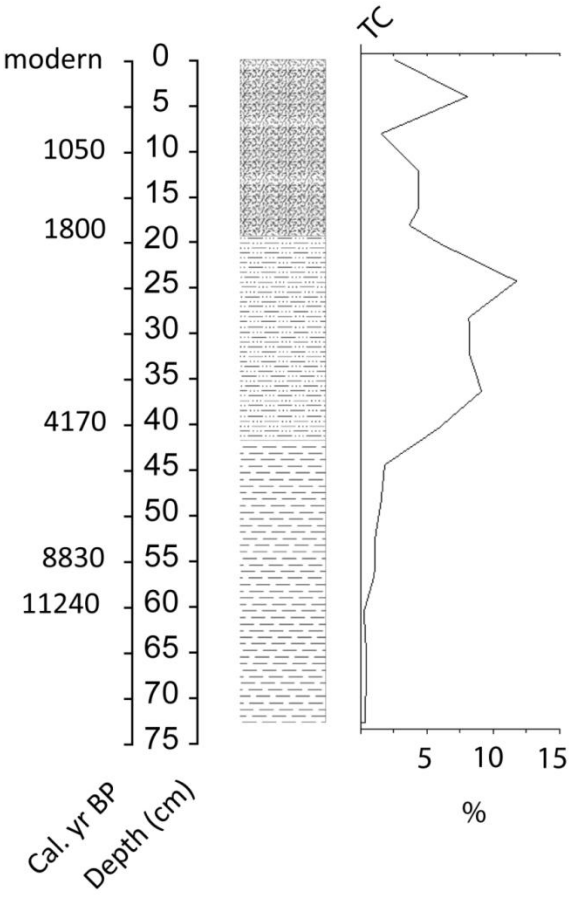

Figure 8. Summary diagram showing the lithology (lithology legend as in fig. 9), and total carbon concentration (TC; %) of the sediment cores of Nishi Ike.

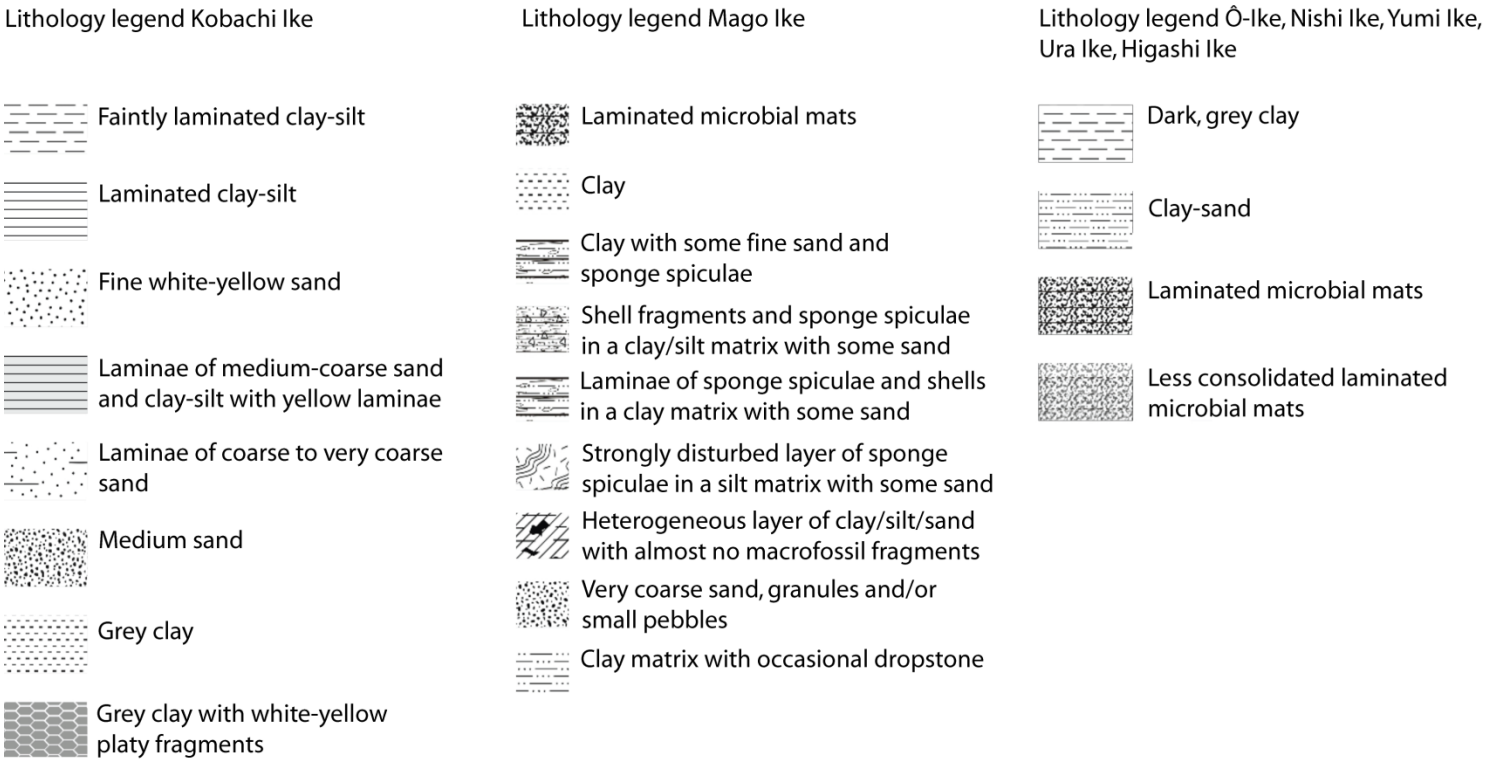

Figure 9. Lithology legends for Kobachi Ike (left), Mago Ike (middle) and the West Ongul lakes (right) (Ô-Ike, Nishi Ike, Yumi Ike, Ura Ike, and Higashi Ike).

Relative sea-level changes

The RSL curves were broadly similar between the Ongul Islands and Skallen but these differed with the one from Skarvsnes (Fig. 10). On West Ongul Island, RSL fall was relatively rapid between c. 5000 and 4800 cal. yr BP and equalled 15 mm/yr. The uplift rate averages 2.1 mm/yr during the past c. 4800 cal. yr BP. The sea-level high stand was below 17 m as indicated by the absence of marine sediments in Ura Ike. In Skallen, RSL fell at a mean rate of 2 mm/yr during the past 4690 ± 100 cal. yr BP; the maximum sea-level high stand is 13 m. Note that the rate of RSL fall is different from that proposed by Takano et al. (2012), because we decided to keep ^{14}C dates uncorrected for the marine reservoir age in the transition zone, following Roberts et al. (2011). In Skarvsnes, RSL fall was relatively rapid between c. 3670 and 1905 cal. yr BP and equalled 14.5 mm/yr. The presence of the cyanobacterial pigment myxoxanthophyll at 115 cm in the Kobachi Ike sediment core is used as the start of the lacustrine zone and hence lake isolation. However, when the higher abundance of the brackish water diatoms compared to the marine diatoms at 165 cm is used as a boundary for lake isolation, the RSL fall is less rapid (12.1 mm/yr) between 4030 and 1905 cal. yr BP. Between c. 1905 and 1500 cal. yr BP, RSL fall dropped to 2.1 mm/yr and from c. 1500 cal. yr BP onwards, it was c. 1.0 mm/yr. The maximum RSL high stand is 32.7 m, which is based on a marine macrofossil of 5410 ± 40 ^{14}C yr old (5265 - 4653 cal. yr BP) preserved in the upper sill of Kobachi Ike (Table 1). Macrofossils from *L. elliptica* and *polychaete* tubes preserved in raised beaches at a height of 8.6 m a.s.l. are respectively 4730 ± 40 and 6800 ± 40 ^{14}C yr old (Table 1).

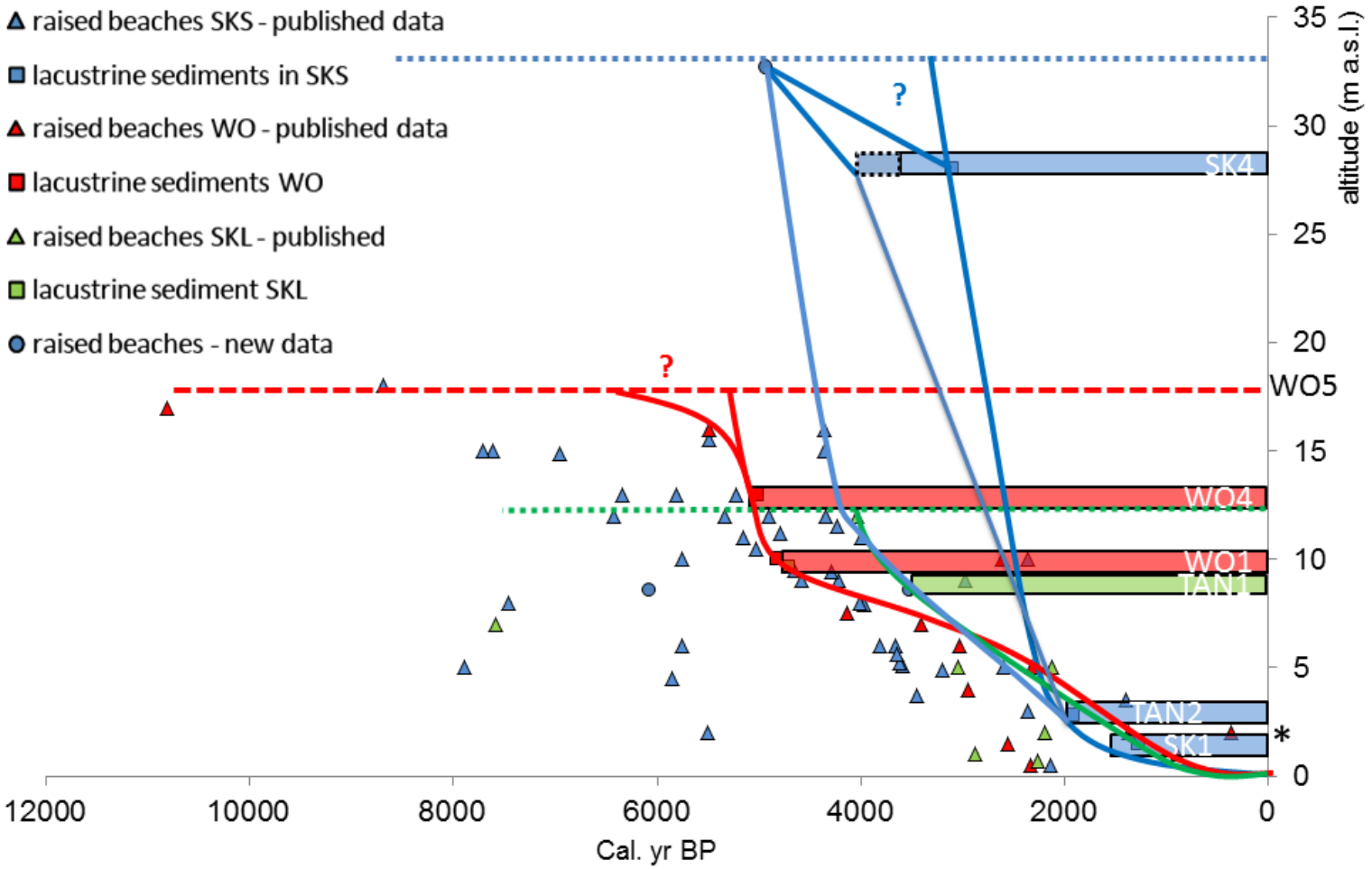
raised beaches SKS - published data
lacustrine sediments in SKS
raised beaches WO - published data
lacustrine sediments WO
raised beaches SKL - published
lacustrine sediment SKL
raised beaches - new data
?
?
SK4
WO5
WO4
WO1
TAN1
TAN2
SK1
*
35
30
25
20
15
10
5
0
altitude (m a.s.l.)
12000
10000
8000
6000
4000
2000
0
Cal. yr BP

Figure 10. Relative sea-level curves for Skarvsnes (SKS; blue), the Ongul Islands (WO; red) and Skallen (SKL; green). The curves are based on the sediment cores from the isolation lakes, of which the lacustrine zones are represented by horizontal bars and on raised beach data. Note that one raised beach data point from West Ongul Island is not consistent with our lake-based approach (indicated with an asterisk on the right). This can be related to post-depositional transportation of the marine fossil. TAN1 and TAN2 are Lake Skallen and Lake Oyako (see Takano et al. 2012 for more information). The maximal marine limit is indicated with horizontal lines. Fossils situated below the actual sea-level and those of LGM ages (see Miura et al. 1998) were excluded from the diagram. Errors of the measured sill heights are <1 cm based on GPS measurements and approximately 0.5 m when the sill height is determined from a geological map. The age range of the dates of the time of isolation should be taken into account: c. 4970-4650 cal. yr BP for Yumi Ike, c. 5300-4580 cal. yr BP for Ô-Ike, c. 1680-1310 cal. yr BP for Mago Ike, and c. 3810-2820 cal. yr BP or 4280-3370 cal. yr BP for Kobachi Ike (depending on whether the detection of myxoxanthophyll or the increase in brackish water diatoms compared to marine diatoms is used as criterion for the delineation between marine and lacustrine sediments. The latter is indicated with a bar with dashed lines.). For the TAN1 and TAN2 lakes derived from the literature, these data are not available.

Discussion and perspectives

Lake origin and evolution

The identification of the transition from marine to lacustrine conditions in three out of the four isolation lakes (Mago Ike, Yumi Ike and Ô-Ike; Figs. 4, 2 & 3) was relatively straightforward due to the presence of brackish-water diatoms and the decrease in marine diatom abundance during a relatively brief phase. This transition zone was subsequently followed by a dominance of freshwater diatoms. Also in the lakes from Skallen, the transition zone was relatively obvious in the TC and TN concentrations (Takano et al. 2012). However, this was not confirmed by a diatom analysis and the other biogeochemical proxies showed gradual or only small changes throughout the cores. Hence, the delineation between marine and lacustrine sediments in this region should be considered as less conclusive compared with the three abovementioned records. Similarly, identifying the transition from marine to lacustrine conditions is less straightforward in the record from Kobachi Ike (Fig. 5) due to the gradual changes in the abundance of brackish water diatoms and the presence of marine taxa throughout the core. This is likely related to peculiar physical and chemical characteristics of the lake with brackish conditions in the bottom waters (specific conductance below 2.4 m equals 11.4 mS/cm) and low salinity waters in the upper part of the water column (5.0 mS/cm) at the time of sampling. This freshwater lens is likely derived from meltwater input from the catchment and/or lake ice (Chapter 5; Kimura et al. 2010). This salinity-driven stratified condition appears to be strong enough to prevent mixing of the bottom water with meltwater. Furthermore, this situation also provides a mechanism for the passage of large fluxes of meltwater without significantly affecting the salinity of the lake as freshwater can pass through the epilimnion and leave the lake via an outflow stream (which was not active during sampling) without diluting the brackish water stored in the hypolimnion. It follows that lake isolation may have started around c. 4030 cal yr BP (165 cm), when the abundance of brackish water diatoms started to increase. Conditions similar to those of today, were likely established around c. 3670 cal. yr BP, when TOC concentrations started to increase, mass-specific MS started to decrease and myxoxanthophyll was present. The latter is linked to the presence of cyanobacteria which

are abundant in East Antarctic lakes (Verleyen et al. 2010) and Kobachi Ike today, but largely absent from the Southern Ocean (Fukuda et al. 1998). The decrease in mass-specific MS around 2160 cal. yr BP (70 cm) also suggest a complete isolation of the lake. This was for example similarly observed in Maritime Antarctic lakes and related to differences in the sedimentary infill of the basins during marine versus lacustrine conditions (Watcham et al. 2011). During the latter, mainly local minerals are transported to the basin while during marine conditions sediments from elsewhere might be transported to the site via ice bergs and redistributed sea ice containing wind-blown particles.

Last Glacial Maximum and deglaciation

The ^{14}C dates in the bottom sediments of the lakes revealed that deglaciation started slightly later in Skarvsnes compared with the Ongul Islands. The oldest ^{14}C date obtained from the Nishi Ike sediment core on West Ongul Island, in the zone in which the TC concentrations start to increase, is c. 11,240 cal. yr BP (Table 1). Below that, TC concentrations were low indicating no/a small amount of primary production. This suggests (scenario 1) that the region was ice-covered during the LGM as a result of the expansion of the EAIS. This is in general agreement with cosmogenic isotope data from Skarvsnes further to the south and a large number of the currently ice-free regions in Antarctica, such as the Schirmacher Oasis, Vestfold Hills (but see Gibson et al. 2009), and the Windmill Islands (see Hall 2009 and Mackintosh et al. 2013 for a review) (Fig. 1). However, scenario 1 contradicts an alternative interpretation (scenario 2) which involves ice-free conditions during the LGM based on raised beaches from the region in which *in situ* shells of *L. elliptica* predating the LGM (Miura et al. 1998) were found. This suggests that the Ongul islands were ice-free during MIS3 and maybe even during earlier isotope stages (Takada et al. 2003). Possibly, the Ongul Islands were indeed ice-free but rather covered with permanent snow banks before, during and after the LGM. This prevented light penetration and hence primary production (cf. Gore 1997). It might be possible that the glacier flowed around the Ongul Islands, through the Fuji Submarine Valley, leaving the region exposed. Another possibility is that both the islands were ice-covered during the LGM and that the shells were well-preserved under a more or less inactive ice-sheet buttressed on the Ongul Islands, and of which the flow lines curved into the glacial troughs between the islands and the continent. This would be in support of scenario 1. A similar process likely resulted in the preservation of Eemian sediments in Progress Lake in the Larsemann Hills, which became ice-free during the Late-Holocene (Hodgson et al. 2006).

The onset of deglaciation of the coastal zone near Skarvsnes seems to occur somewhere around c. 7420 cal. yr BP, as evidenced by the oldest radiocarbon date obtained from the Kobachi Ike sediment cores. This minimum time of deglaciaton is in agreement with that obtained from the radiocarbon dates in the raised beaches (Fig. 10 and Miura et al. 1998); where apart from two dates, none is actually older than c. 8000 cal. yr BP. Moreover, our estimate also corresponds to a cosmogenic isotope dating study which places the deglaciation of Skarvsnes between 10 and 6 ka BP (Yamane et al. 2011). More precisely, the time of deglaciation of the Kobachi Ike basin agrees well with that obtained of nearby Mount Suribati, but slightly postdates that in scenario 1 in the Ongul

Islands. Clearly, if the islands were ice-free during the LGM (scenario 2), the differences in deglaciation history between the ice-free regions in Lützow Holm Bay would be even more pronounced. Such pronounced differences in the deglaciation history between regions only 60-80 km apart from each other are not unlikely. Similar regional and even local-scale differences were for example observed in Stornes in the Larsemann Hills (Hodgson et al. 2005), whereas the other two main peninsulas were ice-covered (Hodgson et al. 2001) together with the nearby Rauer Islands (Berg et al. 2009) (Fig. 1). These differences in glacial history between the ice-free regions in Lützow Holm Bay are furthermore supported by geomorphological evidence and the amount of weathering of the bedrocks. Indeed, rocks in the northernmost part of Sôya Coast are deeply weathered, whereas those in the southern part of the coast (i.e. Skarvsnes and Skallen) are relatively unweathered and intensively striated. It is clear that additional geomorphological research and radiometric dating of land forms and lake sediments is needed to fully resolve the deglaciation history of the Ongul Islands (Mackintosh et al. 2013).

Relative sea-level changes

Our most significant finding is the striking differences in the maximum marine limit between Skallen and the Ongul islands on the one hand and Skarvsnes on the other. On the Ongul Islands, RSL was always below 17 m a.s.l. during the Holocene as indicated by the presence of exclusively lacustrine sediments in the glacial lakes Ura Ike, Higashi Ike and Nishi Ike between c. 11,240 cal. yr BP until present (Fig. 10). This upper marine limit is further confirmed by the absence of marine fossils from the Ongul Islands in deposits above this altitude (Fig. 10). In Skallen, raised beach data suggest that the marine limit was situated at least at 12 m. It is possible that the limit was higher but this needs to be confirmed by additional dating of bottom sediments of glacial lakes. Taken together however, the maximum marine limit in both regions is close to previous estimates based on raised beach data alone (Miura et al. 1998). By contrast, the marine limit in Skarvsnes is up to 15 m higher than that in the Ongul Islands, 20 m higher than in Skallen and 12 m higher than previous estimates based on raised beach data alone (Miura et al. 1998). The shape of the RSL curves and hence the inferred uplift rates are also different between the regions. When the increase in brackish water diatoms at c. 4030 cal. yr BP is considered as the time of isolation, RSL fall is less rapid compared to when the detection of myxoxanthophyll is considered as the time of isolation (3670 cal. yr BP). Given the lack of lake isolation records from between 4 and 28 m a.s.l., it is not possible to conclusively constrain RSL fall until 1905 cal. yr BP. Based on the current data, RSL fall will be within the range 12.1 - 14.5 mm/yr. It appears thus that RSL fall during the Mid- and maybe also Late-Holocene is more or less similar in Skallen and the Ongul Islands, whereas in Skarvsnes it is about 10 times faster than the uplift rate estimated for the past 1000 years in all regions studied. The latter varies between 1 mm/yr (Skarvsnes) and 2.1 mm/yr (West Ongul island), which is similar to the current secular uplift rate as measured using GPS (1.4 - 1.8 mm/yr; Ohzono et al. 2006).

The differences between the RSL curves are potentially underlain by different, non-mutually exclusive processes, namely regional variation in (i) the timing of deglaciation, (ii) local ice-sheet volume and (iii) neotectonic processes. The first process is

less likely, given the relative small changes in the start of deglaciation between the regions. Also the second process can be expected to be negligible, because RSL changes are likely to reflect changes in this part of the EAIS which drains into Lützow Holm Bay rather than local differences in ice-sheet volume. Hence, we speculate that the third hypothesis is more likely, given the small distance between the different sites (Glenn A. Milne & Mike J. Bentley, pers. comm.) and the presence of a fault system on Skarvsnes. Similar findings were for example obtained from Swedish lakes (Risberg et al. 2005) where neotectonic faulting resulted in different RSL curves along the Baltic coast. Lakes situated 50 km apart showed a difference of 5 m in uplift rate as a result of neotectonic processes. Similarly, the fault movement of a bog near Puerto del Hambre (Strait of Magellan, South Chile) was at least 30 m (Bentley & McCulloch 2005). These differences in RSL changes between the islands and peninsulas in Lützow Holm Bay are likely to complicate the constraining of regional GIA models. One way would be to calculate the minimum difference between the ice-sheet volume during/after the LGM and after deglaciation using a suite of existing ice-sheet models (see Bassett et al. 2007 and Watcham et al. 2011).

Apart from the intra-regional difference in shape and maximum sea-level high stand, the RSL curves in Lützow Holm Bay are also different from those obtained from other East Antarctic regions, such as the Larsemann Hills (Verleyen et al. 2005) and the Vestfold Hills (Zwartz et al. 1998) (Fig. 1). In the latter regions, RSL reaches a maximum between c. 8000 and 6000 cal. yr BP, after which a RSL fall occurs due to the outpacing of the eustatic component by isostatic uplift. This is because eustatic sea-level changes are small from the Mid-Holocene onwards because the ice-sheets in the NH reached their current position at that time. By contrast, in Lützow Holm Bay RSL remains at its maximum until c. 4830 cal. yr BP in Skarvsnes and perhaps even later and until 5480 and 4020 cal. yr BP in the Ongul Islands and Skallen respectively. This implies that the neotectonic faulting was complex and that the uplift occurred relatively recently (i.e., after the Mid-Holocene), because ^{14}C dates in raised beaches and cosmogenic isotope dates suggest that ice-sheet thinning and partial deglaciation occurred between 10 and 6 ka BP (Yamane et al. 2011). If deglaciation indeed occurred during the Early-Holocene, isostatic uplift should have been very rapid at least from 6 ka BP onwards which would result in a sea-level maximum that preceded that observed in our data.

Conclusions

The deglaciation history of Skarvsnes agrees well with that derived from a recent cosmogenic isotope dating campaign (Yamane et al. 2011). By contrast, the deglaciation history of West Ongul Island appears to be more complex and not in agreement with previous data from the islands (Miura et al. 1998). This difference might however be explained by extensive snow cover preventing primary production in the glacial lakes.

Of most significance is the difference in (i) Holocene maximum marine limit and (ii) the shape of the RSL curves in Skarvsnes and the Ongul Islands and Skallen. These differences are likely related to neotectonic events, local faulting, on Skarvsnes which complicate a quantitative comparison of the different existing ice-sheet models in order to assess whether they can correctly estimate the volume of the EAIS in this region. One

way to circumvent this problem is to calculate the minimum and maximum ice-sheet thickness in the region.

Acknowledgements

We thank the Belgian Science Policy Office (HOLANT project), the UK Natural Environment Research Council (British Antarctic Survey and Radiocarbon Laboratory), Maaike Vancauwenberghe and the Japanese Antarctic Research Expedition 48 for financial and/or logistical support. EV was a post-doctoral research fellow with the Fund for Scientific Research Flanders and currently funded by Ghent University. IT was funded by the Institute for the Promotion of Innovation by Science and Technology in Flanders.

References

Bassett SE, Milne GA, Bentley MJ, Huybrechts P (2007) Modelling Antarctic sea-level data to explore the possibility of a dominant Antarctic contribution to meltwater pulse IA. *Quaternary Science Revieuws,* **26**: 2113-2127.

Battarbee RW, and Kneen M (1982) The use of electronically counted microspheres in absolute diatom analysis. *Limnology and Oceanography,* **27**: 184-188.

Bentley MJ, and McCulloch (2005) Impact of neotectonics on the record of glacier and sea level fluctuations, Strait of Magellan, southern Chile. *Geografiska Annaler,* **87A**, 393-402.

Bentley MJ, Hodgson DA, Smith JA, Cox NJ (2005) Relative sea-level curves for the South Shetland Islands and Marguerite Bay, Antarctic Peninsula. *Quaternary Science Reviews,* **24**: 1203 – 1216.

Berg S, Wagner B, Cremer H, Leng MJ, Melles M (2010) Late Quaternary environmental and climate history of Rauer Group, East Antarctica. *Palaeogeography, Palaeoclimatology, Palaeoecology*, **297**: 201-213.

Berkman PA, Andrews JT, Bjorck S, Colhoun EA, Emslie SD, Goodwin ID, Hall BL, Hart CP, Hirakawa K, Igarashi A, Ingólfsson O, Lopez-Martinez J, Lyons WB, Mabin MCG, Quilty PG, Taviani M, Yoshida Y (1998) Circum-Antarctic coastal environmental shifts during the Late Quaternary reflected by emerged marine deposits. *Antarctic Science,* **10**: 345-362.

Blaauw M (2010) Methods and code for 'classical' age-modelling of radiocarbon sequences. *Quat Geochr,* **5**: 512-518.

Blaauw M, and Christen JA (2011) Flexible paleoclimate age-depth models using an autoregressive gamma process. *Bayesian Analysis,* **6(3):** 457-474.

Bromwich DH, and Nicolas JP (2010) Sea-level rise: Ice-sheet uncertainty. *Nature Geoscience,* **3**: 596-597.

Chen JL, Wilson CR, Blankenship D, Tapley BD (2009) Accelerated Antarctic ice loss from satellite gravity measurements. *Nature geosciences,* **2**: 859-862.

Cremer H, Gore D, Melles M, Roberts D (2003) Palaeoclimatic significance of Late Quaternary diatom assemblages from Southern Windmill Islands, East Antarctica. *Palaeogeogr. Palaeoclimatol. Palaeoecol.,* **195**: 261–280.

Esposito RMM, Spaulding SA, McKnight DM, Van de Vijver B, Kopalová K, Lubinski D, Hall B, and Whittaker T (2008) Inland diatoms from the McMurdo Dry Valleys and James Ross Island, Antarctica. *Botany,* **86**: 1378-1392.

Fukuda R, Ogawa H, Nagata T, Koike I (1998) Direct determination of carbon and nitrogen contents of natural bacterial assemblages in marine environments. *Applied and Environmental Microbiology,* **64(9):** 3352-3358.

Gibson JAE, Paterson KS, White CA, Swadling KM (2009) Evidence for the continued existence of Abraxas Lake, Vestfold Hills, East Antarctica during the Last Glacial Maximum. *Antarctic Science,* **21(3)**: 269-278.

Goodwin ID, and Zweck C (2000) Glacio-isostasy and glacial ice load at Law Dome, Wilkes Land, East Antarctica. *Quaternary Research,* **53**: 285-293.

Gore DB (1997) Blanketing snow and ice; constraints on radiocarbon dating deglaciation in East Antarctic oases. *Antarctic Science,* **9(3)**: 336-346.

Grimm EC (2004) TGView Version 2.0.2. Illinois State Museum, Springfield, Illinois.

Hall BL (2009) Holocene glacial history of Antarctica and the sub-Antarctic islands. *Quaternary Science Reviews,* **28**: 2213-2230.

Hall BL (2010) Holocene relative sea-level changes and ice fluctuations in the South Shetland Islands. *Global and Planetary Change,* **74**: 15-26.

Hodgson DA, Noon PE, Vyverman W, Bryant CL, Gore DB, Appleby P, Gilmour M, Verleyen E, Sabbe K, Jones VJ, Ellis-Evans JC, Wood PB (2001) Were the Larsemann Hills ice-free through the Last Glacial Maximum? *Antarctic Science,* **13(4)**: 440-454.

Hodgson DA, Verleyen E, Sabbe K, Squier AH, Keely BJ, Leng MJ, Saunders KM, Vyverman W (2005) Late Quaternary climate-driven environmental change in the Larsemann Hills, East Antarctica, multi-proxy evidence from a lake sediment core. *Quat. Res.,* **64**: 83–99.

Hodgson DA, Verleyen E, Squier AH, Sabbe K, Keely BJ, Saunders KM, Vyverman W (2006) Interglacial environments of coastal east Antarctica: comparison of MIS 1 (Holocene) and MIS 5e (Last Interglacial) lake-sediment records. *Quaternary Science Reviews,* **25:** 179-197.

Huybrechts P, Janssens I, Poncin C, Fichefet T (2002) The response of the Greenland ice-sheet to climate changes in the 21st century by interactive coupling of an AOGCM with a thermomechanical ice-sheet model. *Annals of Glaciology,* **35**: 409-415.

Ishikawa T, Tatsumi K, Kizaki K, Yanai H, Ando T, Kikuchi Y, Yoshida Y (1976) Explanatory text of geological map of Langhovde, Antarctica. *Ant. Geol. Map Ser. Sheet 5, Langhovde, Natl. Inst. Polar Res.* 12.

Jeffrey SW, Mantoura RFC, Bjornland T (1997) Data for the identification of 47 key phytoplankton pigments. *In*: Jeffrey SW, Mantoura RFC, Wright SW. Phytoplankton pigments in oceanography, guidelines to modern methods. UNESCO Publishing, Paris, p. 447-554.

Kimura S, Ban S, Imura S, Kudoh S, Matsuzaki M (2010) Limnological characteristics of vertical structures in the lakes of Syowa Oasis, East Antarctica. Polar Science, 3: 262-271.

King P, Kennedy H, Newton PP, Jickells TD, Brand T, Calvert S, Cauwet G, Etcheber H, Head B, Khripounoff A, Manighetti B, Miquel JC (1998) Analysis of total and organic carbon and total nitrogen in settling oceanic particles and a marine sediment: an interlaboratory comparison. *Marine Chemistry,* **60**: 203-216.

Mackintosh AN, Verleyen E, O'Brien PE, White DA, Selwyn Jones R, McKay R, Dunbar R, Gore DB, Fink D, Post AL, Miura H, Leventer A, Goodwin I, Hodgson DA, Lilly K, Crosta X, Golledge NR, Wagner B, Berg S, van Ommen T, Zwartz D, Roberts SJ, Vyverman W, Masse G (2013) Retreat history of the East Antarctic Ice Sheet since the Last Glacial Maximum. *Quaternary Science Reviews,* http://dx.doi.org/10.1016/j.quascirev.2013.07.024.

Nakada M, and Lamback K (1998) The melting history of the late Pleistocene Antarctic ice-sheet. *Nature,* **333**: 36-40.

McCormac F, Hogg A, Blackwell P, Buck C, Higham T, Reimer P (2004) Shcal04 Southern Hemisphere calibration 0-11.0 cal kyr BP. *Radiocarbon,* **46**: 1087-1092.

Miura H, Maemoku H, Igarashi A, Moriwaki K (1998) Late Quaternary raised beach deposits and radiocarbon dates of marine fossils around Lützow Holm Bay. *Special map series of National Institute of Polar Research,* **6:** pp. 46.

Nakada M, Kimura R, Okuno J, Moriwaki K, Miura H, Maemoku H (2000) Late Pleistocene and Holocene melting history of the Antarctic ice-sheet derived from sea-level variations. *Marine Geology,* **167**: 85-103.

Ohtsuka T, Kudoh S, Imura S, Ohtani S (2006) Diatoms composing benthic microbial mats in freshwater lakes of Skarvsnes ice-free area, East Antarctica. *Polar Biosci.,* **20**: 113-130.

Ohzono M, Tabei T, Doi K, Shibuya K, Sagiya T (2006) Crustal movement of Antarctica and Syowa Station based on GPS measurements. *Earth Planets Space,* **58**: 795-804.

Pingree K, Lurie M, Hughes T (2011) Is the East Antarctic ice-sheet stable? Q*uaternary Research,* **75**: 417-429.

Reimer PJ, Baillie MGL, Bard E, Bayliss A, Beck JW, Bertrand CJH, Blackwell PG, Buck CE, Burr GS, Cutler KB, Damon PE, Edwards RL, Fairbanks RG, Friedrich M, Guilderson TP, Hogg AG, Hughen KA, Kromer B, McCormac G, Manning S, Ramsey CB, Reimer RW, Remmele S, Southon JR, Stuiver M, Talamo S, Taylor FW, Van Der Plicht J, Weyhenmeyer CE (2004) Intcal04 Terrestrial radiocarbon age calibration, 0-26 cal kyr BP. *Radiocarbon*, **46**: 1029-1058.

Reimer PJ, Baillie MGL, Bard E, Bayliss A, Beck JW, Blackwell PG, Bronk Ramsey C, Buck CE, Burr GS, Edwards RL, Friedrich M, Grootes PM, Guilderson TP, Hajdas I, Heaton TJ, Hogg AG, Hughen KA, Kaiser KF, Kromer B, McCormac FG, Manning SW, Reimer RW, Richards DA, Southon JR, Talamo S, Turney CSM, van der Plicht J, Weyhenmeyer CE (2009) IntCal09 and Marine09 radiocarbon age calibration curves, 0-50,000 years cal BP. *Radiocarbon*, **51**: 1111-1150.

Renberg I (1990) A procedure for preparing large sets of diatoms slides from sediment cores. *Journal of Paleolimnology,* **4**: 87-90.

Rignot E, Mouginot J, Scheuchl (2011) Ice flow of the Antarctic Ice-sheet. *Science,* **333**: 1427-1430.

Risberg J, Alm G, Goslar T (2005) Variable isostatic uplift patters during the Holocene in southeast Sweden, based on high-resolution AMS radiocarbon datings of lake isolations. *The Holocene,* **15(6)**: 847-857.

Roberts SJ, Hodgson DA, Sterken M, Whitehouse PL, Verleyen E, Vyverman W, Sabbe K, Balbo A, Bentley MJ, Morteton S (2011) Geological constraints on glacio-isostatic adjustment models of relative sea-level change during deglaciation of Prince Gustav Channel, Antarctic Peninsula. *Quaternary Science Reviews,* **30(25-26)**: 3603-3617.

Sabbe K, Verleyen E, Hodgson DA, Vanhoutte K, Vyverman W (2003) Benthic diatom flora of freshwater and saline lakes in the Larsemann Hills and Rauer Islands, East Antarctica. *Antarct Sci,* **15**: 227-248.

Scott FJ, and Thomas DP (2005) Diatoms. *In:* Scott FJ, and Marchant HJ (Eds.) Antarctica marine protists. Hobart, Australia. p. 13 – 201.

Stewart IS, Sauber J, Rose J (2000) Glacio-seismotectonics: ice-sheets, crustal deformation and seismicity. *Quaternary Science Reviews,* **19**: 1367-1389.

Takada M, Tani A, Miura H, Moriwaki K, Nagatomo T (2003) ESR dating of fossil shells in the Lützow Holm Bay region, East Antarctica. *Quaternary Science Reviews,* **22**: 1323-1328.

Takano Y, Tyler JJ, Kojima H, Yokoyama Y, Tanabe Y, Sato T, Ogawa NO, Ohkouchi N, Fukui M (2012) Holocene lake development and glacial-isostatic uplift at Lake Skallen and Lake Oyako, Lützow Holm Bay, East Antarctica, based on biogeochemical facies and molecular signatures. *Applied Geochemistry,* doi: http://dx.doi.org/10.1016/j.apgeochem.2012.08.009

Van Heukelem L, and Thomas CS (2001) Computer-assisted high-performance liquid chromatography method development with applications to the isolation and analysis of phytoplankton pigments. *Journal of Chromatography A*, **910**: 31-49.

Verleyen E, Hodgson DA, Sabbe K, Vanhoutte K, Vyverman W (2004) Coastal oceanographic conditions in the Prydz Bay region (East Antarctica) during the Holocene recorded in an isolation basin. *The Holocene,* **14(2)**: 246-257.

Verleyen E, Hodgson DA, Milne GA, Sabbe K, Vyverman W (2005) Relative sea-level history from the Lambert glacier region, East Antarctica, and its relation to deglaciation and Holocene glacier readvance. *Quaternary Research,* **63**: 45-52.

Verleyen E, Sabbe K, Hodgson DA, Grubisic S, Taton A, Cousin S, Wilmotte A, De Wever A, Van der Gucht K, Vyverman W (2010) Structuring effects of climate-related environmental factors on Antarctic microbial mat communities. *Aquatic Microbial Ecology,* **59:** 11-24.

Verleyen E, Hodgson DA, Gibson J, Imura S, Kaup E, Kudoh S, De Wever A, Hoshino T, McMinn A, Obbels D, Roberts D, Roberts SJ, Sabbe K, Souffreau C, Tavernier I, Van Nieuwenhuyze W, Van Ranst E, Vindevogel N, Vyverman W (2012) Chemical limnology in coastal East Antarctic lakes: monitoring future climate change in centres of endemism and biodiversity. *Antarctic Science,***24(1)**: 23-33.

Watcham EP, Bentley MJ, Hodgson DA, Roberts SJ, Fretwell PT, Lloyd JM, Larter RD, Whitehouse PL, Leng MJ, Monien P, Moreton SG (2011) A new Holocene relative sea-level curve for the South Shetland Islands, Antarctica. *Quaternary Science Reviews,* **30**: 3152-3170.

Whitehouse PL, Bentley MJ, Le Brocq AM (2012) A deglacial model for Antarctica; geological constraints and glaciological modeling as a bias for a new model of Antarctic glacial isostatic adjustment. *Quaternary Science Reviews,* **32**: 1-24.

Wu X, Heflin MB, Schotman H, Vermeersen BLA, Dong D, Gross RS, Ivins ER, Moore AW, Owen SE (2010) Simultaneous estimation of global present-day transport and glacial isostatic adjustment. *Nature Geoscience,* **3**: 642-646.

Wright HE (1967) A square-rod piston sampler for lake sediments. *J Sed Pet,* **37**: 975-976.

Yamane M, Yokoyama Y, Miura H, Maemoku H, Iwasaki S, Matsuzaki H (2011) The last deglacial history of Lützow Holm Bay, East Antarctica. *Journal of Quaternary Science,* **26(1)**: 3-6.

Yokoyama Y, De Deckker P, Lambeck K, Johnston P, Fifield LK (2001) Sea-level at the Last Glacial Maximum: evidence from northwestern Australia to constrain ice volumes for oxygen isotope stage 2. *Palaeogeography, Palaeoclimatology, Palaeoecology,* **165**: 281-297.

Yoshida Y, and Moriwaki K (1979) Some consideration on elevated coastal features and their dates around Syowa Station, Antarctica. *Memoirs of National Institute of Polar Research. Special Issue*, **13**: 220-226.

Zwartz PD, Miura H, Takada M, Moriwaki K (1998) Holocene lake sediments and sea-level change at Mt. Riiser-Larsen. *Polar Geosci,* **11**: 249-259.

Supplementary material

Table S1. Conventional and calibrated radiocarbon dates of the raised beach data. Dates were corrected for the marine reservoir effect (1120 years; Yoshida & Moriwaki 1979). CRA = Conventional Radiocarbon Age.

Sample Code	Description	CRA	Corr. error	Upper cal. range BP	Lower cal. range BP
SK1	Skarvsnes	2540	412	1836	945
SK2	Skarvsnes	3180	564	2767	1443
SK3	Skarvsnes	3370	354	2752	1912
SK4	Skarvsnes	3370	295	2715	1990
SK5	Skarvsnes	3570	322	2969	2168
SK6	Skarvsnes	3870	316	3367	2595
SK7	Skarvsnes	4060	286	3527	2824
SK8	Skarvsnes	4260	286	3807	3070
SK9	Skarvsnes	4380	279	3935	3245
SK10	Skarvsnes	4400	295	3980	3243
SK11	Skarvsnes	4430	316	4061	3265
SK12	Skarvsnes	4430	286	4020	3305
SK13	Skarvsnes	4560	286	4188	3435
SK14	Skarvsnes	4670	286	4350	3575
SK15	Skarvsnes	4690	295	4387	3598
SK16	Skarvsnes	4700	328	4421	3556
SK17	Skarvsnes	4860	286	4601	3814
SK18	Skarvsnes	4870	300	4641	3808
SK19	Skarvsnes	4910	279	4653	3877
SK20	Skarvsnes	4960	328	4793	3913
SK21	Skarvsnes	4970	305	4788	3956
SK22	Skarvsnes	4970	295	4780	3967
SK23	Skarvsnes	5130	322	4974	4108
SK24	Skarvsnes	5190	286	5020	4247
SK25	Skarvsnes	5290	295	5217	4404
SK26	Skarvsnes	5370	412	5437	4366
SK27	Skarvsnes	5460	286	5389	4619
SK28	Skarvsnes	5580	444	5647	4564
SK29	Skarvsnes	5640	354	5623	4803
SK30	Skarvsnes	5720	341	5679	4862
SK31	Skarvsnes	5860	428	5945	4916
SK32	Skarvsnes	5870	494	6026	4848
SK33	Skarvsnes	6090	316	6146	5422
SK34	Skarvsnes	6090	354	5336	5334
SK35	Skarvsnes	6140	354	6209	5433
SK36	Skarvsnes	6180	581	5155	5135
SK37	Skarvsnes	6630	528	6930	5733
SK38	Skarvsnes	6700	444	6911	5909
SK39	Skarvsnes	7170	286	7262	6611
SK40	Skarvsnes	7680	564	7996	6844
SK41	Skarvsnes	7830	617	8209	6951
SK42	Skarvsnes	7950	279	7958	7451
SK43	Skarvsnes	8130	477	8345	7446

SK44	Skarvsnes	8440	382	8581	7785
SK45	Skarvsnes	8860	412	9194	8191
SK46	Skarvsnes	4990	272	4782	4019
SK47	Skarvsnes	4320	272	3854	3175
SK48	Skarvsnes	6390	272	6348	5748
SKL1	Skallen & skallevikhalsen	3240	279	2572	1835
SKL2	Skallen & skallevikhalsen	3290	286	2658	1910
SKL3	Skallen & skallevikhalsen	3790	444	3387	2317
SKL4	Skallen & skallevikhalsen	3180	316	2522	1707
SKL5	Skallen & skallevikhalsen	3930	295	3375	2712
SKL6	Skallen & skallevikhalsen	7810	368	7928	7249
SKL7	Skallen & skallevikhalsen	4720	316	4429	3590
LA1	Langhovde	3480	295	2820	2114
LA2	Langhovde	4040	286	3480	2786
LA3	Langhovde	3960	286	3386	2737
LA4	Langhovde	4300	286	3851	3126
LA5	Langhovde	3660	328	3125	2303
LA6	Langhovde	4000	316	3466	2739
LA7	Langhovde	6440	382	6534	5688
LA8	Langhovde	5370	295	5287	4501
LA9	Langhovde	3730	511	3394	2146
LA10	Langhovde	4540	766	4794	2856
LA11	Langhovde	4640	316	4349	3502
LA12	Langhovde	4920	286	4692	3884
LA13	Langhovde	6070	295	6092	5411
LA14	Langhovde	2000	511	1349	408
LA15	Langhovde	4570	412	4383	3335
LA16	Langhovde	6040	354	6099	5299
LA17	Langhovde	5160	328	5033	4140
LA18	Langhovde	4090	272	3546	2865
LA19	Langhovde	4220	295	3756	2988
LA20	Langhovde	4350	272	3885	3213
LA21	Langhovde	4570	354	4290	3375
LA22	Langhovde	6810	286	6858	6228
LA23	Langhovde	4280	316	3861	3051
LA24	Langhovde	3860	295	2631	2610
LA25	Langhovde	10250	494	11074	9740
LA26	Langhovde	5330	361	5307	4362
LA27	Langhovde	3870	286	3340	2664
LA28	Langhovde	3930	286	3363	2720
LA29	Langhovde	4010	272	3430	2784
LA30	Langhovde	4050	305	3525	2789
LA31	Langhovde	4060	279	3517	2829
LA32	Langhovde	5070	286	4837	4092
LA33	Langhovde	5250	316	5204	4315
LA34	Langhovde	3305	368	2720	1840
LA35	Langhovde	3220	295	2573	1800
LA36	Langhovde	3120	341	2461	1607
LA37	Langhovde	5450	295	5361	4587
LA38	Langhovde	5070	328	4886	4013
LA39	Langhovde	4090	305	3582	2831
LA40	Langhovde	4360	295	3938	3199
LA41	Langhovde	3990	272	3401	2764

LA42	Langhovde	5540	305	4753	4717
LA43	Langhovde	4290	316	3870	3062
LA44	Langhovde	3320	295	2685	1936
LA45	Langhovde	4460	316	4098	3303
LA46	Langhovde	4350	295	3924	3184
LA47	Langhovde	4850	286	4588	3801
LA48	Langhovde	4900	286	4651	3853
LA49	Langhovde	4920	286	4692	3884
LA50	Langhovde	5000	279	4021	4020
LA51	Langhovde	5070	279	4834	4108
LA52	Langhovde	5270	286	5142	4390
LA53	Langhovde	6650	295	6669	5997
LA54	Langhovde	6810	286	6858	6228
LA55	Langhovde	6140	316	6167	5470
LA56	Langhovde	4240	295	3798	3031
LA57	Langhovde	7720	354	7835	7161
LA58	Langhovde	3170	295	2465	1720
LA59	Langhovde	3440	279	2755	2090
LA60	Langhovde	3890	279	3333	2697
LA61	Langhovde	4180	279	3674	2960
LA62	Langhovde	4780	286	4479	3705
LA63	Langhovde	5820	305	5800	5031
OI2	Ongul Islands	1450	341	27	1
OI3	Ongul Islands	2040	316	1214	606
OI4	Ongul Islands	2510	341	1717	971
OI5	Ongul Islands	3330	305	2696	1937
OI6	Ongul Islands	3340	316	2709	1935
OI7	Ongul Islands	3540	316	2919	2147
OI8	Ongul Islands	3590	279	2954	2284
OI9	Ongul Islands	3840	341	3345	2491
OI10	Ongul Islands	3920	286	3357	2713
OI11	Ongul Islands	4230	305	3780	2997
OI12	Ongul Islands	4800	279	4502	3745
OI13	Ongul Islands	5850	328	5860	5052
OI14	Ongul Islands	10590	412	11228	10286

Chapter 7: General discussion

In this thesis, Holocene environmental changes recorded in the sediments of four isolation lakes and three glacial basins in Lützow Holm Bay (East Antarctica; EA) are described with the overall aim to infer common patterns of internal and external forcing and palaeoenvironmental changes. Prior to this study, very few palaeolimnological studies were available for this region. As such, this study contributes to expanding our understanding of the poorly known Holocene environmental history of East Antarctic terrestrial environments. In addition, our record of radiocarbon-dated transitions from marine to lacustrine sediments in the isolation lakes adds much needed new data to results obtained from marine fossils in raised beaches in the region and allows to better constrain the Holocene history of relative sea-level (RSL) change of this understudied region. From a biogeographical perspective, this work adds new distributional and ecological data of lacustrine diatoms, which will lead to a better understanding of colonisation-extinction dynamics and the evolutionary history of Antarctic diatom floras (Vyverman et al. 2010; Verleyen et al. in prep.).

Proxy-based reconstructions, dating of past climate changes and delineating marine and freshwater sediments

The interpretation of Antarctic lake sediment records requires a careful evaluation of potential pitfalls associated with dating and some of the proxies used to infer environmental change, including inferences of past lake water specific conductance and productivity.

With respect to dating, low dating resolution and dating errors due to the presence of old carbon (the so-called reservoir effect) can obviously influence the reliability of inferences with respect to the timing of past events. Apart from the sediment cores from Ura Ike and Higashi Ike, which were mainly used for estimating the minimum age of deglaciation of West Ongul Island (Chapters 4 and 6), the dating resolution of the cores in the present study was relatively high compared with other lacustrine records in Antarctica. In particular around marine-lacustrine transitions the dating effort was high, enabling a relatively reliable reconstruction of RSL changes. In the case of non-sequential dates, additional datings were carried out. In general, age-depth models have been created using the CLAM software (Blaauw 2010). However, as the Kobachi Ike sediments (Chapter 5) appeared to be more challenging, the more advanced, robust and flexible numerical methods behind the Bayesian BACON software were applied. A well-known pitfall might be the presence of a reservoir effect in the marine sediments. Upwelling of old bottom water in the Southern Ocean along with the relative short residence time of surface waters, results in the highest surface-water reservoir ages of all oceans (Key 2004; Ritz et al. 2008; Hall et al. 2010). Although it has been argued to be relatively constant over the past 6 ka (Hall et al. 2010), there is evidence that this reservoir age may have changed over time (Ritz et al. 2008) and can vary regionally

because of regional differences in the upwelling of deep water around the continent (Berkman et al. 1998). In general, the marine reservoir effect has been estimated to be 1300 years in the Southern Ocean (Berkman & Forman 1996). We applied a local reservoir age of 1120 years on marine radiocarbon dates, following Yoshida & Moriwaki (1979) who radiocarbon-dated recent marine specimens near Syowa Station (East Ongul Island). For the lacustrine sediments, dating of the surface sediments revealed that the lakes are in (near) equilibrium with the atmospheric ^{14}C concentration. This was similarly observed in lakes in for example the Larsemann Hills (Hodgson et al. 2001) and the Antarctic Peninsula (AP) (Sterken et al. 2012), because these coastal water bodies are seasonally ice-free (Kimura et al. 2010), thus allowing sufficient CO_2-exchange between the lake-water and the atmosphere. At or shortly after the time of isolation, lake water salinity is relatively high. Saline and brackish lakes have a less extensive ice cover during winter compared with freshwater lakes (Kimura et al. 2010). There is thus no reason to assume a reservoir effect throughout the lacustrine parts of the sediments, including after lake isolation. In Kobachi Ike (Chapter 5), it is possible that a terrestrial carbon influence between 260 and 230 cm resulted in younger ages, as indicated by an increased $C_{organic}/N_{total}$ ratio, which might have originated from the in-wash of terrestrial mosses. For these samples, we did not apply the marine reservoir age. A problem we did encounter was the presence of age reversals in the cores from Mago Ike (Chapter 3), and Ô-Ike (Chapter 4). Reworking of sediments due to wind-induced mixing in lakes or bioturbation in the marine environment, might cause such age reversals. Only in Mago Ike, lithological descriptions revealed sediment disturbances (237-208 cm; Chapter 3). The impact of these age reversals on core interpretation was however minor, because they were identified as outliers before age-depth modelling, and generally confined to zones for which sufficient ^{14}C dates above and below the outliers were available. Therefore, we believe that the age-depth models used for palaeoclimate reconstructions and the reconstruction of the RSL curve are relatively robust.

The quantitative inference of past specific conductance in a number of cores studied here is based on a newly constructed diatom-based transfer function for the Lützow Holm Bay region. In the majority of the cores, modern species analogues are present for fossil assemblages, which add robustness to the specific conductance reconstructions from these fossil assemblages (Fritz et al. 1999). However, a few exceptions occurred. In the sediment cores of Nishi Ike and Yumi Ike (Chapter 4), *Diadesmis gallica* occurred, whereas this species is absent in the diatom surface dataset. Except for one sample in Yumi Ike and one sample in Nishi Ike which are regarded as less reliable, the relative abundance of this species was rather low (maximum 9.7%) and this species only occurred in a limited number of samples, therefore we believe that the specific conductance reconstruction from these lake is relatively unaffected (Ampel et al. 2010). In the transition zone of Yumi Ike, inferred specific conductance exceeded the range used in the dataset to construct the transfer function (0.014 - 5.056 mS/cm), suggesting that the exact specific conductance value is uncertain here and only indicating

brackish-water conditions. For Kobachi Ike (Chapter 5), we were unable to reconstruct specific conductance. Even though it is rather unusual for a lake located at 28 m above sea-level (a.s.l.), it has a high specific conductance (11.4 mS/cm), whereas the surface dataset only contains a low number of brackish-water and saline lakes; 19 out of the 27 lakes have a specific conductance below 1.5 mS/cm (Chapter 3 and Appendix 1). This prevented us from performing a specific conductance reconstruction for this lake. Combining our calibration dataset with those from other regions in EA containing a higher number of brackish and saline lakes was also not possible due to the significant differences in the composition of regional diatom floras in different oases. This prevented the construction of an East Antarctic transfer function or the application of other regional inference models for salinity as for example developed in Verleyen et al. (2003).

These differences in regional diatom community structure are however interesting from a biogeographical point of view. The most abundant diatom species in Syowa Oasis, such as *Halamphora veneta, Diadesmis australis,* and *Craticula antarctica* are also present in other East Antarctic oases. However some species dominating freshwater lakes in for example the Larsemann Hills (Sabbe et al. 2003) and Vestfold Hills (e.g. *Stauroforma inermis* and *Psammothidium abundance*) are apparently absent in Syowa Oasis (Gibson et al. 2006). This is possibly related to differences in the glacial history. While regions in Lützow Holm Bay were likely covered by ice during the Last Glacial Maximum (LGM) (see Chapters 4, 5 and 6), parts of the Larsemann Hills and Vestfold Hills remained ice-free (Mackintosh et al. 2013). This has probably led to the survival of species in the Prydz Bay region (Larsemann Hills) while they became locally extinct in other East Antarctic oases. Hence, those regions that escaped glacial overriding may have acted as glacial refugia for some diatom species as well as for invertebrates (Cromer et al. 2006). It remains to be seen whether these differences in diatom diversity and composition have had an effect on the ecological tolerances and optima of the species shared by the different regions. Although these findings are very interesting from a biological point of view (i.e., the effect of biotic interactions on niche width), it also highlights the necessity to develop regional calibration datasets.

In several cores we combined different proxies to reconstruct past lake (and catchment) productivity. In a given Antarctic lake, primary production is typically directly related to surface air temperature (Doran et al. 2002; Quayle et al. 2002). A higher surface air temperature leads to an increased water temperature and a subsequent increase in the number of ice-free days, which in turn promotes primary production. The run-off by meltwater, thawing of exposed catchment areas, and development of mosses and benthic microbial-mats in them may also increase nutrient availability (Quayle et al. 2002). We reconstructed past lake primary production using a combination of proxies, including organic matter [total carbon (TC), total organic carbon (TOC), and total nitrogen (TN)], absolute diatom abundance and fossil pigments (total chlorophylls and carotenoids). Care should be taken to use TC as a palaeoproductivity indicator as carbonates (i.e. inorganic carbon; TIC) can accumulate in both marine and lacustrine

sediments. Analyses of TC and TOC indicated that only the Kobachi Ike sediments contained significant amounts of TIC. Therefore, in the other lakes, TC was cautiously used as a primary productivity indicator, however in combination with sedimentary pigments, which are routinely used to reconstruct past changes in primary production in Antarctic lake sediments (e.g. Sterken et al. 2012), as well as in Arctic regions (e.g. Antoniades et al. 2007). TN in Antarctic lake sediments was used to reconstruct the abundance of nitrogen-fixing cyanobacteria (cf. Wagner et al. 2004), which are among the dominant organisms in the benthic microbial-mats in these lakes. The total diatom concentration enabled the reconstruction of this component of the autotrophic communities. For all these proxies, fluxes were calculated by taking into account the mass accumulation rate (MAR) of the sediments. This approach was used to calculate the influence of variable sedimentation rates (SRs) and large changes in the proportion of organic, siliciclastic and biogenic components (Street-Perrot et al. 2007) on the proxies for primary production. However, a drawback of this approach is that proxies are made strongly dependent of the age-depth model used which might be problematic in the case of the presence of a significant number of outliers, age reversals, and erroneous ^{14}C ages. In most cores studied here, the different proxies reacted more or less simultaneously in the lacustrine sediments, lending support to our hypotheses of temperature-driven changes in lake primary production. For example, on West Ongul island fluxes of total chlorophylls and carotenoids peaked in the Ô-Ike sediment core between c. 2230 and 2090 cal. yr BP, which falls within a period (c. 2970 - 2010 cal. yr BP) when the TC flux was similarly high (Chapter 4). A notable exception was the core from Kobachi Ike where the diatom flux was low in the lacustrine sediments while fluxes of TOC, TN, chlorophylls and carotenoids were more variable and showed maxima at certain depths (Chapter 5). This might be related to the dominance of cyanobacteria and possibly chlorophytes over diatoms in this brackish lake. By contrast, diatoms are important primary producers in the Southern Ocean leading to high fluxes of diatom abundance in the marine parts of the core. Likewise, the relatively high diatom production observed in the Ô-Ike sediment cores from c. 350 cal. yr BP onwards up to present is not reflected in the fluxes of total chlorophylls and carotenoids (Chapter 4). This might be related to an increase in planktonic primary production in response to climate warming, but this hypothesis is far from certain.

A key set of results of this study concerns the identification and dating of marine-freshwater transitions, which were identified from a combination of proxies. Diatom species composition and fossil pigments, together with mass-specific MS, gamma ray density (GRD), and lithological changes were the main proxies used to define these transitions in Mago Ike (Chapter 3), Yumi Ike and Ô-Ike (Chapter 4). Identification of the transition zone was relatively straightforward in the former lakes as a result of large differences in the composition of microfossils and pigments between marine and lacustrine sediments. By contrast, this was not the case in Kobachi Ike (Chapters 5 and 6) because the lake was not immediately flushed after isolation and remained brackish

during the past c. 3670 years. This resulted in the survival of marine diatoms such as *Chaetoceros* resting spores and *Fragilariopsis* species and hence small and gradual changes in diatom community structure. As a result, the identification of the lacustrine zone was mainly based on changes in sedimentological properties and the pigment composition. More in particular, Kobachi Ike was considered fully isolated when mass-specific MS started to decrease and myxoxanthophyll, a cyanobacteria-specific marker pigment appeared. Alternatively, if the transition zone would be situated at c. 4030 cal. yr BP when the abundance of the brackish water diatoms *Navicula phyllepta* and *Craspedostauros laevissimus* started to increase, RSL fall would have been less steep (12.1 instead of 14.5 mm/yr) between the isolation event and 1905 cal. yr BP.

Deglaciation history of the Lützow Holm Bay region

Our multi-proxy evidence suggests that both West Ongul Island and Skarvsnes became ice-free during the Holocene, although not simultaneously. The oldest radiocarbon date retrieved from Nishi Ike (Chapters 4 and 6) along with the transition of glacial sediments to relatively organic-rich sediments around c. 11,240 cal. yr BP, indicates that West Ongul Island was ice-covered during the LGM and deglaciated during the Early-Holocene. This is in agreement with several other East Antarctic regions, such as the Rauer Islands (Berg et al. 2010) and the Windmill Islands (Kirkup et al. 2002). However, it was previously suggested that this part of Lützow Holm Bay was free of ice during the LGM, based on intact, fragile shells of *Laternula elliptica* found on West Ongul Island which predate the LGM (Miura et al. 1998; Takada et al. 2003). Therefore it might be possible that the Ongul Islands were covered by extensive blankets of snow during the LGM, leading to the lack of biogenic sedimentation and a large gap between the timing of deglaciation and the actual onset of lake primary production. This is a common problem when using ^{14}C but also cosmogenic isotopes to determine the exact age of ice-sheet retreat (Gore 1997). Both islands might have remained ice-free during the LGM if the glacier flowed through the Fuji Submarine Valley, a trough located between the Ongul Islands and the Prince Olav Coast, and diverted around the Ongul Islands. Another hypothesis is that both East and West Ongul Island were ice-covered during the LGM, but that the *L. elliptica* shells were preserved under a more or less inactive and non-erosive glacier. However, given the fragile nature of these shells and the original feeding position they were preserved in, the latter hypothesis can be considered less likely (Mackintosh et al. 2013). Together, this implies that further geomorphological research and radiometric dating [^{14}C, optically stimulated luminescence dating (OSL) and cosmogenic isotopes] of both lake sediments and landforms is required to obtain a better insight into the deglaciation history of the Ongul Islands and Lützow Holm Bay in general.

The deglaciation history of nearby Skarvsnes seems far less complex and occurred around c. 7240 cal. yr BP, as indicated by the oldest radiocarbon date of Kobachi Ike (Chapters 5 and 6). This is in agreement both with dates from raised beaches (Miura et al. 1998) and cosmogenic isotope dating placing the exposure of Mount Suribati, in the

vicinity of Kobachi Ike between c. 8.66 and 6.42 ka BP (Yamane et al. 2011). Skarvsnes appears to have become ice-free slightly later than most other East Antarctic regions where recession of the ice was well underway by the beginning of the Holocene (Hall 2009), although a multi-stage deglaciation pattern can be observed, as some regions only became ice-free as late as the Mid-Holocene (Hodgson et al. 2001). This is similar as in the Northern Hemisphere (NH), where large parts of the ice-sheets started to melt shortly after the LGM and continued to disintegrate in multiple stages until the Late-Holocene (Siegert et al. 2001). In Lützow Holm Bay, this might be related to geomorphological differences of offshore glacial troughs, but marine geological surveys are required to gain more insight into this matter.

Palaeoclimate changes in Lützow Holm Bay during the Mid- to Late-Holocene

There is no evidence for the occurrence of an Early-Holocene Climate optimum (EHCO) on West Ongul Island and Skarvsnes because both regions were then still ice- or snow-covered (see Fig. 1 for an overview figure of inferred climate changes). During the Early-Holocene, the glacial lakes on West Ongul Island were covered by snow or ice (Chapter 4), and near Kobachi Ike on Skarvsnes the period between c. 7240 and 4580 cal. yr BP was characterised by low primary productivity. Between c. 4580 and 4450 cal. yr BP, the presence of an unknown *Navicula* species might indicate that the site was possibly a shallow marine lagoon and only suitable for a limited number of diatom species. In the isolation lakes on West Ongul Island, diatoms thriving in sea-ice and under seasonally stratified conditions were present between c. 6530 and 5000 cal. yr BP. These conditions also prevail today around the islands. Around Skarvsnes, a more diverse diatom community indicated more open-water conditions and the seasonal presence of sea-ice from c. 4450 until 3670 cal. yr BP. In most marine records around Antarctica a warmer period is observed between c. 7.7 and 4 ka BP (Crosta et al. 2008). This marine optimum appeared to be out-of-phase with records on land, or even coincided with cool and dry conditions inferred from lake sediments (Verleyen et al. 2011 in Appendix 2), and with a cooling trend observed in ice cores (Stenni et al. 2010). The disparity between these records might reflect differences in heat capacity between the ocean and the continent (Renssen et al. 2005) and the hypothesis that marine algal assemblages reflect spring, summer and autumn conditions, whereas lacustrine assemblages largely reflect summer conditions, and ice cores reflect winter conditions (Bentley et al. 2008; Hodgson & Smol 2008). However, the latter hypothesis might not entirely be true as it has been shown that lake water column primary production may also occur during spring and autumn, under dim conditions and lake ice cover (Tanabe et al. 2008).

Between c. 4170 and 940 cal. yr BP, a climate optimum could be inferred based on increased fluxes in primary productivity proxies, changes in the moisture balance of the lakes (Chapter 4) and a change in sedimentary properties in Kobacki Ike (Chapter 5). Primary production increased in Nishi Ike and started in Higashi Ike (Chapter 4). These

warmer conditions culminated between c. 2230 and 2090 cal. yr BP, as indicated by a higher accumulation of total carotenoids and chlorophylls in Ô-Ike, overlapping with higher inferred primary production in Yumi Ike (Chapter 4). Reconstructed specific conductance in Nishi Ike was relatively lower during that period, suggesting increased snow melt and hence more diluted lake conditions. Similar observations have been made on Skarvsnes, where Kobachi Ike sediments recorded a decrease in mass-specific MS, a marked change in lithology and an increase in brackish-water diatoms from c. 2010 cal. yr BP onwards (Chapter 5). This was likely related to the disappearance of multi-year snow banks, resulting in a decreased inflow of meltwater and terrigenous material into the lake. This was evidenced by the presence of finer sand, clay and silt in the sediments. The presence of a Mid- to Late-Holocene warm period is in accordance with other East Antarctic lake records, in which it was roughly identified between c. 4.7 and 1 ka BP (Verleyen et al. 2011 in Appendix 2). It was however not pronounced in marine and ice cores, which generally display a Neoglacial cooling from c. 4 ka onwards (Divine et al. 2010).

The period after the Mid- to Late-Holocene warm period, from c. 940 cal. yr BP onwards, can be carefully linked to a Neoglacial cooling. Primary productivity indicators decrease from then onwards in the lakes, and inferred specific conductance stabilises or even increases in the closed basins, possibly related to a lower amount of meltwater entering the lakes (Chapter 4). In the Kobachi Ike sediments, TOC flux slightly decreases from c. 1200 cal. yr BP onwards (Chapter 5). However in the Mago Ike sediments increased primary production was suggested by increased fluxes in chlorophylls, carotenoids, diatoms, TC, and TN between c. 490 and 440 cal. yr BP (Chapter 3). Neoglacial cooling in Lützow Holm Bay is similar to most other East Antarctic regions where distinct colder and/or drier conditions were inferred (Verleyen et al. 2004; 2011 in Appendix 2; Wagner et al. 2004). In contrast to the NH, which is characterised by the occurrence of a Medieval Climate Anomaly (MCA; 1050 - 650 yr BP), Little Ice Age (LIA; 500 - 100 yr BP) and the recent temperature increase (Twentieth-Century Warming, TCW) (Mann et al. 2009), there is no evidence from our lake sediment records for events coeval with these anomalies. This is consistent with the vast majority of the other lake records (Verleyen et al. 2011 in Appendix 2) as well as with ice cores from EA (Goosse et al. 2012).

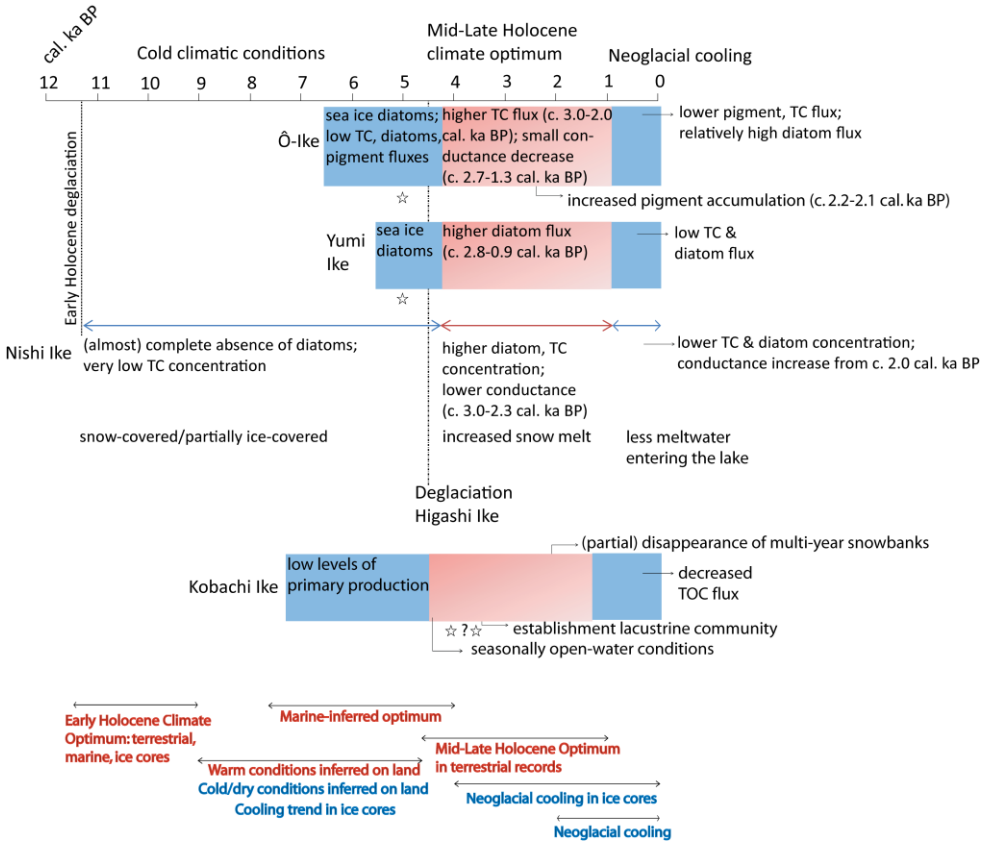

Figure 1. Overview figure of inferred climate changes in West Ongul Island and Skarvsnes during the Holocene, along with a general overview of the literature (see Verleyen et al. 2011 in Appendix 2 and this chapter for detailed references). Red = warm inferred conditions, blue = cold inferred conditions. Star indicates the isolation of the lake (with two possibilities for Kobachi Ike - see Chapters 5 and 6 for a detailed explanation).

Holocene relative sea-level changes in Lützow Holm Bay

We extended an existing RSL curve, which was solely based on marine terraces from Nakada et al. (2000), with published (Takano et al. 2012) and new data from isolation lakes. We obtained a complex RSL history for Lützow Holm Bay, with regional differences in the uplift rate and maximum sea-level high stand, which is likely related to the interplay between glacial isostatic adjustment (GIA) and local neotectonic faulting on Skarvsnes (Chapter 6). Skallen and West Ongul Island experienced a more or less similar RSL history during the Holocene. The upper marine limit in the Ongul Islands and in Skallen agrees well with previous estimates based on fossils from marine terraces (Miura et al. 1998). In Skarvsnes however, the marine limit appears to have been 12 m higher than previous estimates based on raised beach data (Miura et al. 1998) and up to 15 m higher compared to the Ongul Islands. During the Mid- to Late-Holocene, the uplift rate in Skarvsnes was about 10 times higher than the estimated rate during the past 1 ka in all three study regions. On the other hand, the uplift in the Ongul Islands and Skallen appears to have been similar during the Mid- and Late-Holocene. Given the small distance (c. 60 km) between the different sites, the uplift rate in Skarvsnes is more likely related to neotectonic processes (Glenn A. Milne & Mike J. Bentley, pers. comm.). A fault system separating the eastern from the western peninsula of Skarvsnes (Ishikawa et al. 1976) became probably active during the Holocene, possibly triggered by ice-sheet disintegration and the related vertical movement of landmasses. Generally, neotectonic events are considered to be of minor importance in EA, where RSL changes are attributed to eustatic sea-level rise and regional GIA (Stewart et al. 2000). However it has been shown that post-glacial faulting can have a profound influence on RSL changes (Watcham et al. 2011) as has been seen in closely-located regions in Sweden (Risberg et al. 2005), the Strait of Magellan and southern Tierra del Fuego (Bentley & McCulloch 2005), and now probably also in Skarvsnes. This might complicate the use of RSL from this part of EA in validating the numerical ice-sheet models which are used to predict past and future ice-sheet dynamics (Watcham et al. 2011).

Besides these regional differences, the RSL curves from Lützow Holm Bay are also different from those in other East Antarctic regions. In the Larsemann Hills (Verleyen et al. 2005) and Vestfold Hills (Zwartz et al. 1998), sea-level reached a maximum between c. 8 and 6 cal. ka BP, after which RSL fall occurred due to outpacing of the eustatic component by isostatic uplift, whereas in Skarvsnes, sea-level remained at its maximum (32.7 m) at least until c. 4.8 cal. ka BP. These differences are likely related to a relatively recent deglaciation and/or a larger difference in ice-sheet loss in the Lützow Holm Bay region in combination with neotectonics.

Future perspectives

This thesis highlights at least four main lines of potential future research. First, despite several recent studies, high-resolution climate records from the Southern Hemisphere (SH) high-latitudes remain still relatively rare (Mann et al. 2009). Additional records are required to further document and understand regional climate anomalies and the apparent disparity between marine and terrestrial records, and to be able to assess current regional temperature trends observed in the Antarctic in a temporal context (Verleyen et al. 2011 in Appendix 2). This may enable us to better understand the mechanisms behind Holocene climate variability. Although terrestrial archives are present in the ice-free regions of Dronning Maud Land and Enderby Land, a vast sector between 0° and 60°E, very little is known about this area, both in terms of Holocene climate evolution (Verleyen et al. 2011 in Appendix 2) and ice-sheet fluctuations (Mackintosh et al. 2013). Therefore, this study on Lützow Holm Bay, between 35° and 40°E is a first contribution to this gap in our knowledge and highlights the potential of similar regions such as Schirmacher Oasis and the Thalla Hills for palaeolimnological research. Furthermore, also Terre Adélie, between 120° and 150°E remains largely understudied in terms of palaeoclimate changes, with the accompanied problem of the general lack of ice-free land there, leaving shallow marine sediment cores as the only alternative (Verleyen et al. 2011 in Appendix 2). In the future, palaeoclimate studies and studies on ice-sheet dynamics should thus focus on these regions.

Second, the inconclusive deglaciation history of the Ongul Islands requires further radiometric dating (radiocarbon dating, OSL, and cosmogenic isotopes) in combination with geomorphological research. It has been shown that blankets of ice and snow can limit biogenic sedimentation, leading to a hiatus between deglaciation and the actual onset of primary production. As a result, radiocarbon dating of lake sediment cores can only provide a minimum age of deglaciation (Gore 1997). To this end, cosmogenic-exposure age dating, as for instance in Skarvsnes (Yamane et al. 2011) of erratics on hill tops that emerge first from the continental ice is highly recommended (Gore 1997) and might provide additional information on the deglaciation history of East and West Ongul Island. Furthermore, multibeam swath bathymetry and side-scan sonar would be useful in Lützow Holm Bay, and can provide evidence for ice-sheet grounding and flow direction (Shipp et al. 1999; Mosola & Anderson 2006).

Third, as estimates of the contribution of different ice masses to global sea-level rise during Termination I and the Holocene still contain much uncertainty, numerical models need to be validated against precise RSL data (Watcham et al. 2011). This is also the case in Lützow Holm Bay, where a previous study revealed that the models available at that time underestimated the ice-sheet volume during the Last Glacial Maximum (LGM) (Bassett et al. 2007). It remains to be seen whether the most recent models are in agreement with our observations from Lützow Holm Bay and are able to predict the relatively recent deglaciation of Skarvsnes and generate the relative sea-level (RSL) curves

for the different regions. One potential problem in this comparison might be the neotectonic activity in Skarvsnes. Additional sediment cores from isolation lakes situated to the northwestern side of the fault can potentially enable us to better study the influence of neotectonics on RSL changes during the Holocene.

Fourth, as polar lakes are regarded as the 'canaries in the coalmine' because they respond quickly to climate-induced changes (Hodgson & Smol 2008), long-term monitoring in combination with meteorological data will help us understand the ecological implications of future climate anomalies (Verleyen et al. 2012 in Appendix 1). In addition, limnological research of climate-sensitive lakes will also help to refine existing proxies used to reconstruct past productivity and community-level responses to climate-driven environmental change. Good candidate lakes for such studies would have a medium to high salinity and a high surface-area to lake-depth ratio in which meteoric water is the only moisture source as they are very sensitive to changes in snow accumulation in the catchment and in the regional precipitation-evaporation balance (Verleyen et al. 2012 in Appendix 1). Suribati Ike in Lützow Holm Bay is in this respect a suitable candidate (Verleyen et al. 2012 in Appendix 2).

References

Ampel L, Bigler C, Wohlfarth B, Risberg J, Lotter AF, Veres D (2010) Modest summer temperature variability during DO cycles in western Europe. *Quaternary Science Reviews,* **29**: 1322-1327.

Antoniades D, Crawley C, Douglas MSV, Pienitz R, Anderson D, Doran PT, Hawes I, Pollard W, Vincent WF (2007) Abrupt environmental change in Canada's northernmost lake inferred from fossil diatom and pigment stratigraphy. *Geophysical Research Letters,* DOI: 10.1029/2007GL030947.

Bassett SE, Milne GA, Bentley MJ, Huybrechts P (2007) Modelling Antarctic sea-level data to explore the possibility of a dominant Antarctic contribution to meltwater pulse IA. *Quaternary Science Revieuws,* **26**: 2113-2127.

Bentley MJ, and McCulloch (2005) Impact of neotectonics on the record of glacier and sea level fluctuations, Strait of Magellan, southern Chile. *Geografiska Annaler,* **87A**: 393-402.

Bentley MJ, Hodgson DA, Smith JA, Cofaigh CO, Domack EW, Larter RD, Roberts SJ, Brachfeld S, Leventer A, Hjort C, Hillenbrand C-D, Evans J (2008) Mechanisms of Holocene palaeoenvironmental change in the Antarctic Peninsula region. *The Holocene,* **18(8)**: 1-19.

Berg S, Wagner B, Cremer H, Leng MJ, Melles M (2010) Late Quaternary environmental and climate history of Rauer Group, East Antarctica. *Palaeogeography, Palaeoclimatology, Palaeoecology*, **297**: 201-213.

Berkman PA, and Forman SL (1996) Pre-bomb radiocarbon and the reservoir correction for calcarcous marine species in the Southern Ocean. *Geophysical Research Letters,* **23**: 633-636.

Berkman PA, Andrews JT, Bjorck S, Colhoun EA, Emslie SD, Goodwin ID, Hall BL, Hart CP, Hirakawa K, Igarashi A, Ingólfsson O, Lopez-Martinez J, Lyons WB, Mabin MCG, Quilty PG, Taviani M, Yoshida Y (1998) Circum-Antarctic coastal environmental shifts during the Late Quaternary reflected by emerged marine deposits. *Antarctic Science,* **10**: 345-362.

Cromer L, Gibson JAE, Swadling KM, Hodgson DA (2006) Evidence for a lacustrine faunal refuge in the Larsemann Hills, East Antarctica, during the Last Glacial Maximum. *Journal of Biogeography,* **33**: 1314-1323.

Crosta X, Denis D, Ther O (2008) Sea ice seasonality during the Holocene, Adélie Land, East Antarctica. *Marine Micropaleontology,* **66(3-4)**: 222-232.

Divine DV, Koç N, Isaksson E, Nielsen S, Crosta X, Godtliebsen (2010) Holocene Antarctic climate variability from ice and marine sediment cores: Insights on ocean-atmosphere interaction. *Quaternary Science Reviews,* **29**: 303-312.

Doran PT, Priscu JC, Lyons WB, Walsh JE, Fountain AG, McKnight DM, Moorhead DL, Virginia RA, Wall DH, Clow GD, Fritsen CH, McKay CP, Parsons AN (2002) Antarctic climate cooling and terrestrial ecosystem response. *Nature,* **415:** 517-520.

Fritz SC, Cumming BF, Gasse F, Laird KR (1999) Diatoms as indicators of hydrologic and climatic change in saline lakes. *In:* Stoermer EF, and Smol JP (Eds.). The diatom applications for the environmental and earth science. Cambridge university Press. pp. 469.

Gibson JAE, Roberts D, Van de Vijver B (2006) Salinity control of the distribution of diatoms in lakes of the Bunger Hills, East Antarctica. *Polar Biol,* **29**: 694-704.

Goosse H, Braida M, Crosta X, Mairesse A, Masson-Delmotte V, Mathiot P, Neukom R, Oerter H, Philippon G, Renssen H, Stenni B, van Ommen T, Verleyen E (2012) Antarctic temperature changes during the last millennium: evaluation of simulations and reconstructions. *Quaternary Science Reviews,* **55**: 75-90.

Gore DB (1997) Blanketing snow and ice; constraints on radiocarbon dating deglaciation in East Antarctic oases. *Antarctic Science,* **9(3)**: 336-346.

Hall BL (2009) Holocene glacial history of Antarctica and the sub-Antarctic islands. *Quaternary Science Reviews,* **28**: 2213-2230.

Hall BL, Henderson GM, Baroni C, Kellogg TB (2010) Constant Holocene Southern-Ocean ^{14}C reservoir ages and ice-shelf flow rates. *Earth and Planetary Science Letters,* **296**: 115-123.

Hodgson DA, Noon PE, Vyverman W, Bryant CL, Gore DB, Appleby P, Gilmour M, Verleyen E, Sabbe K, Jones VJ, Ellis-Evans JC, Wood PB (2001) Were the Larsemann Hills ice-free through the Last Glacial Maximum? *Antarctic Science,* **13(4)**: 440-454.

Hodgson DA, Smol JP (2008) High latitude palaeolimnology. *In*: Vincent WF, Laybourn-Parry J (Eds.) Polar Lakes and Rivers - Arctic and Antarctic Aquatic Ecosystems. Oxford University Press, Oxford, UK. pp 43-64.

Hu A, Meehl GA, Han W, Yin J (2011) Effect of the potential melting of the Greenland Ice Sheet on the Meridional Overturning Circulation and global climate in the future. *Deep-Sea Research II,* **58**: 1914-1926.

Ishikawa T, Tatsumi K, Kizaki K, Yanai H, Ando T, Kikuchi Y, Yoshida Y (1976) Explanatory text of geological map of Langhovde, Antarctica. *Ant. Geol. Map Ser. Sheet 5, Langhovde, Natl. Inst. Polar Res.* 12.

Key, R.M., 2004. A global ocean carbon climatology: results from the Global Data Analaysis Project (GLODAP). *Global Biogeochemical Cycles,* **18**: doi: 10.1029/2004GB002247.

Kimura S, Ban S, Imura S, Kudoh S, Matsuzaki M (2010) Limnological characteristics of vertical structure in the lakes of Syowa Oasis, East Antarctica. *Polar Science,* **3**: 262-271.

Kirkup H, Melles M, Gore DB (2002) Late Quaternary environment of Southern Windmill Islands, East Antarctica. *Antarct. Sci.,* **14**: 385-394.

Mackintosh AN, Verleyen E, O'Brien PE, White DA, Selwyn Jones R, McKay R, Dunbar R, Gore DB, Fink D, Post AL, Miura H, Leventer A, Goodwin I, Hodgson DA, Lilly K, Crosta X, Golledge NR, Wagner B, Berg S, van Ommen T, Zwartz D, Roberts SJ, Vyverman W, Masse G (2013) Retreat history of the East Antarctic Ice Sheet since the Last Glacial Maximum. *Quaternary Science Reviews*, http://dx.doi.org/10.1016/j.quascirev.2013.07.024.

Mann ME, Zhang ZH, Rutherford S, Bradley RS, Hughes MK, Shindell D, Ammann C, Faluvegi G, Ni FB (2009) Global signatures and dynamical origins of the Little Ice Age and Medieval Climate Anomaly. *Science*, **326**: 1256-1260.

Miura H, Maemoku H, Igarashi A, Moriwaki K (1998) Late Quaternary raised beach deposits and radiocarbon dates of marine fossils around Lützow Holm Bay. *Special map series of National Institute of Polar Research,* **6:** pp. 46.

Mosola AB, and Anderson JB (2006) Expansion and rapid retreat of the West Antarctic Ice Sheet in eastern Ross Sea: possible consequence of over-extended ice streams? *Quaternary Science Reviews,* **25**: 2177-2196.

Nakada M, Kimura R, Okuno J, Moriwaki K, Miura H, Maemoku H (2000) Late Pleistocene and Holocene melting history of the Antarctic ice sheet derived from sea-level variations. *Marine Geology,* **167**: 85-103.

Pfeffer WT, Harper JT, O'Neill S (2008) Kinematic constrains on glacier contributions during the 21st-century sea-level rise. *Science,* **321**: 1340-1343.

Quayle WC, Peck LS, Peat H, Ellis-Evans JC, Harrigan PR (2002) Extreme responses to climate change in Antarctic lakes. *Science,* **295**: 645.

Renssen H, Goosse H, Fichefet T, Masson-Delmotte V, Koc N (2005) Holocene climate evolution in the high-latitude Southern Hemisphere simulated by a coupled atmosphere–sea ice–ocean-vegetation model. *Holocene*, **15 (7)**: 951–964.

Risberg J, Alm G, Goslar T (2005) Variable isostatic uplift patterns during the Holocene in southeast Sweden based on high-resolution AMS radiocarbon datings of lake isolations. *The Holocene,* **15(6)**: 847-857.

Ritz SP, Stocker TF, Müller SA (2008) Modeling the effect of abrupt ocean circulation change on marine reservoir age. *Earth and Planetary Science Letters,* **268**: 202-211.

Sabbe K, Verleyen E, Hodgson DA, Vanhoutte K, Vyverman W (2003) Benthic diatom flora of freshwater and saline lakes in the Larsemann Hills and Rauer Islands, East Antarctica. *Antarct Sci,* **15**: 227-248.

Shipp S, Anderson JB, Domack EW (1999) Seismic signature of the Late Pleistoce fluctuation of the West Antarctic Ice Sheet system in Ross Sea: a new perspective, Part I. *Geological Society of America Bulletin,* **111**: 1486-1516.

Siegert MJ (2001) Ice sheets and late Quaternary environmental change. John Wiley & Sons. 231 pp.

Stenni B, Masson-Delmotte V, Selmo E, Oerter H, Meyer H, Rothlisberger R, Jouzel J, Cattani O, Falourd S, Fischer H, Hoffmann G, Lacumin P, Johnsen SJ, Minster B, Udisti R (2010) The deuterium excess records of EPICA Dome C and Dronning Maud Land ice cores (East Antarctica). *Quatern. Sci. Rev*., **29**: 146–159.

Sterken M, Roberts SJ, Hodgson DA, Vyverman W, Balbo AL, Sabbe K, Moreton SG, Verleyen E (2012) Holocene glacial and climate history of Prince Gustav Channel, northeastern Antarctic Peninsula. *Quaternary Science Reviews,* **31**: 93-111.

Stewart IS, Sauber J, Rose J (2000) Glacio-seismotectonics: ice sheets, crustal deformation and seismicity. *Quaternary Science Reviews,* **19**: 1367-1389.

Street-Perrot FA, Barker PA, Swain DL, Ficken KJ, Wooller MJ, Olago DO, Huang Y (2007) Late Quaternary changes in ecosystems and carbon cycling on Mt. Kenya, East Africa: a landscape-ecological perspective based on multi-proxy lake-sediment fluxes. *Quaternary Science Reviews,* **26**: 1838-1860.

Takada M, Tani A, Miura H, Moriwaki K, Nagatomo T (2003) ESR dating of fossil shells in the Lützow-Holm Bay region, East Antarctica. *Quaternary Science Reviews,* **22**: 1323-1328.

Tanabe Y, Kudoh S, Imura S, Fukuchi M (2008) Phytoplankton blooms under dim and cold conditions in freshwater lakes of East Antarctica. *Polar Biol,* **31**: 199-208.

Takano Y, Tyler JJ, Kojima H, Yokoyama Y, Tanabe Y, Sato T, Ogawa NO, Ohkouchi N, Fukui M (2012) Holocene lake development and glacial-isostatic uplift at Lake Skallen and Lake Oyako, Lützow Holm Bay, East Antarctica, based on biogeochemical facies and molecular signatures. *Applied Geochemistry,* doi: http://dx.doi.org/10.1016/j.apgeochem.2012.08.009

Turner J, Bindschadler R, Convey P, di Prisco G, Fahrbach E, Gutt J, Hodgson D, Mayewski P, Summerhayes C (2009) Antarctic climate change and the Environment. pp 526.

Verleyen E, Hodgson DA, Vyverman W, Roberts D, McMinn A, Vanhoutte K, Sabbe K (2003) Modelling diatom responses to climate induced fluctuations in the moisture balance in continental Antarctic lakes. *J Paleolimnol*, **30**: 195-215.

Verleyen E, Hodgson DA, Sabbe K, Vyverman W (2004) Later Quaternary deglaciation and climate history of the Larsemann Hills (East Antarctica). *Journal of Quaternary Science,* **19(0)**: 1-15.

Verleyen E, Hodgson DA, Milne GA, Sabbe K, Vyverman W (2005) Relative sea-level history from the Lambert glacier region, East Antarctica, and its relation to deglaciation and Holocene glacier readvance. *Quaternary Research,* **63**: 45-52.

Verleyen E, Hodgson DA, Sabbe K, Cremer H, Emslie SD, Gibson J, Hall B, Imura S, Kudoh S, Marshall GJ, McMinn A, Melles M, Newman L, Roberts D, Roberts SJ, Singh SM, Sterken M, Tavernier I, Verkulich S, Van de Vyver E, Van Nieuwenhuyze W, Wagner B, Vyverman W (2011) Post-glacial regional climate variability along the East Antarctic coastal margin - evidence from shallow marine and coastal terrestrial records. *Earth Sci Rev*, **104**: 199-212.

Verleyen E, Hodgson DA, Gibson J, Imura S, Kaup E, Kudoh S, De Wever A, Hoshino T, McMinn A, Obbels D, Roberts D, Roberts SJ, Sabbe K, Souffreau C, Tavernier I, Van Nieuwenhuyze W, Van Ranst E, Vindevogel N, Vyverman W (2012) Chemical limnology in coastal East Antarctic lakes: monitoring future climate change in centres of endemism and biodiversity. *Antarctic Science,***24(1)**: 23-33.

Vyverman W, Verleyen E, Wilmotte A, Hodgson DA, Willems A, Peeters K, Van de Vijver B, De Wever A, Leliaert F, Sabbe K (2010) Evidence for widespread endemism among Antarctic micro-organisms. *Polar Science,* **4(2)**: 103-113.

Wagner B, Cremer H, Hultzsch N, Gore DB, Melles M (2004) Late Pleistocene and Holocene history of Lake Terrasovoje, Amery Oasis, East Antarctica, and its climatic and environmental implications. *J. Paleolimnol.,* **32**: 321-339.

Wanner H, Beer J, Bütikofer J, Crowley TJ, Cubasch U, Flückiger J, Goosse H, Grosjean M, Joos F, Kaplan JO, Küttel M, Müller SA, Prentice IC, Solomina O, Stocker TF, Tarasov P, Wagner M, Widmann M (2008) Mid- to Late Holocene climate change: an overview. *Quaternary Science Reviews,* **27**: 1791-1828.

Watcham EP, Bentley MJ, Hodgson DA, Roberts SJ, Fretwell PT, Lloyd JM, Larter RD, Whitehouse PL, Leng MJ, Monien P, Moreton SG (2011) A new Holocene relative sea-level curve for the South Shetland Islands, Antarctica. *Quaternary Science Reviews,* **30**: 3152-3170.

Yamane M, Yokoyama Y, Miura H, Maemoku H, Iwasaki S, Matsuzaki H (2011) The last deglacial history of Lützow Holm Bay, East Antarctica. *Journal of Quaternary Science,* **26(1)**: 3-6.

Yoshida Y, and Moriwaki K (1979) Some consideration on elevated coastal features and their dates around Syowa Station, Antarctica. *Memoirs of National Institute of Polar Research. Special Issue*, **13**: 220-226.

Zwartz PD, Miura H, Takada M, Moriwaki K (1998) Holocene lake sediments and sea-level change at Mt. Riiser-Larsen. *Polar Geosci,* **11**: 249-259.

Summary

Despite the fact that both Antarctica and the Southern Ocean play a major role in controlling the global climate system (Turner et al. 2009), still relatively few high-resolution climate proxy records have been obtained from the Southern Hemisphere (SH) high latitudes (Mann et al. 2009). Moreover, several vast areas, including Lützow Holm Bay (Hall 2009; Verleyen et al. 2011 in Appendix 2) remain largely understudied. A better knowledge of past climate and ice-sheet fluctuations in East Antarctica (EA) will enable us to understand the mechanisms behind Holocene climate changes and allow us to place recent climate anomalies in a longer-term context.

In this thesis, we analysed biological, geochemical and sedimentological proxies in radiocarbon-dated sediment cores from three glacial and four isolation lakes to infer past climate changes and ice-sheet dynamics in Lützow Holm Bay (EA), between 69 - 70°S and 35 - 40°E. We also developed a regional diatom-based transfer function to reconstruct past changes in lake water specific conductance.

Our multi-proxy evidence suggests that both West Ongul Island and Skarvsnes deglaciated during the Holocene, although not simultaneously. Radiocarbon dates indicate that West Ongul Island deglaciated around 11.2 cal. ka BP. These findings contradict with previous studies which suggested that the islands were ice-free during the Last Glacial Maximum (LGM; Miura et al. 1998). However it is possible that the Ongul Islands were covered by extensive blankets of snow during and after the LGM, leading to a delay in the onset of biogenic sedimentation. Radiocarbon dates from Skarvsnes indicate that the region deglaciated around 7.4 cal. ka BP, which is in agreement with dates from raised beaches (Miura et al. 1998) and cosmogenic isotope dating (Yamane et al. 2011) but slightly later than most other East Antarctic regions (Hall 2009).

Evidence for the occurrence of an Early-Holocene Climate Optimum (EHCO) is lacking from these regions, as they were still snow- or ice-covered. In Skarvsnes, low primary productivity was inferred from marine sediments between 7.4 and 4.6 cal. ka BP. This was followed by a period with increased primary production between c. 4.6 and 3.7 cal. ka BP. Initially, the site was possibly a shallow marine lagoon, only suitable for a limited number of diatom species, after which a more diverse community and seasonally open-water conditions were inferred. Near West Ongul Island, the marine environment was characterised by the presence of diatoms thriving in sea-ice and under seasonally stratified conditions between 6.5 and 5.0 cal. ka BP.

Between 4.2 and 0.9 cal. ka BP, a climate optimum could be inferred, both on West Ongul Island and on Skarvsnes, which culminated between 2230 and 2090 cal. yr BP. In the lakes from West Ongul Island, this was observed as increased primary production and changes in the moisture balance of the lakes, indicating increased snow melt, whereas in Skarvsnes, sedimentological changes could be potentially linked to the disappearance of multi-year snow banks, similarly indicating warmer conditions. The

presence of a Mid- to Late-Holocene warm period is in accordance with other East Antarctic terrestrial records, in which a climate optimum was roughly identified between 4.7 and 1 ka BP (Verleyen et al. 2011 in Appendix 2).

It is likely that Neoglacial cooling occurred from c. 1.2 cal. ka BP onwards, as indicated by decreased primary productivity and stabilised or increased specific conductance in the closed lakes, indicating a lower amount of meltwater entering the lakes, both on Skarvsnes and West Ongul Island. Also in other East Antarctic regions, a similar cooling was observed. We found no evidence for an event coeval with the Northern Hemisphere (NH) Medieval Climate Anomaly (MCA), Little Ice Age (LIA) or Twentieth-Century Warming (TCW), which is consistent with other lake records (Verleyen et al. 2011 in Appendix 2) and ice cores from Antarctica (Goosse et al. in press).

We extended an existing relative sea-level (RSL) curve, which was solely based on marine terraces from Nakada et al. (2000), with published (Takano et al. 2012) and new data from isolation lakes . A complex RSL history for Lützow Holm Bay was obtained, with regional differences in the uplift rate and maximum sea-level high stand, which is likely related to the interplay between glacial isostatic adjustment (GIA) and local neotectonic faulting on Skarvsnes. This RSL curve is furthermore different from RSL curves from other East Antarctic regions, where maximum sea-level was reached between c. 8 and 6 cal. ka BP (Zwartz et al. 1998; Verleyen et al. 2005), after which RSL fall occurred due to outpacing of the eustatic component by isostatic uplift. Moreover, in Skarvsnes, RSL remained at its maximum until at least 4.8 cal. ka BP. These findings suggest a more extended ice-sheet prior to deglaciation and/or a relatively recent disintegration of the ice mass.

Samenvatting

Zowel Antarctica als de Zuidelijke Oceaan controleren in belangrijke mate het globale klimaatsysteem (Turner et al. 2009), maar toch zijn slechts weinig hoge-resolutie klimaatarchieven beschikbaar voor de hoge breedtegraden van de zuidelijke hemisfeer (Mann et al. 2009). Bovendien zijn grote gebieden, zoals Lützow Holm Bay in Oost-Antarctica, onderbestudeerd (Hall 2009; Verleyen et al. 2011 in Appendix 2). Een betere kennis over het vroegere klimaat en de dynamiek van de ijskappen in Oost-Antarctica zal ons toelaten om de huidige klimaatveranderingen in een lange-termijn context te plaatsen.

In deze thesis werden biologische, geochemische en sedimentologische proxies in goed gedateerde sedimentboorkernen uit drie glaciale en vier isolatiemeren bestudeerd, met als doel klimaatveranderingen en ijskapdynamiek te reconstrueren in Lützow Holm Bay (69 - 70°Z en 35 - 40°O). Eveneens werd een regionale transfer functie gebaseerd op diatomeeën opgesteld om veranderingen in conductiviteit te reconstrueren.

De analyses van de sedimentboorkernen toonden aan dat zowel West Ongul Island als Skarvsnes deglacieerden tijdens het Holoceen, hoewel niet gelijktijdig. Dateringen tonen aan dat West Ongul Island deglacieerde rond 11.2 ka BP, wat eerdere suggesties tegenspreekt die stellen dat de Ongul eilanden ijsvrij bleven tijdens het laatste glaciaal maximum (Miura et al. 1998). Het is echter ook mogelijk dat de Ongul eilanden tijdens en na het laatste glaciale maximum door sneeuw of ijs bedekt waren, wat biogene sedimentatie verhinderde. Skarvsnes deglacieerde rond 7.4 ka BP, wat in overeenstemming is met dateringen van mariene terrassen (Miura et al. 1998) en van cosmogene isotopen (Yamane et al. 2011) maar later dan de meeste andere Oost-Antarctische gebieden (Hall 2009).

Aanwijzingen voor een vroeg Holoceen klimaatoptimum werden niet gevonden, aangezien zowel West Ongul Island als Skarvsnes door sneeuw of ijs bedekt waren. In Skarvsnes werd een lage primaire productiviteit waargenomen tussen c. 7.4 en 4.6 ka BP. Deze periode werd dan gevolgd door een hogere productiviteit tussen c. 4.6 en 3.7 ka BP. Initieel was deze site mogelijk een ondiepe mariene lagoon, enkel geschikt voor een beperkt aantal diatomeeënsoorten. Hierna werden een meer diverse gemeenschap en meer open-water condities waargenomen. In de mariene omgeving van West Ongul Island werden diatomeeën waargenomen die voorkomen in zeeijs en bij gestratifieerde condities van de waterkolom, tussen 6.5 en 5.0 ka BP.

Vervolgens werd van 4.2 tot 0.9 ka BP een klimaatoptimum geïnfereerd, zowel in West Ongul Island als in Skarvsnes, dat culmineerde tussen 2.2 en 2.1 ka BP. In de meren op West Ongul Island werd dit waargenomen als een verhoogde primaire productiviteit en veranderingen in de vochtbalans die wijzen op het verhoogd smelten van sneeuw. In Skarvsnes werden sedimentologische veranderingen mogelijks toegeschreven aan het

verdwijnen van sneeuwbanken, eveneens te wijten aan warmere condities. Het voorkomen van een warmere periode komt overeen met andere Oost-Antarctische records en wordt tussen 4.7 en 1 ka BP geplaatst (Verleyen et al. 2011 in Appendix 2).

Vanaf c. 1.2 ka BP trad vermoedelijk een neoglaciale afkoeling op, wat werd waargenomen als een daling in primaire productiviteit en een gestabiliseerde of verhoogde conductiviteit in de meren, wat wijst op een verminderde hoeveelheid smeltwater die in de meren terechtkomt. Dit werd zowel in Skarvsnes als in West Ongul Island waargenomen. Eveneens werd in andere Oost-Antarctische regio's een koudere periode waargenomen. In onze meersedimenten werden geen aanwijzingen gevonden voor klimaatveranderingen die gelinkt kunnen worden aan de Middeleeuws Warme Periode, de Kleine Ijstijd of recente temperatuursstijging, wat in overeenstemming is met andere meersedimentarchieven (Verleyen et al. 2011 in Appendix 2) en ijsboringen (Goosse et al. in press).

Een bestaande relatieve zeespiegelcurve, gebaseerd op mariene terrassen (Nakada et al. 2000), werd uitgebreid met gepubliceerde data (Takano et al. 2012) en nieuwe data van isolatiemeren. De relatieve zeespiegel geschiedenis van Lützow Holm Bay bleek complex, met regionale verschillen in uplift snelheid en maximale zeespiegelhoogstand. Deze is waarschijnlijk te linken aan de wisselwerking tussen isostatische uplift en neotectonische processen op Skarvsnes. Deze relatieve zeespiegelcurve is eveneens sterk verschillend van curves van andere Oost-Antarctische gebieden, waar een zeespiegelhoogstand werd waargenomen tussen 8 en 6 ka BP (Zwartz et al. 1998; Verleyen et al. 2005), waarna de relatieve zeespiegel daalde. In Skarvsnes echter bleef de zeespiegel op zijn maximale hoogte tot 4.8 ka BP, wat erop wijst dat de ijskap uitgebreider was voor deglaciatie optrad, of dat de ijsmassa relatief recent desintegreerde.

Appendix 1. Chemical limnology in coastal East Antarctic lakes: monitoring future climate change in centres of endemism and biodiversity

Running Title: Chemical limnology in East Antarctica

PUBLISHED PAPER. Verleyen E, Hodgson DA, Gibson J, Imura S, Kaup E, Kudoh S, De Wever A, Hoshino T, McMinn A, Obbels D, Roberts D, Roberts SJ, Sabbe K, Souffreau C, Tavernier I, Van Nieuwenhuyze, Van Ranst E, Vindevogel N, Vyverman W (2012) Chemical limnology in coastal East Antarctic lakes: monitoring future climate change in centres of endemism and biodiversity. Antarctic Science, ***24(1)****: 23-33.*

Author's contribution: preparing of the dataset for Lützow Holm Bay

Key-words: Prydz Bay, Lützow Holm Bay, Schirmacher Oasis, specific conductance, hydrological balance, snow accumulation

Abstract

Polar lakes respond quickly to climate-induced environmental changes. We studied the chemical limnological variability in 127 lakes and ponds from eight ice-free regions along the East Antarctic coastline, and compared repeat specific conductance measurements from lakes in the Larsemann Hills and Skarvsnes covering the periods 1987 to 2009 and 1997 to 2008, respectively. Specific conductance, the concentration of the major ions, pH and the concentration of the major nutrients underlie the variation in limnology between and within the regions. This limnological variability is likely related to differences in the time of deglaciation, lake origin and evolution, geology and geomorphology of the lake basins and their catchment areas, sub-regional climate patterns, the distance of the lakes and the lake districts to the ice-sheet and the Southern Ocean, and the presence of particular biota in the lakes and their catchment areas. In regions where repeat surveys were available, inter-annual and inter-decadal variability in specific conductance was relatively large and most pronounced in the non-dilute lakes with a low lake depth to surface area ratio. We conclude that long-term specific conductance measurements in these lakes are complementary to snow accumulation data from ice cores, inexpensive, easy to obtain, and should thus be part of long-term limnological and biological monitoring programs.

Introduction

Polar lakes act as 'early warning systems' because they respond quickly to climate-induced environmental changes (Hodgson & Smol 2008). In the Arctic and Maritime Antarctica, where global warming is particularly amplified, the recent temperature rise has resulted in enhanced primary productivity in lakes (Quayle et al. 2002), a negative precipitation-evaporation balance (Smol & Douglas 2007a), and marked changes in their community structure (Smol et al. 2005). In particular, lakes with a high surface area to volume ratio were shown to respond quickly to changes in the precipitation-evaporation balance and are prone to salinization and desiccation (Smol & Douglas 2007a).

In comparison to these regions, recent climate changes are relatively modest in East Antarctica (EA; Steig et al. 2009) and there are distinct regional differences in, for example, snow accumulation rates (Monaghan et al. 2006). Measurements on the Law Dome ice core show that snow accumulation rates have increased since 1970 and are now outside the natural variability of the past 750 years (van Ommen & Morgan 2010). In contrast, in other EA regions, such as the inner part of the continent and in Dronning Maud Land, the volume of snow has decreased between 1995 and 2004 (Monaghan et al. 2006). The relatively modest warming in EA is likely related to the buffering effect of the 'ozone hole', which has led to stronger circumpolar flow around Antarctica (Marshall et al. 2010). However, it is predicted that when the 'ozone hole' closes, warming will accelerate in EA as well (Turner et al. 2009).

The effect of changes in air surface temperatures, wind speeds and changes in snow accumulation rates on EA lake ecosystems is expected to be complex and will depend, in part, on the geomorphology of the individual lake basins and their catchment areas, and limnological properties. By analogy to well-studied lakes in the Arctic and Maritime Antarctica (Douglas & Smol 1994, Quayle et al. 2002, Smol & Douglas 2007b, Hodgson & Smol 2008) the potential ecosystem changes in EA lakes in response to changing climate variables and weather patterns can be summarized as follows: increased air surface temperatures generally result in higher water temperatures and an increase in the number of ice-free days, which in turn will lead to increased lake primary productivity (Quayle et al. 2002). In closed basin lakes with no multi-year snow banks or glaciers in their catchments, increased air surface temperatures can also lead to enhanced evaporation of the lake water and sublimation of the lake ice resulting in a negative water balance, falling lake levels and increased specific conductance. Conversely, catchments with multiyear snow banks and glaciers may deliver an increased melt water input into lakes. In closed lakes, this will affect the water level, lake water specific conductance and the lakes may become open and develop an outflow stream. In open lakes, increased melt water input leads to increased flushing rates, which also results in a decrease in lake water specific conductance (Verleyen et al. 2003). In addition, soil development in newly exposed ice-free ground in their catchments, results in increased nutrient and organic matter export providing an additional feedback mechanism leading to a further increase of the lake primary productivity (Quayle et al. 2002, Quesada et al. 2006). Decreased wind speeds lead to lower evaporation rates, positively affecting the hydrological balance (e.g. Hodgson et al. 2006). However, this relationship is complicated by the negative effect of both increased temperatures on the evaporation rate, and wind speed on snow accumulation, as slower (katabatic) winds transport less snow from the interior to the coastal regions. The hydrological balance of Antarctic lakes is thus a complex function of melting glaciers and multiyear snow banks in the catchment area, in combination with snowfall (including on the Central Plateau), temperature, and the presence of strong winds to transport it to the lake basin.

Changes in the physical and chemical characteristics of EA lakes are expected to have profound effects on the structure of their communities and the biological and biogeochemical processes occurring in these lakes and their catchments. This is important as EA lakes and ponds are hotspots of biodiversity and microbial production in an otherwise cold desert (Laybourn-Parry & Pearce 2007). Moreover, EA lakes provide

habitats for endemic organisms including rotifers, cladocerans, tardigrades, and several classes and divisions of microorganisms (Convey & Stevens 2007, Vyverman et al. 2010) and may have served as refugia in which organisms have escaped extinction during Pleistocene and Neogene glacial maxima (e.g., Hodgson et al. 2005, Cromer et al. 2006).

In order to better understand the possible trajectory of climate related ecosystem changes in EA, we compiled limnological baseline data on 127 water bodies from 8 ice free regions along the EA coastline (Fig. 1).

We combined existing datasets for the Prydz Bay region (Table S1 in supplementary information) with new data from Prydz Bay and Dronning Maud Land, and compared repeat surveys of specific conductance data for selected lakes from the Larsemann Hills and Skarvsnes. The data set presented here can (i) be used to select regions and lakes which are of particular interest for studies of microbial biodiversity, (ii) serve as baseline data against which future limnological changes can be compared, and (iii) be used to identify lakes which are expected to respond particularly quickly to climate variability and should thus be considered as priority sites for paleolimnological research and long-term biological and limnological monitoring programs.

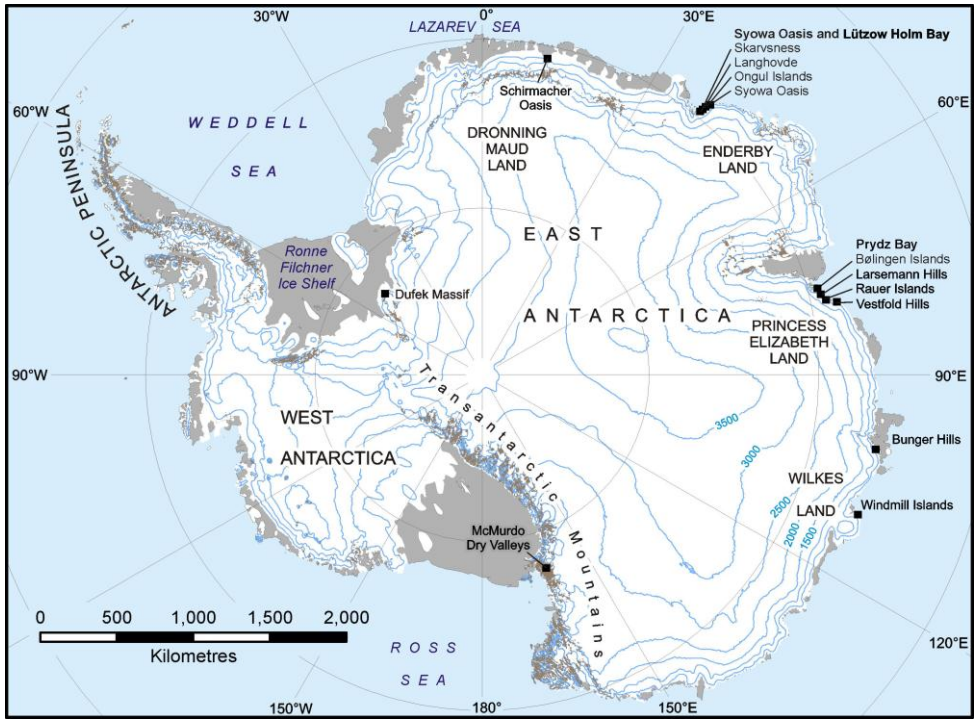

Figure 1. Map of Antarctica showing the locations mentioned in the text.

Study area

Dronning Maud Land

Schirmacher Oasis (70°46'S-11°44'E) in Dronning Maud Land (Fig. 1) is a 17 km long and 2-3 km wide ice free area, with a maximum elevation of 238 m (Bormann & Fritzsche 1995). The region has over 50 ponds and lakes which range in size from 0.02 to 2.2 km² (Vincent & Laybourn-Parry 2008). There is a wide variety of lake types, including epishelf lakes, supraglacial water bodies, ice-dammed lakes, lakes situated on moraines and lakes that have formed in deglaciated basins. Our dataset only contains lakes of the last type, which were formed in ice-free depressions following the retreat of the glaciers that flowed across the Oasis. The presence of former lake terraces show that many of the present day lakes are remnants of larger proglacial lakes (Phartiyal et al. 2011). Sediments in the lakes are generally Holocene in age (Ingólfsson *et al.* 1998) but some of the deeper lakes contain glacial sediments dating back to > 30 ka (Schwab 1998).

In Lützow Holm Bay (Dronning Maud Land; Fig. 1) a series of islands and peninsulas form a c. 200 km² ice-free region, known as Syowa Oasis. Numerous lakes and ponds occur in the region, some of which have been the subject to detailed limnological and biological research programs (e.g., Tominaga & Fukui 1981, Imura et al. 1999, Kimura et al. 2009 and references therein). East and West Ongul Island are the largest islands and are separated by a narrow seaway. East Ongul Island contains mostly small ephemeral ponds and relatively shallow water bodies. West Ongul Island is the larger of the two islands and contains larger and deeper lakes (up to 0.05 km² and 11 m depth). Most regions in Lützow Holm Bay deglaciated during the Holocene, but ^{14}C dates of *in situ* fossils of the marine bivalve *Laternula elliptica* and other marine macrofossils in raised beaches on West Ongul Island suggest that parts of the coastline were ice-free during the Last Glacial Maximum (LGM) and Marine Isotope Stage 3 (Nakada et al. 2000). However, this contradicts a recent ^{14}C dating program of lake sediment cores which revealed that the bottom sediments in none of the 5 lakes studied are of pre-Holocene age (Verleyen et al. unpubl. res.).

Skarvsnes is one of the two largest peninsulas in Lützow-Holm Bay. The water bodies range from small ponds to large lakes (up to 0.5 km^2) and their water chemistry from freshwater to hypersaline (Kimura et al. 2009). The saline lakes are situated on fossil marine beaches and sometimes have water levels below present sea level (e.g. Suribati Ike). The freshwater lakes are known for their luxuriant moss communities, which in some lakes, form pillars up to 60 cm high (Imura et al. 1999). Some of the lakes that were formerly connected to the sea are meromictic, but the majority are holomictic, being mixed throughout the summer ice free period (Vincent & Laybourn-Parry 2008, Kimura et al. 2009).

Langhovde is the other of the two largest peninsulas in Lützow Holm Bay. The Northern part of Langhovde contains lakes and (ephemeral) ponds with varying ionic concentrations, ranging from freshwater to hypersaline. This wide gradient is likely related to differences in wind exposure, sea spray, and altitude, with the most saline lake being isolation lakes.

Princess Elizabeth Land – Prydz Bay

In Prydz Bay near the Lambert Glacier a number of ice-free regions occur, some of which have been the subject of intensive limnological research programs and microbiological studies (e.g. Roberts & McMinn 1996, Laybourn-Parry *et al.* 2001, Verleyen et al. 2010). The Vestfold Hills (68°30' S, 78°00' E) form a 400 km^2 ice-free area (Fig. 1), consisting of three main peninsulas (Mule, Broad and Long Peninsula) and a number of offshore islands. The lakes here also range from freshwater to hypersaline (Roberts & McMinn 1996) and include a number of large permanently stratified meromictic lakes (e.g., Laybourn-Parry et al. (2002), Gibson (1999)). Most of the lakes are of Holocene age but at least one (Abraxas Lake) existed during the LGM (Gibson et al. 2009).

The Larsemann Hills ($69^{o}23'$ S, $76^{o}53'$ E), comprise a 50 km^2 large ice-free area located approximately midway between the eastern extremity of the Amery Ice Shelf and the southern boundary of the Vestfold Hills (Fig. 1). The region consists of two main peninsulas (Stornes and Broknes), together with a number of scattered offshore islands. An inventory of 74 of the 150 freshwater bodies present in the region ranging from small ephemeral ponds to large water bodies is given in Gillieson et al. (1990). Further details on the limnology and microbial communities of 51 of these lakes are described in Sabbe et al. (2004). Parts of the region remained ice-free during the LGM (Hodgson et al. 2001a) whereas others were deglaciated during the Holocene (Verleyen et al. 2004).

The Rauer Islands (68°45' S - 68°55' S and 77°30' E - 78°00' E) are an ice-free coastal archipelago situated approximately 30 km south of the Vestfold Hills (Fig. 1). The region includes 10 major islands and promontories together with numerous minor islands covering a total area of some 300 km^2. A detailed description of the region and of the microbial communities inhabiting 10 out of more than 50 shallow lakes and ponds is given in Hodgson et al. (2001b). The minimum age of deglaciation of the islands is at some time in the Late-Pleistocene/Early-Holocene (White et al. 2009), but the presence of *in situ*, open-marine sediments with radiocarbon ages ranging from 40–30 ka BP to the east of Filla Island suggest that deglaciation of some areas could have commenced much earlier (Berg et al. 2009).

The Bølingen Islands (69°30'S – 75°50'E) are a coastal archipelago, situated north of the Publications Ice Shelf approximately 10 km from the Larsemann Hills (Fig. 1). The limnology and microbial biology of five out of the eight shallow lakes and ephemeral ponds in the islands have been studied (e.g., Sabbe et al. 2004, Hodgson et al. 2004, Verleyen et al. 2010).

Materials and methods

Sampling procedures and limnological measurements

Details of the lake sampling procedures and limnological measurements applied in the Vestfold Hills in the 1994 field season can be found in Roberts and McMinn (1996). Specific conductance was measured using a submersible data logger (Platypus Engineers, Hobart, Tasmania). All samples, except those from Watts Lake and "Pointed" Lake, which were surface samples, were collected from a depth of 2 m. For the methods used in the Larsemann Hills, the Rauer Islands, and Bølingen Islands in the 1997 field season, we refer

to Sabbe et al. (2004) and Hodgson et al. (2001b). Specific conductance was measured using a YSI 6000 meter and the samples were taken in the top 1 to 2 m of the water column when the lake was ice free, or in the top 1 m under ice cover. During 2007, the specific conductance and pH of the lakes in Dronning Maud Land were analysed using a YSI 600 meter and the samples were taken in the top first meter of the water column in deep lakes. In shallow lakes, surface waters were analysed and sampled. During the 2009 field season, specific conductance and pH in the lakes in the Larsemann Hills and Schirmacher Oasis were measured using an IQ170 Scientific Instruments field pH-conductivity meter in the top first meter of the water column, except for Progress Lake and Lake Smirnov which were ice-covered. In Progress Lake the measurements were taken at 3 m and in Lake Smirnov at 4 m. The concentration of the main ions and nutrients in lakes in Dronning Maud Land sampled during the 2007 field season were sampled in the surface waters and analysed in certified laboratories using standard techniques. Measurements were done by atomic absorption spectroscopy (Varian SpectraAA-600) following ISO norms (ISO 7980, 1986; ISO 9964, 1993) and ion chromatography (Dionex ICS-2000) following ISO 10304-1(2007). The major ions in the samples from the Larsemann Hills and Schirmacher Oasis taken in 2009 were analysed using high performance liquid chromatography following the procedures described in Buck et al. (1992).

Repeat measurements of specific conductance from the lakes in the Larsemann Hills, used here to assess long-term changes in the precipitation-evaporation balance were collected first in January and February 1987 by Gillieson et al. (1990). These data were compared with more recent data collected in November-December 1997 and January 2009 using the procedures described above, and during February 1998 as described in Gasparon et al. (2002). The pH measurements from 1997 (Sabbe et al. 2004) were compared with the data extracted from Gillieson et al. (1990). The repeat specific conductivity measurements for the Lützow Holm Bay region were collected in 1997, 2000, 2003, 2004 and 2008 using a Toa Multi Water Quality Meter (MWQ-22A), and compared with measurements taken in January 2007 using the procedures described above (Table 1 in supplementary information).

Data treatment and statistical analyses

Limnological datasets in EA typically differ in the number and type of variables measured and often show missing values resulting from logistical and/or technical problems associated with working in these harsh environments (Table 1 in supplementary information), and the lack of a longer term co-ordinated strategy for data collection. In the multivariate analysis we thus only retained lakes for which at least the following minimal set of environmental variables was available: pH, specific conductance, and the concentration of the major ions (Na^+, K^+, Mg^+, Ca^{2+}, $SO4^{2-}$ and Cl^-), because these factors are known to change in response to climate warming and changes in the hydrological balance (precipitation vs. evaporation and sublimation), brought about by changes in temperature, wind patterns and precipitation (e.g., Roberts et al. 2001, Verleyen et al. 2003). All limnological variables were standardized prior to statistical analyses in order to reduce skewness, to minimize the effect of outlier values, and to enable a comparison of variables measured in different units (ter Braak & Šmilauer 2002). Principal Component

Analysis (PCA) in Canoco 4.5 (ter Braak & Šmilauer 2002) was used to visualize variations in the limnological properties between and within the regions. Two subsets of data were analyzed. Subset A contained the lakes for which measurements of pH, specific conductance and major ions were available. For subset B, the above-mentioned variables together with PO_4-P and NO_3-N were available. For the statistical analysis, nutrient concentrations were divided into classes or threshold values because the data were obtained using different instruments and methods with differing precision (see Table 1 in supplementary material). For PO_4-P, measurements below or equal to 5 µg/L were assigned 0. For NO_3-N, concentrations between 0 and 100 were assigned to class 0, between 100 and 200 to class 1 etc.

Redundancy Analysis (RDA) was applied to explore the relationship between differences in limnology and differences in bedrock geology and/or glacial history of the ice-free regions. To this end, we created a dummy variable for each geographical region (1 when the lake is situated in the region and 0 if not; Table 1 in supplementary material) which represents contrasts in the deglaciation history and a dummy variable denoting bedrock type. Four lakes in the Bølingen Islands (Table S1) were excluded from the RDA and variation partitioning analysis, because no detailed geological information was available for this region. We are aware that inter-regional differences in limnology may also be due to the time of sampling and to different field instruments and laboratory protocols used. We therefore created dummy variables representing the different sampling campaigns (see Table 1 in supplementary information) and subsequently applied variation partitioning analysis (Borcard et al. 1992) to test whether the regional differences hold after accounting for the variation caused by sampling bias. First, the forward selection procedure in Canoco 4.5 was used to select those dummy variables which significantly explain the variation in the limnological conditions. The dummy variables representing the different regions and the sampling campaigns were tested separately. We then treated the significant dummy variables denoting the sampling campaigns as covariables in a RDA with the significant geographical dummy factors as constrained variables. This procedure resulted in 4 fractions, namely (1) the unique effect of geology, geomorphology and glaciation history, (2) the unique effect of the time of sampling and the methods and instruments used, (3) the overlap between (1) and (2), and (4) the unexplained variation.

A scatterplot of the specific conductance and the lake depth to area ratio was used to identify those lakes which are expected to be particularly vulnerable to climate changes, because specific conductance changes are more easily detected in non-dilute lakes. Moreover the lake depth to lake area ratio is a rough measure for basin morphology; shallow lakes with a large surface area are particularly vulnerable to changes in the precipitation evaporation balance as a result of wind and temperature induced changes in the evaporation rate (e.g. Smol & Douglas 2007a).

Results

Limnological variables

Lake water specific conductance ranges from extremely dilute (0.002 mS/cm) in one of the Schirmacher Oasis lakes to hypersaline (131.5 mS/cm) in one of the lakes in the Rauer

Islands (Table 1 in supplementary material). With the exception of a few lakes, the nutrient concentrations and the dissolved organic carbon (DOC) and total organic carbon (TOC) concentrations are low. The latter data are however only available for the lakes in the Larsemann Hills, Bølingen Islands, Rauer Islands, and the ice-free regions in Lützow Holm Bay (Table 1 in supplementary material).

PCA of all lakes (subset A), and all except some lakes from Schirmacher Oasis due to the lack of high precision nutrient data (subset B), revealed that specific conductance and the concentration of major ions are correlated with the first PCA axis and thus govern the main limnological variability within and between the different regions (Fig. 2 & 3).

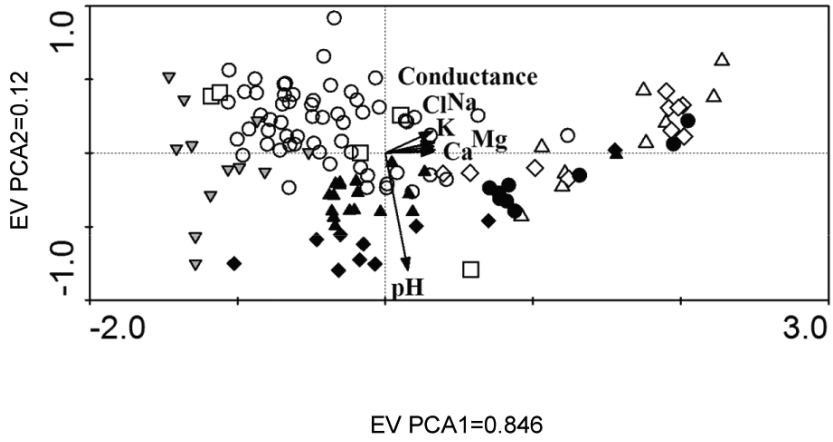

Figure 2. PCA biplot of pH and the environmental properties related to lake water specific conductance and the major ions in Prydz Bay (open symbols): the Vestfold Hills (up-triangle), Rauer Islands (diamonds), Bølingen Islands (squares), Larsemann Hills.

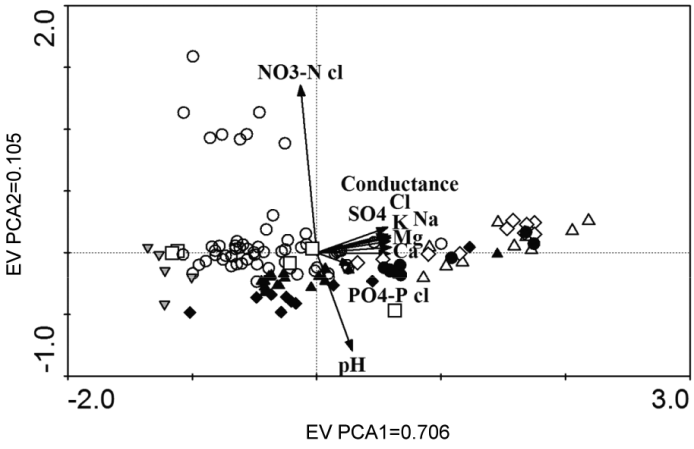

Figure 3. PCA biplot of the lakes for which the following environmental variables were available: pH, specific conductance, Mg2+, Ca2+, Cl-, Na+, K+, SO42-, NO3-N, and PO4-P. Symbols as in Fig.2.

pH is correlated with the second axis in subset A as well as with NO_3 in subset B, while PO_4 governs the third axis (EV=0.08) in subset B (Figure not shown). The lakes in the Rauer Islands, Vestfold Hills, and Langhovde have on average a higher specific conductance than the lakes in the other regions. The lakes in Schirmacher Oasis rank among the most dilute freshwater bodies. There is no clear geographic difference in measured limnological properties between the saline lakes, yet the high PO_4-P concentration in Organic Lake (Table 1 in supplementary material) differentiates it from the other saline water bodies in the Vestfold Hills, the Rauer Islands, and Langhovde (Fig. 3). In Firelight Lake in the Bølingen Islands the PO_4-P concentration is higher than in the other freshwater lakes. The NO_3-N concentration is relatively high in some shallow freshwater lakes in the Larsemann Hills (Fig. 3). There is some geographical overlap between the freshwater systems, yet the lakes in the Lützow Holm Bay region (Ongul Islands and Skarvsnes) are situated on the negative side of the second PCA axis, due to their relatively high pH levels (Fig. 3). In addition, there are inter-and intra-regional differences in the ionic ratios (Table 1 in supplementary material). Lakes close to the ice-sheet and/or situated relatively further away from the ocean, such as the lakes in Schirmacher Oasis, and lakes near the continental ice plateau in the other regions (e.g. L49 in the Larsemann Hills and Lichen Lake in the Vestfold Hills) are characterized by a higher Ca to Na ratio, which is the result of a decreasing marine influence when moving further away from the ocean.

The variation partitioning analysis of subsets A and B revealed that the dummy regional variables explained respectively 51.7% and 42.8% of the variation in limnological conditions, whereas the dummy variables representing sampling bias explained only 20.2% and 19.1% in subsets A and B respectively. The geographical dummy variables independently and significantly ($P \leq 0.005$) explained 34.1% and 30.9% of the limnological variation in subsets A and B respectively, suggesting that a significant part of the difference in limnological properties between the various regions is related to differences in geology, geomorphology and the deglaciation history, and/or with differences in sub regional climate patterns. It is however unclear whether the inter-regional difference in pH is real or related to the month in which sampling took place and related variability in lake-ice cover dynamics. For example, 80% of the pH values taken in 1997 that were measured under lake ice cover in the Larsemann Hills are lower compared with the values from 1987 that were measured during (partly) ice-free conditions (Fig. 4). However, 3 out of the 5 pH values taken in 1997 were higher than those from 2009, also measured during (partly) ice-free conditions.

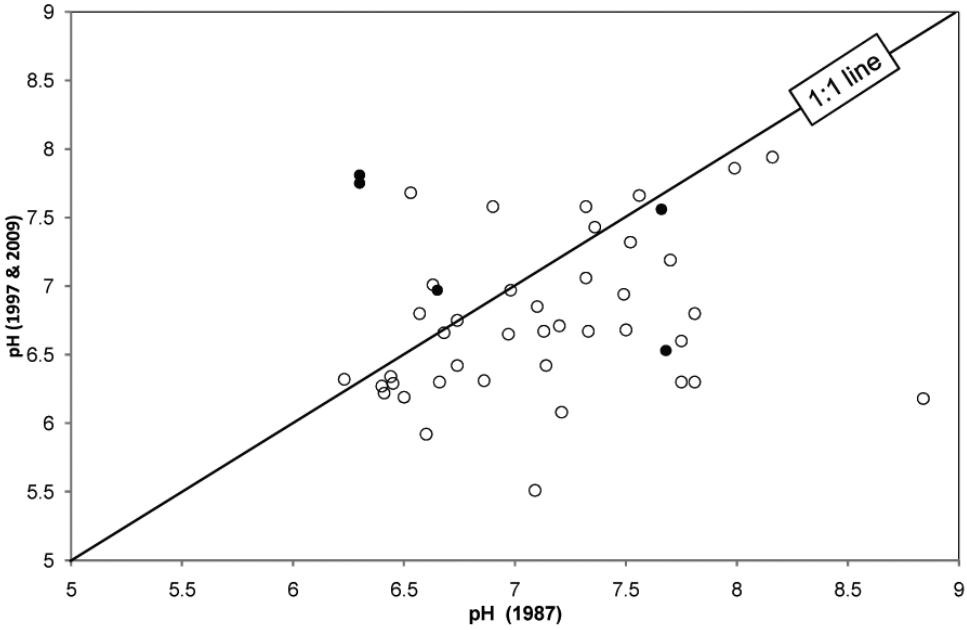

Figure 4. Historical variations in pH in the Larsemann Hills (n=34) showing that the measurements from 1987 are generally higher than those of 1997 (open circles) and 2009 (filled circles), which is likely related to differences in lake ice cover. If a point falls on the 1:1 line, no change in pH has occurred. If the site points are below the 1:1 line, pH has decreased.

Long-term changes in lake water specific conductance

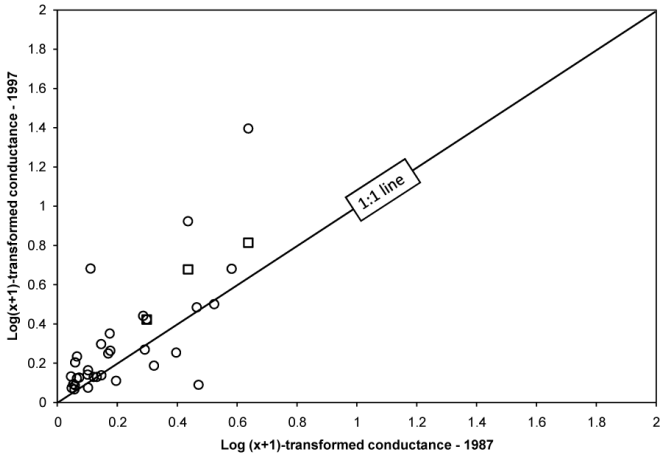

Figure 5. Historical variations in lake water specific conductance in the Larsemann Hills, comparing measurements from the Austral summer of 1987 with those obtained during the Austral spring of 1997 (circles) and the Austral summer (squares).

Changes in specific conductance are generally higher in the more saline lakes as evidenced by their larger deviation from the 1:1 line (Fig. 5, 6, and 7). In the Larsemann Hills (Fig. 5), over 70% of the specific conductance data obtained both during late spring and early summer under respectively ice covered and (partly) ice free conditions in 1997-1998, are higher compared with measurements taken during the summer of 1987 when the majority of the lakes were ice-free

(Gillieson et al. 1990). However, during the Austral summer of 2009, specific conductance was more or less similar in the 6 lakes studied when compared with the data obtained in 1987 (Fig. 6).

In Syowa Oasis, the pattern is less consistent although the lakes were all measured in the Antarctic summer under ice-free conditions (Fig. 7). Specific conductance increased or remained nearly constant in the majority of the lakes in Skarvsnes between 2000 and 2007-2008. The variability in specific conductance was again highest in the most saline lake (Suribati Ike), but decreased from 58.7 mS/cm in January 1997 to 32.9 mS/cm in January 2007, while the Cl concentration in the surface water (29.1 g/L) remained more or less constant over the period between January 1977 and 2007 (Tominaga & Fukui 1981).

The biplot with specific conductance and the surface to lake depth ratio revealed that saline or brackish lakes with a high surface to lake depth ratio are present in nearly all regions studied (Fig. 8). These lakes are therefore identified as priority sites to study changes in the hydrological balance.

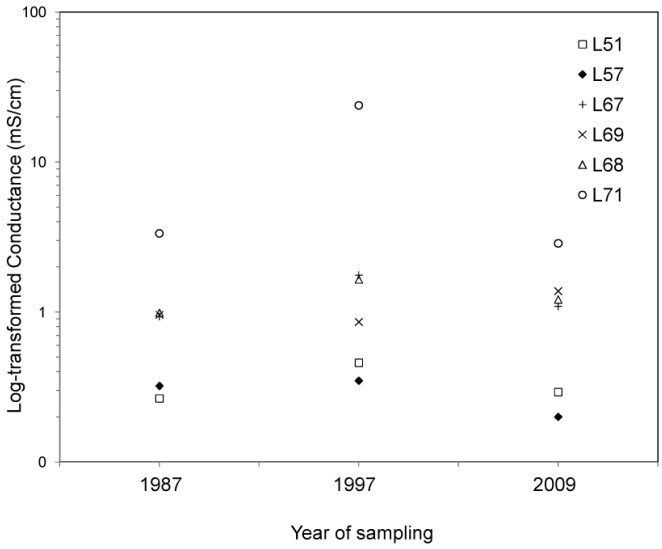

Figure 6. Historical variations in lake water specific conductance in the 6 lakes in the Larsemann Hills sampled during three field campaigns (1987, 1997 and 2009) showing a large inter-annual variability.

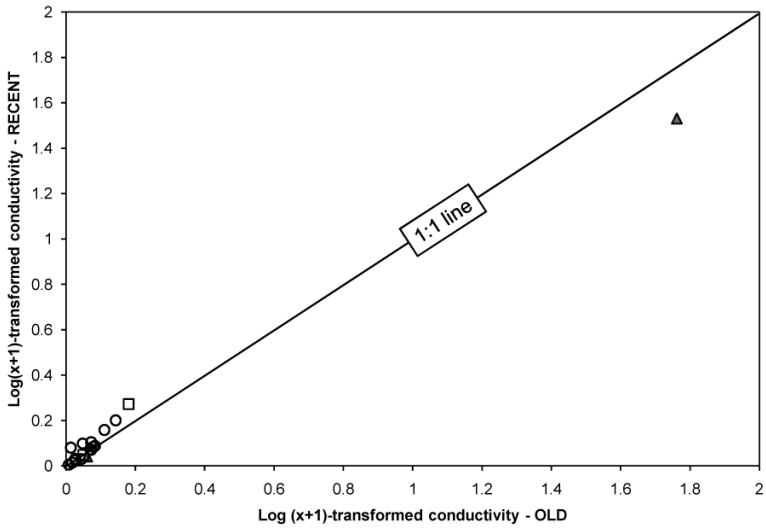

Figure 7. Historical variations in lake water specific conductance in Skarvsnes. All measurements were taken in January under ice-free conditions. Circles denote a comparison between 2000 and 2007-2008, triangles between 1997 and 2007, and squares between 2004 and 2007.

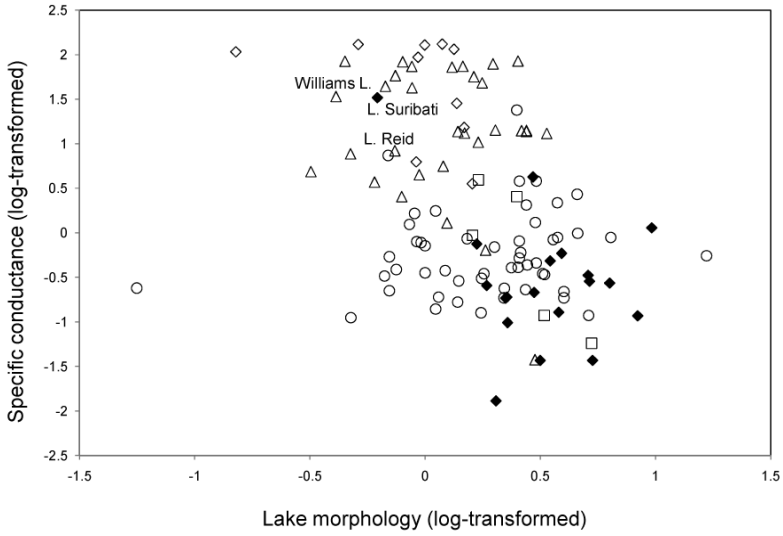

Figure 8. Biplot of the log-transformed lake depth to lake surface area and log-transformed lake water specific conductance. Lakes which are particularly sensitive to changes in the precipitation evaporation balance and should therefore be priority sites for environmental monitoring programs are labeled. Symbols as in Fig. 2.

Discussion

We assessed the limnological variability in eight ice-free regions in a sector between 10 and 80°E along the EA coastline. Our dataset contains a representative set of lakes, although epishelf lakes in Schirmacher Oasis and Amery Oasis were not included neither were the large and well-studied glacial lakes in the McMurdo Dry valleys and a number of other ice-free regions where complimentary datasets were not available (e.g. the Bunger Hills, Windmill Islands, Thala Hills; Vincent & Laybourn-Parry 2008). Moreover, in Schirmacher Oasis, lakes in contact with the East Antarctic Ice-Sheet were not included in our survey. In the Vestfold Hills our dataset was collected to create a diatom-salinity transfer function (Verleyen et al. 2003) and is therefore somewhat biased towards the more saline lakes although freshwater lakes also occur in that region (Roberts & McMinn 1996). Moreover, the nutrient concentration in lakes from the Lützow Holm Bay region and Schirmacher Oasis were measured using less sensitive techniques, and hence we used categorized data, which might underestimate interregional differences in trophic status. Despite this sampling and analytical bias we were able to observe some general trends. EA lakes are in general oligotrophic and span a wide specific conductance gradient, ranging from oligosaline to hypersaline. In the Prydz Bay and the Lützow Holm Bay regions, both freshwater and hypersaline lakes occur, whereas in Schirmacher Oasis only dilute lakes were found. The variation partitioning analysis revealed that the observed differences in chemical limnology are, in part, related to the time of sampling and hence processes related to lake ice dynamics. For example, the lakes in the Larsemann Hills were still ice covered during the field campaign in 1997 and sampled in the upper 1 m under ice-cover, which potentially affected the ionic concentration and the pH. More in particular, the vast majority of the pH measurements taken in 1997 are lower than the values from 1987 and 2009 when the lakes were ice-free or when lake ice cover was less extensive. It is well known that lake ice cover simultaneously limits the photosynthetic drawdown of limnetic CO_2 and traps respired CO_2 within lakes (e.g. Axford et al. 2009). Moreover, ice cover and thawing also affect the concentration of ions in the water column. Ions are expelled out of the lake ice which results in more concentrated lake water. The thawing of the ice can in turn result in an increase or a decrease in ionic concentration and specific conductance, depending on lake-ice and snow cover characteristics. Lake-ice thawing can either result in more diluted lake water due to the addition of meltwater with a low ionic concentration or, on the contrary, it can lead to more concentrated lake water if marine aerosols got accumulated in the snow and ice. However, after accounting for differences in the time of sampling, the geographical and geological dummy variables remain important, hence regional differences in chemical limnology are likely to be real and related to differences in the time of deglaciation, geology, bedrock type and geomorphology of the lake basins and their catchment areas, lake origin and evolution, sub-regional climate patterns, and the distance of the lakes and the lake districts to the ice-sheet and the Southern Ocean. For example, these factors underlie the absence of brackish and (hyper)saline lakes in Schirmacher Oasis. First, all lakes there are situated at elevations above the Holocene relative sea-level limit, which is typically below 25 m a.s.l. in EA (Verleyen et al. 2005; unpublished results). Hence, they are of glacial origin, in contrast to the saline lakes and ponds in EA which are isolation basins and situated at low altitudes. These isolation lakes originated from the sea after

isostatic uplift and the ions trapped in the basins led to brackish conditions (if the flushing rate was relatively low) or hypersaline conditions (if the evaporation-precipitation balance was negative). Second, many of the lakes in Schirmacher Oasis are likely of Holocene age and thus relatively young (Phartiyal et al. 2011). Lakes situated at higher altitudes (above c. 25 m) can only be saline in Antarctica if (i) they have a long history of evaporation and addition of salts by sea spray, such as Lake Reid which is over 100,000 years old (Hodgson et al. 2005), (ii) if the lakes are remnants of very large glacial and old (pre-LGM) lakes, such as Lake Bonney and Lake Fryxell in the McMurdo Dry Valleys in which the ions derived from the large glacial Lake Washburn were concentrated in the bottom waters (Vincent & Laybourn-Parry 2008), or (iii) if they are remnants of larger glacial lakes in ablation dominated areas such as Forlidas Pond in the Dufek Massif (Hodgson et al. 2010). Third, the lakes sampled in Schirmacher Oasis are flushed by meltwater, which flows continuously during summer through small streams originating from the East Antarctic Ice-Sheet or from permanent snow banks upstream. Also the relatively high Ca^{2+} to Na^{+} ratio in the lakes from Schirmacher Oasis are the result from the continuous flushing with glacial meltwater (Table 1 in supplementary information).

The effect of the proximity of the lakes in Schirmacher Oasis to the ice-sheet on their chemical limnology is also apparent within other regions. For example, the freshwater lakes such as Lichen Lake in the Vestfold Hills and L49 in the Larsemann Hills, are situated close to the ice-sheet and show higher Ca^{2+} to Na^{+} ratio (Table 1 in supplementary material), compared with other freshwater lakes which are more influenced by sea spray. Inter- and intra-regional differences in specific conductance and the concentration of the major ions are also related to exposure to winds, in combination with the distance to the sea. The lakes in Langhovde receive salts from the ocean through sea spray and are exposed to the dry katabatic winds which blow over Lützow Holm Bay on the north-eastern part of Langhovde. The lakes there are hypersaline and some were almost completely dried out during the visit in January 2007. In contrast, lakes in the south and south-western part of Langhovde are not exposed to sea spray and hence freshwater lakes and ponds occur there.

Differences in chemical limnology between lakes might also be related to the presence of specific biological communities or the biogeochemistry of the sediments. For example, in some shallow freshwater lakes on Broknes in the Larsemann Hills, the nitrate concentration is higher compared with similar systems in the region and other EA oases, which may be partly underlain by the presence of nitrogen fixing cyanobacteria that are abundantly present there (Sabbe et al. 2004). The PO_4-P concentration is highest in Organic Lake in the Vestfold Hills and in Firelight Lake in the Bølingen Islands. In the latter this is likely related to high density of breeding bird colonies in the catchment area (Sabbe et al. 2004). Organic Lake and the isolation lakes in the Vestfold Hills in general are more nutrient rich, because they contain relict sea water (Vincent & Laybourn-Parry 2008). Alternatively, the age and history of the landscape, along with the gradient and geomorphology of the inflow streams may play an important role in regulating the nutrient input, as observed in the lakes in the McMurdo Dry Valleys (Lyons & Finlay 2008). The fact that the highest nitrate concentrations are found in lakes on Broknes might be related to the relative long period of ice-free conditions over this part of the oasis (Hodgson et al. 2001a). Interestingly, in the lakes of the McMurdo Dry Valleys,

particularly phosphate concentrations were higher on relatively older surfaces and not nitrate (Barrett et al. 2007). It is clear that more detailed studies are required to fully understand the differences in nutrient concentrations between the different water bodies.

Our analyses of repeat survey data revealed relatively large seasonal and inter-annual variability in specific conductance. In most lakes in the Larsemann Hills specific conductance increased between 1987 (Gillieson et al. 1990) and 1997 (Sabbe et al. 2004) and decreased again in 2009 (Fig. 5 and 6), which is likely related to both inter-annual climate variability and weather patterns (Rochera et al. 2010), and the different seasons during which sampling took place. We consider the effect of different field instruments being used as minor, as they were calibrated to fixed standards and the differences in readings in some lakes are more than would be anticipated due to normal instrument error. In 1987 and 2009, samples were taken during the austral summer, whereas in 1997 the lakes were visited during spring when they were still ice covered. It is well known that seasonal differences in specific conductance occur due to changes in lake ice cover and the amount of melt water input (Douglas & Smol 1994, Wetzel 2001). During autumn, ions are frozen out during lake ice formation, which leads to the concentration of the solutes in the remaining lake water and higher specific conductance values compared with summer conditions. During summer, the lake water can be additionally diluted as a result of snow melt draining into the lake from the catchment area. However, seasonal differences in ice cover and snow melt alone fail to explain the increase in specific conductance in three lakes that were consistently sampled under partly ice-free conditions in 1997 (Gasparon et al. 2002). A consistent increase in specific conductance was observed during both spring and late summer 1997, when compared with data obtained in the summers of 1987 (Gillieson et al. 1990), 1992 (Ellis-Evans 1998) and 2009. This increase in specific conductance is consistent with lower snow accumulation rates recorded in ice cores from this part of EA between 1985 and 1994 (Monaghan et al. 2006). The lower specific conductance values after 1997 are in agreement with increased snow accumulation rates between 1995 and 2004 (Monaghan et al. 2006), indicating that part of the long term variation might be related to regional climate variability. The increase in lake water specific conductance in the majority of the lakes is also consistent with long term monitoring data from Deep Lake in the nearby Vestfold Hills, where lake water dropped between 1987 and 1997 (Gibson 2010). Interestingly, the subsequent decrease in specific conductance in six lakes during the 2009 field season is not consistent with the lake level trend in Deep Lake, implying that regional differences in snowfall and snow accumulation are relatively large.

In Syowa Oasis lakes, repeat surveys were carried out in January 1997, 2000, 2007 and 2008, hence inter-lake variations in specific conductance are not biased by seasonal differences in snow melt and lake ice dynamics. The majority of the lakes showed an increase in specific conductance or relatively stable conditions if measurements from 2000 and 2007-2008 are compared. In contrast, if measurements from 1997 in Suribati Ike are compared with data obtained in 2007, specific conductance decreases. Interestingly, the Cl^- concentration analyzed ten years before is similar to the 2007 measurements (Tominaga & Fukui 1981). This large inter-annual and inter-decadal variability is difficult to compare with existing snow thickness data as no direct

measurements are available for this region (Monaghan et al. 2006). Yearly snowfall variability of 20 mm/yr is however common in Antarctica and might underlie this long-term variability (Monaghan et al. 2006), possibly in combination with changes in wind strength.

Our analysis revealed that in terms of the sensitivity of the lakes to climate changes, those lakes with medium to high specific conductance levels and with a high surface area to lake depth ratio in which meteoric water is the only moisture source will respond quickly to changes in the evaporation-precipitation balance and snow accumulation. In EA, such lakes can be found in nearly all regions studied (Fig. 8) and these water bodies should be targeted for long-term limnological and biological monitoring programs. Ideally, however, lakes selected for long term monitoring should not be too shallow so that they are susceptible to complete desiccation, and their sediments should remain undisturbed by ice working so they can be used in paleolimnological studies. Typically, lake depth should exceed 2 m for these purposes; however, sites with shallower water have also accumulated important sedimentary profiles in the Arctic (e.g. Douglas et al. 2004). Based on these criteria, Lake Reid and Williams Lake are the priority sites for long term monitoring programs in respectively the Larsemann Hills and Vestfold Hills (Fig. 8), together with Deep Lake, which is already part of such a program (see Gibson 2010). Lake RI4 is probably too shallow and prone to complete desiccation under future climate warming. In Lützow Holm Bay, Suribati Ike appears to be ideally suited for long term monitoring programs. Additional selection criteria are easy logistic access to the study lakes and the proximity of a weather station. Hence, lakes close to research stations or field huts are preferred. This is the case for Lake Reid in the Larsemann Hills, Williams Lake in the Vestfold Hills and Lake Suribati in Syowa Oasis. Standardized long-term monitoring of these ecosystems in combination with local meteorological data (including precipitation) is thus of primary importance to understand the ecological implications of future climate anomalies. Our data have also shown that it is of utmost importance that in future surveys, the date of sampling and the thickness of the lake ice cover are recorded. Similarly, to monitor the effect of future climate changes on lakes, the specific conductance in these water bodies should be measured, if possible, during the short ice-free period (cf. Smol & Douglas 2007a). In addition, the measurements should be taken at a fixed lake depth, which is particularly important in stratified saline lakes, but also in low-salinity lakes which can be stratified after ice melt during early summer. For some lakes there are basic specific conductance data from at least the late 1980's and, although the data collection has been intermittent, this combined instrumental data is of great value. Such standardized long term specific conductance measurements are complementary to snow accumulation data from ice cores and should thus be part of long-term monitoring, paleolimnological and microbiological research programs. Moreover, in combination with paleolimnological analysis using diatom based transfer functions (e.g. Verleyen et al. 2003, Hodgson et al. 2005, 2006; Table 1 in supplementary material) these programs will allow us to place the recent instrumental data on lacustrine and climate changes in the context of long-term natural variability.

The limnological data presented here can also be used to select regions and lakes for future biodiversity studies, linking the presence of particular taxa to climate-related

environmental conditions (cf. Verleyen et al. 2010). These studies can be used to reveal the ecological conditions under which particular species (including endemics) occur, which is important for the conservation of these unique habitats and their communities. The understudied freshwater lakes in Dronning Maud Land, which appear to differ from the other EA water bodies should be considered as priority sites to study their microbial communities as they might contain other, potentially endemic taxa than those already observed in our analyses of a subset of lakes from the Prydz Bay region and the McMurdo Dry Valleys (Verleyen et al. 2010).

Acknowledgements

This work benefited from the HOLANT and AMBIO projects funded by the Belgian Federal Science Policy Office (BelSPO), the Fund for Scientific Research in Flanders (FWO) project 3G/0533/07, the Natural Environment Research Council (UK), and the MERLIN and REGAL projects funded by the National Institute of Polar Research (Japan). The work was only possible with the logistic support of the Australian Antarctic Division, the British Antarctic Survey, the Japanese National Institute for Polar Research (JARE 48) and the Indian Antarctic Expedition. EV and CS are funded by FWO. IT is financed by the institute for the promotion of Science and Technology in Flanders (Belgium). EK was partly funded by the target grant SF0320080s07 of the Estonian Ministry of Education and Science. Geological maps were provided by the Australian Antarctic Division Data Centre (Henk Brolsma), the National Institute of Polar Research Japan, and the National Centre for Antarctic and Ocean Research India. Prof. Dr. John P. Smol and two anonymous reviewers are thanked for their constructive comments on a previous version of the manuscript.

References

Axford Y, Briner JP, Cooke CA, Francis DR, Michelutti N, Miller GH, Smol JP, Thomas EK, Wilson CR, Wolfe AP (2009) Recent changes in a remote Arctic lake are unique within the past 200,000 years. *Proceedings of the National Academy of Sciences of the United States of America,* **106:** 18443-18446.

Barrett JE, Virginia RA, Lyons WB, McKnight DM, Priscu JC, Doran PT, Fountain AG, Wall DH, Moorhead DL (2007) Biogeochemical stoichiometry of Antarctic Dry Valley ecosystems. *Journal of Geophysical Research-Biogeosciences 112(G1)*: Art. No. G01010.

Berg S, Wagner B, white DA, Cremer H, Bennike O, Melles M (2009) Short Note: New marine core record of Late Pleistocene glaciation history, Rauer Group, East Antarctica. *Antarctic Science*, **21:** 299-300.

Borcard D, Legendre P, Drapeau P (1992) Partialling out the spatial component of ecological variation. *Ecology*, **73:** 1045-1055.

Bormann P, and Fritzsche D (1995) The Schirmacher Oasis, Queen Maud Land, East Antarctica, and its surroundings. Petermanns Geographische Mitteilungen **289**. Gotha: Justus Perthes, 448 pp.

Buck CF, Mayewski PA, Spencera MJ, Whitlowa S, Twicklera MS, Barretta D (1992) Determination of major ions in snow and ice cores by ion chromatography. *Journal of Chromatography A*, **594**: 225-228.

Convey P, and Stevens MI (2007) Antarctic biodiversity. *Science*, **317:** 1877-1878.

Cromer L, Gibson JAE, Swadling KM, Hodgson DA (2006) Evidence for a lacustrine faunal refuge in the Larsemann Hills, East Antarctica, during the Last Glacial Maximum. *Journal of Biogeography*, **33:** 1314-1323.

Douglas MSV, and Smol JP (1994) Limnology of high Arctic ponds (Cape Herschel, Ellesmere Island, N.W.T.). *Archiv für Hydrobiologie*, **131**: 401-434.

Douglas MSV, Smol JP, Blake W (1994) Marked post-18th century environmental change in high Arctic ecosystems. *Science*, **266:** 416-419.

Ellis-Evans JC, Laybourn-Parry J, Bayliss PR, Perriss SJ (1998) Physical, chemical and microbial community characteristics of lakes of the Larsermann Hills, Continental Antarctica. *Archiv fur Hydrobiologie*, **141:** 209-230.

Gasparon M, Lanyon R, Burgess JS, Sigurdsson IA (2002) The freshwater lakes of the Larsemann Hills, East Antarctica: chemical characteristics of the water column. ANARE Report 147. Hobart: Commonwealth of Australia, 28 pp.

Gibson JAE (1999) The meromictic lakes and stratified marine basins of the Vestfold Hills, East Antarctica. *Antarctic Science*, **11:** 175-192.

Gibson JAE (2010) Water levels of Deep Lake, Vestfold Hills.

http://data.aad.gov.au/aadc/soe/display_indicator.cfm?soe_id=62 Accessed 24 June 2010.

Gibson JAE, Paterson KS, White CA, Swadling KM (2009) Evidence for the continued existence of Abraxas Lake, Vestfold Hills, East Antarctica during the Last Glacial Maximum. *Antarctic Science*, **21:** 269-278.

Gillieson D, Burgess J, Spate A, Cochrane A (1990) An atlas of the lakes of the Larsemann Hills, Princess Elizabeth Land, Antarctica. ANARE Research Notes no. 74. Kingston, Tasmania: The Publications Office, Australian Antarctic Division, 173 pp.

Hodgson DA, and Smol JP (2008) High latitude palaeolimnology. *In:* Vincent WF, and Laybourn-Parry J (Eds) Polar Lakes and Rivers - Arctic and Antarctic Aquatic Ecosystems. Oxford: Oxford University Press, pp. 43-64.

Hodgson DA, Vyverman W, Sabbe K (2001b) Limnology and biology of saline lakes in the Rauer Islands, eastern Antarctica. *Antarctic Science*, **13:** 255-270.

Hodgson DA, Roberts D, McMinn A, Verleyen E, Terry B, Corbett C, Vyverman W (2006) Recent rapid salinity rise in three East Antarctic lakes. *Journal of Paleolimnology*, **36:** 385-406.

Hodgson DA, Vyverman W, Verleyen E, Sabbe K, Leavitt PR, Taton A, Squier AH, Keely BJ (2004) Environmental factors influencing the pigment composition of *in situ* benthic microbial communities in east Antarctic lakes. *Aquatic Microbial Ecology*, **37**: 247-263.

Hodgson DA, Verleyen E, Sabbe K, Squier AH, Keely BJ, Leng MJ, Saunders KM, Vyverman W (2005) Late Quaternary climate-driven environmental change in the Larsemann Hills, East Antarctica, multi-proxy evidence from a lake sediment core. *Quaternary Research*,**64:** 83-99.

Hodgson DA, Convey P, Verleyen E, Vyverman W, McIntosh W, Sands CJ, Fernández-Carazo R, Wilmotte A, De Wever A, Peeters K, Tavernier I, Willems A (2010) The limnology and biology of the Dufek Massif, Transantarctic Mountains 82° South. *Polar Science,* **4:** 197-214.

Hodgson DA, Noon PE, Vyverman W, Bryant CL, Gore DB, Appleby P, Gilmour M, Verleyen E, Sabbe K, Jones VJ, Ellis-Evans JC, Wood PB (2001a) Were the Larsemann Hills ice-free through the Last Glacial Maximum? *Antarctic Science*, **13:** 440-454.

Imura S, Bando T, Saito S, Seto K, Kanda H (1999) Benthic moss pillars in Antarctic lakes. *Polar Biology*, **22:** 137-140.

Ingólfsson O, Hjort C, Berkman PA, Bjorck S, Colhoun E, Goodwin ID, Hall B, Hirakawa K, Melles M, Moller P, Prentice ML (1998) Antarctic glacial history since the Last Glacial Maximum: an overview of the record on land. *Antarctic Science,* **10**: 326-344.

Kimura S, Ban S, Imura S, Kudoh S, Matsuzaki M (2009) Limnological characteristics of vertical structure in the lakes of Syowa Oasis, East Antarctica. *Polar Science*, **4**: 262-271.

Laybourn-Parry J, and Pearce DA (2007) The biodiversity and ecology of Antarctic lakes: models for evolution. *Philosophical Transactions of the Royal Society B-Biological Sciences*, **362:** 2273-2289.

Laybourn-Parry J, Hofer JS, Sommaruga R (2001) Viruses in the plankton of freshwater and saline Antarctic lakes. *Freshwater Biology*, **46**: 1279-1287.

Laybourn-Parry J, Quayle W, Henshaw T (2002) The biology and evolution of Antarctic saline lakes in relation to salinity and trophy. *Polar Biology*, **25:** 542-552.

Lyons WB, and Finlay JC (2008) Biogeochemical processes in high-latitude lakes and rivers. *In:* Vincent WF, and Laybourn-Parry J (Eds) Polar Lakes and Rivers - Arctic and Antarctic Aquatic Ecosystems. Oxford: Oxford University Press, pp. 137-156.

Marshall GJ, Di Battista S, Naik SS, Thamban M (2011) Analysis of a regional change in the sign of the SAM–temperature relationship in Antarctica. *Climate Dynamics*, **1-2:** 277-287.

Monaghan AJ, Bromwich DH, Fogt RL, Wang SH, Mayewski PA, Dixon DA, Ekaykin A, Frezzotti M, Goodwin I, Isaksson E, Kaspari SD, Morgan VI, Oerter H, van Ommen TD, Van der Veen CJ, Wen JH (2006) Insignificant change in Antarctic snowfall since the International Geophysical Year. *Science*, **313**: 827-831.

Nakada M, Kimura R, Okuno J, Moriwaki K, Miura H, Maemoku H (2000) Late Pleistocene and Holocene melting history of the Antarctic ice sheet derived from sea-level variations. *Marine Geology*, **167:** 85-103.

Phartiyal B, Sharma A, Bera SK (2011) Glacial lakes and geomorphological evolution of Schirmacher Oasis, East Antarctica, during Late Quaternary. *Quaternary International*, **235**: 128-136.

Quayle WC, Peck LS, Peat H, Ellis-Evans JC, Harrigan PR (2002) Extreme responses to climate change in Antarctic lakes. *Science*, **295:** 645-645.

Quesada A, Vincent WF, Kaup E, Hobbie JE, Laurion I, Pienitz R, Lopez-Martinez J, Duran J-J (2006) Landscape control of high latitude lakes in a changing climate. *In:* Bergstrom D, Convey P, Huiskes A (Eds) Trends in Antarctic Terrestrial and Limnetic Ecosystems. Dordrecht, The Netherlands: Kluwer, pp. 221-251.

Roberts D, and McMinn A (1996) Relationships between surface sediment diatom assemblages and water chemistry gradients in saline lakes of the Vestfold Hills, Antarctica. *Antarctic Science*, **8:** 331-341.

Roberts D, McMinn A, Johnston N, Gore DB, Melles M, Cremer H (2001) An analysis of the limnology and sedimentary diatom flora of fourteen lakes and ponds from the Windmill Islands, East Antarctica. *Antarctic Science*, **13**: 410-419.

Rochera C, Justel A, Fernandez-Valiente E, Banon M, Rico E, Toro M, Camacho A, Quesada A (2010) Interannual meteorological variability and its effects on a lake from maritime Antarctica. *Polar Biology*, **33:** 1615-1628.

Sabbe K, Hodgson DA, Verleyen E, Taton A, Wilmotte A, Vanhoutte K, Vyverman W (2004) Salinity, depth and the structure and composition of microbial mats in continental Antarctic lakes. *Freshwater Biology*, **49:** 296-319.

Schwab MJ (1998) Reconstruction of the Late Quaternary climatic and environmental history of the Schirmacher Oasis and the Wohlthat Massif (East Antarctica). Reports on Polar Research, 293. Bremerhaven: 128 pp.

Smol JP, and Douglas MSV (2007a) Crossing the final ecological threshold in high Arctic ponds. *Proceedings of the National Academy of Sciences of the United States of America*, **104**: 12395-12397.

Smol JP, and Douglas MSV (2007b) From controversy to consensus: making the case for recent climate using lake sediments. *Frontiers in Ecology and the Environment*, **5**: 466-474.

Smol JP, Wolfe AP, Birks HJB, Douglas MSV, Jones VJ, Korhola A, Pienitz R, Ruhland K, Sorvari S, Antoniades D, Brooks SJ, Fallu MA, Hughes M, Keatley BE, Laing TE, Michelutti N, Nazarova L, Nyman M, Paterson AM, Perren B, Quinlan R, Rautio M, Saulnier-Talbot E, Siitoneni S, Solovieva N, Weckstrom J (2005) Climate-driven regime shifts in the biological communities of arctic lakes. *Proceedings of the National Academy of Sciences of the United States of America*, **102:** 4397-4402.

Steig EJ, Schneider DP, Rutherford SD, Mann ME, Comiso JC, Shindell DT (2009) Warming of the Antarctic ice-sheet surface since the 1957 International Geophysical Year. *Nature*, **457:** 459-463.

Ter Braak CJF, and Smilauer P (2002) CANOCO reference manual and user's guide to CANOCO for Windows: software for canonical community ordination (version 4). Ithaca: Microcomputer Power Inc. 351 pp.

Tominaga H, and Fukui F (1981) Saline lakes at Syowa-Oasis, Antarctica. *Hydrobiologia*, **81:** 375-389.

Turner J, Arthern R, Bromwich D, Marshall G, Worby T, Bockheim J, Di Prisco G, Verde C, Convey P, roscoe H, Jones A, Vaughan D, Woodworth P, Scambos T, Cook A, Lenton A, Comiso J, Gugliemin M, Summerhayes C, Meredith M, Naveira-Garabato A, Chown S, Stevens M, Adams B, Worland R, Hennion F, Huiskes A, Bergstrom D, Hodgson DA, Bindschadler R, Bargagli R, Metzl N, Van der Veen K, Monaghan A, Speer K, Rintoul S, Hellmer H, Jacobs S, Heywood K, Holland D, Yamanouchi T, Barbante C, Bertler N, Boutron C, Hong S, Mayewski P, Fastook J, Newsham K, Robinson S, Forcarda J, Trathan P, Smetacek V, Gutt J, Pörtner H-O, Peck L, Gili J-M, Wiencke C, Farhbach E, Atkinson A, Webb D, Isla E, Orejas C, Rossi S, Shanklin J (2009) The Instrumental Period. *in:* Turner J, Convey P, Di Prisco G, Mayewski PA, Hodgson DA, Fahrbach E, Bindschadler R, Gutt J (Eds.) Antarctic Climate Change and the Environment. Cambridge: Scientific Committee for Antarctic Research, pp. 183-298.

Van Ommen TD, and Morgan V (2010) Snowfall increase in coastal East Antarctica linked with southwest Western Australian drought. *Nature Geoscience*, **3**, 267-272.

Verleyen E, Hodgson DA, Milne GA, Sabbe K, Vyverman W (2005) Relative sea-level history from the Lambert Glacier region, East Antarctica, and its relation to deglaciation and Holocene glacier readvance. *Quaternary Research*, **63**, 45-52.

Verleyen E, Hodgson DA, Sabbe K, Vanhoutte K, Vyverman W (2004) Coastal oceanographic conditions in the Prydz Bay region (East Antarctica) during the Holocene recorded in an isolation basin. *Holocene*, **14**, 246-257.

Verleyen E, Hodgson DA, Vyverman W, Roberts D, McMinn A, Vanhoutte K, Sabbe K (2003) Modelling diatom responses to climate induced fluctuations in the moisture balance in continental Antarctic lakes. *Journal of Paleolimnology*, **30**, 195-215.

Verleyen E, Sabbe K, Hodgson DA, Grubisic S, Taton A, Cousin S, Wilmotte A, De Wever A, Van der Gucht K, Vyverman W (2010) Structuring effects of climate-related environmental factors on Antarctic microbial mat communities. *Aquatic Microbial Ecology*, **59**, 11-24.

Vincent WF, and Laybourn-Parry J (2008) *Polar* Lakes and Rivers. Limnology of Arctic and Antarctic Aquatic Ecosystems. Oxford: Oxford University Press, pp. 352.

Vyverman W, Verleyen E, Wilmotte A, Hodgson DA, Willems A, Peeters K, Van de Vijver B, De Wever A, Sabbe K (2010) Evidence for widespread endemism among Antarctic micro-organisms. *Polar Science,* **4**, 103-113.

Wetzel RG (2001) Limnology: Lake and River Ecosystems. Third Edition. San Diego: Academic Press, 1006 pp.

White DA, Bennike O, Berg S, Harley SL, Fink D, Kiernan K, McConnell A, Wagner B (2009) Geomorphology and glacial history of Rauer Group, East Antarctica. *Quaternary Research*, **72**, 80-90.

Supplementary information

Table S1 Complete set of limnological properties in 127 lakes in ice-free regions along the east Antarctic coastline. Fossil diatom assemblages were analysed in sediment cores from lakes marked with an * and hence long-term specific conductance reconstructions are possible or already existing. A reference is given to the original publication. If the data are unpublished, the names of the collectors are given. [a]dummy variable denoting the different regions. [b]year of sampling. [C]dummy variable denoting the type of bedrock obtained using geological maps.

lake code	COND (mS/cm)	pH	Cl (mg/L)	Na (mg/L)	K (mg/L)	Mg (mg/L)	Ca (mg/L)	SO4 (mg/L)	TN (mg/L)	TOC (mg/L)	DOC (mg/L)	Al (mg/L)	Fe (mg/L)	NH4-N (mg/L)	NH4-N class (mg/L)	NO3-N (µg/L)	NO3-N classes	PO4-P (µg/L)	PO4-P classes	elevation (m)	z-max (m)
VAB	14.03	7.68	6150	3560	237	690	76	1076								<1.4	0	2.4	0	13.11	23
VAC*	13.73	8.33	9100	4420	404	1170	58	312								<1.4	0	6	6	8.91	25
VAD	13.04		7400	4470	340	740	182	1788								<1.4	0	27.3	27.3	0.95	6
VAN*	48.22	7.14	33500	16890	1150	5490	500	1740								20.3	0	3.6	0	3.5	21
VBU	78.86	7.39	92700	52830	3130	15020	2310	3320								<1.4	0	82.8	82.8	-0.07	7
VCA	14.23		8200	4500	360	1140	115	520								<1.4	0	9	9		7.4
VCL	10.41	8.7	4400	2370	148	540	24	458								<1.4	0	7.8	7.8	-8.25	60.5
VCO	8.35		4600	2600	174	560	16	84								<1.4	0	3	0	4.99	8.2
VEK	42.52	7.9	26100	13210	1940	3360	430	1975								1.82	0	10.8	10.8	-1.405	39
VGR	1.29		275	132	7.1	28	8.3	17.7								<1.4	0	24	24		3
VHA	5.6		2200	880	87	320	13	8.8								<1.4	0	2.4	0	9.55	29
VHI	4.49		940	510	43	97	26	105								<1.4	0	5.4	5.4	8.3	17.4
VJT	72.51		105300	62610	3820	18000	2750	4010								<1.4	0	8.1	8.1		9.8
VLI	0.64		18	9.8	1.4	1.6	2.5	3.2								<1.4	0	4.2	0		26
VLP1	58.07		45300	26590	1180	7870	530	2610								<1.4	0	3.3	0	7.5 1	4.9
VLP2	84.27		102500	59380	3290	17400	1950	4130								<1.4	0	7.2	7.2	7.51	1.8
VMC	13.76		4800	2750	184	540	20	390								<1.4	0	4.5	0	-1.71	32
VMN	7.71		5850	3050	195	930	50	448								<1.4	0	3	0	27.3	3.8
VOB	83.24		117800	65520	4620	19490	2460	2460								<1.4	0	6.3	6.3	-2.58	14.8

VOR	74.12	6.9	116400	67640	4870	20080	3190	4100					<1.4	0	480	480	2.75	7
VOV	73.88		89700	52830	2900	15020	1730	2250					<1.4	0	28.2	28.2	-28.44	16
VPE	13.17	8.1	7400	4250	296	870	178	1320					<1.4	0	18.3	18.3	3.045	18.4
VPO	4.87		2950	1410	430	460	22	81					<1.4	0	5.4	5.4	5.52	5
VSC	14.09		9200	4500	435	1500	22	122					<1.4	0	4.8	0		10.6
VSH	56.56	7.65	40300	23410	1240	6680	790	2750					<1.4	0	6	6	-6.915	33
VSA	84.81		89700	49180	2760	14430	1810	2400					<1.4	0	13.5	13.5	-0.385	20
VVE	3.71		1950	1050	205	270	38	207					<1.4	0	3	0	0.96	25
VWA	2.55		1200	610	105	215	25	187					<1.4	0	5.4	5.4		29.5
VWE	44.19		33500	17540	2240	4460	430	3485					1.54	0	3.9	0		6
VWI	33.9		25550	12960	1370	3180	570	1910					13.44	0	6.3	6.3	1.165	7
RI1	128.500	7.3	104180	70000	960	3591	210	1730	0	0	0.046	0.046	0	0	0.6	0	10	7
RI2	131.500	7.52	113270	63000	1234	5600	350	2790	5.19	0	0.120	0.120	0	0	0.9	0	10	3
RI3	115.200	7.53	91600	52000	1064	5800	200	490	8.82	0	0.040	0.040	0	0	0	0	3	2.5
RI4	107.700	7.96	84960	53000	1170	4401	550	8630	23.2	8.8	0.028	0.028	0	0	0.6	0	2	1
RI5	93.600	7.83	62230	42000	1149	3768	450	6650	0	0	0.001	0.000	0	0	1.2	0	2	4
RI6	130.300	7.56	97020	71000	1628	4049	250	15940	0	0	0.000	0.000	0	0	0.9	0	15	1
RI7	28.400	8.28	10350	10000	213	351	93	8420	0	0	0.112	0.112	0	0	2.4	0	15	1.5
RI8	6.260	7.86	2380	1200	49	137	29	1040	0	0	0.011	0.011	0	0	0.6	0	18	1
RI9	15.265	7.98	6010	4000	136	272	90	1780	0	0	0.027	0.027	0	0	0.9	0	8	1.5
RI10	3.555	7.77	1380	845	28	79	30	280	0	0	0.000	0.000	0	0	0.3	0	30	1.5
BAL*	2.540	6.85	773	380	21	35	22.6	15	8.79	8.71	0.244	0.244	7	0	0.32	0	20	4
BSU	0.939	7.22	275	161	4.3	19.7	25.6	27	14.2	13.8	0.082	0.082	1.4	0	4.16	0	10	1.8
BFI	3.927	9.38	1500	850	25.3	96	50	50	21.5	19	0.038	0.038	0	0	202.24	202.24	30	1.5
BST	0.118	6.18	15.9	11.6	0.88	1	0.57	0	0	0	0.036	0.036	7	0	0	0	20	2.5

BBA	0.057	6.19	11.6	8.7	0	1.35	0.86	0	0	0	0.010	0.010	1.4	0	0	0	10	15
L71	23.870	7.58	10400	6200	160	824	193	480	16.9	16.9	15.353	15.353	7	0	2.1	0	75	2.5
L72*	0.167	6.31	18.8	12.8	0.65	1.65	0.86	0	0	0	0.318	0.318	11.2	0	3.6	0	15	18
L59	0.410	6.43	134	81	3.2	13	9.14	3.3	0.24	0	0.429	0.429	8.4	0	0	0	20	3.8
L67	1.761	6.68	481	310	9.8	32	21.4	60	2.71	2.51	0.046	0.046	7	0	0	0	45	5
L74	0.692	5.92	183	119	4.3	14.4	15	30.6	0	0	0.375	0.375	1.4	0	0	0	5	4
L63	0.339	6.18	84	60	2.6	6.23	4.29	13.8	0	0	0.166	0.166	1.4	0	0.9	0	60	3.3
L60	0.835	5.51	257	160	8	18.6	18.4	30	0	0	0.890	0.890	14	0	0.6	0	45	5.4
L35	2.170	6.94	795	644	15.2	59	23.3	75	2	2	0.387	0.387	9.8	0	6	6	30	12
L34*	0.387	6.42	110	54	2.6	7.19	3.14	14.8	0	0	0.192	0.192	7	0	3.9	0	5	9
L8	0.355	6.34	94	48	6.5	6.42	3.43	16.6	0	0	0.256	0.256	11.2	0	0.9	0	5	4.8
L7	0.348	6.19	95	51	2.8	5.85	3.71	0	0	0	0.430	0.430	7	0	0	0	25	4.5
L10*	0.327	6.32	90	46.2	2.5	6.42	3.71	12	0	0	0.383	0.383	4.2	0	1.5	0	60	5
L13	0.776	6.67	234	143	5.7	16.3	9.66	0	0	0	0.837	0.837	5.6	0	0.9	0	75	4.8
L14*	1.243	6.71	393	210	9	27.5	13.2	9.5	4.82	4.78	1.074	1.074	1.4	0	1.8	0	60	4.7
L12	0.186	6.22	40.5	25	1.2	3.31	0.57	4.8	0	0	0.114	0.114	2.8	0	5.4	5.4	80	11
LSP	0.308	6.43	84	46	2.2	5.85	3.43	14.8	0	0	0.465	0.465	0	0	1.2	0	5	8.8
L23*	0.985	6.42	277	190	10	18.3	14.5	55	2.44	2.5	0.739	0.739	15.4	0	1.8	0	5	4.6
LBU*	0.186	6.53	43.5	27.8	1.7	3.04	2	5.3	0.23	0	0.057	0.057	4.2	0	0.3	0	40	16
L36	0.230	6.6	57	38.3	0.88	3.92	3.43	10.2	0	0	0.097	0.097	2.8	0	3	0	60	15
LGR	2.705	7.73	860	530	18.2	63	46.6	195	0.17	0	0.313	0.313	2.8	0	0.3	0	50	16
L49	0.127	7.01	16.9	14.9	0.33	1.58	2.29	0	0	0	0.074	0.074	1.4	0	0.9	0	30	3.5
L44	3.800	7.86	1220	780	24	79	43.3	42	3.35	0	0.000	0.000	0	0	0	0	45	7.7
L43	0.599	6.67	140	95	3.2	12.1	11.4	21.2	3.14	0	0.032	0.032	15.4	0	0.3	0	10	6.5
L42	2.050	7.94	599	420	14	46	27.8	60	1.62	1.47	0.029	0.029	5.6	0	0	0	25	11
L69	0.859	6.8	257	172	6.4	15.9	9.31	44	0	0	0.190	0.190	30.8	0	4.5	0	10	3.8
L70*	7.380	7.06	2660	1900	58	176	50	105	14.6	12.9	0.008	0.000	9.8	0	4.8	0	30	3.8
L68*	1.649	6.3	452	280	12.1	30.4	26.1	80	0.14	0	0.020	0.020	14	0	0.6	0	5	4.5

LJA	0.111	6.79	25.4	19.4	0	1.77	1.14	3.8		0	0			0.013	0.013	7	0	0.3	0	85	2
L18	0.376	6.97	97	51	1.32	5.85	5.43	11.1		0	0			0.024	0.024	43.4	0	0.6	0	85	11
L1	3.810	7.19	1240	500	23	80	33.3	27		2.43	0			0.118	0.118	4.2	0	0.9	0	100	7.6
L57*	0.348	6.66	86	46.7	0.88	5.96	3.43	8.3		0	0			0.003	0.000	2.8	0	1.2	0	65	34
L73	0.189	6.08	41.5	24.3	3.5	3.69	1.14	4.8		0.32	0			0.083	0.083	487.2	4	0.3	0	85	4
L51	0.458	6.65	140	95	3.6	11.2	5.43	12.4		0	0			0.037	0.037	7	0	0	0	85	7.6
L58	0.239	6.27	38	25	6.2	2.5	0.57	4.8		0	0			0.063	0.063	14	0	0.6	0	60	0.7
L53b	0.139	6.68	30.8	23.2	0.66	2.19	1.71	3.3		0	0			0.041	0.041	4.2	0	0.6	0	40	0.5
LFO	0.885	7.22	303	180	7.6	16.5	7.93	34		0.35	0			0.040	0.040	8.4	0	1.8	0	30	1
LMA	0.406	6.88	108	51	2.5	7.85	3.71	20.3		3.52	3.48			0.052	0.052	1.4	0	0	0	30	1
LPS	0.520	6.5	171	94	3.3	11.8	5.14	27.7		0.06	0			0.062	0.062	5.6	0	0	0	10	1
LPR	0.807	7.04	247	161	4.7	16.5	8.28	0		0.42	0			0.061	0.061	96.6	0	0	0	10	0.8
L52	0.223	6.75	60	32.7	2.1	3.5	1.43	8.1		0.44	0			0.065	0.065	16.8	0	0	0	80	0.7
L52b	0.237	7.02	67	40.3	1.2	4.88	2.86	9.2		0	0			0.055	0.055	7	0	0	0	80	1
L59b	1.304	7.6	498	310	13.4	58	20	50		3.46	3.67			0.066	0.066	19.6	0	0.3	0	20	0.8
L66	0.795	7.43	285	170	5.5	18.3	18.8	29		0.03	0			0.024	0.024	21	0	0.3	0	25	2.3
L65	0.539	7.32	173	112	3.6	11	8	21		0	0			0.005	0.000	22.4	0	1.5	0	20	0.7
LG1	0.887	7.57	332	200	6.7	21.5	16.7	42		0.19	0			0.047	0.047	200.2	2	0.6	0	65	0.8
LG2	0.219	6.92	54.6	31.1	0.99	3.42	2	8.6		0.24	0			0.000	0.000	8.4	2	0.9	0	65	1
LG4	0.436	7	122	80	3.5	9.5	6	25.8		2.64	0			0.386	0.386	50.4	2	1.2	0	65	1
L64	0.289	6.85	83	49.2	1.87	4.58	3.71	7.4		0	0			0.097	0.097	9.8	2	2.4	0	55	0.7
L64b	0.552	7.16	183	135	5.2	5.66	3.79	3.8		0	0			0.032	0.032	5.6	2	1.8	0		1
LSN	0.118	5.93	27.9	20.1	0.88	2	0.57	6.7		0	0			0.005	0.000	2.8	2	2.7	0		0.8
L61	0.713	6.29	238	148	4.4	17.6	9.66	35.8		0	0			0.016	0.016	7	2	0.3	0	50	0.5
EO10	0.374	7.41	600	316	16.4	44.3	28.7	47.8	0.13	1.1	1.18	<0.002	0.017	<0.010	0.000	<100	0	7	7		
EO11	0.013	7.58	1350	687	29.3	93.7	57	80.4	0.17	1.3	1.4	<0.002	0.033	<0.010	0.000	<100	0	6	6		0.5
EO2	0.229	8.23	158	76.4	3.25	13.2	8.42	5.96	0.07	0.63	0.61	0.008	0.004	0.013	0.013	<100	0	<5	0		1
EO3	1.512	8.26	704	423	30	31.9	16.7	32.9	0.17	1.2	1.11	0.016	0.021	<0.010	0.000	<100	0	<5	0		
EO4	0.456	8.12	363	190	11	25	22.3	19.8	0.28	2.1	2.24	0.007	0.015	0.02	0.02	<100	0	5	5		
EO5	0.345	8.03	255	117	4.87	19.5	13.3	8.39	0.35	2.3	2.41	0.009	0.008	0.024	0.024	<100	0	<5	0		
EO6	0.277	7.87		101	3.88	14.4	8.97		0.09	1		<0.002	0.004								

EO7	0.234	7.6	249	129	5.93	13.2	7.58	11	0.14	1.4	1.49	0.006	0.005	0.013	0.013	<100	0	<5	0	
EO8	0.594	7.82																0	0	
EO9	0.326	8	151	73.5	2.86	13.4	8.32	8.24	0.07	0.63	0.76	<0.002	0.005	<0.010	0	<100	0	<5	0	
LA1*	73.36	7.69	97100	42000	1720	5960	951	1450	2.2	18	18.1	0.283	0.213	1.89	1.89	<100	0	<5	0	4
LA10	2.67	8.28	3530	1970	69	360	161	161	0.4	3.6	3.71	0.121	0.06	0.028	0.028	<100	0	<5	0	
LA2	4.261	8.27	3420	2050	60	269	83.6	137	0.23	1.7	2.07	0.068	0.039	0.024	0.024	<100	0	<5	0	
LA3	26.83	7.93	92600	43800	1560	6280	885	3840	0.66	5.1	5.11	0.278	0.205	2.07	2.07	<100	0	6	6	0.2
LA4	14.72	8.14	12100	5300	167	858	472	700	0.08	1.3	1.39	0.255	0.129	0.99	0.99	<100	0	<5	0	
LA5	91.1	6.92																		
LA6	3.51	8.07	3130	1640	55	251	77.9	152	0.4	2	2.37	0.065	0.037	0.042	0.042	<100	0	<5	0	
LA7	5.046	8.09	3860	2390	74	347	96	275	0.17	1.9	2.1	0.11	0.049	0.025	0.025	<100	0	<5	0	
LA8	3.605	8.48	24500	1520	52	245	106	153	0.22	2.2	1.51	0.069	0.037	0.035	0.035	<100	0	<5	0	
LA9	4.03	8.17	3130	1590	68	252	108	141	0.15	1	1.21	0.083	0.041	0.033	0.033	<100	0	<5	0	
SK1*	0.484	8.95	285	145	6.72	22.7	14.5	14.2	0.58	3.7	3.79	0.003	0.013	0.041	0.041	<100	0	<5	0	5.8
SK10	32.9	7.93	29100	14100	562	1980	195	319	1.4	15	16.8	<0.002	0.15	1.14	1.14	<100	0	<5	0	32
SK2	0.318	8.82	129	61.4	5.66	42.2	12.2	36.7	0.41	2.6	2.76	0.003	0.014	0.017	0.017	<100	0	<5	0	1
SK3	0.178	8.93	70.1	37.9	3.31	18.4	13.6	10.5	0.47	3	3.16	<0.002	0.016	0.022	0.022	<100	0	6	6	
SK4*	4.241	8.64	3850	2230	76	286	16.3	24.9	0.43	4.1	4.48	<0.002	0.062	0.012	0.012	<100	0	<5	0	10.7
SK5	0.014	8.58	4.08	3.08	0.248	1.04	2.01	0.57	0.11	0.84	0.9	0.005	0.015	0.012	0.012	<100	0	<5	0	3.5
SK6	0.945	8.44	500	223	26.7	112	22.3	93.4	0.32	2.3	2.43	0.008	0.042	0.013	0.013	<100	0	<5	0	0.8
SK7	0.382	8.59	183	93.8	7.91	44.3	8.32	10.3	0.33	2.4	2.51	0.02	<0.001	0.02	0.02	<100	0	<5	0	2
SK8	0.098	8.37	226	16.1	1.66	8.98	8.8	11.3	0.13	1.1	3.4	0.008	<0.001	0.029	0.029	<100	0	<5	0	19.5
SK9	0.333	8.38	160	77.2	2.72	19.6	8.21	9.88	0.09	0.81	0.89	<0.002	<0.001	<0.010	0	<100	0	<5	0	2.5
WO1*	0.249	8.1	160	82.7	3.5	13	7.39	8.48	0.15	1.2	1.64	<0.002	<0.001	0.02	0.02	<100	0	<5	0	
WO10	26.8	7.97	25400	12000	432	2270	363	1270	45	270	258	0.343	0.309	16.6	16.6	<100	0	26	26	
WO2	0.451	7.78	272	136	5.78	22.9	13.6	15.6	0.13	1.1	1.26	<0.002	<0.001	0.024	0.024	<100	0	<5	0	
WO3	0.277	7.77	176	91.2	3.47	14.9	7.99	6.93	0.12	0.88	1.05	<0.002	<0.001	0.026	0.026	<100	0	<5	0	
WO4*	0.33	7.63	207	106	4.35	15.4	9.83	9.25	0.3	2	2.22	<0.002	<0.001	0.049	0.049	<100	0	<5	0	
WO5*	0.275	7.59	167	88.5	3.27	15	12.6	11.8	0.14	1.1	1.3	<0.002	<0.001	0.023	0.023	<100	0	<5	0	12

WO6*	0.668	7.64	426	221	7.37	3.8	17.6	14.9	0.27	1.8	2.01	<0.002	<0.001	0.037	0.037	<100	0	<5	0	5
WO7	0.366	8.04	247	121	4.7	19.2	8.84	9.97	0.19	1.5	1.68	<0.002	<0.001	0.031	0.031	<100	0	<5	0	
WO8*	0.273	7.76	167	87.4	3.29	13.9	6.44	6.44	0.2	1.8	1.97	<0.002	<0.001	0.029	0.029	<100	0	<5	0	6
WO9	0.647	7.93	793	421	22.9	58.8	22	16.6	1.1	8.2	8.11	<0.002	<0.001	0.05	0.05	<100	0	<5	0	
SC1	0.006	8.51	0.64	0.50	0.17	0.07	0.17	0.51				<0.5	<0.2			<100	0	<250	ND	
SC2	0.002	6.79	0.77	0.71	0.21	0.12	0.21	0.67				<0.5	<0.2			<100	0	<250	ND	
SC3	0.033	6.58	22.62	17.24	2.79	3.34	2.79	18.07				<0.5	<0.2			<100	0	<250	ND	
SC4	0.031	7.17	10.69	7.89	1.62	1.63	1.62	8.12				<0.5	<0.2			309.00	3.00	<250	ND	
SC5	0.05	7.28	19.46	15.70	2.81	3.13	2.81	13.77				<0.5	<0.2			342.00	3.00	<250	ND	
SC6	0.009	7.5	3.33	2.59	0.61	0.58	0.61	3.08				<0.5	<0.2			<100	0	<250	ND	
SC7	0.154	7.1	44.69	46.00	8.24	8.10	8.24	82.35				<0.5	<0.2			<100	0	<250	ND	
SC8*	0.01	6.77	1.53	1.39	0.3	0.31	1.1	1.59	0.087	1.01				0.01		10		3		5
SC9	0.05	7.16	5.13	3.45	1.2	1.23	2.45	3.15	0.08	0.92				<0.01		<10		<3		7
SC10	0.01	8.08	0.676	0.624	0.21	0.139	0.472	0.608	0.07	0.88				<0,01		10		3		
SC11	0.01	8.69	0.95	1.088	0.17	0.212	0.961	1.202	0.03					0.01		20		3		17
SC12	0.02	6.18	1.525	1.184	0.46	0.374	1.092	1.308	0.16	0.90				0.01		10		3		3
SC13	0.01	5.88	0.795	0.939	0.19	0.138	0.764	0.842	0.11	0.88				<0,01		10		3		36
L51	0.292	6.97	103.3	43.3	1.61	6.94	3.16	7.78	0.343					0.09		10		3		7
L71	2.87	6.9	1428	474	14.24	71.49	26.23	58.6	0.36					0.05		10		7		2.5
L69	1.38	7.81	651	238	8.92	32.44	14.55	84.9	0.31									13		5
L68*	1.21	7.75	700	251	9.58	35.96	14.2	97.3	0.47					0.02		<10				6
L67	1.09	6.53	518	182	6.35	24.74	14.14	40.2	0.35					0.03		10		7		?
L75	2.23	6.92	1085	388	16.87	47.85	25.24	117.9	0.51					0.02		20		7		1
L57*	0.2	7.56	81.7	35.664	1.339	5.172	3.101	35.664						<0,01		20		7		40

lake code	VH[a]	RI[a]	BI[a]	LH[a]	OI[a]	LA[a]	SK[a]	SC[a]	1994[b]	1997[b]	2007[b]	2009[b]	Association 2 (Harvey et al. 1998)[c]	Association 3&4[c]	Association 1[c]	mix association 1 & 3&4[c]	multiple dykes[c]	unknown[c]	Reference or principal collectors	region
VAB	1	0	0	0	0	0	0	0	1	0	0	0	0	0	0	0	0	0	a	0
VAC*	1	0	0	0	0	0	0	0	1	0	0	0	0	0	0	0	0	0	a	0
VAD	1	0	0	0	0	0	0	0	1	0	0	0	0	0	0	0	0	0	a	0
VAN*	1	0	0	0	0	0	0	0	1	0	0	0	0	0	0	0	0	0	a	0
VBU	1	0	0	0	0	0	0	0	1	0	0	0	0	0	0	0	0	0	a	0
VCA	1	0	0	0	0	0	0	0	1	0	0	0	0	0	0	0	0	0	a	0
VCL	1	0	0	0	0	0	0	0	1	0	0	0	0	0	0	0	0	0	a	0
VCO	1	0	0	0	0	0	0	0	1	0	0	0	0	0	0	0	0	0	a	0
VEK	1	0	0	0	0	0	0	0	1	0	0	0	0	0	0	0	0	0	a	0
VGR	1	0	0	0	0	0	0	0	1	0	0	0	0	0	0	0	0	0	a	0
VHA	1	0	0	0	0	0	0	0	1	0	0	0	0	0	0	0	0	0	a	0
VHI	1	0	0	0	0	0	0	0	1	0	0	0	0	0	0	0	0	0	a	0
VJT	1	0	0	0	0	0	0	0	1	0	0	0	0	0	0	0	0	0	a	0
VLI	1	0	0	0	0	0	0	0	1	0	0	0	0	0	0	0	0	0	a	0
VLP1	1	0	0	0	0	0	0	0	1	0	0	0	0	0	0	0	0	0	a	0
VLP2	1	0	0	0	0	0	0	0	1	0	0	0	0	0	0	0	0	0	a	0
VMC	1	0	0	0	0	0	0	0	1	0	0	0	0	0	0	0	0	0	a	0
VMN	1	0	0	0	0	0	0	0	1	0	0	0	0	0	0	0	0	0	a	0
VOB	1	0	0	0	0	0	0	0	1	0	0	0	0	0	0	0	0	0	a	0

VOR	1	0	0	0	0	0	0	0	1	0	0	0	0	0	0	0	0	0	a	0
VOV	1	0	0	0	0	0	0	0	1	0	0	0	0	0	0	0	0	0	a	0
VPE	1	0	0	0	0	0	0	0	1	0	0	0	0	0	0	0	0	0	a	0
VPO	1	0	0	0	0	0	0	0	1	0	0	0	0	0	0	0	0	0	a	0
VSC	1	0	0	0	0	0	0	0	1	0	0	0	0	0	0	0	0	0	a	0
VSH	1	0	0	0	0	0	0	0	1	0	0	0	0	0	0	0	0	0	a	0
VSA	1	0	0	0	0	0	0	0	1	0	0	0	0	0	0	0	0	0	a	0
VVE	1	0	0	0	0	0	0	0	1	0	0	0	0	0	0	0	0	0	a	0
VWA	1	0	0	0	0	0	0	0	1	0	0	0	0	0	0	0	0	0	a	0
VWE	1	0	0	0	0	0	0	0	1	0	0	0	0	0	0	0	0	0	a	0
VWI	1	0	0	0	0	0	0	0	1	0	0	0	0	0	0	0	0	0	a	0
RI1	0	1	0	0	0	0	0	0	0	1	0	0	1	0	0	0	0	0	b	1
RI2	0	1	0	0	0	0	0	0	0	1	0	0	0	1	0	0	0	0	b	1
RI3	0	1	0	0	0	0	0	0	0	1	0	0	1	0	0	0	0	0	b	1
RI4	0	1	0	0	0	0	0	0	0	1	0	0	0	0	1	0	0	0	b	1
RI5	0	1	0	0	0	0	0	0	0	1	0	0	0	0	0	1	0	0	b	1
RI6	0	1	0	0	0	0	0	0	0	1	0	0	0	1	0	0	0	0	b	1
RI7	0	1	0	0	0	0	0	0	0	1	0	0	0	1	0	0	0	0	b	1
RI8	0	1	0	0	0	0	0	0	0	1	0	0	0	0	0	0	1	0	b	1
RI9	0	1	0	0	0	0	0	0	0	1	0	0	0	1	0	0	0	0	b	1
RI10	0	1	0	0	0	0	0	0	0	1	0	0	0	1	0	0	0	0	b	1
BAL*	0	0	1	0	0	0	0	0	0	1	0	0	0	0	0	0	0	1	c,d	3
BSU	0	0	1	0	0	0	0	0	0	1	0	0	0	0	0	0	0	1	c,d	3
BFI	0	0	1	0	0	0	0	0	0	1	0	0	0	0	0	0	0	1	c,d	3
BST	0	0	1	0	0	0	0	0	0	1	0	0	0	0	0	0	0	1	c,d	3

BBA	0	0	1	0	0	0	0	0	0	1	0	0	0	0	0	0	0	0	c,d	3
L71	0	0	0	1	0	0	0	0	0	1	0	0	0	0	0	0	0	0	c,d	4
L72*	0	0	0	1	0	0	0	0	0	1	0	0	0	0	0	0	0	0	c,d	4
L59	0	0	0	1	0	0	0	0	0	1	0	0	0	0	0	0	0	0	c,d	4
L67	0	0	0	1	0	0	0	0	0	1	0	0	0	0	0	0	0	0	c,d	4
L74	0	0	0	1	0	0	0	0	0	1	0	0	0	0	0	0	0	0	c,d	4
L63	0	0	0	1	0	0	0	0	0	1	0	0	0	0	0	0	0	0	c,d	4
L60	0	0	0	1	0	0	0	0	0	1	0	0	0	0	0	0	0	0	c,d	4
L35	0	0	0	1	0	0	0	0	0	1	0	0	0	0	0	0	0	0	c,d	4
L34*	0	0	0	1	0	0	0	0	0	1	0	0	0	0	0	0	0	0	c,d	4
L8	0	0	0	1	0	0	0	0	0	1	0	0	0	0	0	0	0	0	c,d	4
L7	0	0	0	1	0	0	0	0	0	1	0	0	0	0	0	0	0	0	c,d	4
L10*	0	0	0	1	0	0	0	0	0	1	0	0	0	0	0	0	0	0	c,d	4
L13	0	0	0	1	0	0	0	0	0	1	0	0	0	0	0	0	0	0	c,d	4
L14*	0	0	0	1	0	0	0	0	0	1	0	0	0	0	0	0	0	0	c,d	4
L12	0	0	0	1	0	0	0	0	0	1	0	0	0	0	0	0	0	0	c,d	4
LSP	0	0	0	1	0	0	0	0	0	1	0	0	0	0	0	0	0	0	c,d	4
L23*	0	0	0	1	0	0	0	0	0	1	0	0	0	0	0	0	0	0	c,d	4
LBU*	0	0	0	1	0	0	0	0	0	1	0	0	0	0	0	0	0	0	c,d	4
L36	0	0	0	1	0	0	0	0	0	1	0	0	0	0	0	0	0	0	c,d	4
LGR	0	0	0	1	0	0	0	0	0	1	0	0	0	0	0	0	0	0	c,d	4
L49	0	0	0	1	0	0	0	0	0	1	0	0	0	0	0	0	0	0	c,d	4
L44	0	0	0	1	0	0	0	0	0	1	0	0	0	0	0	0	0	0	c,d	4
L43	0	0	0	1	0	0	0	0	0	1	0	0	0	0	0	0	0	0	c,d	4
L42	0	0	0	1	0	0	0	0	0	1	0	0	0	0	0	0	0	0	c,d	4
L69	0	0	0	1	0	0	0	0	0	1	0	0	0	0	0	0	0	0	c,d	4
L70*	0	0	0	1	0	0	0	0	0	1	0	0	0	0	0	0	0	0	c,d	4
L68*	0	0	0	1	0	0	0	0	0	1	0	0	0	0	0	0	0	0	c,d	4

LJA	0	0	0	1	0	0	0	0	0	1	0	0	0	0	0	0	0	0	c,d	4
L18	0	0	0	1	0	0	0	0	0	1	0	0	0	0	0	0	0	0	c,d	4
L1	0	0	0	1	0	0	0	0	0	1	0	0	0	0	0	0	0	0	c,d	4
L57*	0	0	0	1	0	0	0	0	0	1	0	0	0	0	0	0	0	0	c,d	4
L73	0	0	0	1	0	0	0	0	0	1	0	0	0	0	0	0	0	0	c,d	4
L51	0	0	0	1	0	0	0	0	0	1	0	0	0	0	0	0	0	0	c,d	4
L58	0	0	0	1	0	0	0	0	0	1	0	0	0	0	0	0	0	0	c,d	4
L53b	0	0	0	1	0	0	0	0	0	1	0	0	0	0	0	0	0	0	c,d	4
LFO	0	0	0	1	0	0	0	0	0	1	0	0	0	0	0	0	0	0	c,d	4
LMA	0	0	0	1	0	0	0	0	0	1	0	0	0	0	0	0	0	0	c,d	4
LPS	0	0	0	1	0	0	0	0	0	1	0	0	0	0	0	0	0	0	c,d	4
LPR	0	0	0	1	0	0	0	0	0	1	0	0	0	0	0	0	0	0	c,d	4
L52	0	0	0	1	0	0	0	0	0	1	0	0	0	0	0	0	0	0	c,d	4
L52b	0	0	0	1	0	0	0	0	0	1	0	0	0	0	0	0	0	0	c,d	4
L59b	0	0	0	1	0	0	0	0	0	1	0	0	0	0	0	0	0	0	c,d	4
L66	0	0	0	1	0	0	0	0	0	1	0	0	0	0	0	0	0	0	c,d	4
L65	0	0	0	1	0	0	0	0	0	1	0	0	0	0	0	0	0	0	c,d	4
LG1	0	0	0	1	0	0	0	0	0	1	0	0	0	0	0	0	0	0	c,d	4
LG2	0	0	0	1	0	0	0	0	0	1	0	0	0	0	0	0	0	0	c,d	4
LG4	0	0	0	1	0	0	0	0	0	1	0	0	0	0	0	0	0	0	c,d	4
L64	0	0	0	1	0	0	0	0	0	1	0	0	0	0	0	0	0	0	c,d	4
L64b	0	0	0	1	0	0	0	0	0	1	0	0	0	0	0	0	0	0	c,d	4
LSN	0	0	0	1	0	0	0	0	0	1	0	0	0	0	0	0	0	0	c,d	4
L61	0	0	0	1	0	0	0	0	0	1	0	0	0	0	0	0	0	0	c,d	4
EO10	0	0	0	0	1	0	0	0	0	0	1	0	0	0	0	0	0	0	e	5
EO11	0	0	0	0	1	0	0	0	0	0	1	0	0	0	0	0	0	0	e	5
EO2	0	0	0	0	1	0	0	0	0	0	1	0	0	0	0	0	0	0	e	5
EO3	0	0	0	0	1	0	0	0	0	0	1	0	0	0	0	0	0	0	e	5
EO4	0	0	0	0	1	0	0	0	0	0	1	0	0	0	0	0	0	0	e	5
EO5	0	0	0	0	1	0	0	0	0	0	1	0	0	0	0	0	0	0	e	5
EO6	0	0	0	0	1	0	0	0	0	0	1	0	0	0	0	0	0	0	e	5

EO7	0	0	0	0	1	0	0	0	0	0	1	0	0	0	0	0	0	0	e	5
EO8	0	0	0	0	1	0	0	0	0	0	1	0	0	0	0	0	0	0	e	5
EO9	0	0	0	0	1	0	0	0	0	0	1	0	0	0	0	0	0	0	e	5
LA1*	0	0	0	0	0	1	0	0	0	0	1	0	0	0	0	0	0	0	e	6
LA10	0	0	0	0	0	1	0	0	0	0	1	0	0	0	0	0	0	0	e	6
LA2	0	0	0	0	0	1	0	0	0	0	1	0	0	0	0	0	0	0	e	6
LA3	0	0	0	0	0	1	0	0	0	0	1	0	0	0	0	0	0	0	e	6
LA4	0	0	0	0	0	1	0	0	0	0	1	0	0	0	0	0	0	0	e	6
LA5	0	0	0	0	0	1	0	0	0	0	1	0	0	0	0	0	0	0	e	6
LA6	0	0	0	0	0	1	0	0	0	0	1	0	0	0	0	0	0	0	e	6
LA7	0	0	0	0	0	1	0	0	0	0	1	0	0	0	0	0	0	0	e	6
LA8	0	0	0	0	0	1	0	0	0	0	1	0	0	0	0	0	0	0	e	6
LA9	0	0	0	0	0	1	0	0	0	0	1	0	0	0	0	0	0	0	e	6
SK1*	0	0	0	0	0	0	1	0	0	0	1	0	0	0	0	0	0	0	e	7
SK10	0	0	0	0	0	0	1	0	0	0	1	0	0	0	0	0	0	0	e	7
SK2	0	0	0	0	0	0	1	0	0	0	1	0	0	0	0	0	0	0	e	7
SK3	0	0	0	0	0	0	1	0	0	0	1	0	0	0	0	0	0	0	e	7
SK4*	0	0	0	0	0	0	1	0	0	0	1	0	0	0	0	0	0	0	e	7
SK5	0	0	0	0	0	0	1	0	0	0	1	0	0	0	0	0	0	0	e	7
SK6	0	0	0	0	0	0	1	0	0	0	1	0	0	0	0	0	0	0	e	7
SK7	0	0	0	0	0	0	1	0	0	0	1	0	0	0	0	0	0	0	e	7
SK8	0	0	0	0	0	0	1	0	0	0	1	0	0	0	0	0	0	0	e	7
SK9	0	0	0	0	0	0	1	0	0	0	1	0	0	0	0	0	0	0	e	7
WO1*	0	0	0	0	1	0	0	0	0	0	1	0	0	0	0	0	0	0	e	5
WO10	0	0	0	0	1	0	0	0	0	0	1	0	0	0	0	0	0	0	e	5
WO2	0	0	0	0	1	0	0	0	0	0	1	0	0	0	0	0	0	0	e	5
WO3	0	0	0	0	1	0	0	0	0	0	1	0	0	0	0	0	0	0	e	5
WO4*	0	0	0	0	1	0	0	0	0	0	1	0	0	0	0	0	0	0	e	5
WO5*	0	0	0	0	1	0	0	0	0	0	1	0	0	0	0	0	0	0	e	5

WO6*	0	0	0	0	1	0	0	0	0	0	1	0	0	0	0	0	0	0	e	5
WO7	0	0	0	0	1	0	0	0	0	0	1	0	0	0	0	0	0	0	e	5
WO8*	0	0	0	0	1	0	0	0	0	0	1	0	0	0	0	0	0	0	e	5
WO9	0	0	0	0	1	0	0	0	0	0	1	0	0	0	0	0	0	0	e	5
SC1	0	0	0	0	0	0	0	1	0	0	1	0	0	0	0	0	0	0	e	8
SC2	0	0	0	0	0	0	0	1	0	0	1	0	0	0	0	0	0	0	e	8
SC3	0	0	0	0	0	0	0	1	0	0	1	0	0	0	0	0	0	0	e	8
SC4	0	0	0	0	0	0	0	1	0	0	1	0	0	0	0	0	0	0	e	8
SC5	0	0	0	0	0	0	0	1	0	0	1	0	0	0	0	0	0	0	e	8
SC6	0	0	0	0	0	0	0	1	0	0	1	0	0	0	0	0	0	0	e	8
SC7	0	0	0	0	0	0	0	1	0	0	1	0	0	0	0	0	0	0	e	8
SC8*		0	0	0	0	0	0	1	0	0	0	1	0	0	0	0	0	0	f	8
SC9		0	0	0	0	0	0	1	0	0	0	1	0	0	0	0	0	0	f	8
SC10		0	0	0	0	0	0	1	0	0	0	1	0	0	0	0	0	0	f	8
SC11		0	0	0	0	0	0	1	0	0	0	1	0	0	0	0	0	0	f	8
SC12		0	0	0	0	0	0	1	0	0	0	1	0	0	0	0	0	0	f	8
SC13		0	0	0	0	0	0	1	0	0	0	1	0	0	0	0	0	0	f	8
L51		0	0	1	0	0	0	0	0	0	0	1	0	0	0	0	0	0	f	4
L71		0	0	1	0	0	0	0	0	0	0	1	0	0	0	0	0	0	f	4
L69		0	0	1	0	0	0	0	0	0	0	1	0	0	0	0	0	0	f	4
L68*		0	0	1	0	0	0	0	0	0	0	1	0	0	0	0	0	0	f	4
L67		0	0	1	0	0	0	0	0	0	0	1	0	0	0	0	0	0	f	4
L75		0	0	1	0	0	0	0	0	0	0	1	0	0	0	0	0	0	f	4
L57*		0	0	1	0	0	0	0	0	0	0	1	0	0	0	0	0	0	f	4

Appendix 2. Post-glacial regional climate variability along the East Antarctic coastal margin – evidence from shallow marine and coastal terrestrial records

*PUBLISHED PAPER. Verleyen E, Hodgson DA, Sabbe K, Cremer H, Emslie SD, Gibson J, Hall B, Imura S, Kudoh S, Marshall GJ, McMinn A, Melles M, Newman L, Roberts D, Roberts SJ, Singh SM, Sterken M, Tavernier I, Verkulich S, Van de Vyver E, Van Nieuwenhuyze W, Wagner B, Vyverman W. Post-glacial regional climate variability along the East Antarctic coastal margin – evidence from shallow marine and coastal terrestrial records. Earth-Science Reviews, **104**: 199-212.*

Author's contribution: literature study of past climate changes of Lützow Holm Bay

Key-words: Antarctica, Holocene, climate change, warm period, palaeolimnology, marine geology

Abstract

We review the postglacial climate variability along the East Antarctic coastline using terrestrial and shallow marine geological records and compare these reconstructions with data from elsewhere. Nearly all East Antarctic records show a near-synchronous Early-Holocene climate optimum (11.5-9 ka BP), coinciding with the deglaciation of currently ice-free regions and the optimum recorded in Antarctic ice and marine sediment cores. Shallow marine and coastal terrestrial climate anomalies appear to be out of phase after the Early-Holocene warm period, and show complex regional patterns, but an overall trend of cooling in the terrestrial records. A Mid- to Late-Holocene warm period is present in many East Antarctic lake and shallow coastal marine records. Although there are some differences in the regional timing of this warm period, it typically occurs somewhere between 4.7 and 1 ka BP, which overlaps with a similar optimum found in Antarctic Peninsula terrestrial records. The differences in the timing of these sometimes abrupt warm events in different records and regions points to a number of mechanisms that we have yet to identify. Nearly all records show a neoglacial cooling from 2 ka BP onwards. There is no evidence along the East Antarctic coastline for an equivalent to the Northern Hemisphere Medieval Warm Period and there is only weak circumstantial evidence in a few places for a cool event crudely equivalent in time to the Northern Hemisphere's Little Ice Age. There is a need for well-dated, high resolution climate records in coastal East Antarctica and particularly in Terre Adélie, Dronning Maud Land and Enderby Land to fully understand the regional climate anomalies, the disparity between marine and terrestrial records, and to determine the significance of the heterogeneous temperature trends being measured in the Antarctic today.

Introduction

Recent assessments of temperature change have revealed that warming in West Antarctica (WA) has exceeded 0.1°C per decade during the past 50 years (Steig et al., 2009) and that the Antarctic Peninsula (AP) is one of the fastest warming regions on Earth (Vaughan et al., 2003). East Antarctica (EA) shows regional differences but the continent-wide average near-surface temperature trend is positive (Steig et al., 2009). To date little

is known about how this pattern of recent warming in Antarctica relates to past natural variability in these regions, despite this being critical for improved prediction of the impact of future climate anomalies on the cryosphere and ecosystems of the continent. Past climate change reconstructions in Antarctica are largely based on ice cores (e.g. Masson et al., 2000; Mayewski et al., 2009). These records have provided information on, for example, past global atmospheric composition (Petit et al., 1999, Jouzel et al., 2007), and productivity and iron flux in the Southern Ocean over several glacial-interglacial cycles (Wolff et al. 2006). In addition, ice cores have revealed the existence of a bipolar seesaw (Blunier et al. 1998, Broecker, 1998) with warm events being out of phase between the Northern and Southern Hemispheres during glacial periods (e.g. Stocker and Johnsen, 2003; Schneider and Steig, 2008; Barker et al., 2009) and likely also during interglacials (Masson-Delmotte et al. 2010a,b). Over the Pleistocene glacial-interglacial cycles, the climate of Antarctica has traditionally been considered to be largely controlled by changes in the Northern Hemisphere and particularly in the North Atlantic region including changes in the strength of deep water formation; yet recent studies have revealed that the Antarctic warming events preceded those in the North (Ahn and Brook, 2008; Mayewski et al., 2009). The mechanisms behind this forcing are still unclear, but a reduction in the stratification of the Southern Ocean and a subsequent release of CO_2 (Anderson et al., 2009, Hodgson and Sime, in press) and a decrease in sea ice (Stevens and Keeling, 2000) are proposed as playing a critical role.

During the Holocene, the connection between climate changes in both hemispheres is however less clear both because the amplitude of the changes has been smaller (but see Masson-Delmotte et al. 2010a,b), and because the relative impact of regional driving or amplifying mechanisms has been greater. For example, Holocene glacier dynamics in New Zealand have been reported as neither in phase nor strictly anti-phased with glacier changes in both hemispheres (Schaefer et al., 2009). To better understand the past and present regional differences and the links between the climates of the Northern and Southern hemispheres during the Holocene, there is a clear need for well-dated palaeoclimate records, particularly from the high latitudes in the Southern Hemisphere. Ice cores have some disadvantages in this respect because the more subtle climate anomalies such as those occurring during the Holocene (e.g. Mayewski et al., 2004; Wanner et al., 2008) are generally less well resolved in the records from the high central plateau (Masson et al., 2000, but see Schneider and Steig, 2008). This pattern is due to the small variations in isotopic composition in these inland locations compared with those generally observed at coastal sites (Bromwich et al., 1998; Masson et al., 2000). Near the coast, the recovery of reliable ice cores enabling high resolution reconstructions is in turn difficult, because the ice-sheet is often too dynamic. In coastal regions, valuable and often overlooked alternatives are lake sediment cores and shallow marine sediment records (see Hodgson et al., 2004; Hodgson and Smol, 2008 for a review).

Here we aim to synthesise lacustrine and coastal marine records of regional climate and environmental changes along the margin of the East Antarctic Ice-Sheet (EAIS), including the Ross Sea region (RSR), and compare these observations with existing reviews of changes in the AP region (e.g., Ingólfsson et al., 1998; Hjort et al., 2003;

Hodgson et al., 2004; Bentley et al., 2009) and with a variety of Antarctic ice core records (e.g., Masson et al., 2000; Steig et al., 2000, Wolff et al., 2006).

Study area and materials and methods

Physical settings of the study area

The most prominent feature of Antarctica is its ice-sheet, which covers over 99% of the continent and is made up of three distinct morphological zones, consisting of the EAIS, the West Antarctic Ice-Sheet (WAIS) and the glaciers of the AP. The Transantarctic Mountains, which run between Victoria Land and the Ronne and Filchner Ice Shelves (Fig. 1), separate the EAIS from the WAIS. The AP extends north from a line between the southern part of the Weddell Sea and a point on the mainland south of the George VI Ice Shelf. The EAIS comprises by far the largest part of the ice-sheet and drains directly into the Southern Ocean between c. 15°W and 150°E. It also has several outlet glaciers that flow through the Trans-Antarctic Mountains, with some of them draining directly into the Ross Sea and Weddell Sea embayments via ice shelves, and a minority that terminate on land (e.g. Taylor Glacier in the McMurdo Dry Valleys).

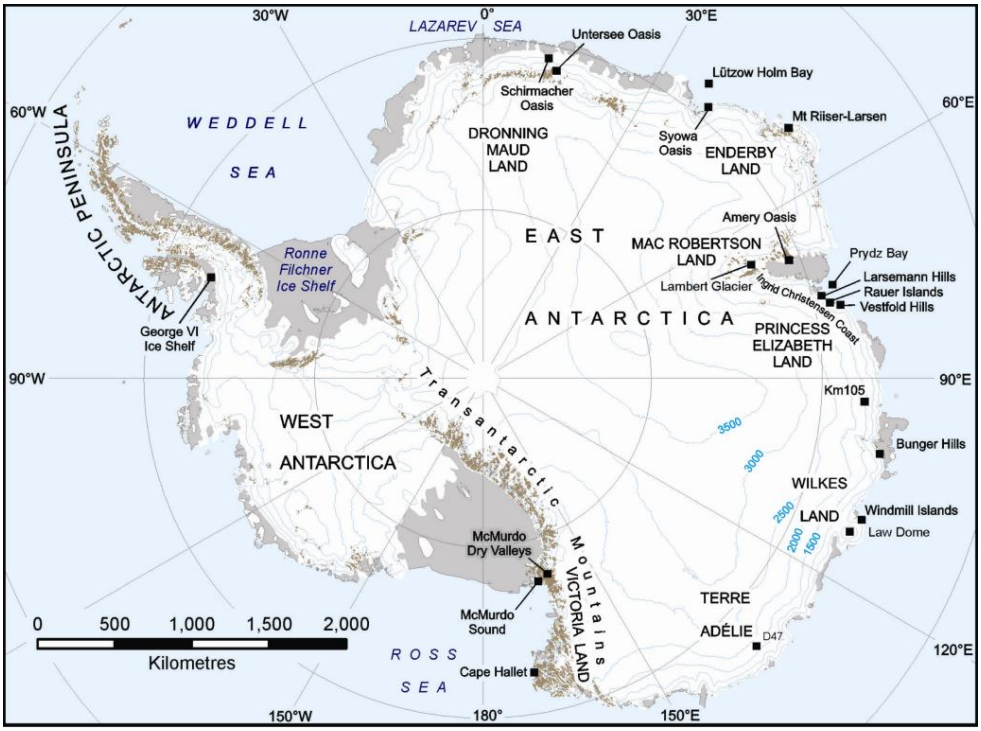

Figure 1. Map of Antarctica showing the locations cited in the text.

The ice-free terrain in EA includes coastal ice-free areas, together with inland nunataks for example in the Transantarctic Mountains, and the Dronning Maud Land regions. It is mainly in the coastal ice free areas that (palaeo)lake sediments and biological, geological and geomorphological evidence is present providing opportunities

to study past climate and environmental changes along the EA coastline. The near shore environment of most of these coastal oases is characterised by bays and fjords, many of which have also been sampled for their marine geological records. The main ice-free regions studied to date are Schirmacher Oasis, the islands and peninsulas in the Lützow Holm Bay region, Amery Oasis, Larsemann Hills, Rauer Islands, Vestfold Hills, Bunger Hills, Windmill Islands and the RSR (Fig. 1). In brief, the Schirmacher Oasis (70°46'S-11°44'E) is a c. 50 km² wide area, bounded by the EAIS to the South and the Lazarev Ice Shelf to the North. Lützow Holm Bay includes several peninsulas and numerous ice free islands that cover a total ice-free area of c. 200 km². Amery Oasis (70°40'S-68°00'E) is a 1800 km² area located some 200 km inland from the front of Amery Ice Shelf in Prydz Bay. The oasis is bordered by the Charybdis Glacier to the north, the EAIS to the west and southwest, and the drainage system of the Amery Ice Shelf/Lambert Glacier to the south and east. The Vestfold Hills (68°30' S, 78°00' E) are a 400 km^2 ice-free area on the Prydz Bay coast (Fig. 1), consisting of three main peninsulas (Mule, Broad and Long Peninsula) and a number of offshore islands. The Larsemann Hills (69°23' S, 76°53' E), is a 50 km^2 ice-free area on the Ingrid Christensen Coast located approximately midway between the eastern extremity of the Amery Ice Shelf and the southern boundary of the Vestfold Hills. The Rauer Islands (68°45' S - 68°55' S and 77°30' E - 78°00' E) are an ice-free coastal archipelago between the Larsemann Hills and the Vestfold Hills (Fig. 1). The Rauer Islands includes 10 major islands and promontories together with numerous minor islands covering a total area of some 300 km^2. The Bunger Hills (66°17'S, 100°47'E) is a 952 km^2 ice-free area of land and marine bays, bordered on the north by the Shackleton Ice Shelf and by the EAIS (with partly floating outlet glaciers) to the south, west and east. The Windmill Islands (66°20' S - 110° 30 E) are a group of ice-free islands and peninsulas on the EA coast north of Law Dome (Fig. 1) and cover a total area of 75-80 km². The RSR contains a number of ice free coastlines, nunataks, and most notably the McMurdo Dry Valleys (77°28' S – 162°31' E), which at 4800 km^2 are the largest relatively ice-free region in Antarctica.

Present day climate

During the instrumental period (past ~50 years) the mean annual temperature in the EA coastal region has been about –10°C (Steig et al., 2009), with positive temperatures generally confined to the summer months, when lakes might become ice-free. During summer, the Antarctic receives more solar radiation than the tropics, but the snow and ice surfaces have a high albedo and reflect much of this radiation back into space (Turner et al. 2009). Where snow melts, exposing large patches of bare (dark) ground, or where sea ice melts exposing ice free (dark) ocean, solar radiation is absorbed rather than reflected, and the environment will locally warm. During winter, the Antarctic stratosphere is extremely cold due to the lack of incoming radiation (Turner et al. 2009), which results in surface cooling, more extensive snow cover and complete lake ice cover in coastal regions. A strong temperature gradient then develops between Antarctica and the Southern Hemisphere mid-latitudes, thereby isolating a pool of very cold air above Antarctica. Very strong winds develop along this thermal gradient. During much of the year a strong temperature inversion exists above the surface, which is maintained by radiative cooling from the highly reflective snow and ice surface. However, when strong katabatic winds, transporting cold, relatively dense air from the interior of Antarctica, reach the coast, they can destroy the inversion through turbulent mixing, leading to

enhanced sensible heat flux towards the surface and an increase in temperature. Thus, near-surface temperatures often co-vary strongly with wind speed. For Antarctica as a whole, studies using reanalysis data and climate models suggest that the season of greatest precipitation is autumn (Marshall 2009) although there is significant regional variation across the continent (e.g. van de Berg et al., 2005). In the coastal regions, the majority of precipitation falls in relation to the passage of synoptic-scale weather systems and associated cloud bands within the circumpolar trough of low pressure that rings the continent (Marshall 2009).

The primary mode of atmospheric circulation variability of the Southern high latitudes is the Southern Annular Mode (SAM), which has a significant influence on EA coastal temperatures (e.g. Thompson and Solomon, 2002; Marshall, 2007). In recent decades the relationship is predominantly negative (r ~ –0.6) so that a more positive SAM leads to colder regional temperatures. Using model data, Van den Broeke and van Lipzig (2003) demonstrated that the negative relationship between the SAM and regional temperatures is a combination of free atmosphere and near-surface effects. A more positive SAM, which is associated with stronger circumpolar westerlies around Antarctica, isolates the continent more effectively from the advection of warm extra-tropical air masses into the coastal region. In addition, positive SAM reduces the speed of katabatic flow over much of EA, hence leading to less disruption of the surface temperature inversion, a sensible heat flux away from the surface and colder temperatures (Van den Broeke and van Lipzig, 2003). There have been statistically significant positive increases in the SAM over the past few decades in austral summer (DJF) and autumn (MAM) (e.g. Marshall, 2003), which will have acted to cool EA temperatures. Nonetheless, over the past 50 years EA coastal temperatures have changed very little so that the changes in the SAM — believed to be principally due to anthropogenic forcing, through ozone depletion and increasing greenhouse gases — can be considered to be buffering the regional impact of global warming.

However, recent work by Marshall et al. (in press) has revealed that the sign of the relationship between the SAM and temperature in EA is not necessarily temporally stable and can indeed reverse on decadal timescales. The changes in sign are related to variability in the positions of the long-waves over the Southern Ocean, the non-annular component of the SAM. Changes in the relative strength and longitude of the two climatological lows located off the EA coast (at ~20°E and 110°E) will impact significantly on the mean advection of temperature and moisture into the region. Using ice core data encompassing the 20th Century, Marshall et al. (in press) showed that such changes are part of natural climate variability. Thus, care needs to be taken in relating proxy indices of the SAM to regional temperature and vice versa.

Materials and methods

The majority of the past climate and environmental change reconstructions in EA reviewed here are based upon lake or shallow near shore marine sediment cores. We are aware that some proxies are more reliable than others in specific settings. Similarly some proxies, such as the occupation of land by biota, might also show a lagged response to climate changes, whereas others respond more quickly (e.g. the response of lacustrine diatom assemblages to salinity changes). Moreover, in contrast to marine sediment and

ice cores in which alkenones and stable isotopes of H and O can be used as palaeothermometers, most proxies used in terrestrial environments provide indirect measurements of past climate changes, for example by reconstructing changes in the moisture balance which can be a function of both temperature and wind speed. In some studies, dating uncertainty can also be high, particularly where only a small number of ^{14}C dates have been used to constrain the timing of past climate and environmental changes. Combined, these shortcomings must be taken into account when formulating a consensus on past regional climate changes.

For an overview of the different proxies used here, the reader is referred to Hodgson et al. (2004) and Hodgson and Smol (2008). In short, lacustrine diatoms are generally used in combination with transfer functions to enable the quantitative reconstruction of past changes in the moisture balance (e.g., Roberts and McMinn, 1998; Verleyen et al., 2003) and/or nutrient levels (Roberts et al., 2004). Marine diatoms are divided into sea-ice related and open water taxa (e.g., Verleyen et al., 2004a) based upon their presence in modern analogue assemblages of the Southern Ocean (e.g., Armand et al., 2005; Crosta et al., 2005). Faunal microfossils are used to study past changes in lake ecology (Cromer et al., 2005, 2006). Fossil pigments enable the reconstruction of changes in the marine and lacustrine autotrophic communities, primary productivity, and changes in ice cover dynamics (e.g., Hodgson et al., 2003; Verleyen et al., 2004a, 2005). Sedimentological and geochemical proxies are used to reconstruct transitions between different sedimentary environments (e.g., glacial vs. lacustrine), primary productivity [e.g., loss-on-ignition, total organic carbon content (TOC)], whether a reduction or oxidation occurs in the water column through reduced or increased ice cover [total sulphur content (TS) e.g., Wagner et al., 2006], or the presence of vegetation in the catchment area (the total carbon vs. total nitrogen content (TC/TN), Wagner et al., 2006). Oxygen and carbon isotopes can be used to infer changes in the moisture balance in closed lakes (e.g., Hodgson et al., 2005).

Other evidence for past climate and environmental changes in EA include the presence of relict deltas on land formed at times of higher lake levels indicating increased meltwater supply (Hall and Denton, 2000a,b) and the presence/absence of seal hairs on land and penguin remains (e.g., Emslie et al., 2007; Hall et al., 2006). For example, the presence of hairs from Southern Elephant Seals has been used to infer changes in sea ice extent in the RSR (Hall et al., 2006), and the remains of past Adélie Penguin colonies and fossilized otoliths of their prey, Antarctic silverfish (Lorenzini et al. 2009), indicate that pack ice was present providing foraging opportunities for penguins during spring; conversely, their absence indicates that cold episodes caused unfavourable marine conditions with permanent sea ice blocking access to nesting sites (Emslie et al., 2007).

Where radiocarbon dating is used to provide a chronology, calibrated ^{14}C dates are cited as reported in the original publications. Similarly, corrections for the radiocarbon reservoir effect are applied as in the original publications. To allow comparison between the studies where ^{14}C dates were used but not calibrated, we list the original ^{14}C dates (^{14}C ka BP), and then carried out our own calibration using CALIB 5.0.2 (http://calib.qub.ac.uk/calib/) citing the upper and lower limits (at 2-std deviations) of the calendar ages (ka BP). In cases where dates were derived from marine organisms,

the radiocarbon dates were corrected for the marine reservoir effect by subtracting 1300 yrs following the Antarctic standard (Berkman et al., 1998) prior to calibration (i.e., the offset from the global marine reservoir (ΔR) was set at 900 years when using the marine calibration curve; Hughen et al., 2004). For lacustrine ^{14}C ages younger than 11 ka BP the Southern Hemisphere atmospheric calibration curve was used (McCormac et al., 2004); in all other cases the Northern Hemisphere atmospheric calibration curve (Reimer et al., 2004) was applied.

The time of deglaciation of the current ice-free regions was derived from published cosmogenic isotope dating of exposed rocks (Gosse and Philips, 2001) and ^{14}C dating of fossils incorporated into raised beaches, organic material and fossils in lake sediments, and (abandoned) bird colonies (e.g. through the radiocarbon dating of stomach oil deposits from snow petrels (*Pagodroma nivea*)). The ^{14}C dates are interpreted as minimum ages since there is an unknown lag time between deglaciation and colonization of the land by biota (e.g., Gore, 1997; Ingólfsson et al., 2003).

Overview of past climate changes

The Pleistocene-Holocene transition

The widespread Antarctic Early-Holocene climate optimum between 11.5 and 9 ka BP observed in all ice cores from coastal and continental sites (Steig et al., 2000, Masson et al., 2000, Masson-Delmotte et al., 2004, 2010; Mayewski et al., 2009), coincided with the onset of biogenic sedimentation in lakes and the occupation of ice-free land by biota between c. 13.5 and 10 ka BP in Princess Elizabeth Land and Mac Robertson Land (Fig. 1 and 2). In the Larsemann Hills, Vestfold Hills and Amery Oasis some areas escaped full glaciation during the Last Glacial Maximum (LGM) (Hodgson et al., 2001; Gibson et al., 2009; Kiernan et al., 2009; Fink et al., 2006; Colhoun et al., 2010; Newman et al. unpubl. res.), whereas other areas were likely completely ice-covered and gradually deglaciated between c. 13.5 and 4 ka BP (Hodgson et al., 2001; White et al., 2009). Diatoms and pigment data point to the establishment of seasonally melting lake ice and snow cover, and the development of microbial mats at c. 10.8 ka BP (Hodgson et al., 2005), with evidence for relatively wet conditions between c. 11.5 and 9.5 ka BP in a lake on one of the northern islands in the Larsemann Hills (Verleyen et al., 2004b). This is consistent with palaeolimnological evidence from the nearby Vestfold Hills, where some lakes became ice-free and diatoms and rotifers inhabited water bodies from c. 11.4 ^{14}C ka BP onwards (c. 13.2-13.4 ka BP; Roberts and McMinn, 1999, Cromer et al., 2005). In the Rauer Islands ice-free conditions were inferred prior to c. 11.6-11.2 ka BP and a marine climate optimum is present between 9.2 and 8.2 ka BP (Berg et al., 2009, 2010). At least parts of Amery Oasis were covered by locally expanded glaciers during the Late Pleistocene (Hambrey et al., 2007), but deglaciation of some areas had started prior to c. 11 ka BP (Wagner et al., 2004, Fink et al., 2006) and biogenic sediments started to accumulate in some lakes from c. 13.4-12.5 ka BP (Wagner et al., 2004; Wagner et al., 2007; Newman et al. unpubl. res.), coincident with deglaciation of coastal regions in Mac Roberston Land from 13 ka BP onwards (Mackintosh et al., 2007). Microfossils indicate a well-developed faunal community in one of the lakes from c. 13 ka BP (Newman et al. unpubl. res.), which was followed by the establishment of a diatom community at c. 10.2 ka BP, likely related

to increased nutrient inputs and a reduction in ice and snow cover, marking the start of relatively warm conditions (Wagner et al., 2004).

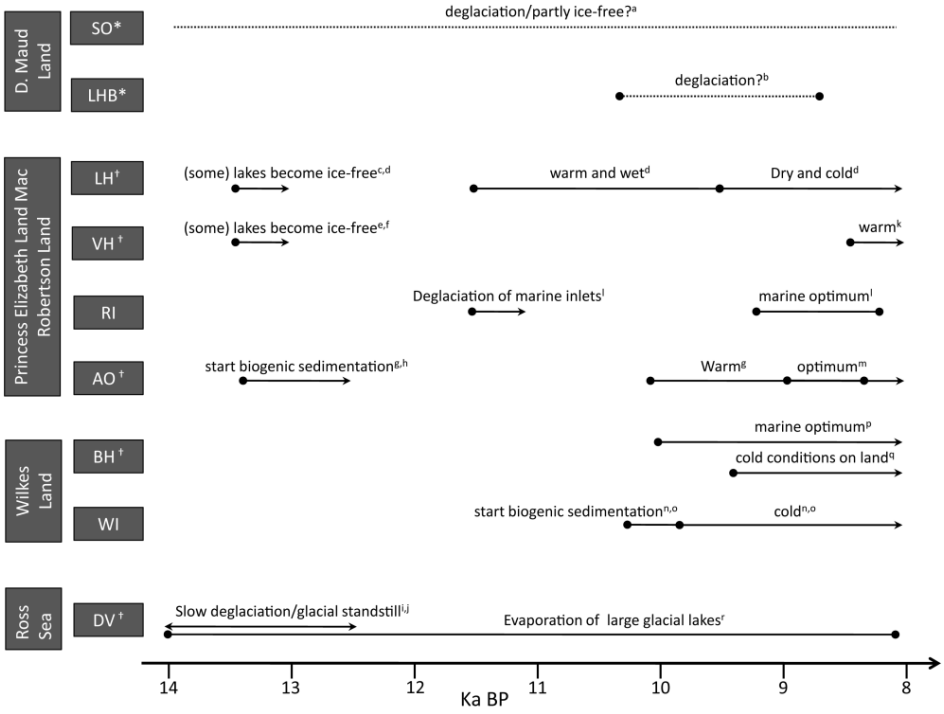

Figure 2. Deglaciation and Early-Holocene warmth in ice-free regions along the East Antarctic coastline. Dashed lines represent poorly dated records. For regions indicated with an asterisk, detailed records are lacking. Regions indicated with a cross were partly ice-free during the LGM. SO: Schirmacher Oasis, LHB: Lützow Holm Bay region, LH: Larsemann Hills, VH: Vestfold Hills, RI: Rauer Islands, AO: Amery Oasis, BH: Bunger Hills, WI: Windmill Islands, and DV: McMurdo Dry Valleys. Superscript numbers refer to the original publications: [a]Gingele et al. (1997), [b]Miura et al. (1998), [c]Hodgson et al. (2005), [d]Verleyen et al. (2004b), [e]Roberts and McMinn (1999), [f]Cromer et al. (2005), [g]Wagner et al. (2004), [h]Fink et al. (2006), [i]Emslie et al. (2007), [j]Hall (2009), [k]Gibson (unpublished results), [l]Berg et al. (2010), [m]Cremer et al. (2007), [n]Cremer et al. (2003), [o]Hodgson et al. (2003), [p]Kulbe et al. (2001), [q]Verkulich et al. 2002), [r]Hendy (2000).

In Wilkes Land, parts of the Bunger Hills remained ice-free during the LGM (Gore et al., 2001), whereas the Windmill Islands (66°20'S-110°30'E) were glaciated (Goodwin, 1993). The minimum ages for deglaciation of the Windmill Islands are also slightly younger than those from the oases near the Lambert Glacier; post-glacial lake sediments accumulated at c. 10.2 ka BP (Roberts et al., 2004), biogenic sedimentation in the marine bays started around c. 10.5 ka BP (Cremer et al., 2003; Hodgson et al., 2003), and penguins occupied the region from at least c. 9 ka BP (Emslie and Woehler, 2005). Despite the temperature optimum recorded in the ice cores, relatively cool summer conditions persisted near the Windmill Islands during the Early-Holocene, probably due to the influence of local glaciers as reflected by the well-developed sea ice diatom assemblages seen in coastal marine sediment cores (Cremer et al., 2003). The Bunger Hills were

occupied by nesting snow petrels from at least 10 ka (Verkulich and Hiller, 1994), and organic sediments started to accumulate in the lakes at the Pleistocene - Holocene boundary in association with extensive and relatively rapid ice melting, which also supports the occurrence of an Early-Holocene warm period at c. 9 +/- 0.5 ka BP (Verkulich et al., 2002). Further radiocarbon evidence suggests that large parts of the southern Bunger Hills were rapidly deglaciated prior to 8 ka BP (Melles et al., 1997).

Although terrestrial climate archives are present in the ice-free regions in Dronning Maud, Enderby, and Mac Robertson Land (Sinha et al., 2000; Bera, 2004, Singh and Tiwari, 2004; Matsumoto et al., 2006), surprisingly little information is available about the deglaciation and post-glacial climate evolution there. At least some areas such as the Untersee Oasis (71°S-13°E) were probably ice-free during the LGM as shown by ^{14}C dating of stomach oil deposits from snow petrels, which indicates occupation during at least the past 34 ka (Hiller et al., 1988). Similarly, coastlines of some islands and peninsulas in Lützow-Holm Bay near Syowa Station (69°00'S-39°35'E) may have been ice-free for at least 40 ka and probably longer, as evidenced by AMS ^{14}C dates of individual *in situ* marine fossils incorporated into raised beaches (Miura et al., 1998). Other areas such as the Schirmacher Oasis likely deglaciated at the Pleistocene - Holocene boundary as indicated by a grounding line retreat in the Lazarev Sea (Gingele et al., 1997). Similarly, parts of Mt. Riiser-Larsen in Enderby Land likely deglaciated at the beginning of the Holocene as evidenced by the onset of organic sedimentation in Lake Richardson (Zwartz et al., 1998).

In the RSR, a grounded ice-sheet fed from the glaciers of the Ross Embayment began filling the McMurdo Sound at ~27 ^{14}C ka BP (Emslie et al., 2007) until reaching its northern extent at the LGM, and remained at its LGM position until c. 12.7 ^{14}C ka BP (c. 14.7-15.2 ka BP). Following the LGM, the ice receded at a very slow rate, or stood still, until c. 10.8 ^{14}C ka BP (c. 12.7-12.9 ka BP) (Denton and Marchant, 2000; Hall and Denton, 2000a; see Hall, 2009 for a review). For example, the Wilson Piedmont Glacier probably maintained its LGM position until c. 10.7 ^{14}C ka BP (c. 12.6-12.8 ka BP) (Hall and Denton, 2000b; Hall et al., 2001) and persisted there into the Early-Holocene (Hall et al., 2000; Hendy, 2000; Hall et al., 2001, 2002). This grounded ice-sheet blocked several valleys in the McMurdo Dry Valleys and fed large proglacial lakes such as glacial Lakes Washburn and Wright, which had water over 500 m deep in some valleys (Hall and Denton, 1995) and existed until the Early-Holocene (Hall et al., 2000; Hendy, 2000; Hall et al., 2002). Between c. 14 ka and 8 ka BP these large proglacial lakes started to evaporate (Hendy, 2000); the evaporation of Lake Washburn starting during the LGM. In the Taylor Valley, evaporation of Lake Fryxell was discontinuous, with a series of high and low stands (Wagner et al., 2006). Significant changes in the rate of carbonate precipitation (measured as Total Inorganic Carbon) in a sediment core from Lake Fryxell between c. 13 and 11 ka BP suggest a significant desiccation event at the Pleistocene-Holocene transition (Wagner et al., 2006, but see Whittaker et al., 2008). Offshore, an Early-Holocene climate optimum with open marine conditions is inferred from the presence of varved diatomaceous ooze in a marine sediment core from Cape Hallett at >9.5-9.4 ka BP (Finocchiaro et al., 2005).

After the Early-Holocene Warm period

The period following deglaciation shows complex and less consistent patterns than those observed at the Pleistocene – Holocene boundary (Fig. 3). In the Larsemann Hills, relatively dry conditions occurred on land between c. 9.5 and 7.4 ka BP, when lake levels dropped below their present position (Verleyen et al., 2004b). The composition of marine sediments deposited in isolation basins between c. 7.4 and 5.2 ka BP is consistent with a marine climate optimum, which is not clearly evident in the terrestrial sediments (Verleyen et al., 2004b; Hodgson et al., 2005). In the Amery Oasis, the slight warming inferred from a minor increase in lake organic matter content during the Early-Holocene at 10.2 ka persisted until c. 6.7 ka BP, when a clear temperature optimum is inferred from geochemical proxies between c. 8.6 and 8.4 ka BP (Cremer et al., 2007). This warming was proposed as being in opposite phase (within dating uncertainty) to the 8.2 ka cold event reported from the North Atlantic region, yet recently obtained ^{14}C dates place this optimum earlier, between 8.9-8.7 ka BP (Newman et al. unpubl. res.), implying that the anomalies in both hemispheres are possibly not related. The optimum was followed by cold conditions from c. 6.7 – 3.7 ka BP (Wagner et al., 2004). In the Vestfold Hills, isostatic rebound and the emergence of isolation lakes from the sea resulted in major ecosystem changes, which hampers detailed palaeoclimatological inferences being made for the period after the Early-Holocene optimum, particularly in lower altitude lakes (Fulford-Smith and Sikes, 1996; Roberts and McMinn, 1999). However, in one of the lakes there is evidence for a warm period between c. 8.5 and 5.5 ka BP and a major cooling event between 5.5 and 5 ka BP (Gibson unpubl. res.). In the Rauer Islands, the cold conditions that started around 8.2 ka BP persisted until 5.7 ka BP were followed by a marine climate optimum which lasted until 3.5 ka BP (Berg et al. 2010). In the Windmill Islands, relatively cool summer conditions were observed in a marine bay with a combination of winter sea-ice and seasonal open water conditions inferred from diatom assemblages between c. 10.5-4 ka BP (Cremer et al., 2003; Hodgson et al., 2003). These open water conditions are partly corroborated in the marine sediments of a nearby isolation basin but have less robust chronological constraints (Roberts et al., 2004). The peak of this (marine) cooling period was pinpointed at about c. 7 ka BP, when penguin colonies where abandoned on one of the peninsulas (Emslie and Woehler, 2005). In the Bunger Hills cold and dry conditions with limited meltwater and extended periods of lake ice cover prevailed on land between c. 9 and 5.5 ka BP (Verkulich et al., 2002), coincident with an expansion in snow petrel colonisation between c. 8 and 6 ka BP (Verkulich and Hiller, 1994). Ainley et al (2006) link slightly elevated $\delta^{13}C$ values in stomach oil deposits from snow petrels to a shift in feeding to ^{13}C enriched prey which was made available by a reduction in sea ice during a marine climate optimum sometime between 7.5 to 5.5 ka BP, yet the temporal resolution of this record is particularly low during this period. Perhaps a better constraint on the timing of this marine optimum can be identified in coastal sediments where high Total Organic Carbon, high C/N and low concentrations of ice related diatoms were present from at least. 9.4 to 7.6 ka BP (Kulbe et al., 2001), followed by cold marine conditions between c. 7.6 and 4.5 ka BP.

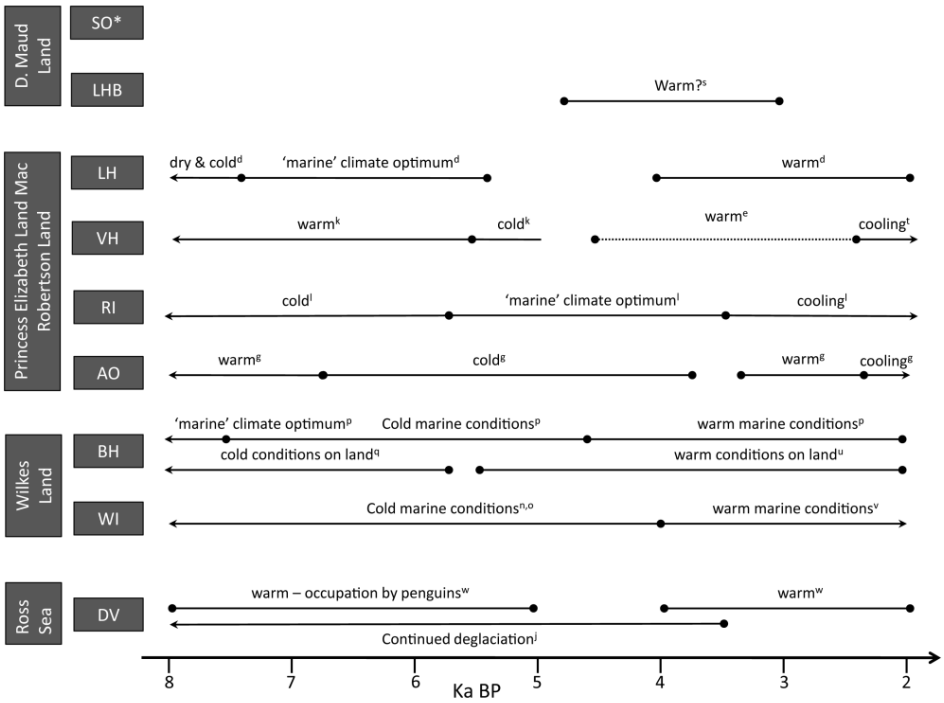

Figure 3. Mid-Holocene climate variability along the East Antarctic coastline. Dashed lines represent poorly dated records. For regions indicated with an asterisk, detailed records are lacking. Abbreviations as in Fig. 2. Superscript numbers refer to the original publications: for a-r see caption of Fig. 2; [s]Okuno et al. (2007), [t]Fulford-Smith and Sikes (1996), [u]Melles et al. (2007), [v]Kirkup et al. (2002).

In the RSR, the last remnants of grounded ice in Taylor Valley post-date c. 8.4 ^{14}C ka BP (c. 9-9.4 ka BP), and penguins did not recolonize the area until c. 8 ka BP, after an absence of c. 19,000 years (Baroni and Orombelli, 1994; Hall et al., 2006; Emslie et al., 2007). Relict lake deltas show an increase in the meltwater supply and increases in lake levels at c. 6 ^{14}C ka BP (c. 6.8 ka BP; Hall and Denton, 2000a,b) coinciding with a major retreat of the Ross Ice-Sheet and a regional deglaciation inferred from radiocarbon dating of remains in raised beaches, till deltas, and marine sediments (c. 6.6 ^{14}C ka BP: c. 7.5 ka BP; Hall et al., 2000a 2004; Hall and Denton, 1999). The recession of parts of the Wilson Piedmont Glacier was delayed until an ice shelf retreat in the area at c. 5.7 ^{14}C ka BP (c. 6.6-6.3 ka BP; Hall and Denton, 1999) and this retreat lasted until at least c. 4.4-3.1 ^{14}C ka BP (c. 5.2-4.8 – 3.5-3.3 ka BP; Hall and Denton, 2000b). This post-dates a secondary climate optimum detected in the ice cores of the RSR, between 8 and 6 ka BP (Masson et al., 2000, p 355). There is also sedimentological and geochemical evidence for increases in inferred salinity between c. 9 and 4 ka BP in a sediment core from Lake Fryxell (Wagner et al., 2006); although subsequent analyses based on stratigraphy, mineralogy and diatom assemblages found generally stable Holocene lake levels after the initial drop in the Early-Holocene, with only a minor low-stand at ~6.4 ka BP (Whittaker et al., 2008). In a marine sediment core from northern Victoria Land, there is evidence for cooling from 9.4 ka and

an abrupt decrease in palaeoproduction markers from 8.0 to 7.8 ka BP when sandy mud sediment suggests a rapid landward recession of the local/regional glaciers, together with the onset of seasonal sea-ice formation (Finocchiaro et al., 2005).

The Mid- to Late-Holocene warm period

A Mid- to Late-Holocene warm period is inferred from various ice, lake and marine core records from Antarctica (see Hodgson et al. (2004) for a review). In the Larsemann Hills this warm period is dated between c. 4 and 2 ka BP (Fig. 3). There, relatively wet conditions resulted in increased lake water levels, which predate then overlap with the coastal marine optimum inferred from the presence of open water marine diatoms in isolation basins at 2.7 to 2.2 ka BP (Verleyen et al., 2004a, 2004b). A short return to dry conditions and low water levels is present in one of the lake records at c. 3.2 ka BP (Verleyen et al., 2004b). The relatively wet period is coincident with ice thinning over Progress Lake and the resumption of biogenic sedimentation at 3.5 ka BP, after at least 40 ka of permanent ice cover (Hodgson et al., 2006a), and the formation of proglacial lakes on Stornes, the eastern of the two main peninsulas in the Larsemann Hills between c. 3.8 and 1.4 ^{14}C ka BP (c. 4.4-4.1 and 1.3 ka BP; Hodgson et al., 2001). In the Amery Oasis, relatively warm conditions between c. 3.2 and 2.3 ka BP are inferred from abundant organic matter deposition in Lake Terrasovoje (Wagner et al., 2004), yet newly obtained ^{14}C dates place this optimum slightly earlier at c. 3.5 and 3.1 ka BP (Newman et al. unpubl. res.). In the Vestfold Hills, a decline in lake salinity could be inferred between c. 4.2 and 2.2 ka BP, but the dates are at low resolution (Roberts and McMinn, 1996, 1999a). This period of low salinity is however broadly supported by the warm and humid conditions between c. 4.7 and 3 ka BP proposed by Björck et al. (1996) after reinterpretation of previously published results (Pickard et al., 1986) and with reduced sea-ice cover in one of the fjords between >3.5 and 2.5 ka BP (McMinn et al., 2001). Following this, a large increase in sea-ice in the fjords suggests cooling occurred between 2.5 and 2 ka BP (McMinn et al., 2001).

In the Windmill Islands, enhanced biological production, probably reflecting more open water conditions and a climate optimum, occurred in the near shore environment between c. 4 and 1 ka BP (Kirkup et al., 2002), with stratified conditions caused by enhanced meltwater input (Cremer et al., 2003). In this area the Mid- to Late-Holocene warm period coincided with the readvance of the Law Dome ice margin after c. 4 ka BP, in response to an increase in precipitation (Goodwin, 1996). In the Bunger Hills, a stepwise increase in primary production was reported in the lakes between c. 4.7 and 2 ka BP (Melles et al., 1997) and was accompanied by the draining of some ice-dammed lakes between c. 5.5 and 2 ka BP (Verkulich et al., 2002). Similarly a gradual near shore marine warming was inferred for this area from c. 4.5 ka BP, followed by an optimum between c. 3.5 and 2.5 ka BP (Kulbe et al., 2001).

In the Lützow-Holm Bay region, a rapid isostatic rebound (6 m in c. 1000 years) occurred between c. 4.7 and 3 ka BP, which was linked to the rapid removal of part of the regional ice mass, most likely as a result of ice melting caused by warming (Okuno et al., 2007). No detailed information is available for other areas in the Dronning Maud Land region.

In the RSR, the presence of hairs from Southern Elephant Seals along with the remains of Adélie Penguins between c. 6 and 4 ^{14}C ka BP (c. 5.6 - 2.8 ka BP), indicates less sea ice than today, but sufficient pack ice for penguins to forage during spring according to Hall et al. (2006), but it is not until 4-2 ka BP that there was extensive occupation by Adélie Penguins along the central to southern coastlines (Baroni and Orombelli, 1994, Emslie et al 2007) after a period of abandonment between 5 and 4 ka BP (Emslie et al., 2007). Moreover, the temporal distribution of otoliths from Antarctic silverfish, which is the preferred prey of Adélie penguins, shows a peak between 4 and 2 ka BP (Lorenzini et al. 2009). In Lake Fryxell, well-developed microbial mats occurred from c. 4 ka BP onwards, which indicates similar environmental conditions and water depths to those found today (Wagner et al., 2006) although minor low stands have been inferred at 4.7, 3.8, and 1.6 ka BP (Whittaker et al., 2008).

Past 2000 years - Neoglacial cooling, the Medieval Warm Period, the Little Ice Age and recent climate change

Much attention has been paid to the fluctuations in climate which in the Northern Hemisphere gave rise to the well-documented Medieval Warm Period (900-1300 AD or 1100-700 BP), and the Little Ice Age (LIA) (1450-1850 AD or 500 and 100 BP). The search in Antarctica for these climate signals is an important element in understanding how the Earth's climate system works, and in particular to determine if Late-Holocene climate events are in phase or exhibit an antiphase or see-saw pattern between the hemispheres.

In the Larsemann Hills, there is some evidence of neoglacial cooling (Fig. 4) leading to dry conditions around 2 ka BP (Hodgson et al., 2005), 700 yr BP and between c. 300 and 150 yr BP in some of the lakes (Verleyen et al., 2004b). These dry conditions parallel declines in sea bird populations during the past 2000 years which have been related to a 'climate deterioration' (Liu et al., 2007). In the Amery Oasis, neoglacial cooling occurred from c. 2.3 ka BP onwards, with a short return to a relatively warmer climate between c. 1.5 and 1 ka BP (Wagner et al., 2004). In the Vestfold Hills, meltwater input into the lakes gradually decreased from 3 ka BP onwards (Fulford-Smith and Sikes, 1996) and an increase in fast ice extent is observed from c. 1.7 ka BP (McMinn, 2000), broadly coincident with the Chelnock Glaciation on land (Adamson and Pickard, 1986). Cold conditions are similarly inferred between c. 1.3 ka BP and 250 yr BP (Bronge, 1992) and low precipitation from c. 1.5 ka ^{14}C BP (c. 1.3-1.5 ka BP, but dating is at low resolution; Roberts and McMinn, 1999). A palaeohydrological model reconstructing changes in lake salinity and water level from a lake sediment core shows no significant change in evaporation for the last c. 700 years, other than a slightly lower evaporation period at c. 150 - 200 yr BP, which is the only hint of a mild LIA-like event in the Vestfold Hills (Roberts et al., 2001).

In the Windmill Islands neoglacial cooling and persistent sea-ice cover were inferred from a decrease in the biogeochemical proxies of production in the marine bays near the Windmill Islands (Kirkup et al., 2002; Cremer et al., 2003). A slow decrease in lake water salinity was observed on nearby islands during the Late-Holocene, and there is no evidence for a LIA-like event there (Hodgson et al., 2006b). Instead, a very rapid salinity rise during the past few decades was present that has likely been brought about by increased wind speed and evaporation (Hodgson et al., 2006b). In the Bunger Hills,

extended settlement by snow petrels after c. 2 ka BP was reported by Verkulich and Hiller (1994) from the presence of stomach oil deposits, and coincides with a lake sediment inferred climate cooling (Melles et al., 1997; Verkulich et al., 2002) and geomorphological evidence of a glacier readvance during recent centuries (Adamson and Colhoun, 1992). Cool conditions persisted from c. 2 ka BP with some minor fluctuations (Verkulich et al., 2002).

In the Lützow-Holm Bay region, lake sediment cores have yet to provide insights in past climate variability during the Late-Holocene but preliminary investigations show excellent preservation of biogeochemical markers (Matsumoto et al., 2006). Detailed palaeoclimatic records are still lacking for the region and for areas in Dronning Maud Land and other regions in Enderby Land.

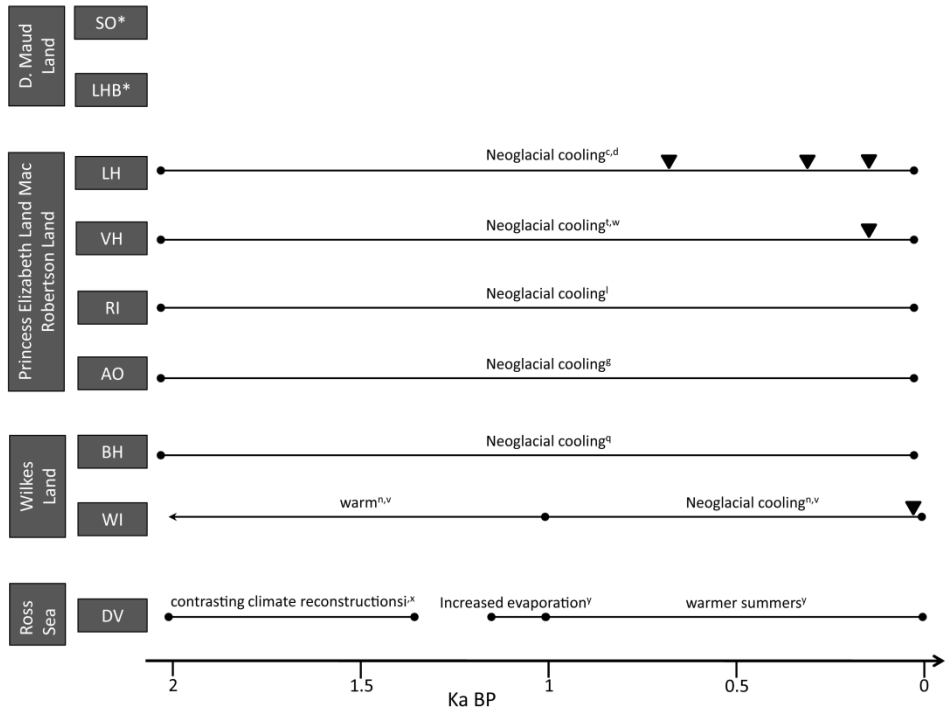

Figure 4 Climate variability along the East Antarctic coastline during the past 2000 years. For regions indicated with an asterisk, detailed records are lacking. Short dry or cold periods are indicated with a triangle. Abbreviations as in Fig.2. Superscript numbers refer to the original publication: for a-w see captions of Fig.2 & 3; [w]McMinn (2000), [x]Hall et al. (2006), [y]Whittaker et al., 2008.

In the RSR, the warmest period of the past 6000 years was inferred between c. 2.3 and 1.1 ka ^{14}C BP (c. 2.6-2.3 and 1.2-0.9 ka BP), based upon an expansion in elephant seal colonies which was linked to a decline in sea ice extent (Hall et al., 2006). However Emslie et al. (2007) conclude that Adélie penguins were absent from the Scott Coast and Ross Island between 2–1.1 ka BP, likely correlated with cooling episodes and extensive sea ice that caused unfavorable marine conditions for breeding in the southern Ross Sea, whilst Hall et al (2006) do not infer there widespread development of land fast ice until after 1.2-0.9 ka BP which led to the abandonment of the elephant seal colonies. These differences in the climate inferences derived from elephant seal versus penguin data have yet to be resolved. Inland enhanced evaporation resulted in Lakes Fryxell, Vanda and Bonney becoming ice-free hypersaline ponds by c. 1.2-1 ka BP (Lyons et al., 1998; Wagner et al., 2006), and at the same time Lake Wilson, a perennially ice-capped, deep (>100 m) lake further South (80°S) in Southern Victoria Land, evaporated to a brine lake (Webster et al., 1996). After 1 ka BP increasing water levels and primary production in the lakes (Lyons et al., 1998; Wagner et al., 2006, Whittaker et al., 2008) are attributed to higher summer temperatures or to an increase in the number of clear, calm and snowless midsummer days (Hendy, 2000). During the last few centuries (< c. 0.2 ^{14}C ka BP, c. 0.4-0.1 ka BP), the Wilson Piedmont Glacier has been more extensive than today as documented by aerial photographs taken in 1956 (Hall and Denton, 2002) but, like other areas of EA there is no clear sign in the McMurdo Dry Valleys of the magnitude and style of glacier advances typical of the Northern Hemisphere Little Ice Age (Hall and Denton, 2002).

Studies in the framework of the US Long Term Ecological Research program have revealed a rapid ecosystem response to local climate cooling in the McMurdo Dry Valleys during recent decades, as evidenced by a decline in lake primary production and declining numbers of soil invertebrates (Doran et al., 2002). However, inter-annual fluctuations are large, as evidenced by the occurrence of an unusually warm summer in 2001-2002, which created sufficient meltwater to replace the prior 14 years of lake level lowering in a period of just three months (Doran et al. 2008).

Synthesis and discussion

Many of the larger currently ice-free regions studied, escaped full glaciation during the LGM, such as the Larsemann Hills (Hodgson et al., 2001, 2009b), the Vestfold Hills (Gibson et al., 2009; Colhoun et al., 2010), Amery Oasis (Fink et al., 2006) and the Bunger Hills (Gore et al., 2001) and possibly also some island and peninsula coastlines in Lützow Holm Bay (Miura et al., 1998), whereas other regions were probably completely glaciated and became gradually ice-free after the Pleistocene-Holocene boundary, with differences in local ice mass and extent causing regional differences in the timing of deglaciation and subsequent colonisation by biota. The onset of deglaciation of the EA oases generally preceded the deglaciation of the AP (Bentley et al., 1999; Anderson et al., 2002; see Hall, 2009 for a review). However, some areas such as Stornes in the Larsemann Hills and parts of the Lützow Holm Bay region became ice-free as recently as the Mid- to Late-Holocene, probably as a result of local ice configurations, further climate warming and ongoing relative sea-level changes. In the RSR, deglaciation started during the transition from the Pleistocene and continued into the Early-Holocene forming a series of large proglacial

lakes. These evaporated to approximately their present size as late as the Mid-Holocene (Hall and Denton, 2000; Wagner et al., 2006). This multi stage deglaciation pattern across EA is similar to that observed in the Northern Hemisphere, where the ice-sheets started to melt immediately after the LGM and continued to disintegrate in various stages until the Late-Holocene (Siegert, 2001). For example, the western part of the North American continent became ice-free during the Pleistocene to Holocene transition (Carlson et al., 2008), whereas the Laurentide Ice-Sheet persisted over the land masses bordering the North Atlantic region during the Early-Holocene. The mechanisms behind these differences in deglaciation patterns along the EA coastline are still unclear. Dating uncertainties are sometimes high which may (partly) underlie the differences in deglaciation history between the different regions. However, it is reasonable to conclude that the main phases of deglaciation were closely linked to the major climate shifts during Termination 1, and the widespread thermal maxima of the Early-Holocene and Mid- to Late-Holocene with regional variations brought about by differences in the response of the ice-sheets to internal glaciological dynamics, the volume of overriding ice at the LGM, global sea-level change, and local climate forcing (cf. Hall, 2009).

The Early-Holocene in EA is characterised by the first thermal optimum, which is well resolved in the majority of terrestrial and coastal marine records between c. 11.5-9.5 ka BP, centred on c. 10 ka BP. This climate optimum is seen in Antarctic ice cores between 11.5 and 9 ka BP (Masson et al., 2000; Stenni et al. 2010), and detected across the continent, for example in a marked phase of deglaciation of the AP Ice-Sheet (e.g. Bentley, 1999; Hall, 2009), and thinning of the WA Ice-Sheet in Marie Byrd Land (Johnson et al., 2008). Moreover, this Early-Holocene optimum on land is also evident in most marine sediment cores (e.g., Finocchiaro et al. 2005, Crosta et al. 2007 and references therein) and coincides with the transition from grounded ice to open marine conditions in some regions of the EA continental shelf, such as in Prydz Bay (Domack et al. 1991; Taylor & McMinn 2002) and Terre Adélie (Denis et al. 2009). The Early-Holocene thermal optimum appears to be a nearly bipolar phenomenon as it is also detected in records from Beringia, Alaska and Northwest America (e.g. Kaufman et al., 2004). However, the North Atlantic region remained cold and didn't experience warmer conditions until c. 2.5 ka later at 7-6 ka BP, as inferred from pollen-based temperature reconstructions for northern Europe (e.g., Davis et al., 2003). The climate at high latitudes in parts of the Southern and Northern Hemisphere (except the North Atlantic region) thus likely responded in phase with the summer insolation maximum at the high latitudes in the Northern Hemisphere during the Early-Holocene (Berger and Loutre, 1991). Interestingly, summer insolation values at the high latitudes in the Southern Hemisphere did not peak during this Early-Holocene period (Berger and Loutre, 1991), but later during the Mid- to Late-Holocene; hence the Early-Holocene climate optimum in Antarctica is likely related to other forcings such as the culmination of the deglacial rise in CO_2 changes in the position and strength of the Southern Westerlies leading to more negative SAM (e.g. Bentley et al., 2009) and/or changes in the thermohaline circulation (THC; Blunier et al., 1998). For the latter scenario geological evidence is still lacking, but it has been suggested that Antarctic interglacial climate optima are caused by transient heat transport redistribution comparable with glacial north-south seesaw abrupt climatic changes (Masson-Delmotte et al. 2010a, b). A possible scenario would then be that decreased

North Atlantic Deep Water formation as a result of the final deglaciation in the Northern Hemisphere during the Early-Holocene weakened the Atlantic Meridional Overturning Circulation (AMOC) and led to warmer conditions over Antarctica. This scenario would then be in agreement with the relatively cold conditions observed in the North Atlantic region (Kaufman et al., 2004).

The period following the Early-Holocene optimum shows complex regional patterns with cold and dry conditions in some regions, coinciding with relatively warmer conditions elsewhere (Fig. 2 and 3), suggesting that regional rather than global forcing mechanisms dominated the climate. This is similar to the marine sediment cores from the continental shelf in which there is also no consensus yet regarding the Early-Holocene climate evolution, but most records there point to the presence of a climate optimum (see Crosta et al. 2008 and reference therein). This thermal optimum either started during the Early-Holocene and lasted until the Mid- or Late-Holocene, or was only shortly interrupted by a cooling trend between 9 and 8 ka BP, after which warmer conditions were re-established until c. 5 ka BP in EA or c. 3 ka BP in West Antarctica (Leventer et al. 1996). For example, less sea ice cover was inferred in the Prydz Bay region between 11,650 and 2600 ^{14}C yr BP (Talyor and McMinn 2002), which was possibly interrupted by a readvance of floating glacial ice between 7400 and 3300 ^{14}C yr BP as observed in the ODP 740A site (Domack et al. 1991). In Adélie Land, a cooler Early-Holocene was followed by a Mid-Holocene warm period (from 7.7 ka BP onwards) with a transition to colder, Neoglacial conditions at c. 4 ka BP (Crosta et al. 2007, 2008). In Victoria Land, the climate cooled from 9.4 ka BP onwards until 8 ka BP, after which seasonal open water conditions and circulation patterns as those of today were established (Finocchiaro et al. 2005). In summary, a marine inferred climate optimum in some areas is apparently out of phase with terrestrially inferred temperatures, or even coincident with cool and dry conditions on land. These anti-phased pattern in climate variability and the disparity between records might reflect (i) differences in heat capacity and hence thermal inertia between the different systems, which is typically higher for the ocean compared with the terrestrial realm (Renssen et al. 2005) and the fact that (ii) the organic fraction in marine sediments reflects spring, summer and autumn conditions (including sea-ice blooms), whereas lacustrine biotic assemblages largely reflect summer conditions when the lakes are ice-free and primary production peaks (Hodgson and Smol, 2008), and (iii) solar insolation maxima during spring, summer and autumn are out of phase at the high latitudes in the Southern Hemisphere during the Holocene (Berger and Loutre, 1991; Bentley et al., 2009). For example, solar insolation was at a maximum during spring at the beginning of the Holocene, whereas the summer insolation was relatively high during the Mid- to Late-Holocene (Renssen et al. 2005). In addition dating uncertainties associated with variable marine reservoir effects in near shore coastal records may also hamper comparison between the different records and anomalies, together with lags in response time of the different archives and proxies used.

In the Amery Oasis there is evidence of a climate optimum between c. 8.6 and 8.4 ka BP (Cremer et al., 2007) or between 8.9 and 8.7 ka BP (Newman et al. unpubl. res.), which slightly predates the colonisation of the RSR by penguins at c. 8 ka BP after an absence of c. 19,000 years (Hall et al., 2006; Emslie et al., 2007). Interestingly, this climate optimum coincides with a cooling trend observed in ice cores (Stenni et al. 2010) and an

open marine record from the South Atlantic Polar Frontal Zone between 9 and 8 ka BP (Nielsen et al. 2004), and, although dating uncertainties are large, it also predates or overlaps (within the dating error) with the well-known temperature decline around 8.2 ka BP in the ice core record from central Greenland (Alley et al., 1997) and between 8.5 and 8 ka BP in records outside the North Atlantic region (Rohling and Pälike, 2005). However, it remains to be seen whether there is a causal link (e.g., seesaw) between the expression of these climate anomalies at the high latitudes in the Northern and Southern hemispheres or if, as some models suggest, these anomalies (after 9 ka) can be explained by the combined effects of local orbital forcing and the long memory of the system (Renssen et al., 2005). Moreover, local processes in the terrestrial realm, such as isostatic uplift and deglaciation, might have had an overriding effect on the regional and global changes such as solar insolation and differences in the thermohaline circulation. Isostatic uplift is known to be high after deglaciation, which, together with glacier and ice-sheet retreat, leads to an increase in the amount of ice-free land which was previously below sea level. This relative increase in ice free ground likely had a negative effect on the local albedo and hence could have led to warmer conditions on land.

The Mid- to Late-Holocene in EA is characterised by the second thermal optimum, which is well resolved along most parts of the coastline but not well resolved in regional ice cores (although secondary warm periods are observed ca. 3 ka BP at Dome C, Dominion Range, and Byrd (Masson et al., 2000, p. 355), and in marine sediment cores from the continental shelf (e.g. Crosta et al. 2007) and near the Antarctic Polar Front (between 50 and 53.2°S; Divine et al. 2010) in which a Neoglacial cooling is observed from 4 ka BP onwards. This Mid- to Late-Holocene warm period in EA can be roughly placed between 4.7 and 1 ka BP and is evidenced by open water coastal marine conditions, increased rates of deglaciation, and wet/warm conditions on land. It is not known if it occurs in coastal Dronning Maud Land, Enderby Land and Terre Adélie due to a lack of long-term high-resolution records in these regions. Similarly, it is not well resolved in the RSR where ice cores point to an earlier secondary warm period at ca. 8-6 ka BP (Masson et al., 2000, p. 355) coincident with an optimum based on the occupation of the region by seals and penguins (Hall et al., 2006). The seal and penguin occupation data then either suggest a later optimum at c. 2.3 and 1.1 ka ^{14}C BP (c. 2.6-2.3 and 1.2-0.9 ka BP) (Hall et al., 2006), or cooling and persistent sea ice (Emslie et al., 2007); a difference in interpretation that requires further research. This is followed by an intensification of Southern circumpolar westerlies at c. 1.2 –1 ka BP, accompanied by relatively cooler conditions in other regions along the EA coastline and in the interior of EA (Masson et al., 2000) and WA (Siple Dome; Mayewski et al., 2009), which is consistent with conditions experienced when the SAM is in its positive mode. In the AP (excluding the northernmost islands), this warm period occurs somewhere between c. 4 and 2 ka BP, whereas in northern sites of the AP it spanned 3.6-3.4 – 0.9 ka BP (see Hodgson et al., 2004 for a review). This Late-Holocene climate optimum in terrestrial environments in Antarctica may be a result of low altitude coastal sites being closer to the 0 °C threshold which would have the effect of amplifying various climate proxies (e.g. Quayle et al. 2002), together with the occurrence of maxima in spring and summer solar radiation during this period (Bentley et al., 2009). Late spring and summer are of high importance in driving primary productivity and inter-annual environmental variability in polar terrestrial and

lake ecosystems (Hodgson & Smol 2008), hence solar insolation maxima during this part of the year are expected to have a profound effect on the records preserved on land. In the AP, an alternative explanation for this warm period is that a poleward displacement of the Southern Westerlies brought warm, moist air to the west side of the AP leading to higher temperatures and precipitation (Bentley et al., 2009). Finally, local processes might also underlie this terrestrial optimum. For example, in the Larsemann Hills, some lakes and likely also their catchments deglaciated during this period which likely led to changes in albedo and a regional warming. It is however unclear whether this deglaciation is the result of the climate optimum, or rather the trigger. This Antarctic Late-Holocene climate optimum is apparently out of phase with anomalies observed in the Northern hemisphere (Mayewski et al., 2004) and in records from the continental shelf (e.g. Crosta et al. 2008). It is clear that there is an urgent need for well-dated records around the EA coastline in order to better compare them with the AP region and with records from the continental shelf and sub-Antarctic regions (e.g. Divine et al. 2010). In addition, these records are needed to study the influence of past climate variability on ecosystem functioning (Hodgson et al., 2004), because the Late-Holocene warming event acts as one of the natural analogues for the climate change that parts of Antarctica are experiencing today.

After 2 ka BP, most areas of EA experienced neoglacial cooling, with markedly cooler or drier events in some regions. With the exception of some ice cores where the most recent cold anomaly is called the 'Antarctic Little Ice Age' (Masson et al., 2000, p354), there is little convincing evidence for a coeval Little Ice Age event (Roberts et al., 2001), nor for anything corresponding convincingly and region-wide to the Medieval Warm Period of the Northern Hemisphere (e.g., Mann et al., 2008).

In the last few decades, a rapid salinity increase has been recorded in lakes in the Windmill Islands region, and a number of ancient moss banks have become desiccated (Wasley, 2006) possibly in response to the increased wind speed observed in some EA coastal regions (Hodgson et al., 2006b). High resolution records from other areas in EA are however lacking. In the RSR, a re-assessment of temperature measurements has revealed that the continent-wide average near-surface temperature trend is positive (Steig et al., 2009). Also in WA, recent measurements and ice core data have revealed that surface temperatures are significantly rising (Schneider and Steig, 2008; Steig et al., 2009). The most vulnerable region in terms of global climate change is without doubt the AP, where temperatures are rising by ~0.55°C per decade, which is six times the global mean (Vaughan et al., 2003). At present, the 'ozone hole' is actually buffering global warming in EA and when it closes, warming is predicted to accelerate there as well (Turner et al., 2009).

Conclusions

Well-dated terrestrial and shallow marine records provide valuable contributions to resolving the magnitude and geographical extent climate changes in EA. Several past climate anomalies appear to be in phase with changes at the higher latitudes in the Northern Hemisphere, whilst others are out of phase (or in anti-phase). There is clear evidence for a nearly Antarctic wide Early-Holocene (11.5-9 ka BP) optimum in phase with changes at Northern Hemisphere high latitudes, but out of phase with changes in the North Atlantic region; and a Mid- to Late-Holocene (4-1 ka BP) optimum near the coast,

subject to regional variations in its precise timing, but occurring well after the orbitally forced (Hewitt and Nitchell, 1998) summer Mid-Holocene warm period experienced between 7-5 ka BP in the Northern Hemisphere high latitudes. There is little or no evidence for a coeval Little Ice Age and Medieval Warm Period in Antarctica. In the most recent period, there is evidence that global warming is starting to significantly impact some ecosystems in various regions in EA, for example through increased primary productivity in lakes, lake level lowering, increases in lake salinity and desiccation of moss banks. At the moment, there is a pressing need for well-dated records to study this present climate anomaly in relation to past natural variability, to reveal the likely ecological consequences and identify both similarities and differences in the respective forcing mechanisms involved. The paucity of data is particularly acute for coastal regions in the Dronning Maud and Enderby Land regions and from Terre Adélie. In the latter region, shallow marine sediments may be the only alternative due to the general lack of ice-free land containing lakes and geological evidence of past environmental changes.

Acknowledgements

This work was initiated by the author's contribution to the special SCAR Antarctic Climate Change and the Environment report. EV is a post-doctoral research fellow with the Fund for Scientific research, Flanders (Belgium). DH is funded by the Natural Environment Research Council (UK). IT is funded by the Institute for the promotion of science and technology in Flanders (Belgium). DR and AM acknowledge the financial support of the Australian Research Council, MM and BW acknowledge the German Research Foundation and SMS acknowledges the National Indian Centre for Antarctic and Ocean Research and the Indian Ministry of Earth Sciences. This work benefited from the HOLANT project funded by the Belgian Federal Science Policy Office and was only possible with the logistic support of the Australian Antarctic Division, the British Antarctic Survey, the Japanese National Institute for Polar Research, Maaike Vancauwenberghe (BelSPO), the Office of Polar Programs of the U.S. National Science Foundation and the Programma Nazionale di Richerche in Antartide (Italy). Fig. 1 was prepared by Peter Fretwell, British Antarctic Survey. Two anonymous reviewers are thanked for their constructive comments on an earlier version of the manuscript.

References

Adamson DA, Colhoun EA (1992) Late Quaternary glaciation and deglaciation of the Bunger Hills, Antarctica. *Ant. Sci.,* **4**: 435-446.

Adamson DA Pickard J (1986) Cainozoic history of the Vestfold Hills. *In*: Pickard J (Eds) Antarctic Oasis, Academic Press, Sydney, pp. 63–97.

Ahn J, Brook EJ (2008) Atmospheric CO_2 and climate on millennial time scales during the Last Glacial Period. *Science*, **322**: 83-85.

Ainley DG, Hobson KA, Crosta X, Rau GH, Wassenaar LI, Augustinus PC (2006) Holocene variation in the Antarctic coastal food web: linking δD and δ^{13}Cin snow petrel diet and marine sediments. *Mar. Ecol. Prog. Ser.,* **306**: 31-40.

Alley RB, Mayewski PA, Sowers T, Stuiver M, Taylor KC, Clark PU (1997) Holocene climatic instability: a prominent, widespread event 8200 yr ago. *Geology*, **25**: 483-486.

Anderson JB, Shipp SS, Lowe AL, Wellner JS, Mosola AB (2002) The Antarctic Ice Sheet during the Last Glacial Maximum and its subsequent retreat history: a review. *Quat. Sci. Rev.,* **21**: 49-70.

Anderson FF, Ali S, Bradtmiller LI, Nielsen SHH, Fleisher MQ, Anderson BE, Burckle LH (2009) Wind-driven upwelling in the Southern Ocean and the deglacial rise in atmospheric CO_2. *Science*, **323**: 1443-1448.

Armand LK, Crosta X, Romero O, Pichon JJ (2005) The biogeography of major diatom taxa in Southern Ocean sediments: 1. sea ice related species. *Palaeogeog. Palaeoclim. Palaeoecol.,* **223**: 93-126.

Barker S, Diz P, Vautravers MJ, Pike J, Knorr G, Hall IR, Broecker WS (2009) Interhemispheric Atlantic seesaw response during the last deglaciation. *Nature*, **457**: 1097-1102.

Baroni C, Orombelli G (1994) Abandoned penguin rookeries as Holocene palaeoclimatic indicators in Antarctica. *Geology*, **22**: 23-26.

Bentley MJ (1999) Volume of Antarctic ice at the Last Glacial Maximum, and its impact on global sea level change. *Quat. Sci. Rev.,* **18**: 1569-1595.

Bentley MJ, Hodgson DA, Smith JA, Cofaigh CO, Domack EW, Larter RD, Roberts SJ, Brachfeld S, Leventer A, Hjort C, Hillenbrand CD, Evans J (2009) Mechanisms of Holocene palaeoenvironmental change in the Antarctic Peninsula region. *Holocene*, **19**: 51-69.

Bera SK (2004) Late Holocene palaeo-winds and climatic changes in Eastern Antarctica as indicated by long-distance transported pollen–spores and local microbiota in polar lake core sediments. *Curr. Sci.,* **86**: 1485-1488.

Berg S, Wagner B, White D, Cremer H, Bennike O, Melles M (2009) Late Pleistocene glaciation history of Rauer Group, East Antarctica. *Ant. Sci.,* **21**: 299-300.

Berg S, Wagner B, Cremer H, Leng MJ, Melles M (2010) Late Quaternary environmental and climate history of Rauer Group, East Antarctica. *Palaeogeog. Palaeoclim. Palaeoecol.,* **297**: 201-213.

Berger A, Loutre MF (1991) Insolation values for the climate of the last 10000000 years. *Quat. Sci. Rev.,* **10**: 297-317.

Berkman PA, Andrews JT, Björck S, Colhoun EA, Emslie SD, Goodwin ID, Hall BL, Hart CP, Hirakawa K, Igarashi A, Ingólfsson O, Lopez-Martinez J, Lyons WB, Mabin MCG, Quilty PG, Taviani M, Yoshida Y (1998) Circum-Antarctic coastal environmental shifts during the Late Quaternary reflected by emerged marine deposits. *Ant. Sci.,* **10**: 345-362.

Björck S, Hjort C, Ingólfsson Ó, Zale R, Ising J (1996) Holocene deglaciation chronology from lake sediments. *In*: López-Martínez J, Thomson MRA, Thomson JW (Eds) Geomorphological map of Byers Peninsula, Livingston Island. BAS GEOMAP Series Sheet 5-A, 49-51. Cambridge, British Antarctic Survey.

Blunier T, Chappellaz J, Schwander J, Dallenbach A, Stauffer B, Stocker TF, Raynaud D, Jouzel J, Clausen HB, Hammer CU, Johnsen SJ (1998) Asynchrony of Antarctic and Greenland climate change during the Last Glacial period. *Nature*, **394**: 739-743.

Broecker WS (1998) Ocean circulation during the Last Deglaciation: a bipolar seesaw? *Palaeoceanography*, **13**: 119-121.

Bromwich DH, Chen B, Hines KM (1998) Global atmospheric impacts induced by year-round open water adjacent to Antarctica. *J. Geophys. Res. – Atmosph.,* **103**: 11173-11189.

Bronge C (1992) Holocene climatic record from lacustrine sediments in a fresh-water lake in the Vestfold Hills, Antarctica. *Geogr. Ann. Ser. A-Phys. Geogr.,* **74**: 47-58.

Carlson AE, Legrande AN, Oppo DW, Came RE, Schmidt GA, Anslow FS, Licciardi JM, Obbink EA (2008) Rapid early Holocene deglaciation of the Laurentide Ice Sheet. *Nature Geoscience*, **1**: 620-624.

Colhoun EA, Kiernan KW, McConnell A, Quilty PG, Fink D, Murray-Wallace CV, Whitehead J (2010) Late Pliocene age of glacial deposits at Heidemann Valley, East Antarctica: evidence for the last major glaciation in the Vestfold Hills. *Ant. Sci.,* **22**: 53-64.

Cremer H, Gore D, Melles M, Roberts D (2003) Palaeoclimatic significance of Late Quaternary diatom assemblages from Southern Windmill Islands, East Antarctica. *Palaeogeogr. Palaeoclimat. Palaeoecol.,* **195**: 261-280.

Cremer H, Heiri O, Wagner B, Wagner B (2007) Abrupt climate warming in East Antarctica during the early Holocene. *Quat. Sci. Rev.,* **26**: 2012-2018.

Cromer L, Gibson JAE, Swadling KM, Ritz DA (2005) Faunal microfossils: indicators of Holocene ecological change in a saline Antarctic lake. *Palaeogeogr. Palaeoclim. Palaeoecol.,* **221**: 83-97.

Cromer L, Gibson JAE, Swadling KM, Hodgson DA (2006) Evidence for a lacustrine faunal refuge in the Larsemann Hills, East Antarctica, during the Last Glacial Maximum. *J. Biogeogr.,* **33**: 1314-1324.

Crosta X, Romero O, Armand LK, Pichon JJ (2005) The biogeography of major diatom taxa in Southern Ocean sediments: 2. open ocean related species. *Palaeogeogr. Palaeoclim. Palaeoecol.,* **223**: 66-92.

Crosta X, Debret M, Denis D, Courty MA, Ther O (2007) Holocene long- and short-term climate changes off Adelie Land, East Antarctica. *Geochemistry Geophysics Geosystems*, **8**: art. Nr. Q11009.

Crosta X, Denis D, Ther O (2008) Sea ice seasonality during the Holocene, Adelie Land, East Antarctica. *Mar. Micropalaeont.,* **66**: 222-232.

Davis BAS, Brewer S, Stevenson AC, Guiot J (2003) The temperature of Europe during the Holocene reconstructed from pollen data. *Quat. Sci. Rev.,* **22**: 1701-1716.

Denis D, Crosta X, Schmidt S, Carson DS, Ganeshram RS, Renssen H, Crespin J, Ther O, Billy I, Giraudeau J (2009) Holocene productivity changes off Adelie Land (East Antarctica). *Palaeoceanography*, **24**: Art. No. PA3207.

Denton GH, Marchant DR (2000) The Geologic basis for a reconstruction of a grounded ice sheet in McMurdo Sound, Antarctica, at the Last Glacial Maximum. *Geogr. Ann. Ser. a-Phys. Geogr.,* **82A**: 167-211.

Divine DV, Koc N, Isaksson E, Nielsen S, Crosta X, Godtliebsen F (2010) Holocene Antarctic climate variability from ice and marine sediment cores: Insights on ocean-atmosphere interaction. *Quat. Sci. Rev.,* **29**: 303-312.

Domack EW, Jull AJT, Nakao S (1991) Advance of fast Antarctic outlet glaciers during the Hypsithermal - Implications for the volume state if the Antarctic Ice-Sheet under global warming. *Geology*, **19**: 1059-1062.

Doran PT, Priscu JC, Lyons WB, Walsh JE, Fountain AG, McKnight DM, Moorhead DL, Virginia RA, Wall DH, Clow GD, Fritsen CH, McKay CP, Parsons AN (2002) Antarctic climate cooling and terrestrial ecosystem response. *Nature*, **415**: 517-520.

Doran PT, McKay CP, Fountain AG, Nylen T, McKnight DM, Jaros C, Barrett JE (2008) Hydrologic response to extreme warm and cold summers in the McMurdo Dry Valleys, East Antarctica. *Ant. Sci.,* **20**: 499-509.

Emslie SD, Woehler EJ (2005) A 9000-year record of Adélie Penguin occupation and diet in the Windmill Islands, East Antarctica. *Ant. Sci.,* **17**: 57-66.

Emslie SD, Coats L, Licht K (2007) A 45,000 yr record of Adélie Penguins and climate change in the Ross Sea, Antarctica. *Geology*, **35**: 61-64.

Fink D, Mckelvey B, Hambrey MJ, Fabel D, Brown R (2006) Pleistocene deglaciation chronology of the Amery Oasis and Radok Lake, Northern Prince Charles Mountains, Antarctica. Earth Planet. Sci. Lett. 243: 229-243.

Finocchiaro F, Langone L, Colizza E, Fontolan G, Giglio F, Tuzzi E (2005) Records of early Holocene warming in a laminated sediment core from Cape Hallett Bay (Northern Victoria Land, Antarctica). *Glob. Planet. Ch.,* **45**: 193-206.

Fulfordsmith SP, Sikes EL (1996) The evolution of Ace Lake, Antarctica, determined from sedimentary diatom assemblages. *Palaeogeogr. Palaeoclim. Palaeoecol.,* **124**: 73-86.

Gibson JAE, Paterson KS, White CA, Swadling KM (2009) Evidence for the continued existence of Abraxas Lake, Vestfold Hills, East Antarctica during the Last Glacial Maximum. *Ant. Sci.,* **21**: 269-278.

Gingele F, Kuhn G, Maus B, Melles M, Schone T (1997) Holocene retreat from the Lazarev Sea shelf, East Antarctica. *Continent. Shel. Res.,* **17**: 137–163.

Goodwin ID (1993) Holocene deglaciation, sea-level change, and the emergence of the Windmill Islands, Budd Coast. *Antarctica. Quat. Res.,* **40**: 70-80.

Goodwin ID (1996) A Mid to Late Holocene readvance of the Law Dome ice margin, Budd Coast, East Antarctica. *Ant. Sci.,* **8**: 395-406.

Gore DB (1997) Blanketing snow and ice; constraints on radiocarbon dating deglaciation in East Antarctic oases. *Ant. Sci.,* **9**: 336-346.

Gore DB, Rhodes EJ, Augustinus PC, Leishman MR, Colhoun EA, Rees-Jones J (2001) Bunger Hills, East Antarctica: ice free at the Last Glacial Maximum. *Geology,* **29**: 1103-1106.

Gosse JC, Phillips FM (2001) Terrestrial *in situ* cosmogenic nuclides: theory and application. *Quat. Sci. Rev.,* **20**: 1475-1560.

Hall BL, and Denton GH (1995) Late Quaternary lake levels in the Dry Valleys, Antarctica. *Ant. J. USA,* **30**: 52-53.

Hall B, and Denton G (1999) New relative sea-level curves for the southern Scott Coast, Antarctica: Evidence for Holocene deglaciation of the western Ross Sea. *J. Quat. Sci.,* **14**: 641-650.

Hall BL, and Denton GH (2000a) Extent and chronology of the Ross Sea Ice Sheet and the Wilson Piedmont Glacier along the Scott Coast at and since the Last Glacial Maximum. *Geogr. Ann. Ser. a-Phys. Geogr.,* **82A**: 337-363.

Hall BL, and Denton GH (2000b) Radiocarbon chronology of Ross Sea Drift, eastern Taylor Valley, Antarctica: Evidence for a grounded ice sheet in the Ross Sea at the Last Glacial Maximum. *Geogr. Ann. Ser. a-Phys. Geogr.,* **82A**: 305-336.

Hall BL, Denton GH, Hendy CH (2000) Evidence from Taylor Valley for a grounded ice sheet in the Ross Sea, Antarctica. *Geogr. Ann. Ser. a-Phys. Geogr.,* **82A**: 275-303.

Hall B, Denton G, Overturf B (2001) Glacial Lake Wright, a high-level Antarctic lake during the LGM and early Holocene. *Ant. Sci.,* **13**: 53-60.

Hall BL, and Denton GH (2002) Holocene history of the Wilson Piedmont Glacier along the Southern Scott Coast, Antarctica. *Holocene*, **12**: 619-627.

Hall BL, Denton GH, Overturf B, Hendy CH (2002) Glacial Lake Victoria, a high-level Antarctic lake inferred from lacustrine deposits in Victoria Valley. *J. Quat. Sci.,* **17**: 697-706.

Hall B, Baroni C, Denton G (2004) Holocene relative sea-level history of the southern Victoria Land Coast, Antarctica. *Glob. Planet. Ch.,* **42**: 241-263.

Hall BL, Hoelzel AR, Baroni C, Denton GH, Le Boeuf BJ, Overturf B, Topf AL (2006) Holocene elephant seal distribution implies warmer-than-present climate in the Ross Sea. *Proc. Nat. Acad. Sci. USA,* **103**: 10213-10217.

Hall BL (2009) Holocene glacial history of Antarctica and the Sub-Antarctic islands. *Quat. Sci. Rev.,* **28**: 2213-2230.

Hambrey MJ, Glasser NF, Mckelvey BC, Sugden DE, Fink D (2007) Cenozoic landscape evolution of an East Antarctic oasis (Radok Lake area, Northern Prince Charles Mountains), and its implications for the glacial and climatic history of Antarctica. *Quat. Sci Rev.,* **26**: 598-626.

Hendy CH (2000) Late Quaternary lakes in the McMurdo Sound region of Antarctica. *Geogr. Ann. Ser. a-Phys. Geogr.,* **82A**: 411-432.

Hewitt CD, and Mitchell JFB (1998) A Fully Coupled GCM Simulation of the Climate of the Mid-Holocene. *Geophys. Res. Lett.,* **25**: 361-364.

Hiller A, Wandu A, Kämpf H, Stackebrandt W (1988) Occupation of the Antarctic continent by petrels during the past 35000 years: inferences from a 14C study of stomach oil deposits. *Polar Biology*, **9**: 69-77.

Hjort C, Ingólfsson O, Bentley MJ, Björck S (2003) The late Pleistocene and Holocene glacial and climate history of the Antarctic Peninsula region as documented by the land and lake sediment records - A review. *In*: Domack E, Leventer A, Burnett A, Bindshadler R, Convey P, Kirby M (Eds.) Antarctic Peninsula climate variability: Historical and palaeonvironmental perspectives. pp. 95-102.

Hodgson DA, Noon PE, Vyverman W, Bryant CL, Gore DB, Appleby P, Gilmour M, Verleyen E, Sabbe K, Jones VJ, Ellis-Evans JC, Wood PB (2001) Were the Larsemann Hills ice-free through the Last Glacial Maximum? *Ant. Sci.,* **13**: 440-454.

Hodgson DA, McMinn A, Kirkup H, Cremer H, Gore D, Melles M, Roberts D, Montiel P (2003) Colonization, succession, and extinction of marine floras during a glacial cycle: a case study from the Windmill Islands (East Antarctica) using biomarkers. *Palaeoceanography,* **18**: doi: 10.1029/2002PA000775.

Hodgson DA, Doran PT, Roberts D, McMinn A (2004) Palaeolimnological studies from the Antarctic and sub-Antarctic islands. *In*: Pienitz R, Douglas MSV, Smol JP (Eds) Developments in palaeoenvironmental research, volume 8. Long-term environmental change in Arctic and Antarctic Lakes, Springer, Dordracht, The Netherlands, pp. 419-474.

Hodgson DA, Verleyen E, Sabbe K, Squier AH, Keely BJ, Leng MJ, Saunders KM, Vyverman W (2005) Late Quaternary climate-driven environmental change in the Larsemann Hills, East Antarctica, multi-proxy evidence from a lake sediment core. *Quat. Res*., **64**: 83-99.

Hodgson DA, Verleyen E, Squier AH, Sabbe K, Keely BJ, Saunders KM, Vyverman W (2006a) Interglacial environments of coastal East Antarctica: Comparison of MIS 1 (Holocene) and MIS 5e (last interglacial) lake-sediment records. *Quat. Sci. Rev.,* **25**: 179-197.

Hodgson DA, Roberts D, McMinn A, Verleyen E, Terry B, Corbett C, Vyverman W (2006b) Recent rapid salinity rise in three east Antarctic lakes. *J. Paleolim.,* **36**: 385-406.

Hodgson DA, and Smol JP (2008) High latitude palaeolimnology. *In*: Vincent WF, and Laybourn-Parry J (Eds) Polar Lakes and Rivers - Limnology of Arctic and Antarctic Aquatic Ecosystems. Oxford University Press, Oxford, UK, pp. 43-64.

Hodgson DA, Abram N, Anderson J, Bargelloni L, Barrett P, Bentley MJ, Bertler NAN, Chown S, Clarke A, Convey P, Crame A, Crosta X, Curran M, di Prisco G, Francis JE, Goodwin I, Gutt J, Massé G, Masson-Delmotte V, Mayewski PA, Mulvaney R, Peck L, Pörtner H-O, Röthlisberger R, Stevens MI, Summerhayes CP, van Ommen T, Verde C, Verleyen E, Vyverman W, Wiencke C, Zane L (2009a) Antarctic climate and environment history in the pre-instrumental period. *In*: Turner J, Convey P, Di Prisco G, Mayewski PA, Hodgson DA, Fahrbach E, Bindschadler R, Gutt J (Eds.) Antarctic Climate Change and the Environment. Scientific Committee for Antarctic Research, Cambridge, pp. 115-182.

Hodgson DA, Verleyen E, Vyverman W, Sabbe K, Leng MJ, Pickering M, Keely BJ (2009b) A geological constraint on relative sea level in Marine Isotope Stage 3 in the Larsemann Hills, Lambert Glacier region, East Antarctica (31 366 - 33 228 cal yr BP). *Quat. Sci. Rev.,* **28**: 2689–2696.

Hodgson DA, and Sime LC (2010) Southern westerlies and CO_2. *Nature Geoscience,* **3(10)**: 666-667.

Hughen KA, Baillie MGL, Bard E, Beck JW, Bertrand CJH, Blackwell PG, Buck CE, Burr GS, Cutler KB, Damon PE, Edwards RL, Fairbanks RG, Friedrich M, Guilderson TP, Kromer B, Mccormac G, Manning S, Ramsey CB, Reimer PJ, Reimer RW, Remmele S, Southon JR, Stuiver M, Talamo S, Taylor FW, Van Der Plicht J, Weyhenmeyer CE (2004) Marine04 marine radiocarbon age calibration, 0-26 cal kyr BP. *Radiocarbon*, **46**: 1059-1086.

Ingólfsson O, Hjort C, Berkman PA, Björck S, Colhoun E, Goodwin ID, Hall B, Hirakawa K, Melles M, Moller P, Prentice ML (1998) Antarctic glacial history since the Last Glacial Maximum: an overview of the record on land. *Ant. Sci.,* **10**: 326-344.

Ingólfsson O, Hjort C, Humlum O (2003) Glacial and climate history of the Antarctic Peninsula since the Last Glacial Maximum. *Arct. Ant. Alp. Res.,* **35**: 175-186.

Johnson JS, Bentley MJ, Ghol K (2008) First exposure ages from the Amundsen Sea embayment, West Antarctica: The late Quaternary context for recent thinning of Pine Island, Smith, and Pope Glaciers. *Geology*, **36**: 223-226.

Jouzel J, Masson-Delmotte V, Cattani O, Dreyfus G, Falourd S, Hoffmann G, Minster B, Nouet J, Barnola JM, Chappellaz J, Fischer H, Gallet JC, Johnsen S, Leuenberger M, Loulergue L, Lueth, D, Oerter H, Parrenin F, Raisbeck G, Raynaud D, Schilt A, Schwander J, Selmo E, Souchez R, Spahni R, Stauffer B, Steffensen JP, Stenni B, Stocker TF, Tison JL, Werner M, Wolff EW (2007) Orbital and millennial Antarctic climate variability over the past 800,000 years. *Science*, **317**: 793-796.

Kaufman DS, Ager TA, Anderson NJ, Anderson PM, Andrews JT, Bartlein PJ, Brubaker LB, Coats LL, Cwynar LC, Duvall ML, Dyke AS, Edwards ME, Eisner WR, Gajewski K, Geirsdottir A, Hu FS, Jennings AE, Kaplan MR, Kerwin MN, Lozhkin AV, Macdonald GM, Miller GH, Mock CJ, Oswald WW, Otto-Bliesner BL, Porinchu DF, Ruhland K, Smol JP, Steig EJ, Wolfe BB (2004) Holocene thermal maximum in the Western Arctic (0-180 degrees W). *Quat. Sci. Rev.,* **23**: 529-560.

Kiernan K, Gore DB, Fink D, White DA, McConnell A, Sigurdsson IA (2009) Deglaciation and weathering of Larsemann Hills, East Antarctica. *Ant. Sci.,* **21**: 373-382.

Kirkup H, Melles M, Gore DB (2002) Late Quaternary environment of Southern Windmill Islands, East Antarctica. *Ant. Sci.,* **14**: 385-394.

Kulbe T, Melles M, Verkulich SR, Pushina ZV (2001) East Antarctic climate and environmental variability over the last 9400 years inferred from marine sediments of the Bunger Oasis. *Arct. Ant. Alp. Res.,* **33**: 223-230.

Leventer A, Domack EW, Ishman SE, Brachfeld S, McClennen CE, Manley P (1996) Productivity cycles of 200-300 years in the Antarctic Peninsula region: Understanding linkages among the sun, atmosphere, oceans, sea ice, and biota. *Geol. Soc. Am. Bull.,* **108**: 1626-1644.

Liu XD, Sun LG, Xie ZQ, Yin XB, Zhu RB, Wang YH (2007) A preliminary record of the historical seabird population in the Larsemann Hills, East Antarctica, from geochemical analyses of Mochou Lake sediments. *Boreas*, **36**: 182-197.

Lorenzini S, Olmastroni S, Pezzo F, Salvatore MC, Baroni C (2009) Holocene Adelie penguin diet in Victoria Land, Antarctica. *Pol. Biol.,* **32**: 1077-1086.

Lyons WB, Tyler SW, Wharton RA, Mcknight DM, Vaughn BH (1998) A Late Holocene desiccation of Lake Hoare and Lake Fryxell, McMurdo Dry Valleys, Antarctica. *Ant. Sci.,* **10**: 247-256.

MacKintosh A, White D, Fink D, Gore DB, Pickard J, Fanning PC (2007) Exposure ages from mountain dipsticks in Mac. Robertson Land, East Antarctica, indicate little change in ice-sheet thickness since the Last Glacial Maximum. *Geology*, **35**: 551-554.

Mann ME, Zhang ZH, Hughes MK, Bradley RS, Miller SK, Rutherford S, Ni FB (2008) Proxy-based reconstructions of hemispheric and global surface temperature variations over the past two millennia. *Proc. Nat. Acad. Sci. USA,* **105**: 13252-13257.

Marshall GJ (2003) Trends in the Southern Annular Mode from observations and reanalyses. *J. Clim*, **16**: 4134–4143.

Marshall GJ (2007) Half-century seasonal relationships between the Southern Annular Mode and Antarctic temperatures. *Int. J. Clim.,* **27**: 373–383.

Marshall GJ (2009) On the annual and semi-annual cycles of precipitation across Antarctica. *Int. J. Clim.,* **29**: 2298-2308.

Marshall GJ, Di Battista S, Naik SS, Thamban M (2011) Analysis of a regional change in the sign of the SAM–temperature relationship in Antarctica. *Climate Dynamics*, **1-2**: 277-287

Masson V, Vimeux F, Jouzel J, Morgan V, Delmotte M, Ciais P, Hammer C, Johnsen S, Lipenkov VY, Mosley-Thompson E, Petit JR, Steig EJ, Stievenard M, Vaikmae R (2000) Holocene climate variability in Antarctica based on 11 ice-core isotopic records. *Quat. Res.,* **54**: 348-358.

Masson-Delmotte V, Stenni B, Jouzel J (2004) Common millennial-scale variability of Antarctic and Southern Ocean temperatures during the past 5000 years reconstructed from the EPICA Dome C ice core. *Holocene*, **14**: 145-151.

Masson-Delmotte V, Stenni B, Pol K, Braconnot P, Cattani O, Falourd S, Kageyama M, Jouzel J, Landais A, Minster B, Barnola JM, Chappellaz J, Krinner G, Johnsen S, Rothlisberger R, Hansen J, Mikolajewicz U, Otto-Bliesner B (2010a) EPICA Dome C record of glacial and interglacial intensities. *Quat. Sci. Rev.,* **29**: 113-128.

Masson-Delmotte V, Stenni B, Blunier T, Cattani O, Chappellaz J, Cheng H, Dreyfus G, Edwards RL, Falourd S, Govin A, Kawamura K, Johnsen SJ, Jouzel J, Landais A, Lemieux-Dudon B, Lourantou A, Marshall G, Minster B, Mudelsee M, Pol K, Rothlisberger R, Selmo E, Waelbroeck C (2010b) Abrupt change of Antarctic moisture origin at the end of Termination II. *Proc. Nat. Acad. Sci. USA,* **107**: 12091-12094.

Matsumoto GI, Komori K, Enomoto A, Imura S, Takemura T, Ohyama Y, Kanda H (2006) Environmental changes in Syowa Station area of Antarctica during the last 2300 years inferred from organic components in lake sediment cores. *Pol. Biosci.,* **19**: 52-61.

Mayewski PA, Rohling EE, Stager JC, Karlen W, Maasch KA, Meeker LD, Meyerson EA, Gasse F, Van Kreveld S, Holmgren K, Lee-Thorp J, Rosqvist G, Rack F, Staubwasser M, Schneider RR, Steig EJ (2004) Holocene climate variability. *Quat. Res.,* **62**: 243-255.

Mayewski PA, Meredith MP, Summerhayes CP, Turner J, Worby A, Barrett PJ, Casassa G, Bertler NAN, Bracegirdle T, Garabato ACN, Bromwich D, Campbell H, Hamilton GS, Lyons WB, Maasch KA, Aoki S, Xiao C, Van Ommen T (2009) State of the Antarctic and Southern Ocean Climate System. *Rev. Geophys.,* **47**: 1-38.

McCormac FG, Hogg AG, Blackwell PG, Buck CE, Higham TFG, Reimer PJ (2004) SHcal04 Southern Hemisphere Calibration, 0-11.0 cal kyr BP. *Radiocarbon*, **46**: 1087-1092.

McMinn A (2000) Late Holocene increase in sea ice extent in fjords of the Vestfold Hills, Eastern Antarctica. *Ant. Sci.,* **12**: 80-88.

McMinn A, Heijnis H, Harle K, McOrist G (2001) Late-Holocene climatic change recorded in sediment cores from Ellis Fjord, eastern Antarctica. *Holocene*, **11**: 291-300.

Melles M, Kulbe T, Verkulich SR, Pushina ZV, Hubberten HW (1997) Late Pleistocene and Holocene environmental history of Bunger Hills, East Antarctica, as revealed by fresh-water and epishelf lake sediments. *In*: Ricci CA (Eds.) The Antarctic Region: Geological Evolution and Processes, Sienna University, Sienna.

Miura H, Moriwaki K, Maemoku H, Hirakawa K (1998) Fluctuations of the East Antarctic Ice Sheet margin since the last glaciation from the stratigraphy of raised beach deposits along the Soya Coast. *Ann. Glaciol.,* **27**: 297-301.

Nielsen SHH, Koc N, Crosta X (2004) Holocene climate in the Atlantic sector of the Southern Ocean: Controlled by insolation or oceanic circulation? *Geology*, **32**: 317-320.

Okuno J, Miura H, Maemoku H (2007) The possibility of the rapid melting of ice sheet in Holocene around the Lützow-Holm Bay, Antarctica. *Geophys. Res.,* Abst. 7.

Petit JR, Jouzel J, Raynaud D, Barkov NI, Barnola JM, Basile I, Bender M, Chappellaz J, Davis M, Delaygue G, Delmotte M, Kotlyakov VM, Legrand M, Lipenkov VY, Lorius C, Pepin L, Ritz C, Saltzman E, Stievenard M (1999) Climate and atmospheric history of the past 420,000 years from the Vostok ice core, Antarctica. *Nature*, **399**: 429-436.

Pickard J, Adamson DA, Heath CW (1986) The evolution of Watts Lake, Vestfold Hills, East Antarctica, from marine inlet to freshwater lake. *Palaeogeogr. Palaeoclim. Palaeoecol.,* **53**: 271-288.

Quayle WC, Peck LS, Peat H, Ellis-Evans JC, Harrigan PR (2002) Extreme responses to climate change in Antarctic lakes. *Science*, **295**: 645-645.

Reimer PJ, Baillie MGL, Bard E, Bayliss A, Beck JW, Bertrand CJH, Blackwell PG, Buck CE, Burr GS, Cutler KB, Damon PE, Edwards RL, Fairbanks RG, Friedrich M, Guilderson TP, Hogg AG, Hughen KA, Kromer B, MccCormac G, Manning S, Ramsey CB, Reimer RW, Remmele S, Southon JR, Stuiver M, Talamo S, Taylor FW, Van Der Plicht J, Weyhenmeyer CE (2004) Intcal04 terrestrial radiocarbon age calibration, 0-26 cal kyr BP. *Radiocarbon*, **46**: 1029-1058.

Renssen H, Goosse H, Fichefet T, Masson-Delmotte V, Koc N (2005) Holocene climate evolution in the high-latitude Southern Hemisphere simulated by a coupled atmosphere-sea ice-ocean-vegetation model. *Holocene*, **15(7)**: 951-964.

Roberts D, McMinn A (1996) Relationships between surface sediment diatom assemblages and water chemistry gradients in saline lakes of the Vestfold Hills, Antarctica. *Ant. Sci.,* **8**: 331-341.

Roberts D, McMinn A (1998) A weighted-averaging regression and calibration model for inferring lake water salinity from fossil diatom assemblages in saline lakes of the Vestfold Hills: a new tool for interpreting Holocene lake histories in Antarctica. *J. palaeolim.,* **19**: 99-113.

Roberts D, McMinn A (1999) A diatom-based palaeosalinity history of Ace Lake, Vestfold Hills, Antarctica. *Holocene*, **9**: 401-408.

Roberts D, Van Ommen TD, McMinn A, Morgan V, Roberts JL (2001) Late-Holocene East Antarctic climate trends from ice-core and lake-sediment proxies. *Holocene*, **11**: 117-120.

Roberts D, McMinn A, Cremer H, Gore DB, Melles M (2004) The Holocene evolution and palaeosalinity history of Beall Lake, Windmill Islands (East Antarctica) using an expanded diatom-based weighted averaging model. *Palaeogeogr. Palaeoclimat. Palaeoecol.,* **208**: 121-140.

Rohling EJ, and Pälike H (2005) Centennial-scale climate cooling with a sudden cold event around 8,200 years ago. *Nature*, **434**: 975-979.

Schaefer JM, Denton GH, Kaplan M, Putnam A, Finkel RC, Barrell DJA, Andersen B G, Schwartz R, Mackintosh A, Chinn T, Schluchter C (2009) High-Frequency Holocene Glacier Fluctuations in New Zealand Differ From the Northern Signature. *Science*, **324**: 622-625.

Schneider DP, Steig EJ (2008) Ice Cores Record Significant 1940s Antarctic Warmth Related to Tropical Climate Variability. *Proc. Nat. Acad. Sci. USA*, **105**: 12154-12158.

Siegert MJ (2001) Ice sheets and late Quaternary environmental change. John Wiley & Sons. 231 pp.

Singh SM, and Tiwari AK (2004) Deep lake sampling in Antarctica using helicopters. *Curr. Sci.,* **87**: 420.

Sinha R, Sharma C, Chauhan MS (2000) Sedimentological and pollen studies of Lake Priyadarshini, Eastern Antarctica. *Palaeobotanist*, **49**: 1-8.

Steig EJ, Morse DL, Waddington ED, Stuiver M, Grootes PM, Mayewski PA, Twickler MS, Whitlow SI (2000) Wisconsinan and Holocene climate history from an ice core at Taylor Dome, Western Ross Embayment, Antarctica. *Geogr. Ann. Ser. a-Phys. Geogr.,* **82A**: 213-235.

Steig EJ, Schneider DP, Rutherford SD, Mann ME, Comiso JC, Shindell DT (2009) Warming of the Antarctic Ice-Sheet surface since the 1957 International Geophysical Year. *Nature*, **457**: 459.

Stenni B, Masson-Delmotte V, Selmo E, Oerter H, Meyer H, Rothlisberger R, Jouzel J, Cattani O, Falourd S, Fischer H, Hoffmann G, Iacumin P, Johnsen SJ, Minster B, Udisti R (2010) The deuterium excess records of EPICA Dome C and Dronning Maud Land ice cores (East Antarctica). *Quat. Sci. Rev.,* **29**: 146-159.

Stocker TF, and Johnsen SJ (2003) A minimum thermodynamic model for the bipolar seesaw. *Palaeoceanography*, **18(4)**: doi 10.1029/2003pa000920.

Taylor F, and McMinn A (2002) Late quaternary diatom assemblages from Prydz Bay, Eastern Antarctica. *Quat. Res.,* 57: 151-161.

Thompson DWJ, and Solomon S (2002) Interpretation of recent Southern Hemisphere climate change. *Science*, **296**: 895-899.

Turner J, Arthern R, Bromwich D, Marshall G, Worby T, Bockheim J, di Prisco G, Verde C, Convey P, Roscoe H, Jones A, Vaughan D, Woodworth P, Scambos T, Cook A, Lenton A, Comiso J, Gugliemin M, Summerhayes C, Meredith M, Naveira-Garabato A, Chown S, Stevens M, Adams B, Worland R, Hennion F, Huiskes A, Bergstrom D, Hodgson DA, Bindschadler R, Bargagli R, Metzl N, van der Veen K, Monaghan A, Speer K, Rintoul S, Hellmer H, Jacobs S, Heywood K, Holland D, Yamanouchi T, Barbante C, Bertler N, Boutron C, Hong S, Mayewski P, Fastook J, Newsham K, Robinson S, Forcarda J, Trathan P, Smetacek V, Gutt J, Pörtner HO, Peck L, Gili JM, Wiencke C, Fahrbach E, Atkinson A, Webb D, Isla E, Orejas C, Rossi S, Shanklin J (2009) The Instrumental Period. *In*: Turner J, Convey P, Di Prisco G, Mayewski PA, Hodgson DA, Fahrbach E, Bindschadler R, Gutt J (Eds.) Antarctic Climate Change and the Environment. Scientific Committee for Antarctic Research, Cambridge, pp. 183-298.

Van de Berg WJ, Van den Broeke MR, Reijmer CH, Van Meijgaard E (2005) Characteristics of the Antarctic surface mass balance, 1958-2002, using a regional atmospheric climate model. *Ann. Glaciol.,* **41**: 97-104.

Van den Broeke MR, van Lipzig NPM (2003) Response of wintertime Antarctic temperatures to the Antarctic Oscillation: results of a regional climate model. *In*: Domack E, Leventer A, Burnett A, Bindschadler R, Convey P, Kirby M (Eds.) Antarctic Peninsula climate variability: Historical and palaeoenvironmental perspectives, Antarctic Research Series, Vol. 79, American Geophysical Union; Washington, DC, pp 43–58.

Vaughan DG, Marshall GJ, Connolley WM, Parkinson C, Mulvaney R, Hodgson DA, King JC, Pudsey CJ, Turner J (2003) Recent rapid regional climate warming on the Antarctic Peninsula. *Clim. Chan.,* **60**: 243-274.

Verkulich SR, Hiller A (1994) Holocene deglaciation of the Bunger Hills revealed by C-14 measurements on stomach oil deposits in snow petrel colonies. *Ant. Sci.,* **6**: 395-399.

Verkulich SR, Melles M, Hubberten HW, Pushina ZV (2002) Holocene environmental changes and development of Figurnoye Lake in the Southern Bunger Hills, East Antarctica. *J. palaeolim.,* **28**: 253-267.

Verleyen E, Hodgson DA, Vyverman W, Roberts D, McMinn A, Vanhoutte K, Sabbe K (2003) Modelling diatom responses to climate induced fluctuations in the moisture balance in continental Antarctic lakes. *J. Paleolim.,* **30**: 195-215.

Verleyen E, Hodgson DA, Sabbe K, Vanhoutte K, Vyverman W (2004a) Coastal oceanographic conditions in the Prydz Bay Region (East Antarctica) during the Holocene recorded in an isolation basin. *Holocene*, **14**: 246-257.

Verleyen E, Hodgson DA, Sabbe K, Vyverman W (2004b) Late Quaternary deglaciation and climate history of the Larsemann Hills (East Antarctica). *J. Quat. Sci.,* **19**: 361-375.

Verleyen E, Hodgson DA, Sabbe K, Vyverman W (2005) Late Holocene changes in ultraviolet radiation penetration recorded in an East Antarctic lake. *J. Paleolim.,* **34**: 191-202.

Wagner B, Cremer H, Hultzsch N, Gore DB, Melles M (2004) Late Pleistocene and Holocene history of Lake Terrasovoje, Amery Oasis, East Antarctica, and its climatic and environmental implications. *J. palaeolim.,* **32**: 321-339.

Wagner B, Melles M, Doran PT, Kenig F, Forman SL, Pierau R, Allen P (2006) Glacial and postglacial sedimentation in the Fryxell Basin, Taylor Valley, Southern Victoria Land, Antarctica. *Palaeogeogr. Palaeoclim. Palaeoecol.,* **241**: 320-337.

Wagner B, Hultzsch N, Melles M, Gore DB (2007) Indications of Holocene sea-level rise in Beaver Lake, East Antarctica. *Ant. Sci.,* **19**: 125-128.

Wanner H, Beer J, Butikofer J, Crowley TJ, Cubasch U, Fluckiger J, Goosse H, Grosjean M, Joos F, Kaplan JO, Kuttel M, Muller SA, Prentice IC, Solomina O, Stocker TF, Tarasov P, Wagner M, Widmann M (2008) Mid- to Late Holocene climate change: an overview. *Quat. Sci. Rev.,* **27**: 1791-1828.

Wasley J, Robinson SA, Lovelock CE, Popp M (2006) Some like it wet – an endemic Antarctic bryophyte likely to be threatened under climate change induced drying. *Functional Plant Biology*, **33**: 443.

Webster J, Hawes I, Downes M, Timperley M, Howardwilliams C (1996) Evidence for regional climate change in the recent evolution of a high latitude pro-glacial lake. *Ant. Sci.,* **8**: 49-59.

White DA, Bennike O, Berg S, Harley SL, Fink D, Kiernan K, Mcconnell A, Wagner B (2009) Geomorphology and glacial history of Rauer Group, East Antarctica. *Quat. Res.,* **72**: 80-90.

Whittaker T, Hall B, Hendy C, Spaulding S (2008) Holocene depositional environments and surface-level changes at Lake Fryxell, Antarctica. *Holocene*, **18**: 775-786.

Wolff EW, Fischer H, Fundel F, Ruth U, Twarloh B, Littot GC, Mulvaney R, Rothlisberger R, De Angelis M, Boutron CF, Hansson M, Jonsell U, Hutterli MA, Lambert F, Kaufmann P, Stauffer B, Stocker TF, Steffensen JP, Bigler M, Siggaard-Andersen ML, Udisti R, Becagli S, Castellano E, Severi M, Wagenbach D, Barbante C, Gabrielli P, Gaspari V (2006) Southern Ocean sea-ice extent, productivity and iron flux over the past eight glacial cycles. *Nature*, **440**: 491-496.

Zwartz DP, Miura H, Takada M, Moriwak, K (1998) Holocene lake sediments and sea-level change at Mt. Riiser-Larsen. *Pol. Geosci.,* **11**: 249-259.